

# Design, Synthesis and Characterization of ABCG2 Inhibitors with a Focus on Water Solubility and Stability in Plasma



## DISSERTATION

ZUR ERLANGUNG DES DOKTORGRADES DER NATURWISSENSCHAFTEN (DR. RER. NAT.)

AN DER FAKULTÄT CHEMIE UND PHARMAZIE DER UNIVERSITÄT REGENSBURG

VORGELEGT VON

**FRAUKE ANTONI**

AUS ERLANGEN

2020



Die vorliegende Arbeit entstand unter Anleitung von Herrn Prof. Dr. Armin Buschauer, der leider viel zu früh verstorben ist, und Herrn Prof. Dr. Günther Bernhardt an der Fakultät für Chemie und Pharmazie der Universität Regensburg.

Promotionsgesuch eingereicht am: 30. September 2020

Tag der mündlichen Prüfung: 09. Dezember 2020

Prüfungsausschuss:

- Prof. Dr. Dominik Horinek (Vorsitzender)
- Prof. Dr. Günther Bernhardt (Erstgutachter)
- Prof. Dr. Pierre Koch (Zweitgutachter)
- Prof. Dr. Joachim Wegener (Drittprüfer)



# Publications

## Articles and Patents

**F. Antoni**, D. Wifling, G. Bernhardt, Water-soluble inhibitors of ABCG2 (BCRP) – a fragment-based and computational approach, *Eur. J. Med. Chem.*, (2020) 112958.

**F. Antoni**, M. Bause, M. Scholler, S. Bauer, S.A. Stark, S.M. Jackson, I. Manolaridis, K.P. Locher, B. König, A. Buschauer, G. Bernhardt, Tariquidar-related triazoles as potent, selective and stable inhibitors of ABCG2 (BCRP), *Eur. J. Med. Chem.*, 191 (2020) 112133.

**F. Antoni**, G. Bernhardt, Derivatives of nitrogen mustard anticancer agents with improved cytotoxicity, *Arch. Pharm.*, n/a (2020) e2000366.

S. Huber, **F. Antoni**, C. Schickaneder, H. Schickaneder, G. Bernhardt, A. Buschauer, Stabilities of neutral and basic esters of bendamustine in plasma compared to the parent compound: kinetic investigations by HPLC, *J. Pharm. Biomed. Anal.*, 104 (2015) 137-143.

H. Schickaneder, C. Schickaneder, A. Buschauer, G. Bernhardt, S. Huber, **F. Antoni**, Preparation of bendamustine derivatives and related compounds for use in treating cancer, WO2015091827A1 (2015).

## Oral Presentations

**F. Antoni**, G. Bernhardt, Approaches to ABCG2 inhibitors with drug-like properties, Barrier and Transporter Meeting (2018, Bad Herrenalb).

**F. Antoni**, G. Bernhardt, Fragment-based discovery of novel ABCG2 inhibitors, Doctoral Colloquium of the Graduate School ChemPharm (2017, Regensburg).

## Poster Presentations

**F. Antoni**, G. Bernhardt, A fragment-based approach to ABCG2 modulators, Summer School Medicinal Chemistry (2018, Regensburg).

**F. Antoni**, G. Bernhardt, A fragment-based approach to ABCG2 inhibitors with drug-like properties, *Frontiers in Medicinal Chemistry* (2018, Jena).

**F. Antoni**, S.A. Stark, M. Scholler, G. Bernhardt, B. König, A. Buschauer, Triazole-type ABCG2 modulators, DPhG Annual Meeting (2016, München).

S.A. Stark, **F. Antoni**, M. Scholler, G. Bernhardt, A. Buschauer, B. König, Synthesis and characterization of triazole-type ABCG2 modulators, Summer School Medicinal Chemistry (2016, Regensburg).

# Contents

<b>1</b>	<b>General Introduction .....</b>	<b>1</b>
1.1	Membrane Transport and ABC Transporters .....	2
1.2	Structure and Mechanism of ABCG2 .....	5
1.3	Functions and Substrates of ABCG2 .....	8
1.3.1	Endogenous Functions .....	9
1.3.2	Barrier Functions .....	9
1.3.3	Function at the Blood-Brain Barrier .....	11
1.3.4	Function in Multidrug Resistance in Cancer .....	12
1.4	Applications of ABCG2 Inhibitors .....	13
1.4.1	Applications as Molecular Tools.....	13
1.4.1.1	Tools for Fundamental Research .....	13
1.4.1.2	Tools for Drug Discovery and Development .....	15
1.4.1.3	Clinical Diagnostic Tools.....	16
1.4.2	Applications as Prospective Drugs .....	16
1.4.2.1	Drugs for Improving Oral Bioavailability .....	16
1.4.2.2	Drugs for Improving Brain Penetration.....	17
1.4.2.3	Drugs for Overcoming Multidrug Resistance in Cancer.....	18
1.5	Reported ABCG2 Inhibitors and Problem Statement .....	20
1.6	Scope and Objectives of the Thesis .....	22
1.7	References .....	24
<b>2</b>	<b>Tariquidar-Related Triazoles as Potent, Selective and Stable Inhibitors of ABCG2 (BCRP).....</b>	<b>33</b>
2.1	Introduction .....	34
2.2	Results and Discussion .....	36
2.2.1	Synthesis.....	36
2.2.2	Inhibition of the ABCG2, ABCB1 and ABCC1 Transport Activity .....	39

2.2.3	Effect on the ABCG2 ATPase Activity .....	42
2.2.4	Thermostabilization of ABCG2 .....	46
2.2.5	Cytotoxicity and Reversal of Drug Resistance .....	47
2.2.6	Stability in Blood Plasma .....	48
<b>2.3</b>	<b>Conclusion .....</b>	<b>49</b>
<b>2.4</b>	<b>Experimental Section .....</b>	<b>51</b>
2.4.1	Chemistry .....	51
2.4.1.1	General Experimental Conditions .....	51
2.4.1.2	Synthesis Protocols and Analytical Data .....	52
2.4.2	Biology .....	75
2.4.2.1	General Experimental Conditions .....	75
2.4.2.2	Cell Culture .....	76
2.4.2.3	Inhibition of ABCG2: Hoechst 33342 Transport Assay .....	77
2.4.2.4	Inhibition of ABCB1: Calcein-AM Transport Assay .....	77
2.4.2.5	Inhibition of ABCC1: Calcein-AM Transport Assay .....	78
2.4.2.6	ABCG2 ATPase Assay .....	78
2.4.2.7	Size-Exclusion Chromatography-Based Thermostability Assay .....	80
2.4.2.8	Chemosensitivity Assay .....	81
2.4.2.9	Chemical Stability Assay (in Blood Plasma) .....	81
<b>2.5</b>	<b>Supplementary Material .....</b>	<b>83</b>
2.5.1	NMR-Spectra of Key Compounds .....	83
2.5.2	Chromatograms (Purity Control) of Key Compounds .....	85
<b>2.6</b>	<b>References .....</b>	<b>88</b>
<b>3</b>	<b>Water-Soluble Inhibitors of ABCG2 (BCRP) – A Fragment-Based and Computational Approach .....</b>	<b>93</b>
<b>3.1</b>	<b>Introduction .....</b>	<b>94</b>
<b>3.2</b>	<b>Results and Discussion .....</b>	<b>97</b>
3.2.1	Design and Synthesis .....	97

3.2.2	Molecular Docking.....	102
3.2.3	Biological Characterization.....	103
3.2.3.1	Inhibition of the ABCG2, ABCB1 and ABCC1 Transport Activity .....	103
3.2.3.2	Cytotoxicity and Reversal of Drug Resistance.....	109
3.2.3.3	Effect on the ATPase Activity .....	110
3.2.3.4	Stability in Blood Plasma.....	112
3.2.4	Aqueous Solubility.....	113
3.2.4.1	Kinetic Solubility.....	114
3.2.4.2	Thermodynamic Solubility .....	118
<b>3.3</b>	<b>Conclusion .....</b>	<b>123</b>
<b>3.4</b>	<b>Experimental Section .....</b>	<b>125</b>
3.4.1	Chemistry .....	125
3.4.1.1	General Experimental Conditions .....	125
3.4.1.2	Synthesis Protocols and Analytical Data .....	126
3.4.2	Molecular Docking.....	167
3.4.3	Biology .....	168
3.4.3.1	General Experimental Conditions .....	168
3.4.3.2	Cell Culture.....	169
3.4.3.3	Inhibition of ABCG2: Hoechst 33342 Transport Assay.....	170
3.4.3.4	Inhibition of ABCB1: Calcein-AM Transport Assay.....	170
3.4.3.5	Inhibition of ABCC1: Calcein-AM Transport Assay.....	170
3.4.3.6	Chemosensitivity Assay.....	170
3.4.3.7	ABCG2 ATPase Assay.....	170
3.4.3.8	Chemical Stability Assay (in Blood Plasma).....	172
3.4.4	Solubility.....	172
3.4.4.1	General Experimental Conditions .....	172
3.4.4.2	Kinetic Solubility Assay.....	173
3.4.4.3	Thermodynamic Solubility Assay .....	173

<b>3.5</b>	<b>Supplementary Material.....</b>	<b>175</b>
3.5.1	Figures 3.13, 3.14 and 3.15 .....	175
3.5.2	NMR Spectra.....	176
3.5.3	Chromatograms (Purity Control).....	213
<b>3.6</b>	<b>References .....</b>	<b>226</b>
<b>4</b>	<b>Summary.....</b>	<b>233</b>
<b>5</b>	<b>Annex: Derivatives of Nitrogen Mustard Anticancer Agents with Improved Cytotoxicity .....</b>	<b>237</b>
<b>5.1</b>	<b>Introduction .....</b>	<b>238</b>
<b>5.2</b>	<b>Results and Discussion .....</b>	<b>241</b>
5.2.1	Synthesis.....	241
5.2.2	Cytotoxicity.....	242
5.2.2.1	Bendamustine and Derivatives .....	243
5.2.2.2	Isobendamustine and Derivatives .....	244
5.2.2.3	Chlorambucil and Derivatives .....	245
5.2.2.4	Melphalan and Derivatives .....	246
<b>5.3</b>	<b>Conclusion .....</b>	<b>247</b>
<b>5.4</b>	<b>Experimental Section .....</b>	<b>249</b>
5.4.1	Chemistry .....	249
5.4.1.1	General Experimental Conditions .....	249
5.4.1.2	Synthesis Protocols and Analytical Data .....	250
5.4.2	Biology .....	257
5.4.2.1	General Experimental Conditions .....	257
5.4.2.2	Cell Culture.....	258
5.4.2.3	Chemosensitivity Assay .....	258
<b>5.5</b>	<b>Supplementary Material.....</b>	<b>260</b>
5.5.1	NMR Spectra.....	260
5.5.2	Chromatograms (Purity Control).....	268

5.6	References .....	271
	Abbreviations.....	273
	Acknowledgements.....	277



# **1 General Introduction**

## 1.1 Membrane Transport and ABC Transporters

Biological membranes are selectively permeable structures, which form the interface between a cell or an organelle and its environment. Membrane transport constitutes one of the most fundamental processes in all living cells – it allows the maintenance of cellular homeostasis [1]. Due to the enormous chemical diversity of the molecules required by or expelled from the cell, it comes to no surprise that the transport mechanisms across biomembranes are multitudinous. In *Escherichia coli*, for example, about 10% of the entire genome encodes membrane-bound and soluble proteins involved in transport processes [2]. The simplest of all transport forms is passive diffusion. While some gases, water and other small polar molecules as well as unpolar compounds can freely permeate a lipid bilayer, ions and larger polar molecules like glucose cannot do so and require transport proteins, such as channel proteins or carriers/transporters, to mediate the passage [3-6]. This process is called passive transport or facilitated diffusion. In case a solute is to be moved against an electrochemical gradient, active transport under the consumption of energy is necessary [4,6]. Active transporters are either driven by an electrochemical potential difference at the biomembrane (secondary active transport) or by the hydrolysis of an energy-carrying molecule, mainly adenosine triphosphate (ATP) (primary active transport) [4,6]. Membrane ATPases are classified into four categories: F-ATPases are mitochondrial or chloroplast ATP synthases; P-ATPases, for instance sodium-potassium pumps or calcium pumps, build an electrochemical gradient; V-ATPases form a proton gradient and are found within many membranes of cell organelles, such as vacuoles in plant cells or endosomes [7]; and ATP-binding cassette (ABC) transporters translocate myriad substrates – inorganic and organic, charged and neutral – across cellular membranes [7-10]. The latter embody by far the largest and most diverse of the transporter families [7,8] and one of the largest protein families in general [11].

The substrates of ABC transporters are beyond number – and so are their functions. They are widespread in all three domains of life. In bacteria and archaea, ABC importers enable the uptake of various nutrients and ABC exporters sequester virulence factors or antibiotics [8,12]. The majority of eukaryotic family members function in the direction of export. On one hand, ABC transporters excrete endogenous metabolites from secretory epithelial cells, such as bile salts in the liver [9,10,13]. On the other hand, at physiological barriers, e.g. the intestinal barrier or the blood-brain barrier (BBB), they protect cells from the entry of diverse xenobiotics, including toxic and carcinogenic substances, but also a wide range of drugs such as cytostatics, antipsychotics or antiepileptic agents [9,10,14,15]. The diversity of the biological roles played by ABC transporters is reflected by their extensive involvement in diseases. A malfunction of ABC transporters is the cause of various severe genetic disorders, such as bile transport

disorders or cystic fibrosis [9,10,13]. Moreover, ABC transporters confer drug resistance (MDR) in cancer [16] or brain diseases [17,18] and they modulate the bioavailability of drugs [9,10,14,15].

Although ABC transporters deserve much attention because of their functions in the human body, they were first discovered and characterized in detail in bacteria, as early as in the 1970s [12,19-22]. Only later it was demonstrated that these proteins are not restricted to prokaryotes. In 1976, Juliano and Ling discovered a drug resistance-related glycoprotein in a mammalian cell line and called it P-glycoprotein (P-gp), because it appeared to confer drug resistance by making the cellular membrane less permeable [23]. It was not until 1986 that studies revealed a strong homology between the DNA sequence of P-gp and the bacterial transport proteins discovered before and it was suggested that P-gp functions as an energy-dependent export pump [24,25]. In the same year, it was recognized by Higgins et al. that highly conserved ATP-binding subunits characterize a large superfamily of transport proteins [26]. The designation ‘ABC transporters’ was first introduced in 1990 by Higgins’ group who named these proteins after their most characteristic feature – the aforementioned ATP-binding cassette [8,27].

Subsequent genome sequencing and phylogenetic analyses confirmed that the ABCs, or nucleotide binding domains (NBDs), are monophyletic, i.e. they have a common evolutionary origin [8,11,26,27]. The NBDs are characterized by highly conserved motifs including the Walker A and B motifs, common to many nucleotide binding proteins [28], and others like the signature motif, which is distinctive of ABC proteins [11,29]. Noteworthy, the ABC protein superfamily also comprises a second, smaller subfamily of cytosolic, non-transporter ABC proteins, which are dedicated to ‘housekeeping’ processes such as protein synthesis [11]. By contrast with the NBDs, the transmembrane domains (TMDs) of ABC transporters are variable and polyphyletic. Bioinformatic analyses showed that the TMDs of exporters have at least three different ancestors [30]. The archetypal ABC transporter comprises two TMDs, each composed of four to eleven (mostly six) transmembrane helices, and two cytosolic NBDs (Figure 1.1) [8,11,27,31-34]. In archaea and bacteria, these four domains often exist as distinct subunits, whereas in eukaryotes usually one NBD and one TMD are fused into half-transporters or all four domains reside in a single polypeptide chain and form a full-transporter [8,11,31-34]. ABC importers additionally comprise an extracytoplasmic solute-binding protein involved in the capture of substrates [12,35].

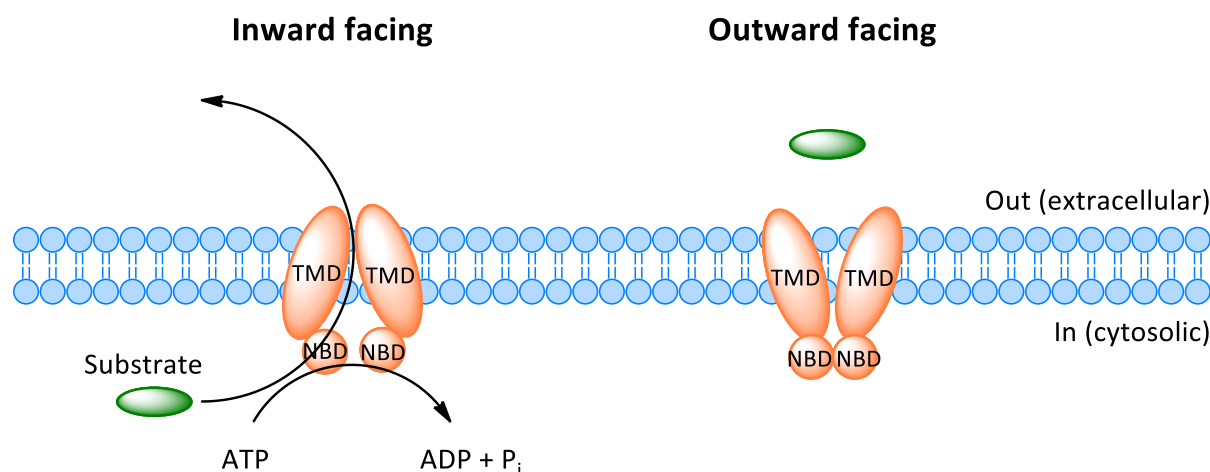


**Figure 1.1.** Cartoon of the structural organization of an archetypal ABC exporter composed of two TMDs and two NBDs. Two conformational states of the transporter – inward facing and outward facing – are depicted to demonstrate the alternating access mechanism of transport. Hydrolysis of ATP to ADP and inorganic phosphate ( $P_i$ ) powers the transport.

In the last two decades structural biology techniques – X-ray crystallography and cryogenic electron microscopy (cryo-EM) – have provided numerous structures of bacterial and human ABC transporters and enabled the visualization of conformational states at high resolutions. The structural organization and mechanism of ABC transporters is depicted in Figure 1.1. Generally, the two TMDs form a translocation pore across the membrane and feature the substrate binding site, whereas the NBDs bind and hydrolyze ATP [10,36-38]. In most ABC transporters the concomitant conformational changes in the NBDs induce a switching of the TMDs between an inward facing and outward facing conformation, thereby translocating the substrate [10,36-38]. It should be noted that there are mechanistic differences between individual ABC transporters, pre-eminently concerning the events at the TMDs, which reflects the variability in the TMDs and differing substrate specificities; even outward-only mechanisms have been proposed for some bacterial subtypes [39].

To date 51 human ABC proteins are known [40]. Due to the progress of the Human Genome Project and to other mass sequencing efforts in the 1990s, 30 human ABC proteins had been identified until 1999 [41]. They were divided into seven subfamilies based on similarity in gene structure (half- vs. full-transporter), on succession of domains, and on sequence homology in the NBDs and TMDs [34,42-45]. The Genome Nomenclature Committee of the Human Genome Organization (HUGO) developed a nomenclature system for the human ABC transporter family, which was implemented in 1999 [37,41]. The seven subfamilies were assigned the designations ABCA to ABCG. The A and C subfamilies are composed of full-transporters, the D and G subfamily of half-transporters and the B subfamily contains both full- and half- transporters; the E and F subfamilies are non-transporter ABC proteins and have no TMDs [34,42-45]. The aforementioned transporter P-gp – the first eukaryotic ABC transporter to be discovered – was termed ABCB1. The human ABC transporter subtypes are of differing

medical relevance. The major drug transporters are ABCB1, ABCG2 and ABCC1 – this triad of efflux pumps seems to mostly account for MDR in cancer [16,46,47] and brain diseases [17], and they play a leading role in tissue defense and the bioavailability of drugs [14,15]. At the BBB, which is one of the most restrictive tissue barrier found within the human body, the predominant transporter was shown to be ABCG2 [48-50].

## 1.2 Structure and Mechanism of ABCG2

In 1990, Chen et al. discovered a novel drug resistance-related membrane protein in a human, doxorubicin-resistant breast cancer cell line [51]. The gene encoding this protein was cloned by Doyle et al. in 1998, who identified the latter as an ABC transporter and named it breast cancer resistance protein (BCRP) [52]. Almost simultaneously, two further articles were published reporting on nearly identical genes expressed in the placenta [53] and in a mitoxantrone-resistant colon carcinoma cell line [54], respectively. Accordingly, the genes were termed ABCP (for the expression in the placenta) and MXR (for mitoxantrone resistance). When the three sequences were eventually compared, they were recognized as essentially identical. Subsequently, the HUGO Genome Nomenclature Committee termed this transporter ABCG2 [55].

The human ABCG subfamily comprises five half transporters [40] (as in all mammals, only rodents have one more) with an NBD at the N-terminus and a TMD at the C-terminus – this is the reverse configuration compared to other ABC subfamilies, where the NBD is at the C-terminus and the TMD at the N-terminus [34,42,44]. The ABCG2 gene spans over 66 kb and encodes a 75 kDa glycoprotein, composed of 655 amino acids [55,56]. Membrane topology analysis of the ABCG2 protein showed that the TMD consists of six transmembrane helices with the N- and C- termini located intracellularly (Figure 1.2A) [57]. As a half-transporter, ABCG2 must dimerize to form a functional transporter, with disulfide bridges contributing to homodimer stabilization [56].

The three-dimensional structure and the transport mechanism of ABCG2 remained a conundrum for almost three decades after its discovery. Generally, integral membrane proteins of mammalian origin are challenging targets for crystallographic studies, because they are often refractory to crystallization and/or difficult to express and purify in sufficient quantities for crystallization [58]. As a case in point, analyses of ABCG2 by electron crystallography provided only low resolution data, precluding insights into the structural details of the transport process [59-62]. In silico homology models did not provide a remedy, since they were not accurate, as demonstrated later by high-resolution techniques [63]. After years of speculations and hazy structural images, a new era was recently inaugurated with the ‘resolution revolution’

in single-particle cryogenic electron microscopy (cryo-EM), mainly driven by direct electron detectors, better microscopes, and improved image processing software [38,58,62]. These novel technologies have made it possible to determine the atomic structure of ABCG2 as well as a broad range of biological macromolecules without crystallization [38,58,62]. In 2017, Locher's group published the first, long-desired high-resolution structure of ABCG2, determined by cryo-EM [63]. One year later, the same group publicized the cryo-EM structures of ABCG2 in complex with two different inhibitors, one of them presented in the thesis in hand, providing a structural basis of small-molecule inhibition of ABCG2 [64]. Later that year, Locher's laboratory provided cryo-EM structures of an ABCG2 mutant trapped in ATP-bound and substrate-bound states, further elucidating the transport mechanism of ABCG2 [65].

The aforementioned studies confirmed conjectures that ABCG2 exhibits an inward open conformation and functions according to the above-mentioned 'switch model' for ABC transport (Figure 1.1). The established membrane fold of the ABCG2 monomer with six transmembrane helices (TMs 1-6) was refined as depicted in Figure 1.2A. The NBD of each monomer is linked to TM1a via a highly charged amino acid sequence. The longest extracellular loop (EL3), between TM5c and TM6a, contains a single *N*-glycosylation site and three cysteine residues, two of which form an intramolecular disulfide bond and the third an intermolecular disulfide bridge to the second monomer. The two monomers form a homodimer with twofold symmetry (Figure 1.2B). The TMD interface is formed by TM2 and TM5 of opposing ABCG2 monomers. At the interface, ABCG2 displays two cavities – the first of these (cavity 1) is accessible from the cytoplasmic side of the membrane and is separated from a second, extracellular site (cavity 2) by a plug formed by two leucine residues of opposing monomers. Cavity 1 was assigned the role of a multidrug binding pocket, accommodating both substrates and inhibitors of ABCG2, the slit-like shape of the cavity favoring flat, polycyclic and hydrophobic molecules. The NBDs are in functionally 'open' conformation in the absence of a substrate, with a gap between the catalytically relevant motifs, but they remain in contact. [63,65]

Upon the binding of a substrate and ATP, conformational changes convert the transporter to an outward facing state (closed NBDs, rotated TMDs with collapsed cavity 1, open 'leucine plug' and cavity 2), the substrate being moved to cavity 2, from where it is expelled into the extracellular space (Figure 1.2B). The binding of two ATP molecules provides the power stroke for these conformational changes, which are induced via strict conformational coupling of the NBDs and TMDs. ATP hydrolysis to ADP and inorganic phosphate ( $P_i$ ) resets the transporter to the inward facing conformation. [63,65]

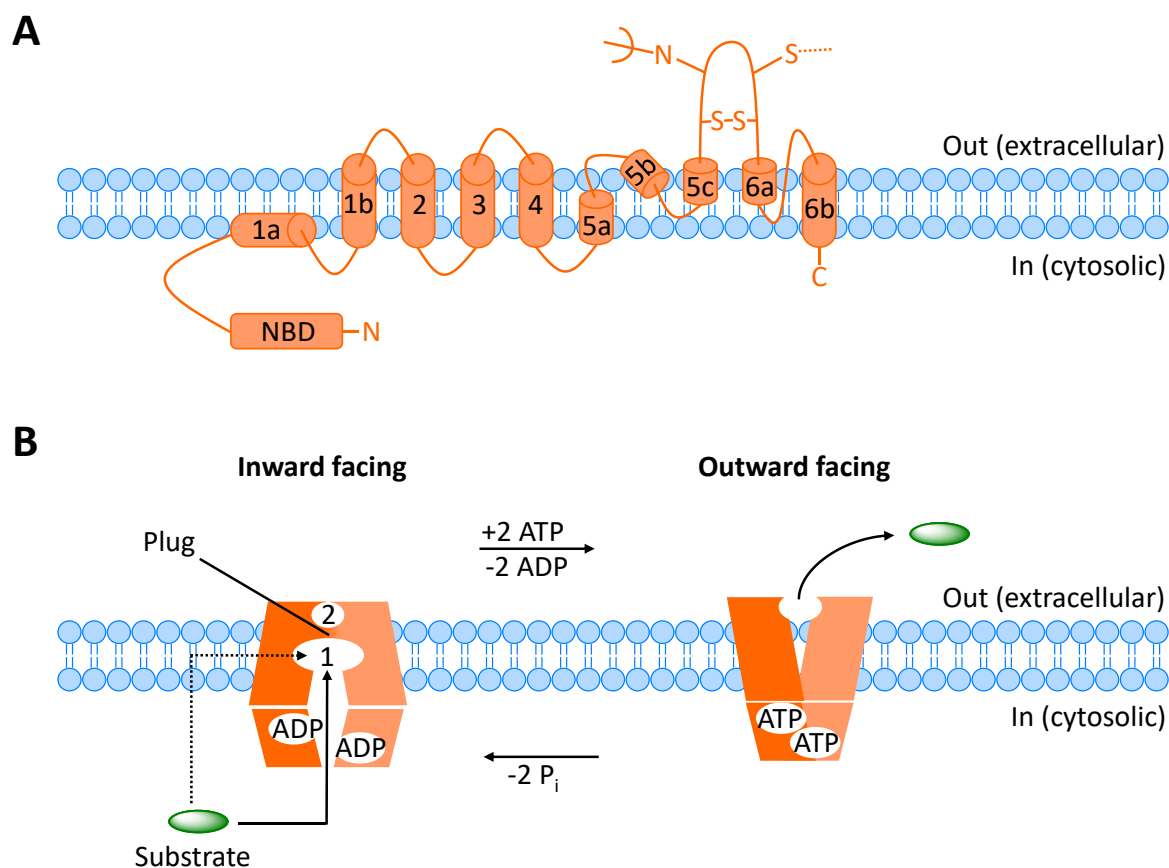


**Figure 1.2.** Cartoon of the structure and mechanism of ABCG2. **(A)** Membrane topology of the ABCG2 monomer. Cysteine residues forming intra- and intermolecular disulfide bonds are indicated, as is the *N*-glycosylation site. **(B)** Transport mechanism of the ABCG2 homodimer. The substrate enters cavity 1 from the cytoplasm or the inner leaflet of the membrane, the 'leucine plug' blocking the access to cavity 2. ATP binding induces the closing of the NBD interface, conversion of the homodimer from the inward to the outward facing state and the release of the substrate to the outside. Hydrolysis of ATP to ADP and  $P_i$  is accompanied by the return of the transporter to the inward facing state.

Small-molecule inhibitors were shown to bind to the central multidrug binding site (cavity 1), just as substrates do. Either one or two molecules – depending on inhibitor size and shape – occupy almost the entire volume of cavity 1, thereby preventing the binding of other molecules, such as transporter substrates; in this sense, the inhibitors act competitively. Simultaneously, they lock the inward open conformation, and due to the conformational coupling of the TMBs to the NBDs, the closing of the NBDs and the ATPase activity, i.e. the ATP hydrolysis, are inhibited. The studies by Locher's group also shed light on the question as to why certain compounds act as substrates, while others are inhibitors of ABCG2. The data corroborated the theory that the key determinant is the binding affinity. Whereas substrates appeared to bind deep in cavity 1, inhibitors were found to fill the cavity completely (one or two molecules) and immobilize the transporter like 'wedges', the numerous contacts to the TM helices explaining the increased binding affinity. [64]

## 1.3 Functions and Substrates of ABCG2

Soon after the discovery of ABCG2 in multidrug-resistant cancer cells, the expression of the protein in normal human tissue was researched in several studies, both on the RNA and on the protein level, the latter by using antibodies against ABCG2, such as 5D3 [66,67]. The tissue distribution pattern emerging from these reports – very similar to ABCB1 – implied that ABCG2 plays a role in the protection against xenobiotics and in the secretion/excretion of endobiotics, apart from conferring MDR to cancer cells [66,67]. Indeed, subsequent studies on *abcg2*-knockout mice and on loss-of-function polymorphisms of ABCG2 in humans confirmed these physiological functions [68,69].

Figure 1.3 shows a schematic overview of the ABCG2 localization in the human organism. The protein is expressed in the apical plasma membrane of epithelial cells throughout the body. It is located in the gastrointestinal tract, the liver and biliary tract, and the kidney, limiting the absorption and promoting the elimination of substrates. The highest expression was observed in the placenta, but also the testes and the brain are protected by ABCG2. The role of ABCG2 in the (lactating) breast is still somewhat enigmatic. Besides epithelial cells, (hematopoietic) stem cells express ABCG2 in the plasma membrane. [66,67,70].

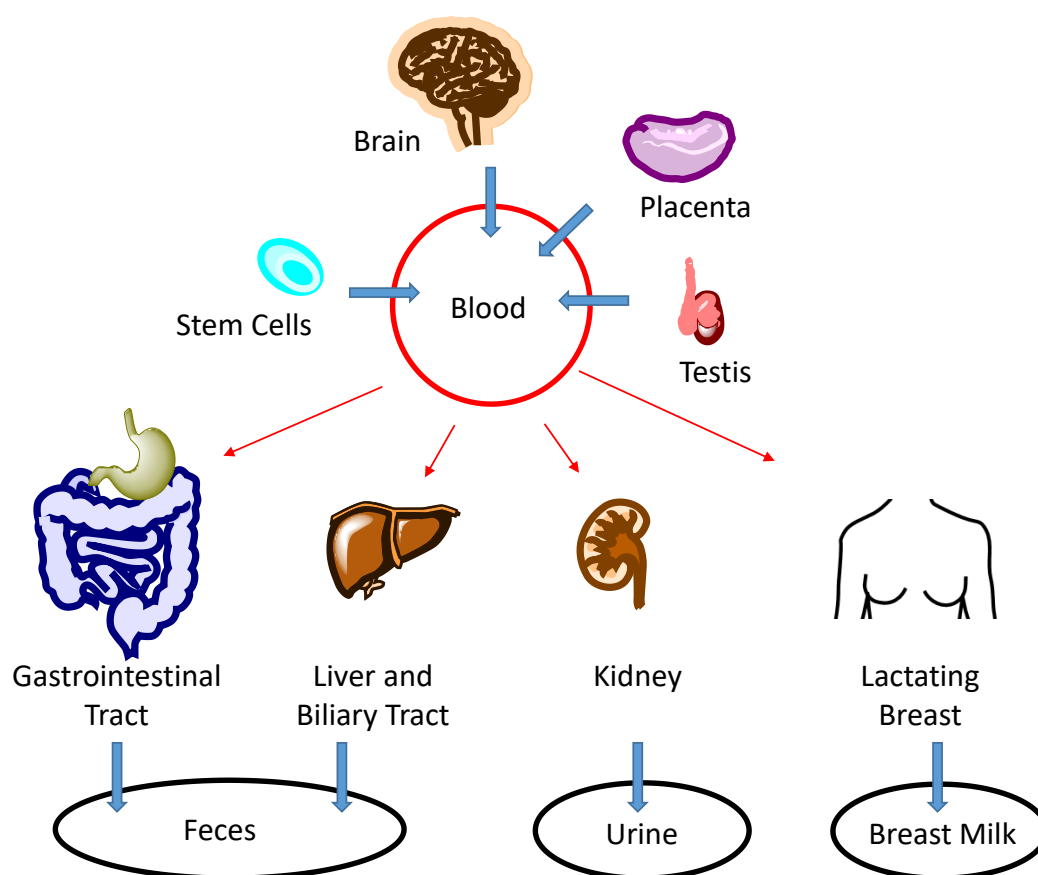


**Figure 1.3.** Schematic overview of ABCG2 expression in normal tissue. Blue arrows indicate the direction of substrate transport.

### 1.3.1 Endogenous Functions

Various studies suggest that transporters involved in drug resistance also have physiological functions: the secretion/excretion of metabolites, nutrients, antioxidants, microbiome products, bile salts, neurotransmitters, other neuro-active molecules, hormones, and signaling molecules [13]. In the case of ABCG2, several endogenous substrates (Figure 1.4) have been discovered. Studies identified sulfated conjugates of steroid hormones as ABCG2 substrates, suggesting an important role in the biliary and renal excretion of these hormones [71] (steroids are converted to water-soluble conjugates for excretion). Also the precursor of steroid hormones, cholesterol, and other sterols are extruded by ABCG2 [72]. Furthermore, it was discovered that ABCG2 is involved in the cellular export of porphyrins and hemes and their biliary excretion, possibly protecting the liver and other cells from an accumulation of these compounds, which is toxic and tends to occur under hypoxic conditions [73]. The abundant expression of ABCG2 in (hematopoietic) stem cells and the ability to survive under hypoxic conditions are thought to be related [73]. Moreover, ABCG2 is an important urate transporter, allowing excretion in the kidney and gastrointestinal tract, and its malfunction is associated with the gout disease [74]. On a final note, ABCG2 also secretes vitamin B<sub>2</sub> (riboflavin) into the breast milk and bile [68]. This finding elucidates the presence of ABCG2 in the mammary gland a little, however it is still controversially discussed why a xenobiotic transporter is used to secrete vitamins into breast milk [68].

### 1.3.2 Barrier Functions

Various lipophilic compounds rapidly pass through biological membranes. By recognizing and removing (often toxic) xenobiotics from the cell, ABC transporters – mainly ABCG2, ABCB1 and ABCC1 – form our cellular defense system [14,75]. ABCG2 is a gatekeeper at all major physiological barriers [14,75]. The first hurdle after ingestion are the pre-systemic barriers, namely the intestinal barrier (gut-blood barrier) and the hepatic barrier (blood-bile barrier). Among the exogenous substrates of ABCG2 (Figure 1.4) are the following dietary toxins: pheophorbide A, a phototoxic chlorophyll metabolite structurally related to porphyrin, which occurs in plant-derived foods [76], PhIP (2-amino-1-methyl-6-phenylimidazo(4,5-b)pyridine), a carcinogen formed during the frying and cooking of meat [77], and aflatoxin B<sub>1</sub>, a carcinogen produced by certain molds [78]. Studies indicate that ABCG2 prevents or limits the absorption of the latter compounds in the gut, and mediates the efflux into the bile. Xeno-substrates that have managed to enter into the systemic circulation are excreted by ABCG2 at the renal barrier (blood-urine barrier). Also distribution to organs is limited by ABCG2 – it is highly expressed at the BBB and the blood-testis barrier, protecting these especially sensitive organs. Moreover,

at the blood-placental barrier (maternal-fetal barrier), ABCG2 defends the fetus against toxic materials ingested by the mother. [14,70,75]

The flipside of the coin is that ABCG2, as well as ABCB1 and ABCC1, also accepts numerous drugs as substrates – with severe consequences. Firstly, the oral bioavailability of such drugs is often poor. For instance, the widely used anticancer drug topotecan exhibits low oral bioavailability of around 30%, which was attributed mainly to its property as an ABCG2 substrate [79,80]. Therefore, intravenous application is standard for many ABCG2-transported drugs, which reduces a patient's quality of life and increases hospital costs, in view of the fact that the patient cannot administer the drug at home [79]. Secondly, drugs that are ABCG2 substrates have only very limited access to the brain – a major obstacle in the treatment of many brain disorders such as HIV infection of the brain or brain cancer, patients with a primary or metastatic brain tumor having a dismal prognosis [17,80]. And thirdly, eponymous for BCRP, expression of the protein in cancer cells confers MDR [70].

Drugs which are substrates of ABCG2 (Figure 1.4) comprise – but are not limited to – anticancer agents such as mitoxantrone, topotecan, methotrexate, and the tyrosine kinase inhibitors imatinib, gefitinib and nilotinib [70,81]; antibiotics like erythromycin [81]; antivirals including anti-HIV drugs such as lamivudine [81]; anti-inflammatory agents like sulfasalazine [81]; and the antiepileptic drug lamotrigine [82]. Noteworthy, also some fluorescent dyes are transported by ABCG2, for instance Hoechst 33342 and rhodamine 123 [81].

Taken together, over 200 transport substrates of ABCG2 have been identified, which considerably overlap with ABCB1 [83].

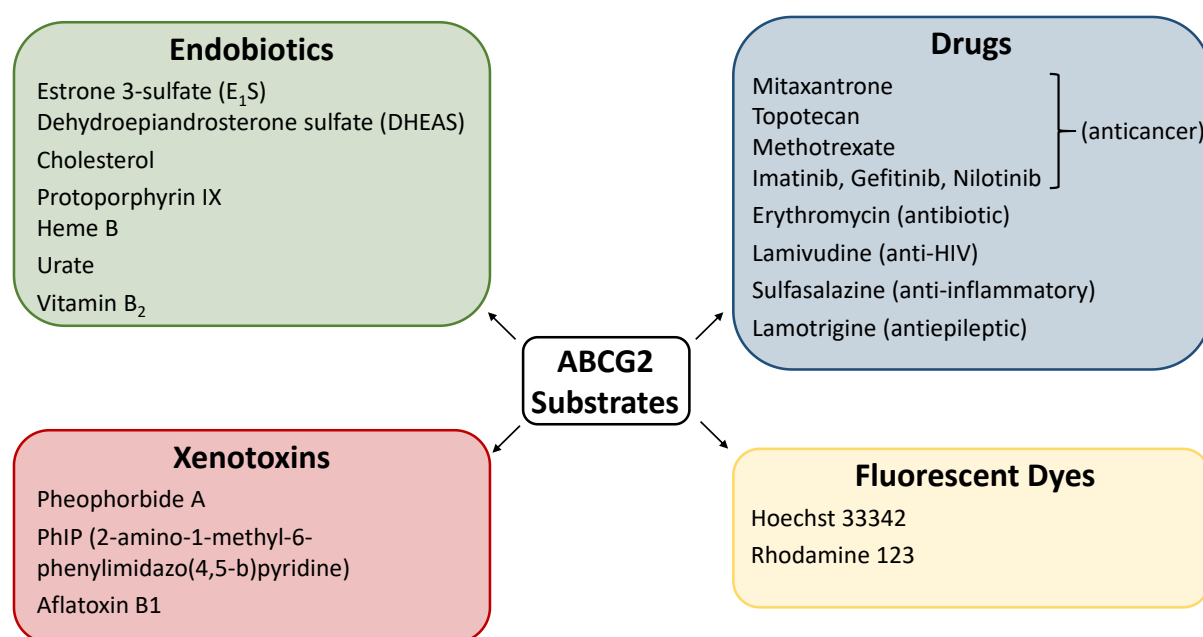


**Figure 1.4.** Selected substrates of ABCG2.

### 1.3.3 Function at the Blood-Brain Barrier

The BBB is one of the most restrictive barriers found within the body [84], which comes to no surprise, considering that the brain is our most critical and most sensitive organ [85]. The BBB is formed primarily by a single monolayer of endothelial cells lining the brain capillaries (Figure 1.5), and represents a dual barrier: physical and biological [84,85]. In contrast to endothelia in peripheral capillaries, these endothelial cells are connected by tight junctions, making the BBB the densest physical barrier in the body (together with the urinary bladder) [17,84,85]. Therefore, paracellular transport of substances into the brain is negligible and the brain endothelium has to be penetrated via the transcellular route, which is restricted biologically by the expression of efflux pumps on the surface of the endothelial cells [17,18,84]. Quantitative (transcriptomic and proteomic) analyses of transporter expression in human brain microvessels revealed that ABCG2 is the most expressed efflux transporter at the BBB, followed by ABCB1 and, to a much lesser extent, by some members of the ABCC subfamily (Figure 1.5) [48-50]. It is worth mentioning that in mice, by contrast, ABCB1 was found to be predominant at the BBB, which led to the initial assumption that this is also the case at the human BBB. This interspecies difference questions the reliability of extrapolating animal data for predicting brain distribution of ABCG2 and ABCB1 substrates in humans [48-50].

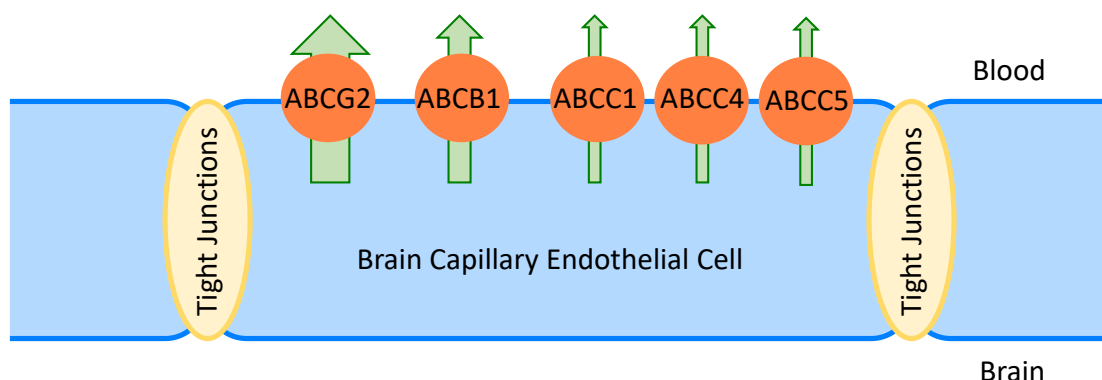


**Figure 1.5.** Expression of ABC transporters (biological barrier) in brain capillary endothelial cells, which are connected by tight junctions (physical barrier) and constitute the principal cellular element of the BBB.

The BBB is almost impermeable to drugs – approximately 98% of small molecule and all large molecule medications are normally excluded from the brain [84]. This is a key mechanism of drug resistance in brain diseases – a complex phenomenon, to which ABCG2 and ABCB1 contribute in two ways: firstly, through their constitutive expression at the BBB and secondly by overexpression (at the BBB or in the target tissue) in some brain diseases, which can be triggered by the activation of nuclear receptors [17,18]. A detailed description of the ABC transporter regulation can be found in an excellent review [86].

In short, the expression of ABCG2 and ABCB1 has been shown to be the main reason for the difficulties in treating brain diseases [17]. Therefore, effective strategies to overcome the restrictions by the BBB, especially ABCG2 and ABCB1, have to be developed.

### **1.3.4 Function in Multidrug Resistance in Cancer**

MDR in cancer is the ability of cancer cells to become simultaneously resistant to multiple, structurally and functionally unrelated drugs – a significant impediment to successful chemotherapy [16,87]. There are several mechanisms that cause drug resistance, including reduced drug uptake, e.g. by endocytosis, activation of detoxifying systems, such as DNA repair and cytochrome P450 oxidases, and defective apoptotic pathways [16]. The most commonly encountered mechanism is an increased efflux of cytostatics mediated by ABC transporters, mainly ABCG2 and its functional homologs ABCB1 and ABCC1 [46]. The notorious activity of ABCG2 in extruding anti-tumor drugs in a variety of cancer cell lines in vitro has been firmly established. By contrast, the clinical relevance of ABCG2 is still sketchy and there have been conflicting reports [70,83]. Studies on clinical samples usually examine the expression of ABCG2, either on the RNA or protein level, and correlate the latter with the outcome of a drug treatment regimen. Most of such studies were carried out for hematological malignancies. There is considerable evidence that ABCG2 (as well as ABCB1) is associated with a poor result in acute myeloid leukemia (AML) and diffuse large B-cell lymphoma, whereas for acute lymphoid leukemia the evidence is less convincing [70,83,88]. Yet, even for AML there exist contradictory studies [70]. Also (leukemic) cancer stem cells express high levels of ABCG2 (and ABCB1), which has been found to correlate with a meager response to chemotherapy [70,83,88]. In solid tumors, the picture is mixed; some studies of solid tumors showed correlation between ABCG2 expression and prognosis, such as for lung or gastric cancer, while others did not. For many solid tumor types, there are not enough studies to draw compelling conclusions [70,83,88].

After almost half a century of research on drug transporters, launched with the discovery of ABCB1 in the 1970's, the role of ABC transporters in clinical MDR has still not yet been clarified, especially that of ABCG2, the latest major drug transporter discovered. Several reasons have been invoked for this deficiency. A great problem is the detection of ABCG2 expression. The detection is variable across laboratories and often not validated at all or validated with a cell line expressing extremely high levels of ABCG2, which one would not expect in clinical samples [70,89]. Besides, ABCG2 is often detected on the RNA level, which does not always directly correlate with the protein level [90]. In addition, ABCG2 has several polymorphic variants, which was not taken into consideration in all studies [90]. A second major challenge is the complexity of MDR mechanisms. Often, the expression of only one

transporter was examined, though the expression of multiple ABC transporters in a single tumor type is common [47,70]. In addition, studies indicate that several other survival factors, such as anti-apoptotic proteins, are up-regulated along with ABCG2, sometimes via the same regulatory machinery [90]. Thus it was suggested that ABCG2 expression by itself is not the sole mechanism behind MDR but rather a marker [90], which is supported by the intriguing observation that ABCG2 expression correlates positively with a resistant phenotype even if the drugs employed are not ABCG2 substrates [83,90].

Apart from chemotherapy, ABCG2 expression is also linked to the failure of photodynamic therapy, since some tumor-selective photosensitizers are substrates of ABCG2 [91].

All in all, studies have shown many correlative links between ABCG2 expression and clinical outcome, yet these have not proved causal. Despite this caveat, it is interesting that the tumor types most refractory to chemotherapy are among those with the highest levels of ABCB1 or ABCG2 expression [47], which suggests that overcoming these transporters may contribute to overcoming MDR in cancer.

## **1.4 Applications of ABCG2 Inhibitors**

In parallel to mechanistic and functional studies, research has also focused on finding inhibitors of ABCG2. Given the wide distribution of the protein in the human body, its various functions including the involvement in diseases and drug response, and all the still open questions in these matters, several applications for ABCG2 inhibitors are obvious. On one hand, they are needed as molecular tools to gain further insight into the mechanism of ABCG2, its role in the human body, and its interaction with drugs. On the other hand, they may be of interest for improving the oral bioavailability of drugs and for overcoming drug resistance in brain diseases and in cancer.

### **1.4.1 Applications as Molecular Tools**

#### **1.4.1.1 Tools for Fundamental Research**

Comprehension of the molecular mechanism of ABC transporters is essential for understanding and modulating their function. High-resolution structural data offer an opportunity to model compounds into the binding pocket, which may facilitate a structure-based inhibitor and drug design or the identification of substrates [63]. ABC transporters are highly dynamic systems and a single structure is merely a snapshot of one conformational state of the protein as it moves its substrate through the membrane [38]. Thus, more than one structural image is necessary in order to understand the transport mechanism in detail, especially also with the protein trapped in a substrate-bound, ATP-bound or inhibitor-bound state. Therefore, inhibitors of ABC

transporters suitable for ‘complexing’ with the respective transporter in structural biology experiments are required. In the case of ABCG2, structures of the protein in complex with two different inhibitors have been published (see Section 1.2) [64], one of which will be presented in Chapter 2 of this thesis.

Fundamental research into the functions of ABCG2 depends heavily on experiments with *abcg2*-knockout mice. The use of selective ABCG2 inhibitors, i.e. a chemical instead of a genetic disruption of the ABCG2 function, complements this approach. Moreover, the application of dual ABCB1/ABCG2 inhibitors is an alternative to double-knockout mice [90,92].

Although the results of animal studies are valuable, the extrapolation to humans is difficult due to interspecies differences. Experiments in humans are restricted to non-invasive methods, positron emission tomography (PET) being used most frequently [93]. For this purpose, a PET imaging probe that interacts with the ABC transporter is necessary: a substrate or inhibitor labeled e.g. with  $^{11}\text{C}$  or  $^{18}\text{F}$  [93]. Usually, transporter imaging probes used in PET studies are not molecules designed de novo, but are marketed drugs or natural food constituents (or metabolites thereof), which are repurposed for this application [93]. The first in vivo evidence for ABC transport activity at the human BBB was produced via PET imaging by Sasongko et al. in 2005. The distribution of the ABCB1-selective substrate [ $^{11}\text{C}$ ]verapamil (an antiarrhythmic drug) to the brain was increased during the inhibition of ABCB1 by cyclosporin A (an immunosuppressant drug) – a proof of ABCB1 activity at the human BBB [94]. This is an excellent example of how inhibition of an ABC transporter enabled pioneering fundamental research.

The visualization of ABCG2 at the human BBB is hampered by the lack of an ABCG2-selective substrate probe. Langer’s group, who has conducted extensive research on imaging ABC transporter functions, developed a protocol in which they used a dual ABCB1/ABCG2 substrate probe and eliminated the influence of ABCB1 efflux by inhibiting this transporter with tariquidar (Figure 1.6) [95,96]. For lack of a clinical ABCG2 inhibitor, another obstacle, they performed experiments on subjects who were either non-carriers or heterozygous carriers of an ABCG2 polymorphism associated with a reduced function of the protein [96]. Indeed, the distribution of the substrate to the brain was increased in the carriers of the polymorphism – the first verification of ABCG2 activity at the human BBB in vivo, reported only four years ago [96]. To date, clinical ABCG2 inhibitors are still quite scarce and selective as well as dual ABCG2/ABCB2 inhibitors (depending on the experimental design) are urgently needed for the PET experiments with labeled substrate probes, as strikingly demonstrated by the elaborate workaround applied by Langer and co-workers. Furthermore, selective ABCG2 inhibitors amenable to PET labeling are of interest as PET imaging agents [97].

### 1.4.1.2 Tools for Drug Discovery and Development

During the discovery and development of new drugs, interactions of the latter with ABC transporters need to be assessed for several reasons. Firstly, it is likely that these drug efflux pumps limit the absorption and distribution of potential medications and promote their elimination; in case of anticancer agents, the uptake by cancer cells may be restrained. Thus, pharmaceutical companies include ABCB1 and ABCG2 transporter assays in early screens in drug discovery to eliminate drug candidates that are substrates of these proteins [98], which can be considered ‘antitargets’ in this respect [99]. Secondly, by contrast, compounds that do have substrate properties are selected in case drugs are not intended to enter the brain. Third generation antihistaminic agents, for example, were designed as substrates of ABC transporters and hence are devoid of central side effects like sleepiness [99,100]. And thirdly, relevant in (pre-) clinical drug development, substrate and inhibitor properties of drugs can cause drug-drug interactions (DDIs). When two drugs which interact with the same ABC transporter are co-administered, one drug may induce transporter inhibition or saturation and thereby change the disposition of the other drug [101]. This phenomenon often causes severe adverse drug reactions in patients [102]. Therefore, the importance of assessing drug-transporter interactions was emphasized in a statement of the International Transporter Consortium in 2010 [102], on the basis of which regulatory authorities – the US Food and Drug Administration (FDA) and the European Medicines Agency (EMA) – recommend in their guidelines that all investigational drugs should be evaluated as substrates or inhibitors of ABCB1 and ABCG2 [103,104].

In the assessment of drug-transporter interactions, prototypical ABC inhibitors are important molecular tools. For instance, in vitro trans-epithelial transport assays, complemented with the use of selective inhibitors, allow probing for ABC transporter substrates [102]. On the examination of DDIs, in vivo studies may be recommended if a drug candidate turns out to be an ABC transporter substrate or inhibitor in vitro [102]. Regulators do not endorse animal studies due to pronounced interspecies differences [105] – DDI studies in humans are the ‘gold standard’ [106]. Healthy volunteers are treated with the drug of interest and an ABC inhibitor, in case the drug is a substrate. Vice versa, if the drug in question is an inhibitor, it is administered together with a substrate. Then, the drug concentration in the blood is assessed and compared to the results achieved when the drug is dosed alone [106]. Some DDIs may lead to changes in the organ distribution of drugs (e.g. brain, liver, kidneys) without affecting plasma concentrations. To elucidate potential DDIs on a tissue level, imaging techniques such as PET can be used. If the drug of interest is an inhibitor, it could be given in an unlabeled form to assess its influence on the distribution of a PET imaging substrate probe [107]. If the drug is a substrate, it may be radiolabeled and used in combination with a transporter inhibitor [107].

As is the case in fundamental research, the shortage of clinically applicable, specific model inhibitors and substrates of ABC transporters as well as probes suitable for imaging studies is well recognized, and represents an area of research that warrants moving forward with drug-transporter interaction and DDI studies [102].

#### **1.4.1.3 Clinical Diagnostic Tools**

Though the role of ABCG2 expression in MDR has not yet been fully elucidated, ABCG2 has been identified as a tumor marker, which could be exploited in the diagnosis of cancer [108]. By analogy with ABCB1 [93], the detection of ABCG2 expression in tumors could be achieved by imaging techniques such as single-photon emission computed tomography (SPECT) or PET, using a labeled substrate probe and an ABCG2 inhibitor, which should increase the accumulation of the imaging probe in ABCG2 expressing tumors. Measuring ABCG2 expression in tumors may also be useful for the prediction and assessment of MDR and response to chemotherapy [47]. This would be a valuable application of clinical ABCG2 inhibitors.

#### **1.4.2 Applications as Prospective Drugs**

To date, no inhibitor targeting an ABC transporter has received marketing authorization by regulatory agencies [47,99,109], though some marketed drugs addressing other targets show off-target, inhibitory activity at ABC transporters [109]. Nevertheless, several potential therapeutic applications of ABCG2 inhibitors have been and are still being explored.

##### **1.4.2.1 Drugs for Improving Oral Bioavailability**

In the light of ABCG2 expression at the intestinal and hepatic barrier, which was shown to limit the oral bioavailability of (anticancer) drugs, the idea of using ABCG2 inhibitors to improve oral bioavailability has been investigated [79,80,110,111]. Preceding preclinical and clinical studies on ABCB1 had already been successful, the most prominent example being the improvement of the oral bioavailability of the anticancer agent paclitaxel when combined with the ABCB1 inhibitor cyclosporin A [79,80,110,111]. Similarly, the oral bioavailability of topotecan was improved when co-administered with the dual ABCB1/ABCG2 inhibitor elacridar (Figure 1.6) in clinical research [112,113]. Since topotecan is a selective substrate for ABCG2, the results suggest that the interaction of the two compounds is due to inhibition of ABCG2 [112,113]. Given the co-expression of ABCB1 and ABCG2 at the intestinal and hepatic barrier and their overlapping substrate ‘specificities’, dual ABCB1/ABCG2 inhibition is of interest for dual substrates, as demonstrated in a clinical trial using the dual ABCB1/ABCG2 substrate irinotecan in combination with the tyrosine kinase inhibitor gefitinib, which also inhibits ABCB1 and ABCG2 [114]. Together, these findings encourage the application of ABCG2 inhibitors to improve oral bioavailability. The reservation must be

made, however, that ABCG2 inhibition can potentially increase brain uptake, which would be undesirable because of possible (neuro)toxic side effects, yet advantageous in case the tumor is located in the brain [111].

#### **1.4.2.2 Drugs for Improving Brain Penetration**

Due to the restrictions by the BBB, the development of drugs targeting the brain shows the highest failure rates in phase I and II clinical trials: 93% to 98% [84]. Clinical strategies to overcome the BBB comprise physical methods such as the administration of drugs directly into the brain region of interest, requiring invasive surgery, and osmotic disruption, e.g. with a mannitol solution, implying increased and unwanted leaking of plasma material into the brain, which is severely toxic for the brain [84]. Neither method is ideal. An alternative in order to specifically increase the brain penetration by drugs which are substrates of ABC transporters is the inhibition of these efflux pumps by the use of inhibitors. In 2002 a first proof-of-concept study in mice demonstrated that the paclitaxel concentration in the brain, which is very low after an intravenous injection, was increased by co-administration with the ABCB1 inhibitor valspodar [115]. Whereas paclitaxel alone did not affect the volume of an implanted brain tumor, co-administration with valspodar reduced the tumor volume by 90% [115]. Several follow-up preclinical studies in mouse or rat models with different substrate/ inhibitor combinations confirmed the principle and showed that it is also applicable to ABCG2 [111,116]. In most cases, however, ABCB1 and ABCG2 work in concert to transport a substrate drug from the brain back into the blood, which can be explained by their prominence and substrate overlap [111,116]. Studies with knockout mice showed that these two export pumps have a cooperative effect at the BBB: the removal of either transporter alone does not result in a significant increase in brain penetration of dual substrates, because it is compensated by the respective other transporter, whereas the complete removal of both efflux pumps has a disproportional effect on brain uptake [111,116]. Consequently, the largest increase in brain accumulation of dual substrate drugs should be achieved by the inhibition of both ABCB1 and ABCG2 [111,116]. This was verified in extensive preclinical research in rodents, mostly using the dual inhibitor elacridar in combination with various dual substrate drugs, not only cytostatics but also drugs for neurological disorders [111,116,117]. Because of interspecies differences, these results do not necessarily translate to humans. The confirmation that this principle – inhibition of ABC transporters to increase drug penetration – is applicable to humans was provided by PET imaging. The aforementioned PET studies, proving the activity of ABCB1 and ABCG2 at the human BBB, were recently followed by a couple of clinical trials focused on improving drug exposure to the brain. [<sup>11</sup>C]Erlotinib, a tyrosine kinase inhibitor, was used as a PET substrate probe. Its brain uptake is limited as it is a substrate of both ABCB1 and ABCG2. The first such study, two years ago, was not successful, which was attributed to

the use of elacridar as a dual inhibitor, as practiced before in numerous preclinical trials [118]. Elacridar is a much more effective inhibitor of ABCB1 than it is of ABCG2, meeting the needs of the rodent BBB, where ABCB1 predominates over ABCG2. Since the situation is vice versa in humans, it was speculated that a better result could be achieved using a dual inhibitor with high potency at ABCG2. Indeed a proof-of-concept study carried out by Langer's group only one year ago accomplished a much better outcome [119]. They found out that erlotinib is not only a dual substrate, but at a supratherapeutic dose it functions as an inhibitor of ABCB1 and ABCG2. Using erlotinib, they were able to achieve an increase in brain distribution of [ $^{11}\text{C}$ ]erlotinib [119]. However, the clinical application of supratherapeutic doses of erlotinib may be hampered by safety concerns [119], which is why further research on clinically applicable, potent dual ABCB1/ABCG2 inhibitors is desirable.

Together, the preclinical and clinical data make a compelling case for the application of ABCG2 and dual ABCB1/ABCG2 inhibitors as drugs to improve brain penetration.

#### **1.4.2.3 Drugs for Overcoming Multidrug Resistance in Cancer**

As the human ABC transporters were first discovered in cancer cells, where they extrude anticancer drugs, the use of ABC inhibitors to improve the response to chemotherapy stood to reason. Already in the 1980's, less than 10 years after the discovery of ABCB1, the first clinical trials on combination chemotherapy – an anticancer drug together with an ABCB1 inhibitor – were carried out and dozens more followed [46]. Nevertheless, this is by far the most uncertain and most disputed potential application of ABC inhibitors – no wonder, considering that the role of ABC transporter expression in MDR is still unclear.

Initially, drugs which had been approved for other indications and noted to inhibit ABCB1 (first generation inhibitors) were used in clinical trials, for instance verapamil or cyclosporin A [46,47,120,121]. Owing to their low inhibitory potency, higher doses than those required for their individual therapeutic activity were applied, which consequently led to unacceptable toxic side effects [46,47,120,121]. Second generation inhibitors were analogs of the initial agents developed solely for the purpose of altering drug resistance, the cyclosporin derivative valspodar being tested most frequently in clinical trials [46,47,120,121]. These inhibitors were more potent and less toxic, but induced pharmacokinetic interactions that limited the clearance and metabolism of anticancer drugs and thereby elevated their plasma concentrations beyond acceptable toxicity, for instance by inhibiting cytochrome P450 enzymes [46,47,120,121]. This usually prompted dose reductions of the anticancer agents down to ineffective levels [46,47,120,121]. Third generation inhibitors, such as elacridar and tariquidar, were designed with increased specificity to overcome these disadvantages [46,47,120,121]. Indeed, they displayed either no or only minor pharmacokinetic interactions with different anticancer agents,

yet several clinical studies failed to show a conclusive benefit of the addition of an ABCB1 inhibitor to standard therapy and some were closed early owing to toxicity [46,47,120,121]. Therefore, the conduction of further trials was generally discouraged. However, the point must be made that the clinical trial designs were often flawed. Typically, ABCB1 was not assayed in tumors and there was no selection of patients whose tumors displayed overexpression of ABCB1 [46,120,122]. Furthermore, many studies enrolled patients following multiple lines of therapy, so that drug resistance was likely to be multifactorial, yet other drug efflux mechanisms or a lack of uptake mechanisms were not controlled [46,120,122]. Thus the idea of overcoming MDR by inhibiting ABCB1 was not adequately tested [46,120,122].

Given the lack of success with the preceding trials on ABCB1 inhibitors and the restricted knowledge about which cancers express ABCG2, only very few clinical trials aimed at overcoming ABCG2-mediated drug resistance have been carried through, and the picture is very similar to ABCB1. In the last decade, a couple of trials investigated the combination of topotecan with the tyrosine kinase inhibitor lapatinib, which also inhibits ABCG2 [88,123,124]. Unfortunately, the results did not demonstrate an advantage over the application of topotecan alone, although ABCG2 expression was detected [88,123-126]. This failure was attributed mainly to other mechanisms being involved in the resistance and also toxicity was a problem in some cases [88,123,124].

It is worth noting that an explanation for toxicity problems despite the lack of pharmacokinetic interactions could be the ABCB1/ABCG2 inhibition in cells, where these transporters are known to play a protective role, e.g. in bone marrow stem cells, yet in many cases there was no clear evidence for such an effect [120,123].

Taken together, there is still no definite answer to the question if inhibitors of ABC transporters can effectively reverse drug resistance in humans. It could be speculated, however, that in case proper patient populations were selected, whose tumors show ABC transporter-dominated resistance, successful reversal of drug resistance by ABC inhibitors might be feasible [46,47,120,124]. Given the expression of multiple ABC transporters in tumors, compounds that inhibit ABCB1 and ABCG2 (and ABCC1) may be advantageous [120].

Moreover, apart from chemotherapy, also photodynamic therapy (PDT) could profit from ABCG2 inhibition. As mentioned above, a couple of PDT agents were shown to be ABCG2 substrates and high ABCG2 expression was correlated with decreased potency of the latter [91]. Thus, ABCG2 inhibitors may improve the response to PDT.

## 1.5 Reported ABCG2 Inhibitors and Problem Statement

The research into inhibitors of ABC transporters began in 1981 with the serendipitous finding that the calcium channel blocker verapamil inhibited ABCB1-mediated drug efflux in resistant tumor cells [116,127]. Subsequently, numerous chemicals were screened for their potential to inhibit ABCB1 [116] and, as outlined in the previous section, a couple of ABCB1 inhibitors with higher potency were developed, in particular the two benzanilides elacridar (by Glaxo) [128] and tariquidar (by Xenova) [129] (Figure 1.6). Both are non-marketed, experimental compounds, which have been used in clinical trials.

After the discovery of ABCG2, the ability of the hitherto developed ABCB1 inhibitors to impede also ABCG2-mediated drug efflux was investigated. Indeed, both elacridar [130] and tariquidar [131] happen to inhibit ABCG2, albeit less potently than ABCB1. The first selective inhibitor of ABCG2 reported was the fungal toxin fumitremorgin C (FTC) [132,133] (Figure 1.6), which, however, is precluded from the use in vivo due to its severe neurotoxic side effects. A number of other natural and dietary compounds were identified as ABCG2 inhibitors, primarily flavonoids [134,135]. Of these constituents, only curcumin (Figure 1.6) was evaluated clinically as an ABCG2 inhibitor [103,136]. This substance was also shown to inhibit ABCB1 and ABCC1, yet with lower potency [136]. Disadvantageously, it shows poor absorption and extensive metabolic instability [137]. Furthermore, various drugs on the market were investigated for interaction with ABCG2. The immunosuppressant cyclosporin A (Figure 1.6) is a very unspecific ABCG2 inhibitor, since it also inhibits ABCB1 and other transporters, as well as cytochrome P enzymes [92,138]. With tyrosine kinase inhibitors emerging as anticancer drugs in the beginning of this century, they were evaluated in this regard and some turned out to be ABCG2 inhibitors, notably erlotinib [139] and lapatinib [103,140] (Figure 1.6), which were used in some of the clinical trials mentioned in Section 1.4. At higher concentrations, they inhibit ABCB1 as well [103,139,140]. Recently, the platelet-increasing agent eltrombopag (Figure 1.6) was demonstrated to be an ABCG2 inhibitor [92,141]. However, the use of drugs for in vivo experiments may cause safety problems due to the effects they were originally designated for.

Of course, medicinal chemists did not remain idle and synthesized compounds designed solely for the purpose of inhibiting ABCG2. Soon after the discovery that the mycotoxin FTC is a selective ABCG2 inhibitor, analogs thereof, featuring lower toxicity and higher potency, were reported [142]. In particular Ko143 [142] (Figure 1.6), which is still among the most potent ABCG2 inhibitors published so far, has to be pointed out. Later it was shown that it is not entirely selective for ABCG2 and interacts with ABCB1 and ABCC1, but only at high

concentrations [143]. A drawback of Ko143 is its poor metabolic stability caused by the labile ester group [143,144]. Since the report on Ko143, many more ABCG2 inhibitors have been created, mostly derivatives of the aforementioned compounds. They were extensively reviewed elsewhere [135,145,146] and some prominent examples will be highlighted in Chapter 2.

Nevertheless, to the best of the author's knowledge, none of these have been developed for the use in humans. Hence, the aforementioned drugs and dietary compounds have to be repurposed, with all the detriments indicated above. For clinical DDI studies, for instance, the FDA recommends the use of cyclosporin A, eltrombopag and curcumin as ABCG2 inhibitors [147]. In some articles on the subject, the utilization of lapatinib is suggested [92,103].

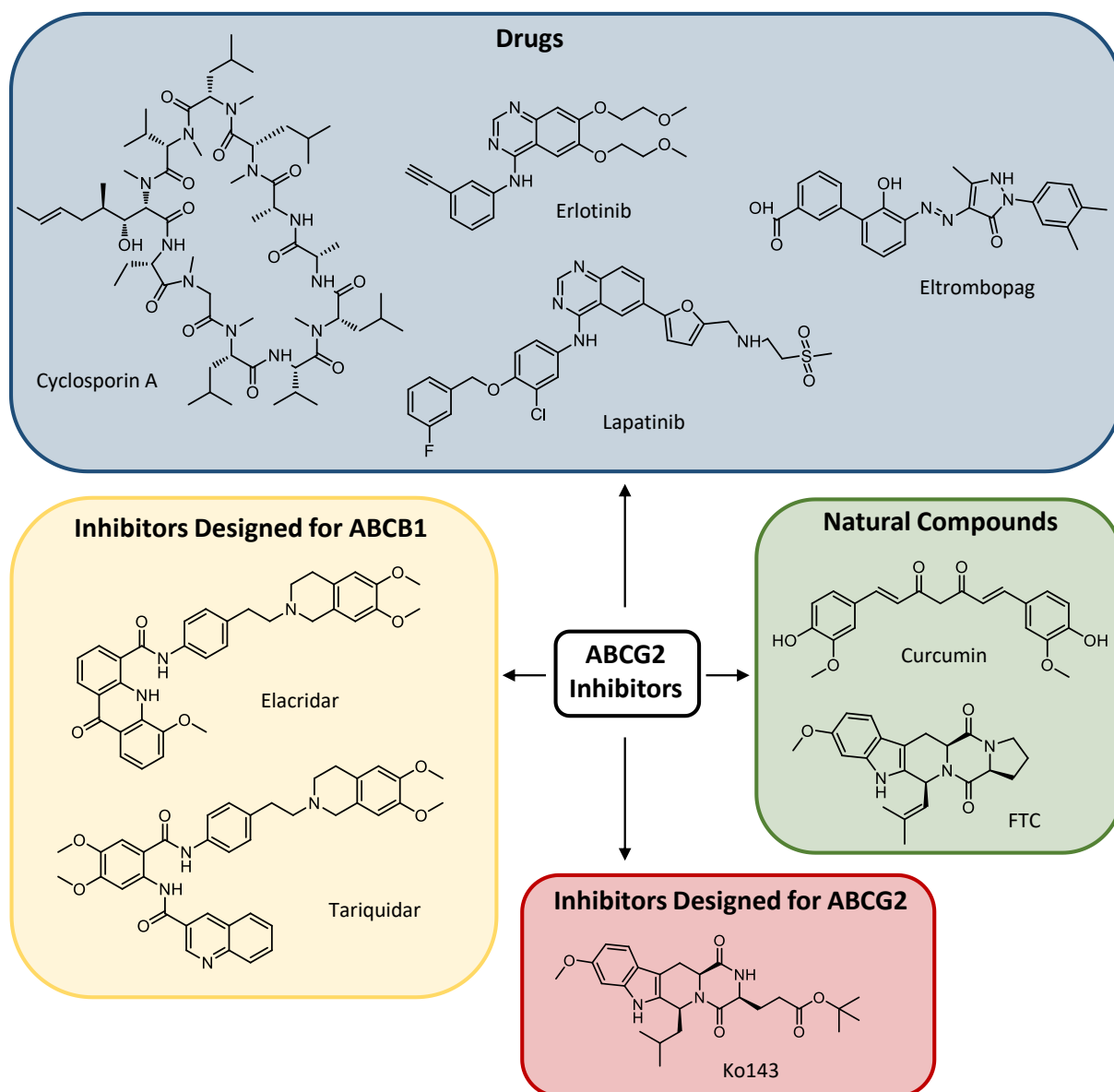


**Figure 1.6.** Structures of selected inhibitors of ABCG2.

A thorough literature research by the author of this thesis brought to light a dilemma: researchers of many different disciplines lament the lack of clinically usable ABCG2 inhibitors, impeding their research into applications of the latter, while on the other hand, as many applications are not yet fully developed, medicinal chemists treat the discovery of ABCG2 inhibitors as an end in itself, strikingly focusing on improved in vitro potency, thereby neglecting in vivo applicability. Therefore, in the author's opinion, the research into novel ABCG2 inhibitors needs redirecting towards a more application-oriented design. More precisely, not only the pharmacodynamic but also the pharmacokinetic (i.e. absorption, distribution, the metabolism and excretion; ADME) and toxicity (Tox) properties should be optimized – only drug-like molecules, i.e. such ones with sufficiently favorable ADME-Tox properties, can be effective in vivo [148].

Two major shortcomings of ABCG2 inhibitors in terms of drug-like properties are particularly eminent. Firstly, ABCG2 inhibitors are typically very lipophilic compounds with high molecular weight, which generally entails low water solubility, compromising absorption and distribution. Considering that the inhibitors have to address the large and distinctly hydrophobic multidrug binding site of ABCG2 (see Section 1.2) [64], this is not surprising. Secondly, ABCG2 inhibitors often contain labile groups such as amide and ester moieties or Michael systems, which are susceptible to hydrolysis or other nucleophilic attack, thus causing metabolic instability.

Consequently, the present thesis is devoted to the creation of ABCG2 inhibitors that are not only potent, but also drug-like, in particular water-soluble and stable.

## 1.6 Scope and Objectives of the Thesis

The ABCG2 transporter is involved in multidrug resistance of cancer and a functional component of the blood-brain-barrier. Inhibitors of this drug efflux pump are investigated to overcome the aforementioned obstacles. The research on ABCG2 inhibitors has concentrated on potency, while drug-like properties have been disregarded. Since the latter are an indispensable precondition for application in vivo and, ultimately, in humans, the present thesis is dedicated to the design, synthesis and characterization of novel, drug-like ABCG2 inhibitors, focusing on stability in blood plasma and water solubility.

During preceding studies on the dual ABCB1/ABCG2 inhibitor tariquidar (Figure 1.6) by our working group, it had been found by serendipity that minimal structural modifications resulted in a drastic change in activity in favor of ABCG2 inhibition [149]. In contrast to tariquidar, which shows higher potency at the ABCB1 transporter, its analog UR-ME22-1 is selective for ABCG2. However, the aforementioned modifications rendered the molecule prone to

hydrolysis in blood plasma [150]. In cooperation with members of Prof. König's group (Institute of Organic Chemistry, University of Regensburg), who provided the synthesis, the labile moieties in UR-ME22-1 were bioisosterically replaced by more stable groups. The key feature was a central triazole core. With the novel compounds in hand, our working group carried out biological assays. Furthermore, one of the inhibitors was forwarded to Prof. Locher's group (Institute of Molecular Biology and Biophysics, ETH Zürich), which allowed the group to elucidate the structure of ABCG2 in an inhibitor-bound state in a cryo-EM experiment – a study they already published [64], which is outlined in Section 1.2. The first objective of the thesis in hand (Chapter 2) was the completion of the chemical and biological characterization of the new, tariquidar-related triazoles (among others the determination of the stability in blood plasma), the synthesis of known ABCG2 inhibitors as a reference, and the comparative analysis of the biological data collected in our as well as Prof. Locher's working group, not least to gain deeper insight into the underlying transport inhibition mechanisms, which, heretofore, had still been an enigma.

Subsequently, the focus of this thesis was directed on water solubility, which is a fundamental prerequisite for all bioactive compounds. The preceding, tariquidar-related triazoles acted as potent and effective ABCG2 inhibitors. Accordingly, they appeared to stay in solution at least for the short time span of the biological assays. Their equilibrium solubility, however, was very poor, a severe impediment for application, particularly in vivo. This is typical of ABCG2 inhibitors, which are usually very large and lipophilic. Therefore, the second objective of the thesis in hand (Chapter 3) was the design and synthesis of novel potent and stable ABCG2 inhibitors with improved equilibrium water solubility, using the previous inhibitors as a starting point. It was planned to pursue a fragment-based approach, which was considered suitable because ligands optimized in such an approach are more likely to be relatively small and hydrophilic [151,152]. On 'growing' the optimized fragments into potent and soluble inhibitors, it was devised to take advantage of a cryo-EM structure of ABCG2 [63] and to use molecular docking studies in order to optimize protein-ligand interactions. In addition to a thorough biological characterization, it was planned to establish solubility assays suitable for analyzing compounds in the comparatively low solubility range of ABCG2 inhibitors.

## 1.7 References

- [1] I. Cho, M.R. Jackson, J. Swift, Roles of Cross-Membrane Transport and Signaling in the Maintenance of Cellular Homeostasis, *Cell. Mol. Bioeng.*, 9 (2016) 234-246.
- [2] F.R. Blattner, G. Plunkett, C.A. Bloch, N.T. Perna, V. Burland, M. Riley, J. Collado-Vides, J.D. Glasner, C.K. Rode, G.F. Mayhew, J. Gregor, N.W. Davis, H.A. Kirkpatrick, M.A. Goeden, D.J. Rose, B. Mau, Y. Shao, The Complete Genome Sequence of *Escherichia coli* K-12, *Science*, 277 (1997) 1453.
- [3] A. Missner, P. Pohl, 110 Years of the Meyer–Overton Rule: Predicting Membrane Permeability of Gases and Other Small Compounds, *ChemPhysChem*, 10 (2009) 1405-1414.
- [4] N.J. Yang, M.J. Hinner, Getting Across the Cell Membrane: An Overview for Small Molecules, Peptides, and Proteins, in: A. Gautier, M.J. Hinner (Eds.) *Site-Specific Protein Labeling: Methods and Protocols*, Springer New York, New York, NY, 2015, pp. 29-53.
- [5] W. Shinoda, Permeability across lipid membranes, *Biochim. Biophys. Acta, Biomembr.*, 1858 (2016) 2254-2265.
- [6] S. Sahoo, M. Aurich, J. Jonsson, I. Thiele, Membrane transporters in a human genome-scale metabolic knowledgebase and their implications for disease, *Front. Physiol.*, 5 (2014).
- [7] P.L. Pedersen, Transport ATPases: Structure, Motors, Mechanism and Medicine: A Brief Overview, *J. Bioenerg. Biomembr.*, 37 (2005) 349-357.
- [8] C.F. Higgins, ABC Transporters: From Microorganisms to Man, *Annu. Rev. Cell Biol.*, 8 (1992) 67-113.
- [9] P. Borst, R.O. Elferink, Mammalian ABC Transporters in Health and Disease, *Annu. Rev. Biochem.*, 71 (2002) 537-592.
- [10] S. Wilkens, Structure and mechanism of ABC transporters, *F1000Prime Rep.*, 7 (2015) 1-9.
- [11] E. Dassa, Natural history of ABC systems: not only transporters, *Essays Biochem.*, 50 (2011) 19-42.
- [12] A.L. Davidson, E. Dassa, C. Orelle, J. Chen, Structure, Function, and Evolution of Bacterial ATP-Binding Cassette Systems, *Microbiol. Mol. Biol. Rev.*, 72 (2008) 317.
- [13] S.K. Nigam, What do drug transporters really do?, *Nat. Rev. Drug Discov.*, 14 (2015) 29-44.
- [14] E.M. Leslie, R.G. Deeley, S.P.C. Cole, Multidrug resistance proteins: role of P-glycoprotein, MRP1, MRP2, and BCRP (ABCG2) in tissue defense, *Toxicol. Appl. Pharmacol.*, 204 (2005) 216-237.
- [15] G. Szakács, A. Váradi, C. Özvegy-Laczka, B. Sarkadi, The role of ABC transporters in drug absorption, distribution, metabolism, excretion and toxicity (ADME–Tox), *Drug Discov. Today*, 13 (2008) 379-393.
- [16] M.M. Gottesman, T. Fojo, S.E. Bates, Multidrug resistance in cancer: role of ATP-dependent transporters, *Nat. Rev. Cancer*, 2 (2002) 48-58.
- [17] A. Mahringer, G. Fricker, ABC transporters at the blood-brain barrier, *Expert Opin. Drug Metab. Toxicol.*, 12 (2016) 499-508.
- [18] W. Löscher, H. Potschka, Drug resistance in brain diseases and the role of drug efflux transporters, *Nat. Rev. Neurosci.*, 6 (2005) 591-602.
- [19] G.F.-L. Ames, J. Lever, Components of Histidine Transport: Histidine-Binding Proteins and hisP Protein, *Proc. Natl. Acad. Sci. U. S. A.*, 66 (1970) 1096.
- [20] O. Kellermann, S. Szmelcman, Active Transport of Maltose in *Escherichia coli* K12, *Eur. J. Biochem.*, 47 (1974) 139-149.
- [21] S. Szmelcman, M. Schwartz, T.J. Silhavy, W. Boos, Maltose Transport in *Escherichia coli* K12, *Eur. J. Biochem.*, 65 (1976) 13-19.

- [22] T. Ferenci, W. Boos, M. Schwartz, S. Szmelcman, Energy-Coupling of the Transport System of *Escherichia coli* Dependent on Maltose-Binding Protein, *Eur. J. Biochem.*, 75 (1977) 187-193.
- [23] R.L. Juliano, V. Ling, A surface glycoprotein modulating drug permeability in Chinese hamster ovary cell mutants, *Biochim. Biophys. Acta, Biomembr.*, 455 (1976) 152-162.
- [24] J.H. Gerlach, J.A. Endicott, P.F. Juranka, G. Henderson, F. Sarangi, K.L. Deuchars, V. Ling, Homology between P-glycoprotein and a bacterial haemolysin transport protein suggests a model for multidrug resistance, *Nature*, 324 (1986) 485-489.
- [25] P. Gros, J. Croop, D. Housman, Mammalian multidrug resistance gene: Complete cDNA sequence indicates strong homology to bacterial transport proteins, *Cell*, 47 (1986) 371-380.
- [26] C.F. Higgins, I.D. Hiles, G.P.C. Salmond, D.R. Gill, J.A. Downie, I.J. Evans, I.B. Holland, L. Gray, S.D. Buckel, A.W. Bell, M.A. Hermodson, A family of related ATP-binding subunits coupled to many distinct biological processes in bacteria, *Nature*, 323 (1986) 448-450.
- [27] S.C. Hyde, P. Emsley, M.J. Hartshorn, M.M. Mimmack, U. Gileadi, S.R. Pearce, M.P. Gallagher, D.R. Gill, R.E. Hubbard, C.F. Higgins, Structural model of ATP-binding proteing associated with cystic fibrosis, multidrug resistance and bacterial transport, *Nature*, 346 (1990) 362-365.
- [28] J.E. Walker, M. Saraste, M.J. Runswick, N.J. Gay, Distantly related sequences in the alpha- and beta-subunits of ATP synthase, myosin, kinases and other ATP-requiring enzymes and a common nucleotide binding fold, *EMBO J.*, 1 (1982) 945-951.
- [29] E. Schneider, S. Hunke, ATP-binding-cassette (ABC) transport systems: Functional and structural aspects of the ATP-hydrolyzing subunits/domains, *FEMS Microbiol. Rev.*, 22 (1998) 1-20.
- [30] B. Wang, M. Dukarevich, E.I. Sun, M.R. Yen, M.H. Saier, Membrane Porters of ATP-Binding Cassette Transport Systems Are Polyphyletic, *J. Membr. Biol.*, 231 (2009) 1.
- [31] G.F.-L. Ames, C.S. Mimura, S.R. Holbrook, V. Shyamala, Traffic ATPases: A Superfamily of Transport Proteins Operating from *Escherichia coli* to Humans, *Advances in Enzymology and Related Areas of Molecular Biology*, 65 (1992) 1-47.
- [32] K.J. Linton, C.F. Higgins, The *Escherichia coli* ATP-binding cassette (ABC) proteins, *Molecular Microbiology*, 28 (1998) 5-13.
- [33] I.B. Holland, M. A. Blight, ABC-ATPases, adaptable energy generators fuelling transmembrane movement of a variety of molecules in organisms from bacteria to humans, *J. Mol. Biol.*, 293 (1999) 381-399.
- [34] J. Xiong, J. Feng, D. Yuan, J. Zhou, W. Miao, Tracing the structural evolution of eukaryotic ATP binding cassette transporter superfamily, *Sci. Rep.*, 5 (2015) 16724.
- [35] G.F.-L. Ames, Bacterial periplasmic transport systems: structure, mechanism, and evolution, *Annu. Rev. Biochem.*, 55 (1986) 397-425.
- [36] D.C. Rees, E. Johnson, O. Lewinson, ABC transporters: the power to change, *Nat. Rev. Mol. Cell Biol.*, 10 (2009) 218-227.
- [37] P.M. Jones, M.L. O'Mara, A.M. George, ABC transporters: a riddle wrapped in a mystery inside an enigma, *Trends Biochem. Sci.*, 34 (2009) 520-531.
- [38] C. Thomas, R. Tampé, Multifaceted structures and mechanisms of ABC transport systems in health and disease, *Curr. Opin. Struct. Biol.*, 51 (2018) 116-128.
- [39] K.P. Locher, Mechanistic diversity in ATP-binding cassette (ABC) transporters, *Nat. Struct. Mol. Biol.*, 23 (2016) 487-493.
- [40] HUGO Genome Nomenclature Committee, Gene group: ATP binding cassette transporters (ABC), <https://www.genenames.org/data/genegroup/#!/group/417> (accessed May 13, 2020).
- [41] I. Klein, B. Sarkadi, A. Váradi, An inventory of the human ABC proteins, *Biochim. Biophys. Acta, Biomembr.*, 1461 (1999) 237-262.
- [42] M. Dean, A. Rzhetsky, R. Allikmets, The human ATP-binding cassette (ABC) transporter superfamily, *Genome Res.*, 11 (2001) 1156-1166.

- [43] M. Dean, R. Allikmets, Complete Characterization of the Human ABC Gene Family, *J. Bioenerg. Biomembr.*, 33 (2001) 475-479.
- [44] M. Dean, T. Annilo, Evolution of the ATP-binding cassette (ABC) transporter superfamily in vertebrates, *Annu. Rev. Genomics Hum. Genet.*, 6 (2005) 123-142.
- [45] M. Dean, The Genetics of ATP-Binding Cassette Transporters, in: *Methods in Enzymology*, Academic Press, 2005, pp. 409-429.
- [46] G. Szakács, J.K. Paterson, J.A. Ludwig, C. Booth-Genthe, M.M. Gottesman, Targeting multidrug resistance in cancer, *Nat. Rev. Drug Discov.*, 5 (2006) 219-234.
- [47] R.W. Robey, K.M. Pluchino, M.D. Hall, A.T. Fojo, S.E. Bates, M.M. Gottesman, Revisiting the role of ABC transporters in multidrug-resistant cancer, *Nat. Rev. Cancer*, 18 (2018) 452-464.
- [48] S. Dauchy, F. Dutheil, R.J. Weaver, F. Chassoux, C. Daumas-Duport, P.-O. Couraud, J.-M. Scherrmann, I. De Waziers, X. Decleves, ABC transporters, cytochromes P450 and their main transcription factors: expression at the human blood-brain barrier, *J. Neurochem.*, 107 (2008) 1518-1528.
- [49] R. Shawahna, Y. Uchida, X. Decleves, S. Ohtsuki, S. Yousif, S. Dauchy, A. Jacob, F. Chassoux, C. Daumas-Duport, P.-O. Couraud, T. Terasaki, J.-M. Scherrmann, Transcriptomic and Quantitative Proteomic Analysis of Transporters and Drug Metabolizing Enzymes in Freshly Isolated Human Brain Microvessels, *Mol. Pharmaceutics*, 8 (2011) 1332-1341.
- [50] Y. Uchida, S. Ohtsuki, Y. Katsukura, C. Ikeda, T. Suzuki, J. Kamiie, T. Terasaki, Quantitative targeted absolute proteomics of human blood-brain barrier transporters and receptors, *J. Neurochem.*, 117 (2011) 333-345.
- [51] Y.N. Chen, L.A. Mickley, A.M. Schwartz, E.M. Acton, J. Hwang, A.T. Fojo, Characterization of adriamycin-resistant human breast cancer cells which display overexpression of a novel resistance-related membrane protein, *J. Biol. Chem.*, 265 (1990) 10073-10080.
- [52] L.A. Doyle, W. Yang, L.V. Abruzzo, T. Krogmann, Y. Gao, A.K. Rishi, D.D. Ross, A multidrug resistance transporter from human MCF-7 breast cancer cells, *Proc. Natl. Acad. Sci. U. S. A.*, 96 (1999) 2569.
- [53] R. Allikmets, L.M. Schriml, A. Hutchinson, V. Romano-Spica, M. Dean, A Human Placenta-specific ATP-Binding Cassette Gene (ABCP) on Chromosome 4q22 That Is Involved in Multidrug Resistance, *Cancer Res.*, 58 (1998) 5337.
- [54] K. Miyake, L. Mickley, T. Litman, Z. Zhan, R. Robey, B. Cristensen, M. Brangi, L. Greenberger, M. Dean, T. Fojo, S.E. Bates, Molecular Cloning of cDNAs Which Are Highly Overexpressed in Mitoxantrone-resistant Cells, *Cancer Res.*, 59 (1999) 8.
- [55] F. Staud, P. Pavék, Breast cancer resistance protein (BCRP/ABCG2), *Int. J. Biochem. Cell Biol.*, 37 (2005) 720-725.
- [56] Z. Ni, Z. Bikadi, M.F. Rosenberg, Q. Mao, Structure and function of the human breast cancer resistance protein (BCRP/ABCG2), *Curr. Drug Metab.*, 11 (2010) 603-617.
- [57] H. Wang, E.-W. Lee, X. Cai, Z. Ni, L. Zhou, Q. Mao, Membrane Topology of the Human Breast Cancer Resistance Protein (BCRP/ABCG2) Determined by Epitope Insertion and Immunofluorescence, *Biochemistry*, 47 (2008) 13778-13787.
- [58] Y. Cheng, Single-Particle Cryo-EM at Crystallographic Resolution, *Cell*, 161 (2015) 450-457.
- [59] C.A. McDevitt, R.F. Collins, M. Conway, S. Modok, J. Storm, I.D. Kerr, R.C. Ford, R. Callaghan, Purification and 3D Structural Analysis of Oligomeric Human Multidrug Transporter ABCG2, *Structure*, 14 (2006) 1623-1632.
- [60] M.F. Rosenberg, Z. Bikadi, J. Chan, X. Liu, Z. Ni, X. Cai, R.C. Ford, Q. Mao, The Human Breast Cancer Resistance Protein (BCRP/ABCG2) Shows Conformational Changes with Mitoxantrone, *Structure*, 18 (2010) 482-493.

- [61] M.F. Rosenberg, Z. Bikadi, E. Hazai, T. Starborg, L. Kelley, N.E. Chayen, R.C. Ford, Q. Mao, Three-dimensional structure of the human breast cancer resistance protein (BCRP/ABCG2) in an inward-facing conformation, *Acta Cryst. D*, 71 (2015) 1725-1735.
- [62] P. Kapoor, A.J. Horsey, M.H. Cox, I.D. Kerr, ABCG2: does resolving its structure elucidate the mechanism?, *Biochem. Soc. Trans.*, 46 (2018) 1485-1494.
- [63] N.M.I. Taylor, I. Manolaridis, S.M. Jackson, J. Kowal, H. Stahlberg, K.P. Locher, Structure of the human multidrug transporter ABCG2, *Nature*, 546 (2017) 504-509.
- [64] S.M. Jackson, I. Manolaridis, J. Kowal, M. Zechner, N.M.I. Taylor, M. Bause, S. Bauer, R. Bartholomaeus, G. Bernhardt, B. Koenig, A. Buschauer, H. Stahlberg, K.-H. Altmann, K.P. Locher, Structural basis of small-molecule inhibition of human multidrug transporter ABCG2, *Nat. Struct. Mol. Biol.*, 25 (2018) 333-340.
- [65] I. Manolaridis, S.M. Jackson, N.M.I. Taylor, J. Kowal, H. Stahlberg, K.P. Locher, Cryo-EM structures of a human ABCG2 mutant trapped in ATP-bound and substrate-bound states, *Nature*, 563 (2018) 426-430.
- [66] L.A. Doyle, D.D. Ross, Multidrug resistance mediated by the breast cancer resistance protein BCRP (ABCG2), *Oncogene*, 22 (2003) 7340-7358.
- [67] P.A. Fetsch, A. Abati, T. Litman, K. Morisaki, Y. Honjo, K. Mittal, S.E. Bates, Localization of the ABCG2 mitoxantrone resistance-associated protein in normal tissues, *Cancer Lett.*, 235 (2006) 84-92.
- [68] M.L.H. Vlaming, J.S. Lagas, A.H. Schinkel, Physiological and pharmacological roles of ABCG2 (BCRP): Recent findings in *Abcg2* knockout mice, *Adv. Drug Delivery Rev.*, 61 (2009) 14-25.
- [69] W. Zhang, S. Sun, W. Zhang, Z. Shi, Polymorphisms of ABCG2 and its impact on clinical relevance, *Biochem. Biophys. Res. Commun.*, 503 (2018) 408-413.
- [70] R.W. Robey, C. Ierano, Z. Zhan, S.E. Bates, The challenge of exploiting ABCG2 in the clinic, *Curr. Pharm. Biotechnol.*, 12 (2011) 595-608.
- [71] M. Suzuki, H. Suzuki, Y. Sugimoto, Y. Sugiyama, ABCG2 Transports Sulfated Conjugates of Steroids and Xenobiotics, *J. Biol. Chem.*, 278 (2003) 22644-22649.
- [72] T. Janvilisri, H. Venter, S. Shahi, G. Reuter, L. Balakrishnan, H.W. Van Veen, Sterol Transport by the Human Breast Cancer Resistance Protein (ABCG2) Expressed in *Lactococcus lactis*, *J. Biol. Chem.*, 278 (2003) 20645-20651.
- [73] P. Krishnamurthy, T. Xie, J.D. Schuetz, The role of transporters in cellular heme and porphyrin homeostasis, *Pharmacol. Ther.*, 114 (2007) 345-358.
- [74] M.C. Cleophas, L.A. Joosten, L.K. Stamp, N. Dalbeth, O.M. Woodward, T.R. Merriman, ABCG2 polymorphisms in gout: insights into disease susceptibility and treatment approaches, *Pharmacogenomics Pers. Med.*, 10 (2017) 129-142.
- [75] I. Nagy, B. Tóth, Z. Gáborik, F. Erdo, P. Krajcsi, Membrane Transporters in Physiological Barriers of Pharmacological Importance, *Curr. Pharm. Des.*, 22 (2016) 5347-5372.
- [76] J.W. Jonker, M. Buitelaar, E. Wagenaar, M.A. Van der Valk, G.L. Scheffer, R.J. Scheper, T. Plosch, F. Kuipers, R.P.J.O. Elferink, H. Rosing, J.H. Beijnen, A.H. Schinkel, The breast cancer resistance protein protects against a major chlorophyll-derived dietary phototoxin and protoporphyria, *Proc. Natl. Acad. Sci. U. S. A.*, 99 (2002) 15649-15654.
- [77] A.E. van Herwaarden, J.W. Jonker, E. Wagenaar, R.F. Brinkhuis, J.H.M. Schellens, J.H. Beijnen, A.H. Schinkel, The Breast Cancer Resistance Protein (Bcrp1/Abcg2) Restricts Exposure to the Dietary Carcinogen 2-Amino-1-methyl-6-phenylimidazo[4,5-b]pyridine, *Cancer Res.*, 63 (2003) 6447.
- [78] A.E. van Herwaarden, E. Wagenaar, B. Karnekamp, G. Merino, J.W. Jonker, A.H. Schinkel, Breast cancer resistance protein (Bcrp1/Abcg2) reduces systemic exposure of the dietary carcinogens aflatoxin B1, IQ and Trp-P-1 but also mediates their secretion into breast milk, *Carcinogenesis*, 27 (2005) 123-130.

- [79] C.M.F. Kruijtzer, J.H. Beijnen, J.H.M. Schellens, Improvement of Oral Drug Treatment by Temporary Inhibition of Drug Transporters and/or Cytochrome P450 in the Gastrointestinal Tract and Liver: An Overview, *Oncologist*, 7 (2002) 516-530.
- [80] P. Breedveld, J.H. Beijnen, J.H.M. Schellens, Use of P-glycoprotein and BCRP inhibitors to improve oral bioavailability and CNS penetration of anticancer drugs, *Trends Pharmacol. Sci.*, 27 (2006) 17-24.
- [81] W. Mo, J.-T. Zhang, Human ABCG2: structure, function, and its role in multidrug resistance, *Int J Biochem Mol Biol*, 3 (2012) 1-27.
- [82] K. Römermann, R. Helmer, W. Löscher, The antiepileptic drug lamotrigine is a substrate of mouse and human breast cancer resistance protein (ABCG2), *Neuropharmacology*, 93 (2015) 7-14.
- [83] A.J. Horsey, M.H. Cox, S. Sarwat, I.D. Kerr, The multidrug transporter ABCG2: still more questions than answers, *Biochem. Soc. Trans.*, 44 (2016) 824-830.
- [84] P. Karande, J.P. Trasatti, D. Chandra, Novel Approaches for the Delivery of Biologics to the Central Nervous System, in: M. Singh, M. Salnikova (Eds.) *Novel Approaches and Strategies for Biologics, Vaccines and Cancer Therapies*, Academic Press, San Diego, 2015, pp. 59-88.
- [85] A. Mahringer, M. Ott, G. Fricker, The Blood–Brain Barrier: An Introduction to Its Structure and Function, in: G. Fricker, M. Ott, A. Mahringer (Eds.) *The Blood Brain Barrier (BBB)*, Springer, Berlin, Heidelberg, 2013.
- [86] D.S. Miller, Regulation of ABC transporters at the blood–brain barrier, *Clin. Pharm. Ther.*, 97 (2015) 395-403.
- [87] M. Liscovitch, Y. Lavie, Cancer multidrug resistance: A review of recent drug discovery research, *IDrugs*, 5 (2002) 349-355.
- [88] M.H. Hasanabady, F. Kalalinia, ABCG2 inhibition as a therapeutic approach for overcoming multidrug resistance in cancer, *J. Biosci.*, 41 (2016) 313-324.
- [89] R.W. Robey, O. Polgar, J. Deeken, K.W. To, S.E. Bates, ABCG2: determining its relevance in clinical drug resistance, *Cancer Metastasis Rev.*, 26 (2007) 39-57.
- [90] M. Jani, C. Ambrus, R. Magnan, K. Tauberné Jakab, E. Beéry, J.K. Zolnercijs, P. Krajcsi, Structure and function of BCRP, a broad specificity transporter of xenobiotics and endobiotics, *Arch. Toxicol.*, 88 (2014) 1205-1248.
- [91] D. Westover, F. Li, New trends for overcoming ABCG2/BCRP-mediated resistance to cancer therapies, *J. Exp. Clin. Cancer Res.*, 34 (2015) 159.
- [92] Z. Safar, E. Kis, F. Erdo, J.K. Zolnercijs, P. Krajcsi, ABCG2/BCRP: variants, transporter interaction profile of substrates and inhibitors, *Expert Opin. Drug Metab. Toxicol.*, 15 (2019) 313-328.
- [93] N. Tournier, B. Stieger, O. Langer, Imaging techniques to study drug transporter function in vivo, *Pharmacol. Ther.*, 189 (2018) 104-122.
- [94] L. Sasongko, J.M. Link, M. Muzi, D.A. Mankoff, X. Yang, A.C. Collier, S.C. Shoner, J.D. Unadkat, Imaging P-glycoprotein Transport Activity at the Human Blood-brain Barrier with Positron Emission Tomography, *Clin. Pharm. Ther.*, 77 (2005) 503-514.
- [95] T. Wanek, C. Kuntner, J.P. Bankstahl, S. Mairinger, M. Bankstahl, J. Stanek, M. Sauberer, T. Filip, T. Erker, M. Müller, W. Löscher, O. Langer, A Novel PET Protocol for Visualization of Breast Cancer Resistance Protein Function at the Blood–Brain Barrier, *J. Cereb. Blood Flow Metab.*, 32 (2012) 2002-2011.
- [96] M. Bauer, K. Römermann, R. Karch, B. Wulkersdorfer, J. Stanek, C. Philippe, A. Maier-Salamon, H. Haslacher, C. Jungbauer, W. Wadsak, W. Jäger, W. Löscher, M. Hacker, M. Zeitlinger, O. Langer, Pilot PET Study to Assess the Functional Interplay Between ABCB1 and ABCG2 at the Human Blood–Brain Barrier, *Clin. Pharm. Ther.*, 100 (2016) 131-141.
- [97] S. Mairinger, V. Zoufal, T. Wanek, A. Traxl, T. Filip, M. Sauberer, J. Stanek, C. Kuntner, J. Pahnke, M. Müller, O. Langer, Influence of breast cancer resistance protein and P-

glycoprotein on tissue distribution and excretion of Ko143 assessed with PET imaging in mice, *Eur. J. Pharm. Sci.*, 115 (2018) 212-222.

[98] I.B. Holland, ABC proteins, the fascination, the politics, the potential for applications for improving human health, in: I.B. Holland, S.P.C. Cole, K. Kuchler, C.F. Higgins (Eds.) *ABC Proteins*, Academic Press, London, 2003, pp. 619-623.

[99] G.F. Ecker, ABC Transporters: From Targets to Antitargets and Back, in: H.H. Sitte, G.F. Ecker, G. Folkers, R. Mannhold, H. Buschmann, R.P. Clausen (Eds.) *Transporters as Drug Targets*, Wiley, 2017, pp. 107-118.

[100] S.K. Bagal, P.J. Bungay, Minimizing Drug Exposure in the CNS while Maintaining Good Oral Absorption, *ACS Med. Chem. Lett.*, 3 (2012) 948-950.

[101] T. Wanek, A. Traxl, C. Kuntner, O. Langer, Investigation of Transporter-Mediated Drug-Drug Interactions Using PET/MRI, in: C. Kuntner-Hannes, Y. Haemisch (Eds.) *Image Fusion in Preclinical Applications*, Springer, 2019, pp. 117-133.

[102] K.M. Giacomini, S.-M. Huang, D.J. Tweedie, L.Z. Benet, K.L.R. Brouwer, X. Chu, A. Dahlin, R. Evers, V. Fischer, K.M. Hillgren, K.A. Hoffmaster, T. Ishikawa, D. Keppler, R.B. Kim, C.A. Lee, M. Niemi, J.W. Polli, Y. Sugiyama, P.W. Swaan, J.A. Ware, S.H. Wright, S. Wah Yee, M.J. Zamek-Gliszczynski, L. Zhang, Membrane transporters in drug development, *Nat. Rev. Drug Discov.*, 9 (2010) 215-236.

[103] C.A. Lee, M.A. O'Connor, T.K. Ritchie, A. Galetin, J.A. Cook, I. Ragueneau-Majlessi, H. Ellens, B. Feng, M.E. Taub, M.F. Paine, J.W. Polli, J.A. Ware, M.J. Zamek-Gliszczynski, Breast Cancer Resistance Protein (ABCG2) in Clinical Pharmacokinetics and Drug Interactions: Practical Recommendations for Clinical Victim and Perpetrator Drug-Drug Interaction Study Design, *Drug Metab. Dispos.*, 43 (2015) 490-509.

[104] F. Montanari, G.F. Ecker, Prediction of drug-ABC-transporter interaction — Recent advances and future challenges, *Adv. Drug Delivery Rev.*, 86 (2015) 17-26.

[105] S. Jaiswal, A. Sharma, M. Shukla, K. Vaghasiya, N. Rangaraj, J. Lal, Novel pre-clinical methodologies for pharmacokinetic drug-drug interaction studies: spotlight on “humanized” animal models, *Drug Metab. Rev.*, 46 (2014) 475-493.

[106] B. Wulkersdorfer, T. Wanek, M. Bauer, M. Zeitlinger, M. Müller, O. Langer, Using Positron Emission Tomography to Study Transporter-Mediated Drug-Drug Interactions in Tissues, *Clin. Pharm. Ther.*, 96 (2014) 206-213.

[107] O. Langer, Use of PET Imaging to Evaluate Transporter-Mediated Drug-Drug Interactions, *J. Clin. Pharmacol.*, 56 (2016) 143-156.

[108] M. Wang, D.X. Zheng, M.B. Luo, M. Gao, K.D. Miller, G.D. Hutchins, Q.-H. Zheng, Synthesis of carbon-11-labeled tariquidar derivatives as new PET agents for imaging of breast cancer resistance protein (ABCG2), *Appl. Radiat. Isot.*, 68 (2010) 1098-1103.

[109] A. Traxl, S. Mairinger, T. Filip, M. Sauberer, J. Stanek, S. Poschner, W. Jäger, V. Zoufal, G. Novarino, N. Tournier, M. Bauer, T. Wanek, O. Langer, Inhibition of ABCB1 and ABCG2 at the Mouse Blood-Brain Barrier with Marketed Drugs To Improve Brain Delivery of the Model ABCB1/ABCG2 Substrate [11C]erlotinib, *Mol. Pharmaceutics*, 16 (2019) 1282-1293.

[110] R.L. Oostendorp, J.H. Beijnen, J.H.M. Schellens, The biological and clinical role of drug transporters at the intestinal barrier, *Cancer Treat. Rev.*, 35 (2009) 137-147.

[111] S. Durmus, J.J.M.A. Hendriks, A.H. Schinkel, Apical ABC Transporters and Cancer Chemotherapeutic Drug Disposition, in: J.D. Schuetz, T. Ishikawa (Eds.) *Advances in Cancer Research*, Academic Press, 2015, pp. 1-41.

[112] C.M.F. Kruijtzter, J.H. Beijnen, H. Rosing, W.W. ten Bokkel Huinink, M. Schot, R.C. Jewell, E.M. Paul, J.H.M. Schellens, Increased Oral Bioavailability of Topotecan in Combination With the Breast Cancer Resistance Protein and P-Glycoprotein Inhibitor GF120918, *J. Clin. Oncol.*, 20 (2002) 2943-2950.

[113] I.E.L.M. Kuppens, E.O. Witteveen, R.C. Jewell, S.A. Radema, E.M. Paul, S.G. Mangum, J.H. Beijnen, E.E. Voest, J.H.M. Schellens, A Phase I, Randomized, Open-Label, Parallel-

- Cohort, Dose-Finding Study of Elacridar (GF120918) and Oral Topotecan in Cancer Patients, *Clin. Cancer Res.*, 13 (2007) 3276.
- [114] W.L. Furman, F. Navid, N.C. Daw, M.B. McCarville, L.M. McGregor, S.L. Spunt, C. Rodriguez-Galindo, J.C. Panetta, K.R. Crews, J. Wu, A.J. Gajjar, P.J. Houghton, V.M. Santana, C.F. Stewart, Tyrosine Kinase Inhibitor Enhances the Bioavailability of Oral Irinotecan in Pediatric Patients With Refractory Solid Tumors, *J. Clin. Oncol.*, 27 (2009) 4599-4604.
- [115] S. Fellner, B. Bauer, D.S. Miller, M. Schaffrik, M. Fankhänel, T. Spruß, G. Bernhardt, C. Graeff, L. Färber, H. Gschaidmeier, A. Buschauer, G. Fricker, Transport of paclitaxel (Taxol) across the blood-brain barrier in vitro and in vivo, *J. Clin. Invest.*, 110 (2002) 1309-1318.
- [116] S. Agarwal, A. Hartz, M. S., W. Elmquist, F., B. Bauer, Breast Cancer Resistance Protein and P-Glycoprotein in Brain Cancer: Two Gatekeepers Team Up, *Curr. Pharm. Des.*, 17 (2011) 2793-2802.
- [117] W. Zhang, M. Liu, L. Yang, F. Huang, Y. Lan, H. Li, H. Wu, B. Zhang, H. Shi, X. Wu, P-glycoprotein inhibitor tariquidar potentiates efficacy of astragaloside iv in experimental autoimmune encephalomyelitis mice, *Molecules*, 24 (2019) 561/561-561/515.
- [118] R.B. Verheijen, M. Yaqub, E. Sawicki, O. van Tellingen, A.A. Lammertsma, B. Nuijen, J.H.M. Schellens, J.H. Beijnen, A.D.R. Huitema, N.H. Hendrikse, N. Steeghs, Molecular Imaging of ABCB1 and ABCG2 Inhibition at the Human Blood–Brain Barrier Using Elacridar and <sup>11</sup>C-Erlotinib PET, *J. Nucl. Med.*, 59 (2018) 973-979.
- [119] M. Bauer, R. Karch, B. Wulkersdorfer, C. Philippe, L. Nics, E.-M. Klebermass, M. Weber, S. Poschner, H. Haslacher, W. Jaeger, N. Tournier, W. Wadsak, M. Hacker, M. Zeitlinger, O. Langer, A proof-of-concept study to inhibit ABCG2- and ABCB1- mediated efflux transport at the human blood-brain barrier, *J. Nucl. Med.*, 60 (2019) 486-491.
- [120] E. Fox, S.E. Bates, Tariquidar (XR9576): a P-glycoprotein drug efflux pump inhibitor, *Expert Rev. Anticancer Ther.*, 7 (2007) 447-459.
- [121] Z. Binkhathlan, A. Lavasanifar, P-glycoprotein Inhibition as a Therapeutic Approach for Overcoming Multidrug Resistance in Cancer: Current Status and Future Perspectives, *Curr. Cancer Drug Targets*, 13 (2013) 326-346.
- [122] R.W. Robey, P. Massey, R., L. Amiri-Kordestani, S. Bates, E., ABC Transporters: Unvalidated Therapeutic Targets in Cancer and the CNS, *Anti-Cancer Agents Med. Chem.*, 10 (2010) 625-633.
- [123] J.W. Ricci, D. Lovato, R.S. Larson, ABCG2 Inhibitors: Will They Find Clinical Relevance?, *J. Develop. Drugs*, 4 (2015) 1-6.
- [124] D.J. Brackman, K.M. Giacomini, Reverse Translational Research of ABCG2 (BCRP) in Human Disease and Drug Response, *Clin. Pharm. Ther.*, 103 (2018) 233-242.
- [125] S.J. Weroha, A.L. Oberg, K.L.A. Ziegler, S.R. Dakhilm, K.M. Rowland, L.C. Hartmann, D.F. Moore, Jr., G.L. Keeney, P.P. Peethambaram, P. Haluska, Phase II trial of lapatinib and topotecan (LapTop) in patients with platinum-refractory/resistant ovarian and primary peritoneal carcinoma, *Gynecol. Oncol.*, 122 (2011) 116-120.
- [126] S. Lheureux, S. Krieger, B. Weber, P. Pautier, M. Fabbro, F. Selle, H. Bourgeois, T. Petit, A. Lortholary, A. Plantade, M. Briand, A. Leconte, N. Richard, P. Vilquin, B. Clarisse, C. Blanc-Fournier, F. Joly, Expected Benefits of Topotecan Combined With Lapatinib in Recurrent Ovarian Cancer According to Biological Profile: A Phase 2 Trial, *Int. J. Gynecol. Cancer*, 22 (2012) 1483.
- [127] T. Tsuruo, H. Iida, S. Tsukagoshi, Y. Sakurai, Overcoming of Vincristine Resistance in P388 Leukemia in Vivo and in Vitro through Enhanced Cytotoxicity of Vincristine and Vinblastine by Verapamil, *Cancer Res.*, 41 (1981) 1967.
- [128] F. Hyafil, C. Vergely, P. Du Vignaud, T. Grand-Perret, In vitro and in vivo reversal of multidrug resistance by GF120918, an acridonecarboxamide derivative, *Cancer Res.*, 53 (1993) 4595-4602.

- [129] M. Roe, A. Folkes, P. Ashworth, J. Brumwell, L. Chima, S. Hunjan, I. Pretswell, W. Dangerfield, H. Ryder, P. Charlton, Reversal of P-glycoprotein mediated multidrug resistance by novel anthranilamide derivatives, *Bioorg. Med. Chem. Lett.*, 9 (1999) 595-600.
- [130] M. de Bruin, K. Miyake, T. Litman, R. Robey, S.E. Bates, Reversal of resistance by GF120918 in cell lines expressing the ABC half-transporter, MXR, *Cancer Lett.*, 146 (1999) 117-126.
- [131] R.W. Robey, K. Steadman, O. Polgar, K. Morisaki, M. Blayney, P. Mistry, S.E. Bates, Pheophorbide a Is a Specific Probe for ABCG2 Function and Inhibition, *Cancer Res.*, 64 (2004) 1242-1246.
- [132] S.K. Rabindran, H. He, M. Singh, E. Brown, K.I. Collins, T. Annable, L.M. Greenberger, Reversal of a novel multidrug resistance mechanism in human colon carcinoma cells by fumitremorgin C, *Cancer Res.*, 58 (1998) 5850-5858.
- [133] S.K. Rabindran, D.D. Ross, L.A. Doyle, W. Yang, L.M. Greenberger, Fumitremorgin C Reverses Multidrug Resistance in Cells Transfected with the Breast Cancer Resistance Protein, *Cancer Res.*, 60 (2000) 47.
- [134] S. Zhang, X. Yang, M.E. Morris, Flavonoids Are Inhibitors of Breast Cancer Resistance Protein (ABCG2)-Mediated Transport, *Mol. Pharmacol.*, 65 (2004) 1208.
- [135] A. Boumendjel, S. Macalou, G. Valdameri, A. Pozza, C. Gauthier, O. Arnaud, E. Nicolle, S. Magnard, P. Falson, R. Terreux, P.A. Carrupt, L. Payen, A. Di Pietro, Targeting the Multidrug ABCG2 Transporter with Flavonoidic Inhibitors: In Vitro Optimization and In Vivo Validation, *Curr. Med. Chem.*, 18 (2011) 3387.
- [136] W. Chearwae, S. Shukla, P. Limtrakul, S.V. Ambudkar, Modulation of the function of the multidrug resistance-linked ATP-binding cassette transporter ABCG2 by the cancer chemopreventive agent curcumin, *Mol. Cancer Ther.*, 5 (2006) 1995-2006.
- [137] V. Lopes-Rodrigues, E. Sousa, M.H. Vasconcelos, Curcumin as a Modulator of P-Glycoprotein in Cancer: Challenges and Perspectives, *Pharmaceuticals*, 9 (2016) 71.
- [138] M. Qadir, K.L. Loughlin, S.M. Fricke, N.A. Williamson, W.R. Greco, H. Minderman, M.R. Baer, Cyclosporin A Is a Broad-Spectrum Multidrug Resistance Modulator, *Clin. Cancer Res.*, 11 (2005) 2320.
- [139] Z. Shi, X.-X. Peng, I.-W. Kim, S. Shukla, Q.-S. Si, R.W. Robey, S.E. Bates, T. Shen, C.R. Ashby, L.-W. Fu, S.V. Ambudkar, Z.-S. Chen, Erlotinib (Tarceva, OSI-774) Antagonizes ATP-Binding Cassette Subfamily B Member 1 and ATP-Binding Cassette Subfamily G Member 2-Mediated Drug Resistance, *Cancer Res.*, 67 (2007) 11012.
- [140] C.-I. Dai, A.K. Tiwari, C.-P. Wu, X.-d. Su, S.-R. Wang, D.-g. Liu, C.R. Ashby, Y. Huang, R.W. Robey, Y.-j. Liang, L.-m. Chen, C.-J. Shi, S.V. Ambudkar, Z.-S. Chen, L.-w. Fu, Lapatinib (Tykerb, GW572016) Reverses Multidrug Resistance in Cancer Cells by Inhibiting the Activity of ATP-Binding Cassette Subfamily B Member 1 and G Member 2, *Cancer Res.*, 68 (2008) 7905.
- [141] K. Takeuchi, T. Sugiura, K. Matsubara, R. Sato, T. Shimizu, Y. Masuo, M. Horikawa, N. Nakamichi, N. Ishiwata, Y. Kato, Interaction of Novel Platelet-Increasing Agent Eltrombopag with Rosuvastatin via Breast Cancer Resistance Protein in Humans, *Drug Metab. Dispos.*, 42 (2014) 726.
- [142] J.D. Allen, A. Van Loevezijn, J.M. Lakhai, M. Van der Valk, O. Van Tellingen, G. Reid, J.H.M. Schellens, G.-J. Koomen, A.H. Schinkel, Potent and specific inhibition of the breast cancer resistance protein multidrug transporter in vitro and in mouse intestine by a novel analogue of fumitremorgin C, *Mol. Cancer Ther.*, 1 (2002) 417-425.
- [143] L.D. Weidner, S.S. Zoghbi, S. Lu, S. Shukla, S.V. Ambudkar, V.W. Pike, J. Mulder, M.M. Gottesman, R.B. Innis, M.D. Hall, The inhibitor Ko143 is not specific for ABCG2, *J. Pharmacol. Exp. Ther.*, 354 (2015) 384-393.
- [144] K. Liu, J. Zhu, Y. Huang, C. Li, J. Lu, M. Sachar, S. Li, X. Ma, Metabolism of Ko143, an ABCG2 inhibitor, *Drug Metab. Pharmacokinet.*, 32 (2017) 193-200.

- [145] F. Lecerf-Schmidt, B. Peres, G. Valdameri, C. Gauthier, E. Winter, L. Payen, A. Di Pietro, A. Boumendjel, ABCG2: recent discovery of potent and highly selective inhibitors, *Future Med. Chem.*, 5 (2013) 1037-1045.
- [146] D. Peña-Solórzano, S.A. Stark, B. König, C.A. Sierra, C. Ochoa-Puentes, ABCG2/BCRP: Specific and Nonspecific Modulators, *Medicinal Research Reviews*, 37 (2017) 987-1050.
- [147] FDA, Drug Development and Drug Interactions: Table of Substrates, Inhibitors and Inducers, <https://www.fda.gov/drugs/drug-interactions-labeling/drug-development-and-drug-interactions-table-substrates-inhibitors-and-inducers#table5-2> (accessed July 14, 2020).
- [148] L. Di, E.H. Kerns, G.T. Carter, Drug-like property concepts in pharmaceutical design, *Curr. Pharm. Des.*, 15 (2009) 2184-2194.
- [149] M. Kühnle, M. Egger, C. Müller, A. Mahringer, G. Bernhardt, G. Fricker, B. König, A. Buschauer, Potent and Selective Inhibitors of Breast Cancer Resistance Protein (ABCG2) Derived from the p-Glycoprotein (ABCB1) Modulator Tariquidar, *J. Med. Chem.*, 52 (2009) 1190-1197.
- [150] S. Bauer, C. Ochoa-Puentes, Q. Sun, M. Bause, G. Bernhardt, B. Koenig, A. Buschauer, Quinoline Carboxamide-Type ABCG2 Modulators: Indole and Quinoline Moieties as Anilide Replacements, *ChemMedChem*, 8 (2013) 1773-1778.
- [151] G.G. Ferenczy, G.M. Keserű, Enthalpic Efficiency of Ligand Binding, *J. Chem. Inf. Model.*, 50 (2010) 1536-1541.
- [152] G.G. Ferenczy, G.M. Keserű, On the enthalpic preference of fragment binding, *MedChemComm*, 7 (2016) 332-337.

## **2 Tariquidar-Related Triazoles as Potent, Selective and Stable Inhibitors of ABCG2 (BCRP)**

Prior to the submission of this thesis, this chapter was published slightly modified:

F. Antoni\*, M. Bause, M. Scholler, S. Bauer, S.A. Stark, S.M. Jackson, I. Manolaridis, K.P. Locher, B. König\*, A. Buschauer, G. Bernhardt, Tariquidar-related triazoles as potent, selective and stable inhibitors of ABCG2 (BCRP), *Eur. J. Med. Chem.*, 191 (2020) 112133.

<https://doi.org/10.1016/j.ejmech.2020.112133>

Author contributions:

The junior authors performed the experiments and analyzed the data with supervision from B.K., K.P.L., A.B and G.B. The synthesis was performed by M.B., S.A.S. and F.A. The transport assays were carried out by S.B., F.A., M.S. and S.A.S.; M.S. performed the ATPase Assays. S.M.J. and I.M. carried out the thermostability assays. F.A. performed the chemosensitivity assays and the chemical stability assays. F.A. wrote the manuscript with input from all co-authors.

\*Corresponding author

## 2.1 Introduction

In 1990, a novel drug resistance-related membrane protein was discovered in a doxorubicin resistant breast cancer cell line [1] and in 1998 it was identified as the most recent member of the human ABC transporter superfamily and named breast cancer resistance protein (BCRP) [2]. The Human Genome Nomenclature Committee termed the transporter ABCG2 [3]. ABCG2 as well as other ABC transporter subtypes such as ABCB1 (P-gp) und ABCC1 (MRP1) are not only associated with the chemoresistance of malignant tumors [4-7], but they are also expressed at the blood-brain barrier (BBB), preventing the entry of a broad variety of xenobiotics, including numerous drugs, into the central nervous system [8-10]. Therefore, co-administration of an ABC inhibitor and a cytostatic drug represents an attractive strategy to overcome the BBB and multidrug resistance (MDR) of various malignancies. This has been demonstrated by several proof-of-concept studies, although ABC inhibitors are not in clinical use yet [11-16]. ABCG2 has come into focus since apart from being one of the three major subtypes conferring MDR in cancer cells (in addition to ABCB1 and ABCC1), it also appears to be the most abundant subtype at the human BBB [17,18].

Figure 2.1 shows a selection of ABCG2 inhibitors described so far. Among the first substances found to affect ABCG2 activity are inhibitors of the ABCB1 transporter, primarily the benzanilides elacridar (**2.01**) and tariquidar (**2.02**) [19-22]. Fumitremorgin C (FTC) (**2.03**), a fungal toxin from *A. fumigatus* Fresen. containing a tetrahydro- $\beta$ -carboline backbone, was the first known specific inhibitor of the ABCG2 subtype [23]. Its neurotoxic effects, however, preclude its use in vivo. Its nontoxic analog Ko143 (**2.04**) was developed in 2002 and is still among the most potent known ABCG2 inhibitors [24]. It was recently reported, though, that it also interferes with both, ABCB1 and ABCC1 transport, but only at higher concentrations (low micromolar range) [25]. The suitability of Ko143 for in vivo studies is compromised by the poor metabolic stability of the ester moiety [26,27]. Lately, further derivatives of FTC have been prepared, e.g. compound **2.05** [28]. Besides the fungal toxin FTC, other natural compounds and derivatives thereof were reported to antagonize ABCG2, the main structural class being flavonoids such as flavones, chalcones and curcuminoids [29-34]. Chromone is a partial structure present in many active flavonoids and was derivatized to create novel, potent and nontoxic ABCG2 inhibitors such as compounds **2.06** and **2.07** [35]. The stability of these compounds still remains to be determined, though. In an ongoing search for potent, selective and stable inhibitors for ABCG2, further structure types have emerged, for instance the relatively small acrylonitrile YHO-13177 (**2.08**) [36,37].

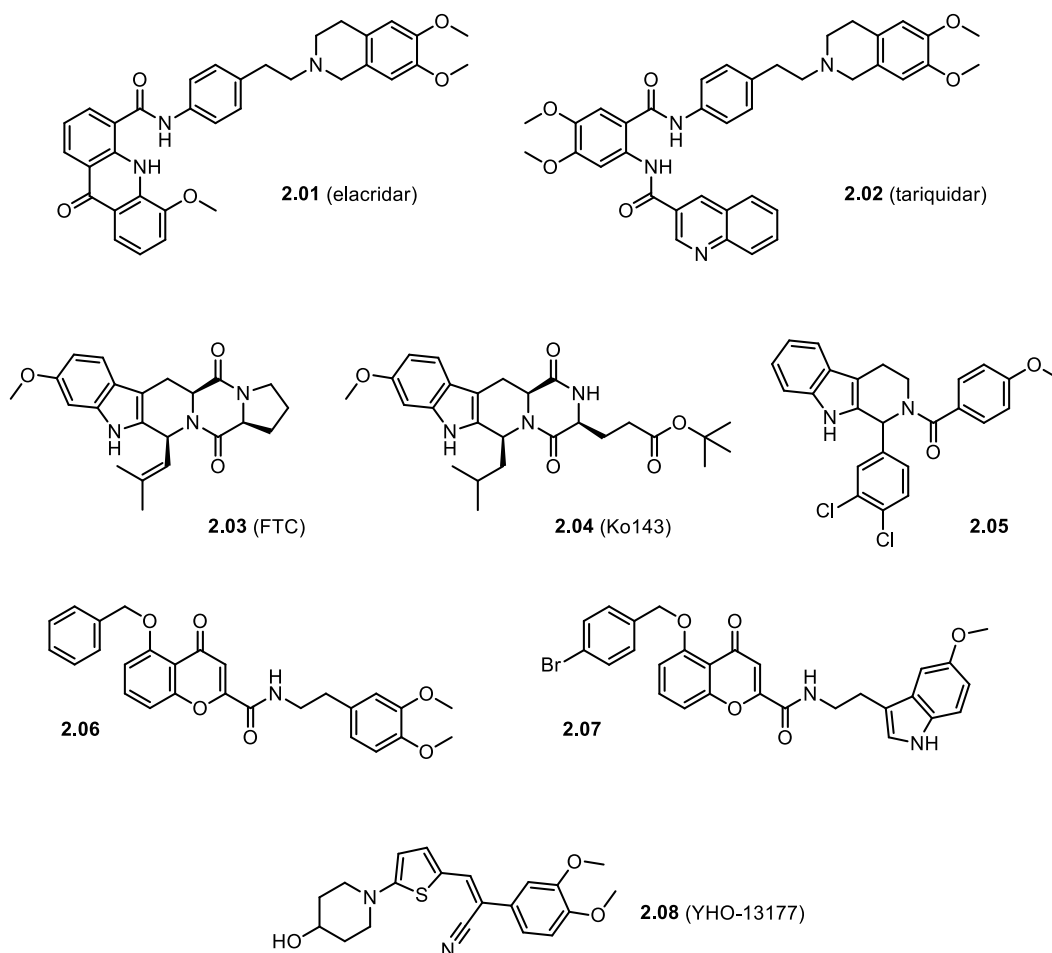


**Figure 2.1.** Structures of known ABCG2 inhibitors: elacridar (**2.01**), tariquidar (**2.02**), fumitremorgin C (**2.03**), Ko143 (**2.04**), the  $\beta$ -carboline derivative **2.05**, the chromones **2.06** and **2.07** and the acrylonitrile YHO-13177 (**2.08**).

Until recently, the mechanism of ABCG2 inhibition could only be speculated about, since there were no high-resolution structural data for ABCG2. The breakthrough came in 2017 with the high-resolution cryo-EM structure of ABCG2 [38]. One year later, we determined the structure of ABCG2 in complex with two different inhibitors, including UR-MB136 (**2.59**), a member of the series we present here [39]. The synthetic route to **2.59**, the appertaining series of novel ABCG2 inhibitors and their biological characterization have not been published yet, and are subject of the present study. Heretofore, we modified the dual ABCB1/ABCG2 inhibitor tariquidar (**2.02**) to obtain the selective ABCG2 inhibitor UR-ME22-1 (**2.09**) (Figure 2.2) [40]. The main, selectivity-yielding modification was the shift of the hetarycarboxamido moiety from the *ortho*- to the *meta*-position of the central benzamide core. However, this shift rendered the central benzamide bond prone to hydrolysis in murine plasma, presumably due to inadequate steric hindrance, facilitating the attack of the amide bond by plasma hydrolases. In an attempt to gain stable tariquidar analogs, the labile amide moiety was replaced by an indole ring, yielding more stable inhibitors with higher efficacy than **2.09** [41]. However, it was shown that these compounds were still hydrolyzed to a certain extent, namely at the ester bond attached to the central, trisubstituted phenyl ring. Here we present the synthesis and pharmacological

evaluation of novel tariquidar derivatives. As shown in Figure 2.2, we introduced a triazole core as a bioisoster to the labile amide group in **2.09**, which can be more conveniently synthesized than an indole moiety. Furthermore, we synthesized compounds in which the labile ester moiety was replaced by ketone groups. We aimed at ABCG2 inhibitors that are potent, effective, selective, and suitable for complexing with ABCG2 in cryo-EM experiments and, moreover, also stable in blood plasma, a prerequisite for in vivo studies.

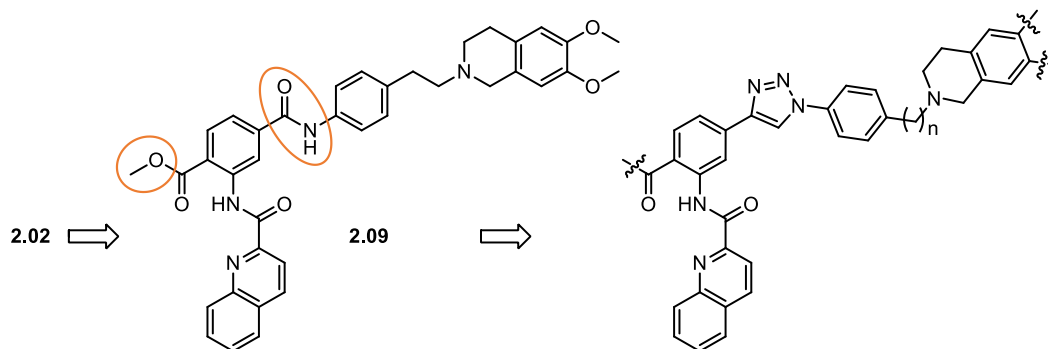


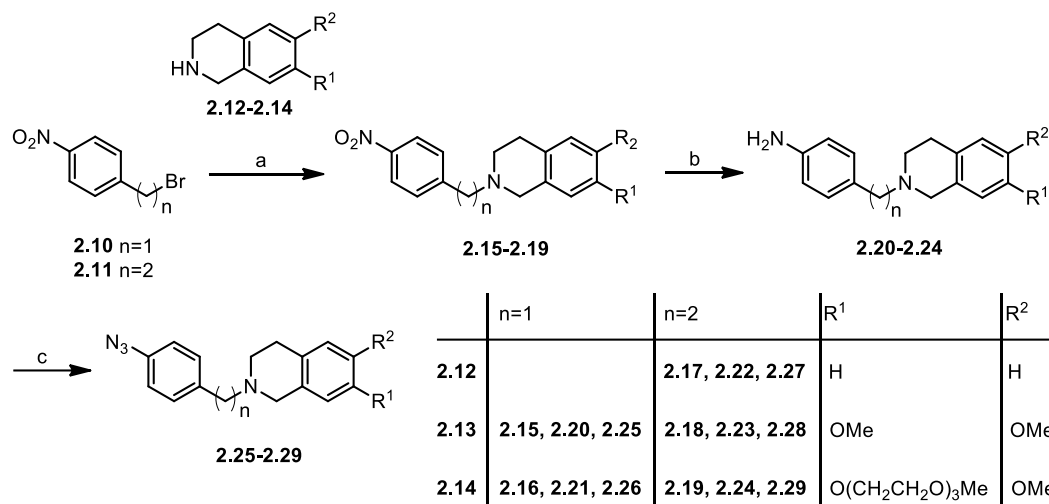
**Figure 2.2.** Structure of UR-ME22-1 (**2.09**) and general structure of the title compounds developed from **2.09**.

In order to rank our novel series we also purchased or prepared compounds **2.02-2.08** as reference substances and investigated them in our assays.

## 2.2 Results and Discussion

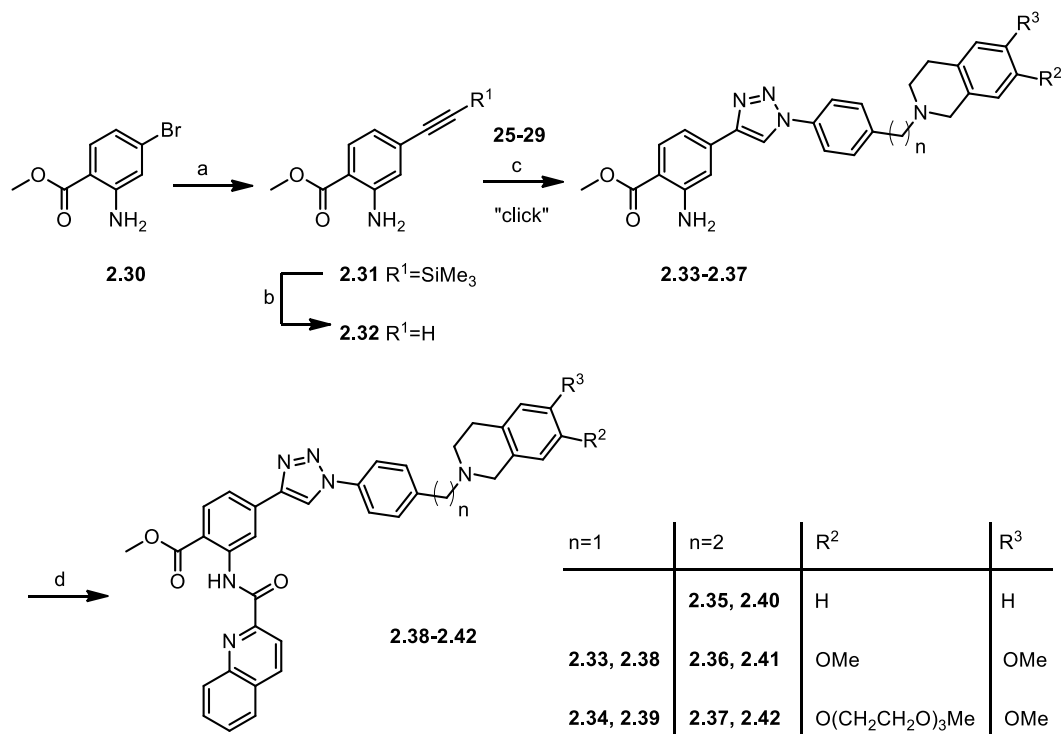
### 2.2.1 Synthesis

“Key” step in the convergent synthesis of the title compounds was the production of the triazole core in a copper-catalyzed azide-alkyne cycloaddition (CuAAC), a stepwise variant of the Huisgen cycloaddition process, and the most often used “click” reaction [42]. Here we used the polytriazole TBTA as a copper(I)-stabilizing ligand [43]. The azides for the CuAAC were prepared in three steps (Scheme 2.1). In order to vary the linker length between the tetrahydroisoquinoline moiety and the phenyl ring, either 1-(bromomethyl)-4-nitrobenzene (**2.10**) or 1-(2-bromoethyl)-4-nitrobenzene (**2.11**) was combined with the respective tetrahydroisoquinoline derivative (**2.12-2.14**) in an *N*-alkylation reaction affording compounds **2.15-2.19**. In our previous studies on tariquidar analogs it proved to be advantageous in terms of efficacy to introduce a polyethylene glycol (PEG) chain at the tetrahydroisoquinoline moiety, which was explained by a solubilizing effect [41,44,45]. For this reason, we also synthesized the PEGylated tetrahydroisoquinoline derivative **2.14** according to our previous report [44] and alkylated the nitrogen. In the next two steps, the nitro group in compounds **2.15-2.19** was reduced to an amine group, resulting in compounds **2.20-2.24**, and then converted into an azide moiety, affording compounds **2.25-2.29**.



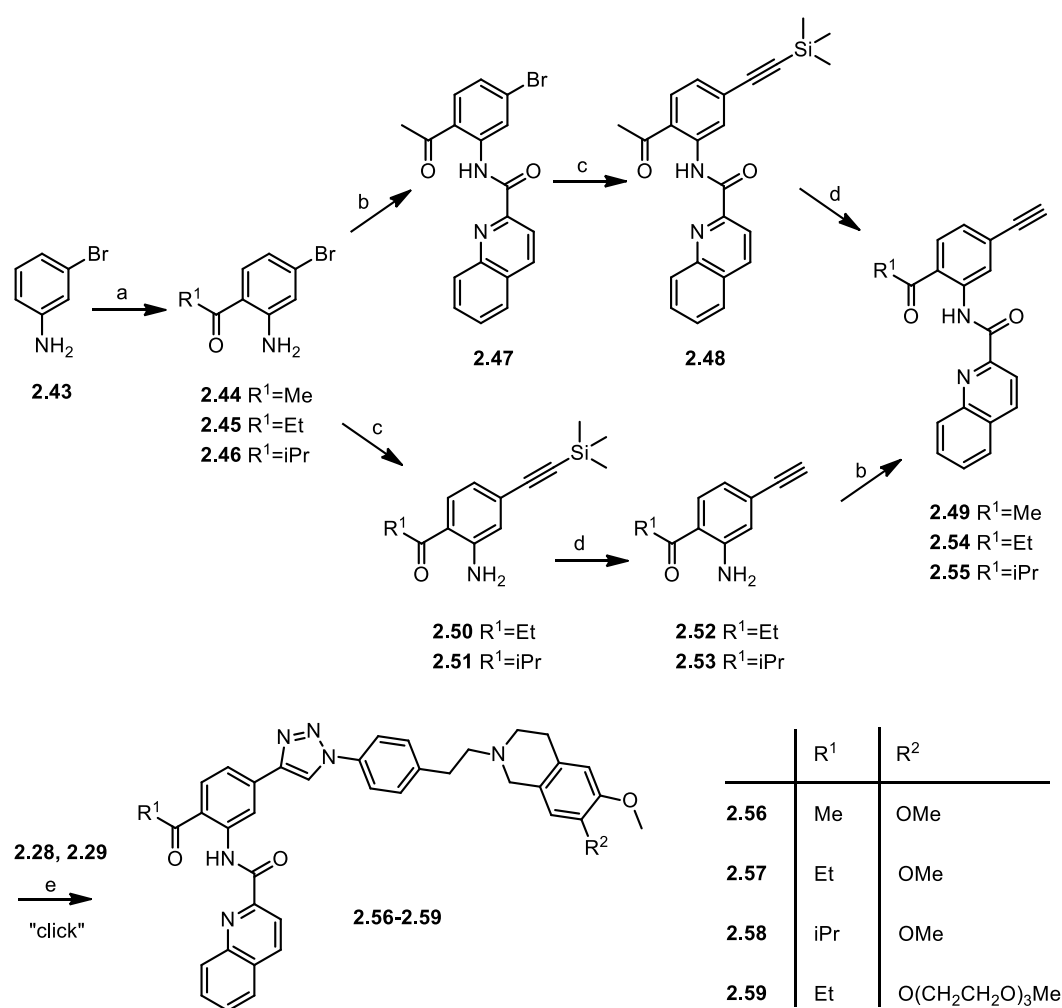
**Scheme 2.1.** Synthesis of the azides for the “click” reactions. Reagents and conditions: (a)  $K_2CO_3$ , MeCN, reflux, overnight; (b) Pd/C,  $H_2$  (40 bar), EtOH, rt, overnight or  $SnCl_2$ , EtOH, reflux, 2 h; (c) (I)  $NaNO_2$ , 6 M HCl aq.,  $-5\text{ }^\circ\text{C}$ , 1 h; (II)  $NaN_3$ ,  $-5\text{ }^\circ\text{C}$ , 1 h.

The synthesis of the target compounds containing an ester group is shown in Scheme 2.2. Firstly, the alkyne **2.32** as the second reactant in the “click” reactions was prepared by Sonogashira coupling of methyl 2-amino-4-bromobenzoate (**2.30**) and trimethylsilylacetylene to **2.31** and subsequent TMS-deprotection (to compound **2.32**). Then **2.32** was combined with the azides **2.25-2.29**, affording the triazoles **2.33-2.37** and the quinoline moiety was introduced by amide coupling with quinoline-2-carboxylic acid, yielding the inhibitors **2.38-2.42**.



**Scheme 2.2.** Synthesis of the inhibitors **2.38-2.42** bearing an ester moiety. Reagents and conditions: (a) ethynyltrimethylsilane,  $Pd(PPh_3)_2Cl_2$ , CuI,  $NEt_3$ , THF,  $60\text{ }^\circ\text{C}$ , overnight; (b) TBAF, THF,  $0\text{ }^\circ\text{C}$ , 2 h; (c)  $CuSO_4$ , sodium ascorbate, TBTA, DMF, rt, 24 h; (d) quinoline-2-carboxylic acid, HBTU, DIPEA, DCM,  $0\text{ }^\circ\text{C} \rightarrow \text{rt}$ , 24 h.

In the second subseries, the labile ester moiety was replaced by different ketone groups (Scheme 2.3). 3-Bromoaniline (**2.43**) was acylated in a Sugawara reaction, a specific *ortho*-acylation of anilines, to form the ketones **2.44-2.46**. Compound **2.44** was first treated with quinoline-2-carboxylic acid to form the amide **2.47** and then submitted to a Sonogashira coupling with trimethylsilylacetylene (resulting in **2.48**) and deprotected to **2.49**. Precursors **2.45** and **2.46** were first coupled with trimethylsilylacetylene under Sonogashira conditions (forming **2.50** and **2.51**), deprotected (to **2.52** and **2.53**), and then treated with quinoline-2-carboxylic acid to form the amide bond (yielding **2.54** and **2.55**). The final step was the “click” reaction of the alkynes **2.49**, **2.54**, and **2.55** with the azides **2.28** or **2.29** to form the inhibitors **2.56-2.59**.



**Scheme 2.3.** Synthesis of the inhibitors **2.56-2.59** bearing a ketone moiety. Reagents and conditions: (a) (I) BCl<sub>3</sub>, DCM, 0 °C, 20 min; (II) AlCl<sub>3</sub>, respective nitrile, reflux, 24 h; (III) 2 M HCl aq, 0 °C, 10 min → 80 °C, 1 h; (b) quinoline-2-carboxylic acid, HBTU, DIPEA, DCM, 0 °C → rt, 24 h; (c) ethynyltrimethylsilane, Pd(PPh<sub>3</sub>)<sub>2</sub>Cl<sub>2</sub>, CuI, NEt<sub>3</sub>, THF, 60 °C, overnight; (d) TBAF, THF, 0 °C, 2 h; (e) CuSO<sub>4</sub>, sodium ascorbate, TBTA, DMF or THF, rt, 24 h.

The reference compounds **2.03** and **2.04** were commercially available; **2.02** [21], **2.05** [28], **2.06** [35], **2.07** [35], and **2.08** [36,37] were synthesized according to literature.

## 2.2.2 Inhibition of the ABCG2, ABCB1 and ABCC1 Transport Activity

The newly synthesized compounds (**2.38-2.42** and **2.56-2.59**), as well as our previous tariquidar analog **2.09** and the reference compounds **2.02-2.08**, were analyzed for inhibition of the ABCG2 transport activity in a Hoechst 33342 microplate assay. The DNA stain Hoechst 33342, which emits blue fluorescence when bound to DNA, is a substrate of the ABCG2 transporter and therefore extruded from ABCG2-expressing cells such as the MCF-7/Topo cells utilized in this assay. When the ABCG2 transport function is inhibited, Hoechst 33342 accumulates in the cells and can be detected fluorometrically, which allows for determination of the inhibitory potency and efficacy of the target compounds. Examples of concentration-response curves are shown in Figure 2.3. In order to assess the selectivity of the inhibitors, they were also analyzed in a calcein-AM microplate assays with respect to inhibition of the ABCB1 and ABCC1 transporter activity, using KB-V1 and MDCK.2-MRP1 cells, respectively. The assay principle is analogous to the Hoechst 33342 assay. The dual ABCB1 and ABCC1 substrate calcein-AM is added to the cells and exported by the respective transporter. Upon inhibition of the transport, calcein-AM accumulates in the cells, becomes cleaved to calcein by intracellular esterases and complexes  $\text{Ca}^{2+}$ -ions, resulting in a strong green fluorescence. The fluorescence can be detected and correlated with the inhibitory potencies of the test compounds. The results of the transport assays are summarized in Table 2.1.

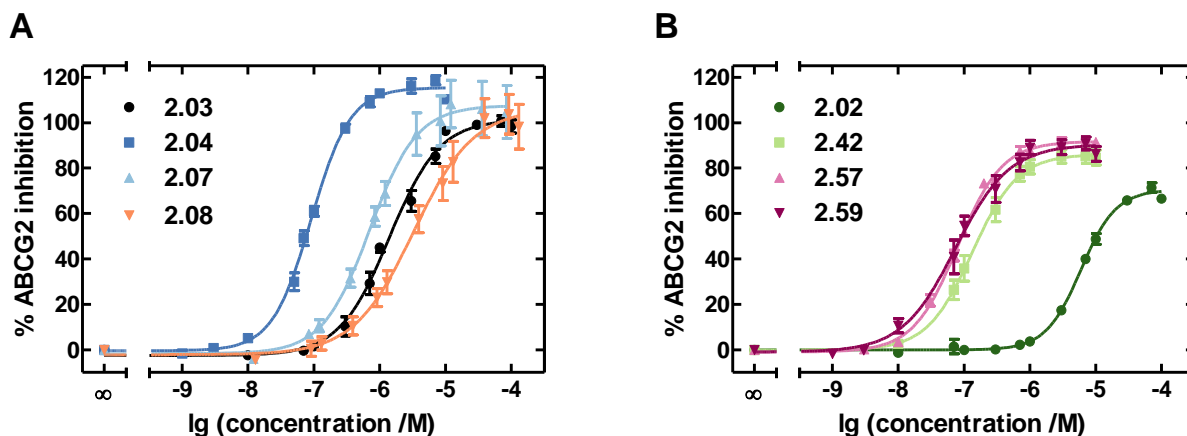


**Figure 2.3.** Concentration-dependent inhibition of ABCG2-mediated Hoechst 33342 efflux in MCF-7/Topo cells by (A) the reference compounds FTC (**2.03**), Ko143 (**2.04**), **2.07** and **2.08** as well as (B) tariquidar (**2.02**) and its novel analogs **2.42**, **2.57** and **2.59**. The inhibition is expressed relative to the maximal effect in the presence of 10  $\mu\text{M}$  FTC set to 100%.

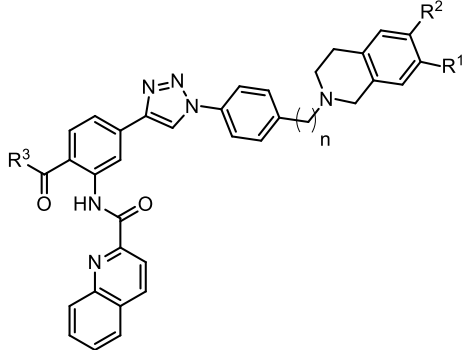
FTC (**2.03**), its well-known analog Ko143 (**2.04**) and the more recent analog **2.05**, which all comprise a tetrahydro- $\beta$ -carboline moiety, were similarly effective at ABCG2 with an  $I_{\text{max}}$  value of 102%, 116% and 111%, respectively. However **2.04**, with an  $\text{IC}_{50}$  value of 92 nM, was over ten times more potent than the other two tetrahydro- $\beta$ -carboline derivatives in our assay. Whereas **2.04** is reported to be more potent than its precursor **2.03** [24], the  $\text{IC}_{50}$  value of **2.05** determined here (1.1  $\mu\text{M}$ ) was about five times higher than reported in literature (lit. 233 nM in Hoechst 33342 assay [28]; 237 nM in pheophorbide A assay [28]). This discrepancy

probably reflects differences in the assay set-up, for instance different concentrations of Hoechst 33342 were applied (it was higher in our assay). In accordance with previous reports [25], **2.04** was not entirely selective; in contrast to **2.03** and **2.05** it showed potency at the ABCB1 and ABCC1 transporter. The reference compounds **2.06-2.08** were almost equieffective with **2.04**, but less potent. The chromone **2.07** inhibited ABCG2 with an  $IC_{50}$  value of 707 nM (lit. 110 nM [35]), being almost three times more potent than the chromone **2.06**, which showed an  $IC_{50}$  value of 1.8  $\mu$ M (lit. 170 nM [35]). Here again, the  $IC_{50}$  values determined by us were higher than those reported in literature. Furthermore, chromone **2.07**, as opposed to chromone **2.06**, showed very low inhibition of ABCB1 and ABCC1. The acrylonitrile **2.08** inhibited ABCG2 with a far higher  $IC_{50}$  value (3.3  $\mu$ M) than **2.04**. This compound is interesting insofar as it appears to be a triple ABCG2, ABCB1 and ABCC1 inhibitor, which might have a different application than specific inhibitors.

In accordance with previous publications [22], tariquidar (**2.02**) was a dual ABCG2 and ABCC1 inhibitor, but showed much higher inhibitory potency and also higher efficacy at the ABCB1 than at the ABCG2 transporter. Structural modifications at the benzamide core of **2.02** led to a drastic increase in selectivity for ABCG2 over ABCB1 (compound **2.09**), confirming our previous results [40]. Compound **2.09** showed only very low inhibition of ABCB1, but inhibited ABCG2 with an  $IC_{50}$  value of 101 nM. The maximal response of 99% was higher than that determined in a flow cytometric mitoxantrone efflux assay we used before. The replacement of the labile amide moiety in **2.09** by a triazole ring resulted in the novel inhibitors **2.38-2.42**. This replacement was well-tolerated, the efficacy of the new compounds being 85-95% and the potencies in the three-digit nanomolar range. Apparently the length of the linker between the tetrahydroisoquinoline moiety and the phenyl ring does not clearly correlate with the inhibitory potency. Compounds **2.38** and **2.41**, as well as **2.39** and **2.42**, only differ in the length of the linker (one vs. two methylene groups). Whereas compounds **2.39** and **2.42** were equipotent ( $IC_{50}$  values of about 150 nM), compound **2.38** ( $IC_{50}$  of 350 nM) was almost twice as potent as **2.41**. The introduction of a PEG chain increased the potency by a factor of two (**2.38** vs. **2.39**) or four (**2.41** vs. **2.42**). The replacement of the two methoxy groups at the tetrahydroisoquinoline moiety by hydrogen atoms (**2.40**) increased the potency slightly. Taken together, variations in the linker and the moieties attached to the tetrahydroisoquinoline ring seem to be well-tolerated. In terms of selectivity, compounds **2.38-2.42** showed great differences. While all of them were inactive at ABCC1, they showed very dissimilar effects on ABCB1. Here again, there was no correlation between the length of the linker and ABCB1 inhibition. Both **2.38** and **2.39**, with an identical linker (one methylene group), inhibited ABCB1 with a maximal response between 20% and 30% (up to 100  $\mu$ M). **2.40**, **2.41** and **2.42** (two methylene groups) diverged very much depending on the substituents at the

tetrahydroisoquinoline moiety. **2.41** was inactive, **2.40** was 11% effective (up to 100  $\mu$ M) and **2.42**, containing the PEG chain, was 80% effective and exhibited an  $IC_{50}$  value in the low micromolar range, making it a dual ABCG2 and ABCB1 inhibitor. It seems as if the PEG chain can confer potency at ABCB1. Since, however, this was not the case for **2.39**, compared to **2.38**, this effect appears to depend on the specific structure.

**Table 2.1.** Inhibitory effect of the reference compounds **2.02-2.08**, our previous tariquidar analog **2.09** and the new inhibitors **2.38-2.42** and **2.56-2.59** on the transport activity of ABCG2, ABCB1 and ABCC1.

	n=1	n=2	R <sup>1</sup>	R <sup>2</sup>	R <sup>3</sup>
		<b>2.40</b>	H	H	OMe
	<b>2.38</b>	<b>2.41</b>	OMe	OMe	OMe
	<b>2.39</b>	<b>2.42</b>	O(CH <sub>2</sub> CH <sub>2</sub> O) <sub>3</sub> Me	OMe	OMe
		<b>2.56</b>	OMe	OMe	Me
		<b>2.57</b>	OMe	OMe	Et
		<b>2.58</b>	OMe	OMe	iPr
		<b>2.59</b>	O(CH <sub>2</sub> CH <sub>2</sub> O) <sub>3</sub> Me	OMe	Et

Compound	ABCG2 <sup>a</sup>		ABCB1 <sup>b</sup>		ABCC1 <sup>c</sup>	
	$IC_{50}$ [nM] <sup>d</sup>	$I_{max}$ [%] <sup>d,e</sup>	$IC_{50}$ [nM] <sup>d</sup>	$I_{max}$ [%] <sup>d,f</sup>	$IC_{50}$ [nM] <sup>d</sup>	$I_{max}$ [%] <sup>d,g</sup>
<b>2.02</b> (tariquidar)	6223 $\pm$ 707	72 $\pm$ 3	356 $\pm$ 3	100 $\pm$ 3	inactive <sup>h,i</sup>	–
<b>2.03</b> (FTC)	1483 $\pm$ 194	102 $\pm$ 3	inactive	–	inactive	–
<b>2.04</b> (Ko143)	92 $\pm$ 9	116 $\pm$ 2	$\geq$ 25520 <sup>j</sup>	$\geq$ 11	6650 $\pm$ 2856	29 $\pm$ 8
<b>2.05</b>	1115 $\pm$ 32	111 $\pm$ 3	inactive	–	inactive	–
<b>2.06</b>	1800 $\pm$ 300 <sup>i</sup>	108 $\pm$ 5 <sup>i</sup>	inactive <sup>i</sup>	–	inactive <sup>i</sup>	–
<b>2.07</b>	707 $\pm$ 98	109 $\pm$ 12	6756 $\pm$ 946	10 $\pm$ 1	3599 $\pm$ 302	15 $\pm$ 1
<b>2.08</b> (YHO-13177)	3345 $\pm$ 342	106 $\pm$ 9	$\geq$ 65480	$\geq$ 53	$\geq$ 39750	$\geq$ 81
<b>2.09</b> (UR-ME22-1)	101 $\pm$ 17	99 $\pm$ 1	$\geq$ 12080	$\geq$ 14	inactive	–
<b>2.38</b> (UR-MB86)	350 $\pm$ 53	87 $\pm$ 2	$\geq$ 10730	$\geq$ 25	inactive	–
<b>2.39</b> (UR-MB84)	153 $\pm$ 12	85 $\pm$ 3	$\geq$ 25030	$\geq$ 21	inactive	–
<b>2.40</b> (UR-MB81)	486 $\pm$ 5	95 $\pm$ 5	$\geq$ 38270	$\geq$ 11	inactive	–
<b>2.41</b> (UR-MB19)	617 $\pm$ 179	90 $\pm$ 3	inactive	–	inactive	–
<b>2.42</b> (UR-MB95)	144 $\pm$ 35	86 $\pm$ 3	1623 $\pm$ 405	80 $\pm$ 7	inactive	–
<b>2.56</b> (UR-St1)	140 $\pm$ 40	97 $\pm$ 2	inactive	–	inactive	–
<b>2.57</b> (UR-MB108)	79 $\pm$ 5	91 $\pm$ 2	inactive	–	inactive	–
<b>2.58</b> (UR-St2)	295 $\pm$ 28	90 $\pm$ 0.4	$\geq$ 21830	$\geq$ 24	$\geq$ 19040	$\geq$ 14
<b>2.59</b> (UR-MB136)	81 $\pm$ 16	90 $\pm$ 3	$\geq$ 44460	$\geq$ 42	inactive	–

<sup>a</sup> Hoechst 33342 microplate assay using ABCG2-expressing MCF-7/Topo cells.

<sup>b</sup> Calcein-AM microplate assay using ABCB1-expressing KB-V1 cells.

<sup>c</sup> Calcein-AM microplate assay using ABCC1-expressing MDCK.2-MRP1 cells.

<sup>d</sup> Mean values  $\pm$  SEM from two to seven independent experiments, each performed in triplicate.

<sup>e</sup> Maximal inhibitory effect ( $I_{max}$ ) relative to the response to FTC at a concentration of 10  $\mu$ M (100%).

<sup>f</sup> Maximal inhibitory effect ( $I_{max}$ ) relative to the response to tariquidar at a concentration of 10  $\mu$ M (100%).

<sup>g</sup> Maximal inhibitory effect ( $I_{max}$ ) relative to the response to reversan at a concentration of 30  $\mu$ M (100%).

<sup>h</sup> Inactive: response  $\leq$  10% up to a concentration of 100  $\mu$ M.

<sup>i</sup> Data taken from our previous studies [46].

<sup>j</sup> No plateau was reached up to a concentration of 100  $\mu$ M. In these cases, minimum  $IC_{50}$  values and  $I_{max}$  values were stated.

The second modification of **2.09** was the replacement of the labile ester moiety at the central, trisubstituted phenyl core by ketones, yielding the inhibitors **2.56-2.59**. This alteration increased the efficacy at ABCG2 to 90-97%. The IC<sub>50</sub> values were in the two- to low three-digit nanomolar range. The length of the acyl group attached to the benzamide core was varied. The propionyl group (in **2.57**) proved to be superior to the smaller acetyl group (in **2.56**) and also to the bulkier isobutyryl moiety (in **2.58**) in terms of inhibitory potency and selectivity, **2.58** showing moderate ABCB1 and ABCC1 activity. In this subseries, the introduction of a PEG chain (**2.59**) left the inhibitory potency at ABCG2 unchanged, but, here again, caused an inhibitory effect on ABCB1, with the maximal response being 42% (up to a concentration of 100  $\mu$ M). It is conceivable that the PEG chain confers affinity to the binding site in ABCB1. Except for **2.58**, none of the ketone-containing inhibitors showed inhibition of ABCC1.

### 2.2.3 Effect on the ABCG2 ATPase Activity

On the basis of the results obtained from the functional transport assays, the two most potent novel inhibitors (**2.57** and **2.59**), their precursor **2.09** and the reference compounds **2.02-2.08** were examined with regard to their effect on ABCG2 ATPase activity. The ATPase assay, requiring relatively high levels of transporter protein, was performed with ABCG2-expressing Sf9 membranes. ABC transporters gain the energy for the transport of their substrates from ATP hydrolysis to ADP and inorganic phosphate. The latter was determined in a colorimetric reaction after incubation of the membrane preparations with different concentrations of test compounds, resulting in concentration-response curves (examples depicted in Figure 2.4A+B). In a variant of this assay, the ABCG2 transporters in the membranes were additionally stimulated with the ABCG2 substrate sulfasalazine to investigate whether the test compounds reverse the activating effect caused by sulfasalazine, or not (Figure 2.4C+D). The results of the two assay variants are summarized in Table 2.2.

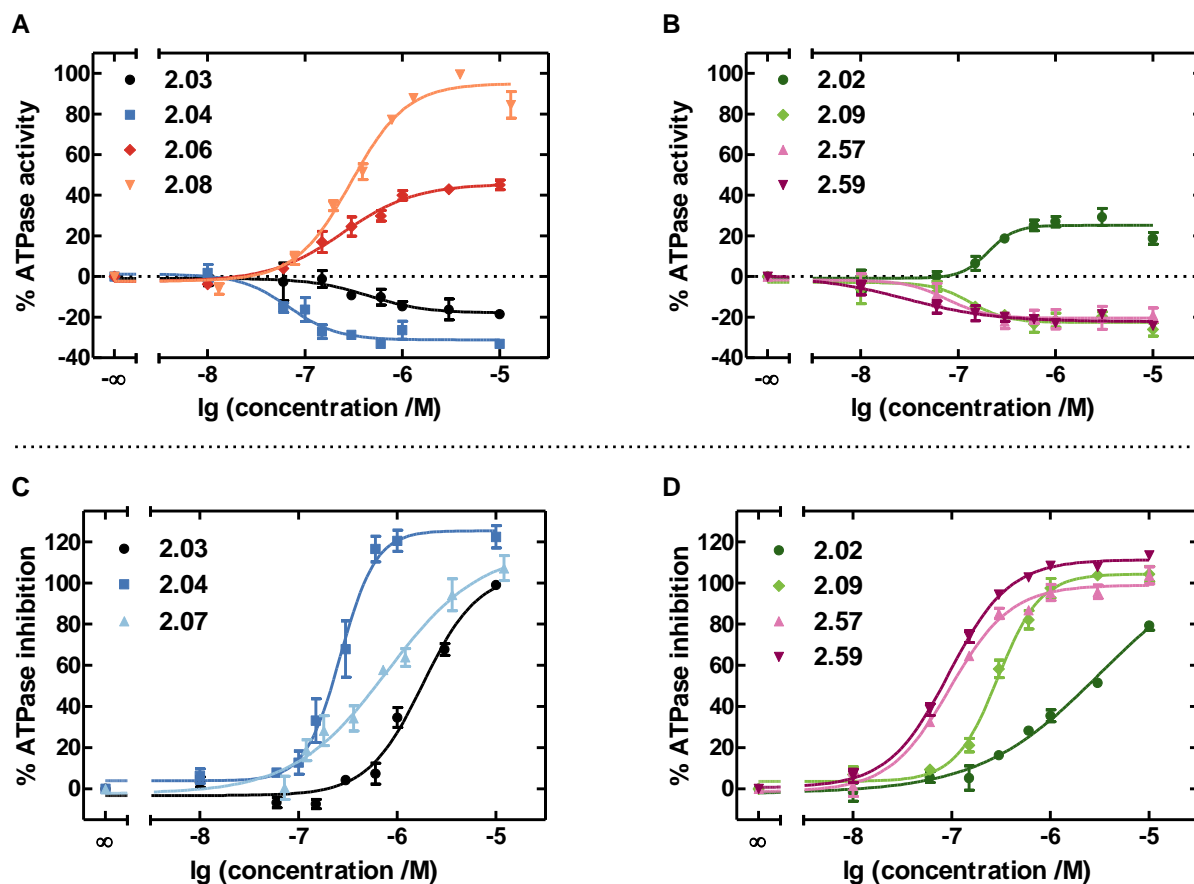
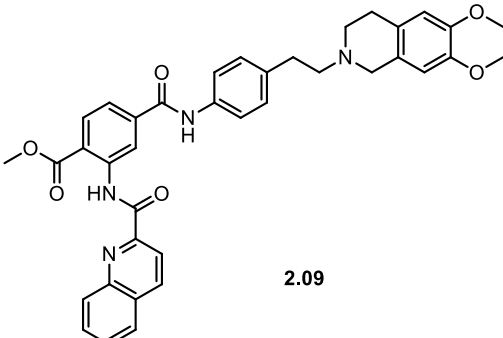


**Figure 2.4.** (A+B) Concentration-dependent stimulation or suppression of the ATPase activity in ABCG2-expressing Sf9 membranes by (A) the reference compounds FTC (2.03), Ko143 (2.04), 2.06 and 2.08 as well as (B) tariquidar (2.02), its analog UR-ME22-1 (2.09) and its novel analogs 2.57 and 2.59. The effect is expressed relative to the basal ATPase activity (0%) and the maximal stimulatory effect in the presence of 30  $\mu\text{M}$  sulfasalazine set to 100%. (C+D) Concentration-dependent inhibition of the sulfasalazine (3  $\mu\text{M}$ )-stimulated ATPase activity in ABCG2-expressing Sf9 membranes by (C) the reference compounds FTC (2.03), Ko143 (2.04) and 7 as well as (D) tariquidar (2.02), its analog UR-ME22-1 (2.09) and its novel analogs 2.57 and 2.59. The inhibition is expressed relative to the maximal inhibitory effect in the presence of 10  $\mu\text{M}$  FTC set to 100%.

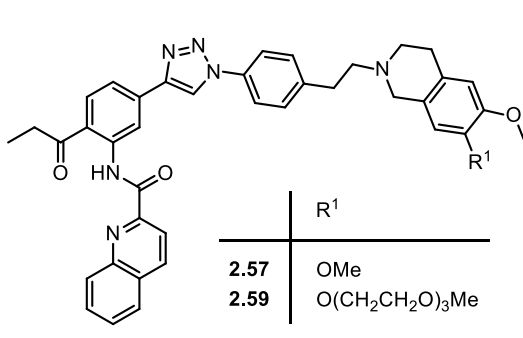
In the absence of inhibitors, ABCG2 showed relatively high basal ATPase activity, which was set to zero in our assay. The test compounds, all being transport inhibitors, behaved in three different manners with respect to ABCG2 ATPase activity. Firstly, most of them decreased it to a level below the basal activity (below zero) or secondly, had no effect on it. In these two cases it can be assumed that the test compounds are not transported and the inhibition of the transport of other substrates may be, at least in part, attributed to the inhibition of the ATPase activity of the transporter. A reduction of the ATPase activity was evoked by FTC (2.03) and its analogs Ko143 (2.04) and 2.05, and the tariquidar analogs 2.09, 2.57 and 2.59, their maximal effects being between -20% and -37% and their potencies in the two-digit (2.04, 2.57 and 2.59) to three-digit (2.03, 2.05 and 2.09) nanomolar range. The compounds were also able to inhibit sulfasalazine-stimulated ATPase activity with an efficacy around 100% (2.03, 2.09, 2.57 and 2.59) or more (2.04, 2.05) and potencies again in the two-digit (2.57 and 2.59) to three-digit (2.04, 2.05 and 2.09) nanomolar range. Only 2.03 showed a higher  $\text{IC}_{50}$  value of 1.8  $\mu\text{M}$ . The chromone 2.07 exhibited no effect on the basal ATPase activity, but was able to reverse activation by sulfasalazine.

Thirdly, some compounds increased the ATPase activity and can therefore be considered transporter substrates, although the coupling of ATP-hydrolysis to transport has been challenged [47]. It is conceivable that transport inhibitors that are strong ATPase activators at the same time compete with other substrates, e.g. Hoechst 33342, for transport by diffusing rapidly back into the cell (so-called “fast-diffusers”) [48]. To explore if they also compete for the same binding site, further interaction type analyses would be required. It seems probable, though, because we recently identified one central multidrug-binding site [39] (i.e. for substrates and inhibitors). The acrylonitrile **2.08** activated the ATPase activity as efficiently as the standard activator sulfasalazine (namely with 99%) and even exhibited a lower EC<sub>50</sub> value (327 nM vs. 916 nM for sulfasalazine). Compound **2.08** might be such a “fast-diffuser”, an assumption also supported by its low molecular mass.

**Table 2.2.** Effect of the reference compounds **2.02-2.08**, our previous tariquidar analog **2.09** and the new inhibitors **2.57** and **2.59** on the ATPase activity of ABCG2 with and without pre-stimulation with sulfasalazine.



**2.09**



	R <sup>1</sup>
<b>2.57</b>	OMe
<b>2.59</b>	O(CH <sub>2</sub> CH <sub>2</sub> O) <sub>3</sub> Me

Compound	Effect on ATPase activity <sup>a</sup>		Inhibition on stimulated ATPase activity <sup>b</sup>	
	EC <sub>50</sub> [nM] <sup>c,d</sup>	E <sub>max</sub> [%] <sup>c,e</sup>	IC <sub>50</sub> [nM] <sup>c</sup>	I <sub>max</sub> [%] <sup>c,f</sup>
Sulfasalazine	916 ± 2	96 ± 4	–	–
<b>2.02</b> (tariquidar)	211 ± 31	25 ± 3	≥ 1180	≥ 79
<b>2.03</b> (FTC)	412 ± 240	- 20 ± 2	1808 ± 203	104 ± 2
<b>2.04</b> (Ko143)	70 ± 17	- 31 ± 1	271 ± 44	124 ± 5
<b>2.05</b>	134 ± 3	- 37 ± 2	226 ± 30	141 ± 8
<b>2.06</b>	274 ± 86	45 ± 3	194 ± 128	19 ± 4
<b>2.07</b>	–	0 ± 1	745 ± 74	113 ± 4
<b>2.08</b> (YHO-13177)	327 ± 34	99 ± 7	–	–
<b>2.09</b> (UR-ME22-1)	105 ± 14	- 27 ± 7	294 ± 17	105 ± 3
<b>2.57</b> (UR-MB108)	70 ± 28	- 21 ± 4	96 ± 2	99 ± 3
<b>2.59</b> (UR-MB136)	52 ± 38	- 23 ± 0.1	93 ± 8	112 ± 1

<sup>a</sup> ATPase microplate assay using ABCG2-expressing Sf9 membranes.

<sup>b</sup> ATPase microplate assay using ABCG2-expressing Sf9 membranes; ABCG2 stimulated with sulfasalazine at a concentration of 3 μM.

<sup>c</sup> Mean values ± SEM from two to four independent experiments, each performed in duplicate.

<sup>d</sup> Half-maximal effective concentrations were termed EC<sub>50</sub> (not IC<sub>50</sub>) values, even if the ATPase activity was reduced, in order to avoid confusion with the data from the ATPase assay with sulfasalazine stimulation.

<sup>e</sup> Maximal effect (E<sub>max</sub>) on the ATPase activity relative to the basal ATPase activity (0%) and to the response to sulfasalazine at a concentration of 30 μM (100%).

<sup>f</sup> Maximal inhibitory effect (I<sub>max</sub>) relative to the response to FTC at a concentration of 10 μM (100%).

Transport inhibitors that exert only a partially activating effect on the ATPase activity were tariquidar (**2.02**), showing a maximal effect of 25% and standing in contrast with its ATPase-suppressing analogs (**2.09**, **2.57** and **2.59**), and the chromone **2.06** (45%), as opposed to the chromone **2.07** with no effect. Nonetheless, both **2.02** and **2.07** were able to partly antagonize ATPase stimulation by sulfasalazine.

The ATPase results from our novel tariquidar derivatives are consistent with the structural data on ABCG2 inhibition we published recently [39]. We showed that compound **2.59** and a derivative of **2.04** both bound to the multidrug-binding site identified in these experiments (cavity 1; located in the transmembrane domains) and locked the inward-facing conformation, thereby inhibiting the ATPase activity (of the cytoplasmic, nucleotide-binding domains) due to conformational coupling.

Figure 2.5 shows the comportment of the reference compounds FTC (**2.03**) and its analogs Ko143 (**2.04**) and **2.05**, in relation to our previous tariquidar analog **2.09** and our most potent novel analogs **2.57** and **2.59**, all of which suppressed the ABCG2 ATPase activity. Depicted are half-maximal (effective or inhibitory) concentrations, determined in the three different functional assays performed, namely the Hoechst 33342 transport assay and the ATPase assay with and without pre-stimulation with sulfasalazine. Of course, it is expected that half-maximal concentrations differ when determined in different assays, depending on the experimental conditions. However, plotting the functional data obtained from different assays in a radar chart, we were able to show commonality and to identify outliers. Ko143 (**2.04**) and the tariquidar analogs **2.09**, **2.57** and **2.59** showed similar behavior – their potencies in the three assays coincided fairly well. FTC (**2.03**) and its derivative **2.05**, on the other hand, did not show comparable half-maximal concentrations. Their potencies determined in the Hoechst transport assay were much higher than those in the ATPase assay and compound **2.03** also showed a higher half-maximal concentration in the ATPase assay with sulfasalazine-stimulation than without. Our previous structural study [39] showed that one **2.59** molecule or two molecules of a derivative of **2.04** completely occupied the volume of cavity 1. We concluded that these inhibitors act competitively at the binding site with substrates, which was the second inhibition mechanism identified, apart from ATPase inhibition. So one could speculate that not only **2.59** but also the other inhibitors compete for the binding site with substrates, and similar potencies in the three assays might suggest that the inhibitors **2.04**, **2.09**, **2.57** and **2.59** bind to ABCG2 with higher affinities than the substrates Hoechst 33342 and sulfasalazine. Vice versa, higher potencies in assays in the presence of substrates might be taken as a hint to displaceability of **2.03** and **2.05** by the respective substrates at the concentrations employed.

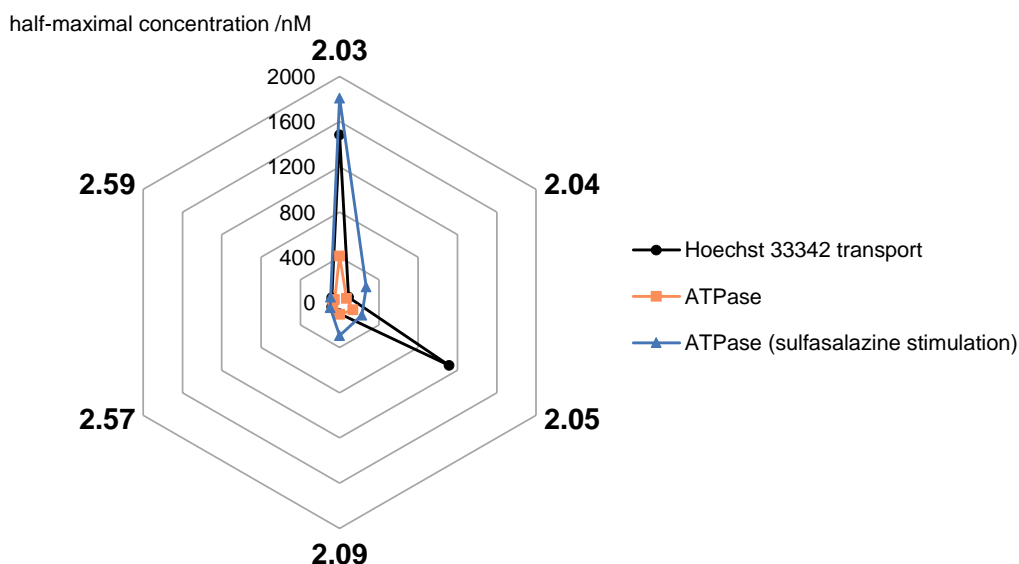


**Figure 2.5.** Comparison of half-maximal effective/ inhibitory concentrations produced by the compounds **2.03**, **2.04**, **2.05**, **2.07**, **2.09**, **2.57** and **2.59** in the Hoechst 33342 transport assay (black), the ATPase assay (orange) and the ATPase assay with pre-stimulation with sulfasalazine (blue).

## 2.2.4 Thermostabilization of ABCG2

We analyzed the thermostabilization of ABCG2 by our two most potent novel tariquidar analogs (**2.57** and **2.59**) and the reference compound Ko143 (**2.04**) in a size-exclusion chromatography-based thermostability assay (SEC-TS). For this purpose, purified ABCG2 was incubated with or without an inhibitor at increasing temperatures and subjected to SEC. The main peak heights were plotted against the temperature to obtain the “melting points” ( $T_m$  values) of ABCG2. The curves for ABCG2 in the presence and absence of compound **2.57** are depicted in Figure 2.6; the curves for ABCG2 in the presence and absence of compounds **2.04** and **2.59** were included in our previous report [39] (on the cryo-EM structure of ABCG2 in complex with inhibitors).

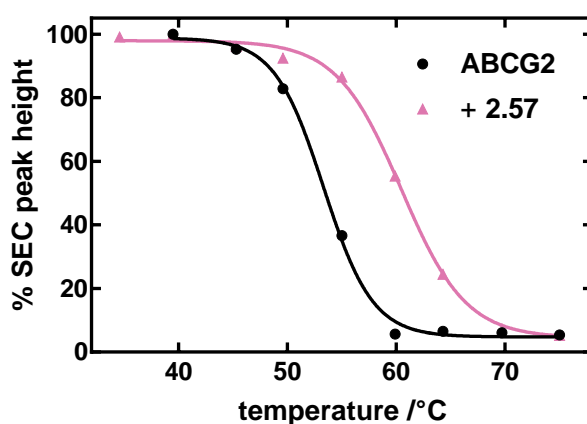


**Figure 2.6.** SEC-TS of ABCG2 before or after the addition of **2.57** at a concentration of 10  $\mu$ M. The peak heights are expressed relative to the peak height of ABCG2 without inhibitor at 4 °C (HP-SEC analysis, UV detection at 280 nm).

The melting points determined in this assay are listed in Table 2.3. Compounds **2.04**, **2.57** and **2.59** showed approximately 7 °C thermostabilization of purified ABCG2. Since the three compounds stabilized ABCG2 to the same extent, it can be deduced that these compounds bind to ABCG2 with similar affinities.

**Table 2.3.** T<sub>m</sub> values of ABCG2 alone and in complex with **2.04**, **2.57** or **2.59** determined in a SEC-TS.

sample	T <sub>m</sub> [°C] <sup>a</sup>
ABCG2	53.3 ± 0.3
<b>2.04</b> (Ko143)	60.0 ± 0.3
<b>2.57</b> (UR-MB108)	60.5 ± 0.3
<b>2.59</b> (UR-MB136)	59.0 ± 0.5

<sup>a</sup> Best fit values ± SD.

## 2.2.5 Cytotoxicity and Reversal of Drug Resistance

The effect of the two most potent novel transport and ATPase inhibitors (**2.57** and **2.59**) and the most potent reference compound Ko143 (**2.04**) on the proliferation as well as the ability to overcome drug resistance of MCF-7/Topo cells were investigated in a kinetic chemosensitivity assay, using the inhibitors alone and in combination with the cytostatic topotecan, an ABCG2 substrate. The results are shown in Figure 2.7. Incubation of the cells with **2.04** had no effect on cell proliferation up to a concentration of 3 µM. A slight cytotoxic effect was observed at a concentration of 10 µM. When incubated with topotecan alone at a concentration of 100 nM, the cells were not affected due to their resistance against the cytostatic. By contrast, the combination of 100 nM topotecan with a per se nontoxic concentration of **2.04** led to a complete reversal of resistance. Inhibitor **2.57** was nontoxic up to a concentration of 1 µM. At higher concentrations, however, it showed cytotoxicity, which might be an interesting property in view of addressing tumor stem cells [49]. By analogy with **2.04**, **2.57** reversed topotecan resistance when administered at nontoxic concentrations in combination with the cytostatic (100 nM). The inhibitor **2.59**, which only differs from **2.57** in the PEG chain attached to the tetrahydroisoquinoline moiety, was also able to reverse drug resistance in MCF-7/Topo cells and was superior to **2.57** in so far as it did not exhibit marked cytotoxicity at concentrations up to 10 µM.

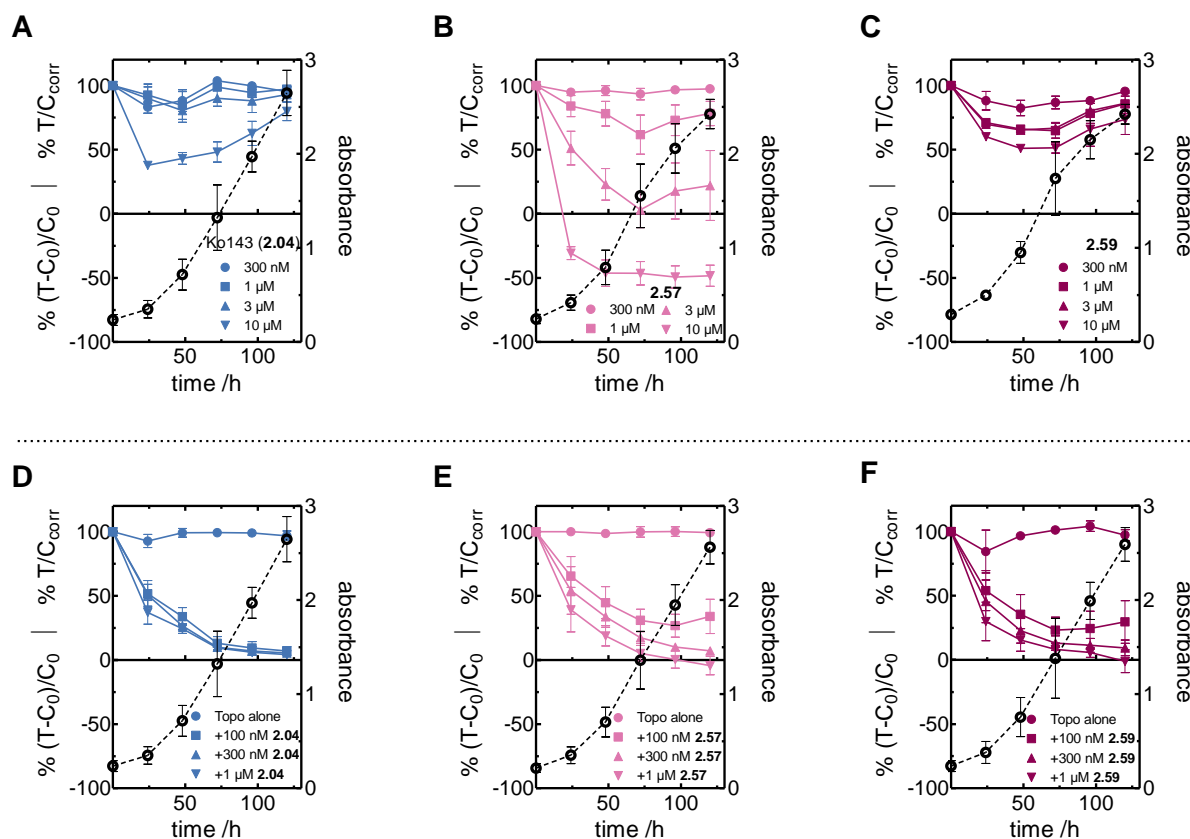


**Figure 2.7.** (A-C) Antiproliferative activities of Ko143 (**2.04**) (A) and the novel tariquidar analogs **2.57** (B) and **2.59** (C) against MCF-7/Topo cells upon long-term incubation. (D-F) Reversal of ABCG2-mediated drug resistance against topotecan on proliferating MCF-7/Topo cells: effect of 100 nM topotecan (Topo) alone and in combination with different concentrations of **2.04** (D), **2.57** (E) or **2.59** (F). Antiproliferative effects correspond to the left y-axes. The growth curves of untreated control cells (open circles) correspond to the right y-axes. Data are mean values  $\pm$  SEM of two to four independent experiments, each performed in octuplicate.

In conclusion, the reversal of drug resistance in MCF-7/Topo cells by the compounds **2.04**, **2.57** and **2.59** is in good agreement with the data from the transport assays (Figure 2.3, Table 2.1) and confirms the three substances as inhibitors of ABCG2-mediated drug efflux.

## 2.2.6 Stability in Blood Plasma

A prerequisite for in vivo studies is the stability of the test compounds in blood plasma. We first replaced the labile benzamide bond in **2.09** by a triazole core (affording compounds **2.38**-**2.42**) and then introduced ketones at the central trisubstituted phenyl ring as alternatives to the labile ester moiety, resulting in the inhibitors **2.56**-**2.59**. Exemplarily, the stability of **2.59** upon incubation in murine blood plasma at 37 °C was demonstrated by HPLC-analysis. As depicted in Figure 2.8, the peak area of **2.59** remains virtually unchanged over a period of 24 hours and no additional peaks were detected at 220 nm. This experiment demonstrates that the bioisosteric replacement of the labile amide and ester moieties in **2.09** provided for stable inhibitors.

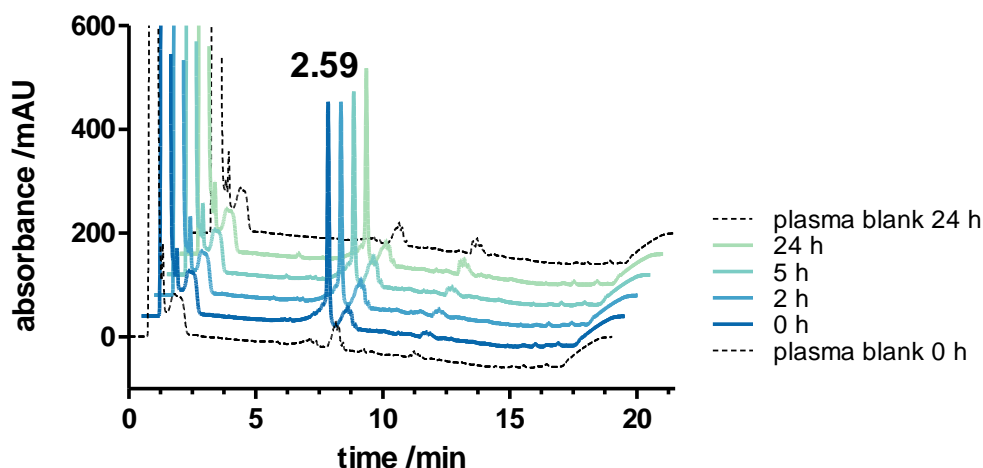


**Figure 2.8.** Chromatograms illustrating the stability of compound **2.59** upon incubation in murine blood plasma at 37 °C over a period of 24 h. RP-HPLC analysis, UV detection at 220 nm.

## 2.3 Conclusion

The study presented is a continuation of our previous investigations on tariquidar analogs as ABCG2 inhibitors. Among the title compounds, UR-MB108 (**2.57**) and UR-MB136 (**2.59**) excelled in terms of inhibitory potency in the Hoechst 33342 transport assay. With  $IC_{50}$  values of around 80 nM, they are among the most potent ABCG2 inhibitors known so far. Reversal of drug resistance in MCF-7/Topo breast cancer cells confirmed their ability to inhibit drug efflux. The PEGylated compound **2.59** also showed low potency at ABCB1, whereas **2.57** was highly ABCG2-selective. Both compounds suppressed the basal ABCG2 ATPase activity and were able to antagonize the ATPase-activating effect of sulfasalazine. Furthermore, the two compounds thermostabilized ABCG2 to the same extent, suggesting comparable binding affinities. Compound **2.59** was already analyzed in our precedent cryo-EM study [39] of ABCG2 in complex with inhibitors, in which we showed that one **2.59** molecule occupied the cavity for multidrug binding (in the transmembrane domain), locked the inward-facing conformation and inhibited the cytosolic ATPase subunit via conformational coupling. Compounds **2.57** and **2.59** differ only in the PEG chain attached at the tetrahydroisoquinoline moiety in **2.59** and it is probable that they bind similarly to the central multidrug binding site, an assumption which is supported by their same behavior in the functional assays and the thermostability assay.

Respecting future research, we expect compounds **2.57** and **2.59** to be of potential value as reference substances in mechanistic studies on ABCG2 regarding transport and inhibition. Compound **2.57** is beneficial, because it is more conveniently synthesized than **2.59**. Furthermore, in the light of their stability in blood plasma, compounds **2.57** and **2.59** can be employed as pharmacological tools for in vivo investigations on the (patho-)physiological role of the ABCG2 transporter and as a means to overcome MDR and the BBB. The high specificity

of compound **2.57** towards ABCG2 makes it convenient, for instance, as PET tracer for imaging the ABCG2 transporter at the BBB, the two methoxy groups in **2.57** being suited for  $^{11}\text{C}$ -PET labeling. In addition, **2.57** could be used for in vivo studies with pharmacological interventions specifically on the ABCG2 subtype, for example to improve the efficacy of photodynamic therapy of non-melanoma skin cancer.

## 2.4 Experimental Section

### 2.4.1 Chemistry

#### 2.4.1.1 General Experimental Conditions

**Chemicals and solvents** were purchased from commercial suppliers (Sigma Aldrich, Munich, Germany; Merck, Darmstadt, Germany; VWR, Darmstadt, Germany; Thermo Fisher Scientific, Waltham, MA, USA; TCI, Eschborn, Germany) and used without further purification unless stated otherwise. The catalyst  $\text{Pd}(\text{PPh}_3)_2\text{Cl}_2$  [50] for the Sonogashira couplings and the ligand tris[(1-benzyl-1*H*-1,2,3-triazol-4-yl)methyl]amine (TBTA) [43] for the CuAAC were synthesized according to published procedures. Per analysis grade solvents were used for reaction mixtures and technical grade solvents for chromatography (automated flash column chromatography and TLC). Reactions requiring anhydrous conditions were carried out in dried reaction vessels under an atmosphere of nitrogen and anhydrous solvents were used. Millipore water was used throughout for the preparation of buffers and HPLC eluents. Acetonitrile for analytical and preparative HPLC (gradient grade) was obtained from Merck (Darmstadt, Germany).

**Thin layer chromatography** was performed on TLC Silica gel 60 F<sub>254</sub> aluminium plates (Merck, Darmstadt, Germany). Visualization was accomplished by UV irradiation at wavelengths of 254 nm and 366 nm or by staining with potassium permanganate or Ehrlich's reagent.

**Automated flash column chromatography** was performed on an Isolera Spektra One device (Biotage, Uppsala, Sweden). Silica gel 60 (0.040-0.063 mm) for flash column chromatography (Merck, Darmstadt, Germany) was used.

**Melting points** were determined in open capillaries on an OptiMelt MPA 100 apparatus (Stanford Research Systems, Sunnyvale, CA, USA) and are uncorrected.

**NMR spectra** were recorded on an Avance 300 instrument (7.05 T, <sup>1</sup>H: 300.1 MHz, <sup>13</sup>C: 75.5 MHz), an Avance 400 instrument (9.40 T, <sup>1</sup>H: 400 MHz, <sup>13</sup>C: 101 MHz) or an Avance 600 instrument with cryogenic probe (14.1 T, <sup>1</sup>H: 600 MHz, <sup>13</sup>C: 151 MHz) (Bruker, Karlsruhe, Germany) with TMS as external standard.

**High-resolution mass spectrometry** (HRMS) analysis was performed on an Agilent 6540 UHD Accurate-Mass Q-TOF LC/MS system (Agilent Technologies, Santa Clara, CA, USA), using an ESI source.

**IR spectra** were recorded with a Golden Gate Single Reflection Diamond ATR System (Specac, Orpington, UK) in an Excalibur FTS 3000 FT-IR-Spectrometer (Bio-Rad, München, Germany).

**Preparative HPLC** was performed on a system from Knauer (Berlin, Germany), consisting of two K-1800 pumps and a K-2001 detector. A Kinetex® XB-C18 (5 µm, 100 Å, 250 mm x 21.2 mm; Phenomenex, Aschaffenburg, Germany) served as RP-column at a flow-rate of 15 mL/min. Mixtures of acetonitrile and 0.1% aq TFA were used as mobile phase. The detection wavelength was set to 220 nm throughout. The solvent mixtures were removed by lyophilization, using an Alpha 2-4 LD lyophilization apparatus (Christ, Osterode am Harz, Germany) equipped with an RZ 6 rotary vane vacuum pump (Vacuubrand, Wertheim, Germany).

**Analytical HPLC** was performed on a system from Agilent Technologies (Santa Clara, CA, USA) (Series 1100) composed of a G1312A binary pump equipped with a G1379A degasser, a G1329A ALS autosampler, a G1316A COLCOM thermostated column compartment and a G1314A VWD detector. A Kinetex® C8 (2.6 µm, 100 Å, 100 mm × 4.6 mm; Phenomenex, Aschaffenburg, Germany) served as RP-column at a flow rate of 1 mL/min. Oven temperature was set to 30 °C throughout. Mixtures of acetonitrile (A) and 0.05% aq TFA (B) were used as mobile phase. The detection wavelength was set to 220 nm throughout. Solutions for injection (40 µM) were prepared by diluting a stock solution in DMSO with a mixture of A and B corresponding to the mixture at the start of the gradient. The injection volume was 50 µL. The following linear gradient was applied: 0-12 min: A/B 30:70-95:5, 12-15 min: A/B 95:5.

#### 2.4.1.2 Synthesis Protocols and Analytical Data

##### General Procedure for N-Alkylation

The 1,2,3,4-tetrahydroisoquinoline derivative (1 eq), 1-(bromomethyl)-4-nitrobenzene (1 eq) or 1-(2-bromoethyl)-4-nitrobenzene (1 eq) and K<sub>2</sub>CO<sub>3</sub> (3 eq) were refluxed in MeCN overnight. The reaction mixture was cooled to rt, filtered and the filtrate concentrated under reduced pressure. The residual solid was taken up in DCM and washed with H<sub>2</sub>O twice. The organic layer was dried over MgSO<sub>4</sub>, the solvent removed under reduced pressure and the residue purified by flash column chromatography.

##### General Procedure for the Reduction of Nitro Compounds

The nitrobenzene derivative (1 eq) was dissolved in EtOH, a 10% Pd/C catalyst (10 wt%) was added and the suspension was stirred rapidly in a hydrogen atmosphere (40 bar) at rt overnight. The catalyst was filtered off, the solvent was evaporated and the residue was subjected to flash column chromatography.

**General Procedure for Azide Formation**

The amine (1 eq) was dissolved in 6 M HCl aq and cooled to - 5 °C. An aqueous solution of NaNO<sub>2</sub> (1.0 eq) was added and the mixture was stirred for 1 h. The solution was neutralized with an aqueous solution of NaOAc while being cooled continuously. An aqueous solution of NaN<sub>3</sub> (1.2 eq) was added dropwise. After another h of cooling, the mixture was slowly warmed to rt, and the product was extracted with EtOAc. The combined organic layers were washed with H<sub>2</sub>O and brine, dried over MgSO<sub>4</sub> and concentrated. The product was used for subsequent conversion without further purification.

**General Procedure for the Ortho Acylation of 3-Bromoaniline**

To a cooled (0 °C) solution of BCl<sub>3</sub> (1 M solution in heptane, 1.1 eq) in DCM 3-bromoaniline (1 eq) was added under a stream of nitrogen gas. The mixture was stirred for 20 min and AlCl<sub>3</sub> (1.1 eq) and the respective nitrile (1 eq) were added subsequently. Stirring continued for 24 h under reflux. After cooling to 0 °C, 2 M HCl aq was added. The mixture was stirred rapidly for 10 min and heated again to 80 °C for 1 h. The product was extracted with DCM and the organic phase washed with 1 M NaOH aq, dried and concentrated. The residue was subjected to flash column chromatography.

**General Procedure for the Sonogashira Reaction**

The bromobenzene derivative (1 eq), CuI (0.1 eq) and Pd(PPh<sub>3</sub>)<sub>2</sub>Cl<sub>2</sub> (0.05 eq) were placed in a sealed vial under nitrogen. A mixture of degassed THF and NEt<sub>3</sub> (2:1) and ethynyltrimethylsilane (1.5 eq) was added. The solution was stirred at 60 °C overnight. H<sub>2</sub>O was added and the product was extracted with DCM. The organic phase was separated, concentrated and purified by flash column chromatography.

**General Procedure for TMS Deprotection**

A solution of the respective trimethylsilyl-protected alkyne (1 eq) in THF was cooled in an ice bath. Under stirring, TBAF (1.5 M in THF, 1.5 eq) was added and stirring was continued until TLC analysis revealed complete consumption of the starting material (approximately 2 h). The solvent was evaporated, saturated NH<sub>4</sub>Cl solution was added and the compound extracted with DCM. The organic layer was separated, dried over Mg<sub>2</sub>SO<sub>4</sub> and the solvent was evaporated. In case of sufficient purity the product was used for subsequent reaction without further purification. Otherwise, flash column chromatography was used to remove traces of the starting material.

**General Procedure for Amide Formation**

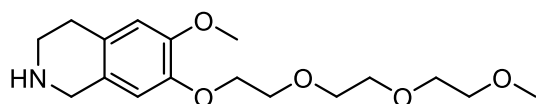
DIPEA (10 eq), HBTU (3 eq) and quinoline-2-carboxylic acid (3 eq) were dissolved in anhydrous DCM under a nitrogen atmosphere and cooled to 0 °C. The amine derivative was

added in small portions and the mixture was allowed to reach rt and stirred for 24 h. The solution was washed with H<sub>2</sub>O and brine, twice each, dried and concentrated. The residue was subjected to flash column chromatography.

### General Procedure for the CuAAC

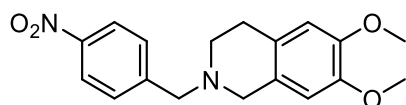
The azide (1.0-1.5 eq), the alkyne (1.0-1.3 eq), CuSO<sub>4</sub>·6H<sub>2</sub>O (0.1 eq), sodium ascorbate (0.5 eq) and TBTA (0.1 eq) were dissolved in DMF or, in case of UR-St1 and UR-St2, in THF and stirred for 24 h under a nitrogen atmosphere. DCM was added and the organic layer was washed with H<sub>2</sub>O, dried over MgSO<sub>4</sub> and concentrated. The crude mixture was purified by flash column chromatography.

### 6-Methoxy-7-(2-(2-(2-methoxyethoxy)ethoxy)ethoxy)-1,2,3,4-tetrahydroisoquinoline (2.14) [44]



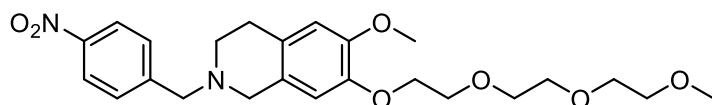
Compound **2.14** was prepared as described previously [44].

### 6,7-Dimethoxy-2-(4-nitrobenzyl)-1,2,3,4-tetrahydroisoquinoline (2.15) [51,52]



Compound **2.15** was prepared according to the general procedure for N-alkylation and was described elsewhere [51,52].

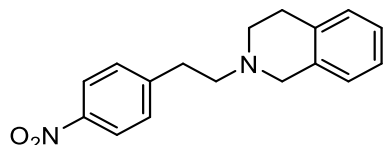
### 6-Methoxy-7-(2-(2-(2-methoxyethoxy)ethoxy)ethoxy)-2-(4-nitrobenzyl)-1,2,3,4-tetrahydroisoquinoline (2.16)



Compound **2.16** was prepared from **2.14** (2.44 mmol) according to the general procedure for N-alkylation. Flash column chromatography (PE:EtOAc 1:1) afforded a brownish oil. **Yield:** 843 mg (1.83 mmol, 75%). **R<sub>f</sub>** (PE:EtOAc 1:1): 0.38. **<sup>1</sup>H NMR** (400 MHz, CDCl<sub>3</sub>, δ): 2.72 (t, *J*=5.8 Hz, 2H), 2.82 (t, *J*=5.7 Hz, 2H), 3.35 (s, 3H), 3.49-3.55 (m, 4H), 3.60-3.67 (m, 4H), 3.68-3.73 (m, 2H), 3.75 (s, 2H), 3.80 (s, 3H), 3.83 (t, *J*=5.2 Hz, 2H), 4.09 (t, *J*=5.2 Hz, 2H), 6.52 (s, 1H), 6.60 (s, 1H), 7.57 (d, *J*=8.7 Hz, 2H), 8.18 (d, *J*=8.7 Hz, 2H). **<sup>13</sup>C NMR** (101 MHz, CDCl<sub>3</sub>, δ): 28.7, 50.9, 55.7, 56.0, 59.0, 61.9, 68.7, 69.6, 70.5, 70.6, 70.8, 71.9, 112.1, 112.2, 123.6 (2C), 126.3, 126.7, 126.9, 129.5 (2C), 146.6, 147.2, 148.3. **IR** [cm<sup>-1</sup>]: 2899.0 (m, br), 1602.8 (m), 1516.0 (s), 1450.5 (m), 1342.5 (s), 1255.7 (m), 1226.7 (m), 1128.4 (s), 1105.2 (s), 854.5 (m),

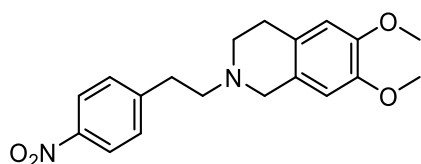
632.7 (s), 536.2 (s), 497.6 (s), 414.7 (s). **HRMS-ESI** ( $m/z$ ):  $[M + H]^+$  calcd. for  $C_{24}H_{33}N_2O_7^+$  461.2282; found 461.2285.  **$C_{24}H_{32}N_2O_7$**  (460.53).

### 2-(4-Nitrophenethyl)-1,2,3,4-tetrahydroisoquinoline (2.17) [53]



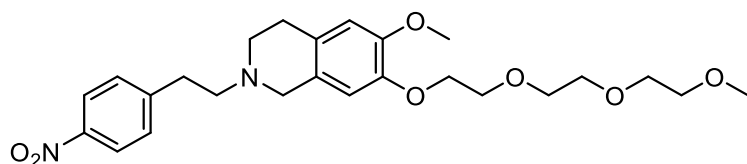
Compound **2.17** was prepared according to the general procedure for N-alkylation and was described elsewhere [53].

### 6,7-Dimethoxy-2-(4-nitrophenethyl)-1,2,3,4-tetrahydroisoquinoline (2.18) [53-55]



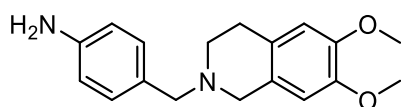
Compound **2.18** was prepared according to the general procedure for N-alkylation and was described elsewhere [53-55].

### 6-Methoxy-7-(2-(2-(2-methoxyethoxy)ethoxy)ethoxy)-2-(4-nitrophenethyl)-1,2,3,4-tetrahydroisoquinoline (2.19) [44]

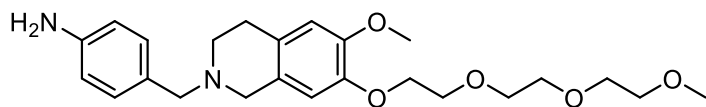


Compound **2.19** was prepared from **2.14** according to the general procedure for N-alkylation and was described previously [44].

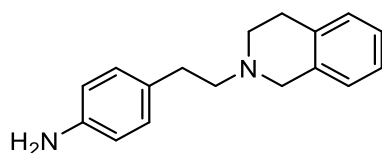
### 4-((6,7-Dimethoxy-3,4-dihydroisoquinolin-2(1H)-yl)methyl)aniline (2.20) [52]



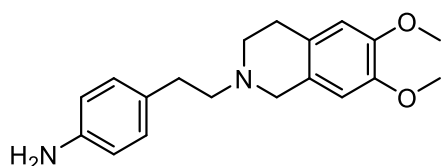
Compound **2.20** was prepared from **2.15** according to the general procedure for the reduction of nitro compounds and was described elsewhere [52].

**4-((6-Methoxy-7-(2-(2-(2-methoxyethoxy)ethoxy)ethoxy)ethoxy)-3,4-dihydroisoquinolin-2(1H)-yl)methyl)aniline (2.21)**

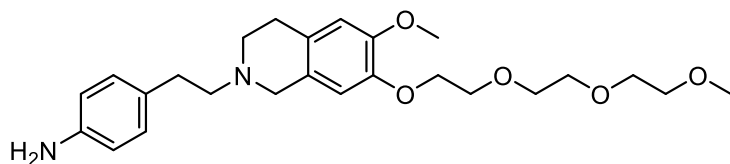
Compound **2.16** (1.58 mmol) was dissolved in EtOH before  $\text{SnCl}_2 \cdot 2\text{H}_2\text{O}$  (6 eq) was added. The solution was refluxed under a nitrogen atmosphere for 2 h. The solvent was evaporated and EtOAc was added. The organic solution was washed with 1 M NaOH aq,  $\text{H}_2\text{O}$  and brine, dried over  $\text{MgSO}_4$  and concentrated. The crude product was purified in two subsequent flash column chromatography runs (1<sup>st</sup> run:  $\text{CHCl}_3:\text{MeOH}:\text{NEt}_3$  89:10:1, 2<sup>nd</sup> run: EtOH) to obtain **2.21** as a yellow oil. **Yield:** 327 mg (0.76 mmol, 48%). **R<sub>f</sub>** ( $\text{CHCl}_3:\text{MeOH}:\text{NEt}_3$  89:10:1): 0.37, **R<sub>f</sub>** (EtOH): 0.25. **<sup>1</sup>H NMR** (400 MHz,  $\text{CDCl}_3$ ,  $\delta$ ): 2.68 (t,  $J=5.8$  Hz, 2H), 2.79 (t,  $J=5.7$  Hz, 2H), 3.37 (s, 3H), 3.49 (s, 2H), 3.52-3.56 (m, 4H), 3.62-3.68 (m, 6H), 3.70-3.73 (m, 2H), 3.79 (s, 3H), 3.83 (t,  $J=5.2$  Hz, 2H), 4.10 (t,  $J=5.2$  Hz, 2H), 6.53 (s, 1H), 6.58 (s, 1H), 6.65 (d,  $J=8.2$  Hz, 2H), 7.15 (d,  $J=8.2$  Hz, 2H). **<sup>13</sup>C NMR** (101 MHz,  $\text{CDCl}_3$ ,  $\delta$ ): 28.8, 50.5, 55.5, 56.0, 59.0, 62.3, 68.7, 69.7, 70.5, 70.6, 70.8, 72.0, 112.1, 112.4, 115.0 (2C), 127.0, 127.1, 128.1, 130.3 (2C), 145.6, 146.4, 148.1. **IR** [ $\text{cm}^{-1}$ ]: 3450.6 (w, br), 3358.1 (w, br), 2887.4 (m, br), 2353.1 (w), 2324.2 (w), 1734 (w), 1612.5 (m), 1516 (s), 1450.5 (m), 1363.7 (m), 1255.7 (m), 1224.8 (m), 1122.6 (s), 833.2 (m), 632.7 (s), 536.2 (s), 497.6 (s), 403.1 (s). **HRMS-ESI** ( $m/z$ ):  $[\text{M} + \text{H}]^+$  calcd. for  $\text{C}_{24}\text{H}_{35}\text{N}_2\text{O}_5$  431.2540; found 431.2542. **C<sub>24</sub>H<sub>34</sub>N<sub>2</sub>O<sub>5</sub>** (430.55).

**4-(2-(3,4-Dihydroisoquinolin-2(1H)-yl)ethyl)aniline (2.22) [53]**

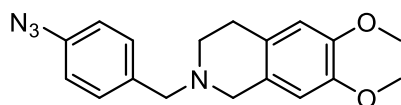
Compound **2.22** was prepared from **2.17** according to the general procedure for the reduction of nitro compounds and was described elsewhere [53].

**4-(2-(6,7-Dimethoxy-3,4-dihydroisoquinolin-2(1H)-yl)ethyl)aniline (2.23) [53-55]**

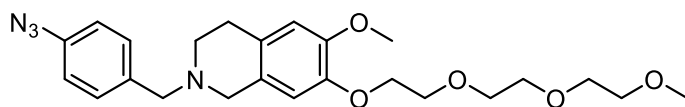
Compound **2.23** was prepared from **2.18** according to the general procedure for the reduction of nitro compounds and was described elsewhere [53-55].

**4-(2-(6-Methoxy-7-(2-(2-(2-methoxyethoxy)ethoxy)ethoxy)-3,4-dihydroisoquinolin-2(1H)-yl)ethyl)aniline (2.24) [44]**

Compound **2.24** was prepared from **2.19** according to the general procedure for the reduction of nitro compounds and was described previously [44].

**2-(4-azidobenzyl)-6,7-dimethoxy-1,2,3,4-tetrahydroisoquinoline (2.25)**

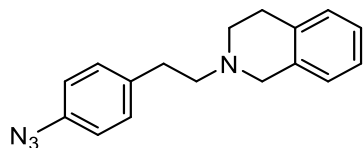
Compound **2.25** was prepared from **2.20** (0.84 mmol) according to the general procedure for azide formation. **Yield:** 269 mg (0.83 mmol, 99%), brown oil. **<sup>1</sup>H NMR** (400 MHz, CDCl<sub>3</sub>, δ): 2.78-2.88 (m, 4H), 3.61 (s, 2H), 3.74 (s, 2H), 3.81 (s, 3H), 3.84 (s, 3H), 6.48 (s, 1H), 6.60 (s, 1H), 7.01 (d, *J*=8.4 Hz, 2H), 7.39 (d, *J*=8.4 Hz, 2H). **<sup>13</sup>C NMR** (101 MHz, CDCl<sub>3</sub>, δ): 27.9, 50.1, 54.7, 55.9 (2C), 61.1, 109.5, 111.4, 119.0 (2C), 125.5, 125.6, 130.9 (2C), 139.3, 147.4, 147.7 (one quaternary carbon not apparent). **IR** [cm<sup>-1</sup>]: 2939.5 (w, br), 2117.8 (s), 1714.7 (m), 1519.9 (m), 1363.7 (w), 1286.5 (m), 1261.4 (m), 1124.5 (m), 1055.1 (w), 1010.7 (w), 881.5 (vw), 825.5 (vw), 632.7 (m), 536.2 (s), 495.7 (s), 405.1 (s). **HRMS-ESI** (*m/z*): [M + H]<sup>+</sup> calcd. for C<sub>18</sub>H<sub>21</sub>N<sub>4</sub>O<sub>2</sub><sup>+</sup> 325.1659; found 325.1664. C<sub>18</sub>H<sub>20</sub>N<sub>4</sub>O<sub>2</sub> (324.38).

**2-(4-Azidobenzyl)-6-methoxy-7-(2-(2-(2-methoxyethoxy)ethoxy)ethoxy)-1,2,3,4-tetrahydroisoquinoline (2.26)**

Compound **2.26** was prepared from **2.21** (0.53 mmol) according to the general procedure for azide formation. **Yield:** 242 mg (0.53 mmol, 100%), brownish oil. **<sup>1</sup>H NMR** (400 MHz, CDCl<sub>3</sub>, δ): 2.90 (t, *J*=6.0 Hz, 2H), 3.06 (t, *J*=6.1 Hz, 2H), 3.36 (s, 3H), 3.51-3.56 (m, 2H), 3.61-3.67 (m, 4H), 3.69-3.73 (m, 2H), 3.78-3.82 (m, 5H), 3.84 (t, *J*=5.1 Hz, 2H), 3.95 (s, 2H), 4.09 (t, *J*=5.1 Hz, 2H), 6.52 (s, 1H), 6.59 (s, 1H), 7.02 (d, *J*=8.4 Hz, 2H), 7.39 (d, *J*=8.4 Hz, 2H). **<sup>13</sup>C NMR** (101 MHz, CDCl<sub>3</sub>, δ): 25.9, 48.8, 52.6, 56.0, 58.8, 59.0, 68.6, 69.6, 70.5, 70.6, 70.8, 71.9, 111.8, 112.0, 119.3 (2C), 122.7, 125.0, 130.3, 131.8 (2C), 140.3, 147.0, 148.8. **IR** [cm<sup>-1</sup>]: 2910.6 (m, br), 2115.9 (s), 1708.9 (w), 1608.6 (w), 1516.0 (m, br), 1462.0 (w), 1363.7 (w), 1286.5 (m, br), 1257.6 (w), 1228.7 (w), 1128.4 (m, br), 632.7 (s), 536.2 (s), 497.6 (s), 401.2 (s).

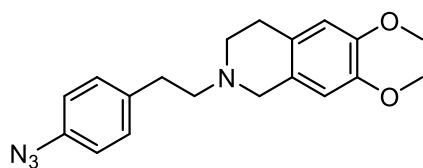
**HRMS-ESI** ( $m/z$ ):  $[M + H]^+$  calcd. for  $C_{24}H_{33}N_4O_5^+$  457.2445 found 457.2446.  $C_{24}H_{32}N_4O_5$  (456.54).

### 2-(4-Azidophenethyl)-1,2,3,4-tetrahydroisoquinoline (2.27)



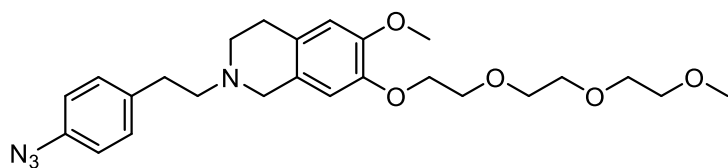
Compound **2.27** was prepared from **2.22** (1.19 mmol) according to the general procedure for azide formation. **Yield**: 292 mg (0.98 mmol, 82%), yellow oil.  **$^1H$  NMR** (400 MHz,  $CDCl_3$ ,  $\delta$ ): 2.88-3.06 (m, 8H), 3.91 (s, 2H), 6.94-6.99 (m, 2H), 7.03-7.07 (m, 1H), 7.11-7.19 (m, 3H), 7.21-7.24 (m, 2H).  **$^{13}C$  NMR** (101 MHz,  $CDCl_3$ ,  $\delta$ ): 27.3, 32.1, 49.9, 54.5, 58.4, 119.2 (2C), 126.2, 126.77, 126.81, 128.7, 130.2 (2C), 132.3, 133.2, 136.0, 138.2. **IR** [ $cm^{-1}$ ]: 2939.5 (vw, br), 2112.0 (m), 1714.7 (w), 1674.2 (w), 1506.4 (w), 1286.5 (w, br), 632.7 (m), 534.3 (s), 497.6 (s), 405.1 (s). **HRMS-ESI** ( $m/z$ ):  $[M + H]^+$  calcd. for  $C_{17}H_{19}N_4^+$  279.1604; found 279.1604.  $C_{17}H_{18}N_4$  (278.36).

### 2-(4-Azidophenethyl)-6,7-dimethoxy-1,2,3,4-tetrahydroisoquinoline (2.28) [56]



Compound **2.28** was prepared from **2.23** (1.28 mmol) according to the general procedure for azide formation. **Yield**: 260 mg (0.77 mmol, 60%), colorless solid.  **$^1H$  NMR** (400 MHz,  $[D_6]DMSO$ ,  $\delta$ ): 2.60-2.74 (m, 6H), 2.77-2.86 (m, 2H), 3.52 (s, 2H), 3.69 (s, 3H), 3.70 (s, 3H), 6.62 (s, 1H), 6.65 (s, 1H), 7.02 (d,  $J=8.4$  Hz, 2H), 7.30 (d,  $J=8.4$  Hz, 2H).  **$^{13}C$  NMR** (101 MHz,  $[D_6]DMSO$ ,  $\delta$ ): 24.6, 29.0, 48.8, 51.4, 55.4, 55.5, 55.9, 109.6, 111.5, 119.3 (2C), 123.4, 130.2 (2C), 134.2, 137.8, 147.5, 148.1 (one quaternary carbon not apparent). **HRMS-ESI** ( $m/z$ ):  $[M + H]^+$  calcd. for  $C_{19}H_{23}N_4O_2^+$  339.1816; found 339.1817.  $C_{19}H_{22}N_4O_2$  (338.41).

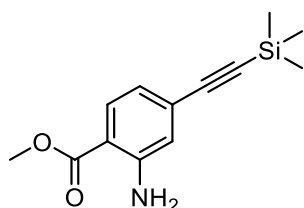
### 2-(4-Azidophenethyl)-6-methoxy-7-(2-(2-(2-methoxyethoxy)ethoxy)ethoxy)-1,2,3,4-tetrahydroisoquinoline (2.29)



Compound **2.29** was prepared from **2.24** (1.33 mmol) according to the general procedure for azide formation. **Yield**: 344 mg (0.73 mmol, 55%), brown oil.  **$^1H$  NMR** (400 MHz,  $CDCl_3$ ,  $\delta$ ): 2.70-2.90 (m, 8H), 3.37 (s, 3H), 3.53-3.57 (m, 2H), 3.61 (s, 2H), 3.63-3.69 (m, 4H), 3.72-3.76

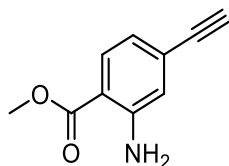
(m, 2H), 3.81 (s, 3H), 3.86 (t,  $J=5.2$  Hz, 2H), 4.13 (t,  $J=5.2$  Hz, 2H), 6.58 (s, 1H), 6.59 (s, 1H), 6.96 (d,  $J=8.4$  Hz, 2H), 7.22 (d,  $J=8.4$  Hz, 2H).  $^{13}\text{C}$  NMR (101 MHz,  $\text{CDCl}_3$ ,  $\delta$ ): 28.7, 33.4, 51.0, 55.7, 56.0, 59.1, 60.1, 68.8, 69.7, 70.6, 70.7, 70.8, 72.0, 112.0, 112.4, 119.0 (2C), 126.5, 126.9, 130.1 (2C), 137.2, 137.8, 146.5, 148.3. IR [ $\text{cm}^{-1}$ ]: 2922.1 (w, br), 2110.1 (m), 1734.0 (vw, br), 1510.3 (m), 1452.4 (w), 1371.4 (w), 1286.5 (w), 1257.6 (w), 1228.7 (w), 1126.4 (w), 632.7 (m), 536.2 (s), 497.6 (s), 403.1 (s). HRMS-ESI ( $m/z$ ):  $[\text{M} + \text{H}]^+$  calcd. for  $\text{C}_{25}\text{H}_{35}\text{N}_4\text{O}_5^+$  471.2602; found 471.2604.  $\text{C}_{25}\text{H}_{34}\text{N}_4\text{O}_5$  (470.57).

### Methyl 2-amino-4-((trimethylsilyl)ethynyl)benzoate (2.31) [41]



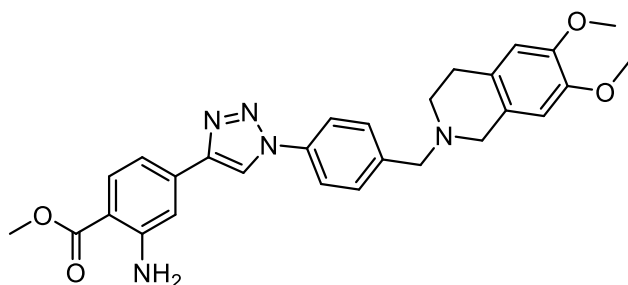
Compound **2.31** was prepared from methyl 2-amino-4-bromobenzoate according to the general procedure for the Sonogashira reaction and was described previously [41].

### Methyl 2-amino-4-ethynylbenzoate (2.32) [41]



Compound **2.32** was prepared from **2.31** according to the general procedure for TMS deprotection and was described previously [41].

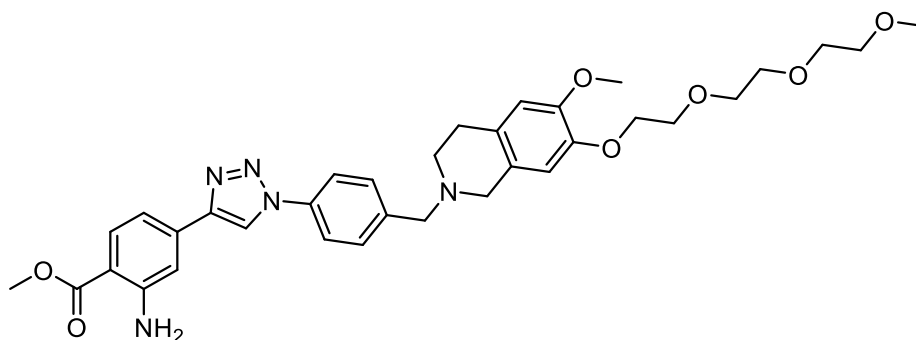
### Methyl 2-amino-4-(1-(4-((6,7-dimethoxy-3,4-dihydroisoquinolin-2(1H)-yl)methyl)-phenyl)-1H-1,2,3-triazol-4-yl)benzoate (2.33)



Compound **2.33** was prepared from **2.25** (0.86 mmol, 1.0 eq) and **2.32** (1.12 mmol, 1.3 eq) according to the general procedure for the CuAAC. The crude product was purified in two subsequent flash column chromatography runs (1<sup>st</sup> run:  $\text{CHCl}_3$ :MeOH 49:1, 2<sup>nd</sup> run: DCM:acetone 4:1). **Yield**: 255 mg, (0.51 mmol, 59%), colorless solid.  $R_f$  ( $\text{CHCl}_3$ :MeOH 49:1): 0.08,  $R_f$  (DCM:acetone 4:1): 0.09. **MP**: 197 °C.  $^1\text{H}$  NMR (400 MHz,  $\text{CDCl}_3$ ,  $\delta$ ): 2.77 (t,

$J=5.7$  Hz, 2H), 2.85 (t,  $J=5.7$  Hz, 2H), 3.58 (s, 2H), 3.75 (s, 2H), 3.81 (s, 3H), 3.85 (s, 3H), 3.89 (s, 3H), 5.86 (br s, 2H), 6.49 (s, 1H), 6.62 (s, 1H), 7.09 (dd,  $J=1.6, 8.3$  Hz, 1H), 7.35 (d,  $J=1.6$  Hz, 1H), 7.59 (d,  $J=8.5$  Hz, 2H), 7.75 (d,  $J=8.5$  Hz, 2H), 7.94 (d,  $J=8.3$  Hz, 1H), 8.21 (s, 1H).  $^{13}\text{C}$  NMR (101 MHz,  $\text{CDCl}_3$ ,  $\delta$ ): 28.7, 50.9, 51.6, 55.7, 56.0 (2C), 62.0, 109.5, 110.5, 111.5, 113.4, 113.8, 118.5, 120.6 (2C), 126.1, 126.4, 130.3 (2C), 132.1, 135.4, 135.9, 139.9, 147.3, 147.4, 147.6, 150.9, 168.3. IR [ $\text{cm}^{-1}$ ]: 3471.9 (m), 3361.9 (m), 3138.2 (w), 2941.4 (m), 2912.5 (m), 2837.3 (w), 2787.1 (w), 2756.3 (w), 1680 (s), 1626 (m), 1593.2 (m), 1518 (s), 1450.5 (m), 1431.2 (m), 1365.6 (m), 1298.1 (m), 1226.7 (s), 1186.2 (m), 1124.5 (m), 1099.4 (m), 1039.6 (m), 887.3 (m), 850.6 (m), 812 (m), 781.2 (m), 700.2 (m), 555.5 (m), 403.1 (m). HRMS-ESI ( $m/z$ ):  $[\text{M} + \text{H}]^+$  calcd. for  $\text{C}_{28}\text{H}_{30}\text{N}_5\text{O}_4^+$  500.2292; found 500.2301.  $\text{C}_{28}\text{H}_{29}\text{N}_5\text{O}_4$  (499.57).

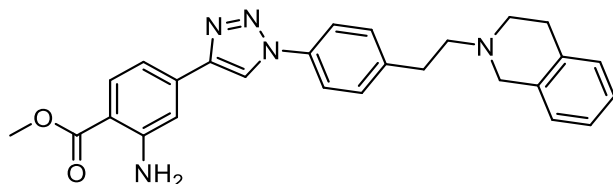
**Methyl 2-amino-4-(1-(4-((6-methoxy-7-(2-(2-(2-methoxyethoxy)ethoxy)ethoxy)-3,4-dihydroisoquinolin-2(1H)-yl)methyl)phenyl)-1H-1,2,3-triazol-4-yl)benzoate (2.34)**



Compound **2.34** was prepared from **2.26** (0.40 mmol, 1.0 eq) and **2.32** (0.52 mmol, 1.3 eq) according to the general procedure for the CuAAC and purified by flash column chromatography (DCM:acetone:MeOH 13:6:1). For removal of residual TBTA, the mixture was subjected once more to column chromatography ( $\text{CH}_3\text{COOH}$ :EtOAc 1:4 and then EtOAc:NEt<sub>3</sub> 4:1). The eluate was washed with  $\text{H}_2\text{O}$ , dried over  $\text{MgSO}_4$  and concentrated. **Yield**: 0.25 mmol (63%), yellow solid. **R<sub>f</sub>** ( $\text{CH}_2\text{Cl}_2$ :acetone:MeOH 13:6:1): 0.60. **MP**: 111 °C.  $^1\text{H}$  NMR (400 MHz,  $\text{CDCl}_3$ ,  $\delta$ ): 2.78 (m, 2H), 2.84 (m, 2H), 3.36 (s, 3H), 3.51-3.55 (m, 2H), 3.57 (m, 2H), 3.61-3.68 (m, 4H), 3.68-3.74 (m, 2H), 3.76 (m, 2H), 3.81 (s, 3H), 3.84 (t,  $J=5.2$  Hz, 2H), 3.89 (s, 3H), 4.11 (t,  $J=5.2$  Hz, 2H), 5.87 (br s, 2H), 6.54 (s, 1H), 6.61 (s, 1H), 7.09 (dd,  $J=1.6, 8.3$  Hz, 1H), 7.35 (d,  $J=1.5$  Hz, 1H), 7.59 (d,  $J=8.5$  Hz, 2H), 7.75 (d,  $J=8.5$  Hz, 2H), 7.93 (d,  $J=8.3$  Hz, 1H), 8.22 (s, 1H).  $^{13}\text{C}$  NMR (101 MHz,  $\text{CDCl}_3$ ,  $\delta$ ): 28.6, 50.7, 51.6, 55.5, 56.0, 59.0, 61.8, 68.8, 69.6, 70.5, 70.6, 70.8, 71.9, 110.5, 112.1, 112.3, 113.4, 113.8, 118.6, 120.6 (2C), 126.3 (HMBC), 126.7, 130.4 (2C), 132.1, 135.4, 136.0, 139.3 (HMBC), 146.6, 147.4, 148.4, 150.9, 168.3. IR [ $\text{cm}^{-1}$ ]: 3481.5 (w), 3365.8 (w), 2922.1 (m, br), 2877.8 (m, br), 1681.9 (m), 1624.1 (m), 1595.1 (m), 1560.4 (m), 1516.0 (s), 1448.5 (m), 1365.6 (m), 1296.2 (m), 1234.4 (s), 1190.1 (m), 1097.5 (s), 1035.8 (m), 935.5 (w), 850.6 (m), 814.0 (m),

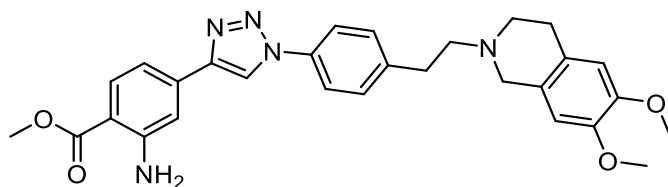
781.2 (m), 700.2 (m), 461.0 (w). **HRMS-ESI** ( $m/z$ ):  $[M + H]^+$  calcd. for  $C_{34}H_{42}N_5O_7^+$  632.3079 found 632.3084.  $C_{34}H_{41}N_5O_7$  (631.73).

**Methyl 2-amino-4-(1-(4-(2-(3,4-dihydroisoquinolin-2(1H)-yl)ethyl)phenyl)-1H-1,2,3-triazol-4-yl)benzoate (2.35)**



Compound **2.35** was prepared from **2.27** (1.56 mmol, 1.0 eq) and **2.32** (2.03 mmol, 1.3 eq) according to the general procedure for the CuAAC. The crude product was purified in three subsequent flash column chromatography runs (1<sup>st</sup> run:  $CHCl_3$ :MeOH 19:1, 2<sup>nd</sup> run:  $CHCl_3$ :MeOH 49:1, 3<sup>rd</sup> run: EtOAc:NEt<sub>3</sub> 49:1). **Yield**: 367 mg (0.81 mmol, 52%), colorless crystals. **R<sub>f</sub>** ( $CHCl_3$ :MeOH 19:1): 0.39, **R<sub>f</sub>** ( $CHCl_3$ :MeOH 49:1): 0.04, **R<sub>f</sub>** (EtOAc:NEt<sub>3</sub> 49:1): 0.23. **MP**: 191 °C. **<sup>1</sup>H NMR** (400 MHz,  $CDCl_3$ ,  $\delta$ ): 2.78-2.86 (m, 4H), 2.91-3.02 (m, 4H), 3.74 (s, 2H), 3.89 (s, 3H), 5.85 (br s, 2H), 7.01-7.17 (m, 5H), 7.34 (d,  $J$ =1.4 Hz, 1H), 7.42 (d,  $J$ =8.4 Hz, 2H), 7.69 (d,  $J$ =8.4 Hz, 2H), 7.93 (d,  $J$ =8.3 Hz, 1H), 8.17 (s, 1H). **<sup>13</sup>C NMR** (101 MHz,  $CDCl_3$ ,  $\delta$ ): 29.1, 33.5, 51.0, 51.6, 56.1, 59.8, 110.5, 113.4, 113.8, 118.5, 120.6 (2C), 125.7, 126.2, 126.6, 128.7, 130.1 (2C), 132.1, 134.2, 134.6, 135.2, 135.5, 141.7, 147.4, 150.9, 168.3. **IR** [ $cm^{-1}$ ]: 3469.9 (m), 3363.8 (m), 3122.7 (w), 2922.1 (m), 2854.6 (w), 2802.6 (w), 2347.4 (w), 2324.2 (w), 1683.9 (s), 1618.3 (m), 1583.6 (s), 1516 (m), 1448.5 (m), 1294.2 (m), 1238.3 (s), 1193.9 (m), 1097.5 (s), 1037.7 (m), 889.2 (m), 829.4 (s), 785 (s), 742.6 (s), 698.2 (s), 511.1 (s, br). **HRMS-ESI** ( $m/z$ ):  $[M + H]^+$  calcd. for  $C_{27}H_{28}N_5O_2^+$  454.2238 found 454.2239.  $C_{27}H_{27}N_5O_2$  (453.55).

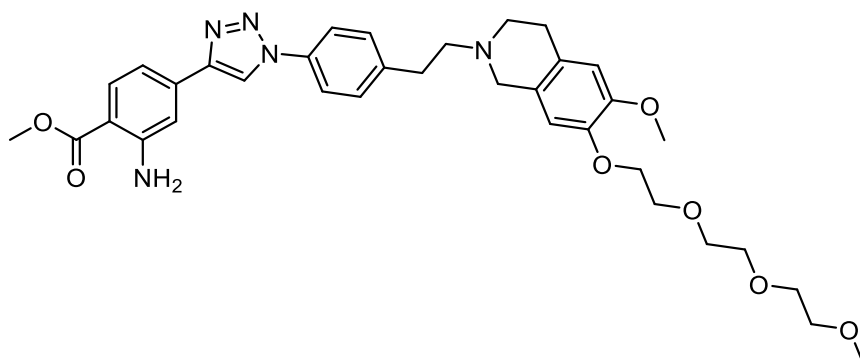
**Methyl 2-amino-4-(1-(4-(2-(6,7-dimethoxy-3,4-dihydroisoquinolin-2(1H)-yl)ethyl)phenyl)-1H-1,2,3-triazol-4-yl)benzoate (2.36)**



Compound **2.36** was prepared from **2.28** (0.24 mmol, 1.0 eq) and **2.32** (0.31 mmol, 1.3 eq) according to the general procedure for the CuAAC and purified by flash column chromatography (EtOAc:NEt<sub>3</sub> 99:1). **Yield**: 62 mg (0.12 mmol, 51%), yellowish solid. **R<sub>f</sub>** (EtOAc:NEt<sub>3</sub> 99:1): 0.12. **<sup>1</sup>H NMR** (400 MHz,  $CDCl_3$ ,  $\delta$ ): 2.73-2.87 (m, 6H), 2.92-3.00 (m, 2H), 3.65 (s, 2H), 3.82 (s, 3H), 3.83 (s, 3H), 3.86 (s, 3H), 5.87 (br s, 2H), 6.53 (s, 1H), 6.59 (s, 1H), 7.07 (dd,  $J$ =1.3, 8.3 Hz, 1H), 7.31 (d,  $J$ =1.1 Hz, 1H), 7.38 (d,  $J$ =8.3 Hz, 2H), 7.66 (d,

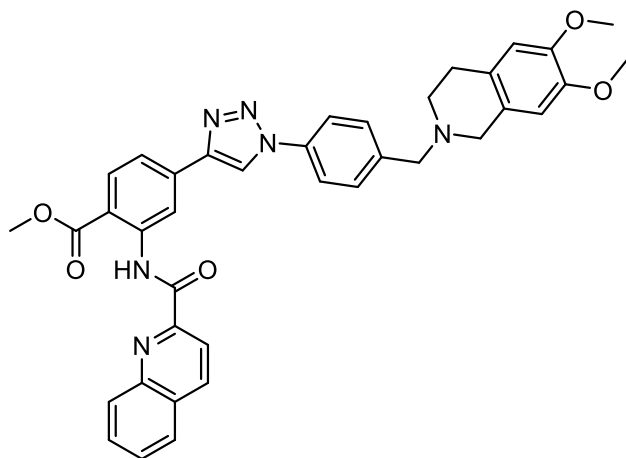
$J=8.3$  Hz, 2H), 7.90 (d,  $J=8.3$  Hz, 1H), 8.17 (s, 1H).  $^{13}\text{C}$  NMR (101 MHz,  $\text{CDCl}_3$ ,  $\delta$ ): 28.7, 33.6, 51.1, 51.6, 55.7, 55.97, 56.01, 59.7, 109.6, 110.5, 111.5, 113.4, 113.8, 118.6, 120.6 (2C), 126.1, 126.4, 130.1 (2C), 132.1, 135.2, 135.5, 141.7, 147.3, 147.4, 147.7, 150.9, 168.3. MS-ESI ( $m/z$ ):  $[\text{M} + \text{H}]^+$  calcd. for  $\text{C}_{29}\text{H}_{32}\text{N}_5\text{O}_4^+$  514.2; found 514.1.  $\text{C}_{29}\text{H}_{31}\text{N}_5\text{O}_4$  (513.60).

**Methyl 2-amino-4-(1-(4-(2-(6-methoxy-7-(2-(2-(2-methoxyethoxy)ethoxy)ethoxy)ethoxy)-3,4-dihydroisoquinolin-2(1H)-yl)ethyl)phenyl)-1H-1,2,3-triazol-4-yl)benzoate (2.37)**



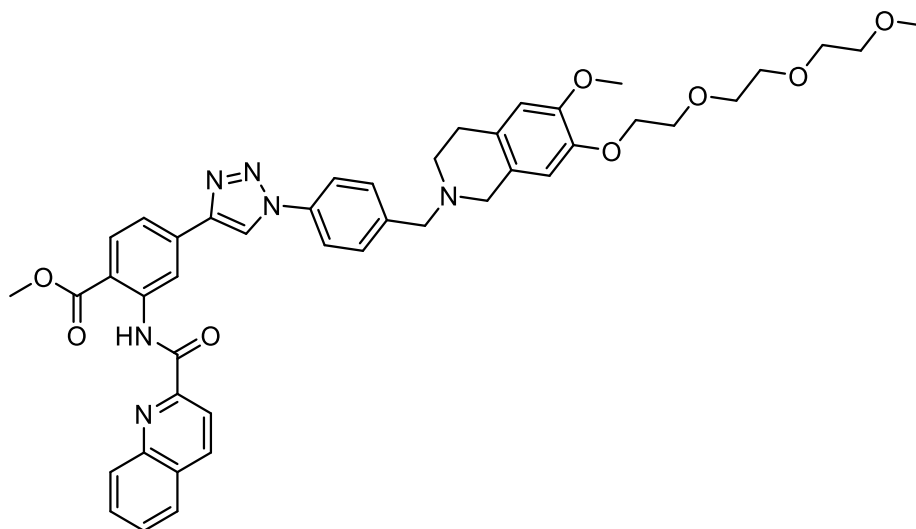
Compound **2.37** was prepared from **2.29** (0.51 mmol, 1.0 eq) and **2.32** (0.66 mmol, 1.3 eq) according to the general procedure for the CuAAC and purified by flash column chromatography (DCM:acetone:MeOH 13:6:1). **Yield**: 220 mg (0.34 mmol, 67%), yellow solid. **R<sub>f</sub>** (DCM:acetone:MeOH 13:6:1): 0.15. **MP**: 99 °C.  $^1\text{H}$  NMR (400 MHz,  $\text{CDCl}_3$ ,  $\delta$ ): 2.77-2.88 (m, 6H), 2.94-3.02 (m, 2H), 3.37 (s, 3H), 3.53-3.56 (m, 2H), 3.63-3.69 (m, 6H), 3.71-3.75 (m, 2H), 3.81 (s, 3H), 3.86 (t,  $J=5.2$  Hz, 2H), 3.88 (s, 3H), 4.13 (t,  $J=5.2$  Hz, 2H), 5.86 (br s, 2H), 6.59 (s, 1H), 6.60 (s, 1H), 7.09 (dd,  $J=1.5, 8.3$  Hz, 1H), 7.34 (d,  $J=1.4$  Hz, 1H), 7.41 (d,  $J=8.4$  Hz, 2H), 7.69 (d,  $J=8.4$  Hz, 2H), 7.93 (d,  $J=8.3$  Hz, 1H), 8.19 (s, 1H).  $^{13}\text{C}$  NMR (101 MHz,  $\text{CDCl}_3$ ,  $\delta$ ): 28.7, 33.5, 51.0, 51.6, 55.6, 56.02, 59.05, 59.7, 68.8, 69.7, 70.6, 70.7, 70.8, 72.0, 110.5, 112.0, 112.4, 113.4, 113.8, 118.6, 120.6 (2C), 126.4, 126.9, 130.1 (2C), 132.1, 135.2, 135.5, 141.6, 146.5, 147.4, 148.3, 150.9, 168.3. **IR** [ $\text{cm}^{-1}$ ]: 3468.0 (w, br), 3361.9 (w, br), 2920.2 (m, br), 2873.9 (m), 2810.3 (w), 1732.1 (m), 1689.6 (s), 1622.1 (m), 1591.3 (m), 1518.0 (s), 1448.5 (m), 1348.2 (w), 1301.9 (m), 1242.2 (s), 1224.8 (s), 1126.4 (s), 1097.5 (s), 1033.8 (m), 987.6 (w), 943.2 (w), 891.1 (w), 842.9 (m), 815.9 (m), 777.3 (m), 700.2 (w), 528.5 (w), 453.3 (w). **HRMS-ESI** ( $m/z$ ):  $[\text{M} + \text{H}]^+$  calcd. for  $\text{C}_{35}\text{H}_{44}\text{N}_5\text{O}_7$  646.3235; found 646.3237.  $\text{C}_{35}\text{H}_{43}\text{N}_5\text{O}_7$  (645.76).

**Methyl 4-(1-(4-((6,7-dimethoxy-3,4-dihydroisoquinolin-2(1H)-yl)methyl)phenyl)-1H-1,2,3-triazol-4-yl)-2-(quinoline-2-carboxamido)benzoate (2.38)**

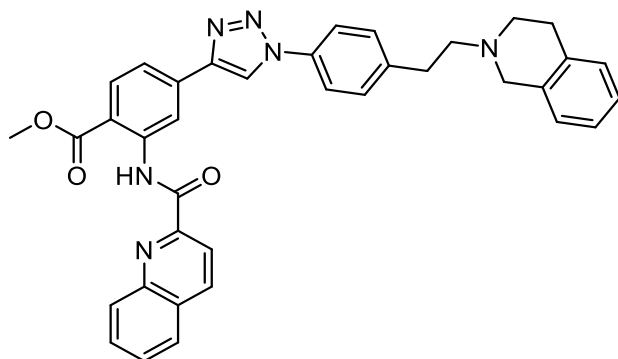


Compound **2.38** was prepared from **2.33** (0.20 mmol) according to the general procedure for amide formation. It was purified by flash column chromatography (1<sup>st</sup> CHCl<sub>3</sub>:MeOH 20:1, 2<sup>nd</sup> DCM:acetone:MeOH 12:7:1). **Yield:** 72 mg (0.11 mmol, 55%), yellowish solid. **R<sub>f</sub>** (CHCl<sub>3</sub>:MeOH 20:1): 0.46; **R<sub>f</sub>** (DCM:acetone:MeOH 12:7:1): 0.66. **MP:** 135 °C. **<sup>1</sup>H NMR** (400 MHz, CD<sub>2</sub>Cl<sub>2</sub>, δ): 2.85 (s, 4H), 3.63 (s, 2H), 3.70-3.91 (m, 8H), 4.07 (s, 3H), 6.50 (s, 1H), 6.62 (s, 1H), 7.55-8.01 (m, 8H), 8.14-8.54 (m, 5H), 9.51 (s, 1H), 13.28 (s, 1H). **<sup>13</sup>C NMR** (101 MHz, CD<sub>2</sub>Cl<sub>2</sub>, δ): 27.6, 50.1, 51.6, 54.5, 55.0 (2C), 60.8, 108.9, 110.9, 115.3, 116.3, 118.0, 118.5, 119.1, 119.7 (2C), 125.1, 127.0, 127.5, 128.7, 129.2, 129.6, 129.7 (3C), 131.2, 135.2, 135.3, 137.0, 140.6, 145.8, 146.4, 146.7, 147.1, 149.3, 162.8, 166.9 (one quaternary carbon not apparent). **HRMS-ESI** (*m/z*): [M + H]<sup>+</sup> calcd. for C<sub>38</sub>H<sub>35</sub>N<sub>6</sub>O<sub>5</sub><sup>+</sup> 655.2663; found 655.2661. **C<sub>38</sub>H<sub>34</sub>N<sub>6</sub>O<sub>5</sub>** (654.73).

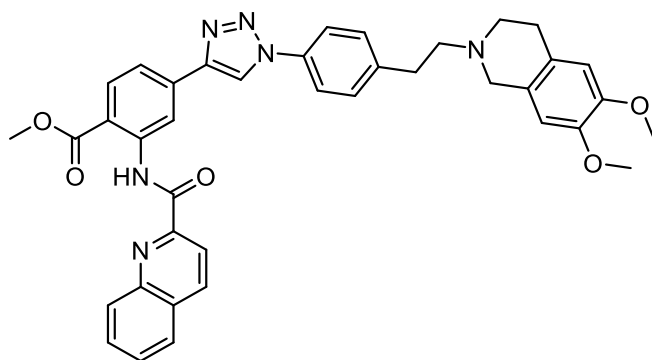
**Methyl 4-(1-(4-((6-methoxy-7-(2-(2-(2-methoxyethoxy)ethoxy)ethoxy)-3,4-dihydroisoquinolin-2(1H)-yl)methyl)phenyl)-1H-1,2,3-triazol-4-yl)-2-(quinoline-2-carboxamido)benzoate (2.39)**



Compound **2.39** was prepared from **2.34** (0.15 mmol) according to the general procedure for amide formation. It was purified with flash column chromatography (CHCl<sub>3</sub>:MeOH 100:7). **Yield:** 73 mg (0.09 mmol, 59%). **R<sub>f</sub>** (CHCl<sub>3</sub>:MeOH 100:7): 0.40. **MP:** 138 °C. **<sup>1</sup>H NMR** (400 MHz, CDCl<sub>3</sub>, δ): 2.74-2.81 (m, 2H), 2.82-2.88 (m, 2H), 3.36 (s, 3H), 3.51-3.55 (m, 2H), 3.59 (s, 2H), 3.62-3.68 (m, 4H), 3.70-3.74 (m, 2H), 3.76 (s, 2H), 3.82 (s, 3H), 3.85 (t, *J*=5.2 Hz, 2H), 4.09 (s, 3H), 4.12 (t, *J*=5.2 Hz, 2H), 6.56 (s, 1H), 6.62 (s, 1H), 7.61 (d, *J*=8.4 Hz, 2H), 7.64-7.69 (m, 1H), 7.80 (d, *J*=8.5 Hz, 2H), 7.82-7.86 (m, 1H), 7.90-7.94 (m, 1H), 7.99 (dd, *J*=1.7, 8.3 Hz, 1H), 8.25 (d, *J*=8.3 Hz, 1H), 8.36 (d, *J*=8.5 Hz, 1H), 8.38 (s, 2H), 8.45 (s, 1H), 9.46 (d, *J*=1.6 Hz, 1H), 13.41 (s, 1H). **<sup>13</sup>C NMR** (101 MHz, CDCl<sub>3</sub>, δ): 28.6, 50.8, 52.5, 55.6, 56.1, 59.0, 62.0, 68.8, 69.7, 70.6, 70.7, 70.8, 72.0, 112.1, 112.3, 116.0, 117.3, 118.8, 119.1, 120.2, 120.5 (2C), 126.8, 127.7, 128.4, 129.4, 130.3 (4C), 132.2, 136.0, 137.8, 141.3, 146.6, 146.7, 147.4, 148.3, 150.0, 163.9, 167.8 (three quaternary carbons not apparent). **HRMS-ESI** (*m/z*): [M + H]<sup>+</sup> calcd. for C<sub>44</sub>H<sub>47</sub>N<sub>6</sub>O<sub>8</sub><sup>+</sup> 787.3450; found 787.3436. **C<sub>44</sub>H<sub>46</sub>N<sub>6</sub>O<sub>8</sub>** (786.89).

**Methyl 4-(1-(4-(2-(3,4-dihydroisoquinolin-2(1H)-yl)ethyl)phenyl)-1H-1,2,3-triazol-4-yl)-2-(quinoline-2-carboxamido)benzoate (2.40)**

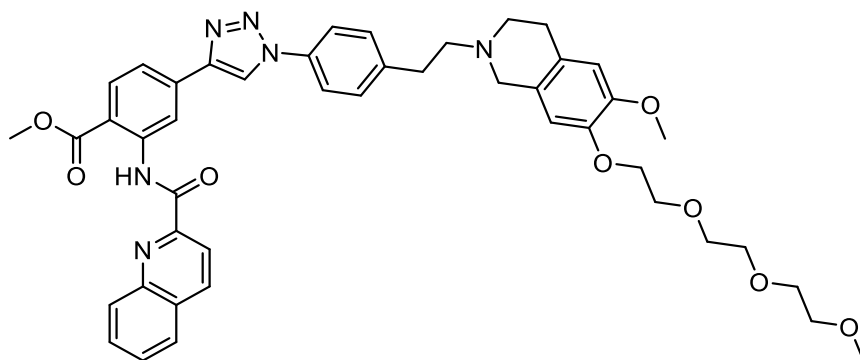
Compound **2.40** was prepared from **2.35** (0.22 mmol) according to the general procedure for amide formation. It was purified by flash column chromatography (EtOAc:MeOH 19:1). **Yield:** 81 mg (0.13 mmol, 59%), yellowish solid. **R<sub>f</sub>** (EtOAc:MeOH 19:1): 0.42. **MP:** 131 °C. **<sup>1</sup>H NMR** (400 MHz, CDCl<sub>3</sub>, δ): 2.81-2.89 (m, 4H), 2.93-3.05 (m, 4H), 3.77 (s, 2H), 4.09 (s, 3H), 7.03-7.08 (m, 1H), 7.10-7.16 (m, 3H), 7.44 (d, *J*=8.4 Hz, 2H), 7.65-7.70 (m, 1H), 7.75 (d, *J*=8.4 Hz, 2H), 7.82-7.87 (m, 1H), 7.91-7.95 (m, 1H), 7.99 (dd, *J*=1.6, 8.3 Hz, 1H), 8.25 (d, *J*=8.3 Hz, 1H), 8.34-8.44 (m, 4H), 9.45 (d, *J*=1.6 Hz, 1H), 13.42 (s, 1H). **<sup>13</sup>C NMR** (101 MHz, CDCl<sub>3</sub>, δ): 29.0, 33.5, 51.0, 52.5, 56.1, 59.8, 116.0, 117.3, 118.8, 119.1, 120.2, 120.6 (2C), 125.7, 126.3, 126.6, 127.7, 128.4, 128.7, 129.4, 130.1 (2C), 130.31, 130.34, 132.2, 134.2, 135.2, 136.0, 137.8, 141.3, 141.6, 146.7, 147.4, 150.0, 163.9, 167.8 (one quaternary carbon not apparent). **HRMS-ESI** (*m/z*): [M + H]<sup>+</sup> calcd. for C<sub>37</sub>H<sub>33</sub>N<sub>6</sub>O<sub>3</sub><sup>+</sup> 609.2609; found 609.2611. C<sub>37</sub>H<sub>32</sub>N<sub>6</sub>O<sub>3</sub> (608.70).

**Methyl 4-(1-(4-(2-(6,7-dimethoxy-3,4-dihydroisoquinolin-2(1H)-yl)ethyl)phenyl)-1H-1,2,3-triazol-4-yl)-2-(quinoline-2-carboxamido)benzoate (2.41)**

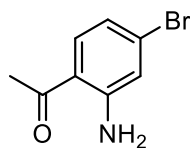
Compound **2.41** was prepared from **2.36** (0.12 mmol) according to the general procedure for amide formation. It was purified by flash column chromatography (EtOAc:NEt<sub>3</sub> 99:1). **Yield:** 60 mg (0.09 mmol, 75%), yellowish solid. **R<sub>f</sub>** (EA: NEt<sub>3</sub> 99:1): 0.34. **MP:** 129 °C. **<sup>1</sup>H NMR** (400 MHz, CDCl<sub>3</sub>, δ): 2.80-2.89 (m, 6H), 2.97-3.04 (m, 2H), 3.69 (s, 2H), 3.82-3.88 (m, 6H),

4.06 (s, 3H), 6.55 (s, 1H), 6.61 (s, 1H), 7.43 (d,  $J=8.4$  Hz, 2H), 7.66 (t,  $J=7.5$  Hz, 1H), 7.75 (d,  $J=8.4$  Hz, 2H), 7.80-7.86 (m, 1H), 7.91 (d,  $J=8.0$  Hz, 1H), 7.98 (dd,  $J=1.6, 8.3$  Hz, 1H), 8.24 (d,  $J=8.3$  Hz, 1H), 8.33-8.40 (m, 3H), 8.43 (s, 1H), 9.44 (d,  $J=1.5$  Hz, 1H), 13.40 (s, 1H).  $^{13}\text{C}$  NMR (101 MHz,  $\text{CDCl}_3$ ,  $\delta$ ): 28.5, 33.4, 51.0, 52.5, 55.6, 55.9, 56.0, 59.6, 109.5, 111.4, 116.0, 117.3, 118.8, 119.1, 120.1, 120.6 (2C), 126.0, 126.1, 127.7, 128.3, 129.4, 130.1 (2C), 130.29, 130.32, 132.1, 135.2, 136.0, 137.7, 141.3, 141.4, 146.6, 147.3, 147.4, 147.7, 150.0, 163.9, 167.8. IR [ $\text{cm}^{-1}$ ]: 3130.5 (vw), 2922.1 (m, br), 2852.7 (w), 1691.6 (s), 1612.5 (w), 1568.1 (m), 1500.6 (s), 1427.3 (m), 1230.6 (s), 1126.4 (m), 1103.3 (m), 1037.7 (m), 819.7 (w), 767.7 (s), 696.3 (m), 528.5 (m), 478.3 (m), 457.1 (m). MS-ESI ( $m/z$ ):  $[\text{M} + \text{H}]^+$  calcd. for  $\text{C}_{39}\text{H}_{37}\text{N}_6\text{O}_5^+$  669.2820; found 669.2833.  $\text{C}_{39}\text{H}_{36}\text{N}_6\text{O}_5$  (668.75).

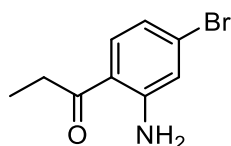
**Methyl 4-(1-(4-(2-(6-methoxy-7-(2-(2-(2-methoxyethoxy)ethoxy)ethoxy)-3,4-dihydroisoquinolin-2(1H)-yl)ethyl)phenyl)-1H-1,2,3-triazol-4-yl)-2-(quinoline-2-carboxamido)benzoate (2.42)**



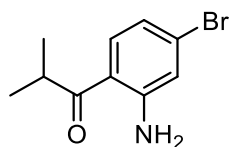
Compound **2.42** was prepared from **2.37** (25 mmol) according to the general procedure for amide formation. It was purified by flash column chromatography ( $\text{CHCl}_3$ :MeOH 100:7). **Yield**: 120 mg (15 mmol, 60%), colorless solid. **MP**: 129 °C.  $^1\text{H}$  NMR (600 MHz,  $\text{CDCl}_3$ ,  $\delta$ ): 2.79-2.89 (m, 6H), 2.99-3.04 (m, 2H), 3.37 (s, 3H), 3.53-3.56 (m, 2H), 3.64-3.70 (m, 6H), 3.72-3.75 (m, 2H), 3.82 (s, 3H), 3.86 (t,  $J=5.3$  Hz, 2H), 4.08 (s, 3H), 4.15 (t,  $J=5.3$  Hz, 2H), 6.61 (s, 2H), 7.43 (d,  $J=8.5$  Hz, 2H), 7.63-7.69 (m, 1H), 7.75 (d,  $J=8.5$  Hz, 2H), 7.82-7.85 (m, 1H), 7.90-7.93 (m, 1H), 7.98 (dd,  $J=1.7, 8.3$  Hz, 1H), 8.24 (d,  $J=8.3$  Hz, 1H), 8.36 (d,  $J=8.6$  Hz, 1H), 8.38 (s, 2H), 8.42 (s, 1H), 9.45 (d,  $J=1.6$  Hz, 1H), 13.40 (s, 1H).  $^{13}\text{C}$  NMR (151 MHz,  $\text{CDCl}_3$ ,  $\delta$ ): 28.6, 33.5, 51.0, 52.4, 55.5, 56.0, 59.0, 59.6, 68.8, 69.6, 70.5, 70.6, 70.8, 71.9, 112.0, 112.4, 116.0, 117.3, 118.8, 119.0, 120.2, 120.6 (2C), 126.8 (2C), 127.6, 128.3, 129.4, 130.1 (2C), 130.26, 130.29, 132.1, 135.1, 136.0, 137.7, 141.3, 141.5, 146.5, 146.6, 147.3, 148.3, 150.0, 163.9, 167.8. HRMS-ESI ( $m/z$ ):  $[\text{M} + \text{H}]^+$  calcd. for  $\text{C}_{45}\text{H}_{49}\text{N}_6\text{O}_8^+$  801.3606; found 801.3640.  $\text{C}_{45}\text{H}_{48}\text{N}_6\text{O}_8$  (800.91).

**1-(2-Amino-4-bromophenyl)ethan-1-one (2.44)**

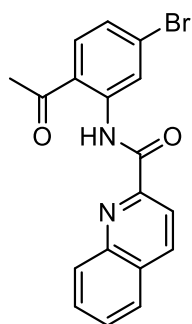
Compound **2.44** was synthesized according to the general procedure for the ortho acylation of 3-bromoaniline (15.64 mmol) and purified by flash column chromatography. **Yield:** 569 mg (2.66 mmol, 17%). **<sup>1</sup>H NMR** (400 MHz, CDCl<sub>3</sub>, δ): 2.54 (s, 3H), 6.32 (br s, 2H), 6.76 (dd, *J*=1.9, 8.6 Hz, 1H), 6.83 (d, *J*=1.9 Hz, 1H), 7.55 (d, *J*=8.6 Hz, 1H). **<sup>13</sup>C NMR** (101 MHz, CDCl<sub>3</sub>, δ): 27.9, 117.1, 119.0, 119.5, 129.0, 133.3, 151.0, 200.1. **HRMS-ESI** (*m/z*): [M + H]<sup>+</sup> calcd. for C<sub>8</sub>H<sub>9</sub>BrNO<sup>+</sup> 213.9862; found 213.9860. **C<sub>8</sub>H<sub>8</sub>BrNO** (214.06).

**1-(2-Amino-4-bromophenyl)propan-1-one (2.45) [57]**

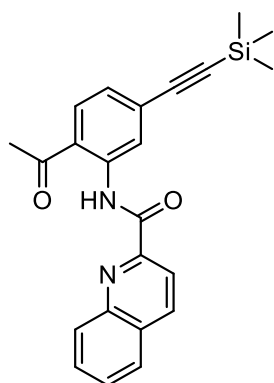
Compound **2.45** was synthesized according to the general procedure for the ortho acylation of 3-bromoaniline (46.3 mmol) and purified with by column chromatography (PE:EtOAc 4:5). **Yield:** 550 mg (11.6 mmol, 25%). **R<sub>f</sub>** (PE:EtOAc 4:5): 0.58. **<sup>1</sup>H NMR** (400 MHz, CD<sub>3</sub>OD, δ): 1.14 (t, *J*=7.3 Hz, 3H), 2.92 (q, *J*=7.3 Hz, 2H), 6.68 (dd, *J*=2.0, 8.7 Hz, 1H), 6.93 (d, *J*=2.0 Hz, 1H), 7.65 (d, *J*=8.7 Hz, 1H). **<sup>13</sup>C NMR** (101 MHz, CD<sub>3</sub>OD, δ): 9.2, 33.2, 117.2, 119.0, 120.4, 129.7, 133.9, 153.6, 204.4. **HRMS-ESI** (*m/z*): [M + H]<sup>+</sup> calcd. for C<sub>9</sub>H<sub>11</sub>BrNO<sup>+</sup> 228.0019; found 228.0018. **C<sub>9</sub>H<sub>10</sub>BrNO** (228.09).

**1-(2-Amino-4-bromophenyl)-2-methylpropan-1-one (2.46) (CAS 1598834-65-1)**

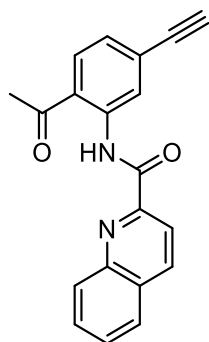
Compound **2.46** was synthesized according to the general procedure for the ortho acylation of 3-bromoaniline (45.5 mmol) and purified by flash column chromatography (DCM). **Yield:** 1.20 g (5.0 mmol, 11%). **<sup>1</sup>H NMR** (400 MHz, CDCl<sub>3</sub>, δ): 1.18 (d, *J*=6.8 Hz, 6H), 3.50 (m, 1H), 6.37 (br s, 2H), 6.75 (dd, *J*=1.9, 8.6 Hz, 1H), 6.83 (d, *J*=1.9 Hz, 1H), 7.59 (d, *J*=8.7 Hz, 1H). **<sup>13</sup>C NMR** (101 MHz, CDCl<sub>3</sub>, δ): 19.6 (2C), 35.5, 115.6, 119.0, 119.8, 128.7, 132.3, 151.7, 206.5. **C<sub>10</sub>H<sub>12</sub>BrNO** (242.12).

***N*-(2-Acetyl-5-bromophenyl)quinoline-2-carboxamide (2.47)**

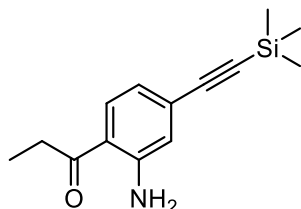
Compound **2.47** was prepared from **2.44** (2.57 mmol) according to the general procedure for amide formation. It was purified by flash column chromatography (DCM). **Yield:** 417 mg (1.13 mmol, 44%). **R<sub>f</sub>** (DCM): 0.55. **<sup>1</sup>H NMR** (400 MHz, CDCl<sub>3</sub>, δ): 2.73 (s, 3H), 7.32 (dd, *J*=2.0, 8.5 Hz, 1H), 7.63-7.69 (m, 1H), 7.78-7.85 (m, 2H), 7.88-7.93 (m, 1H), 8.34-8.37 (m, 2H), 8.38-8.42 (m, 1H), 9.33 (d, *J*=2.0 Hz, 1H), 13.84 (s, 1H). **<sup>13</sup>C NMR** (101 MHz, CDCl<sub>3</sub>, δ): 28.7, 118.9, 121.8, 123.9, 125.9, 127.6, 128.4, 129.4, 129.8, 130.3, 130.5, 132.7, 137.7, 141.2, 146.7, 149.7, 164.3, 201.1. **HRMS-ESI** (*m/z*): [M + H]<sup>+</sup>; calcd. for C<sub>18</sub>H<sub>14</sub>BrN<sub>2</sub>O<sub>2</sub><sup>+</sup> 369.0233; found 369.0230. **C<sub>18</sub>H<sub>13</sub>BrN<sub>2</sub>O<sub>2</sub>** (369.22).

***N*-(2-Acetyl-5-((trimethylsilyl)ethynyl)phenyl)quinoline-2-carboxamide (2.48)**

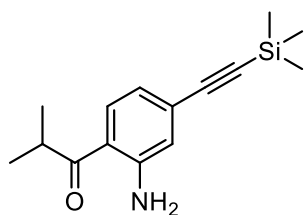
Compound **2.48** was prepared from **2.47** (1.14 mmol) according to the general procedure for the Sonogashira reaction. It was purified by flash column chromatography (PE:DCM 1:1). **Yield:** 336 mg (0.87 mmol, 76%). **R<sub>f</sub>** (PE:DCM 1:1): 0.33. **<sup>1</sup>H NMR** (400 MHz, CDCl<sub>3</sub>, δ): 0.28 (s, 9H), 2.73 (s, 3H), 7.24 (dd, *J*=1.6, 8.3 Hz, 1H), 7.62-7.68 (m, 1H), 7.79-7.85 (m, 1H), 7.87-7.92 (m, 2H), 8.36 (s, 2H), 8.40 (d, *J*=8.4 Hz, 1H), 9.18 (d, *J*=1.5 Hz, 1H), 13.79 (s, 1H). **<sup>13</sup>C NMR** (101 MHz, CDCl<sub>3</sub>, δ): 0.0 (3C), 28.8, 98.6, 104.1, 119.1, 122.8, 124.4, 126.0, 127.8, 128.5, 129.6, 129.8, 130.4, 130.6, 131.6, 137.8, 140.3, 146.8, 150.1, 164.3, 201.5. **MS-ESI** (*m/z*): [M + H]<sup>+</sup>; calcd. for C<sub>23</sub>H<sub>23</sub>N<sub>2</sub>O<sub>2</sub>Si<sup>+</sup> 387.1523; found 387.1523. **C<sub>23</sub>H<sub>22</sub>N<sub>2</sub>O<sub>2</sub>Si** (386.15).

**N-(2-Acetyl-5-ethynylphenyl)quinoline-2-carboxamide (2.49)**

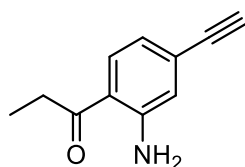
Compound **2.49** was prepared from **2.48** (0.85 mmol) according to the general procedure for TMS deprotection and purified by flash column chromatography (DCM). **Yield:** 200 mg (0.64 mmol, 75%). **R<sub>f</sub>** (DCM): 0.57. **MP:** 187 °C. **<sup>1</sup>H NMR** (300 MHz, CDCl<sub>3</sub>, δ): 2.74 (s, 3H), 3.27 (s, 1H), 7.25-7.30 (m, 1H, signals interfering with the solvent signal), 7.62-7.68 (m, 1H), 7.77-7.86 (m, 1H), 7.87-7.95 (m, 2H), 8.35 (s, 2H), 8.40 (d, *J*=8.6 Hz, 1H), 9.22 (d, *J*=1.5 Hz, 1H), 13.78 (s, 1H). **<sup>13</sup>C NMR** (75 MHz, CDCl<sub>3</sub>, δ): 28.7, 80.6, 82.8, 118.9, 122.9, 124.4, 126.1, 127.6, 128.3, 128.5, 129.4, 130.2, 130.5, 131.5, 137.6, 140.2, 146.7, 149.9, 164.2, 201.3. **HRMS-ESI** (*m/z*): [M + H]<sup>+</sup> calcd. for C<sub>20</sub>H<sub>15</sub>N<sub>2</sub>O<sub>2</sub><sup>+</sup> 315.1128; found 315.1137. **C<sub>20</sub>H<sub>14</sub>N<sub>2</sub>O<sub>2</sub>** (314.34).

**1-(2-Amino-4-((trimethylsilyl)ethynyl)phenyl)propan-1-one (2.50)**

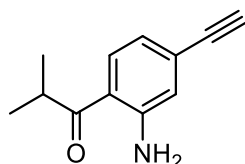
Compound **2.50** was synthesized from **2.45** (3.9 mmol) according to the general procedure for the Sonogashira reaction and purified by flash column chromatography (PE:EtOAc 7:1). **Yield:** 850 mg (3.5 mmol, 89%). **R<sub>f</sub>** (PE:EtOAc 7:1): 0.38. **<sup>1</sup>H NMR** (400 MHz, CDCl<sub>3</sub>, δ): 0.25 (s, 9H), 1.19 (t, *J*=7.3 Hz, 3H), 2.95 (q, *J*=7.3 Hz, 2H), 6.25 (br s, 2H), 6.71 (dd, *J*=1.5, 8.3 Hz, 1H), 6.76 (d, *J*=1.4 Hz, 1H), 7.67 (d, *J*=8.3 Hz, 1H). **<sup>13</sup>C NMR** (101 MHz, CDCl<sub>3</sub>, δ): 0.0 (3C), 8.8, 32.5, 96.9, 104.4, 117.7, 119.3, 120.6, 128.6, 131.0, 149.9, 203.0. **HRMS-ESI** (*m/z*): [M + H]<sup>+</sup> calcd. for C<sub>14</sub>H<sub>20</sub>NOSi<sup>+</sup> 246.1309; found 246.1313. **C<sub>14</sub>H<sub>19</sub>NOSi** (245.40).

**1-(2-Amino-4-((trimethylsilyl)ethynyl)phenyl)-2-methylpropan-1-one (2.51)**

Compound **2.51** was prepared from **2.46** (4.80 mmol) according to the general procedure for the Sonogashira reaction. It was purified by flash column chromatography (PE:EtOAc 9:1). **Yield:** 510 mg (1.97 mmol, 41%). **R<sub>f</sub>** (PE:EtOAc 9:1): 0.55. **<sup>1</sup>H NMR** (400 MHz, CDCl<sub>3</sub>, δ): 0.25 (s, 9H), 1.19 (d, *J*=6.8 Hz, 6H), 3.54 (m, 1H), 6.21 (br s, 2H), 6.73 (dd, *J*=1.5, 8.3 Hz, 1H), 6.80 (d, *J*=1.4 Hz, 1H), 7.68 (d, *J*=8.4 Hz, 1H). **<sup>13</sup>C NMR** (101 MHz, CDCl<sub>3</sub>, δ): 0.0 (3C), 19.7 (2C), 35.6, 97.1, 104.3, 116.9, 119.6, 121.1, 128.7, 131.0, 150.1, 206.7. **HRMS-ESI** (*m/z*): [M + H]<sup>+</sup>; calcd. for C<sub>15</sub>H<sub>22</sub>NOSi<sup>+</sup> 260.1465; found 260.1467. **C<sub>15</sub>H<sub>21</sub>NOSi** (259.42).

**1-(2-amino-4-ethynylphenyl)propan-1-one (2.52)**

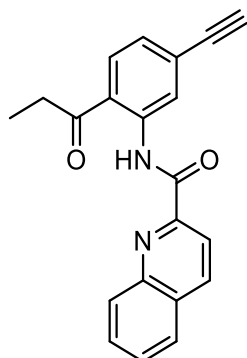
Compound **2.52** was prepared from **2.50** (3.1 mmol) according to the general procedure for TMS deprotection. It was purified by flash column chromatography (0-20% EtOAc in PE). **Yield:** 359 mg (2.1 mmol, 68%). **R<sub>f</sub>** (PE:EtOAc 7:1): 0.31. **<sup>1</sup>H NMR** (400 MHz, CDCl<sub>3</sub>, δ): 1.20 (t, *J*=7.3 Hz, 3H), 2.95 (q, *J*=7.3 Hz, 2H), 3.14 (s, 1H), 6.27 (s, 2H), 6.74 (dd, *J*=1.6, 8.3 Hz, 1H), 6.78 (d, *J*=1.5 Hz, 1H), 7.69 (d, *J*=8.3 Hz, 1H). **<sup>13</sup>C NMR** (101 MHz, CDCl<sub>3</sub>, δ): 8.7, 32.4, 79.2, 83.0, 117.8, 119.2, 120.8, 127.5, 131.0, 149.8, 202.9. **HRMS-ESI** (*m/z*): [M + H]<sup>+</sup> calcd. for C<sub>11</sub>H<sub>12</sub>NO<sup>+</sup> 174.0913; found 174.0915. **C<sub>11</sub>H<sub>11</sub>NO** (173.22).

**1-(2-Amino-4-ethynylphenyl)-2-methylpropan-1-one (2.53)**

Compound **2.53** was prepared from **2.51** (1.34 mmol) according to the general procedure for TMS deprotection. It was purified by flash column chromatography (PE:EtOAc 9:1). **Yield:** 238 mg (1.27 mmol, 95%). **R<sub>f</sub>** (PE:EtOAc 9:1): 0.45. **<sup>1</sup>H NMR** (400 MHz, CDCl<sub>3</sub>, δ): 1.19 (d, *J*=6.8 Hz, 6H), 3.14 (s, 1H), 3.54 (m, 1H), 5.99 (br s, 2H), 6.75 (dd, *J*=1.6, 8.3 Hz, 1H), 6.81 (d, *J*=1.6 Hz, 1H), 7.70 (d, *J*=8.3 Hz, 1H). **<sup>13</sup>C NMR** (101 MHz, CDCl<sub>3</sub>, δ): 19.5 (2C), 35.5,

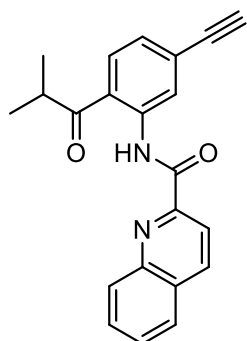
79.2, 83.0, 116.9, 119.3, 121.1, 127.5, 131.0, 150.2, 206.6. **HRMS-ESI** ( $m/z$ ):  $[M + H]^+$ ; calcd. for  $C_{12}H_{14}NO^+$  188.1070; found 188.1073.  **$C_{12}H_{13}NO$**  (187.24).

***N*-(5-Ethynyl-2-propionylphenyl)quinoline-2-carboxamide (2.54)**



Compound **2.54** was prepared from **2.52** (1.2 mmol) according to the general procedure for amide formation and was purified by flash column chromatography (PE:EtOAc 7:1). **Yield:** 379 mg (1.2 mmol, 100%).  **$R_f$**  (PE:EtOAc 7:1): 0.2.  **$^1H$  NMR** (400 MHz,  $CDCl_3$ ,  $\delta$ ): 1.31 (t,  $J=7.2$  Hz, 3H), 3.09 (q,  $J=7.2$  Hz, 2H), 3.26 (s, 1H), 7.24-7.28 (m, 1H, signals interfering with the solvent signal), 7.61-7.68 (m, 1H), 7.79-7.85 (m, 1H), 7.89 (d,  $J=8.2$  Hz, 1H), 7.92 (d,  $J=8.2$  Hz, 1H), 8.35 (s, 2H), 8.40 (d,  $J=8.5$  Hz, 1H), 9.21 (d,  $J=1.5$  Hz, 1H), 13.79 (s, 1H).  **$^{13}C$  NMR** (101 MHz,  $CDCl_3$ ,  $\delta$ ): 8.7, 33.5, 80.4, 82.8, 118.9, 122.7, 124.6, 126.1, 127.6, 128.1, 128.3, 129.4, 130.2, 130.5, 130.6, 137.6, 140.1, 146.7, 150.0, 164.1, 203.8. **HRMS-ESI** ( $m/z$ ):  $[M + H]^+$  calcd. for  $C_{21}H_{17}N_2O_2^+$  329.1285; found 329.1287.  **$C_{21}H_{16}N_2O_2$**  (328.37).

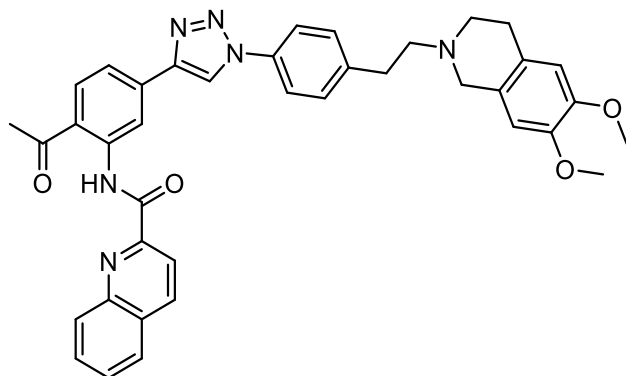
***N*-(5-Ethynyl-2-isobutyrylphenyl)quinoline-2-carboxamide (2.55)**



Compound **2.55** was prepared from **2.53** (0.58 mmol) according to the general procedure for amide formation. It was purified by flash column chromatography (PE:EtOAc 8:2). **Yield:** 171 mg (0.50 mmol, 86%). **MP:** 196 °C.  **$R_f$**  (PE:EtOAc 8:2): 0.52.  **$^1H$  NMR** (300 MHz,  $CDCl_3$ ,  $\delta$ ): 1.30 (d,  $J=6.8$  Hz, 6H), 3.26 (s, 1H), 3.66 (m, 1H), 7.29 (dd,  $J=8.2, 1.6$  Hz, 1H), 7.64-7.70 (m, 1H), 7.81-7.88 (m, 1H), 7.89-7.96 (m, 2H), 8.37 (s, 2H), 8.44 (d,  $J=8.4$  Hz, 1H), 9.20 (d,  $J=1.6$  Hz, 1H), 13.72 (s, 1H).  **$^{13}C$  NMR** (75 MHz,  $CDCl_3$ ,  $\delta$ ): 19.6 (2C), 36.8, 80.5, 82.9, 119.1, 122.3, 124.9, 126.2, 127.7, 128.1, 128.4, 129.5, 130.3, 130.5, 130.6, 137.8, 140.6, 146.8, 150.1,

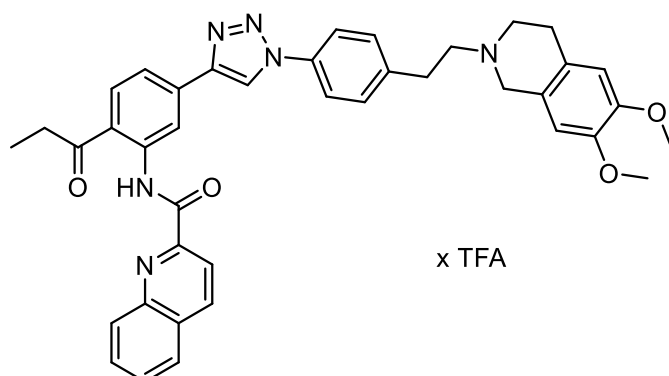
164.2, 207.5. **HRMS-ESI** (m/z): [M + H]<sup>+</sup> calcd. for C<sub>22</sub>H<sub>19</sub>N<sub>2</sub>O<sub>2</sub><sup>+</sup> 343.1441; found 343.1449. C<sub>22</sub>H<sub>18</sub>N<sub>2</sub>O<sub>2</sub> (342.40).

***N*-(2-Acetyl-5-(1-(4-(2-(6,7-dimethoxy-3,4-dihydroisoquinolin-2(1*H*)-yl)ethyl)-phenyl)-1*H*-1,2,3-triazol-4-yl)phenyl)quinoline-2-carboxamide (2.56)**



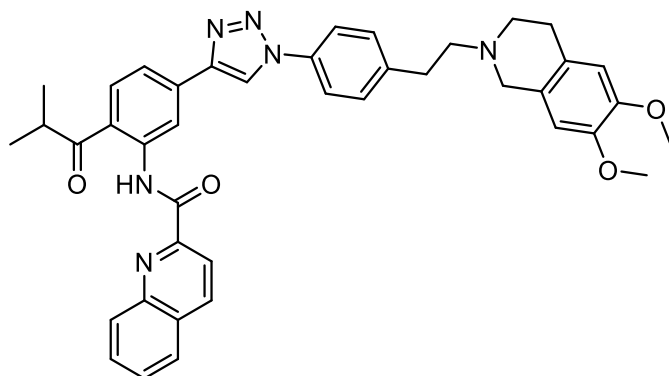
Compound **2.56** was synthesized from **2.28** (0.33 mmol, 1.5 eq) and **2.49** (0.22 mmol, 1.0 eq) according to the general procedure for the CuAAC. It was purified in two subsequent flash column chromatography runs (1<sup>st</sup> run: DCM:MeOH 95:5, 2<sup>nd</sup> run: PE:acetone 1:1). **Yield:** 24 mg (0.04 mmol, 18%), dark yellowish solid. **R<sub>f</sub>** (DCM:MeOH 95:5): 0.32. **<sup>1</sup>H NMR** (300 MHz, CDCl<sub>3</sub>, δ): 2.80 (s, 3H), 2.81-2.91 (m, 6H), 2.97-3.07 (m, 2H), 3.69 (m, 2H), 3.83-3.88 (m, 6H), 6.55 (s, 1H), 6.62 (s, 1H), 7.44 (d, *J*=8.4 Hz, 2H), 7.64-7.71 (m, 1H), 7.76 (d, *J*=8.4 Hz, 2H), 7.81-7.88 (m, 1H), 7.89-7.95 (m, 1H), 8.03 (dd, *J*=1.6, 8.3 Hz, 1H), 8.11 (d, *J*=8.4 Hz, 1H), 8.37 (m, 2H), 8.41-8.48 (m, 2H), 9.48 (d, *J*=1.5 Hz, 1H), 13.98 (s, 1H). **<sup>13</sup>C NMR** (75 MHz, CDCl<sub>3</sub>, δ): 28.8, 28.9, 33.7, 51.2, 55.8, 56.0, 56.1, 59.9, 109.5, 111.4, 117.7, 118.9, 119.4, 120.1, 120.7 (2C), 122.8, 126.2, 126.4, 127.7, 128.5, 129.5, 130.2 (2C), 130.4, 130.7, 132.8, 135.2, 136.4, 137.8, 141.0, 141.8, 146.8, 147.3, 147.4, 147.7, 150.1, 164.7, 201.7. **HRMS-ESI** (m/z): [M + H]<sup>+</sup> calcd. for C<sub>39</sub>H<sub>37</sub>N<sub>6</sub>O<sub>4</sub><sup>+</sup> 653.2871; found 653.2874. C<sub>39</sub>H<sub>36</sub>N<sub>6</sub>O<sub>4</sub> (652.76).

***N*-(5-(1-(4-(2-(6,7-Dimethoxy-3,4-dihydroisoquinolin-2(1*H*)-yl)ethyl)phenyl)-1*H*-1,2,3-triazol-4-yl)-2-propionylphenyl)quinoline-2-carboxamide hydrotrifluoroacetate (**2.57**)**



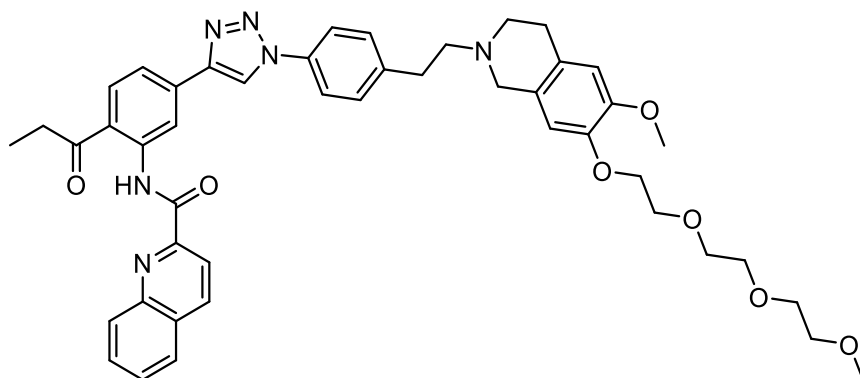
Compound **2.57** was prepared from **2.28** (0.38 mmol, 1.0 eq) and **2.54** (0.49 mmol, 1.3 eq) according to the general procedure for the CuAAC. It was purified by flash column chromatography (CHCl<sub>3</sub>:MeOH 100:7) and recrystallization (CHCl<sub>3</sub>). **Yield**: 118 mg (0.18 mmol, 48%), colorless solid. **R<sub>f</sub>** (CHCl<sub>3</sub>:MeOH 100:7): 0.38. **MP**: 170 °C. For further purification, the substance was subjected to preparative HPLC (gradient: 0-30 min: MeCN/0.1% aq TFA 51:49-87:13, *t<sub>R</sub>* = 12.5 min). Analytical and pharmacological characterization was performed with the HPLC purified substance. **<sup>1</sup>H NMR** (600 MHz, [D<sub>6</sub>]DMSO, δ): 1.22 (t, *J*=7.1 Hz, 3H), 2.99-3.14 (m, 2H), 3.19-3.28 (m, 4H), 3.38 (m, 1H), 3.55 (m, 2H), 3.75 (s, 3H), 3.76 (s, 3H), 3.81 (m, 1H), 4.33 (m, 1H), 4.56 (m, 1H), 6.81 (s, 1H), 6.86 (s, 1H), 7.61 (d, *J*=8.5 Hz, 2H), 7.79-7.84 (m, 2H), 7.96-8.01 (m, 1H), 8.04 (d, *J*=8.4 Hz, 2H), 8.17 (d, *J*=8.0 Hz, 1H), 8.27 (d, *J*=8.3 Hz, 1H), 8.31-8.36 (m, 2H), 8.70 (d, *J*=8.5 Hz, 1H), 9.50 (s, 1H), 9.57 (d, *J*=1.6 Hz, 1H), 10.07 (br s, 1H), 13.76 (s, 1H). **<sup>13</sup>C NMR** (151 MHz, [D<sub>6</sub>]DMSO, δ): 8.5, 24.6, 29.2, 32.9, 49.3, 51.9, 55.5, 55.6, 55.6, 109.6, 111.5, 116.6, 118.6, 119.8, 120.0, 120.4 (2C), 121.1, 122.5, 123.1, 128.2, 128.7, 129.1, 129.4, 130.3 (2C), 131.0, 132.4, 135.4, 135.5, 137.7, 138.5, 139.8, 145.9, 146.3, 147.8, 148.5, 149.5, 163.3, 204.2. **HRMS-ESI** (*m/z*): [M + H]<sup>+</sup> calcd. for C<sub>40</sub>H<sub>39</sub>N<sub>6</sub>O<sub>4</sub><sup>+</sup> 667.3027; found 667.3029. **C<sub>40</sub>H<sub>38</sub>N<sub>6</sub>O<sub>4</sub> · C<sub>2</sub>HF<sub>3</sub>O<sub>2</sub>** (666.78 + 114.02).

***N*-(5-(1-(4-(2-(6,7-Dimethoxy-3,4-dihydroisoquinolin-2(1*H*)-yl)ethyl)phenyl)-1*H*-1,2,3-triazol-4-yl)-2-isobutyrylphenyl)quinoline-2-carboxamide (2.58)**



Compound **2.58** was prepared from **2.28** (0.38 mmol, 1.5 eq) and **2.55** (0.25 mmol, 1.0 eq) according to the general procedure for the CuAAC. It was purified in three subsequent flash column chromatography runs (1<sup>st</sup> run: DCM:MeOH 95:5, 2<sup>nd</sup> run: PE:acetone 1:1). **Yield:** 16 mg (0.02 mmol, 8%), beige solid. **R<sub>f</sub>** (DCM:MeOH 95:5): 0.29. **<sup>1</sup>H NMR** (300 MHz, CDCl<sub>3</sub>, δ) 1.34 (d, *J*=6.8 Hz, 6H), 2.79-2.91 (m, 6H), 2.98-3.06 (m, 2H), 3.69 (s, 2H), 3.72-3.81 (m, 1H), 3.84-3.87 (m, 6H), 6.56 (s, 1H), 6.62 (s, 1H), 7.45 (d, *J*=8.5 Hz, 2H), 7.64-7.72 (m, 1H), 7.76 (d, *J*=8.5 Hz, 2H), 7.82-7.90 (m, 1H), 7.91-7.95 (m, 1H), 8.05 (dd, *J*=1.7, 8.3 Hz, 1H), 8.14 (d, *J*=8.6 Hz, 1H), 8.38 (m, 2H), 8.43-8.48 (m, 2H), 9.47 (d, *J*=1.6 Hz, 1H), 13.97 (s, 1H). **HRMS-ESI** (*m/z*): [M + H]<sup>+</sup> calcd. for C<sub>41</sub>H<sub>41</sub>N<sub>6</sub>O<sub>4</sub><sup>+</sup> 681.3184; found 681.3188. **C<sub>41</sub>H<sub>40</sub>N<sub>6</sub>O<sub>4</sub>** (680.81).

***N*-(5-(1-(4-(2-(6-Methoxy-7-(2-(2-(2-methoxyethoxy)ethoxy)ethoxy)-3,4-dihydroisoquinolin-2(1*H*)-yl)ethyl)phenyl)-1*H*-1,2,3-triazol-4-yl)-2-propionylphenyl)quinoline-2-carboxamide (2.59)[39]**



We described compound **2.59** recently [39]. For clarity it is also included here. **2.59** was prepared from **2.29** (0.37 mmol, 1.0 eq) and **2.54** (0.48 mmol, 1.3 eq) according to the general procedure for the CuAAC. It was purified by column chromatography (DCM:MeOH 95:5). **Yield:** 160 mg (0.20 mmol, 54%). **MP:** 168 °C. **<sup>1</sup>H NMR** (600 MHz, CDCl<sub>3</sub>, δ): 1.34 (t, *J*=7.2 Hz, 3H), 2.79-2.88 (m, 6H), 2.96-3.01 (m, 2H), 3.14 (q, *J*=7.2 Hz, 2H), 3.36 (s, 3H),

3.53-3.55 (m, 2H), 3.63-3.69 (m, 6H), 3.71-3.75 (m, 2H), 3.81 (s, 3H), 3.86 (t,  $J=5.2$  Hz, 2H), 4.14 (t,  $J=5.2$  Hz, 2H), 6.60 (m, 2H), 7.42 (d,  $J=8.3$  Hz, 2H), 7.63-7.67 (m, 1H), 7.74 (d,  $J=8.4$  Hz, 2H), 7.81-7.85 (m, 1H), 7.89 (d,  $J=8.0$  Hz, 1H), 7.98 (dd,  $J=1.6, 8.3$  Hz, 1H), 8.09 (d,  $J=8.3$  Hz, 1H), 8.33-8.35 (m, 2H), 8.41-8.44 (m, 2H), 9.44 (d,  $J=1.6$  Hz, 1H), 13.96 (s, 1H).  $^{13}\text{C}$  NMR (151 MHz,  $\text{CDCl}_3$ ,  $\delta$ ): 8.7, 28.6, 33.3, 33.5, 50.9, 55.5, 55.9, 59.0, 59.6, 68.7, 69.6, 70.5, 70.6, 70.7, 71.9, 111.9, 112.3, 117.6, 118.7, 119.1, 119.9, 120.5 (2C), 122.3, 126.3, 126.8, 127.5, 128.3, 129.3, 130.0 (2C), 130.2, 130.5, 131.6, 135.1, 135.9, 137.6, 140.7, 141.5, 146.5, 146.7, 147.1, 148.3, 150.0, 164.4, 203.9. **HRMS-ESI** ( $m/z$ ):  $[\text{M} + \text{H}]^+$  calcd. for  $\text{C}_{46}\text{H}_{51}\text{N}_6\text{O}_7^+$  799.3814; found 799.3823.  $\text{C}_{46}\text{H}_{50}\text{N}_6\text{O}_7 \cdot \text{C}_2\text{HF}_3\text{O}_2$  (798.94 + 114.02).

## 2.4.2 Biology

### 2.4.2.1 General Experimental Conditions

**Materials.** Commodity chemicals and solvents were purchased from commercial suppliers (Sigma Aldrich, Munich, Germany; Merck, Darmstadt, Germany; VWR, Darmstadt, Germany; Thermo Fisher Scientific, Waltham, MA, USA; Invitrogen, Karlsruhe, Germany). Topotecan and vinblastine were obtained from Sigma Aldrich. Hoechst 33342 and calcein-AM were procured from Biotium (Fremont, CA, USA). FTC was from Merck. Tariquidar was synthesized in our laboratory according to literature [21] with slight modifications [58]. Reversan was obtained from Tocris (Wiesbaden-Nordenstadt, Germany). Cholesterol/RAMEB, a complex of 5.4% cholesterol and randomly methylated  $\beta$ -cyclodextrin, was acquired from CycloLab (Cyclodextrin Research and Development Laboratory, Budapest, Hungary). Millipore water was used throughout for the preparation of buffers, aqueous reagent solutions and HPLC eluents. The pH of buffers and aqueous reagent solutions was adjusted with NaOH aq or HCl aq unless stated otherwise. Acetonitrile for HPLC (gradient grade) was obtained from Merck. Mammalian cell lines were purchased from the ATCC (American Type Culture Collection; Manassas, VA, USA), Sf9 cells were obtained from CLS (Eppelheim, Germany). Tissue culture flasks were procured from Sarstedt (Nümbrecht, Germany). Dulbecco's Modified Eagle's Medium - high glucose (DMEM/High; with 4500 mg/L glucose, sodium pyruvate and sodium bicarbonate, without L-glutamine, liquid, sterile-filtered, suitable for cell culture) and L-glutamine solution (200 mM, sterile-filtered, BioXtra, suitable for cell culture) were from Sigma Aldrich. Insect-Xpress Medium was obtained from Lonza (Verviers, Belgium). Fetal calf serum (FCS) and trypsin/EDTA and were from Biochrom (Berlin, Germany). For all assays in microplate format, 96-well plates (PS, clear, F-bottom, with lid, sterile) from Greiner Bio-One (Frickenhausen, Germany) were used. The BaculoGold transfection kit was bought from BD Biosciences (San Jose, CA, USA). The Bio-Rad protein assay kit was purchased from Bio-Rad Laboratories (Munich, Germany). Syringe filters

(Phenex-RC, 4 mm, 0.2  $\mu$ m) used in the chemical stability assay were from Phenomenex (Aschaffenburg, Germany).

**Stock solutions.** Topotecan and vinblastine were dissolved in 70% EtOH to give 100  $\mu$ M stock solutions. Hoechst 33342 stock solution (0.8 mM) was prepared in water and calcein-AM stock solution (100  $\mu$ M) in DMSO. The test compounds and the reference compounds fumitremorgin C, tariquidar, reversan and sulfasalazine were dissolved in DMSO at 100 times the final concentrations in the transport assays and the ATPase assay and at 1000 times the final concentrations in the chemosensitivity assay. A 1.5 mM stock solution of sulfasalazine in DMSO was prepared for stimulating ABCG2 in the inhibition mode of the ATPase Assay. Furthermore, 3 mM stock solutions of the test compounds in DMSO were prepared for the stability assay in blood plasma. If not stated otherwise, water served as solvent for other assay reagents.

**Instruments.** Fluorescence and absorbance measurements in microplates were carried out with a GENios Pro microplate reader (equipped with a Xenon arc lamp; Tecan, Grödig, Austria). Analytical HPLC of compound **2.59** after incubation in murine plasma was performed on a system from Agilent described in Section 2.4.1.1. The HPLC conditions were as described, yet with two alterations. The following linear gradient was applied: 0-12 min: A/B 20:80-95:5, 12-15 min: A/B 95:5. The injection volume was 100  $\mu$ L.

**Software.** All biological data were analyzed with GraphPad Prism 5 (GraphPad Software, San Diego, CA, USA).

#### 2.4.2.2 Cell Culture

All mammalian cells were cultured in DMEM/High supplemented with 2% (v/v) of a 200 mM L-glutamine solution and 10% (v/v) FCS at 37 °C in a water-saturated atmosphere containing 5% CO<sub>2</sub>.

**MCF-7/Topo** cells, an ABCG2-overexpressing variant of the MCF-7 cell line (ATCC<sup>®</sup> HTB-22), were obtained by passaging the MCF-7 cells with increasing amounts of topotecan in the culture medium to achieve a maximum concentration of 550 nM within a period of about 40 d; after 3 passages at the maximum concentration the treated cells expressed sufficient quantities of ABCG2 [40,59]. They were cultured with 550 nM topotecan to maintain overexpression of the ABCG2 transporter.

**KB-V1** cells, an ABCB1-overexpressing variant of the KB cell line (ATCC<sup>®</sup> CCL-17), were obtained by passaging the KB cells with increasing amounts of vinblastine in the culture medium to achieve a maximum concentration of 330 nM within a period of about 90 d; after 3 passages at the maximum concentration the treated cells expressed sufficient quantities of

ABCB1 transporter [58,60]. They were cultured with 330 nM vinblastine to maintain overexpression of the ABCB1 transporter.

**MDCK.2-MRP1** cells were a kind gift from Prof. Dr. P. Borst from the Netherland Cancer Institute (Amsterdam, NL). They were obtained by transfecting MDCK.2 cells (ATCC® CRL-2936) with human ABCC1 [61,62]. Due to the strong adherence of this cell line, trypsinization was performed using 2X trypsin/EDTA (0.1%./0.04%) for 30 min.

**Sf9** cells (CLS 604328) were cultured in Insect Xpress medium supplemented with 5% (v/v) FCS in 250 or 500 mL disposable Erlenmeyer flasks at 28 °C and under rotation at 150 rpm.

All cells were routinely monitored for mycoplasma contamination by PCR using the Venor®GeM mycoplasma detection kit (Minerva Biolabs, Berlin, Germany) and were negative.

#### **2.4.2.3 Inhibition of ABCG2: Hoechst 33342 Transport Assay [44]**

MCF-7/Topo cells were seeded into 96-well plates at a density of 20,000 cells per well (100 µL/well) and allowed to attach to the surface of the microplates at 37 °C in a water-saturated atmosphere containing 5% CO<sub>2</sub> overnight. The next day, the culture medium was removed and the cells were incubated with loading suspension (DMEM, supplemented as described above, 8 µM Hoechst 33342 and the test compounds at increasing concentrations; 100 µL/well) for 2 h (37 °C, water-saturated atmosphere containing 5% CO<sub>2</sub>). FTC at a final concentration of 10 µM served as reference compound (positive control); the vehicle DMSO (1%) served as negative control. Each concentration was measured in triplicate, positive and negative control 12-fold each. The supernatants were drained and the cells were fixed with 4% (w/w) PFA in PBS (100 µL/well) under light protection for 20 min. Afterwards, the MCF-7/Topo cells were washed with PBS twice (250 µL/well each time) to remove residual dye and overlaid with PBS (100 µL/well). The relative fluorescence intensities ( $\lambda_{exc}$ =340 nm,  $\lambda_{em}$ =485 nm) were determined using a GENios Pro microplate reader. On each plate, the optimal gain was calculated by the determination of the fluorescence intensities in the presence of the reference substance FTC.

The data were normalized relative to the fluorescence intensity in the absence of an ABCG2 inhibitor (negative control) and the response elicited by the FTC (positive) control, which was defined as 100% inhibition of the Hoechst 33342 efflux. IC<sub>50</sub> values were calculated using four parameter sigmoidal fits. Errors were expressed as standard error of the mean (SEM).

#### **2.4.2.4 Inhibition of ABCB1: Calcein-AM Transport Assay [44]**

KB-V1 cells were seeded into 96-well plates at a density of 20,000 cells per well (100 µL/well) and allowed to attach to the surface of the microplates at 37 °C in a water-saturated atmosphere containing 5% CO<sub>2</sub> overnight. The next day, the culture medium was removed and the cells

were washed with loading buffer (120 mM NaCl, 5 mM KCl, 2 mM MgCl<sub>2</sub>, 1.5 mM CaCl<sub>2</sub>, 25 mM HEPES, 10 mM glucose, pH 7.4) in order to remove unspecific serum esterases. Afterwards, the cells were incubated with loading suspension (loading buffer, 5 mg/mL BSA, 1.25 µL/mL 20% (w/w) Pluronic® F-127 in DMSO, 0.5 µM calcein-AM and the test compounds at increasing concentrations; 100 µL/well) for 10 min (37 °C, water-saturated atmosphere containing 5% CO<sub>2</sub>). Tariquidar at a final concentration of 10 µM served as reference compound (positive control); the vehicle DMSO (1%) served as negative control. Each concentration was measured in triplicate, positive and negative control 12-fold each. The supernatants were drained and the cells were fixed with 4% (w/w) PFA in PBS (100 µL/well) under light protection for 20 min. Afterwards, the KB-V1 cells were washed with PBS twice (250 µL/well each time) to remove residual dye and overlaid with PBS (100 µL/well). The relative fluorescence intensities ( $\lambda_{\text{exc}}=485$  nm,  $\lambda_{\text{em}}=535$  nm) were determined using a GENios Pro microplate reader. On each plate, the optimal gain was calculated by the determination of the fluorescence intensities in the presence of the reference substance tariquidar.

The data were normalized relative to the fluorescence intensity in the absence of an ABCB1 inhibitor (negative control) and the response elicited by the tariquidar (positive) control, which was defined as 100% inhibition of the calcein-AM efflux. IC<sub>50</sub> values were calculated using four parameter sigmoidal fits. Errors were expressed as standard error of the mean (SEM).

#### **2.4.2.5 Inhibition of ABCC1: Calcein-AM Transport Assay [41]**

MDCK.2-MRP1 cells were seeded into 96-well plates at a density of 20,000 cells per well (100 µL/well) and allowed to attach to the surface of the microplates in a water-saturated atmosphere containing 5% CO<sub>2</sub> at 37 °C overnight. The assay was performed and the data evaluated as described for the calcein-AM transport assay for analyzing ABCB1 inhibition with two exceptions: reversan at a final concentration of 30 µM served as positive control and the incubation time was 1 h.

#### **2.4.2.6 ABCG2 ATPase Assay**

**Generation of recombinant baculoviruses** encoding the ABCG2 protein (in the pVL1392 vector) was performed in Sf9 insect cells using the BD BaculoGold transfection kit according to the manufacturer's protocol. High-titer virus stock solutions were generated by 2-3 sequential amplifications. The supernatant fluid from the last amplification was stored at 4 °C under light protection.

**Membrane preparation.** The protocol is based on the work of Sarkadi et al. [63]. Sf9 cells with a density of 3 x 10<sup>6</sup> cells/mL (100 mL) were infected 1:500 with a high-titer ABCG2 baculovirus stock, incubated for 48 h and harvested by centrifugation at 4 °C and 500 g for 10 min. The cell pellet was re-suspended in Tris mannitol buffer (50 mM Tris, 300 mM

mannitol, 0.5 mM phenylmethylsulfonyl fluoride (PMSF), pH 7; 100 mL) and centrifuged again. Then the pellet was lysed and homogenized in TMEP buffer (50 mM Tris, 50 mM mannitol, 1 mM EDTA, 10 µg/mL leupeptin, 10 µg/mL benzamidine, 0.5 mM PMSF, 2 mM DTT, pH 7; 60 mL) by a Potter Elvehjem tissue homogenizer. Undisrupted cells and cellular debris were pelleted by centrifugation at 4 °C and 500 g for 10 min and the supernatant, containing the membranes, was removed carefully. For cholesterol loading [64,65], 2.5 mg/mL Cholesterol/RAMEB complex (cholesterol content 5.4%) was added (150 mg total) and the membranes were incubated at 4 °C for 20 min. After centrifugation at 4 °C and 100,000 g for 1 h the pellet (containing the membranes) was re-suspended in TMEP buffer (30 mL), giving a protein concentration of 2.0-3.0 mg/mL, and homogenized with a Potter Elvehjem tissue homogenizer. All procedures during the membrane preparation were performed at 4 °C and aliquots (500-1000 µL) were stored at - 80 °C until use.

**Protein quantification** was performed by the method of Bradford using the Bio-Rad protein assay kit according to the manual.

**Assay procedure.** The assay was performed by analogy with the ABCB1 ATPase assay procedure described by Sarkadi et al. [63]. The ATPase activity of the ABCG2 transporter was estimated by measuring inorganic phosphate liberation. It was determined as orthovanadate-sensitive ATPase activity in the presence of inhibitors in ABCG2 Sf9 membrane preparations. The assay was carried out in the activation mode, i.e. without stimulation of ABCG2, and in the inhibition mode, where the ABCG2 transporters in the membranes were stimulated with sulfasalazine.

Membranes containing 2.0-2.5 mg total protein were thawed on ice and pelleted by centrifugation at 4 °C and 16,200 g for 10 min. Then they were suspended in assay buffer (50 mM MOPS-Tris (100 mM MOPS, pH adjusted to 7.0 with 1.7 M Tris), 50 mM KCl, 5 mM NaN<sub>3</sub>, 2 mM EGTA, 2 mM DTT, 1 mM ouabain; 4.2 mL), mixed with 10% (w/w) CHAPS (42 µL; decreases the high basal ABCG2 ATPase activity) and homogenized using a syringe and a needle (27G). When the assay was performed in the inhibition mode, 1.5 mM sulfasalazine (10.5 µL; final conc. 3 µM) was added to the suspension to activate ABCG2. The suspension was split into 2 portions (2.0 mL each) and one portion was supplemented with orthovanadate (100 mM Na<sub>3</sub>VO<sub>4</sub>, pH 10; 50 µL; final conc. 2 mM), the other with the same amount of purified water. The two suspensions (w. and wo. orthovanadate) were transferred into a 96-well plate on ice (40 µL/well; 20-25 µg protein/well) and pre-incubated at 37 °C for 3 min.

The ATPase reaction was started by adding the reference and test compounds in assay buffer containing 20 mM ATP (10 µL/well, giving a final volume of 50 µL/well; final conc. 4 mM) with a multichannel pipette and the plate was incubated at 37 °C in a microplate shaker for 1 h.

For this purpose, an ATP solution (200 mM  $Mg_xATP$ , 400 mM  $MgCl_2$ , pH adjusted to 7.0 with 1.7 M Tris) was diluted 1:10 (v/v) with assay buffer and the test and reference compounds were added 5-fold concentrated. Sulfasalazine at a final concentration of 30  $\mu M$  served as reference activator (positive control) in the activation mode; FTC at a final concentration of 10  $\mu M$  served as reference inhibitor (positive control) in the inhibition mode; the vehicle DMSO (1% final content) served as negative control. Each concentration (w. and wo. orthovanadate) was measured in duplicate, positive and negative control in quadruplicate each.

The reaction was stopped by the addition of 10% (w/w) SDS (30  $\mu L$ /well); background control (phosphate stemming from the assay buffer) (w. and wo. orthovanadate) was stopped before starting the reaction with  $MgATP$  and was measured in duplicate.

Phosphate standards (0, 0.05, 0.1, 0.25, 1.5 and 2.0 mM  $NaH_2PO_4$  in assay buffer; 50  $\mu L$ /well; each concentration measured in duplicate) were included on each plate for calibration.

The amount of phosphate was determined by adding a colorimetric reagent (1 part of reagent A (35 mM ammonium molybdate, 15 mM zinc acetate) mixed with 4 parts of reagent B (5% (w/w) ascorbic acid, pH 5.0; freshly prepared); 200  $\mu L$ /well) and by incubating at 37 °C for further 20 min. The absorbance (820 nm) as a parameter proportional to the phosphate amount was measured, using a GENios Pro microplate reader.

The data obtained under the treatment with orthovanadate were subtracted from the data without orthovanadate to obtain phosphate liberation resulting from ABCG2 activity. The ensuing data were normalized relative to the absorbance in the absence of an ABCG2 activator/inhibitor (negative control) and the response elicited by the sulfasalazine (positive) control, which was defined as 100% ATPase activity in the activation mode, or the response elicited by the FTC (positive) control, which was defined as 100% ATPase inhibition in the inhibition mode of the assay, where the membranes were activated with sulfasalazine.  $IC_{50}$  values were calculated using four parameter sigmoidal fits. Errors were expressed as standard error of the mean (SEM).

#### **2.4.2.7 Size-Exclusion Chromatography-Based Thermostability Assay (SEC-TS)**

**Expression and purification of human ABCG2** was performed as described in our previous report [39].

**Assay procedure.** The assay was carried out as described in our previous study [39]. In short: Detergent-purified ABCG2 was incubated with or without the test compound at a concentration of 10  $\mu M$  for 10 min at room temperature. Samples were aliquoted (100  $\mu L$  each) and heated at one temperature, ranging from 30-75 °C, for 10 min in a Bio-Rad Thermocycler. Then the samples were cooled on ice, centrifuged at 4 °C and 100,000 g for 20 min and subjected to HP-SEC, using a TSKgel G3000SWxl column (Tosoh Biosciences) as stationary phase and a

detection wavelength of 280 nm.  $T_m$  values were calculated using four parameter sigmoidal fits. Errors were expressed as standard deviation (SD) of the best fit values.

#### 2.4.2.8 Chemosensitivity Assay [66]

MCF-7/Topo cells were seeded into 96-well plates at a density of 1500 cells per well (100  $\mu$ L/well) and allowed to attach to the surface of the microplates in a water-saturated atmosphere containing 5% CO<sub>2</sub> at 37 °C overnight. The next day, fresh medium containing the test compounds at 2-fold final concentrations was added (100  $\mu$ L/well; giving a final volume of 200  $\mu$ L/well). On each plate, vinblastine at a final concentration of 300 nM served as reference cytostatic (positive control); the vehicle DMSO (0.1%) served as negative control to monitor cell growth in the absence of a drug. Each concentration was measured 8-fold, positive and negative control 16-fold each. Growth of the cells was stopped after different periods of time by removal of medium and fixation with 2% (v/v) glutardialdehyde in PBS. All the plates were stored at 4 °C until the end of the experiment and afterwards stained with 0.02% crystal violet (100  $\mu$ L/well) for 20 min. Excess dye was removed by rinsing the plates with water three times. Crystal violet bound by the fixed cells was re-dissolved in 70% EtOH (180  $\mu$ L/well) while shaking the microplates for 2-3 h. The absorbance (580 nm) as a parameter proportional to the cell mass was measured using a GENios Pro microplate reader.

Cytotoxic effects were expressed as corrected T/C-values according to

$$T / C_{corr} [\%] = \frac{T - C_0}{C - C_0} \cdot 100$$

where T is the mean absorbance of the treated cells, C the mean absorbance of the negative controls and  $C_0$  the mean absorbance of the cells at the time of compound addition ( $t_0$ ). When the absorbance of treated cells T was lower than at the beginning of the experiment ( $C_0$ ), the extent of cell killing was calculated as cytotoxic effect according to

$$Cytotoxic\ effect\ [\%] = \frac{T - C_0}{C_0} \cdot 100$$

#### 2.4.2.9 Chemical Stability Assay (in Blood Plasma) [41]

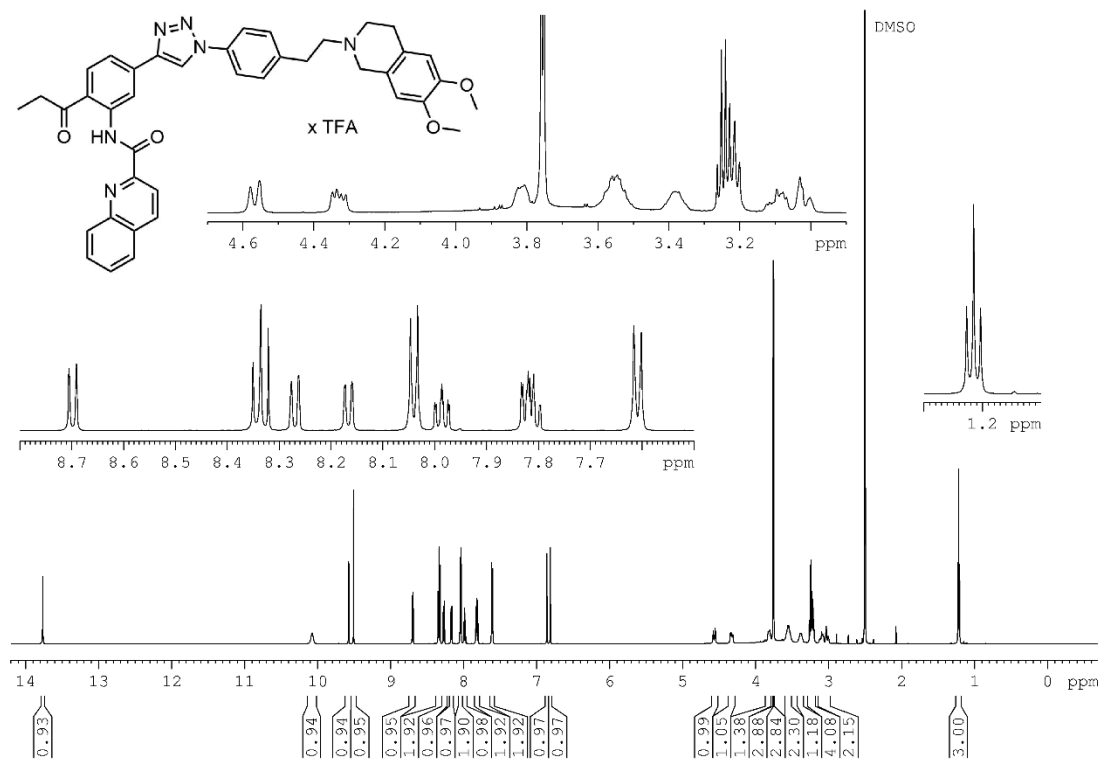
The blood from NMRI (nu/nu) mice was collected by cardiac puncture in deep anesthesia using heparinized syringes. To remove cellular components, the samples were immediately centrifuged at 4 °C and 4500 g for 7 min and the supernatant was carefully removed. The plasma samples were stored at - 80 °C.

Stock solutions of the test compounds (3 mM in DMSO) were diluted 1:50 with murine plasma giving a concentration of 60  $\mu$ M. The samples were vortexed shortly and incubated at 37 °C.

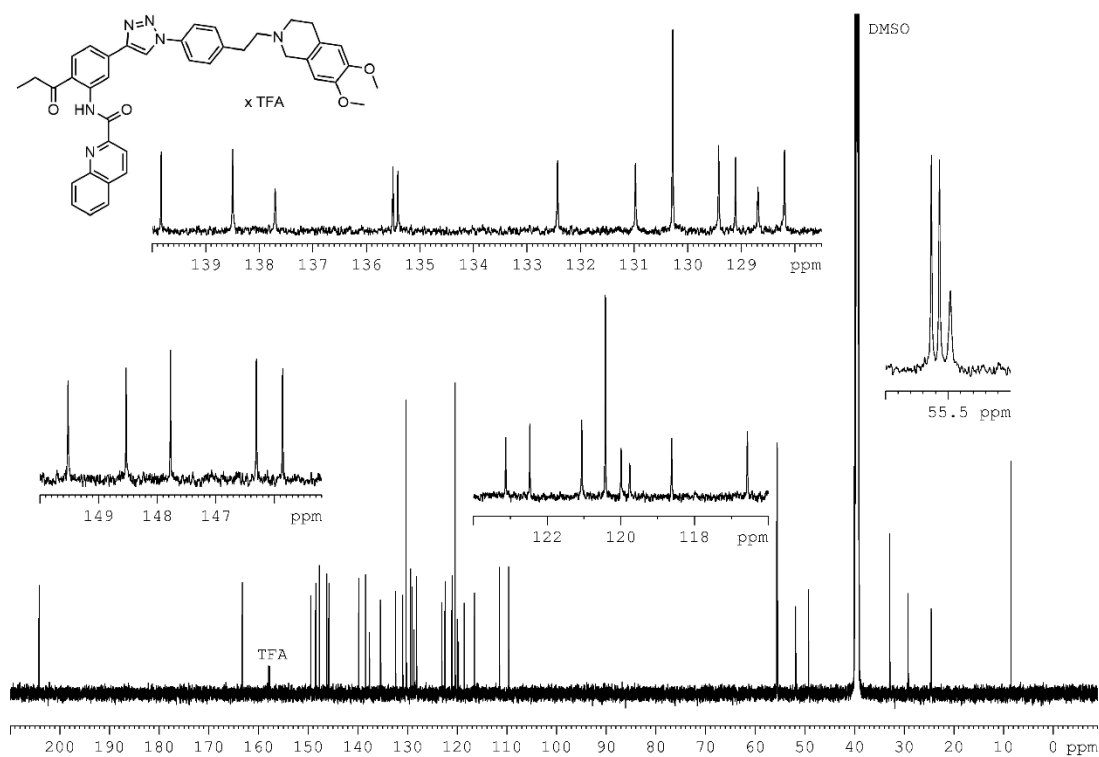
After different periods of time, aliquots were taken and deproteinated by adding two parts of ice-cold MeCN, vortexing and storing at 4 °C for 30 min. Samples were centrifuged at 4 °C and 14,000 g for 5 min and the supernatants were filtered with syringe filters, diluted 1:1 with MeCN and stored at - 80 °C until analyzed. They were thawed at room temperature and analyzed with HPLC.

## 2.5 Supplementary Material

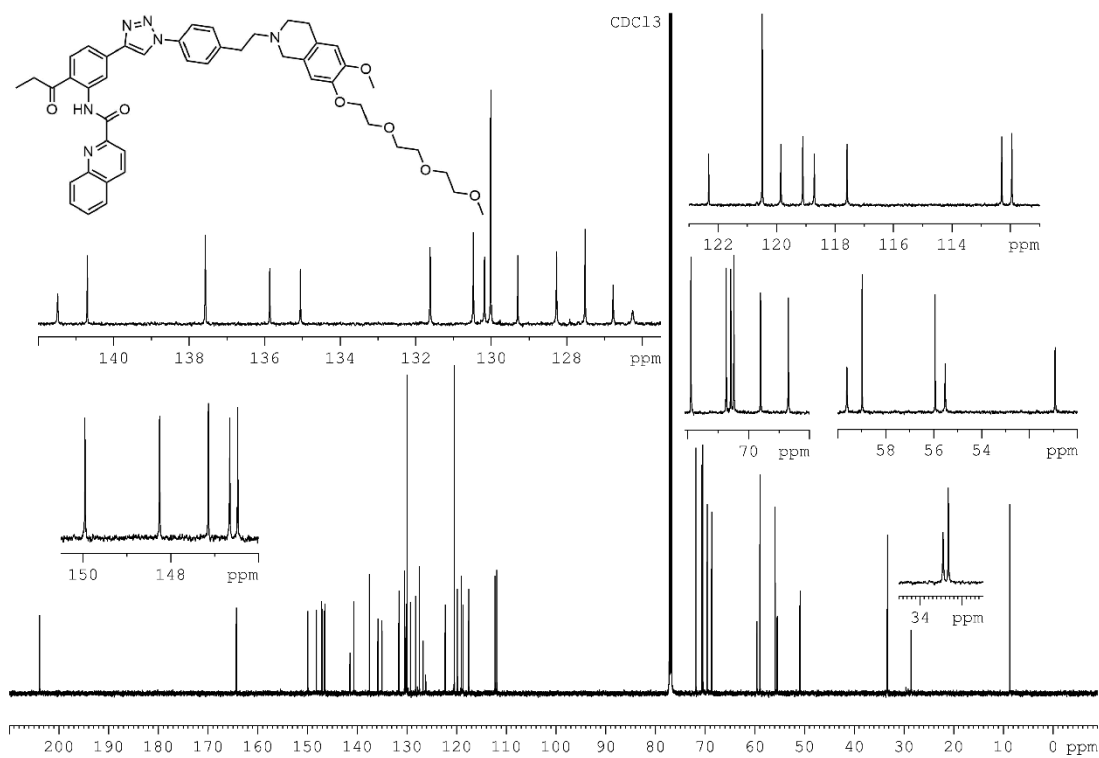
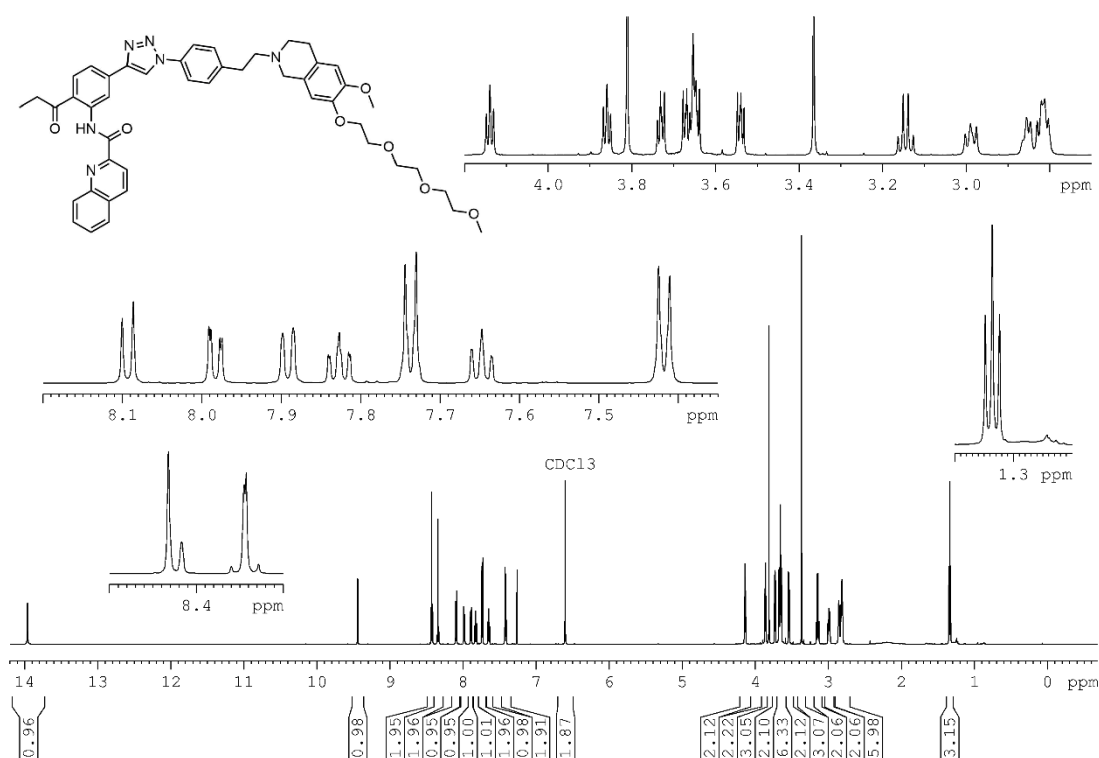
### 2.5.1 NMR-Spectra of Key Compounds



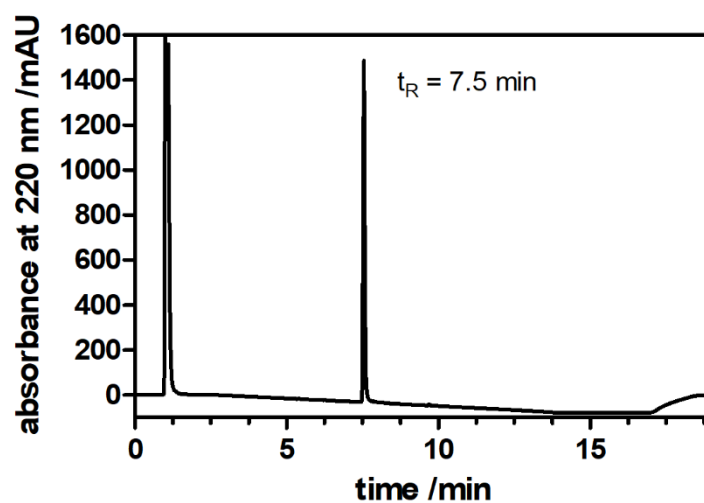
<sup>1</sup>H NMR spectrum (600 MHz, DMSO-*d*<sub>6</sub>) of compound 2.57.



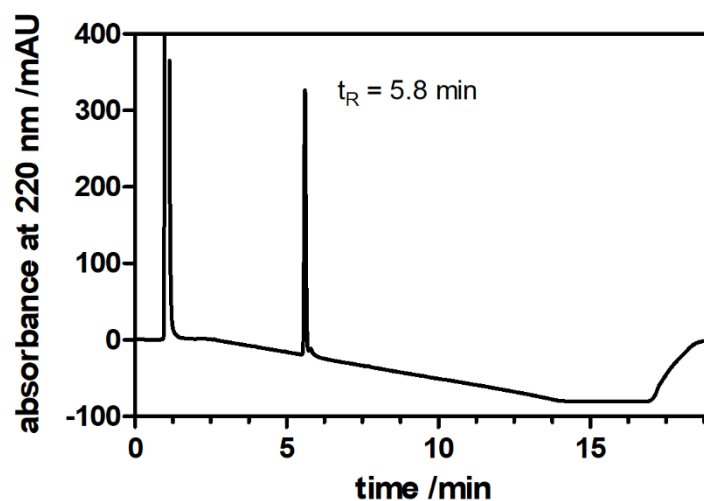
<sup>13</sup>C NMR spectrum (151 MHz, DMSO-*d*<sub>6</sub>) of compound 2.57.



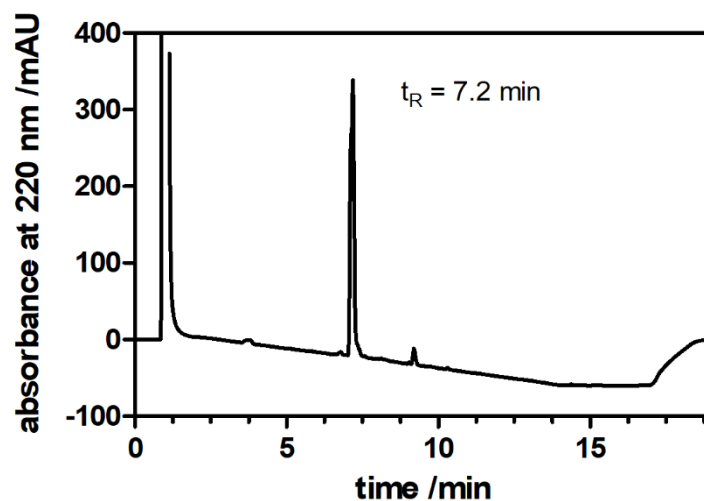
## 2.5.2 Chromatograms (Purity Control) of Key Compounds



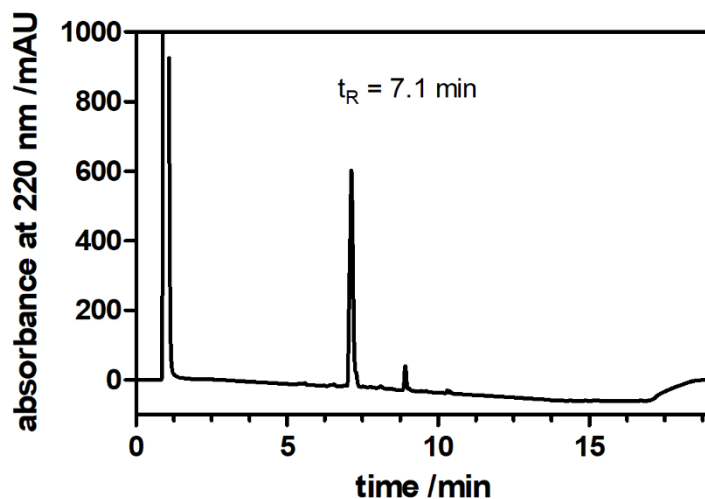
Chromatogram (purity control) of **2.07** (RP-HPLC).



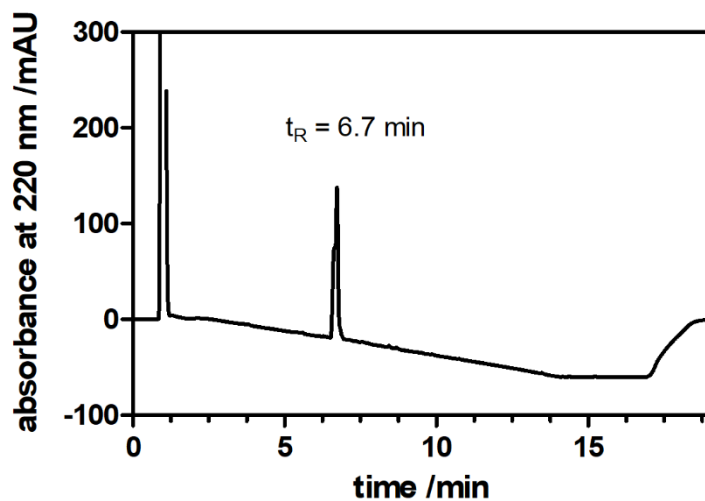
Chromatogram (purity control) of **2.08** (RP-HPLC).



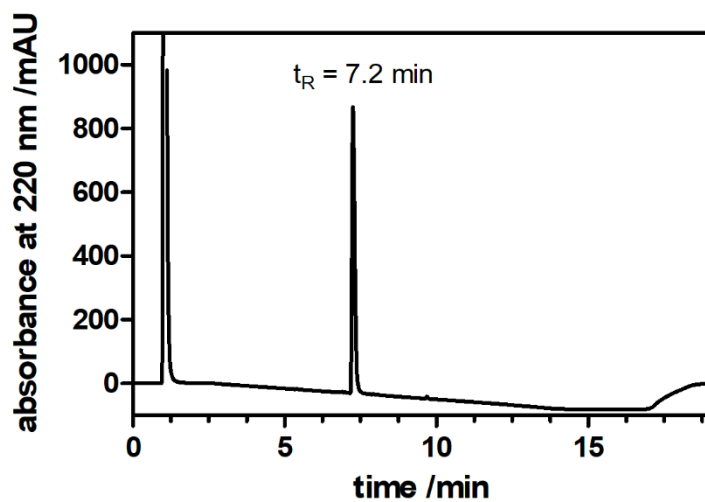
Chromatogram (purity control) of **2.41** (RP-HPLC).



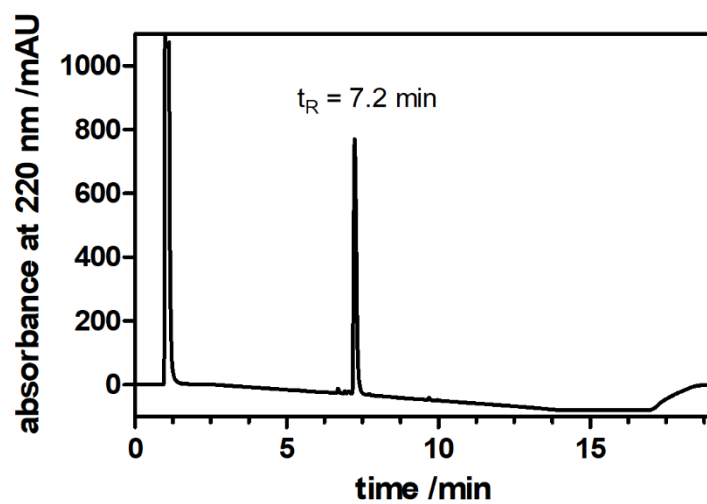
Chromatogram (purity control) of **2.42** (RP-HPLC).



Chromatogram (purity control) of **2.56** (RP-HPLC).



Chromatogram (purity control) of **2.57** (RP-HPLC).



Chromatogram (purity control) of **2.59** (RP-HPLC).

## 2.6 References

- [1] Y.N. Chen, L.A. Mickley, A.M. Schwartz, E.M. Acton, J. Hwang, A.T. Fojo, Characterization of adriamycin-resistant human breast cancer cells which display overexpression of a novel resistance-related membrane protein, *J. Biol. Chem.*, 265 (1990) 10073-10080.
- [2] L.A. Doyle, W. Yang, L.V. Abruzzo, T. Krogmann, Y. Gao, A.K. Rishi, D.D. Ross, A multidrug resistance transporter from human MCF-7 breast cancer cells, *Proc. Natl. Acad. Sci. U. S. A.*, 96 (1999) 2569.
- [3] F. Staud, P. Pavlek, Breast cancer resistance protein (BCRP/ABCG2), *Int. J. Biochem. Cell Biol.*, 37 (2005) 720-725.
- [4] M.M. Gottesman, T. Fojo, S.E. Bates, Multidrug resistance in cancer: role of ATP-dependent transporters, *Nat. Rev. Cancer*, 2 (2002) 48-58.
- [5] H.R. Mellor, R. Callaghan, Resistance to Chemotherapy in Cancer: A Complex and Integrated Cellular Response, *Pharmacology*, 81 (2008) 275-300.
- [6] B.C. Baguley, Multiple Drug Resistance Mechanisms in Cancer, *Mol. Biotechnol.*, 46 (2010) 308-316.
- [7] R.W. Robey, K.M. Pluchino, M.D. Hall, A.T. Fojo, S.E. Bates, M.M. Gottesman, Revisiting the role of ABC transporters in multidrug-resistant cancer, *Nat. Rev. Cancer*, 18 (2018) 452-464.
- [8] D.J. Begley, ABC transporters and the blood-brain barrier, *Curr. Pharm. Des.*, 10 (2004) 1295-1312.
- [9] C. Ghosh, V. Puvenna, J. Gonzalez-Martinez, D. Janigro, N. Marchi, Blood-brain barrier P450 enzymes and multidrug transporters in drug resistance: a synergistic role in neurological diseases, *Curr. Drug Metab.*, 12 (2011) 742-749.
- [10] A. Mahringer, G. Fricker, ABC transporters at the blood-brain barrier, *Expert Opin. Drug Metab. Toxicol.*, 12 (2016) 499-508.
- [11] M. Hubensack, C. Mueller, P. Hoecherl, S. Fellner, T. Spruss, G. Bernhardt, A. Buschauer, Effect of the ABCB1 modulators elacridar and tariquidar on the distribution of paclitaxel in nude mice, *J. Cancer Res. Clin. Oncol.*, 134 (2008) 597-607.
- [12] M.H. Hasanabady, F. Kalalinia, ABCG2 inhibition as a therapeutic approach for overcoming multidrug resistance in cancer, *J. Biosci.*, 41 (2016) 313-324.
- [13] J.W. Ricci, D.M. Lovato, V. Severns, L.A. Sklar, R.S. Larson, Novel ABCG2 Antagonists Reverse Topotecan-Mediated Chemotherapeutic Resistance in Ovarian Carcinoma Xenografts, *Mol. Cancer Ther.*, 15 (2016) 2853-2862.
- [14] M.C. de Gooijer, N.A. de Vries, T. Buckle, L.C.M. Buil, J.H. Beijnen, W. Boogerd, O. van Tellingen, Improved Brain Penetration and Antitumor Efficacy of Temozolomide by Inhibition of ABCB1 and ABCG2, *Neoplasia*, 20 (2018) 710-720.
- [15] A. Karbownik, K. Sobańska, W. Płotek, T. Grabowski, A. Klupczynska, S. Plewa, E. Grześkowiak, E. Szałek, The influence of the coadministration of the p-glycoprotein modulator elacridar on the pharmacokinetics of lapatinib and its distribution in the brain and cerebrospinal fluid, *Invest. New Drugs*, (2019) Ahead of Print.
- [16] M. Bauer, R. Karch, B. Wulkersdorfer, C. Philippe, L. Nics, E.-M. Klebermass, M. Weber, S. Poschner, H. Haslacher, W. Jaeger, N. Tournier, W. Wadsak, M. Hacker, M. Zeitlinger, O. Langer, A proof-of-concept study to inhibit ABCG2- and ABCB1- mediated efflux transport at the human blood-brain barrier, *J. Nucl. Med.*, 60 (2019) 486-491.
- [17] S. Dauchy, F. Dutheil, R.J. Weaver, F. Chassoux, C. Daumas-Duport, P.-O. Couraud, J.-M. Scherrmann, I. De Waziers, X. Decleves, ABC transporters, cytochromes P450 and their main transcription factors: expression at the human blood-brain barrier, *J. Neurochem.*, 107 (2008) 1518-1528.

- [18] R. Shawahna, Y. Uchida, X. Decleves, S. Ohtsuki, S. Yousif, S. Dauchy, A. Jacob, F. Chassoux, C. Daumas-Duport, P.-O. Couraud, T. Terasaki, J.-M. Scherrmann, Transcriptomic and Quantitative Proteomic Analysis of Transporters and Drug Metabolizing Enzymes in Freshly Isolated Human Brain Microvessels, *Mol. Pharmaceutics*, 8 (2011) 1332-1341.
- [19] F. Hyafil, C. Vergely, P. Du Vignaud, T. Grand-Perret, In vitro and in vivo reversal of multidrug resistance by GF120918, an acridonecarboxamide derivative, *Cancer Res.*, 53 (1993) 4595-4602.
- [20] M. de Bruin, K. Miyake, T. Litman, R. Robey, S.E. Bates, Reversal of resistance by GF120918 in cell lines expressing the ABC half-transporter, MXR, *Cancer Lett.*, 146 (1999) 117-126.
- [21] M. Roe, A. Folkes, P. Ashworth, J. Brumwell, L. Chima, S. Hunjan, I. Pretswell, W. Dangerfield, H. Ryder, P. Charlton, Reversal of P-glycoprotein mediated multidrug resistance by novel anthranilamide derivatives, *Bioorg. Med. Chem. Lett.*, 9 (1999) 595-600.
- [22] R.W. Robey, K. Steadman, O. Polgar, K. Morisaki, M. Blayney, P. Mistry, S.E. Bates, Pheophorbide a Is a Specific Probe for ABCG2 Function and Inhibition, *Cancer Res.*, 64 (2004) 1242-1246.
- [23] S.K. Rabindran, H. He, M. Singh, E. Brown, K.I. Collins, T. Annable, L.M. Greenberger, Reversal of a novel multidrug resistance mechanism in human colon carcinoma cells by fumitremorgin C, *Cancer Res.*, 58 (1998) 5850-5858.
- [24] J.D. Allen, A. Van Loevezijn, J.M. Lakhai, M. Van der Valk, O. Van Tellingen, G. Reid, J.H.M. Schellens, G.-J. Koomen, A.H. Schinkel, Potent and specific inhibition of the breast cancer resistance protein multidrug transporter in vitro and in mouse intestine by a novel analogue of fumitremorgin C, *Mol. Cancer Ther.*, 1 (2002) 417-425.
- [25] L.D. Weidner, S.S. Zoghbi, S. Lu, S. Shukla, S.V. Ambudkar, V.W. Pike, J. Mulder, M.M. Gottesman, R.B. Innis, M.D. Hall, The inhibitor Ko143 is not specific for ABCG2, *J. Pharmacol. Exp. Ther.*, 354 (2015) 384-393.
- [26] S.A.L. Zander, J.H. Beijnen, O. van Tellingen, Sensitive method for plasma and tumor Ko143 quantification using reversed-phase high-performance liquid chromatography and fluorescence detection, *J. Chromatogr. B: Anal. Technol. Biomed. Life Sci.*, 913-914 (2013) 129-136.
- [27] K. Liu, J. Zhu, Y. Huang, C. Li, J. Lu, M. Sachar, S. Li, X. Ma, Metabolism of Ko143, an ABCG2 inhibitor, *Drug Metab. Pharmacokinet.*, 32 (2017) 193-200.
- [28] A. Spindler, K. Stefan, M. Wiese, Synthesis and Investigation of Tetrahydro- $\beta$ -carboline Derivatives as Inhibitors of the Breast Cancer Resistance Protein (ABCG2), *J. Med. Chem.*, 59 (2016) 6121-6135.
- [29] W. Chearwae, S. Shukla, P. Limtrakul, S.V. Ambudkar, Modulation of the function of the multidrug resistance-linked ATP-binding cassette transporter ABCG2 by the cancer chemopreventive agent curcumin, *Mol. Cancer Ther.*, 5 (2006) 1995-2006.
- [30] E. Nicolle, J. Boccard, D. Guilet, M.-G. Dijoux-Franca, F. Zelefac, S. Macalou, J. Grosselin, J. Schmidt, P.-A. Carrupt, A. Di Pietro, A. Boumendjel, Breast cancer resistance protein (BCRP/ABCG2): New inhibitors and QSAR studies by a 3D linear solvation energy approach, *Eur. J. Pharm. Sci.*, 38 (2009) 39-46.
- [31] K. Takada, N. Imamura, K.R. Gustafson, C.J. Henrich, Synthesis and structure-activity relationship of botryllamides that block the ABCG2 multidrug transporter, *Bioorg. Med. Chem. Lett.*, 20 (2010) 1330-1333.
- [32] J. Gallus, K. Juvala, M. Wiese, Characterization of 3-methoxy flavones for their interaction with ABCG2 as suggested by ATPase activity, *Biochim. Biophys. Acta, Biomembr.*, 1838 (2014) 2929-2938.
- [33] N. Sjostedt, K. Holvikari, P. Tammela, H. Kidron, Inhibition of Breast Cancer Resistance Protein and Multidrug Resistance Associated Protein 2 by Natural Compounds and Their Derivatives, *Mol. Pharmaceutics*, 14 (2017) 135-146.

- [34] K. Silbermann, C.P. Shah, N.U. Sahu, K. Juvalé, S.M. Stefan, P.S. Kharkar, M. Wiese, Novel chalcone and flavone derivatives as selective and dual inhibitors of the transport proteins ABCB1 and ABCG2, *Eur. J. Med. Chem.*, 164 (2019) 193-213.
- [35] G. Valdameri, E. Genoux-Bastide, B. Peres, C. Gauthier, J. Guitton, R. Terreux, S.M.B. Winnischofer, M.E.M. Rocha, A. Boumendjel, A. Di Pietro, Substituted Chromones as Highly Potent Nontoxic Inhibitors, Specific for the Breast Cancer Resistance Protein, *J. Med. Chem.*, 55 (2012) 966-970.
- [36] R. Yamazaki, H. Hatano, T. Yaegashi, Y. Igarashi, O. Yoshida, Y. Sugimoto, Preparation of 3-[4-(4-hydroxypiperidin-1-yl)thiophen-2-yl]-2-phenylacrylonitrile 2-(cyclic amino)acetyl esters as breast cancer resistance protein (ABCG2) inhibitors, WO2009072267A1, 2009.
- [37] R. Yamazaki, Y. Nishiyama, T. Furuta, H. Hatano, Y. Igarashi, N. Asakawa, H. Kodaira, H. Takahashi, R. Aiyama, T. Matsuzaki, N. Yagi, Y. Sugimoto, Novel Acrylonitrile Derivatives, YHO-13177 and YHO-13351, Reverse BCRP/ABCG2-Mediated Drug Resistance In Vitro and In Vivo, *Mol. Cancer Ther.*, 10 (2011) 1252-1263.
- [38] N.M.I. Taylor, I. Manolaridis, S.M. Jackson, J. Kowal, H. Stahlberg, K.P. Locher, Structure of the human multidrug transporter ABCG2, *Nature*, 546 (2017) 504-509.
- [39] S.M. Jackson, I. Manolaridis, J. Kowal, M. Zechner, N.M.I. Taylor, M. Bause, S. Bauer, R. Bartholomaeus, G. Bernhardt, B. Koenig, A. Buschauer, H. Stahlberg, K.-H. Altmann, K.P. Locher, Structural basis of small-molecule inhibition of human multidrug transporter ABCG2, *Nat. Struct. Mol. Biol.*, 25 (2018) 333-340.
- [40] M. Kühnle, M. Egger, C. Müller, A. Mahringer, G. Bernhardt, G. Fricker, B. König, A. Buschauer, Potent and Selective Inhibitors of Breast Cancer Resistance Protein (ABCG2) Derived from the p-Glycoprotein (ABCB1) Modulator Tariquidar, *J. Med. Chem.*, 52 (2009) 1190-1197.
- [41] S. Bauer, C. Ochoa-Puentes, Q. Sun, M. Bause, G. Bernhardt, B. Koenig, A. Buschauer, Quinoline Carboxamide-Type ABCG2 Modulators: Indole and Quinoline Moieties as Anilide Replacements, *ChemMedChem*, 8 (2013) 1773-1778.
- [42] L. Liang, D. Astruc, The copper(I)-catalyzed alkyne-azide cycloaddition (CuAAC) "click" reaction and its applications. An overview, *Coord. Chem. Rev.*, 255 (2011) 2933-2945.
- [43] T.R. Chan, R. Hilgraf, K.B. Sharpless, V.V. Fokin, Polytriazoles as Copper(I)-Stabilizing Ligands in Catalysis, *Org. Lett.*, 6 (2004) 2853-2855.
- [44] C.O. Puentes, P. Höcherl, M. Kühnle, S. Bauer, K. Bürger, G. Bernhardt, A. Buschauer, B. König, Solid phase synthesis of tariquidar-related modulators of ABC transporters preferring breast cancer resistance protein (ABCG2), *Bioorg. Med. Chem. Lett.*, 21 (2011) 3654-3657.
- [45] C. Ochoa-Puentes, S. Bauer, M. Kühnle, G. Bernhardt, A. Buschauer, B. König, Benzanilide-Biphenyl Replacement: A Bioisosteric Approach to Quinoline Carboxamide-Type ABCG2 Modulators, *ACS Med. Chem. Lett.*, 4 (2013) 393-396.
- [46] J.E. Obrique-Balboa, Q. Sun, G. Bernhardt, B. König, A. Buschauer, Flavonoid derivatives as selective ABCC1 modulators: Synthesis and functional characterization, *Eur. J. Med. Chem.*, 109 (2016) 124-133.
- [47] S. Kraege, K. Stefan, K. Juvalé, T. Ross, T. Willmes, M. Wiese, The combination of quinazoline and chalcone moieties leads to novel potent heterodimeric modulators of breast cancer resistance protein (BCRP/ABCG2), *Eur. J. Med. Chem.*, 117 (2016) 212-229.
- [48] T. Litman, T.E. Druley, W.D. Stein, S.E. Bates, From MDR to MXR: new understanding of multidrug resistance systems, their properties and clinical significance, *Cell. Mol. Life Sci.*, 58 (2001) 931-959.
- [49] T. Reya, S.J. Morrison, M.F. Clarke, I.L. Weissman, Stem cells, cancer, and cancer stem cells, *Nature*, 414 (2001) 105-111.
- [50] H. Itatani, J.C. Bailar, Homogenous catalysis in the reactions of olefinic substances. V. Hydrogenation of soybean oil methyl ester with triphenylphosphine and triphenylarsine palladium catalysts, *J. Am. Oil Chem. Soc.*, 44 (1967) 147-151.

- [51] G. Palmisano, G. Lesma, M. Nali, B. Rindone, S. Tollari, A mild and chemoselective reduction of cyclic iminium salts, *Synthesis*, (1985) 1072-1074.
- [52] A. Heckel, R. Walter, W. Grell, J.C.A. Van Meel, N. Redemann, Aminomethyleneindolinones with antitumor activity, WO9962882A1, 1999.
- [53] W. Klinkhammer, H. Mueller, C. Globisch, I.K. Pajeva, M. Wiese, Synthesis and biological evaluation of a small molecule library of 3rd generation multidrug resistance modulators, *Bioorg. Med. Chem.*, 17 (2009) 2524-2535.
- [54] T.A. Davidson, R.C. Griffith, N-[Amino(or hydroxy)phenethyl]-1,2,3,4-tetrahydroisoquinolines and precursors, EP51190A2, 1982.
- [55] N. Dodic, B. Dumaitre, A. Daugan, P. Pianetti, Synthesis and Activity against Multidrug Resistance in Chinese Hamster Ovary Cells of New Acridone-4-carboxamides, *J. Med. Chem.*, 38 (1995) 2418-2426.
- [56] B. Liu, Q. Qiu, T. Zhao, L. Jiao, J. Hou, Y. Li, H. Qian, W. Huang, Discovery of Novel P-Glycoprotein-Mediated Multidrug Resistance Inhibitors Bearing Triazole Core via Click Chemistry, *Chem. Biol. Drug Des.*, 84 (2014) 182-191.
- [57] G.A. Gazzaeva, M.I. Khasanov, S.S. Mochalov, N.S. Zefirov, 4H-3,1-Benzoxazines from ortho-aminoacylbenzenes, *Chem. Heterocycl. Compd.*, 43 (2007) 799-810.
- [58] M. Hubensack, Approaches to Overcome the Blood-Brain Barrier in the Chemotherapy of Primary and Secondary Brain Tumors: Modulation of P-glycoprotein 170 and Targeting of the Transferrin Receptor, Dissertation, University of Regensburg, 2005, <https://epub.uni-regensburg.de/10297/>.
- [59] C.-H. Yang, E. Schneider, M.-L. Kuo, E.L. Volk, E. Rocchi, Y.-C. Chen, BCRP/MXR/ABCP expression in topotecan-resistant human breast carcinoma cells, *Biochem. Pharmacol.*, 60 (2000) 831-837.
- [60] K. Kohno, J. Kikuchi, S. Sato, H. Takano, Y. Saburi, K. Asoh, M. Kuwano, Vincristine-resistant human cancer KB cell line and increased expression of multidrug-resistance gene, *Jpn. J. Cancer Res.*, 79 (1988) 1238-1246.
- [61] R. Evers, M. Kool, L. van Deemter, H. Janssen, J. Calafat, L.C. Oomen, C.C. Paulusma, R.P. Oude Elferink, F. Baas, A.H. Schinkel, P. Borst, Drug export activity of the human canalicular multispecific organic anion transporter in polarized kidney MDCK cells expressing cMOAT (MRP2) cDNA, *J. Clin. Invest.*, 101 (1998) 1310-1319.
- [62] E. Bakos, R. Evers, G. Szakacs, G.E. Tusnady, E. Welker, K. Szabo, M. De Haas, L. Van Deemter, P. Borst, A. Varadi, B. Sarkadi, Functional multidrug resistance protein (MRP1) lacking the N-terminal transmembrane domain, *J. Biol. Chem.*, 273 (1998) 32167-32175.
- [63] B. Sarkadi, E.M. Price, R.C. Boucher, U.A. Germann, G.A. Scarborough, Expression of the human multidrug resistance cDNA in insect cells generates a high activity drug-stimulated membrane ATPase, *J. Biol. Chem.*, 267 (1992) 4854-4858.
- [64] A. Telbisz, M. Mueller, C. Ozvegy-Laczka, L. Homolya, L. Szente, A. Varadi, B. Sarkadi, Membrane cholesterol selectively modulates the activity of the human ABCG2 multidrug transporter, *Biochim. Biophys. Acta, Biomembr.*, 1768 (2007) 2698-2713.
- [65] A. Pal, D. Mehn, E. Molnar, S. Gedey, P. Meszaros, T. Nagy, H. Glavinas, T. Janaky, O. von Richter, G. Bathori, L. Szente, P. Krajcsi, Cholesterol potentiates ABCG2 activity in a heterologous expression system: improved in vitro model to study function of human ABCG2, *J. Pharmacol. Exp. Ther.*, 321 (2007) 1085-1094.
- [66] G. Bernhardt, H. Reile, H. Birnböck, T. Spruß, H. Schönenberger, Standardized kinetic microassay to quantify differential chemosensitivity on the basis of proliferative activity, *J. Cancer Res. Clin. Oncol.*, 118 (1992) 35-43.



# **3 Water-Soluble Inhibitors of ABCG2 (BCRP) – A Fragment-Based and Computational Approach**

Prior to the submission of this thesis, this chapter was submitted slightly modified for publication:

F. Antoni\*, D. Wifling, G. Bernhardt, Water-soluble inhibitors of ABCG2 (BCRP) – a fragment-based and computational approach, Eur. J. Med. Chem., (2020) 112958.

<https://doi.org/10.1016/j.ejmech.2020.112958>

Author contributions:

F.A. conceived the project with input from the co-authors. F.A. designed the target structures; **3.48**, **3.49** and **3.50** were designed by F.A. and D.W. together. D.W. performed the molecular docking studies. F.A. performed the synthesis, the biological assays, the solubility assays and the data analysis with G.B. as a supervisor. F.A. wrote the manuscript with input from all co-authors.

\*Corresponding author

## 3.1 Introduction

Water solubility of a compound is indispensable for its biological activity: undissolved, a molecule cannot reach its target. This is a simple fact, however often undervalued. There is a general tendency in drug discovery towards large and lipophilic molecules – such compounds are more likely to be identified as ‘hits’ in high-throughput screenings (in which the compounds are added ‘pre-dissolved’ in DMSO) [1,2], and during the optimization of the ‘hits’ often additional lipophilic substituents are attached [3]. The dilemma is that higher lipophilicity is strongly connected with increased in vitro activity [2,4], because hydrophobic interactions are the dominant driving forces in small-molecule ligand-protein binding processes [5,6]. Frequently, drug discovery strategies lead to a substance with high activity and selectivity but very poor aqueous solubility [1,2].

This phenomenon causes immense problems, because aqueous solubility plays an essential role in virtually every phase of the discovery and development of pharmacological tools and drugs [3,7]. It already begins in the purification process, where RP-HPLC is commonly the method of choice, for which the substance needs to be dissolved in a water-containing eluent. In biological in vitro studies, low solubility leads to erratic and erroneous assay results [3]. If precipitation occurs before the compound can reach its target, the actual concentration is lower than intended and the substance appears less active [3,8]. Hence, structure-activity relationship analyses are compromised [9] and off-target activities may become undetectable [3]. In vivo, after oral administration, poor water solubility results in inadequate resorption [1-3,8,10]. Self-evidently, the compound needs to be dissolved in the aqueous gastrointestinal fluids in order to cross the intestinal membranes, and the flux (passive diffusion) is directly proportional to the concentration gradient of the agent between the intestinal lumen and the blood [1]. Poorly soluble compounds are particularly susceptible to food effects (on drug absorption) and often special excipients are required, which can impair the results of in vivo studies [3]. Not only oral drug forms, but also parenteral formulations depend heavily on sufficient aqueous solubility, water being the solvent of choice for intravenous administration [10]. Furthermore, in organisms, poorly soluble drugs may precipitate at high concentrations and cause adverse effects such as phlebitis [11]. Taken together, sufficient aqueous solubility is of major importance for both drugs and pharmacological tools and low solubility of drug candidates has been the cause of numerous failures in drug development [12].

When addressing solubility problems, formulation technology can help, but this approach is expensive and there is no guarantee of success [1-3,9]. Therefore, the primary strategy should be to improve solubility by adequate alterations of the chemical structure of the molecule [2,9,13]. Such structural changes fall into three categories: they aim either at (I) decreasing the

crystal packing energy, e.g. by disrupting planarity, [2,7,13-15] (II) increasing the solvation energy, for example by attaching polar or ionizable groups [2,7,13,15] or at (III) reducing the cavitation energy [16] – required to form a cavity in the water structure in order to host the solute molecule, which results in a concomitant decrease in entropy – for instance by reducing the size of the molecule [2,15]. Whether these structural changes actually enhance the solubility is hard to predict, also when *in silico* methods are applied [2]. In 1997, Lipinski et al. published their seminal article on the well-known ‘rule of five’ (Ro5) [1]. Using a library of drugs with ‘good’ resorption properties (i.e. drugs that passed clinical Phase II selection), the group identified four calculable parameters to estimate resorption by free diffusion, a process which is dependent on sufficient solubility and permeability. The authors concluded that resorption problems are more likely to occur, when there are more than five H-bond donors, ten H-bond acceptors, the molecular weight (MWT) is higher than 500 Da and the calculated logP (clogP) is higher than five (all values are five or multiples thereof) [1]. Since then, a couple of drugs that are Ro5-outliers have emerged (e.g. the anticancer drug Navitoclax [17]), but the bottom line of articles on the subject is mostly the same: the development of ‘beyond-Ro5’ drugs is feasible and for some targets necessary, but extremely difficult, and there is a high probability of failure [18-20]. Therefore, medicinal chemists are well-advised to take the Ro5 into consideration when designing novel chemical entities.

Ultimately, with the designed compound in hand, solubility can be assessed experimentally to find out if the solubility-optimization process was successful. Usually a distinction is made between the kinetic and the thermodynamic (equilibrium) solubility of a compound (c.f. Section 3.2.4). What levels of equilibrium solubility are required for pharmacological tools and drugs is debated, but a range between 1  $\mu$ M to 0.1 M may be considered as a drug solubility window [21]. As a rule of thumb, the solubility of a compound should be at least three times its IC<sub>50</sub> value [22].

The target we address in this study – ABCG2 – is a member of the ATP-binding cassette (ABC) transporter superfamily [23]. It functions as an exporter and is predominantly expressed in the plasma membrane [24]. Inhibitors of ABCG2 have been developed as pharmacological tools to study the patho(physiological) role of this transporter and as a means to overcome the blood-brain barrier (BBB) [25] or multidrug resistance (MDR) in cancer [26]. During the development of ABCG2 inhibitors the focus has been on optimizing their potency and selectivity. In a few cases [27,28], efforts have been made to improve some of their drug-like (i.e. ADME-Tox) properties, mainly to increase their stability or decrease their toxicity. But their physicochemical properties, especially their water solubility, have been neglected so far. Aqueous solubility has not been a parameter much taken into consideration and up to now no solubility-driven optimization of ABCG2 inhibitors has been reported. The outcome is that most ABCG2

inhibitors described so far are relatively large and lipophilic molecules. Increasing the aqueous solubility of ABCG2 inhibitors is a great challenge, because ABCG2, much more than many other targets, requires ligands that show high lipophilicity and size. In contrast to ligands of membrane-spanning receptors, an ABCG2 inhibitor must permeate through the cell membrane to reach its target, i.e. the multidrug binding site, which was recently identified by cryo-EM studies [29,30]. Moreover, as revealed in the aforementioned structural studies, the binding site is comparatively large and markedly hydrophobic.

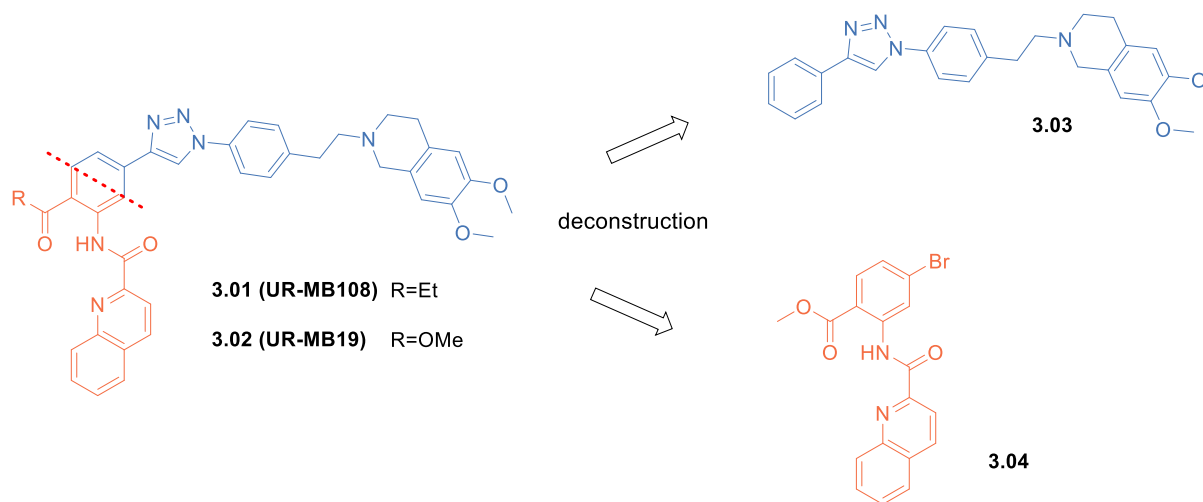


**Figure 3.1.** Our previous tariquidar-related ABCG2 inhibitors UR-MB108 (**3.01**) and UR-MB19 (**3.02**) and rationale of our fragment-based approach: deconstruction of **3.02** to the fragments **3.03** and **3.04**.

Previously we reported on tariquidar-related triazoles (such as UR-MB108 (**3.01**); Figure 3.1 as selective and stable inhibitors of ABCG2 [28]. Inhibitor **3.01** acted as a potent and effective ABCG2 transport and ATPase inhibitor. Accordingly, it appeared to stay in solution at least for the short time span of the transport and ATPase assay. Unfortunately – preempting one result of the present study – the equilibrium solubility of inhibitor **3.01** was as low as 78 nM, neither reaching the level of at least 1  $\mu$ M mentioned above, nor fulfilling the rule of thumb, the  $IC_{50}$  value of **3.01** also being around 80 nM. In the present study, we set out to design and prepare potent and stable ABCG2 inhibitors with improved equilibrium water solubility, using our previous inhibitors (**3.01** and UR-MB19 (**3.02**); Figure 3.1) as a starting point. To this end, we pursued a fragment-based approach, which we considered suitable for our predicament because of the following reasons: high-affinity ligands that are small have been shown to bind with favorable enthalpy, dominated by optimal polar interactions [31,32], whereas for larger ligands entropy changes become increasingly important (coming mainly from the desolvation; water molecules from the solvation shell are released and join bulk water) [31,32]. Therefore, ligands optimized in a fragment-based approach are more likely to be relatively low in hydrophobicity and small in size [31,32]. Moreover, fragments are easier to prepare synthetically, so this strategy is also time-saving. Figure 3.1 shows the rationale of our fragment-based approach:

compound **3.02** was ‘deconstructed’ to the fragments **3.03** and **3.04** for analysis and optimization. When ‘enlarging’ the new fragments to obtain potent and soluble inhibitors, we took advantage of the recently published cryo-EM structure of ABCG2 in complex with inhibitors [29], too, and used molecular docking studies to optimize protein-ligand interactions. In addition, we considered Lipinski’s Ro5 when designing our novel inhibitors. Furthermore, we established thermodynamic and kinetic solubility assays suitable for analyzing compounds in the comparatively low solubility range of ABCG2 inhibitors.

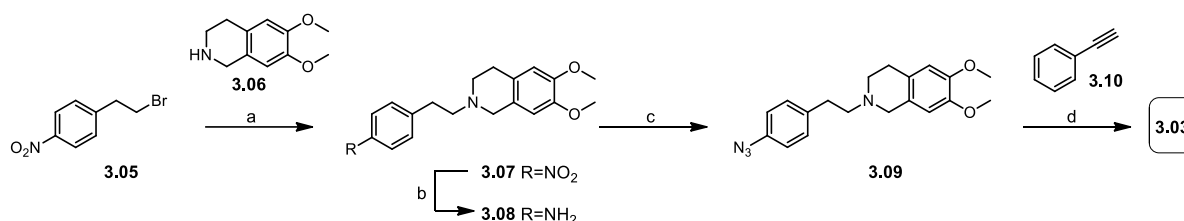
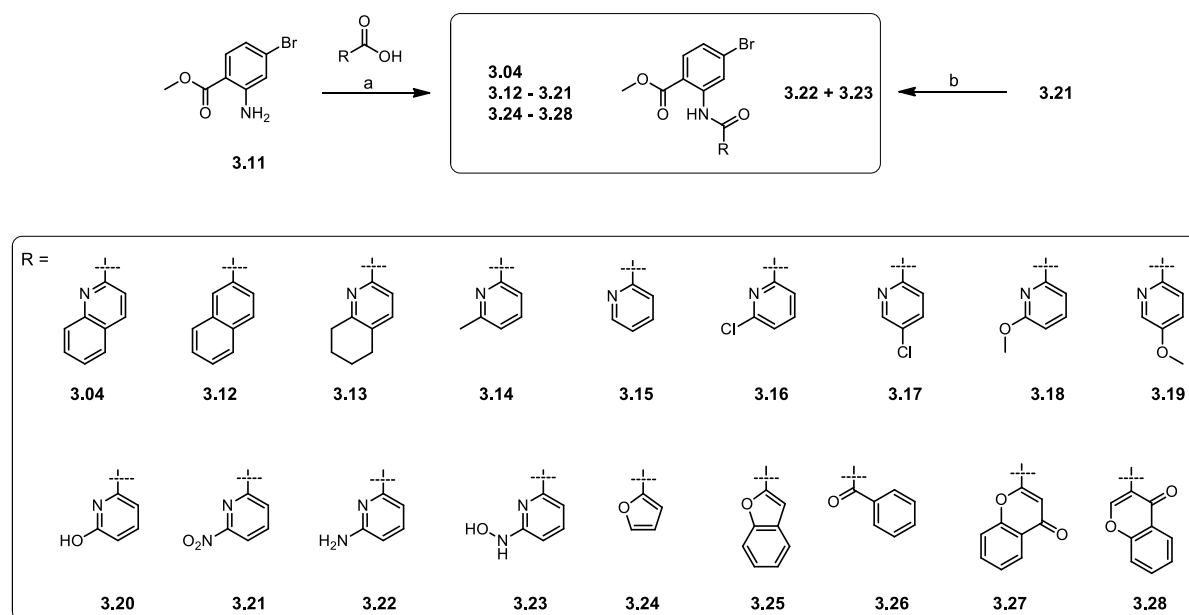
## 3.2 Results and Discussion

### 3.2.1 Design and Synthesis

We designed fragment **3.04** in a way that it contains a more readily accessible ester moiety (like in **3.02**), instead of a more stable ketone function (as in **3.01**), because stability was not an issue in case of the fragments; they merely served as a starting point for structural optimizations and ‘enlarging’ or merging/linking with other fragments to obtain potent inhibitors. The introduction of a ketone group only gave very low yields, whereas the building block comprising the ester was commercially available.

The synthesis of the fragments **3.03** and **3.04** is shown in Scheme 3.1. Compound **3.03** was prepared in a copper-catalyzed azide-alkyne cycloaddition (CuAAC), belonging to a set of synthetic procedures termed ‘click’ reactions due to their convenience, versatility and achievement of high yields [33]. The azide for the ‘click’ reaction was synthesized according to our previous report [28]. 1-(2-bromoethyl)-4-nitrobenzene (**3.05**) was treated with 6,7-dimethoxy-1,2,3,4-tetrahydroisoquinoline (**3.06**) in an N-alkylation reaction to give compound **3.07**, then the nitro group was hydrogenated to an amine group (yielding **3.08**) and converted to an azide, resulting in compound **3.09**, which was introduced into a ‘click’ reaction with phenylacetylene (**3.10**). In this variant of the CuAAC we used the polytriazole TBTA as a copper(I)-stabilizing ligand.

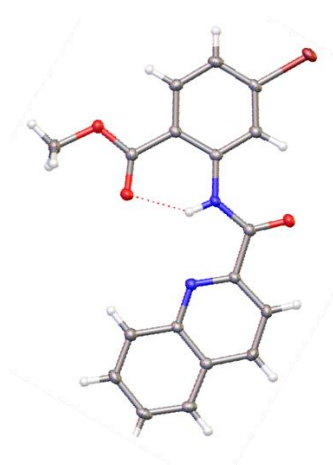
Fragment **3.04** was synthesized by amide bond formation from methyl 2-amino-4-bromobenzoate (**3.11**) and quinoline-2-carboxylic acid, using TBTU as a coupling reagent. Compound **3.11** is a building block of our previous inhibitor **3.02** and was therefore abundantly available in our laboratory. In pursuit of convenient, fast and economic procedures, we used **3.11** for synthesizing compound **3.04** (and further fragments), which is the reason for the presence of bromine in the respective substructure.

**A**

**B**


**Scheme 3.1.** (A) Synthesis of fragment **3.03**. Reagents and conditions: (a)  $\text{K}_2\text{CO}_3$ , MeCN,  $130^\circ\text{C}$  (microwave), 70 min; (b) Pd/C,  $\text{H}_2$  (10 bar), EtOH, rt, overnight; (c) (I)  $\text{NaNO}_2$ , 6 M HCl aq,  $0^\circ\text{C}$ , 1 h; (II)  $\text{NaN}_3$ ,  $0^\circ\text{C} \rightarrow \text{rt}$ , 2 h; (d)  $\text{CuSO}_4$ , sodium ascorbate, TBTA,  $\text{CHCl}_3$ , reflux, 1 d. (B) Synthesis of the fragments **3.04** and **3.12-3.28**. Reagents and conditions: (a) respective carboxylic acid, TBTU, DIPEA, DMF,  $80^\circ\text{C}$  (microwave), 30 min; or respective carboxylic acid chloride (carboxylic acid,  $\text{SOCl}_2$ , pyridine, toluene, reflux, 2 h), DIPEA, DCM,  $0^\circ\text{C}$ , overnight; (b)  $\text{HSiCl}_3$ , DIPEA, DCM,  $0^\circ\text{C} \rightarrow \text{rt}$ , overnight.

Based on the inhibitory potency and efficacy of the two fragments **3.03** and **3.04**, fragment **3.04** was selected for further optimization and study. We replaced the quinoline moiety by 17 different groups, yielding the novel fragments **3.12-3.28** (Scheme 3.1B). Our strategy for designing the fragment library derived from compound **3.04** was as follows: we performed structural changes aiming at improved solubility and/or introduced substructures known to confer inhibitory potency at ABCG2. In order to gain structural information, we performed an X-ray analysis of a crystal of **3.04** (Figure 3.2). This showed that the molecule was present in a flat conformation and that there was a hydrogen bond between the ester carbonyl oxygen and the amide hydrogen. The quinoline nitrogen faced the amide hydrogen, probably due to dipole-dipole interaction. As a trend, the higher the planarity the more  $\pi$ - $\pi$  stacking is possible, contributing to crystal lattice stability [4]. The solubility can be increased by disrupting planarity, thus decreasing the crystal lattice energy. We implemented this idea by substituting the quinoline nitrogen by a carbon (**3.12**) (in the hope of decreasing the dipole-dipole

interactions with the amide hydrogen, thereby allowing rotation), by increasing the fraction of  $sp^3$ -hybridized carbon (**3.13**, **3.14**) and by omitting one aromatic ring (**3.15**). Destabilizing the crystal lattice is a useful approach, when high lipophilicity is required by targets such as ABCG2. We also made efforts to decrease the logP value by introducing polar groups (substituting one aromatic ring) (**3.16-3.23**) or by substituting the quinoline nitrogen by oxygen (more electronegative), hence increasing polarity (**3.24-3.26**). Fragments **3.18** and **3.19** bear methoxy groups, which are present in many known ABCG2 inhibitors [35-37], and compound **3.21** contains a nitro group, also found in a number of ABCG2 inhibitors [38,39]. Furthermore, chromone is a very prominent substructure of numerous ABCG2 inhibitors reported [40-42] and is a structural element of the fragments **3.27** and **3.28**.



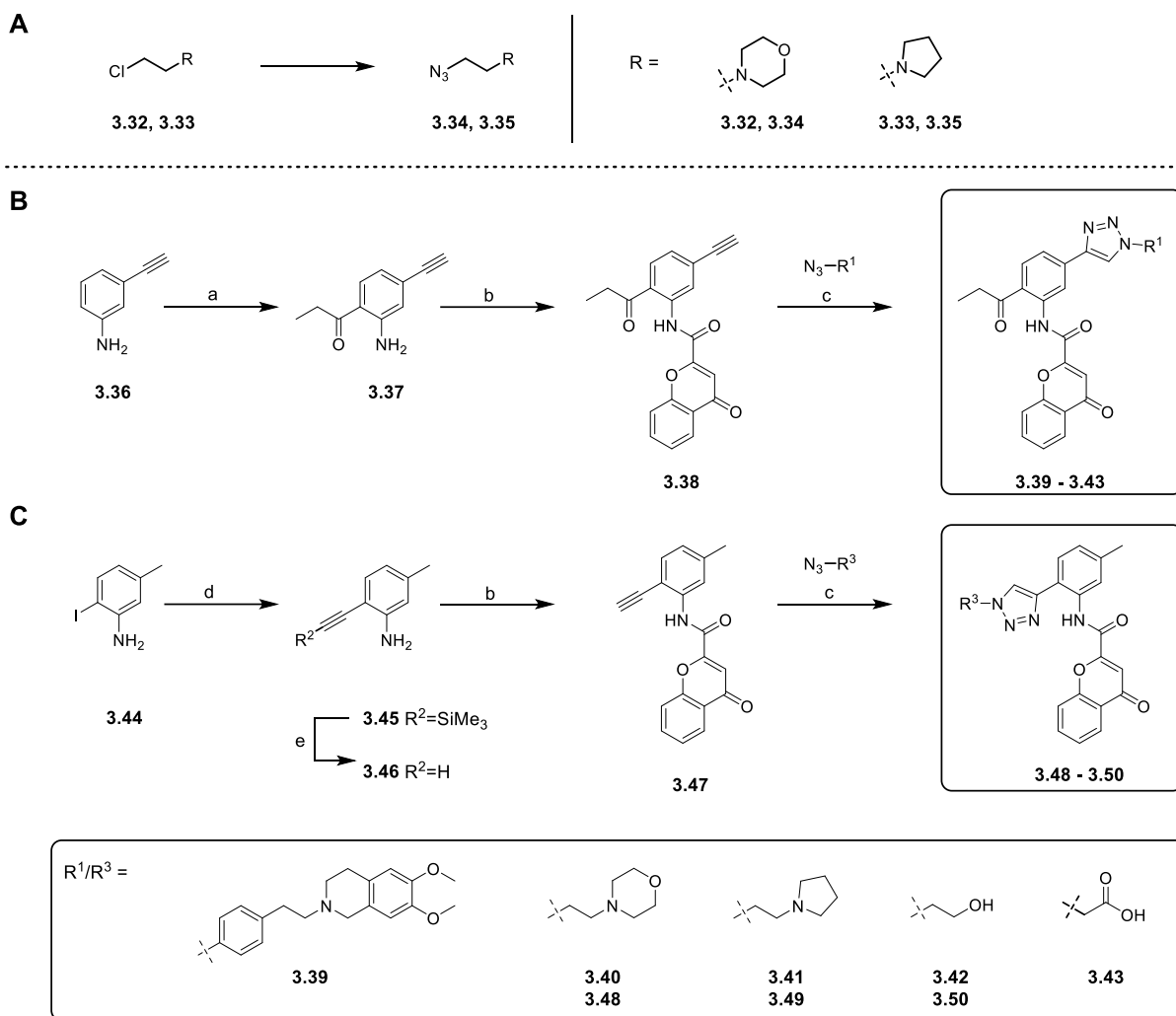
**Figure 3.2.** Structure of compound **3.04**, determined by X-ray analysis.

Like their precursor **3.04**, the fragments **3.12-3.21** and **3.24-3.28** were synthesized from **3.11** and the respective carboxylic acid by amide bond formation (Scheme 3.1B). The carboxylic acids employed were all commercially available, except the corresponding acid for fragment **3.13**. The acid was synthesized according to literature [34]. 5,6,7,8-Tetrahydroquinoline was oxidized at the nitrogen with 3-chlorobenzoperoxoic acid, yielding 5,6,7,8-tetrahydroquinoline 1-oxide (**3.29**), then treated with trimethylsilyl cyanide and dimethylcarbamoyl chloride to form 5,6,7,8-tetrahydroquinoline-2-carbonitrile (**3.30**) and afterwards hydrolyzed with hydrochloric acid to 5,6,7,8-tetrahydroquinoline-2-carboxylic acid (**3.31**). The fragments **3.22** and **3.23** were obtained by reduction of the nitro group in compound **3.21** to an amino group (in **3.22**) and a hydroxyl amino group (in **3.23**), using trichlorosilane.

According to the biological results of the novel fragments, we chose compound **3.27**, containing a chromone moiety, for further optimization and ‘decorating’, yielding a chromone-based series of inhibitors (comprising two subsets; Scheme 3.2) Aiming at increased solubility, we introduced solubilizing groups such as basic, acidic and hydroxyl moieties.

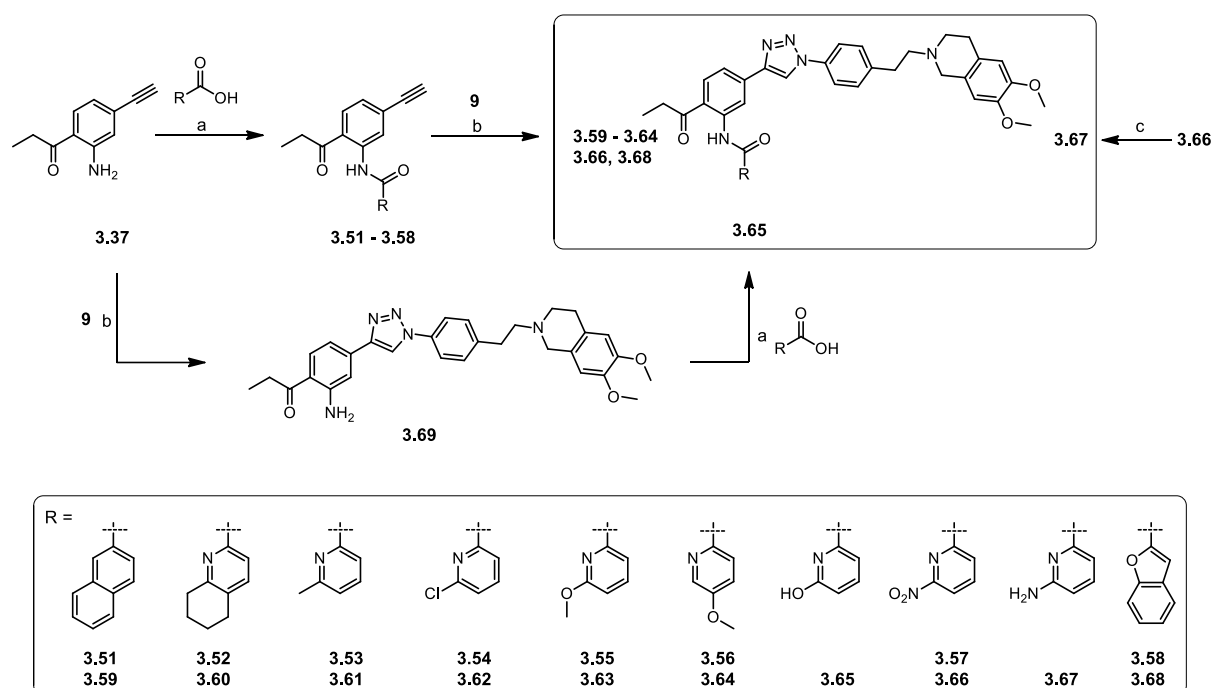
In a first chromone subset, we introduced solubilizing groups via ‘click’ chemistry in meta-position to the amide moiety (replacing the bromine), analogous to our previous inhibitors **3.01** and **3.02**, which bear a triazole ring in an equivalent position. For this purpose, we converted protonatable 2-morpholinoethyl chloride (**3.32**) and 2-pyrrolidoethyl chloride (**3.33**) into the corresponding azides (**3.34** and **3.35**) (Scheme 3.2A). Besides, we employed the azide **3.09** and commercially available azides containing a hydroxyl group or a carboxylic acid. For stability reasons, we also substituted the ester moiety by a ketone. The latter was synthesized by acylating 3-ethynylaniline (**3.36**) in ortho-position to the amine group in a variant of the Sugasawa reaction, using GaCl<sub>3</sub> as a Lewis acid (forming **3.37**). Then the chromone-2-carboxylic acid was introduced by amide bond formation, giving compound **3.38**, which was treated with the respective azide in a ‘click’ reaction to form the inhibitors **3.39-3.43** (Scheme 3.2B).

We performed molecular docking experiments with fragment **3.27**, using the recently published cryo-EM structure of ABCG2 (see Section 3.2.2). Based on these experiments, we created a second chromone subset, in which we introduced solubilizing groups (also via ‘click’) in ortho-position to the amide moiety, substituting the ester group, and a methyl group meta to the amide group (substituting the bromine). The synthesis started from 2-iodo-5-methylaniline (**3.44**), which was coupled with trimethylsilylacetylene in a Sonogashira reaction (yielding the alkyne **3.45**), deprotected with potassium carbonate to **3.46**, treated with chromone-2-carboxylic acid to form the amide **3.47** and then submitted to CuAAC with the respective azide, resulting in the inhibitors **3.48-3.50** (Scheme 3.2C).



**Scheme 3.2.** (A) Synthesis of the azide building blocks **3.34** and **3.35**. Reagents and conditions:  $\text{NaN}_3$ ,  $\text{H}_2\text{O}$ ,  $130\text{ }^\circ\text{C}$  (microwave), 1 h. (B+C) Synthesis of the inhibitors **3.39-3.43** (B) and **3.48-3.50** (C), bearing a chromone moiety. Reagents and conditions: (a) (I) propionitrile,  $\text{BCl}_3$ ,  $\text{CHCl}_3$ ,  $0\text{ }^\circ\text{C}$ ; (II)  $\text{GaCl}_3$ ,  $0\text{ }^\circ\text{C}$ , 10 min  $\rightarrow$  rt  $\rightarrow$  reflux, overnight; (III) 2 M  $\text{HCl}$  aq,  $0\text{ }^\circ\text{C} \rightarrow 70\text{ }^\circ\text{C}$ , 2 h; (b) 4-oxo-4*H*-chromene-2-carboxylic acid, TBUTU, DIPEA, DMF,  $80\text{ }^\circ\text{C}$  (microwave), 30 min; (c) respective azide,  $\text{CuSO}_4$ , sodium ascorbate, TBTA,  $\text{CHCl}_3$ , reflux, 2-3 d; (d) trimethylsilylacetylene,  $\text{Pd}(\text{PPh}_3)_2\text{Cl}_2$ ,  $\text{CuI}$ ,  $\text{NEt}_3$ , THF, rt, 90 min; (e)  $\text{K}_2\text{CO}_3$ , MeOH, rt, 2 h.

In addition to the compounds derived from fragment **3.27**, we prepared a second series (Scheme 3.3), in which we merged fragments showing activity similar to their precursor **3.04**, with fragment **3.03**. By analogy with our previous inhibitor **3.01**, we also replaced the ester moiety by a ketone group in order to provide for chemical stability. This series was synthesized from compound **3.37**, which was treated with the corresponding carboxylic acids to form the amides **3.51-3.58** and then introduced into a ‘click’ reaction with the azide **3.09**, yielding the inhibitors **3.59-3.64**, **3.66** and **3.58**. Compound **3.65** could not be synthesized in this way – the CuAAC failed – so **3.65** was formed by treating **3.37** with **3.09** under ‘click’ conditions first (resulting in **3.69**) and then introducing the corresponding carboxylic acid to form the amide bond. By analogy with the corresponding fragment **3.22**, compound **3.67** was synthesized from **3.66** by reducing the nitro group with ammonium formate, using palladium on charcoal as a catalyst.



**Scheme 3.3.** Synthesis of the inhibitors **3.59-3.68**. Reagents and conditions: (a) corresponding carboxylic acid, TBTU, DIPEA, DMF, 80 °C (microwave), 30 min; or corresponding carboxylic acid chloride (carboxylic acid, SOCl<sub>2</sub>, pyridine, toluene, reflux, 2 h), DIPEA, DCM, 0 °C, overnight; (b) CuSO<sub>4</sub>, sodium ascorbate, TBTA, CHCl<sub>3</sub> or THF or DMSO/2-propanol, reflux, 1-3 d; (c) ammonium formate, Pd/C, THF/MeOH, reflux, overnight.

### 3.2.2 Molecular Docking

We performed molecular (induced-fit) docking experiments with our most potent fragment **3.27** (see Table 3.1), using the recently reported cryo-EM structure of the ABCG2 transporter (PDB ID: 5NJ3 [30]). Based on our calculations, the most probable binding site is located between the two ABCG2 monomers in the center of the transmembrane domain (Figure 3.3A), which is in agreement with a cryo-EM structure of ABCG2 in complex with small molecule inhibitors [29]. Within this cavity, the carbonyl oxygen in the ester moiety of **3.27** formed a hydrogen bond with N436 of the first monomer, and the chromone ring structure established  $\pi$ - $\pi$  contacts with the phenyl ring of F439 belonging to the second monomer (Figure 3.3B). Noteworthy, one molecule of compound **3.27** bound to both ABCG2 monomers and connected them with each other (as did our much larger previous inhibitor UR-MB136 in the cryo-EM structure [29]). In contrast, two molecules of MZ29, also rather a small inhibitor, proved [29] to bind to the ABCG2 transporter. Fragment **3.27** served as a starting point for structural optimization. Retaining the *N*-phenyl-chromone-2-carboxamide scaffold, we varied both, the nature and the position of the substituents at the central phenyl ring. Thereby we considered stability as well as solubility aspects, e.g. by substituting the labile ester moiety and introducing polar groups such as heterocycles and hydroxyl groups. Guided by a low XP Gscore, visual inspection of the binding poses and synthetic feasibility, we selected compound **3.48** (Figure 3.3C) for synthesis and characterization. Compounds **3.49** and **3.50** were derived from **3.48**. Compound **3.48**

seemed favorable because it showed interactions similar to those of **3.27**, which had already been proven very potent in the biological assays: there was a hydrogen bond between the triazole ring and N436 (first monomer) and  $\pi$ - $\pi$  stacking between the chromone ring and the phenyl ring of F439 (second monomer). We chose a methyl group in para position to the triazole ring to optimally occupy the hydrophobic pocket formed by F431, F432 and two other residues not depicted in the figure (M549 and L555). The position of the triazole ring was chosen not only because of the favorable hydrogen bond, but also because the rather spacious morpholine ring, which is attached to the triazole ring via an ethylene linker, is directed towards the wide, intracellular part of the pore between the two ABCG2 monomers.

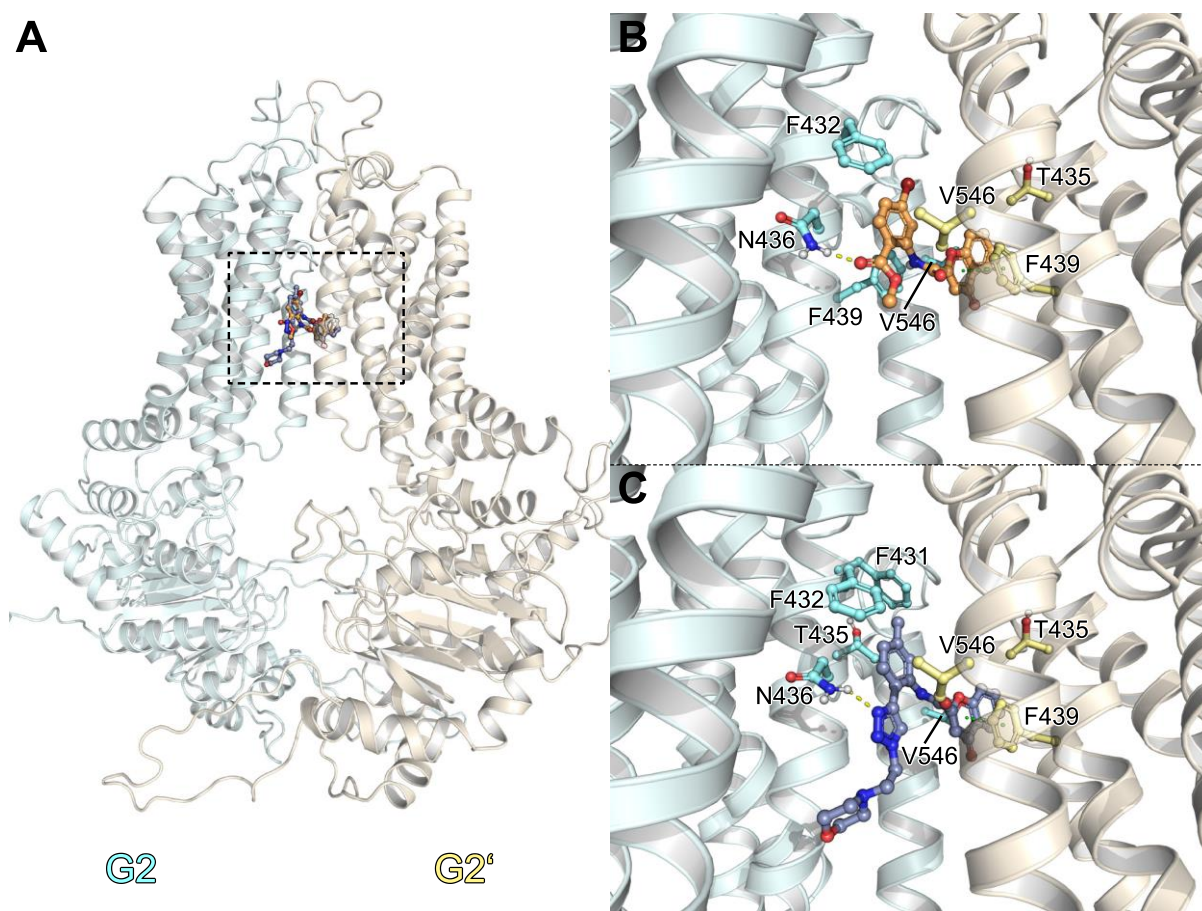


**Figure 3.3.** Binding poses of **3.27** and **3.48** obtained from induced-fit docking to the ABCG2 transporter. (A) Ribbon illustration of the ABCG2 homodimer, with individual G2 monomers colored blue and yellow. Bound ligand (**3.27** and **3.48**) molecules are colored orange and violet, respectively. (B+C) Specific interactions between **3.27** (B) or **3.48** (C) and ABCG2 residues within the binding pocket are highlighted: the respective residues are labelled, hydrogen bonds are indicated as yellow, and  $\pi$ - $\pi$  stacking as green, dashed lines.

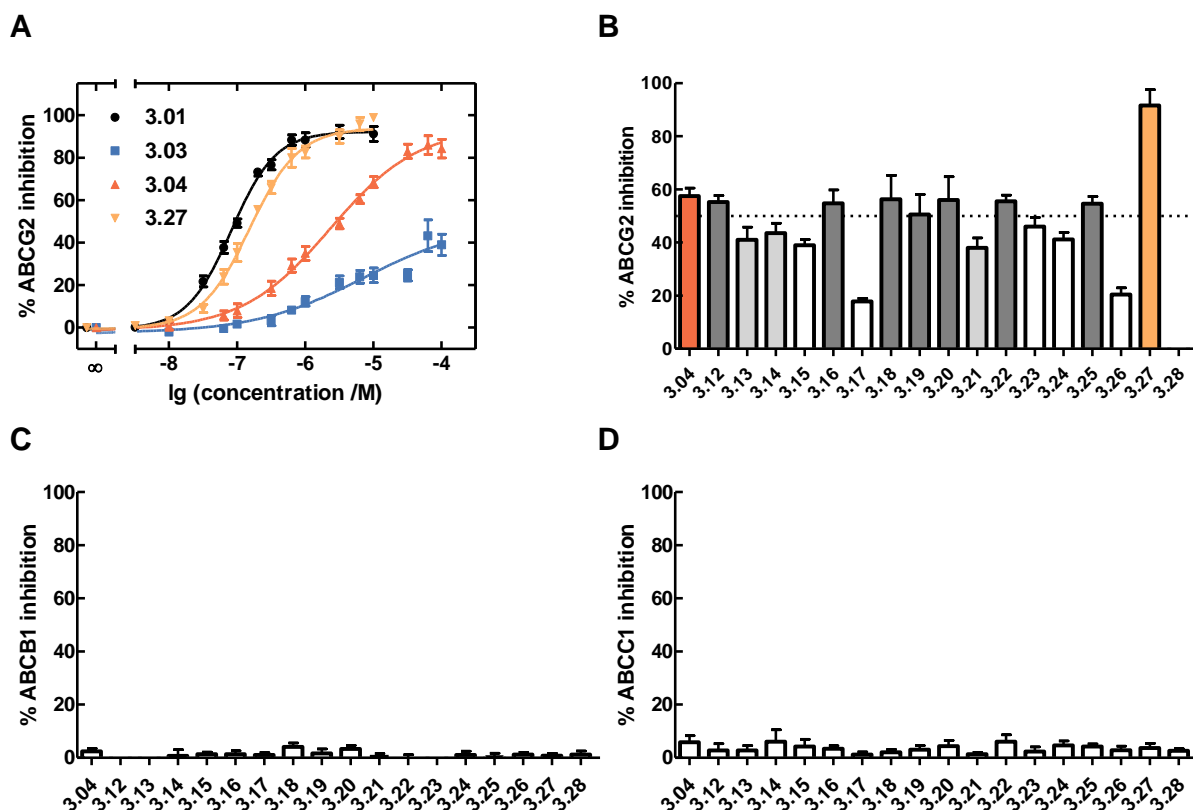
### 3.2.3 Biological Characterization

#### 3.2.3.1 Inhibition of the ABCG2, ABCB1 and ABCC1 Transport Activity

In order to investigate an inhibition of ABCG2-mediated transport activity by our compounds, we performed a Hoechst 33342 microplate assay, using ABCG2-expressing MCF-7/Topo cells. Hoechst 33342 is a substrate of ABCG2, which accumulates in the cells upon ABCG2

inhibition and can be detected fluorometrically (after DNA-intercalation). In addition, we analyzed the effect on the transport activity of ABCB1 and ABCC1 in a calcein-AM microplate assay, using KB-V1 and MDCK.2-MRP1 cells, respectively. By analogy with the Hoechst 33342 assay, the accumulation of the dual ABCB1/C1 substrate calcein-AM is determined by measuring the fluorescence after intracellular cleavage to calcein, which fluoresces in complex with  $\text{Ca}^{2+}$ -ions.

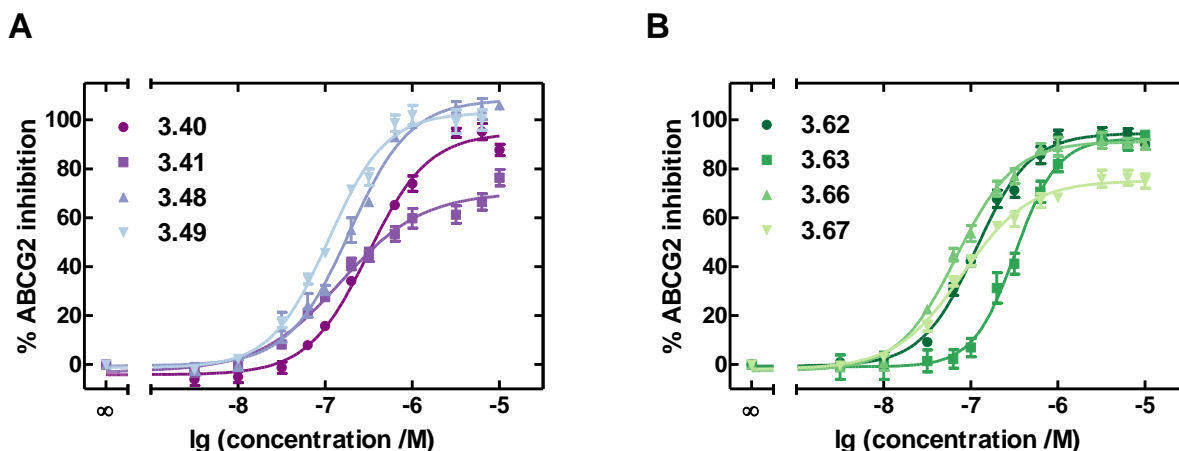
The fragments **3.03** and **3.04**, representing partial structures of our previous, tariquidar-related ABCG2 inhibitors (**3.01** and **3.02**), showed distinct behavior in the Hoechst 33342 assay. Whereas compound **3.03** was only 41% effective, fragment **3.04** was as effective as **3.01** and **3.02**, namely 86%, and showed a moderate  $\text{IC}_{50}$  value of 1.9  $\mu\text{M}$  (Figure 3.4A and Table 3.1). Therefore, we considered **3.04** as a starting point for optimization. The novel fragments derived from **3.04** (compounds **3.12-3.28**), in which the quinoline moiety was replaced by other groups, were analyzed for inhibition of ABCG2, ABCB1 and ABCC1 at a concentration of 10  $\mu\text{M}$  (Figure 3.4B-D). The highest signal in the Hoechst 33342 assay at this concentration was detected in the case of the chromone-bearing fragment **3.27**. When analyzed in a concentration-dependent manner in the Hoechst 33342 assay, **3.27** proved to be as potent as inhibitor **3.01** (Figure 3.4A and Table 3.1). This is astonishing in so far, as it is a variant of only a part of compound **3.01**; it has a much lower MWT than **3.01**, hence a much higher ligand efficiency [43]. Therefore, we prepared a series of ABCG2 inhibitors derived from **3.27** (chromone series, compounds **3.39-3.43** and **3.48-3.50**). Fragments **3.12**, **3.16**, **3.18**, **3.19**, **3.20**, **3.22** and **3.25** inhibited ABCG2 to the same extent as fragment **3.04** (at 10  $\mu\text{M}$ ), namely by more than 50%. These fragments, as well as **3.13**, **3.14** and **3.21**, were selected as a basis for our second series of ABCG2 inhibitors (compounds **3.59-3.68**). Fragments **3.13**, **3.14** and **3.21**, although they inhibited ABCG2 by less than 50% (at 10  $\mu\text{M}$ ), were considered interesting: the inhibitors derived from **3.13** and **3.14** were likely to show higher solubilities (increase in the fraction of  $\text{sp}^3$ -hybridized carbon, disrupting planarity) and **3.21** bears a nitro group, reportedly conferring activity at ABCG2, which we hoped would influence larger molecules more than the fragments. Fragment **3.28**, differing from **3.27** only in the position of the carboxamido substituent at the chromone moiety, turned out to be instable in aqueous solution (data not shown), which is most probably the reason for its inactivity. All fragments were selective towards ABCG2. They did not show inhibition of ABCB1 and ABCC1 at 10  $\mu\text{M}$ .



**Figure 3.4.** (A, B) Inhibition of ABCG2-mediated Hoechst 33342 efflux in MCF-7/Topo cells (A) by our previous tariquidar-related inhibitor **3.01**, the two substructures **3.03** and **3.04** and the novel fragment **3.27** (derived from **3.04**) in a concentration-dependent manner as well as (B) by compounds **3.04** and **3.12-3.28** at a concentration of 10  $\mu$ M. The inhibition is expressed relative to the maximal effect in the presence of 10  $\mu$ M FTC set to 100%. (C, D) Inhibition of ABCB1 (C) and ABCC1 (D)-mediated calcein-AM efflux in KB-V1 (C) and MDCK.2-MRP1 (D) cells by the fragments **3.04** and **3.12-3.28** at a concentration of 10  $\mu$ M. The inhibition is expressed relative to the maximal effect in the presence of 10  $\mu$ M tariquidar (C) and 30  $\mu$ M reversan (D) set to 100%. Presented are mean values  $\pm$  SEM from at least three independent experiments, each performed in triplicate.

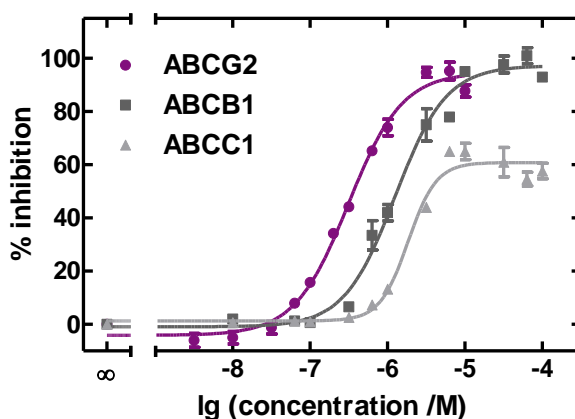
The results of the transport assays for two series of inhibitors are depicted in Figure 3.5 and Figure 3.6, showing exemplary concentration-response curves, and are summarized in Table 3.1. The introduction of polar groups into the structure of **3.27** via ‘click’ chemistry and the substitution of the methoxycarbonyl moiety by a propionyl group yielded the first subset (compounds **3.39-3.43**) of a chromone series. Compound **3.39**, which contains a 6,7-dimethoxy-1,2,3,4-tetrahydroisoquinoline moiety connected to the triazole ring with a phenylethyl linker (analogous to **3.01** and **3.02**), was only 65% effective. The comparison with fragment **3.27** (91% effective), as well as solubility considerations, suggested the introduction of much smaller moieties. Therefore, we conceived structures with only an ethylene or methylene linker between a polar group and the triazole ring. Compound UR-Ant116 (**3.40**), containing a morpholine ring, proved to be very effective (95%) and potent, showing an  $IC_{50}$  value of 312 nM (Figure 3.5). Compound UR-Ant121 (**3.41**), bearing a pyrrolidine ring, was even a bit more potent ( $IC_{50}$  value of 158 nM), but less effective (70%) (Figure 3.5). The introduction of a hydroxyl group (compound **3.42**) decreased potency to an  $IC_{50}$  value above 1  $\mu$ M. When a carboxylic acid (compound **3.43**) was introduced, the ability to inhibit ABCG2

was abolished. It is very probable that the acid moiety, which on the one hand should increase solubility, on the other hand prevents the compound from entering the cell membrane.



**Figure 3.5.** Concentration-dependent inhibition of ABCG2-mediated Hoechst 33342 efflux in MCF-7/Topo cells by (A) the chromones **3.40**, **3.41**, **3.48** and **3.49** as well as (B) the compounds **3.62**, **3.63**, **3.66** and **3.67**. The inhibition is expressed relative to the maximal effect in the presence of 10  $\mu$ M FTC set to 100%. Presented are mean values  $\pm$  SEM from at least three independent experiments, each performed in triplicate.

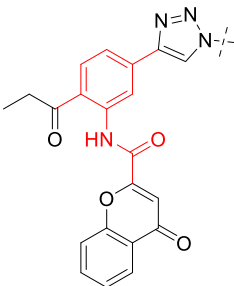
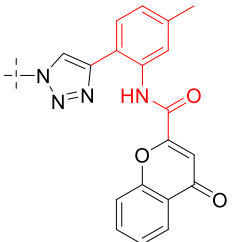
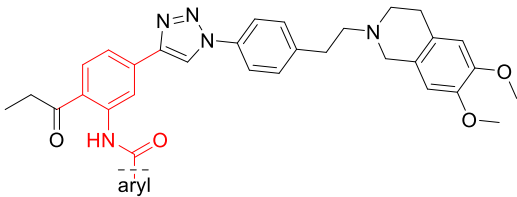
With respect to selectivity, the first subset of the chromone series showed interesting results. Compound **3.39** was selective for ABCG2. The smaller compounds **3.40-3.43**, though structurally extremely similar, behaved very differently. Whereas **3.41**, bearing a pyrrolidine ring, was selective for ABCG2, compound **3.40**, differing from **3.41** in the morpholine ring, was a triple ABCG2, ABCB1 and ABCC1 inhibitor (Figure 3.6). These two compounds could have different applications. For pharmacological tools selectivity is usually a necessity. For some clinical uses, however, inhibition of the three transporter subtypes may be advantageous. Especially ABCG2 and ABCB1 often have a concerted effect. Their expression overlaps at many physiological barriers (e.g. the GBB and the BBB), they share a number of clinically relevant substrates (such as topotecan), and a loss of function of one of these transporter subtypes can be compensated by an increase in the function of the respective other subtype [44,45]. Therefore a dual ABCB1/ABCG2 inhibitor may be necessary to overcome physiological barriers and MDR. Compound **3.42** showed low inhibition of ABCB1 and ABCC1. **3.43** was not only inactive at ABCG2, but also at ABCB1 and ABCC1. This is in agreement with the assumption that the acid is not capable of penetrating the cell membrane.



**Figure 3.6.** Concentration-dependent inhibition of ABCG2-mediated Hoechst 33342 efflux in MCF-7/Topo cells and of ABCB1 and ABCC1-mediated calcein-AM efflux in KB-V1 and MDCK.2-MRP1 cells, respectively, by compound **3.40**. The inhibition is expressed relative to the maximal effect in the presence of 10  $\mu$ M FTC, 10  $\mu$ M tariquidar and 30  $\mu$ M reversan, respectively, all set to 100%. Presented are mean values  $\pm$  SEM from at least three independent experiments, each performed in triplicate.

The second subset (compounds **3.48-3.50**) of the chromone series features different substitution at the central phenyl ring and results from molecular docking studies with fragment **3.27**. Compounds UR-Ant131 (**3.48**), containing a morpholine ring, and UR-Ant132 (**3.49**) with a pyrrolidine ring were highly effective (over 100%) and highly potent in the Hoechst 33342 assay ( $IC_{50}$  values of 188 nM for **3.48** and 109 nM for **3.49**) (Figure 3.5); as was compound **3.50** (bearing a hydroxyl group), though a bit less so than the other two inhibitors ( $I_{max}$  91%,  $IC_{50}$  447 nM). Also these three compounds showed different selectivities. Contrary to **3.49** and **3.50**, which were specific ABCG2 inhibitors, compound **3.48** also inhibited ABCB1 and ABCC1, though only to a small extent (13% and 22%, respectively). It seems as if a morpholine ring can confer inhibitory potency at ABCB1 and ABCC1, since we observed the same effect – much more pronounced – in case of compound **3.40**.

**Table 3.1.** Inhibitory effects of our previous, tariquidar-related inhibitors **3.01** and **3.02**, the two substructures **3.03** and **3.04** and the novel fragment **3.27** (derived from **3.04**), as well as of the novel inhibitors **3.39-3.43**, **3.48-3.50** and **3.59-3.68** on the transport activity of ABCG2, ABCB1 and ABCC1.

<div style="display: flex; justify-content: space-around; align-items: center;"> <div style="text-align: center;">  <p><b>3.39 - 3.43</b></p> </div> <div style="text-align: center;">  <p><b>3.48 - 3.50</b></p> </div> <div style="text-align: center;">  <p><b>3.59 - 3.68</b></p> </div> </div>						
Compound	ABCG2 <sup>a</sup>		ABCB1 <sup>b</sup>		ABCC1 <sup>c</sup>	
	IC <sub>50</sub> [nM] <sup>d</sup>	I <sub>max</sub> [%] <sup>d,e</sup>	IC <sub>50</sub> [nM] <sup>d</sup>	I <sub>max</sub> [%] <sup>d,f</sup>	IC <sub>50</sub> [nM] <sup>d</sup>	I <sub>max</sub> [%] <sup>d,g</sup>
<b>3.01</b> (UR-MB108) <sup>h</sup>	79 ± 5	91 ± 2	inactive <sup>i</sup>	–	inactive	–
<b>3.02</b> (UR-MB19) <sup>h</sup>	617 ± 179	90 ± 3	inactive	–	inactive	–
<b>3.03</b> (UR-Ant74)	3606 ± 271	41 ± 5	inactive	–	inactive	–
<b>3.04</b> (UR-Ant31)	1918 ± 482	86 ± 5	inactive	–	inactive	–
<b>3.27</b> (UR-Ant56)	140 ± 14	91 ± 3	inactive	–	inactive	–
<b>3.39</b> (UR-Ant71)	80 ± 25	65 ± 4	inactive	–	inactive	–
<b>3.40</b> (UR-Ant116)	312 ± 14	95 ± 2	1342 ± 176	92 ± 3	2076 ± 163	66 ± 2
<b>3.41</b> (UR-Ant121)	158 ± 22	70 ± 4	inactive	–	inactive	–
<b>3.42</b> (UR-Ant127)	≥ 1102 <sup>j</sup>	≥ 71 <sup>j</sup>	≥ 2285 <sup>j</sup>	≥ 41 <sup>j</sup>	≥ 1963 <sup>j</sup>	≥ 33 <sup>j</sup>
<b>3.43</b> (UR-Ant122)	inactive	–	inactive	–	inactive	–
<b>3.48</b> (UR-Ant131)	188 ± 21	108 ± 3	≥ 1601 <sup>j</sup>	≥ 13 <sup>j</sup>	≥ 1469 <sup>j</sup>	≥ 22 <sup>j</sup>
<b>3.49</b> (UR-Ant132)	109 ± 6	103 ± 4	inactive	–	inactive	–
<b>3.50</b> (UR-Ant133)	447 ± 27	91 ± 4	inactive	–	inactive	–
<b>3.59</b> (UR-Ant124)	249 ± 20	70 ± 2	inactive	–	inactive	–
<b>3.60</b> (UR-Ant115)	180 ± 15	63 ± 3	inactive	–	inactive	–
<b>3.61</b> (UR-Ant110)	166 ± 24	81 ± 6	≥ 9972 <sup>k</sup>	≥ 19 <sup>k</sup>	inactive	–
<b>3.62</b> (UR-Ant68)	116 ± 9	95 ± 2	inactive	–	inactive	–
<b>3.63</b> (UR-Ant105)	322 ± 32	92 ± 2	inactive	–	inactive	–
<b>3.64</b> (UR-Ant108)	116 ± 21	68 ± 5	≥ 2775 <sup>k</sup>	≥ 13 <sup>k</sup>	inactive	–
<b>3.65</b> (UR-Ant112)	328 ± 48	75 ± 1	≥ 18450 <sup>k</sup>	≥ 14 <sup>k</sup>	inactive	–
<b>3.66</b> (UR-Ant111)	70 ± 7	91 ± 2	inactive	–	inactive	–
<b>3.67</b> (UR-Ant113)	82 ± 10	75 ± 3	inactive	–	inactive	–
<b>3.68</b> (UR-Ant62)	120 ± 8	78 ± 1	inactive	–	inactive	–

<sup>a</sup> Hoechst 33342 microplate assay, using ABCG2-expressing MCF-7/Topo cells.

<sup>b</sup> Calcein-AM microplate assay, using ABCB1-expressing KB-V1 cells.

<sup>c</sup> Calcein-AM microplate assay, using ABCC1-expressing MDCK.2-MRP1 cells.

<sup>d</sup> Mean values ± SEM from at least three independent experiments, each performed in triplicate.

<sup>e</sup> Maximal inhibitory effect (I<sub>max</sub>) relative to the response to FTC at a concentration of 10 μM (100%).

<sup>f</sup> Maximal inhibitory effect (I<sub>max</sub>) relative to the response to tariquidar at a concentration of 10 μM (100%).

<sup>g</sup> Maximal inhibitory effect (I<sub>max</sub>) relative to the response to reversan at a concentration of 30 μM (100%).

<sup>h</sup> Data taken from our previous study [28].

<sup>i</sup> Inactive: response ≤ 10% up to a concentration of 100 μM.

<sup>j</sup> No plateau was reached at the kinetic solubility limit; minimum IC<sub>50</sub> values and I<sub>max</sub> values were stated.

<sup>k</sup> No plateau was reached up to a concentration of 100 μM; minimum IC<sub>50</sub> values and I<sub>max</sub> values were stated.

The second series (compounds **3.59-3.68**) originating from the fragment screening, are analogs of compound **3.01**, the quinoline group being substituted with aryl moieties that compared favorably in the fragment analysis. They all showed  $IC_{50}$  values in the two- to low three-digit nM range. The most effective substances from this series, with an  $I_{max}$  value of over 90%, were compound **3.62**, with a 2-chloropyridine moiety, compound **3.63**, containing a 2-methoxypyridine group, and compound **3.66**, featuring 2-nitropyridine, which was the most potent substance of this series with an  $I_{50}$  value of 70 nM (Figure 3.5). Compound **3.61**, comprising a 2-methylpyridine moiety, was with 81% only a little less effective. Compounds **3.59**, **3.60**, **3.64**, **3.65**, **3.67** and **3.68** showed efficacies somewhat below 80%. Compound **3.67**, with a 2-aminopyridine group, was the most potent among the latter substances, showing an  $IC_{50}$  value of 82 nM (and an  $I_{max}$  value of 75%) (Figure 3.5). All members of this series were highly selective for ABCG2, except for compounds **3.61**, **3.64** and **3.65**. The latter also inhibited ABCB1, but only by less than 20% and only at very high concentrations (100  $\mu$ M). They showed a clear preference for ABCG2 and thus are rather selective.

### 3.2.3.2 Cytotoxicity and Reversal of Drug Resistance

The cytotoxicity and the ability to reverse the resistance of MCF-7/Topo cells toward the cytostatic drug topotecan was investigated exemplarily in a kinetic chemosensitivity assay for the inhibitors **3.40** and **3.48** as representatives of the two subsets of the chromone series and compound **3.63**, a member of the second series. As shown in Figure 3.7, against MCF-7/Topo cells, compound **3.40** was nontoxic up to a concentration of 1  $\mu$ M and exhibited a cytotoxic effect only at higher concentrations. Upon incubation with topotecan at a concentration of 100 nM, the cells were not affected due to their resistance, whereas the addition of **3.40** at per se nontoxic concentrations entirely reversed the resistance. Inhibitor **3.48** did not show any cytotoxicity, even at a concentration as high as 10  $\mu$ M. Analogous to **3.40**, **3.48** was able to reverse topotecan resistance; the same was true of inhibitor **3.63**, when administered at a nontoxic concentration, which was up to 1  $\mu$ M. At higher concentrations **3.63** displays a cytotoxic effect. In sum, this assay disclosed that the compounds analyzed prevented the topotecan efflux, which is in accordance with the results of the Hoechst 33342 transport assay.

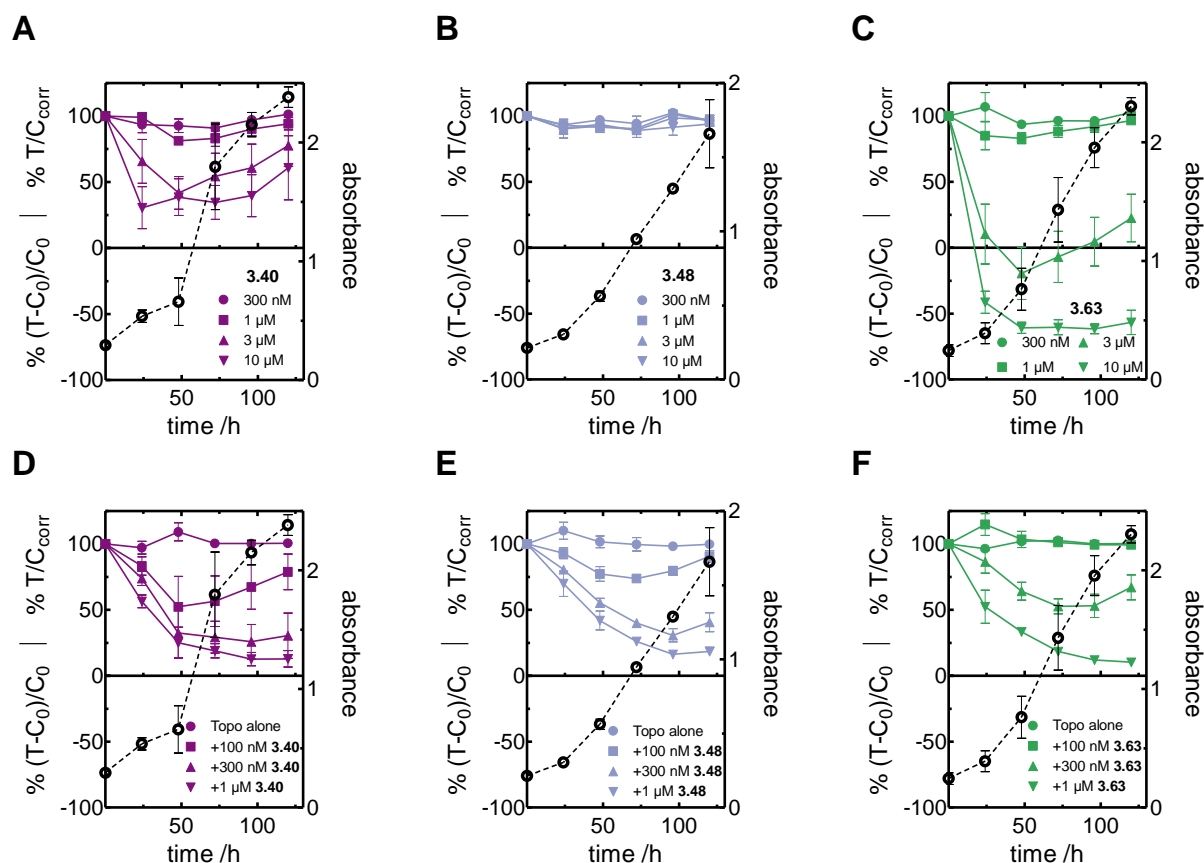


**Figure 3.7.** (A–C) Antiproliferative activities of the inhibitors **3.40** (A), **3.48** (B) and **3.63** (C) against MCF-7/Topo cells upon long-term incubation. (D–F) Reversal of ABCG2-mediated drug resistance against topotecan on proliferating MCF-7/Topo cells: effect of 100 nM topotecan (Topo) alone and in combination with different concentrations of **3.40** (D), **3.48** (E) or **3.63** (F). Antiproliferative effects correspond to the left y-axes. The growth curves of untreated control cells (open circles) correspond to the right y-axes. Data are mean values  $\pm$  SEM of two to three independent experiments, each performed in octuplicate.

### 3.2.3.3 Effect on the ATPase Activity

For comprehensive biological characterization, we investigated our most advantageous transport inhibitors in terms of potency and solubility, UR-Ant116 (**3.40**), UR-Ant121 (**3.41**), UR-Ant131 (**3.48**) and UR-Ant132 (**3.49**), in an ATPase assay, which gives information on the type of inhibition. We performed the assay with membrane preparations of human ABCG2 overexpressing MCF-7/Topo breast cancer cells in order to provide a membrane environment for native protein structure and function. Transport of substrates by ABCG2 is an alternating process, whereby the substrate-bound, inward-open conformation is converted to an outward facing state that can release the substrate to the outside [30]. ABCG2 gains the energy for this process by ATP-hydrolysis to ADP and inorganic phosphate. The latter was determined by a molybdenum blue reaction after incubation of the membranes for a certain period of time (with and without a transport inhibitor) as an estimate for the ABCG2-associated ATPase activity, thereby assessing the influence of test compounds on the ATPase activity of ABCG2. In the absence of an ATPase stimulating agent, ABCG2 typically displays basal ATPase activity, presumably induced by endogenous substrates (e.g. lipids) [46] present in the membrane

preparations, which was set to zero in our assay. As depicted in Figure 3.8A, both compounds **3.40** and **3.41**, belonging to the first subset of the chromone series, at concentrations of 1  $\mu\text{M}$  and 10  $\mu\text{M}$ , suppressed the ATPase activity to a level even below the basal ATPase activity. This led to the conclusion that these two compounds are not substrates of ABCG2. It has been shown that the inhibition of the ATPase and of the transport activity are closely connected. A recent cryo-EM study [29] suggested that ABCG2 transport inhibitors, including one member of our preceding tariquidar analogs (UR-MB136), bind to a central multidrug binding site located in the transmembrane domain, lock the inward-facing conformation of ABCG2 and inhibit the ATPase activity through conformational coupling with the cytoplasmic nucleotide-binding domain. Based on these results, it can be assumed that the inhibition of the ATPase activity by compounds **3.40** and **3.41** contributes to the overall inhibition of ABCG2 transport. In contrast to the compounds **3.40** and **3.41**, the transport inhibitors **3.48** and **3.49**, members of the second subset of the chromone series displaying different substitution at the central phenyl ring, showed a very distinct behavior in the ATPase assay – they did not suppress, but stimulate the ATPase activity of ABCG2 (at concentrations of 1  $\mu\text{M}$  and 10  $\mu\text{M}$ ) and therefore are most likely substrates of the transporter rather than ATPase inhibitors. In order to find out to which degree they activate the ABCG2 ATPase activity, we determined concentration-response curves of the two compounds. As shown in Figure 3.8B, **3.48** and **3.49** exhibited  $I_{\text{max}}$  values of 46% and 29%, respectively, and potencies of 96 nM and 62 nM, respectively. It is conceivable that they compete with other substrates, such as Hoechst 33342, for transport and thereby reduce their transport. However, they do not fully activate the ATPase activity; it can also be supposed that by being transported more slowly, they occupy the multidrug binding site of the transporter, so that it is not at disposal for other substrates.

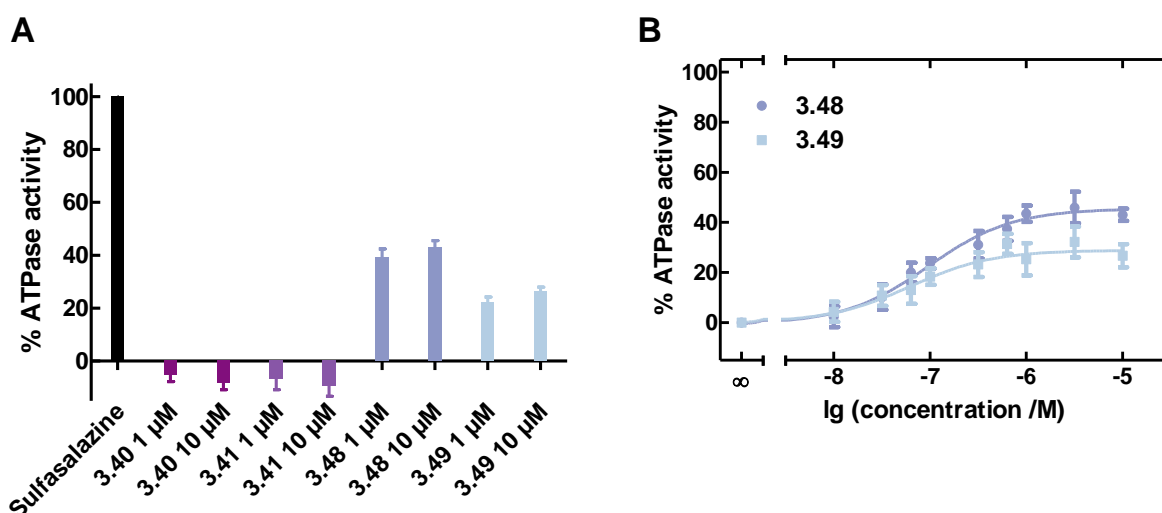


**Figure 3.8.** Stimulation or suppression of the ATPase activity in ABCG2-expressing MCF-7/Topo membrane preparations by the compounds **3.40**, **3.41**, **3.48** and **3.49** at a concentration of 1  $\mu\text{M}$  and 10  $\mu\text{M}$  (A) and concentration-dependent stimulation of the ATPase activity by the compounds **3.48** and **3.49** (B). The effect is expressed relative to the basal ATPase activity (0%) and the maximal stimulatory effect in the presence of 30  $\mu\text{M}$  sulfasalazine set to 100%. Presented are mean values  $\pm$  SEM from at least three independent experiments each performed in triplicate.

It is interesting that minor structural changes have such an impact on the type of inhibition. This shows that it is possible to modulate the inhibition type according to the needs of the desired application. ATPase activators and suppressors may have different applications. Whereas ATPase activators deplete the cell of ATP, a compelling effect when addressing resistant tumor cells [47], ATPase suppressors do not interfere with the ATP balance of the cell.

#### 3.2.3.4 Stability in Blood Plasma

Having analyzed the biological activity and selectivity of our inhibitors, investigations on their drug-like properties were pending. After studying cytotoxicity we determined the stability in blood plasma, which is a precondition for in vivo studies. Chromone is a structural element quite common in natural products and drugs and can be considered a privileged scaffold [48,49] in drug discovery, not least due to its synthetic availability, structural diversity and low toxicity (confirmed in our cytotoxicity assay, using MCF-7/Topo cells, see Figure 3.7). However, chromones may be susceptible to hydrolysis, depending on the substitution pattern. 3-Substituted chromones are very reactive towards the attack of nucleophiles, such as water [50]. We observed this behavior with fragment **3.28**, a 3-substituted chromone, which hydrolyzed rapidly in aqueous solution, explaining the lack of biological activity. By contrast, fragment **3.27**, a chromone substituted in 2-position, exhibited excellent inhibition of ABCG2 and was the foundation of our chromone series. Exemplarily of this series, compound **3.49** was incubated in human plasma and analyzed via HPLC with UV detection at 220 nm (Figure 3.9A). The peak area of **3.49** decreased by about 58% over a period of 24 hours, yet no additional peaks were detected. On the off chance that a possible degradation product may not be detectable by this method (due to lacking UV-absorption or retention), the samples were also analyzed by HPLC-MS coupling (0 h and 24 h). Also with this hyphenated technique, applying a different gradient, no additional peaks were detected (data not shown). Therefore, we attributed the decrease in the peak area to adsorption, either to the vial surface or to plasma proteins, and concluded that **3.49** is in fact stable in blood plasma. Moreover, the main decrease in peak height occurred in the first five hours and after that, the peak area remained almost unchanged, which supports our assumption that the decrease is due to adsorption, not to hydrolysis.

Furthermore, as a representative of the second series, inhibitor **3.65** was studied in the same manner (Figure 3.9B). The situation was the same as with compound **3.49** – the peak area of **3.65** decreased but no additional peaks were detected, also upon HRMS analysis (data not shown). Hence, we again concluded that the compound was adsorbed to a certain extent.

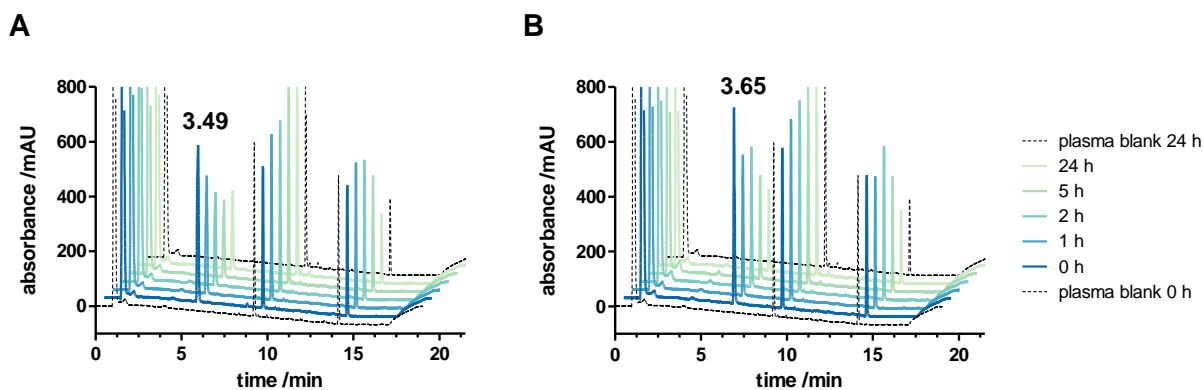


**Figure 3.9.** Chromatograms illustrating the stability of the compounds **3.49** (A) and **3.65** (B) upon incubation in human blood plasma at 37 °C over a period of 24 h. RP-HPLC analysis, UV detection at 220 nm.

### 3.2.4 Aqueous Solubility

When determining the solubility of chemical entities, it is fundamental to understand the distinction between thermodynamic and kinetic solubility. Thermodynamic – or equilibrium – solubility is defined as the maximum concentration of a solute in a solvent in a state of complete thermodynamic equilibrium, i.e. a saturated solution at equilibrium with an excess of undissolved solid and at a fixed temperature and pressure [51,52]. It is usually determined by the classical shake-flask method (using a solid in a buffer) with subsequent HPLC-analysis [1,8,13,53]. By contrast, in kinetic solubility assays no equilibrium is reached. Most often the compound, ‘pre-dissolved’ in DMSO, is added into an aqueous buffer and precipitation is measured turbidimetrically or nephelometrically after a short period of time [54-56]. The concentration of the compound in the buffer at which a precipitate appears is termed kinetic solubility [1,8,13]. Unlike thermodynamic solubility assays, kinetic assays can be performed in microplates in high throughput and they are useful to verify concentration-response data – making sure that precipitation does not occur on the time scale of the biological assay. They are also used as an early estimate of solubility in drug discovery [1,8,55]. However, the apparent solubility in a kinetic assay is always – sometimes dramatically – higher than the thermodynamic ‘true’ solubility and therefore should not be used for decision-making, otherwise the optimization process may be driven towards the synthesis of compounds with the slowest precipitation rather than the highest solubility [1,2,8,57].

Here, we established both a kinetic solubility assay mainly to verify our biological data and a thermodynamic solubility assay in order to rank our ABCG2 inhibitors in terms of solubility and thereby to assess if our efforts met our objective – potent ABCG2 inhibitors with improved solubility.

### 3.2.4.1 Kinetic Solubility

**Assay Adaptation.** We conducted the kinetic solubility assay in microplates under conditions identical to those in the biological assays. Inhibitor solutions in DMSO at increasing concentrations were diluted 1:100 in the respective aqueous buffer, resulting in a uniform DMSO concentration (1%) in each well. The plates were incubated at 37 °C for two hours – the time span of the Hoechst 33342 assay, which is the most time-consuming assay among the ATPase and transport assays. While handling the plates, attention was paid to avoiding scratches on the plates that might have interfered with the readouts. Then the extinction was measured as a function of the inhibitor concentration. The extinction of electromagnetic radiation, when passed through a suspension, is due to the processes of absorption, scattering, diffraction and reflection. When the extinction is measured at a wavelength at which the test compound does not absorb any light, a sharp increase in the extinction values at a certain concentration arises from scattering due to precipitation, corresponding to the solubility limit of the respective compound [54]. At that point, the clear solution turns into a turbid suspension containing solid particles.

Since ABCG2 inhibitors show poor solubility, we strove for a detection limit as low as possible, thus a signal intensity as high as possible. Therefore, we needed to adjust the changeable assay parameters, namely sample volume and measurement wavelength, accordingly. In order to get an estimate for the detection limit we required a substance with extremely low aqueous solubility as a reference. We chose coronene, a polycyclic aromatic compound comprising six peri-fused benzene rings, which shows an aqueous solubility as low as 0.5 nM [58] (detected fluorometrically). When performing the assay with this compound, it can be assumed that the concentration at which the sharp increase in extinction occurs indicates the detection limit of the assay rather than the solubility limit of coronene, because coronene is practically insoluble in water and experiments showed that precipitation takes place quickly – after the addition of the DMSO stock solution to the buffer the concentration-extinction curve was measured repeatedly and remained almost constant for 24 hours (data not shown). Using coronene, we explored the effects of the sample volume and of the wavelength on the signal intensity, thus the detection limit of the assay. As expected, the signal intensity increased with the sample volume (data not shown). Therefore, we employed the highest volume possible per microplate well in the assay, namely 300 µL. For analyzing the dependence of the signal intensity on the wavelength, we considered the spectral properties of coronene, DMSO and polystyrene (microplate material). The latter shows absorption between 200 nm and 290 nm, which decreases rapidly above 290 nm [59]. DMSO exhibits a sharp absorption maximum at a wavelength of around 250 nm and practically no absorption above 265 nm [61]. The main absorption bands of coronene are located between 300 nm and 350 nm and there is only very

low absorption above 350 nm [60]. Therefore, we performed the experiment at different wavelengths ranging from 380 nm to 830 nm, where the aforementioned compounds do not absorb radiation (Figure 3.10A). Light scattering drastically decreases with increasing wavelength, though this effect depends on the particle size and is more pronounced for small particles [62]. Accordingly, when measuring the extinction as a function of the coronene concentration, we found the highest signal intensity at a wavelength of 380 nm and the lowest at 830 nm. To find the lowest wavelength compatible, we measured the UV/VIS absorption spectra of our inhibitors (examples thereof depicted in Figure 3.10B) and found that they have a cut-off wavelength of 380 nm, which we chose as measurement wavelength for our assay.

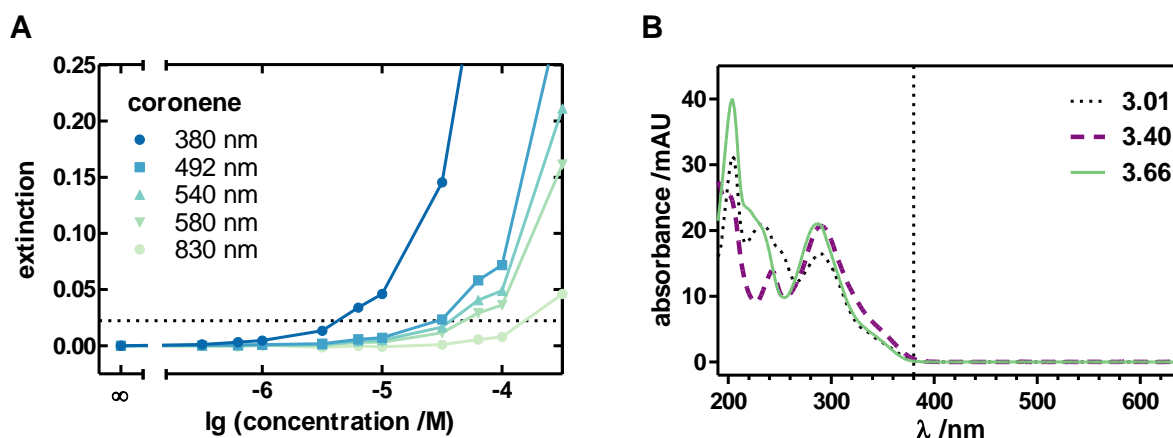


**Figure 3.10.** (A) Effect of the wavelength on the signal intensity in a kinetic solubility assay: extinction (mainly due to scattering) as a function of the concentration of the ‘insoluble’ standard coronene at different wavelengths. The data were normalized to the blank value. Presented are mean values  $\pm$  SEM from one experiment performed in octuplicate. (B) UV/VIS absorption spectra of the inhibitors **3.01**, **3.40** and **3.66**, revealing a shared cut-off wavelength of 380 nm.

By analogy with a recently published study [63] covering the solubility of a detergent (sodium lauroyl isethionate), we estimated the kinetic solubility of the test compounds as the highest concentration at which more than 95% of the radiation is transmitted, i.e. the extinction is lower than 0.0223, the data having been normalized to the blank value (1% DMSO in buffer). The threshold is indicated as a dashed line in Figure 3.10A and Figure 3.11. In the case of coronene, the highest concentration below the threshold was 1  $\mu$ M, which we identified as the detection limit. It should be noted that the detection limit determined in this assay is only applicable under the assumption that the inhibitors precipitate with particle size and form similar to coronene.

**Assay Results.** We examined our previous inhibitor UR-MB108 (**3.01**), fragment **3.27**, and all our novel inhibitors (**3.39-3.43**, **3.48-3.50** and **3.59-3.68**) in the kinetic solubility assay, using PBS (pH 7.4) as a solvent. We included coronene in every batch of assays as a control for precipitation. Exemplary concentration-extinction curves are depicted in Figure 3.11. The estimated kinetic solubility limits are listed in Table 3.2.

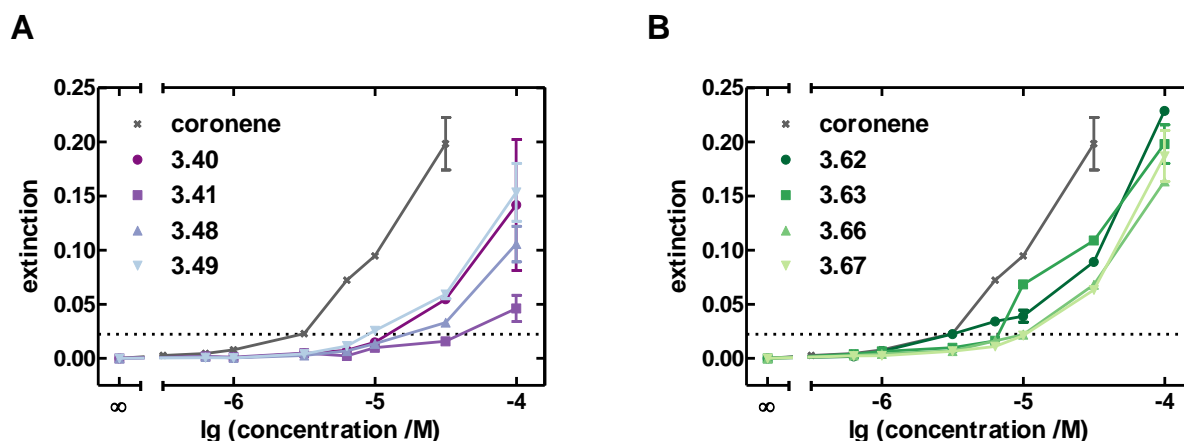


**Figure 3.11.** Concentration-dependent extinction (at 380 nm) due to scattering in a kinetic solubility assay in PBS caused by (A) the chromone inhibitors **3.40**, **3.41**, **3.48** and **3.49** as well as (B) the inhibitors **3.62**, **3.63**, **3.66** and **3.67**. The data were normalized to the blank value. Presented are mean values  $\pm$  SEM from two to three independent experiments, each performed in triplicate.

We compared the concentration-dependent curves in the functional assays with the kinetic solubility limits in order to decide if the biological data were compromised by precipitation (c.f. Figure 3.13 in the supplementary material, Section 3.5.1). If a curve reached a plateau before the solubility limit was achieved, we concluded that the curve was unaffected by solubility constraints and that the values derived from the curve ( $I_{\max}$  and  $IC_{50}$ ) are valid. Our previous inhibitor **3.01** and fragment **3.27** showed a solubility limit of 3  $\mu$ M and 10  $\mu$ M, respectively. The curves of both compounds reached a plateau in the Hoechst 33342 transport assay at around 1  $\mu$ M, meaning that the biological data are reliable. The chromone inhibitors exhibited solubility limits between 3  $\mu$ M and 30  $\mu$ M and all of them, except for one, achieved a plateau in the Hoechst 33342 assay before the solubility limit was reached. Only the curve of compound **3.42**, which was less potent than the other chromones, did not reach a plateau; the values increased up to a concentration of 3  $\mu$ M and then suddenly dropped. This reflects the results of the kinetic solubility assay, according to which the solubility limit was reached at 3  $\mu$ M. This consistency indicates that the kinetic solubility assay is reliable. We marked insufficient solubility as the cause for the incomplete curve in a footnote to Table 3.1. We also investigated some of our chromone inhibitors – compounds **3.40**, **3.41**, **3.48** and **3.49** – in the ATPase assay. Since the highest concentration employed there was 10  $\mu$ M, the ATPase data are largely not compromised by insufficient solubility.

Our second series of inhibitors, compounds **3.59-3.68**, showed kinetic solubilities up to 10  $\mu$ M. The curves of compounds **3.60**, **3.63** and **3.65-3.68** all reached a plateau in the Hoechst 33342 assay at concentrations lower than the respective kinetic solubility limit. The curves of compounds **3.59**, **3.61** and **3.64** also reached a plateau, although this was at concentrations that slightly exceeded their respective kinetic solubility limit. It is possible that with higher solubility, their  $I_{\max}$  values might be slightly higher. The curve of compound **3.62** reached a

plateau at about 3  $\mu\text{M}$  and this inhibitor exhibited a solubility limit of 1  $\mu\text{M}$ , which is around the detection limit. The first values of the concentration-extinction curve coincided with the ones from the control coronene but a strong increase occurred only at higher concentrations, at around 10  $\mu\text{M}$ . Therefore it is improbable that the biological data of compound **3.62** are impaired.

We did not only test our substances for interaction with ABCG2, but we also assessed their selectivity and therefore examined them for inhibition of ABCB1 and ABCC1 in the calcein-AM assay. Most of the inhibitors analyzed were selective towards ABCG2 or just exhibited very low inhibitory potency at the other two transporters. At concentrations higher than their solubility limits – we studied the inhibitors at concentrations up to 100  $\mu\text{M}$  – they might appear more selective than they actually are. Since this concerns only quite high concentrations, however, we considered this not very relevant. Three compounds were not selective, namely the chromones **3.40**, **3.42** and **3.48**. Regarding compound **3.42**, the situation is the same as with the Hoechst 33342 assay; no plateau was reached at the solubility limit (as we indicated in the footnote to Table 3.1). The curves of compound **3.40**, which is a triple ABCB1/ABCC1/ABCG2 inhibitor, plateaued in both calcein-AM assays before the solubility limit of 10  $\mu\text{M}$  was reached. Compound **3.48** also showed some potency at ABCB1 and ABCC1, but did not reach a plateau in the calcein-AM assays at concentrations below the solubility limit of 10  $\mu\text{M}$ , which we indicated in Table 3.1.

Altogether, with a few exceptions, the biological data were not affected much by kinetic solubility limits.

**Table 3.2:** Estimated kinetic solubility limits of our previous tariquidar analog **3.01**, fragment **3.27**, and the chromone inhibitors (**3.39-3.43**, **3.48-3.50**) as well as the second series of inhibitors (**3.59-3.68**).

Compound	Kinetic Solubility [ $\mu\text{M}$ ] <sup>a</sup>	Compound	Kinetic Solubility [ $\mu\text{M}$ ] <sup>a</sup>
<b>3.01</b> (UR-MB108) <sup>h</sup>	3	<b>3.59</b> (UR-Ant124)	3
<b>3.27</b> (UR-Ant56)	10	<b>3.60</b> (UR-Ant115)	7
<b>3.39</b> (UR-Ant71)	7	<b>3.61</b> (UR-Ant110)	3
<b>3.40</b> (UR-Ant116)	10	<b>3.62</b> (UR-Ant68)	1
<b>3.41</b> (UR-Ant121)	30	<b>3.63</b> (UR-Ant105)	7
<b>3.42</b> (UR-Ant127)	3	<b>3.64</b> (UR-Ant108)	3
<b>3.43</b> (UR-Ant122)	10	<b>3.65</b> (UR-Ant112)	7
<b>3.48</b> (UR-Ant131)	10	<b>3.66</b> (UR-Ant111)	10
<b>3.49</b> (UR-Ant132)	7	<b>3.67</b> (UR-Ant113)	10
<b>3.50</b> (UR-Ant133)	3	<b>3.68</b> (UR-Ant62)	7

<sup>a</sup> Highest concentration in the kinetic solubility assay in PBS (data normalized to the blank value), at which transmission was higher than 95%, i.e. the extinction was lower than 0.0223.

The buffer used in the transport assays also contained serum albumin. Since this can influence precipitation, we also performed kinetic solubility assays in a buffer containing bovine serum albumin (BSA). We found that the addition of BSA did not change the data significantly, which

is shown exemplarily for compound **3.01** in Figure 3.14 in the supplementary material (Section 3.5.1).

#### 3.2.4.2 Thermodynamic Solubility

**Assay Adaption.** To determine thermodynamic solubility the traditional shake-flask technique was modified. In the course of the optimization of the assay, we repeatedly faced major challenges due to the high lipophilicity and low solubility range of ABCG2 inhibitors.

We scaled the procedure down in order to facilitate handling and to minimize the amount of substance required. On downscaling it should be borne in mind that the surface to volume ratio is larger the smaller the flask. Therefore adsorption of the solute to the vial surface may have a greater effect on the thermodynamic equilibrium between the saturated solution and the undissolved solid. To minimize adsorption we tested different vial materials regarding the ability to adsorb compounds such as **3.01**. Indeed there were distinct differences. We found the most pronounced adsorption with untreated glass vials (maybe due to ionic interactions between the negatively charged silanol glass surface and the positively charged, protonated heterocycle in **3.01**), followed by untreated polypropylene (PP), ‘siliconized’ PP (i.e. PP treated with a siliconizing agent) and the least with ‘siliconized’ glass, which we chose for the assay (graph see Figure 3.15 in the supplementary material, Section 3.5.1).

With respect to in vitro as well as in vivo studies we used PBS at a pH value of 7.4 as a solvent. This is the usual pH value in the biological assays and the pH value in the small intestine as well as many other body fluids, such as blood plasma, lymph, cerebrospinal fluid and cytoplasm. It is common practice to use an aqueous buffer as a simplistic surrogate of the intestinal content in solubility studies [2,64]. Typically, the sample is prepared by adding solid to the buffer. This turned out to be practically impossible with our substances – they showed very poor wettability and tended to float on the surface, even after shaking, making it impossible to take out a homogeneous aliquot for HPLC analysis without some of the solid adhering to the pipette tip. This behavior may be attributed to their lipophilicity. Unfortunately, the lipophilicity also made it impossible to remove floating substance by filtration – adsorption to the filter (different materials tested) was so pronounced that not only the floating substance, but also the dissolved compound was removed from the solution and after filtration there was no signal detectable by HPLC. We solved this problem by adding a stock solution in DMSO to the buffer instead of adding solid. Of course, the presence of DMSO influences the solubility of a compound. It has been shown that a DMSO content over 5‰ can distort the results of thermodynamic solubility assays [65]. So we kept the DMSO content at only 1‰.

After the sample preparation, we incubated it in a shaker at 25 °C. Studies showed that a thermodynamic equilibrium is usually established after 24 hours of stirring [66]. We shook our

samples for 36-40 hours to make sure an equilibrium had been reached and then allowed sedimentation for another 24 hours. In case a compound did not sediment properly, we centrifuged the sample.

Another challenge associated with the low solubility and high lipophilicity of the inhibitors was the transfer of the samples into the HPLC vials. After transferring compound **3.01**, we did not detect any peak and found out that the reason was adsorption of **3.01** to the pipette tip. After pipetting the sample into an HPLC vial containing acetonitrile and rinsing the tip, a peak was detectable.

Having established a procedure for the thermodynamic solubility assay, we validated it with haloperidol as a reference substance. The solubility of the latter is referred to as 37  $\mu\text{M}$  in literature [67]. We determined a solubility of  $40 \pm 1 \mu\text{M}$ .

**Assay Results.** We investigated fragment **3.27**, our novel inhibitors (**3.39-3.42**, **3.48-3.50** and **3.59-3.68**) as well as our previous tariquidar analog **3.01** in the thermodynamic solubility assay (Table 3.3). As already stated in the introduction, compound **3.01** exhibited an equilibrium solubility of only 78 nM. Furthermore it violates two of the Ro5 due to its size and high clogP. The first series of inhibitors is based on fragment **3.27**, a substructure of **3.01**, containing a chromone instead of a quinoline moiety. Though much smaller, **3.27** was equipotent with **3.01**. Its solubility, however, with 109 nM, was not much higher than the solubility of **3.01**, despite its low molecular weight and conformity with the Ro5. This can probably be attributed to the lack of a protonatable nitrogen. The inhibitors derived from fragment **3.27** all contain a polar or ionizable moiety. Compounds **3.39-3.42**, the first subset of the chromone inhibitors, display very different solubilities. Merging **3.27** with fragment **3.03** led to the inhibitor **3.39**, which was only slightly more soluble than **3.01** (149 nM). However, when far smaller polar moieties were introduced (compounds **3.40-3.42**), the solubility could be enhanced markedly and in contrast to **3.39** the compounds complied with the Ro5, or in case of **3.40**, almost complied (only the MWT was slightly higher than 500 g/mol). Compounds **3.41** and **3.42** both contain a heterocycle (morpholine in **3.40** and pyrrolidine in **3.41**) and exhibit solubilities of ca. 1 and 1.5  $\mu\text{M}$ , respectively – 13-fold and 19-fold the solubility of inhibitor **3.01**. The introduction of a hydroxyl group into compound **3.42** increased the solubility to 575 nM. Compound **3.43**, containing a carboxyl group, was not measured because it did not inhibit ABCG2. The second subset of the chromone inhibitors, compounds **3.48-3.50**, differs structurally from the first subset, the main difference being the absence of an acyl moiety. The inhibitors obey the Ro5 and, here again, the compounds containing an ionizable ring – **3.48** and **3.49** – showed high solubilities (1.1 and 1.3  $\mu\text{M}$ , respectively) compared to **3.01**. The introduction of a hydroxyl group (in compound **3.50**) did not increase the solubility.

The second series of inhibitors (**3.59-3.68**) is structurally more similar to compound **3.01**. The compounds are analogs of **3.01**, the quinoline moiety being replaced by other ring structures. They have MWTs similar to **3.01** and, therefore, violate at least one Ro5. However, we were able to increase the fraction of sp<sup>3</sup>-hybridized carbon or decrease the clogP values compared to **3.01**, i.e. by introducing polar groups. The latter strategy, of course, also led to an increase in the number of H-donors or H-acceptors and in some cases to Ro5 violations.

Compound **3.59**, containing a naphthalene ring and designed with regard to improved rotation around the amide bond and reduced planarity, did not show improved solubility. Compound **3.60** contains a tetrahydroquinoline ring to reduce aromaticity, thus planarity and  $\pi$ - $\pi$  stacking and ultimately crystal packing. This substitution did not increase the solubility, either. However, when the phenyl ring in the quinoline moiety was replaced by a smaller group containing sp<sup>3</sup>-hybridized carbon, namely a methyl group (compound **3.61**), the solubility was six-fold increased to 445 nM. The introduction of polar moieties, replacing the phenyl ring, yielded different results. Compound **3.62**, an organic chloride, did not display increased solubility. Though electronegative, chlorine confers lipophilicity due to its size. Also the introduction of a methoxy group, attached in different positions in compounds **3.63** and **3.64**, did not solve the solubility problem; neither did the attachment of a nitro (in **3.66**) or an amino (in **3.67**) group. Here, a general problem of increasing solubility by introducing polar groups becomes apparent – on one hand, polarity will indeed be increased by this approach and the heteroatoms can form stabilizing H-bonds with water, but on the other hand also polar intermolecular interactions may be increased. This could lead to enhanced crystal packing, counteracting the solubilizing effect of the polar groups. Fortunately, this strategy proved successful, nevertheless. Compound **3.65**, displaying a hydroxyl group, is over ten times more soluble than **3.01** (855 nM). We find it surprising that the introduction of an amino group did not have the same effect. Lastly, the replacement of the quinoline moiety by a slightly smaller and less lipophilic benzofuran ring (in **3.68**) did not improve the solubility.

**Table 3.3.** Ro5 compliance and thermodynamic solubilities of our previous tariquidar analog **3.01**, fragment **3.27**, and the chromone inhibitors (**3.39-3.43**, **3.48-3.50**) as well as the second series of inhibitors (**3.59-3.68**).

Compound	MWT [g/mol]	ClogP <sup>a</sup>	H-Donors	H-Acceptors	Ro5 Violations	Thermodynamic Solubility [nM] <sup>b</sup>
<b>3.01</b> (UR-MB108)	666.77	5.42	1	10	2	78 ± 5
<b>3.27</b> (UR-Ant56)	402.20	3.23	1	6	0	109 ± 18
<b>3.39</b> (UR-Ant71)	683.75	3.64	1	11	2	149 ± 36
<b>3.40</b> (UR-Ant116)	501.53	1.75	1	10	(1)	999 ± 189
<b>3.41</b> (UR-Ant121)	485.53	2.81	1	9	0	1483 ± 383
<b>3.42</b> (UR-Ant127)	432.43	1.51	2	9	0	575 ± 144
<b>3.43</b> (UR-Ant122)	446.41	1.85	2	10	0	n. d. <sup>c</sup>
<b>3.48</b> (UR-Ant131)	459.50	1.71	1	9	0	1144 ± 203
<b>3.49</b> (UR-Ant132)	443.50	2.76	1	8	0	1228 ± 106
<b>3.50</b> (UR-Ant133)	390.39	1.47	2	8	0	< 100
<b>3.59</b> (UR-Ant124)	665.78	5.63	1	9	2	< 100
<b>3.60</b> (UR-Ant115)	670.80	5.41	1	10	2	< 100
<b>3.61</b> (UR-Ant110)	630.74	4.46	1	10	1	445 ± 48
<b>3.62</b> (UR-Ant68)	651.15	4.47	1	10	1	< 100
<b>3.63</b> (UR-Ant105)	646.73	5.25	1	11	3	< 100
<b>3.64</b> (UR-Ant108)	646.73	4.21	1	11	2	119 ± 29
<b>3.65</b> (UR-Ant112)	632.71	4.30	2	11	2	855 ± 242
<b>3.66</b> (UR-Ant111)	661.71	4.05	1	13	2	< 100
<b>3.67</b> (UR-Ant113)	631.72	3.60	3	11	2	< 100
<b>3.68</b> (UR-Ant62)	655.74	5.04	1	10	2	< 100

<sup>a</sup> Calculated LogP values, using ACD/Structure Designer.<sup>b</sup> Thermodynamic solubility assay: shake-flask experiment in PBS with subsequent HPLC analysis. Mean values ± SEM from at least six independent experiments, each performed in duplicate.<sup>c</sup> n. d.: not determined.

When comparing the two series of inhibitors it becomes obvious that the chromone inhibitors, which are smaller and structurally more different from **3.01**, are superior to the members of the second series in terms of solubility and Ro5 compliance. The fragment-based approach led to the discovery of fragment **3.27**, which is a very potent and effective ABCG2 inhibitor on its own. Thus it was possible to obtain much smaller and more polar inhibitors, which exhibited up to 19-fold increased solubility. Furthermore, it became apparent that if a compound complies with the Ro5 plus contains a protonatable nitrogen, it is a good predictor for improved solubility.

As a side note it should be mentioned that in silico methods (we used the ACD/Structure Designer) failed to predict the solubility of our substances. Another common approach to estimate solubility is to use experimentally easily accessible parameters for guidance. For instance, the retention time in RP-HPLC analysis is linked to the lipophilicity of a compound [68] and the crystal lattice energy can be estimated from the melting point [2]. This approach turned out to be rather productive. For example, when comparing compound **3.49** with

compound **3.01**, marked decreases in retention time (3.8 min vs. 7.2 min) and melting point (ca. 180 °C vs. 219 °C) were observed, in parallel with the increase in solubility (1.2  $\mu$ M vs. 78 nM). Another operating experience worth disclosing is that adsorption of the substances to the vial surface can be critical. A case in point is compound **3.65**, which showed a 3-fold higher solubility when ‘siliconized’ PP vials (higher adsorption) were used instead of ‘siliconized’ glass vials (2.9  $\mu$ M vs. 855 nM). Apparently, the presence of a layer of molecules adhering to the vial surface can influence the equilibrium in favor of higher solubility values.

Figure 3.12 summarizes the properties of the novel inhibitors that are most promising in terms of potency and solubility, specifically **3.40**, **3.41**, **3.48**, **3.49** and **3.65**, in comparison to our previous inhibitor **3.01** and fragment **3.27**. Depicted are  $IC_{50}$  values in the Hoechst 33342 assay and kinetic and thermodynamic solubility limits. As mentioned before, medicinal chemists often face the dilemma of improving solubility at the expense of diminished biological activity, due to the positive correlation of lipophilicity and affinity to hydrophobic binding pockets in drug targets [31]. The chart shows that by virtue of a fragment-based and rational approach we were able to circumvent this predicament and increase the equilibrium solubility of our compounds while maintaining inhibitory potency. Whereas compound **3.01** and fragment **3.27** exhibited equilibrium solubilities in the range of their potencies, the chromone inhibitors **3.40**, **3.41**, **3.48**, and **3.49** showed equilibrium solubilities that were three to nine times higher than their  $IC_{50}$  values. Compound **3.65**, the most soluble compound of the second series, showed an equilibrium solubility 2.5 times higher than its  $IC_{50}$  value.

As expected, the kinetic solubilities were considerably higher than the thermodynamic equilibrium solubilities. This means that by adding a DMSO stock solution to the buffer, a supersaturated solution was produced in the concentration range between the thermodynamic and the kinetic solubility limit. Here it becomes obvious that time is a critical factor. On the time scale of the biological assays performed in this study, namely up to two hours, the precipitation of our previous inhibitor **3.01** was slow enough to allow for reliable results. However, since the thermodynamic (equilibrium) solubility of **3.01** was in the range of its  $IC_{50}$  value, compound **3.01** is not suited for in vitro assays requiring long time-periods of incubation and especially in vivo studies can be impaired. By contrast, the novel inhibitors with improved equilibrium solubility qualify for such examinations.

Lastly, there was no clear correlation between the thermodynamic and kinetic solubility, but as a tendency, higher kinetic solubility can be taken as a hint to increased equilibrium solubility.

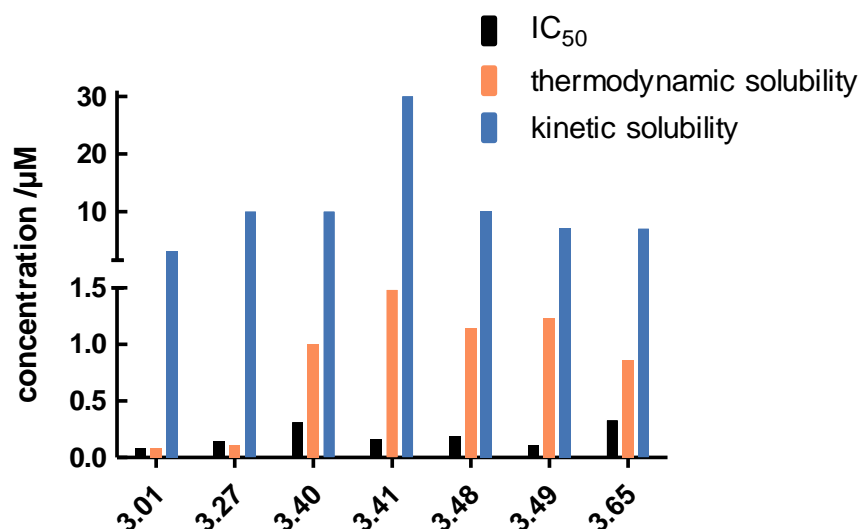


**Figure 3.12.** Comparison of the IC<sub>50</sub> values in the Hoechst 33342 assay and kinetic and thermodynamic solubility limits of our previous tariquidar analog **3.01**, fragment **3.27**, the novel chromone inhibitors **3.40**, **3.41**, **3.48** and **3.49** as well as the novel, **3.01**-related inhibitor **3.65**.

### 3.3 Conclusion

Poor aqueous solubility has been reported to cause major problems with purification as well as in vitro and in vivo studies of biologically active compounds [3]. ABCG2 inhibitors are especially prone to solubility issues due to their size and lipophilic nature. Our previous, tariquidar-related inhibitor UR-MB108 (**3.01**) [28] shows high potency (79 nM), but extremely low equilibrium solubility (78 nM). This study comprises a solubility-driven discovery of novel ABCG2 inhibitors based on **3.01**. In a fragment-based approach, we synthesized and tested substructures of **3.01** for inhibitory potency, optimized them and included molecular docking experiments to grow the most promising fragments into inhibitors. The novel compounds inhibited ABCG2 with IC<sub>50</sub> values in the two- to low three-digit nanomolar range, categorizing them among the most potent known ABCG2 inhibitors. Their ability to inhibit ABCG2 transport was not only assessed in a Hoechst 33342 transport assay, but also confirmed by their ability to reverse the drug resistance in MCF7-Topo cells. The most promising compounds in terms of potency and solubility were the inhibitors UR-Ant116 (**3.40**), UR-Ant121 (**3.41**), UR-Ant131 (**3.48**) and UR-Ant132 (**3.49**), all of which displayed an *N*-phenyl-chromone-2-carboxamide scaffold. Their equilibrium solubility ranged between 1 μM and 1.5 μM, which puts them at the lower edge of the drug solubility window. Compared to **3.01**, this is an up to 19-fold improvement of equilibrium solubility. As a rule of thumb, the solubility of a potential drug should be at least three times its IC<sub>50</sub> value. Compounds **3.40**, **3.41**, **3.48** and **3.49** exhibit solubilities of three to nine times their IC<sub>50</sub> value – sufficient to exert their maximal effect. Moreover they do not or, in case of **3.40** only slightly, violate Lipinski's Ro5, which predicts good absorption properties in vivo. These four compounds differ in their biological profile.

Whereas **3.41** was a triple ABCB1/ABCC1/ABCG2 inhibitor, compounds **3.42** and **3.49** were selective for ABCG2 and **3.48** was almost selective – it inhibited the other two subtypes only with very low potency and efficacy. Besides, the substances showed different modes of inhibition. An ATPase assay revealed that compounds **3.40** and **3.41** decreased the ATPase activity, whereas **3.48** and **3.49**, both differing structurally from the aforementioned two inhibitors, were partial ATPase activators. As a prerequisite for in vivo studies, we demonstrated the stability of the compounds in blood plasma and their non-toxicity.

Taken together, we offer scientists investigating ABCG2 a set of potent, selective and non-selective inhibitors that are stable, non-toxic and water-soluble ( $> 1 \mu\text{M}$ ). To the best of our knowledge, this is the first study on ABCG2 inhibitors focusing on improved aqueous solubility and the first report providing not only biological, but also solubility information on the compounds. We expect them to be of great value for in vitro examinations requiring long time-periods of incubation such as structural biology studies on protein-ligand interactions using X-ray crystallography or NMR. Such studies depend on sufficient equilibrium solubility of the ligands; insufficient solubility has been identified as the cause of crystallography failures and as limitation to the method [69]. In the light of their stability in blood plasma and low toxicity, our substances are promising candidates for in vivo investigations, their aqueous solubility increasing the chances of success. For instance, due to their high selectivity, UR-Ant121 (**3.41**) and UR-Ant132 (**3.49**) should be well-suited as pharmacological tools for PET studies of ABCG2, e.g. at the BBB, provided that appropriate radioactive labeling can be achieved. Up to now, inhibitors of ABCG2 are not in clinical use yet [70]. Potential therapeutic applications were explored in several in vivo studies [70,71], for instance as a means to overcome the BBB and MDR. Since ABCB1 and ABCG2 (and to a lesser extent ABCC1) act in concert at many physiological barriers [72], the triple ABCB1/ABCC1/ABCG2 inhibitor UR-Ant116 (**3.40**) is an attractive candidate for therapeutic studies.

## 3.4 Experimental Section

### 3.4.1 Chemistry

#### 3.4.1.1 General Experimental Conditions

**Chemicals and solvents** were purchased from commercial suppliers (Sigma Aldrich, Munich, Germany; Merck, Darmstadt, Germany; VWR, Darmstadt, Germany; Thermo Fisher Scientific, Waltham, MA, USA; TCI, Eschborn, Germany) and used without further purification unless stated otherwise. Reactions requiring anhydrous conditions were carried out in dry reaction vessels under an atmosphere of argon and anhydrous solvents were used. Millipore water was used throughout for the preparation of buffers and HPLC eluents. Acetonitrile for HPLC (gradient grade) was obtained from Merck.

**Microwave** reactions were carried out in an Initiator 8 microwave reactor (Biotage, Uppsala, Sweden).

**Thin layer chromatography** was performed on TLC Silica gel 60 F<sub>254</sub> aluminium plates (Merck, Darmstadt, Germany). Visualization was accomplished by UV irradiation at wavelengths of 254 nm and 366 nm or by staining with ninhydrin (1.5 g ninhydrin, 5 mL acetic acid, 500 mL 95% ethanol).

For **column chromatography** Geduran<sup>®</sup> Silica 60 gel (0.040-0.063 mm; Merck, Darmstadt, Germany) was used.

**Automated flash column chromatography** was performed on a 971-FP Flash Purification System (Agilent Technologies, Santa Clara, CA, USA) using pre-packed SuperFlash Silica 50 columns (Agilent Technologies). The crude products were dissolved in a suitable solvent, mixed with Geduran<sup>®</sup> Silica 60 gel (0.040-0.063 mm; Merck, Darmstadt, Germany), concentrated under reduced pressure and placed in a load cartridge prior to the run.

**Melting points** were determined with a Büchi B-540 apparatus (Büchi Labortechnik, Essen, Germany) and are uncorrected.

**NMR spectra** were recorded on an Avance 300 instrument (7.05 T, <sup>1</sup>H: 300.1 MHz, <sup>13</sup>C: 75.5 MHz), an Avance 400 instrument (9.40 T, <sup>1</sup>H: 400 MHz, <sup>13</sup>C: 101 MHz) or an Avance 600 instrument with cryogenic probe (14.1 T, <sup>1</sup>H: 600 MHz, <sup>13</sup>C: 151 MHz) (Bruker, Karlsruhe, Germany) with TMS as external standard.

**High-resolution mass spectrometry** (HRMS) analysis was performed on an Agilent 6540 UHD Accurate-Mass Q-TOF LC/MS system (Agilent Technologies, Santa Clara, CA, USA) using an ESI source.

**Low-resolution mass spectrometry (MS)** was performed on a Finnigan MAT SSQ 710 A GC/MS system (Finnigan MAT, now Thermo Fisher Scientific, Waltham, MA, USA).

**Preparative HPLC** was performed on a system from Knauer (Berlin, Germany) consisting of two K-1800 pumps and a K-2001 detector. A Kinetex® XB-C18 (5  $\mu$ m, 100 Å, 250 mm x 21.2 mm; Phenomenex, Aschaffenburg, Germany) served as RP-column at a flow-rate of 15 mL/min. Mixtures of acetonitrile and 0.1% aq TFA were used as mobile phase. The detection wavelength was set to 220 nm throughout. The solvent mixtures were removed by lyophilization using an Alpha 2-4 LD lyophilization apparatus (Christ, Osterode am Harz, Germany) equipped with an RZ 6 rotary vane vacuum pump (Vacuubrand, Wertheim, Germany).

**Analytical HPLC** was performed on a system from Agilent Technologies (Santa Clara, CA, USA) (Series 1100) composed of a G1312A binary pump equipped with a G1379A degasser, a G1329A ALS autosampler, a G1316A COLCOM thermostated column compartment and a G1314A VWD detector. A Kinetex® C8 (2.6  $\mu$ m, 100 Å, 100 mm  $\times$  4.6 mm; Phenomenex, Aschaffenburg, Germany) served as RP-column at a flow rate of 1 mL/min. Oven temperature was set to 30 °C throughout. Mixtures of acetonitrile (A) and 0.05% aq TFA (B) were used as mobile phase. The detection wavelength was set to 220 nm throughout. Solutions for injection (40  $\mu$ M) were prepared by diluting a stock solution in DMSO with a mixture of A and B corresponding to the composition of the eluent at the start of the gradient. The following linear gradient was applied: 0-12 min: A/B 30:70-95:5, 12-15 min: A/B 95:5. Retention (capacity) factors were calculated from retention times ( $t_R$ ) according to  $k = (t_R - t_0)/t_0$  ( $t_0$  = dead time).

**X-Ray analysis.** Single clear colorless prism-shaped crystals of compound **3.04** were obtained by recrystallization from  $\text{CHCl}_3$ . A crystal (0.35 $\times$ 0.21 $\times$ 0.20) was selected and mounted on a MITIGEN holder oil on a SuperNova, Single source at offset, Atlas diffractometer. The crystal was kept at  $T = 123.00(10)$  K during data collection. Using Olex2 (Dolomanov et al., 2009), the structure was solved with the ShelXT (Sheldrick, 2015) structure solution program, using the Direct Methods solution method. The model was refined with olex2.refine (Bourhis et al., 2015) using Gauss-Newton minimization.

### 3.4.1.2 Synthesis Protocols and Analytical Data

All compounds were characterized by  $^1\text{H}$  and  $^{13}\text{C}$  NMR spectroscopy, (HR)MS, and melting point (if applicable). In addition, final compounds were characterized by RP-HPLC (purity control). The purity of the final compounds was  $\geq 95\%$  throughout.

#### General Procedure for N-Acylation of Anilines 1

Under dry conditions the carboxylic acid (1.0-1.5 eq) was dissolved in anhydrous DMF (0.5 M) in a microwave reaction vessel. DIPEA (2.0-3.0 eq) and the coupling reagent TBTU (1.0-

1.5 eq) were added and the solution was stirred at rt for 5 min. The aniline (1.0-1.1 eq) was added and stirring was continued at 80 °C for another 30 min in a microwave reactor. The mixture was diluted either with DCM or EtOAc and washed with H<sub>2</sub>O, saturated NH<sub>4</sub>Cl-solution and brine. The organic layer was dried over Na<sub>2</sub>SO<sub>4</sub>, and the volatiles were removed under reduced pressure. The residue was subjected to column chromatography (eluent: PE/EtOAc) and/ or to recrystallization in EtOAc or CHCl<sub>3</sub>.

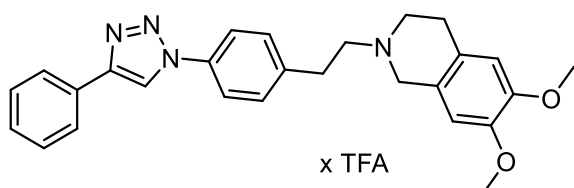
### General Procedure for N-acylation of Anilines 2

Under dry conditions the carboxylic acid (1.0 eq) was dissolved in anhydrous toluene (0.5 M) and treated with SOCl<sub>2</sub> (2.0 eq) and pyridine (2.0 eq). After 2 h of refluxing, the volatiles were removed under reduced pressure. The residue was redissolved in DCM and added dropwise to a stirred solution of the aniline (1.0 eq) and DIPEA (4.0 eq) in DCM at 0 °C. Stirring was continued at rt overnight. The mixture was diluted with DCM and washed with H<sub>2</sub>O and saturated NH<sub>4</sub>Cl-solution. The organic layer was dried over Na<sub>2</sub>SO<sub>4</sub>, and the solvent was evaporated. The residue was subjected to recrystallization in EtOAc or to flash column chromatography (eluent: PE/EtOAc).

### General Procedure for CuAAC [73,74]

The alkyne (1.0 eq), the azide (1.2 - 1.5 eq), CuSO<sub>4</sub>·5H<sub>2</sub>O (0.15 eq), sodium ascorbate (0.7 eq) and TBTA (0.15 eq) were dissolved/suspended in CHCl<sub>3</sub>, THF or DMSO/isopropanol and refluxed for 1 to 3 d. In a few cases a washing step followed. After removal of the solvent under reduced pressure the remaining crude material was purified by (flash) column chromatography (eluent: DCM/MeOH) and subsequent preparative HPLC (eluent: MeCN/0.1% aq TFA).

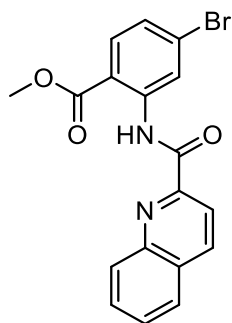
### 6,7-Dimethoxy-2-(4-(4-phenyl-1*H*-1,2,3-triazol-1-yl)phenethyl)-1,2,3,4-tetrahydroisoquinoline (3.03)



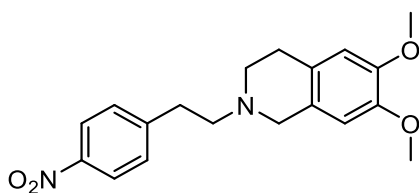
Compound **3.03** was prepared according to the general procedure for the CuAAC. The reaction was carried out using ethynylbenzene (21.5 µL, 0.196 mmol, 1.0 eq), 2-(4-azidophenethyl)-6,7-dimethoxy-1,2,3,4-tetrahydroisoquinoline (**3.09**) (99.4 mg, 0.294 mmol, 1.5 eq), CuSO<sub>4</sub>·5H<sub>2</sub>O (7.3 mg, 0.029 mmol, 0.15 eq), sodium ascorbate (27.2 mg, 0.137 mmol, 0.7 eq) and TBTA (15.6 mg, 0.029 mmol, 0.15 eq) in CHCl<sub>3</sub> (2 mL). Refluxing lasted for 1 d. Column chromatography (eluent: DCM/MeOH 19:1, *R<sub>f</sub>* = 0.2) followed by preparative HPLC (gradient: 0-30 min: MeCN/ 0.1% aq TFA 33:67-69:31, *t<sub>R</sub>* = 11.0 min) afforded the product as a yellowish solid (71.8 mg, 0.129 mmol, 66%), **mp** 193-195 °C. <sup>1</sup>H NMR (600 MHz, CDCl<sub>3</sub>) δ (ppm)

12.96 (br s, 1H), 8.19 (s, 1H), 7.88 (m, 2H), 7.74 (d,  $J = 8.2$  Hz, 2H), 7.45 (m, 2H), 7.41 (d,  $J = 8.2$  Hz, 2H), 7.37 (m, 1H), 6.64 (s, 1H), 6.54 (s, 1H), 4.65 (d,  $J = 14.5$  Hz, 1H), 4.07 (d,  $J = 14.5$  Hz, 1H), 3.86 (s, 3H), 3.83 (s, 3H), 3.76 (m, 1H), 3.51-3.21 (m, 6H), 2.97 (m, 1H).  **$^{13}\text{C}$  NMR** (151 MHz,  $\text{CDCl}_3$ )  $\delta$  (ppm) 162.0 (TFA), 161.8 (TFA), 149.5, 148.9, 148.7, 136.8, 136.4, 130.4 (2C), 130.1, 129.1 (2C), 128.7, 126.0 (2C), 122.4, 121.2 (2C), 118.1, 117.8, 117.1 (TFA), 115.2 (TFA), 111.3, 109.3, 56.2, 56.1, 55.7, 52.5, 49.5, 30.5, 24.1. **RP-HPLC** (220 nm): 99% ( $t_R = 4.5$  min,  $k = 3.3$ ). **HRMS** (ESI):  $m/z$   $[M+H]^+$  calcd. for  $\text{C}_{27}\text{H}_{29}\text{N}_4\text{O}_2^+$ : 441.2285, found: 441.2310.  $\text{C}_{27}\text{H}_{28}\text{N}_4\text{O}_2 \cdot \text{C}_2\text{HF}_3\text{O}_2$  (440.54 + 114.02).

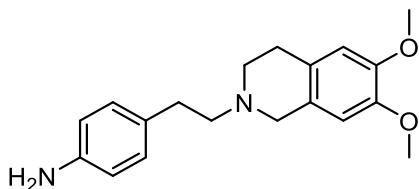
### Methyl 4-bromo-2-(quinoline-2-carboxamido)benzoate (**3.04**)



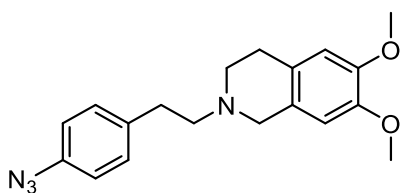
**3.04** was prepared according to the general procedure 1 for N-acylation of anilines. The reaction was carried out using quinoline-2-carboxylic acid (113 mg, 0.652 mmol, 1.5 eq), TBTU (209 mg, 0.652 mmol, 1.5 eq), DIPEA (222  $\mu\text{L}$ , 1.30 mmol, 3.0 eq) and methyl 2-amino-4-bromobenzoate (100 mg, 0.435 mmol, 1.0 eq) and DMF (1 mL). Dilution with EtOAc preceded the washing steps. Purification by column chromatography (eluent: PE/EtOAc = 4:1,  $R_f = 0.3$ ) and recrystallization in EtOAc afforded **3.04** as slightly yellowish crystals (144 mg, 0.374 mmol, 86%), **mp** 184-186  $^{\circ}\text{C}$ .  **$^1\text{H}$  NMR** (300 MHz,  $\text{CDCl}_3$ )  $\delta$  (ppm) 13.26 (s, 1H), 9.26 (d,  $J = 2.0$  Hz, 1H), 8.33 (s, 2H), 8.29 (d,  $J = 8.5$  Hz, 1H), 7.92 (d,  $J = 8.6$  Hz, 1H), 7.87 (dd,  $J = 0.9, 8.2$  Hz, 1H), 7.80 (m, 1H), 7.63 (m, 1H), 7.29-7.22 (m, 1H, signals interfering with the solvent signal), 4.03 (s, 3H).  **$^{13}\text{C}$  NMR** (75 MHz,  $\text{CDCl}_3$ )  $\delta$  (ppm) 167.6, 163.7, 149.7, 146.6, 141.7, 137.8, 132.4, 130.4, 130.3, 129.5, 129.4, 128.5, 127.8, 126.1, 123.5, 119.0, 115.2, 52.7. **RP-HPLC** (220 nm): 98% ( $t_R = 10.1$  min,  $k = 8.7$ ). **HRMS** (ESI):  $m/z$   $[M+H]^+$  calcd. for  $\text{C}_{18}\text{H}_{14}\text{BrN}_2\text{O}_3^+$ : 385.0182, found: 385.0189.  $\text{C}_{18}\text{H}_{13}\text{BrN}_2\text{O}_3$  (385.21).

**6,7-Dimethoxy-2-(4-nitrophenethyl)-1,2,3,4-tetrahydroisoquinoline (3.07) [75,76]**

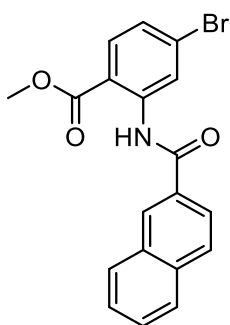
1-(2-Bromoethyl)-4-nitrobenzene (300 mg, 1.30 mmol, 1.0 eq), 6,7-dimethoxy-1,2,3,4-tetrahydroisoquinoline hydrochloride (330.8 mg, 1.43 mmol, 1.1 eq) and  $K_2CO_3$  (721 mg, 5.22 mmol, 4.0 eq) were suspended in MeCN (10 mL) in a microwave vessel and kept in a microwave reactor at 130 °C for 70 min. The suspension was filtered, and the filtrate concentrated under reduced pressure. The residue was subjected to flash column chromatography (4 g column, gradient: 0-20 min: DCM/MeOH 100:0-96:4,  $R_f$  = 0.3 in DCM/MeOH 96:4), yielding **3.07** as an orange solid (276 mg, 0.806 mmol, 62%), **mp** 102-108 °C (lit. [76,77] mp 118 °C).  **$^1H$  NMR** (300 MHz,  $CDCl_3$ )  $\delta$  (ppm) 8.14 (d,  $J$  = 8.8 Hz, 2H), 7.40 (d,  $J$  = 8.7 Hz, 2H), 6.60 (s, 1H), 6.52 (s, 1H), 3.84 (s, 3H), 3.83 (s, 3H), 3.68 (s, 2H), 3.08-2.99 (m, 2H), 2.90-2.78 (m, 6H).  **$^{13}C$  NMR** (75 MHz,  $CDCl_3$ )  $\delta$  148.2, 147.8, 147.5, 146.7, 129.7 (2C), 125.8, 125.7, 123.8 (2C), 111.4, 109.5, 59.0, 56.1, 56.0, 55.5, 51.0, 33.7, 28.4. **HRMS** (ESI):  $m/z$   $[M+H]^+$  calcd. for  $C_{19}H_{23}N_2O_4^+$ : 343.1652, found: 343.1654.  **$C_{19}H_{22}N_2O_4$**  (342.39).

**4-(2-(6,7-Dimethoxy-3,4-dihydroisoquinolin-2(1H)-yl)ethyl)aniline (3.08) [75-77]**

6,7-Dimethoxy-2-(4-nitrophenethyl)-1,2,3,4-tetrahydroisoquinoline (**3.07**) (894 mg, 2.61 mmol, 1.0 eq) was dissolved in EtOH (18 mL) and a 10% Pd/C catalyst (100 mg) was added. The suspension was stirred under a hydrogen atmosphere (10 bar) overnight and the catalyst was filtered off. Column chromatography (eluent: DCM/MeOH = 14:1,  $R_f$  = 0.2) yielded **3.08** as a yellow solid (577 mg, 1.85 mmol, 71%), **mp** 120-122 °C (lit. [77] mp 120 °C).  **$^1H$  NMR** (300 MHz,  $CDCl_3$ )  $\delta$  (ppm) 7.02 (d,  $J$  = 8.3 Hz, 2H), 6.66-6.58 (m, 3H), 6.53 (s, 1H), 3.84 (s, 3H), 3.83 (s, 3H), 3.68 (s, 2H), 3.62 (br s, 2H), 2.92-2.69 (m, 8H).  **$^{13}C$  NMR** (75 MHz,  $CDCl_3$ )  $\delta$  (ppm) 147.7, 147.3, 144.7, 130.0, 129.6 (2C), 126.4, 126.0, 115.4 (2C), 111.4, 109.5, 60.4, 56.0, 56.0, 55.6, 51.0, 33.0, 28.4. **HRMS** (ESI):  $m/z$   $[M+H]^+$  calcd. for  $C_{19}H_{25}N_2O_2^+$ : 313.1911, found: 313.1912.  **$C_{19}H_{24}N_2O_2$**  (312.41).

**2-(4-Azidophenethyl)-6,7-dimethoxy-1,2,3,4-tetrahydroisoquinoline (3.09) [78]**

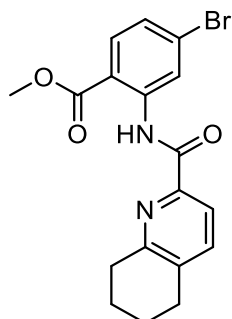
4-(2-(6,7-Dimethoxy-3,4-dihydroisoquinolin-2(1*H*)-yl)ethyl)aniline (**3.08**) (560 mg, 1.79 mmol, 1.0 eq) was dissolved in 6 M HCl aq (10 mL) and cooled to 0 °C using an ice bath. A solution of NaNO<sub>2</sub> (148 mg, 2.15 mmol, 1.2 eq) in H<sub>2</sub>O (2 mL) was added dropwise, and stirring was continued for 1 h. Thereafter, a solution of NaN<sub>3</sub> (233 mg, 3.59 mmol, 2.0 eq) was added dropwise, and the mixture was brought to rt and stirred for another 2 h. Then, the mixture was diluted with H<sub>2</sub>O, and the product was extracted with DCM (3 x 100 mL). The combined organic layers were dried over Na<sub>2</sub>SO<sub>4</sub> and the volatiles were removed under reduced pressure, affording **3.09** as a yellow solid (556 mg, 1.64 mmol, 92%), **mp** 168-175 °C (lit. [78] mp 68-70°C). **<sup>1</sup>H NMR** (300 MHz, CDCl<sub>3</sub>) δ (ppm) 7.23 (d, *J* = 8.5 Hz, 2H), 6.93 (d, *J* = 8.5 Hz, 2H), 6.61 (s, 1H), 6.53 (s, 1H), 4.64-4.51 (m, 1H), 4.07-3.96 (m, 1H), 3.83 (s, 3H), 3.81 (s, 3H), 3.72-3.56 (m, 1H), 3.47-3.19 (m, 6H), 2.98-2.84 (m, 1H). **<sup>13</sup>C NMR** (75 MHz, CDCl<sub>3</sub>) δ (ppm) 149.3, 148.7, 139.3, 132.7, 130.3 (2C), 122.5, 119.6 (2C), 118.0, 111.2, 109.3, 56.1, 56.1, 55.8, 52.2, 49.3, 30.1, 24.0. **HRMS** (ESI): *m/z* [*M*+*H*]<sup>+</sup> calcd. for C<sub>19</sub>H<sub>23</sub>N<sub>4</sub>O<sub>2</sub><sup>+</sup>: 339.1816, found: 339.1818. C<sub>19</sub>H<sub>22</sub>N<sub>4</sub>O<sub>2</sub> (338.41).

**Methyl 2-(2-naphthamido)-4-bromobenzoate (3.12)**

**3.12** was prepared according to the general procedure 2 for N-acylation of anilines. The reaction was carried out using 2-naphthoic acid (100 mg, 0.581 mmol, 1.0 eq), thionyl chloride (84 µL, 1.162 mmol, 2.0 eq), pyridine (94 µL, 1.162 mmol, 2.0 eq), methyl 2-amino-4-bromobenzoate (134 mg, 0.581 mmol, 1.0 eq), DIPEA (405 µL, 2.323 mmol, 4.0 eq), and toluene (1 mL). After the washing steps, recrystallization in EtOAc afforded **3.12** as a beige-colored solid (104 mg, 0.271 mmol, 47%), **mp** 145-146 °C. **<sup>1</sup>H NMR** (400 MHz, CDCl<sub>3</sub>) δ (ppm) 12.21 (s, 1H), 9.26 (d, *J* = 1.9 Hz, 1H), 8.57 (s, 1H), 8.11-7.87 (m, 5H), 7.64-7.54 (m, 2H), 7.29-7.24 (m, 1H, signals interfering with the solvent signal), 3.99 (s, 3H). **<sup>13</sup>C NMR** (101 MHz, CDCl<sub>3</sub>) δ (ppm) 168.8, 165.9, 142.8, 135.2, 132.9, 132.1, 131.7, 130.0, 129.6, 128.9, 128.6, 128.2, 127.9, 127.0,

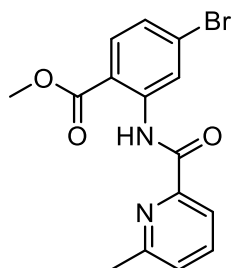
126.0, 123.6, 123.5, 113.9, 52.8. **RP-HPLC** (220 nm): 97% ( $t_R$  = 10.4 min,  $k$  = 8.9). **HRMS** (ESI):  $m/z$   $[M+H]^+$  calcd. for  $C_{19}H_{15}BrNO_3^+$ : 384.0230, found: 384.0236.  **$C_{19}H_{14}BrNO_3$**  (384.23).

### Methyl 4-bromo-2-(5,6,7,8-tetrahydroquinoline-2-carboxamido)benzoate (**3.13**)



**3.13** was prepared according to the general procedure 1 for N-acylation of anilines. The reaction was carried out using 5,6,7,8-tetrahydroquinoline-2-carboxylic acid (**3.31**) (100 mg, 0.564 mmol, 1.0 eq), TBTU (181 mg, 0.564 mmol, 1.0 eq), DIPEA (197  $\mu$ L, 1.129 mmol, 2.0 eq) and methyl 2-amino-4-bromobenzoate (143 mg, 0.621 mmol, 1.1 eq) and DMF (2 mL). Dilution with DCM preceded the washing steps. Recrystallization in EtOAc afforded **3.13** as beige-colored crystals (30 mg, 0.077 mmol, 14%), **mp** 142-143 °C.  **$^1H$  NMR** (400 MHz,  $CDCl_3$ )  $\delta$  (ppm) 12.92 (s, 1H), 9.24 (d,  $J$  = 1.9 Hz, 1H), 7.99 (d,  $J$  = 7.8 Hz, 1H), 7.93 (d,  $J$  = 8.6 Hz, 1H), 7.55 (d,  $J$  = 7.8 Hz, 1H), 7.28-7.22 (m, 1H, signals interfering with the solvent signal), 4.00 (s, 3H), 3.08 (t,  $J$  = 6.3 Hz, 2H), 2.86 (t,  $J$  = 6.2 Hz, 2H), 1.92 (m, 4H).  **$^{13}C$  NMR** (101 MHz,  $CDCl_3$ )  $\delta$  (ppm) 167.6, 164.1, 156.7, 147.1, 141.8, 138.2, 136.5, 132.4, 129.4, 126.0, 123.6, 120.2, 115.3, 52.6, 32.7, 29.1, 23.0, 22.7. **RP-HPLC** (220 nm): 97% ( $t_R$  = 10.5 min,  $k$  = 9.0). **HRMS** (ESI):  $m/z$   $[M+H]^+$  calcd. for  $C_{18}H_{18}BrN_2O_3^+$ : 389.0495, found: 389.0498.  **$C_{18}H_{17}BrN_2O_3$**  (386.15).

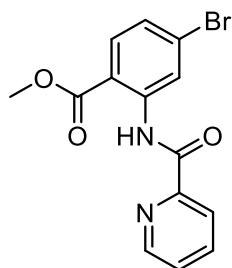
### Methyl 4-bromo-2-(6-methylpicolinamido)benzoate (**3.14**)



**3.14** was prepared according to the general procedure 1 for N-acylation of anilines. The reaction was carried out using 6-methylpicolinic acid (100 mg, 0.729 mmol, 1.0 eq), TBTU (234 mg, 0.729 mmol, 1.0 eq), DIPEA (254  $\mu$ L, 1.458 mmol, 2.0 eq) and methyl 2-amino-4-bromobenzoate (185 mg, 0.802 mmol, 1.1 eq) and DMF (2 mL). Dilution with DCM preceded the washing steps. Purification by column chromatography (eluent: PE/EtOAc = 10:1,  $R_f$  = 0.3)

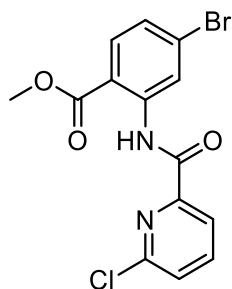
afforded **3.14** as a yellowish solid (198 mg, 0.567 mmol, 78%), **mp** 157-158 °C. **<sup>1</sup>H NMR** (300 MHz, CDCl<sub>3</sub>)  $\delta$  (ppm) 13.02 (s, 1H), 9.24 (d,  $J$  = 2.0 Hz, 1H), 8.09 (d,  $J$  = 7.7 Hz, 1H), 7.94 (d,  $J$  = 8.6 Hz, 1H), 7.80 (t,  $J$  = 7.7 Hz, 1H), 7.36 (d,  $J$  = 7.7 Hz, 1H), 7.30-7.23 (m, 1H, signals interfering with the solvent signal), 4.00 (s, 3H), 2.73 (s, 3H). **<sup>13</sup>C NMR** (75 MHz, CDCl<sub>3</sub>)  $\delta$  (ppm) 167.6, 163.7, 157.7, 149.3, 141.7, 138.0, 132.4, 129.4, 126.6, 126.2, 123.7, 120.1, 115.3, 52.7, 24.5. **RP-HPLC** (220 nm): 98% ( $t_R$  = 9.1 min,  $k$  = 7.7). **HRMS** (ESI):  $m/z$  [ $M+H$ ]<sup>+</sup> calcd. for C<sub>15</sub>H<sub>14</sub>BrN<sub>2</sub>O<sub>3</sub><sup>+</sup>: 349.0182, found: 349.0195. C<sub>15</sub>H<sub>13</sub>BrN<sub>2</sub>O<sub>3</sub> (349.18).

### Methyl 4-bromo-2-(picolinamido)benzoate (**3.15**)



**3.15** was prepared according to the general procedure 1 for N-acylation of anilines. The reaction was carried out using picolinic acid (80 mg, 0.652 mmol, 1.5 eq), TBTU (209 mg, 0.652 mmol, 1.5 eq), DIPEA (122  $\mu$ L, 1.30 mmol, 3.0 eq) and methyl 2-amino-4-bromobenzoate (100 mg, 0.435 mmol, 1.0 eq) and DMF (1 mL). Dilution with EtOAc preceded the washing steps. Purification by column chromatography (eluent: PE/EtOAc = 4:1,  $R_f$  = 0.3) afforded **3.15** as a white, fluffy solid (109 mg, 0.325 mmol, 75%), **mp** 179-181 °C. **<sup>1</sup>H NMR** (300 MHz, CDCl<sub>3</sub>)  $\delta$  (ppm) 13.05 (s, 1H), 9.26 (d,  $J$  = 1.9 Hz, 1H), 8.78 (d,  $J$  = 4.3 Hz, 1H), 8.29 (d,  $J$  = 7.8 Hz, 1H), 7.98-7.87 (m, 2H), 7.55-7.46 (m, 1H), 7.31-7.26 (m, 1H, signals interfering with the solvent signal), 4.00 (s, 3H). **<sup>13</sup>C NMR** (75 MHz, CDCl<sub>3</sub>)  $\delta$  (ppm) 167.8, 163.6, 150.1, 148.8, 141.9, 137.7, 132.4, 129.6, 126.8, 126.3, 123.7, 123.0, 115.0, 52.8. **RP-HPLC** (220 nm): 98% ( $t_R$  = 8.2 min,  $k$  = 6.9). **HRMS** (ESI):  $m/z$  [ $M+H$ ]<sup>+</sup> calcd. for C<sub>14</sub>H<sub>12</sub>BrN<sub>2</sub>O<sub>3</sub><sup>+</sup>: 335.0031, found: 335.0031. C<sub>14</sub>H<sub>11</sub>BrN<sub>2</sub>O<sub>3</sub> (335.15).

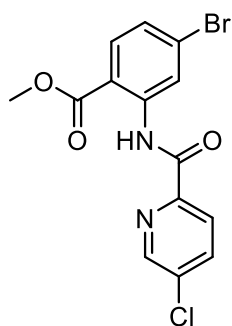
### Methyl 4-bromo-2-(6-chloropicolinamido)benzoate (**3.16**)



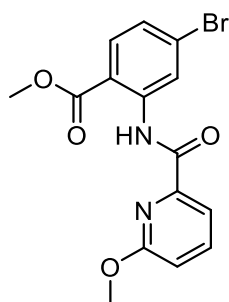
**3.16** was prepared according to the general procedure 1 for N-acylation of anilines. The reaction was carried out using 6-chloropicolinic acid (500 mg, 3.174 mmol, 1.0 eq), TBTU (1019 mg,

3.174 mmol, 1.0 eq), DIPEA (1106  $\mu$ L, 6.347 mmol, 2.0 eq) and methyl 2-amino-4-bromobenzoate (803 mg, 3.491 mmol, 1.1 eq) and DMF (8 mL). Dilution with EtOAc preceded the washing steps. Recrystallization in  $\text{CHCl}_3$  afforded **3.16** as a white solid (272 mg, 0.736 mmol, 23%), **mp** 167-169  $^{\circ}\text{C}$ .  **$^1\text{H}$  NMR** (300 MHz,  $\text{CDCl}_3$ )  $\delta$  (ppm) 12.82 (s, 1H), 9.18 (d,  $J = 1.9$  Hz, 1H), 8.20 (s, 1H), 7.98-8.16 (m, 2H), 7.53 (d,  $J = 7.9$  Hz, 1H), 7.29 (dd,  $J = 2.0$ , 8.6 Hz, 1H), 4.05 (s, 3H).  **$^{13}\text{C}$  NMR** (75 MHz,  $\text{CDCl}_3$ )  $\delta$  (ppm) 167.4, 162.0, 150.6, 150.5, 141.1, 140.4, 132.6, 129.4, 127.7, 126.6, 123.6, 121.6, 115.5, 52.9. **RP-HPLC** (220 nm): 99% ( $t_R = 9.1$  min,  $k = 7.7$ ). **HRMS** (ESI):  $m/z$   $[M+H]^+$  calcd. for  $\text{C}_{14}\text{H}_{11}\text{BrClN}_2\text{O}_3^+$ : 368.9636, found: 368.9639.  **$\text{C}_{14}\text{H}_{10}\text{BrClN}_2\text{O}_3$**  (369.60).

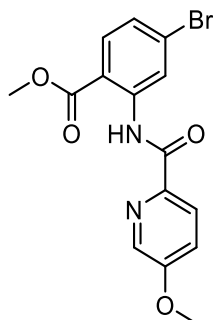
### Methyl 4-bromo-2-(5-chloropicolinamido)benzoate (**3.17**)



**3.17** was prepared according to the general procedure 1 for N-acylation of anilines. The reaction was carried out using 5-chloropicolinic acid (500 mg, 3.174 mmol, 1.0 eq), TBTU (1019 mg, 3.174 mmol, 1.0 eq), DIPEA (1106  $\mu$ L, 6.347 mmol, 2.0 eq) and methyl 2-amino-4-bromobenzoate (803 mg, 3.491 mmol, 1.1 eq) and DMF (8 mL). Dilution with EtOAc preceded the washing steps. Recrystallization in  $\text{CHCl}_3$  afforded **3.17** as a white solid (178 mg, 0.482 mmol, 15%), **mp** 195-199  $^{\circ}\text{C}$ .  **$^1\text{H}$  NMR** (400 MHz,  $\text{CDCl}_3$ )  $\delta$  (ppm) 12.94 (s, 1H), 9.21 (d,  $J = 1.7$  Hz, 1H), 8.71 (d,  $J = 2.2$  Hz, 1H), 8.23 (d,  $J = 8.4$  Hz, 1H), 7.94 (d,  $J = 8.6$  Hz, 1H), 7.88 (dd,  $J = 2.3$ , 8.4 Hz, 1H), 7.28 (dd,  $J = 1.8$ , 8.6 Hz, 1H), 3.99 (s, 3H).  **$^{13}\text{C}$  NMR** (101 MHz,  $\text{CDCl}_3$ )  $\delta$  (ppm) 167.8, 162.7, 148.3, 147.9, 141.7, 137.4, 135.7, 132.4, 129.6, 126.4, 124.0, 123.7, 115.0, 52.8. **RP-HPLC** (220 nm): 98% ( $t_R = 9.3$  min,  $k = 7.9$ ). **HRMS** (ESI):  $m/z$   $[M+H]^+$  calcd. for  $\text{C}_{14}\text{H}_{11}\text{BrClN}_2\text{O}_3^+$ : 368.9636, found: 368.9640.  **$\text{C}_{14}\text{H}_{10}\text{BrClN}_2\text{O}_3$**  (369.60).

**Methyl 4-bromo-2-(6-methoxypicolinamido)benzoate (3.18)**

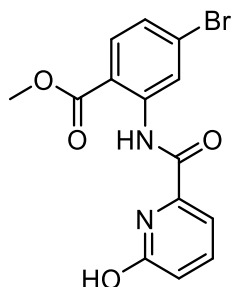
**3.18** was prepared according to the general procedure 1 for N-acylation of anilines. The reaction was carried out using 6-methoxypicolinic acid (100 mg, 0.653 mmol, 1.0 eq), TBTU (210 mg, 0.653 mmol, 1.0 eq), DIPEA (228  $\mu$ L, 1.306 mmol, 2.0 eq) and methyl 2-amino-4-bromobenzoate (165 mg, 0.718 mmol, 1.1 eq) and DMF (1.5 mL). Dilution with DCM preceded the washing steps. Recrystallization in EtOAc afforded **3.18** as a white solid (77 mg, 0.211 mmol, 32%), **mp** 177-179 °C. **<sup>1</sup>H NMR** (300 MHz, CDCl<sub>3</sub>)  $\delta$  (ppm) 13.03 (s, 1H), 9.26 (d,  $J$  = 2.0 Hz, 1H), 7.95-7.83 (m, 2H), 7.80-7.72 (m, 1H), 7.29-7.22 (m, 1H, signals interfering with the solvent signal), 6.95 (dd,  $J$  = 0.8, 8.2 Hz, 1H), 4.19 (s, 3H), 3.92 (s, 3H). **<sup>13</sup>C NMR** (75 MHz, CDCl<sub>3</sub>)  $\delta$  (ppm) 167.6, 163.6, 163.2, 147.4, 142.0, 139.9, 132.1, 129.5, 126.1, 123.6, 116.1, 115.1, 115.0, 54.4, 52.4. **RP-HPLC** (220 nm): 98% ( $t_R$  = 9.4 min,  $k$  = 8.0). **HRMS** (ESI):  $m/z$  [ $M+H$ ]<sup>+</sup> calcd. for C<sub>15</sub>H<sub>14</sub>BrN<sub>2</sub>O<sub>4</sub><sup>+</sup>: 365.0131, found: 365.0147. **C<sub>15</sub>H<sub>13</sub>BrN<sub>2</sub>O<sub>4</sub>** (365.18).

**Methyl 4-bromo-2-(5-methoxypicolinamido)benzoate (3.19)**

**3.19** was prepared according to the general procedure 1 for N-acylation of anilines. The reaction was carried out using 5-methoxypicolinic acid (100 mg, 0.653 mmol, 1.0 eq), TBTU (210 mg, 0.653 mmol, 1.0 eq), DIPEA (228  $\mu$ L, 1.306 mmol, 2.0 eq) and methyl 2-amino-4-bromobenzoate (165 mg, 0.718 mmol, 1.1 eq) and DMF (1 mL). Dilution with EtOAc preceded the washing steps. Purification by column chromatography (eluent: PE/EtOAc = 4:1,  $R_f$  = 0.2) afforded **3.19** as a white solid (70 mg, 0.192 mmol, 29%), **mp** 162-164 °C. **<sup>1</sup>H NMR** (300 MHz, CDCl<sub>3</sub>)  $\delta$  (ppm) 12.89 (s, 1H), 9.24 (d,  $J$  = 2.0 Hz, 1H), 8.42 (d,  $J$  = 2.3 Hz, 1H), 8.23 (d,  $J$  = 8.6 Hz, 1H), 7.92 (d,  $J$  = 8.6 Hz, 1H), 7.33 (dd,  $J$  = 2.4, 8.6 Hz, 1H), 7.26-7.20 (m, 1H, signals interfering with the solvent signal), 3.98 (s, 3H), 3.93 (s, 3H). **<sup>13</sup>C NMR** (75 MHz, CDCl<sub>3</sub>)  $\delta$  (ppm) 167.9, 163.5, 158.3, 142.7, 142.1, 136.9, 132.3, 129.5, 125.9, 124.3, 123.5,

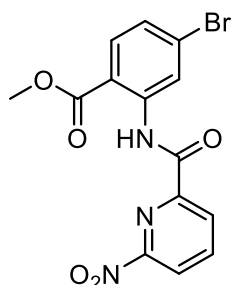
120.8, 114.8, 56.0, 52.7. **RP-HPLC** (220 nm): 100% ( $t_R$  = 8.5 min,  $k$  = 7.2). **HRMS** (ESI):  $m/z$  [ $M+H$ ]<sup>+</sup> calcd. for C<sub>15</sub>H<sub>14</sub>BrN<sub>2</sub>O<sub>4</sub><sup>+</sup>: 365.0131, found: 365.0138. **C<sub>15</sub>H<sub>13</sub>BrN<sub>2</sub>O<sub>4</sub>** (365.18).

### Methyl 4-bromo-2-(6-hydroxypicolinamido)benzoate (**3.20**)



**3.20** was prepared according to the general procedure 1 for N-acylation of anilines. The reaction was carried out using 6-hydroxypicolinic acid (100 mg, 0.719 mmol, 1.0 eq), TBTU (230 mg, 0.719 mmol, 1.0 eq), DIPEA (250  $\mu$ L, 1.438 mmol, 2.0 eq) and methyl 2-amino-4-bromobenzoate (182 mg, 0.797 mmol, 1.1 eq) and DMF (2 mL). Dilution with DCM preceded the washing steps. The crude product was subjected to column chromatography (eluent: DCM/MeOH = 50:1,  $R_f$  = 0.3) and for further purification to preparative HPLC (gradient: 0-30 min: MeCN/ 0.1% aq TFA 55:45-90:10,  $t_R$  = 12.0 min). Removal of the solvent from the eluate through evaporation and lyophilization afforded **3.20** as a white solid (94 mg, 0.268 mmol, 37%), **mp** 182-184 °C. **<sup>1</sup>H NMR** (400 MHz, DMSO-*d*<sub>6</sub>)  $\delta$  12.43 (s, 1H), 11.22 (s, 1H), 9.02 (d,  $J$  = 1.6 Hz, 1H), 7.97 (d,  $J$  = 8.6 Hz, 1H), 7.88 (t,  $J$  = 7.8 Hz, 1H), 7.65 (d,  $J$  = 6.9 Hz, 1H), 7.45 (dd,  $J$  = 2.0, 8.5 Hz, 1H), 6.98 (d,  $J$  = 8.2 Hz, 1H), 3.96 (s, 3H). **<sup>13</sup>C NMR** (151 MHz, DMSO-*d*<sub>6</sub>)  $\delta$  (ppm) 166.5, 162.9, 162.7, 147.2, 140.8 (2C), 132.8, 127.9, 126.2, 122.7, 115.6, 114.6, 114.4, 52.9. **RP-HPLC** (220 nm): 100% ( $t_R$  = 6.8 min,  $k$  = 5.5). **HRMS** (ESI):  $m/z$  [ $M+H$ ]<sup>+</sup> calcd. for C<sub>14</sub>H<sub>12</sub>BrN<sub>2</sub>O<sub>4</sub><sup>+</sup>: 350.9975, found: 350.9976. **C<sub>14</sub>H<sub>11</sub>BrN<sub>2</sub>O<sub>4</sub>** (351.16).

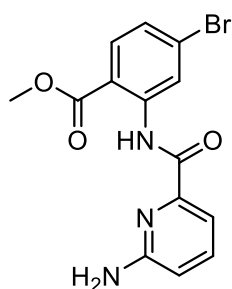
### Methyl 4-bromo-2-(6-nitropicolinamido)benzoate (**3.21**)



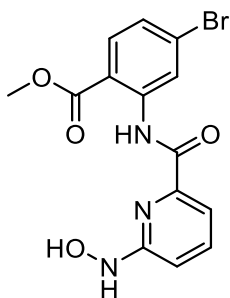
**3.21** was prepared according to the general procedure 1 for N-acylation of anilines. The reaction was carried out using 6-nitropicolinic acid (100 mg, 0.595 mmol, 1.0 eq), TBTU (191 mg, 0.595 mmol, 1.0 eq), DIPEA (207  $\mu$ L, 1.190 mmol, 2.0 eq) and methyl 2-amino-4-bromobenzoate (151 mg, 0.654 mmol, 1.1 eq) and DMF (2 mL). Dilution with DCM preceded

the washing steps. Recrystallization in EtOAc afforded **3.21** as a yellowish solid (82 mg, 0.216 mmol, 36%), **mp** 222-223 °C. **<sup>1</sup>H NMR** (300 MHz, CDCl<sub>3</sub>)  $\delta$  (ppm) 13.02 (s, 1H), 9.19 (d,  $J$  = 2.0 Hz, 1H), 8.67 (dd,  $J$  = 0.8, 7.7 Hz, 1H), 8.47 (dd,  $J$  = 0.8, 8.0 Hz, 1H), 8.30 (t,  $J$  = 7.9 Hz, 1H), 7.99 (d,  $J$  = 8.6 Hz, 1H), 7.34 (dd,  $J$  = 2.0, 8.6 Hz, 1H), 4.07 (s, 3H). **<sup>13</sup>C NMR** (75 MHz, CDCl<sub>3</sub>)  $\delta$  (ppm) 167.8, 161.1, 155.4, 149.9, 142.0, 141.0, 132.6, 129.5, 128.2, 127.1, 123.7, 120.8, 115.6, 53.1. **RP-HPLC** (220 nm): 100% ( $t_R$  = 8.1 min,  $k$  = 6.8). **HRMS** (ESI):  $m/z$  [ $M+H$ ]<sup>+</sup> calcd. for C<sub>14</sub>H<sub>11</sub>BrN<sub>3</sub>O<sub>5</sub><sup>+</sup>: 379.9877, found: 379.9879. C<sub>14</sub>H<sub>10</sub>BrN<sub>3</sub>O<sub>5</sub> (386.15).

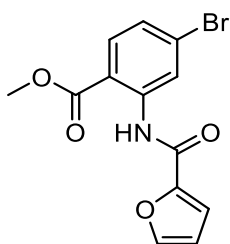
### Methyl 2-(6-aminopicolinamido)-4-bromobenzoate (**3.22**)



Methyl 4-bromo-2-(6-nitropicolinamido)benzoate (**3.21**) (30 mg, 0.079 mmol, 1.0 eq) was dissolved in anhydrous DCM (1 mL) and DIPEA (69  $\mu$ L, 0.395 mmol, 5.0 eq) was added. The stirred solution was cooled down to 0 °C using an ice bath, HSiCl<sub>3</sub> was added dropwise and stirring was continued at rt overnight. The reaction was quenched with H<sub>2</sub>O followed by extraction with DCM. The combined organic layers were dried over Na<sub>2</sub>SO<sub>4</sub> and the volatiles were removed under reduced pressure. Purification by column chromatography (eluent: DCM/MeOH = 100:1,  $R_f$  = 0.2) was not sufficient to separate the product entirely from the byproduct methyl 4-bromo-2-(6-(hydroxyamino)picolinamido)benzoate (**3.23**) ( $R_f$  = 0.1). Therefore the mixture was subjected to preparative HPLC (gradient: 0-30 min: MeCN/ 0.1% aq TFA 46:54-82:18,  $t_R$  = 12.8 min). Removal of the solvent from the eluate through evaporation and lyophilization afforded **3.22** as a brownish solid (8.3 mg, 0.024 mmol, 30%), **mp** 186-188 °C. **<sup>1</sup>H NMR** (400 MHz, CDCl<sub>3</sub>)  $\delta$  (ppm) 12.88 (s, 1H), 9.23 (d,  $J$  = 2.0 Hz, 1H), 7.92 (d,  $J$  = 8.6 Hz, 1H), 7.66-7.59 (m, 2H), 7.27-7.23 (m, 1H, signals interfering with the solvent signal), 6.74-6.67 (m, 1H), 3.97 (s, 3H), 3.66 (2H). **<sup>13</sup>C NMR** (101 MHz, CDCl<sub>3</sub>)  $\delta$  (ppm) 167.7, 163.8, 157.3, 148.2, 142.0, 139.3, 132.3, 129.5, 126.0, 123.6, 115.0, 113.4, 112.4, 52.6. **RP-HPLC** (220 nm): 97% ( $t_R$  = 6.1 min,  $k$  = 4.8). **HRMS** (ESI):  $m/z$  [ $M+H$ ]<sup>+</sup> calcd. for C<sub>14</sub>H<sub>13</sub>BrN<sub>3</sub>O<sub>3</sub><sup>+</sup>: 350.0135, found: 350.0164. C<sub>14</sub>H<sub>12</sub>BrN<sub>3</sub>O<sub>3</sub> (350.17).

**Methyl 4-bromo-2-(6-(hydroxyamino)picolinamido)benzoate (3.23)**

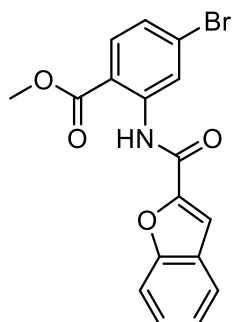
**3.23** is a side product of the synthesis of **3.22**. Preparative HPLC (gradient: 0-30 min: MeCN/0.1% aq TFA 46:54-82:18,  $t_R$  = 14.5 min) and removal of the solvent from the eluate through evaporation and lyophilization afforded **3.23** as a white solid (3.9 mg, 0.011 mmol, 13%), **mp** 252-255 °C. Due to a slow rotation around the amide group on the NMR time scale, two isomers (ratio ca 1:0.3) were evident in the NMR spectra. **<sup>1</sup>H NMR** (600 MHz, DMSO-*d*<sub>6</sub>)  $\delta$  (ppm) 12.48 (s, 0.3H), 12.40 (s, 1H), 9.05 (d,  $J$  = 2.0 Hz, 0.3H), 9.04 (d,  $J$  = 2.0 Hz, 1H), 8.99 (s, 1H), 8.82 (d,  $J$  = 1.5 Hz, 1H), 7.96 (d,  $J$  = 8.5 Hz, 1.3H), 7.87 (t,  $J$  = 7.8 Hz, 1H), 7.63 (m, 0.3H), 7.55 (m, 1H), 7.45 (m, 1.3H), 7.33 (m, 0.3H), 7.14 (d,  $J$  = 8.2 Hz, 1H), 6.75 (dd,  $J$  = 0.7, 8.3 Hz, 0.3H), 6.18 (s, 0.5H), 3.98 (s, 3H), 3.97 (s, 0.9H). **<sup>13</sup>C NMR** (151 MHz, DMSO-*d*<sub>6</sub>)  $\delta$  (ppm) 166.3, 163.2, 162.3, 146.9, 140.6, 139.4, 132.9, 127.9, 126.1, 122.6, 115.7, 113.6, 110.9, 52.9. **RP-HPLC** (220 nm): 96% ( $t_R$  = 6.4 min,  $k$  = 5.1). **HRMS** (ESI):  $m/z$  [ $M+H$ ]<sup>+</sup> calcd. for C<sub>14</sub>H<sub>13</sub>BrN<sub>3</sub>O<sub>4</sub><sup>+</sup>: 366.0084, found: 366.0087. **C<sub>14</sub>H<sub>12</sub>BrN<sub>3</sub>O<sub>4</sub>** (366.17).

**Methyl 4-bromo-2-(furan-2-carboxamido)benzoate (3.24)**

**3.24** was prepared according to the general procedure 1 for N-acylation of anilines. The reaction was carried out using furan-2-carboxylic acid (73 mg, 0.652 mmol, 1.5 eq), TBTU (209 mg, 0.652 mmol, 1.5 eq), DIPEA (122  $\mu$ L, 1.30 mmol, 3.0 eq) and methyl 2-amino-4-bromobenzoate (100 mg, 0.435 mmol, 1.0 eq) and DMF (1 mL). Dilution with EtOAc preceded the washing steps. The crude product was subjected to column chromatography (eluent: PE/EtOAc = 6:1,  $R_f$  = 0.2) and for further purification to preparative HPLC (gradient: 0-20 min: MeCN/0.1% aq TFA 50:50-95:5,  $t_R$  = 14.3 min). Removal of the solvent from the eluate through evaporation and lyophilization afforded **3.24** as a white, fluffy solid (4.63 mg, 0.014 mmol, 3%), **mp** 142-144 °C. **<sup>1</sup>H NMR** (300 MHz, DMSO-*d*<sub>6</sub>)  $\delta$  (ppm) 11.85 (s, 1H), 8.88 (d,  $J$  = 2.0 Hz, 1H), 8.06 (m, 1H), 7.95 (d,  $J$  = 8.6 Hz, 1H), 7.44 (dd,  $J$  = 2.0, 8.6 Hz, 1H),

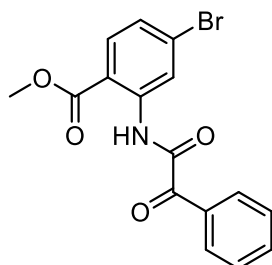
7.34 (dd,  $J = 0.5, 3.5$  Hz, 1H), 6.77 (dd,  $J = 1.7, 3.5$  Hz, 1H), 3.91 (s, 3H).  $^{13}\text{C}$  NMR (101 MHz, DMSO- $d_6$ )  $\delta$  (ppm) 167.4, 155.8, 146.9, 146.6, 141.1, 132.5, 128.0, 126.1, 122.4, 116.2, 114.9, 112.9, 52.9. **RP-HPLC** (220 nm): 97% ( $t_R = 7.9$  min,  $k = 6.6$ ). **HRMS** (ESI):  $m/z$  [ $M+H$ ] $^+$  calcd. for  $\text{C}_{13}\text{H}_{11}\text{BrNO}_4^+$ : 323.9866, found: 323.9868. **C<sub>13</sub>H<sub>10</sub>BrNO<sub>4</sub>** (324.13).

### Methyl 2-(benzofuran-2-carboxamido)-4-bromobenzoate (**3.25**)



**3.25** was prepared according to the general procedure 1 for N-acylation of anilines. The reaction was carried out using benzofuran-2-carboxylic acid (106 mg, 0.652 mmol, 1.5 eq), TBTU (209 mg, 0.652 mmol, 1.5 eq), DIPEA (122  $\mu\text{L}$ , 1.30 mmol, 3.0 eq) and methyl 2-amino-4-bromobenzoate (100 mg, 0.435 mmol, 1.0 eq) and DMF (1 mL). Dilution with EtOAc preceded the washing steps. Purification by column chromatography (eluent: PE/EtOAc = 4:1,  $R_f = 0.3$ ) and recrystallization in EtOAc afforded **3.25** as white crystals (63 mg, 0.168 mmol, 39%), **mp** 163-165  $^{\circ}\text{C}$ .  $^1\text{H}$  NMR (300 MHz,  $\text{CDCl}_3$ )  $\delta$  (ppm) 12.26 (s, 1H), 9.17 (d,  $J = 1.9$  Hz, 1H), 7.94 (d,  $J = 8.6$  Hz, 1H), 7.73-7.64 (m, 2H), 7.62 (d,  $J = 1.0$  Hz, 1H), 7.50-7.43 (m, 1H), 7.36-7.26 (m, 2H, signals interfering with the solvent signal), 4.01 (s, 3H).  $^{13}\text{C}$  NMR (75 MHz,  $\text{CDCl}_3$ )  $\delta$  (ppm) 168.3, 157.5, 155.3, 148.7, 141.9, 132.2, 129.8, 127.7, 127.5, 126.4, 124.0, 123.7, 122.9, 114.3, 112.5, 112.0, 52.9. **RP-HPLC** (220 nm): 96% ( $t_R = 9.6$  min,  $k = 8.2$ ). **HRMS** (ESI):  $m/z$  [ $M+H$ ] $^+$  calcd. for  $\text{C}_{17}\text{H}_{13}\text{BrNO}_4^+$ : 374.0028, found: 374.0029. **C<sub>17</sub>H<sub>12</sub>BrNO<sub>4</sub>** (374.19).

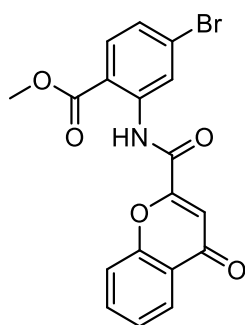
### Methyl 4-bromo-2-(2-oxo-2-phenylacetamido)benzoate (**3.26**)



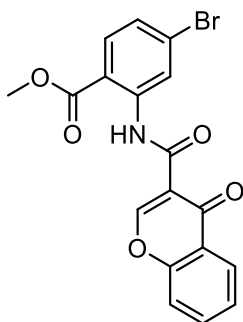
**3.26** was prepared according to the general procedure 1 for N-acylation of anilines. The reaction was carried out using 2-oxo-2-phenylacetic acid (326 mg, 2.173 mmol, 1.0 eq), TBTU (698 mg, 2.173 mmol, 1.0 eq), DIPEA (757  $\mu\text{L}$ , 4.347 mmol, 2.0 eq) and methyl 2-amino-4-bromobenzoate (500 mg, 2.391 mmol, 1.1 eq) and DMF (5 mL). Dilution with EtOAc preceded

the washing steps. Recrystallization in  $\text{CHCl}_3$  afforded **3.26** as a yellow solid (326 mg, 0.900 mmol, 41%), **mp** 171-173 °C.  **$^1\text{H}$  NMR** (300 MHz,  $\text{CDCl}_3$ )  $\delta$  (ppm) 12.54 (s, 1H), 9.09 (d,  $J = 1.9$  Hz, 1H), 8.45-8.36 (m, 2H), 7.95 (d,  $J = 8.6$  Hz, 1H), 7.71-7.61 (m, 1H), 7.57-4.47 (m, 2H), 7.33 (dd,  $J = 1.9, 8.6$  Hz, 1H), 3.98 (s, 3H).  **$^{13}\text{C}$  NMR** (75 MHz,  $\text{CDCl}_3$ )  $\delta$  (ppm) 186.8, 167.8, 160.1, 140.9, 134.8, 133.1, 132.4, 131.5 (2C), 129.6, 128.7 (2C), 127.1, 123.5, 115.2, 53.0. **RP-HPLC** (220 nm): 97% ( $t_R = 9.5$  min,  $k = 8.1$ ). **HRMS** (ESI):  $m/z$   $[M+H]^+$  calcd. for  $\text{C}_{16}\text{H}_{13}\text{BrNO}_4^+$ : 362.0022, found: 362.0022.  **$\text{C}_{16}\text{H}_{12}\text{BrNO}_4$**  (362.17).

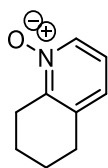
### Methyl 4-bromo-2-(4-oxo-4H-chromene-2-carboxamido)benzoate (**3.27**)



**3.27** was prepared according to the general procedure 1 for N-acylation of anilines. The reaction was carried out using 4-oxo-4H-chromene-2-carboxylic acid (500 mg, 2.63 mmol, 1.0 eq), TBTU (844 mg, 6.63 mmol, 1.0 eq), DIPEA (916  $\mu\text{L}$ , 5.26 mmol, 2.0 eq) and methyl 2-amino-4-bromobenzoate (665 mg, 2.89 mmol, 1.1 eq) and DMF (5 mL). Dilution with DCM preceded the washing steps. Recrystallization in  $\text{CHCl}_3$  afforded **3.27** as a white solid (490 mg, 1.22 mmol, 46%), **mp** 257-260 °C.  **$^1\text{H}$  NMR** (300 MHz,  $\text{CDCl}_3$ )  $\delta$  (ppm) 12.83 (s, 1H), 9.12 (d,  $J = 1.9$  Hz, 1H), 8.23 (dd,  $J = 1.4, 8.0$  Hz, 1H), 7.97 (d,  $J = 8.6$  Hz, 1H), 7.84-7.70 (m, 2H), 7.49 (m, 1H), 7.35 (dd,  $J = 1.9, 8.6$  Hz, 1H), 7.27-7.24 (m, 1H, signals interfering with the solvent signal), 4.03 (s, 3H).  **$^{13}\text{C}$  NMR** (75 MHz,  $\text{CDCl}_3$ )  $\delta$  (ppm) 178.4, 168.3, 157.9, 155.4, 154.6, 141.0, 134.9, 132.3, 130.0, 127.4, 126.3, 126.1, 124.4, 123.7, 118.7, 114.8, 112.7, 53.0. **RP-HPLC** (220 nm): 99% ( $t_R = 8.5$  min,  $k = 7.1$ ). **HRMS** (ESI):  $m/z$   $[M+H]^+$  calcd. for  $\text{C}_{18}\text{H}_{13}\text{BrNO}_5^+$ : 401.9972, found: 401.9972.  **$\text{C}_{18}\text{H}_{12}\text{BrNO}_5$**  (402.20).

**Methyl 4-bromo-2-(4-oxo-4H-chromene-3-carboxamido)benzoate (3.28)**

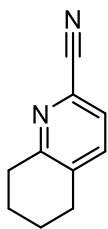
**3.28** was prepared according to the general procedure 1 for N-acylation of anilines. The reaction was carried out using 4-oxo-4*H*-chromene-3-carboxylic acid (500 mg, 2.63 mmol, 1.0 eq), TBTU (844 mg, 6.63 mmol, 1.0 eq), DIPEA (916  $\mu$ L, 5.26 mmol, 2.0 eq) and methyl 2-amino-4-bromobenzoate (665 mg, 2.89 mmol, 1.1 eq) and DMF (5 mL). Dilution with DCM preceded the washing steps. Recrystallization in  $\text{CHCl}_3$  afforded **3.28** as a yellow solid (393 mg, 0.98 mmol, 37%), **mp** 215–217  $^{\circ}\text{C}$ . Due to a slow rotation around the amide group on the NMR time scale, two isomers (ratio ca 1:0.4) were evident in the NMR spectra.  **$^1\text{H}$  NMR** (300 MHz,  $\text{CDCl}_3$ )  $\delta$  (ppm) 14.78–14.44 (m, 1H), 13.68–13.48 (m, 0.3H), 9.09–8.99 (m, 0.4H), 8.95–8.85 (m, 1H), 8.24–8.16 (m, 1H), 8.15–8.09 (m, 0.4H), 8.05–7.95 (m, 1.4H), 7.84–7.77 (m, 1.4H), 7.66–7.55 (m, 1.4H), 7.49–7.41 (m, 1.4H), 7.33–7.21 (m, 2.8H, signals interfering with the solvent signal), 4.07 (m, 3H), 4.05 (m, 1.1H).  **$^{13}\text{C}$  NMR** (75 MHz,  $\text{CDCl}_3$ )  $\delta$  (ppm) 181.3, 166.2, 164.0, 155.0, 152.9, 151.9, 141.0, 135.2, 133.7, 133.5, 129.7, 129.2, 126.9, 126.8, 124.6, 124.4, 120.5, 119.9, 117.7, 117.5, 117.4, 101.2, 53.4. **RP-HPLC** (220 nm): 77% ( $t_{\text{R}}$  = 7.4 min,  $k$  = 6.1). **HRMS** (ESI):  $m/z$   $[M+H]^+$  calcd. for  $\text{C}_{18}\text{H}_{13}\text{BrNO}_5$ : 401.9972, found: 401.9974.  **$\text{C}_{18}\text{H}_{12}\text{BrNO}_5$**  (402.20).

**5,6,7,8-Tetrahydroquinoline 1-oxide (3.29) [79,80]**

5,6,7,8-Tetrahydroquinoline (300 mg, 2.252 mmol, 1.0 eq) and 3-chlorobenzoperoxoic acid (466 mg, 2.703 mmol, 1.2 eq) were dissolved in DCM (10 mL) and stirred at rt overnight. The reaction was quenched with 1 M NaOH aq (15 mL) and the product extracted with DCM. The combined organic layers were dried over  $\text{Na}_2\text{SO}_4$  and the solvent was evaporated. Purification by column chromatography (eluent: DCM/MeOH = 19:1,  $R_{\text{f}}$  = 0.3) afforded **3.29** as a yellowish solid (271 mg, 1.816 mmol, 81%), **mp** 52–53  $^{\circ}\text{C}$  (lit. [79] mp 77–79  $^{\circ}\text{C}$ ).  **$^1\text{H}$  NMR** (300 MHz,  $\text{CDCl}_3$ )  $\delta$  (ppm) 8.14–8.04 (m, 1H), 7.06–6.91 (m, 2H), 2.90 (t,  $J$  = 6.4 Hz, 2H), 2.74 (t,  $J$  = 6.0 Hz, 2H), 1.93–1.66 (m, 4H).  **$^{13}\text{C}$  NMR** (75 MHz,  $\text{CDCl}_3$ )  $\delta$  (ppm) 148.8, 136.9, 136.5,

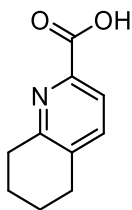
126.4, 122.1, 28.7, 24.8, 21.9, 21.7. **GC-MS** (EI<sup>+</sup>): *m/z* (%) 149.08310 (4) [M]<sup>+</sup>, 133.08776 (74) [M-O]<sup>+</sup>, 132.08048 (100) [M-O-H]<sup>+</sup>. **C<sub>9</sub>H<sub>11</sub>NO** (149.19).

### 5,6,7,8-Tetrahydroquinoline-2-carbonitrile (**3.30**) [81,82]

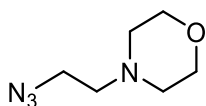


5,6,7,8-Tetrahydroquinoline-1-oxide (**3.29**) (714 mg, 4.79 mmol, 1.0 eq), trimethylsilyl cyanide (1317  $\mu$ l, 10.53 mmol, 2.2 eq) and dimethylcarbamoyl chloride (1132 mg, 10.53 mmol, 2.2 eq) were dissolved in DCM (7 ml) and stirred at rt overnight. The reaction was quenched with 3 M NaOH aq (10 ml) and stirring was continued for 10 min. After extraction with DCM, the combined organic layers were dried over Na<sub>2</sub>SO<sub>4</sub> and concentrated under reduced pressure. Purification by column chromatography (eluent: DCM (*R<sub>f</sub>* = 0.35) to DCM/MeOH 19:1) yielded **3.30** as a white solid (589 mg, 3.72 mmol, 78%), **mp** 75-76 °C (lit. **mp** 79-80 °C). **<sup>1</sup>H NMR** (400 MHz, CDCl<sub>3</sub>)  $\delta$  (ppm) 7.44 (m, 2H), 2.94 (t, *J* = 6.5 Hz, 2H), 2.84 (t, *J* = 6.3 Hz, 2H), 1.87 (m, 4H). **<sup>13</sup>C NMR** (101 MHz, CDCl<sub>3</sub>)  $\delta$  (ppm) 160.1, 137.4, 137.3, 130.7, 125.7, 117.8, 32.5, 29.2, 22.6, 22.2. **GC-MS** (EI<sup>+</sup>): *m/z* (%) 158.08320 (94) [M]<sup>+</sup>, 157.07600 (100) [M-H]<sup>+</sup>, 143.06009 (36) [M-CH<sub>3</sub>]<sup>+</sup>, 130.05276 (63) [M-C<sub>2</sub>H<sub>4</sub>]<sup>+</sup>. **C<sub>10</sub>H<sub>10</sub>N<sub>2</sub>** (158.20).

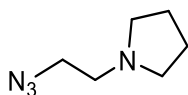
### 5,6,7,8-Tetrahydroquinoline-2-carboxylic acid (**3.31**) [34,83]



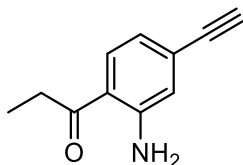
5,6,7,8-Tetrahydroquinoline-2-carbonitrile (**3.30**) (569 mg, 3.597 mmol, 1.0 eq) was dissolved in 6 M HCl aq (15 mL) and refluxed for 2 d. The product was extracted with DCM, the combined organic layers dried over Na<sub>2</sub>SO<sub>4</sub> and the solvent evaporated to give **3.31** as a beige-colored solid (543 mg, 3.06 mmol, 85%), which was used in the next step without further purification, **mp** 131-132 °C. **<sup>1</sup>H NMR** (400 MHz, CDCl<sub>3</sub>)  $\delta$  7.95 (d, *J* = 7.8 Hz, 1H), 7.62 (d, *J* = 7.8 Hz, 1H), 6.64 (s, 1H), 2.98 (t, *J* = 6.4 Hz, 2H), 2.88 (t, *J* = 6.3 Hz, 2H), 1.99-1.80 (m, 4H). **<sup>13</sup>C NMR** (101 MHz, CDCl<sub>3</sub>)  $\delta$  (ppm) 164.5, 156.7, 143.2, 139.4, 138.3, 121.1, 31.9, 29.0, 22.6, 22.3. **HRMS** (ESI): *m/z* [*M*+H]<sup>+</sup> calcd. for C<sub>10</sub>H<sub>12</sub>NO<sub>2</sub><sup>+</sup>: 178.0863, found: 178.0864. **C<sub>10</sub>H<sub>11</sub>NO<sub>2</sub>** (177.20).

**4-(2-Azidoethyl)morpholine (3.34) [84,85]**

4-(2-Chloroethyl)morpholine hydrochloride (1000 mg, 5.37 mmol, 1 eq) and NaN<sub>3</sub> (524 mg, 8.06 mmol, 1.5 eq) were dissolved in H<sub>2</sub>O (10 mL) in a microwave vessel and kept in a microwave reactor at 130 °C for 1 h. The solution was basicified with 0.1 M NaOH aq (1 mL) and the product was extracted with ether (100 mL) several times. The combined organic layers were dried over Na<sub>2</sub>SO<sub>4</sub> and the volatiles were removed under reduced pressure, affording **3.34** as a yellowish oil (240 mg, 1.54 mmol, 29%). <sup>1</sup>H NMR (300 MHz, CDCl<sub>3</sub>) δ (ppm) 3.73-3.64 (m, 4H), 3.36-3.27 (m, 2H), 2.60-2.51 (m, 2H), 2.50-2.41 (m, 4H). <sup>13</sup>C NMR (75 MHz, CDCl<sub>3</sub>) δ (ppm) 66.8 (2C), 57.6, 53.6 (2C), 47.8. HRMS (ESI): *m/z* [*M*+H]<sup>+</sup> calcd. for C<sub>6</sub>H<sub>13</sub>N<sub>4</sub>O<sup>+</sup>: 157.1084, found: 157.1088. C<sub>6</sub>H<sub>12</sub>N<sub>4</sub>O (156.19).

**1-(2-Azidoethyl)pyrrolidine (3.35) [85,86]**

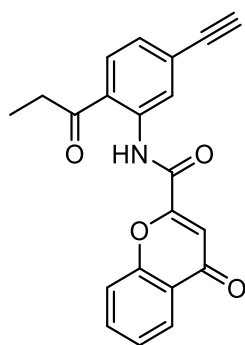
1-(2-Chloroethyl)pyrrolidine (1000 mg, 5.88 mmol, 1.0 eq) and NaN<sub>3</sub> (573 mg, 8.82 mmol, 1.5 eq) were dissolved in H<sub>2</sub>O (10 mL) in a microwave vessel and kept in a microwave reactor at 130 °C for 1 h. The solution was basicified with 1 M NaOH aq (1 mL) and the product extracted with DCM (3 x 150 mL). The combined organic layers were dried over Na<sub>2</sub>SO<sub>4</sub> and the volatiles removed under reduced pressure, affording **3.35** as a brown oil (174 mg, 1.24 mmol, 21%). <sup>1</sup>H NMR (300 MHz, CDCl<sub>3</sub>) δ (ppm) 4.09-3.99 (m, 2H), 3.92-3.74 (m, 2H), 3.27-3.15 (m, 2H), 2.97-2.78 (m, 2H), 2.30-1.98 (m, 4H). <sup>13</sup>C NMR (75 MHz, CDCl<sub>3</sub>) δ 54.5 (2C), 53.7, 47.0, 23.4 (2C). HRMS (ESI): *m/z* [*M*+H]<sup>+</sup> calcd. for C<sub>6</sub>H<sub>12</sub>N<sub>4</sub><sup>+</sup>: 141.1135, found: 141.1138. C<sub>6</sub>H<sub>12</sub>N<sub>4</sub> (140.19).

**1-(2-Amino-4-ethynylphenyl)propan-1-one (3.37) [28] (Sugasawa [87] reaction)**

Under dry conditions 3-ethynylaniline (5.00 g, 42.7 mmol, 1.0 eq) and propionitrile (6.10 mL, 85.4 mmol, 2.0 eq) were dissolved in CHCl<sub>3</sub> (40 mL) and cooled down to 0 °C using an ice bath. 1 M heptane solution of BCl<sub>3</sub> (46.9 mL, 46.9 mmol, 1.1 eq) was added very slowly (with a drip rate of 1-2 drops per second) in order to avoid aggregation. A white, milky suspension was formed. With stirring at 0 °C, GaCl<sub>3</sub> (8.27 g, 46.9 mmol, 1.1 eq) was added and the milky

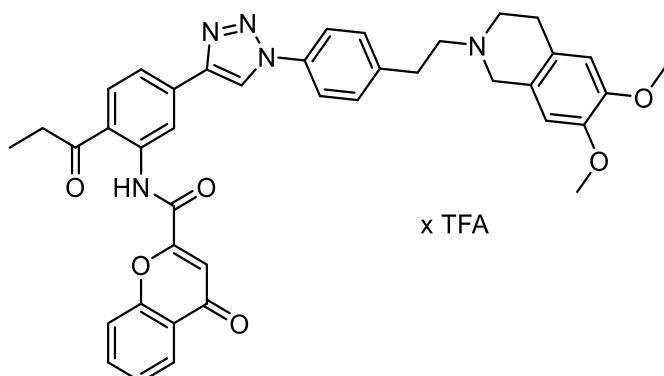
suspension turned into an emulsion of a dark brown oil in a yellow solution. The mixture was stirred for 10 min at 0 °C, brought to rt and then refluxed overnight, the color turning from pale yellow to orange. After cooling to rt 2 M HCl aq (55 ml) was added very slowly (extremely exothermic reaction) and the mixture was stirred for 2 h at 70 °C, cooled to rt and transferred into a separation funnel with DCM and H<sub>2</sub>O. The two phases were separated and rests of the product extracted from the aqueous layer with DCM. The combined organic layers were dried over Na<sub>2</sub>SO<sub>4</sub> and the volatiles were removed under reduced pressure. Transfer and extraction were hampered by the dark brown, viscid oil formed in the reaction. After purification by column chromatography (eluent: PE/EA 10:1, *R<sub>f</sub>* = 0.2), an orange solid (1.05 g, 6.09 mmol, 14%) was obtained, **mp** 64-69 °C. <sup>1</sup>H NMR (300 MHz, CDCl<sub>3</sub>) δ (ppm) 7.68 (d, *J* = 8.3 Hz, 1H), 6.79 (d, *J* = 1.4 Hz, 1H), 6.74 (dd, *J* = 1.5, 8.3 Hz, 1H), 6.25 (br s, 2H), 3.14 (s, 1H), 2.95 (q, *J* = 7.3 Hz, 2H), 1.19 (t, *J* = 7.3 Hz, 3H). <sup>13</sup>C NMR (75 MHz, CDCl<sub>3</sub>) δ (ppm) 203.0, 149.6, 131.1, 127.5, 121.0, 119.4, 118.0, 83.1, 79.3, 32.5, 8.7. HRMS (ESI): *m/z* [*M*+H]<sup>+</sup> calcd. for C<sub>11</sub>H<sub>12</sub>NO<sup>+</sup>: 174.0913, found: 174.0914. C<sub>11</sub>H<sub>11</sub>NO (173.22).

### ***N*-(5-Ethynyl-2-propionylphenyl)-4-oxo-4H-chromene-2-carboxamide (3.38)**

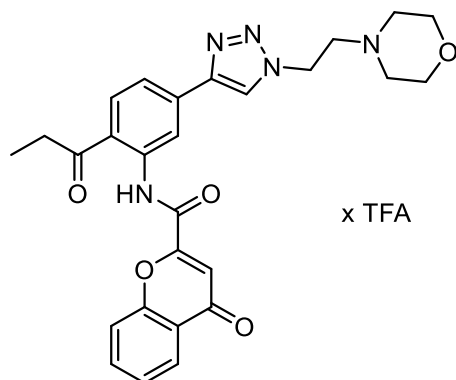


**3.38** was prepared according to the general procedure 1 for N-acylation of anilines. The reaction was carried out using 4-oxo-4*H*-chromene-2-carboxylic acid (494 mg, 2.60 mmol, 1.5 eq), TBTU (834 mg, 2.60 mmol, 1.5 eq), DIPEA (905 μL, 5.20 mmol, 3.0 eq) and 1-(2-amino-4-ethynylphenyl)propan-1-one (**37**) (300 mg, 1.73 mmol, 1.0 eq) and DMF (6 mL). Dilution with DCM preceded the washing steps. Purification by column chromatography (eluent: DCM/MeOH = 100:1, *R<sub>f</sub>* = 0.4) and recrystallization in CHCl<sub>3</sub> afforded **3.38** as a yellow solid (181 mg, 0.52 mmol, 30%), **mp** 262-266 °C (decomp.). <sup>1</sup>H NMR (600 MHz, CDCl<sub>3</sub>) δ (ppm) 13.45 (s, 1H), 9.07 (d, *J* = 1.3 Hz, 1H), 8.25 (dd, *J* = 1.5, 7.8 Hz, 1H), 7.98 (d, *J* = 8.3 Hz, 1H), 7.87-7.81 (m, 2H), 7.52-7.48 (m, 1H), 7.34 (dd, *J* = 1.4, 8.2 Hz, 1H), 7.27 (s, 1H), 3.30 (s, 1H), 3.13 (q, *J* = 7.2 Hz, 2H), 1.31 (t, *J* = 7.2 Hz, 3H). <sup>13</sup>C NMR (151 MHz, CDCl<sub>3</sub>) δ (ppm) 205.0, 178.6, 158.2, 155.6, 155.0, 139.6, 135.0, 130.9, 129.1, 127.3, 126.3, 126.1, 124.7, 124.4, 122.1, 118.8, 112.6, 82.5, 81.4, 33.5, 8.7. HRMS (ESI): *m/z* [*M*+H]<sup>+</sup> calcd. for C<sub>21</sub>H<sub>16</sub>NO<sub>4</sub><sup>+</sup>: 346.1074, found: 346.1072. C<sub>21</sub>H<sub>15</sub>NO<sub>4</sub> (345.35).

***N*-(5-(1-(4-(2-(6,7-Dimethoxy-3,4-dihydroisoquinolin-2(1*H*)-yl)ethyl)phenyl)-1*H*-1,2,3-triazol-4-yl)-2-propionylphenyl)-4-oxo-4*H*-chromene-2-carboxamide hydrotrifluoroacetate (3.39)**

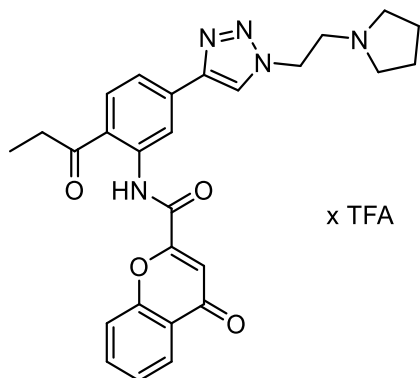


**3.39** was prepared according to the general procedure for the click reaction. The reaction was carried out using *N*-(5-ethynyl-2-propionylphenyl)-4-oxo-4*H*-chromene-2-carboxamide (**3.38**) (45.0 mg, 0.130 mmol, 1.0 eq), 2-(4-azidophenethyl)-6,7-dimethoxy-1,2,3,4-tetrahydroisoquinoline (**3.09**) (66.1 mg, 0.195 mmol, 1.5 eq), CuSO<sub>4</sub>·5H<sub>2</sub>O (4.9 mg, 0.020 mmol, 0.15 eq), sodium ascorbate (18.1 mg, 0.091 mmol, 0.7 eq) and TBTA (10.4 mg, 0.020 mmol, 0.15 eq) in CHCl<sub>3</sub> (10 mL). Refluxing lasted for 3 d. Flash column chromatography (4 g column, gradient: 0-20 min: DCM/MeOH 100:0-95:5, *R<sub>f</sub>* = 0.3 in DCM/MeOH 95:5) followed by preparative HPLC (gradient: 0-30 min: MeCN/ 0.1% aq TFA 42:58-78:22, *t<sub>R</sub>* = 16.0 min) afforded the product as a yellowish solid (14.9 mg, 0.019 mmol, 14%), **mp** 221-225 °C (decomp.). **<sup>1</sup>H NMR** (600 MHz, DMSO-*d*<sub>6</sub>) δ (ppm) 13.30 (s, 1H), 10.11 (s, 1H), 9.51 (s, 1H), 9.33 (d, *J* = 1.6 Hz, 1H), 8.35 (d, *J* = 8.4 Hz, 1H), 8.11 (dd, *J* = 1.6, 7.9 Hz, 1H), 8.01 (m, 3H), 7.87 (dd, *J* = 1.6, 8.2 Hz, 1H), 7.81 (d, *J* = 8.3 Hz, 1H), 7.61 (m, 3H), 7.01 (s, 1H), 6.86 (s, 1H), 6.81 (s, 1H), 4.56 (d, *J* = 15.1 Hz, 1H), 4.32 (dd, *J* = 7.8, 14.9 Hz, 1H), 3.81 (m, 1H), 3.76 (s, 3H), 3.75 (s, 3H), 3.54 (m, 2H), 3.38 (m, 1H), 3.26 (q, *J* = 7.1 Hz, 2H), 3.21 (t, *J* = 8.3 Hz, 2H), 3.14-2.98 (m, 2H), 1.21 (t, *J* = 7.1 Hz, 3H). **<sup>13</sup>C NMR** (151 MHz, DMSO-*d*<sub>6</sub>) δ (ppm) 205.2, 177.3, 158.2 (TFA), 158.0 (TFA), 157.7, 154.9, 154.9, 148.5, 147.8, 146.0, 139.0, 137.8, 135.8, 135.5, 135.4, 132.6, 130.3 (2C), 126.4, 125.2, 123.7, 123.1, 122.5, 121.2, 120.9, 120.4 (2C), 119.8, 118.4, 116.7, 111.5, 111.2, 109.6, 55.6, 55.6, 55.5, 51.8, 49.3, 32.9, 29.2, 24.6, 8.4. **RP-HPLC** (220 nm): 99% (*t<sub>R</sub>* = 6.4 min, *k* = 5.2). **HRMS** (ESI): *m/z* [*M*+*H*]<sup>+</sup> calcd. for C<sub>40</sub>H<sub>38</sub>N<sub>5</sub>O<sub>6</sub><sup>+</sup>: 684.2817, found: 684.2829. **C<sub>40</sub>H<sub>37</sub>N<sub>5</sub>O<sub>6</sub> · C<sub>2</sub>HF<sub>3</sub>O<sub>2</sub>** (683.75 + 114.02).

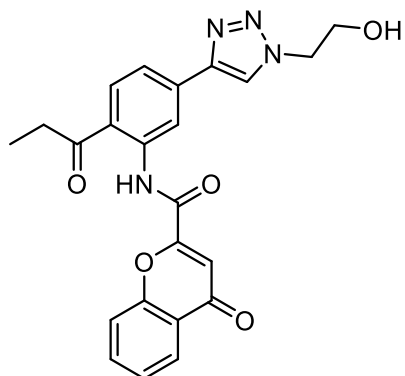
***N*-(5-(1-(2-Morpholinoethyl)-1*H*-1,2,3-triazol-4-yl)-2-propionylphenyl)-4-oxo-4*H*-chromene-2-carboxamide hydrotrifluoroacetate (**3.40**)**

**3.40** was prepared according to the general procedure for the click reaction. The reaction was carried out using *N*-(5-ethynyl-2-propionylphenyl)-4-oxo-4*H*-chromene-2-carboxamide (**3.38**) (37.0 mg, 0.107 mmol, 1.0 eq), 4-(2-azidoethyl)morpholine (**3.34**) (25.1 mg, 0.161 mmol, 1.5 eq), CuSO<sub>4</sub>·5H<sub>2</sub>O (4.0 mg, 0.016 mmol, 0.15 eq), sodium ascorbate (14.9 mg, 0.075 mmol, 0.7 eq) and TBTA (8.5 mg, 0.016 mmol, 0.15 eq) in CHCl<sub>3</sub> (7 mL). Refluxing lasted for 3 d. Flash column chromatography (4 g column, gradient: 0-20 min: DCM/MeOH 100:0-95:5, *R<sub>f</sub>* = 0.2 in DCM/MeOH 95:5) followed by preparative HPLC (gradient: 0-30 min: MeCN/0.1% aq TFA 33:67-69:31, *t<sub>R</sub>* = 12.0 min) afforded the product as a white solid (50.3 mg, 0.082 mmol, 76%), **mp** 232-234 °C (decomp.). **<sup>1</sup>H NMR** (600 MHz, DMSO-*d*<sub>6</sub>, D<sub>2</sub>O 10%) δ (ppm) 9.19 (d, *J* = 1.6 Hz, 1H), 8.77 (s, 1H), 8.26 (d, *J* = 8.4 Hz, 1H), 8.06 (dd, *J* = 1.5, 7.9 Hz, 1H), 7.96 (m, 1H), 7.74 (m, 2H), 7.57 (m, 1H), 6.95 (s, 1H), 4.89 (t, *J* = 6.4 Hz, 2H), 3.82 (m, 4H), 3.73 (m, 2H), 3.29 (m, 4H), 3.18 (q, *J* = 7.1 Hz, 2H), 1.16 (t, *J* = 7.1 Hz, 3H) (the NH protons are not apparent because of the addition of D<sub>2</sub>O). **<sup>13</sup>C NMR** (151 MHz, DMSO-*d*<sub>6</sub>, D<sub>2</sub>O 10%) δ (ppm) 205.5, 177.8, 158.7 (TFA), 158.5 (TFA), 157.8, 155.1, 155.1, 145.6, 139.2, 136.3, 135.8, 132.9, 126.8, 125.5, 124.1, 123.8, 122.3, 120.9, 118.7, 116.7, 111.4, 63.7 (2C), 55.0, 51.8 (2C), 44.3, 33.1, 8.6. **RP-HPLC** (220 nm): 99% (*t<sub>R</sub>* = 4.1 min, *k* = 3.0). **HRMS** (ESI): *m/z* [*M*+*H*]<sup>+</sup> calcd. for C<sub>27</sub>H<sub>28</sub>N<sub>5</sub>O<sub>5</sub><sup>+</sup>: 502.2085, found: 502.2090. C<sub>27</sub>H<sub>27</sub>N<sub>5</sub>O<sub>5</sub> · C<sub>2</sub>HF<sub>3</sub>O<sub>2</sub> (501.54 + 114.02).

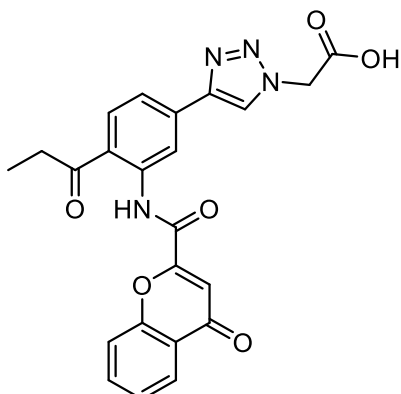
**4-Oxo-*N*-(2-propionyl-5-(1-(2-(pyrrolidin-1-yl)ethyl)-1*H*-1,2,3-triazol-4-yl)phenyl)-4*H*-chromene-2-carboxamide hydrotrifluoroacetate (3.41)**



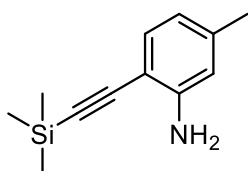
**3.41** was prepared according to the general procedure for the click reaction. The reaction was carried out using *N*-(5-ethynyl-2-propionylphenyl)-4-oxo-4*H*-chromene-2-carboxamide (**3.38**) (40.0 mg, 0.116 mmol, 1.0 eq), 1-(2-azidoethyl)pyrrolidine (**3.35**) (24.4 mg, 0.174 mmol, 1.5 eq), CuSO<sub>4</sub>·5H<sub>2</sub>O (4.3 mg, 0.017 mmol, 0.15 eq), sodium ascorbate (16.1 mg, 0.081 mmol, 0.7 eq) and TBTA (9.2 mg, 0.017 mmol, 0.15 eq) in CHCl<sub>3</sub> (10 mL). Refluxing lasted for 2 d. Flash column chromatography (4 g column, gradient: 0-20 min: DCM/MeOH 100:0-90:10, 20-30 min: DCM/MeOH 90:10, *R<sub>f</sub>* = 0.3 in DCM/MeOH 90:10) followed by preparative HPLC (gradient: 0-30 min: MeCN/ 0.1% aq TFA 33:67-69:31, *t<sub>R</sub>* = 11.5 min) afforded the product as a white solid (58.3 mg, 0.097 mmol, 84%), **mp** 228-234 °C (decomp.). **<sup>1</sup>H NMR** (600 MHz, DMSO-*d*<sub>6</sub>) δ (ppm) 13.32 (s, 1H), 9.86 (s, 1H), 9.24 (m, 1H), 8.87 (m, 1H), 8.32 (m, 1H), 8.10 (m, 1H), 8.00 (m, 1H), 7.79 (m, 2H), 7.60 (m, 1H), 6.99 (m, 1H), 4.88 (t, *J* = 6.2 Hz, 2H), 3.83 (m, 2H), 3.59 (m, 2H), 3.23 (q, *J* = 7.1 Hz, 2H), 3.11 (m, 2H), 2.09-1.82 (m, 4H), 1.20 (t, *J* = 7.1 Hz, 3H). **<sup>13</sup>C NMR** (151 MHz, DMSO-*d*<sub>6</sub>) δ (ppm) 205.2, 177.3, 158.1 (TFA), 157.9 (TFA), 157.7, 154.8 (2C), 145.3, 139.1, 136.1, 135.5, 132.7, 126.4, 125.2, 123.9, 123.7, 122.1, 120.5, 118.4, 116.4, 111.2, 53.7 (2C), 52.8, 45.9, 32.8, 22.6 (2C), 8.4. **RP-HPLC** (220 nm): 97% (*t<sub>R</sub>* = 4.3 min, *k* = 3.1). **HRMS** (ESI): *m/z* [*M*+*H*]<sup>+</sup> calcd. for C<sub>27</sub>H<sub>28</sub>N<sub>5</sub>O<sub>4</sub><sup>+</sup>: 486.2136, found: 486.2139. **C<sub>27</sub>H<sub>27</sub>N<sub>5</sub>O<sub>4</sub> · C<sub>2</sub>HF<sub>3</sub>O<sub>2</sub>** (485.54 + 114.02).

***N*-(5-(1-(2-Hydroxyethyl)-1*H*-1,2,3-triazol-4-yl)-2-propionylphenyl)-4-oxo-4*H*-chromene-2-carboxamide (**3.42**)**

**3.42** was prepared according to the general procedure for the click reaction. The reaction was carried out using *N*-(5-ethynyl-2-propionylphenyl)-4-oxo-4*H*-chromene-2-carboxamide (**3.38**) (40.0 mg, 0.116 mmol, 1.0 eq), 2-azidoethan-1-ol (15.1 mg, 0.174 mmol, 1.5 eq), CuSO<sub>4</sub>·5H<sub>2</sub>O (4.3 mg, 0.017 mmol, 0.15 eq), sodium ascorbate (16.1 mg, 0.081 mmol, 0.7 eq) and TBTA (9.2 mg, 0.017 mmol, 0.15 eq) in CHCl<sub>3</sub> (6 mL). Refluxing lasted for 2 d. Flash column chromatography (4 g column, gradient: 0-20 min: DCM/MeOH 100:0-95:5, 20-25 min: DCM/MeOH 95:5, *R<sub>f</sub>* = 0.3 in DCM/MeOH 95:5) followed by preparative HPLC (gradient: 0-30 min: MeCN/ 0.1% aq TFA 44:56-80:20, *t<sub>R</sub>* = 11.0 min) afforded the product as a slightly yellow solid (30.3 mg, 0.070 mmol, 60%), **mp** 273-275 °C (decomp.). **<sup>1</sup>H NMR** (600 MHz, DMSO-*d*<sub>6</sub>) δ (ppm) 13.30 (s, 1H), 9.24 (d, *J* = 1.6 Hz, 1H), 8.75 (s, 1H), 8.30 (d, *J* = 8.4 Hz, 1H), 8.12 (dd, *J* = 1.6, 8.0 Hz, 1H), 8.01 (m, 1H), 7.81 (m, 2H), 7.61 (m, 1H), 7.01 (s, 1H), 5.10 (t, *J* = 5.4 Hz, 1H), 4.49 (t, *J* = 5.3 Hz, 2H), 3.86 (m, 2H), 3.24 (q, *J* = 7.1 Hz, 2H), 1.20 (t, *J* = 7.1 Hz, 3H). **<sup>13</sup>C NMR** (151 MHz, DMSO-*d*<sub>6</sub>) δ (ppm) 205.2, 177.3, 157.7, 154.9, 154.9, 144.8, 139.0, 136.6, 135.5, 132.5, 126.4, 125.2, 123.7, 123.6, 122.1, 120.6, 118.4, 116.4, 111.2, 59.7, 52.6, 32.8, 8.4. **RP-HPLC** (220 nm): 100% (*t<sub>R</sub>* = 5.1 min, *k* = 3.9). **HRMS** (ESI): *m/z* [*M*+H]<sup>+</sup> calcd. for C<sub>23</sub>H<sub>21</sub>N<sub>4</sub>O<sub>5</sub><sup>+</sup>: 433.1506, found: 433.1508. **C<sub>23</sub>H<sub>20</sub>N<sub>4</sub>O<sub>5</sub>** (432.44).

**2-(4-(3-(4-Oxo-4H-chromene-2-carboxamido)-4-propionylphenyl)-1H-1,2,3-triazol-1-yl)acetic acid (3.43)**

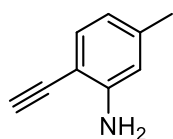
**3.43** was prepared according to the general procedure for the click reaction. The reaction was carried out using *N*-(5-ethynyl-2-propionylphenyl)-4-oxo-4H-chromene-2-carboxamide (**3.38**) (40.0 mg, 0.116 mmol, 1.0 eq), 2-azidoacetic acid (130  $\mu$ L, 0.174 mmol, 1.5 eq), CuSO<sub>4</sub>·5H<sub>2</sub>O (4.3 mg, 0.017 mmol, 0.15 eq), sodium ascorbate (16.1 mg, 0.081 mmol, 0.7 eq) and TBTA (9.2 mg, 0.017 mmol, 0.15 eq) in CHCl<sub>3</sub> (10 mL). Refluxing lasted for 3 d. Flash column chromatography (4 g column, gradient: 0-20 min: DCM/MeOH 95:5-75:25, 20-30 min: DCM/MeOH 75:25, *R<sub>f</sub>* = 0.2 in DCM/MeOH 75:25) followed by preparative HPLC (gradient: 0-30 min: MeCN/ 0.1% aq TFA 45:55-75:25, *t<sub>R</sub>* = 14.0 min) afforded the product as a white solid (16.7 mg, 0.037 mmol, 32%), **mp** 295-297 °C (decomp.). **<sup>1</sup>H NMR** (600 MHz, DMSO-*d*<sub>6</sub>)  $\delta$  (ppm) 13.51 (s, 1H), 13.30 (s, 1H), 9.24 (d, *J* = 1.6 Hz, 1H), 8.78 (s, 1H), 8.31 (d, *J* = 8.5 Hz, 1H), 8.11 (dd, *J* = 1.6, 7.9 Hz, 1H), 8.00 (m, 1H), 7.80 (m, 2H), 7.61 (m, 1H), 7.00 (s, 1H), 5.38 (s, 2H), 3.24 (q, *J* = 7.1 Hz, 2H), 1.20 (t, *J* = 7.1 Hz, 3H). **<sup>13</sup>C NMR** (151 MHz, DMSO-*d*<sub>6</sub>)  $\delta$  (ppm) 205.2, 177.3, 168.5, 157.7, 154.9, 154.9, 145.0, 139.1, 136.3, 135.5, 132.6, 126.4, 125.2, 124.5, 123.7, 122.2, 120.6, 118.4, 116.5, 111.2, 50.8, 32.8, 8.4. **RP-HPLC** (220 nm): 98% (*t<sub>R</sub>* = 5.4 min, *k* = 4.2). **HRMS** (ESI): *m/z* [*M*+H]<sup>+</sup> calcd. for C<sub>23</sub>H<sub>19</sub>N<sub>4</sub>O<sub>6</sub><sup>+</sup>: 447.1299, found: 447.1298. C<sub>23</sub>H<sub>18</sub>N<sub>4</sub>O<sub>6</sub> (446.42).

**5-Methyl-2-((trimethylsilyl)ethynyl)aniline (3.45) [88] (Sonogashira [89] coupling)**

The liquids used in this reaction (THF, NEt<sub>3</sub> and trimethylsilylacetylene) were deoxygenated by bubbling with argon for 30 min. Under an atmosphere of argon, 2-Iodo-5-methylaniline (907 mg, 3.89 mmol, 1 eq), Pd(PPh<sub>3</sub>)<sub>2</sub>Cl<sub>2</sub> (137 mg, 0.195 mmol, 0.05 eq) and CuI (37.1 mg, 0.195 mmol, 0.05 eq) were placed in a dried Schlenk flask and dissolved THF. NEt<sub>3</sub> (1085  $\mu$ L, 7.784 mmol, 2 eq) was added and the mixture was deoxygenated again by bubbling with argon.

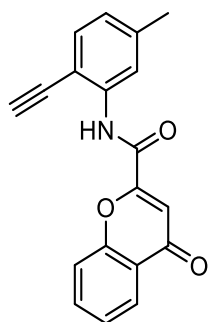
Trimethylsilylacetylene (825  $\mu$ L, 5.84 mmol, 1.5 eq) was added dropwise, resulting in a color change from yellow over red to green. After 1.5 h of stirring at rt the volatiles were removed under reduced pressure and the residue subjected to flash column chromatography (15 g column, gradient: 0-20 min: PE/EtOAc 100:0-90:10,  $R_f$  = 0.3 in DCM/MeOH 90:10), which afforded **3.45** as a yellow oil (720 mg, 3.54 mmol, 91%).  **$^1\text{H}$  NMR** (400 MHz,  $\text{CH}_2\text{Cl}_2$ )  $\delta$  (ppm) 7.18 (d,  $J$  = 7.7 Hz, 1H), 6.52-6.47 (m, 2H), 4.27 (br s, 2H), 2.25 (s, 3H), 0.27 (s, 9H).  **$^{13}\text{C}$  NMR** (101 MHz,  $\text{CH}_2\text{Cl}_2$ )  $\delta$  (ppm) 148.3, 140.4, 132.2, 119.0, 114.9, 105.2, 102.2, 99.1, 21.8, 0.3 (3C). **GC-MS** ( $\text{EI}^+$ ):  $m/z$  (%) 203.11332 (65)  $[\text{M}]^+$ , 188.09008 (100)  $[\text{M}-\text{CH}_3]^+$ .  $\text{C}_{12}\text{H}_{17}\text{NSi}$  (203.36).

### 2-Ethynyl-5-methylaniline (**3.46**) [90]



5-Methyl-2-((trimethylsilyl)ethynyl)aniline (**3.45**) (684 mg, 3.36 mmol, 1.0 eq) was dissolved in MeOH (10 mL) and  $\text{K}_2\text{CO}_3$  (697 mg, 5.05 mmol, 1.5 eq) was added. The suspension was stirred at rt for 2 h, diluted with  $\text{H}_2\text{O}$  and the product was extracted with DCM (3x). The combined organic layers were dried over  $\text{Na}_2\text{SO}_4$  and the solvent evaporated to give **3.46** as a brown solid (331 mg, 2.52 mmol, 75%), which was used for the subsequent reaction without further purification, **mp** 44-47  $^\circ\text{C}$ .  **$^1\text{H}$  NMR** (400 MHz,  $\text{CDCl}_3$ )  $\delta$  (ppm) 7.21 (d,  $J$  = 7.7 Hz, 1H), 6.54-6.48 (m, 2H), 4.18 (br s, 2H), 3.34 (s, 1H), 2.26 (s, 3H).  **$^{13}\text{C}$  NMR** (101 MHz,  $\text{CDCl}_3$ )  $\delta$  (ppm) 148.6, 140.7, 132.6, 119.1, 115.1, 104.0, 81.9, 81.0, 21.8. **GC-MS** ( $\text{EI}^+$ ):  $m/z$  (%) 131.06984 (100)  $[\text{M}]^+$ , 130.06257 (89)  $[\text{M}-\text{H}]^+$ .  $\text{C}_9\text{H}_9\text{N}$  (131.18).

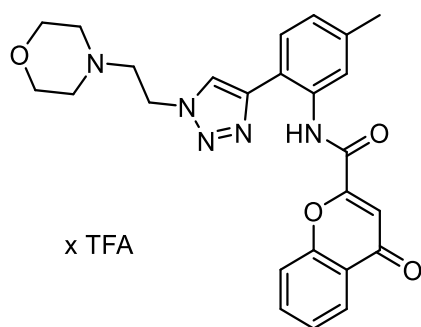
### *N*-(2-Ethynyl-5-methylphenyl)-4-oxo-4*H*-chromene-2-carboxamide (**3.47**)



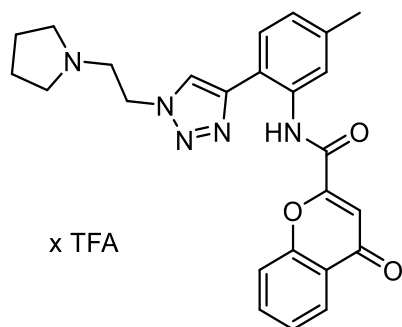
**3.47** was prepared according to the general procedure 1 for *N*-acylation of anilines. The reaction was carried out using 4-oxo-4*H*-chromene-2-carboxylic acid (544 mg, 2.86 mmol, 1.5 eq), TBTU (918 mg, 2.86 mmol, 1.5 eq), DIPEA (996  $\mu$ L, 5.72 mmol, 3.0 eq) and 2-ethynyl-5-methylaniline (**3.46**) (250 mg, 1.91 mmol, 1.0 eq) and DMF (4 mL). Dilution with DCM preceded the washing steps. Purification by flash column chromatography (8 g column,

gradient: 0-20 min: DCM/MeOH 100:0-99:1,  $R_f = 0.4$  in DCM/MeOH 99:1) and recrystallization in  $\text{CHCl}_3$  afforded **3.47** as yellow crystals (331 mg, 1.09 mmol, 57%). **mp** 260-277 °C (decomp.).  **$^1\text{H}$  NMR** (400 MHz,  $\text{CDCl}_3$ )  $\delta$  (ppm) 9.55 (s, 1H), 8.43 (s, 1H), 8.26 (dd,  $J = 1.3, 7.9$  Hz, 1H), 7.81-7.74 (m, 1H), 7.54-7.47 (m, 2H), 7.44 (d,  $J = 7.9$  Hz, 1H), 7.28 (s, 1H), 7.01-6.96 (m, 1H), 3.67 (s, 1H), 2.42 (s, 3H).  **$^{13}\text{C}$  NMR** (101 MHz,  $\text{CDCl}_3$ )  $\delta$  (ppm) 178.2, 156.9, 155.3, 154.6, 141.5, 138.3, 134.9, 132.3, 126.4, 126.4, 125.8, 124.5, 120.3, 118.1, 112.8, 108.9, 84.4, 79.4, 22.2. **HRMS** (ESI):  $m/z$   $[M+H]^+$  calcd. for  $\text{C}_{19}\text{H}_{14}\text{NO}_3^+$ : 304.0968, found: 304.0974.  **$\text{C}_{19}\text{H}_{13}\text{NO}_3$**  (303.32).

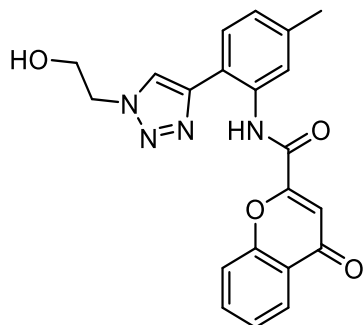
***N*-(5-Methyl-2-(1-(2-morpholinoethyl)-1*H*-1,2,3-triazol-4-yl)phenyl)-4-oxo-4*H*-chromene-2-carboxamide hydrotrifluoroacetate (**3.48**)**



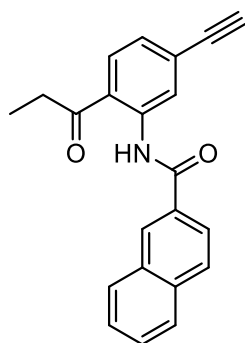
**3.48** was prepared according to the general procedure for the click reaction. The reaction was carried out using *N*-(2-ethynyl-5-methylphenyl)-4-oxo-4*H*-chromene-2-carboxamide (**3.47**) (40.0 mg, 0.132 mmol, 1.0 eq), 4-(2-azidoethyl)morpholine (**3.34**) (30.9 mg, 0.198 mmol, 1.5 eq),  $\text{CuSO}_4 \cdot 5\text{H}_2\text{O}$  (4.9 mg, 0.020 mmol, 0.15 eq), sodium ascorbate (18.3 mg, 0.092 mmol, 0.7 eq) and TBTA (10.5 mg, 0.020 mmol, 0.15 eq) in  $\text{CHCl}_3$  (9 mL). Refluxing lasted for 3 d. Flash column chromatography (4 g column, gradient: 0-40 min: DCM/MeOH 100:0-95:5,  $R_f = 0.3$  in DCM/MeOH 95:5), followed by preparative HPLC (gradient: 0-30 min: MeCN/0.1% aq TFA 28:72-64:36,  $t_R = 11.0$  min), afforded the product as a slightly yellow solid (47.3 mg, 0.082 mmol, 63%), **mp** 233-235 °C (decomp.).  **$^1\text{H}$  NMR** (600 MHz,  $\text{DMSO}-d_6$ )  $\delta$  (ppm) 13.02 (s, 1H), 10.21 (br s, 1H), 8.86 (s, 1H), 8.49 (s, 1H), 8.11 (dd,  $J = 1.5, 7.9$  Hz, 1H), 7.97 (m, 1H), 7.88 (d,  $J = 8.3$  Hz, 1H), 7.74 (d,  $J = 7.9$  Hz, 1H), 7.60 (m, 1H), 7.16 (m, 1H), 6.99 (s, 1H), 4.99 (t,  $J = 6.2$  Hz, 2H), 4.04-3.14 (m, 10H), 2.39 (s, 3H).  **$^{13}\text{C}$  NMR** (151 MHz,  $\text{DMSO}-d_6$ )  $\delta$  (ppm) 177.3, 158.6 (TFA), 158.4 (TFA), 158.1 (TFA), 157.9 (TFA), 157.2, 155.2, 154.9, 146.2, 138.7, 135.2, 134.5, 127.6, 126.3, 125.9, 125.2, 123.7, 123.6, 121.5, 118.4, 117.0 (TFA), 116.3, 115.03 (TFA), 111.0, 63.4 (2C), 54.6, 51.6 (2C), 44.3, 21.2. **RP-HPLC** (220 nm): 100% ( $t_R = 3.6$  min,  $k = 2.4$ ). **HRMS** (ESI):  $m/z$   $[M+H]^+$  calcd. for  $\text{C}_{25}\text{H}_{26}\text{N}_5\text{O}_4^+$ : 460.1979, found: 460.2015.  **$\text{C}_{25}\text{H}_{25}\text{N}_5\text{O}_4 \cdot \text{C}_2\text{HF}_3\text{O}_2$**  (459.51 + 114.02).

***N*-(5-Methyl-2-(1-(2-(pyrrolidin-1-yl)ethyl)-1*H*-1,2,3-triazol-4-yl)phenyl)-4-oxo-4*H*-chromene-2-carboxamide hydrotrifluoroacetate (3.49)**

**3.49** was prepared according to the general procedure for the click reaction. The reaction was carried out using *N*-(2-ethynyl-5-methylphenyl)-4-oxo-4*H*-chromene-2-carboxamide (**3.47**) (40.0 mg, 0.132 mmol, 1.0 eq), 1-(2-azidoethyl)pyrrolidine (**3.35**) (27.7 mg, 0.198 mmol, 1.5 eq), CuSO<sub>4</sub>·5H<sub>2</sub>O (4.9 mg, 0.020 mmol, 0.15 eq), sodium ascorbate (18.3 mg, 0.092 mmol, 0.7 eq) and TBTA (10.5 mg, 0.020 mmol, 0.15 eq) in CHCl<sub>3</sub> (9 mL). Refluxing lasted for 2 d. Flash column chromatography (4 g column, gradient: 0-40 min: DCM/MeOH 100:0-90:10, *R<sub>f</sub>* = 0.4 in DCM/MeOH 90:10), followed by preparative HPLC (gradient: 0-30 min: MeCN/0.1% aq TFA 32:68-68:32, *t<sub>R</sub>* = 11.5 min), afforded the product as a slightly yellow solid (33.6 mg, 0.044 mmol, 34%), **mp** 177-183 °C (decomp.). **<sup>1</sup>H NMR** (600 MHz, DMSO-*d*<sub>6</sub>) δ (ppm) 13.00 (s, 1H), 9.95 (s, 1H), 8.87 (s, 1H), 8.49 (s, 1H), 8.11 (dd, *J* = 1.5, 7.9 Hz, 1H), 7.97 (m, 1H), 7.89 (d, *J* = 8.3 Hz, 1H), 7.74 (d, *J* = 7.9 Hz, 1H), 7.60 (m, 1H), 7.16 (m, 1H), 6.99 (s, 1H), 4.95 (t, *J* = 6.2 Hz, 2H), 3.85 (m, 2H), 3.61 (m, 2H), 3.12 (m, 2H), 2.39 (s, 3H), 2.08-1.80 (m, 4H). **<sup>13</sup>C NMR** (151 MHz, DMSO-*d*<sub>6</sub>) δ (ppm) 177.3, 158.2 (TFA), 158.0 (TFA), 157.2, 155.2, 154.9, 146.2, 138.7, 135.2, 134.5, 127.6, 126.3, 125.9, 125.2, 123.7, 123.7, 121.5, 118.4, 116.3, 111.0, 53.7 (2C), 52.7, 46.1, 22.6 (2C), 21.2. **RP-HPLC** (220 nm): 100% (*t<sub>R</sub>* = 3.8 min, *k* = 2.6). **HRMS** (ESI): *m/z* [*M*+H]<sup>+</sup> calcd. for C<sub>25</sub>H<sub>26</sub>N<sub>5</sub>O<sub>3</sub><sup>+</sup>: 444.2023, found: 444.2050. **C<sub>25</sub>H<sub>25</sub>N<sub>5</sub>O<sub>3</sub> · C<sub>2</sub>HF<sub>3</sub>O<sub>2</sub>** (443.51 + 114.02).

***N*-(2-(1-(2-Hydroxyethyl)-1*H*-1,2,3-triazol-4-yl)-5-methylphenyl)-4-oxo-4*H*-chromene-2-carboxamide (3.50)**

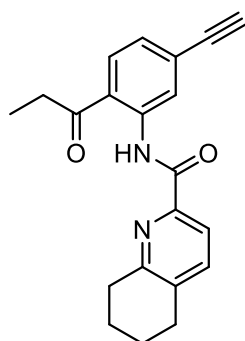
**3.50** was prepared according to the general procedure for the click reaction. The reaction was carried out using *N*-(2-ethynyl-5-methylphenyl)-4-oxo-4*H*-chromene-2-carboxamide (**3.47**) (40.0 mg, 0.132 mmol, 1.0 eq), 2-azidoethan-1-ol (17.2 mg, 0.198 mmol, 1.5 eq), CuSO<sub>4</sub>·5H<sub>2</sub>O (4.9 mg, 0.020 mmol, 0.15 eq), sodium ascorbate (18.3 mg, 0.092 mmol, 0.7 eq) and TBTA (10.5 mg, 0.020 mmol, 0.15 eq) in CHCl<sub>3</sub> (9 mL). Refluxing lasted for 2 d. Flash column chromatography (4 g column, gradient: 0-30 min: DCM/MeOH 100:0-95:05, 30-35 min: DCM/MeOH 95:5, *R<sub>f</sub>* = 0.3 in DCM/MeOH 95:5) followed by preparative HPLC (gradient: 0-30 min: MeCN/ 0.1% aq TFA 42:58-78:22, *t<sub>R</sub>* = 12.0 min) afforded the product as a yellow solid (37.4 mg, 0.096 mmol, 73%), **mp** 319-321 °C (decomp.). **<sup>1</sup>H NMR** (600 MHz, DMSO-*d*<sub>6</sub>) δ (ppm) 13.25 (s, 1H), 8.78 (s, 1H), 8.54 (m, 1H), 8.10 (dd, *J* = 1.5, 7.9 Hz, 1H), 8.00 (m, 1H), 7.91 (d, *J* = 8.2 Hz, 1H), 7.77 (d, *J* = 8.0 Hz, 1H), 7.59 (m, 1H), 7.12 (m, 1H), 6.98 (s, 1H), 5.13 (t, *J* = 5.4 Hz, 1H), 4.57 (t, *J* = 5.4 Hz, 2H), 3.90 (m, 2H), 2.38 (s, 3H). **<sup>13</sup>C NMR** (151 MHz, DMSO-*d*<sub>6</sub>) δ (ppm) 177.4, 157.1, 155.3, 154.9, 145.8, 138.3, 135.3, 134.5, 127.5, 126.3, 125.7, 125.1, 123.7, 123.3, 121.1, 118.4, 116.3, 110.9, 59.8, 52.9, 21.2. **RP-HPLC** (220 nm): 100% (*t<sub>R</sub>* = 5.2 min, *k* = 4.0). **HRMS** (ESI): *m/z* [*M*+H]<sup>+</sup> calcd. for C<sub>21</sub>H<sub>19</sub>N<sub>4</sub>O<sub>4</sub><sup>+</sup>: 391.1401, found: 491.1405. C<sub>21</sub>H<sub>18</sub>N<sub>4</sub>O<sub>4</sub> (390.40).

***N*-(5-Ethynyl-2-propionylphenyl)-2-naphthamide (3.51)**

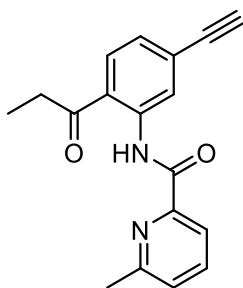
**3.51** was prepared according to the general procedure 2 for N-acylation of anilines. The reaction was carried out using 2-naphthoic acid (100 mg, 0.581 mmol, 1.0 eq), thionyl chloride (84 μL, 1.162 mmol, 2.0 eq), pyridine (94 μL, 1.162 mmol, 2.0 eq), 1-(2-amino-4-

ethynylphenyl)propan-1-one (**3.37**) (100.6 mg, 0.581 mmol, 1.0 eq), DIPEA (405  $\mu$ L, 2.323 mmol, 4.0 eq) and toluene (1 mL). After the washing steps, flash column chromatography (4 g column, gradient: 0-20 min: PE/EtOAc 100:0-90:10,  $R_f$  = 0.2 in DCM/MeOH 90:10) afforded **3.51** as a yellowish solid (135 mg, 0.412 mmol, 71%), **mp** 149-153 °C. **<sup>1</sup>H NMR** (400 MHz, CDCl<sub>3</sub>)  $\delta$  12.87 (s, 1H), 9.19 (d,  $J$  = 1.5 Hz, 1H), 8.61 (d,  $J$  = 1.2 Hz, 1H), 8.12 (dd,  $J$  = 1.9, 8.6 Hz, 1H), 8.08-8.03 (m, 1H), 8.01-7.88 (m, 3H), 7.63-7.55 (m, 2H), 7.28-7.24 (m, 1H, signals interfering with the solvent signal), 3.28 (s, 1H), 3.12 (q,  $J$  = 7.2 Hz, 2H), 1.28 (d,  $J$  = 14.5 Hz, 3H). **<sup>13</sup>C NMR** (101 MHz, CDCl<sub>3</sub>)  $\delta$  (ppm) 205.3, 166.3, 141.4, 135.2, 132.9, 132.0, 130.8, 129.6, 128.9 (2C), 128.7, 128.2, 127.9, 126.9, 126.0, 124.6, 123.8, 121.6, 82.9, 80.9, 33.5, 8.8. **HRMS** (ESI):  $m/z$  [ $M+H$ ]<sup>+</sup> calcd. for C<sub>22</sub>H<sub>18</sub>NO<sub>2</sub><sup>+</sup>: 328.1332, found: 328.1335. C<sub>22</sub>H<sub>17</sub>NO<sub>2</sub> (327.38).

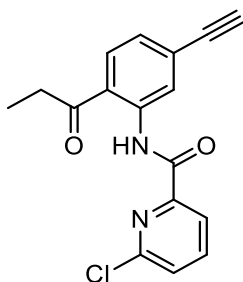
#### ***N*-(5-Ethynyl-2-propionylphenyl)-5,6,7,8-tetrahydroquinoline-2-carboxamide (3.52)**



**3.52** was prepared according to the general procedure 1 for N-acylation of anilines. The reaction was carried out using 5,6,7,8-tetrahydroquinoline-2-carboxylic acid (31 mg, 0.17 mmol, 1.5 eq), TBTU (56 mg, 0.17 mmol, 1.5 eq), DIPEA (60  $\mu$ L, 0.35 mmol, 3.0 eq) and 1-(2-amino-4-ethynylphenyl)propan-1-one (**3.37**) (20 mg, 0.12 mmol, 1.0 eq) and DMF (1 mL). Dilution with DCM preceded the washing steps. Purification by column chromatography (eluent: PE/EtOAc = 7:1,  $R_f$  = 0.2) afforded **3.52** as a yellow solid (33 mg, 0.10 mmol, 86%), **mp** 150-154 °C. **<sup>1</sup>H NMR** (300 MHz, CDCl<sub>3</sub>)  $\delta$  13.44 (s, 1H), 9.15 (d,  $J$  = 1.6 Hz, 1H), 7.96 (d,  $J$  = 7.8 Hz, 1H), 7.87 (d,  $J$  = 8.3 Hz, 1H), 7.52 (d,  $J$  = 7.9 Hz, 1H), 7.21 (dd,  $J$  = 1.6, 8.2 Hz, 1H), 3.23 (s, 1H), 3.13 (t,  $J$  = 6.4 Hz, 2H), 3.04 (q,  $J$  = 7.2 Hz, 2H), 2.84 (t,  $J$  = 6.3 Hz, 2H), 2.01-1.79 (m, 4H), 1.25 (t,  $J$  = 7.2 Hz, 3H). **<sup>13</sup>C NMR** (75 MHz, CDCl<sub>3</sub>)  $\delta$  (ppm) 202.8, 163.5, 155.8, 146.3, 139.3, 137.0, 135.2, 129.5, 127.1, 124.9, 123.6, 121.7, 119.0, 82.0, 79.3, 32.5, 31.7, 28.0, 22.0, 21.6, 7.8. **HRMS** (ESI):  $m/z$  [ $M+H$ ]<sup>+</sup> calcd. for C<sub>21</sub>H<sub>21</sub>N<sub>2</sub>O<sub>3</sub><sup>+</sup>: 333.1598, found: 333.1607. C<sub>21</sub>H<sub>20</sub>N<sub>2</sub>O<sub>2</sub> (332.40).

***N*-(5-Ethynyl-2-propionylphenyl)-6-methylpicolinamide (3.53)**

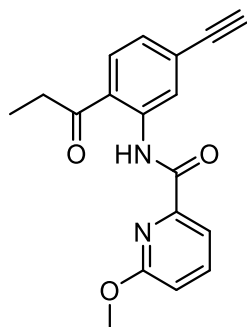
**3.53** was prepared according to the general procedure 1 for N-acylation of anilines. The reaction was carried out using 6-methylpicolinic acid (238 mg, 1.73 mmol, 1.5 eq), TBTU (556 mg, 1.73 mmol, 1.5 eq), DIPEA (603  $\mu$ L, 3.46 mmol, 3.0 eq) and 1-(2-amino-4-ethynylphenyl)propan-1-one (**3.37**) (200 mg, 1.16 mmol, 1.0 eq) and DMF (3 mL). Dilution with DCM preceded the washing steps. Purification by column chromatography (eluent: PE/EtOAc = 4:1,  $R_f$  = 0.3) afforded **3.53** as a beige-colored solid (269 mg, 0.92 mmol, 80%), **mp** 135-139 °C.  $^1\text{H}$  NMR (400 MHz,  $\text{CDCl}_3$ )  $\delta$  (ppm) 13.53 (s, 1H), 9.17 (d,  $J$  = 1.5 Hz, 1H), 8.07 (d,  $J$  = 7.6 Hz, 1H), 7.90 (d,  $J$  = 8.2 Hz, 1H), 7.81-7.74 (m, 1H), 7.35 (d,  $J$  = 7.7 Hz, 1H), 7.24 (dd,  $J$  = 1.6, 8.2 Hz, 1H), 3.24 (s, 1H), 3.06 (q,  $J$  = 7.2 Hz, 2H), 2.76 (s, 3H), 1.27 (t,  $J$  = 7.2 Hz, 3H).  $^{13}\text{C}$  NMR (101 MHz,  $\text{CDCl}_3$ )  $\delta$  (ppm) 203.8, 164.3, 157.8, 149.6, 140.2, 137.7, 130.6, 128.2, 126.4, 126.1, 124.7, 122.9, 120.0, 82.9, 80.4, 33.6, 24.5, 8.8. HRMS (ESI):  $m/z$   $[M+H]^+$  calcd. for  $\text{C}_{18}\text{H}_{17}\text{N}_2\text{O}_2^+$ : 293.1285, found: 293.1285.  $\text{C}_{18}\text{H}_{16}\text{N}_2\text{O}_2$  (292.34).

**6-Chloro-*N*-(5-ethynyl-2-propionylphenyl)picolinamide (3.54)**

**3.54** was prepared according to the general procedure 1 for N-acylation of anilines. The reaction was carried out using 6-chloropicolinic acid (177 mg, 1.13 mmol, 1.5 eq), TBTU (361 mg, 1.13 mmol, 1.5 eq), DIPEA (392  $\mu$ L, 2.25 mmol, 3.0 eq) and 1-(2-amino-4-ethynylphenyl)propan-1-one (**3.37**) (130 mg, 0.75 mmol, 1.0 eq) and DMF (2 mL). Dilution with DCM preceded the washing steps. Purification by column chromatography (eluent: PE/EtOAc = 4:1,  $R_f$  = 0.3) afforded **3.54** as a brownish solid (191 mg, 0.61 mmol, 81%), **mp** 160-163 °C.  $^1\text{H}$  NMR (300 MHz,  $\text{CDCl}_3$ )  $\delta$  (ppm) 13.45 (s, 1H), 9.10 (d,  $J$  = 1.5 Hz, 1H), 8.19 (dd,  $J$  = 0.8, 7.6 Hz, 1H), 7.95-7.82 (m, 2H), 7.53 (dd,  $J$  = 0.8, 7.9 Hz, 1H), 7.29-7.23 (m, 1H, signals interfering with the solvent signal), 3.25 (s, 1H), 3.07 (q,  $J$  = 7.2 Hz, 2H), 1.28 (t,  $J$  = 7.2 Hz, 3H).  $^{13}\text{C}$  NMR (75 MHz,  $\text{CDCl}_3$ )  $\delta$  (ppm) 204.1, 162.6, 150.9, 150.6, 140.2, 139.9,

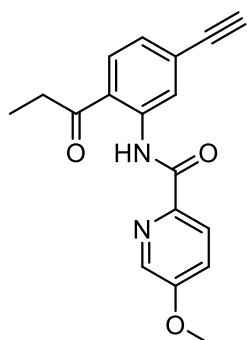
130.7, 128.3, 127.5, 126.5, 124.6, 122.6, 121.5, 82.8, 80.6, 33.5, 8.8. **HRMS** (ESI):  $m/z$   $[M+H]^+$  calcd. for  $C_{17}H_{14}ClN_2O_2^+$ : 313.0738, found: 313.0743.  **$C_{17}H_{13}ClN_2O_2$**  (312.75).

***N*-(5-Ethynyl-2-propionylphenyl)-6-methoxypicolinamide (3.55)**



**3.55** was prepared according to the general procedure 1 for N-acylation of anilines. The reaction was carried out using 6-methoxypicolinic acid (265 mg, 1.73 mmol, 1.5 eq), TBTU (556 mg, 1.73 mmol, 1.5 eq), DIPEA (603  $\mu$ L, 3.46 mmol, 3.0 eq) and 1-(2-amino-4-ethynylphenyl)propan-1-one (**3.37**) (200 mg, 1.16 mmol, 1.0 eq) and DMF (2 mL). Dilution with DCM preceded the washing steps. Purification by column chromatography (eluent: PE/EtOAc = 10:1,  $R_f$  = 0.2) afforded **3.55** as a yellow solid (275 mg, 0.89 mmol, 77%), **mp** 170-173 °C.  **$^1H$  NMR** (400 MHz,  $CDCl_3$ )  $\delta$  (ppm) 13.45 (s, 1H), 9.18 (d,  $J$  = 1.5 Hz, 1H), 7.90-7.83 (m, 2H), 7.78-7.72 (m, 1H), 7.24 (dd,  $J$  = 1.6, 8.2 Hz, 1H), 6.95 (dd,  $J$  = 0.7, 8.2 Hz, 1H), 4.29 (s, 3H), 3.24 (s, 1H), 3.05 (q,  $J$  = 7.2 Hz, 2H), 1.21 (t,  $J$  = 7.2 Hz, 3H).  **$^{13}C$  NMR** (101 MHz,  $CDCl_3$ )  $\delta$  (ppm) 203.6, 163.9, 163.3, 147.7, 140.1, 139.8, 130.5, 128.2, 126.1, 124.6, 123.0, 116.1, 115.0, 82.9, 80.4, 54.5, 33.4, 8.5. **HRMS** (ESI):  $m/z$   $[M+H]^+$  calcd. for  $C_{18}H_{17}N_2O_3^+$ : 309.1234, found: 309.1242.  **$C_{18}H_{16}N_2O_3$**  (308.33).

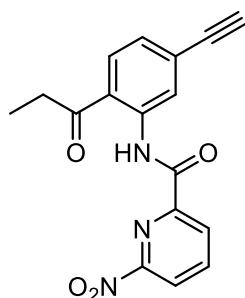
***N*-(5-Ethynyl-2-propionylphenyl)-5-methoxypicolinamide (3.56)**



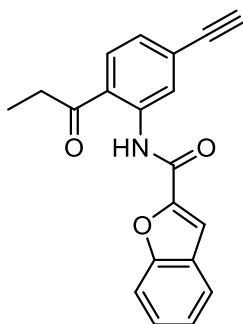
**3.56** was prepared according to the general procedure 1 for N-acylation of anilines. The reaction was carried out using 5-methoxypicolinic acid (265 mg, 1.73 mmol, 1.5 eq), TBTU (556 mg, 1.73 mmol, 1.5 eq), DIPEA (603  $\mu$ L, 3.46 mmol, 3.0 eq) and 1-(2-amino-4-ethynylphenyl)propan-1-one (**3.37**) (200 mg, 1.16 mmol, 1.0 eq) and DMF (3 mL). Dilution with DCM preceded the washing steps. Purification by column chromatography (eluent:

PE/EtOAc = 4:1,  $R_f$  = 0.2) afforded **3.56** as a yellow solid (296 mg, 0.96 mmol, 83%), **mp** 175-178 °C.  **$^1\text{H}$  NMR** (400 MHz,  $\text{CDCl}_3$ )  $\delta$  (ppm) 13.37 (s, 1H), 9.17 (d,  $J$  = 1.5 Hz, 1H), 8.48 (d,  $J$  = 2.8 Hz, 1H), 8.23 (d,  $J$  = 8.7 Hz, 1H), 7.91 (d,  $J$  = 8.2 Hz, 1H), 7.33 (dd,  $J$  = 2.8, 8.7 Hz, 1H), 7.23 (dd,  $J$  = 1.5, 8.2 Hz, 1H), 3.94 (s, 3H), 3.24 (s, 1H), 3.08 (q,  $J$  = 7.2 Hz, 2H), 1.27 (t,  $J$  = 7.2 Hz, 3H).  **$^{13}\text{C}$  NMR** (101 MHz,  $\text{CDCl}_3$ )  $\delta$  (ppm) 204.2, 164.0, 158.2, 143.1, 140.5, 136.9, 130.7, 128.3, 125.9, 124.7, 124.2, 122.5, 120.9, 83.0, 80.5, 56.0, 33.6, 8.8. **HRMS** (ESI):  $m/z$   $[M+H]^+$  calcd. for  $\text{C}_{18}\text{H}_{17}\text{N}_2\text{O}_3^+$ : 309.1234, found: 309.1236.  **$\text{C}_{18}\text{H}_{16}\text{N}_2\text{O}_3$**  (308.34).

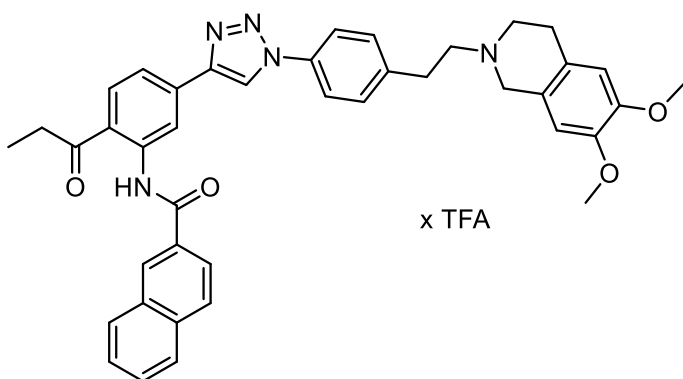
### ***N*-(5-Ethynyl-2-propionylphenyl)-6-nitropicolinamide (3.57)**



**3.57** was prepared according to the general procedure 1 for N-acylation of anilines. The reaction was carried out using 6-nitropicolinic acid (437 mg, 2.60 mmol, 1.5 eq), TBTU (834 mg, 2.60 mmol, 1.5 eq), DIPEA (905  $\mu\text{L}$ , 5.20 mmol, 3.0 eq) and 1-(2-amino-4-ethynylphenyl)propan-1-one (**3.37**) (300 mg, 1.73 mmol, 1.0 eq) and DMF (4 mL). Dilution with DCM preceded the washing steps. Purification by column chromatography (eluent: PE/EtOAc = 3:1,  $R_f$  = 0.2) afforded **3.57** as a yellow solid (460 mg, 1.42 mmol, 82%), **mp** 184-193 °C. Due to a slow rotation around the amide group on the NMR time scale, two isomers (ratio ca 1:0.3) were evident in the NMR spectra.  **$^1\text{H}$  NMR** (400 MHz,  $\text{CDCl}_3$ )  $\delta$  (ppm) 13.72 (s, 0.2H), 13.67 (s, 1H), 9.31 (d,  $J$  = 1.8 Hz, 0.2H), 9.11 (d,  $J$  = 1.2 Hz, 1H), 8.69-8.61 (m, 1.3H), 8.49-8.42 (m, 1.3H), 8.32-8.25 (m, 1.3H), 8.04-7.93 (m, 1.3H), 7.49 (dd,  $J$  = 1.9, 8.5 Hz, 0.2H), 7.31 (dd,  $J$  = 1.4, 8.2 Hz, 1H), 3.27 (s, 1.1H), 3.12 (m, 2.6H), 1.32 (m, 3.9H).  **$^{13}\text{C}$  NMR** (101 MHz,  $\text{CDCl}_3$ )  $\delta$  (ppm) 204.4, 161.6, 155.5, 150.3, 141.8, 139.7, 130.9, 128.5, 128.1, 127.0, 124.7, 122.7, 120.6, 82.7, 80.9, 33.5, 8.7. **HRMS** (ESI):  $m/z$   $[M+H]^+$  calcd. for  $\text{C}_{17}\text{H}_{14}\text{N}_3\text{O}_4^+$ : 324.0979, found: 324.0980.  **$\text{C}_{17}\text{H}_{13}\text{N}_3\text{O}_4$**  (323.31).

***N*-(5-Ethynyl-2-propionylphenyl)benzofuran-2-carboxamide (3.58)**

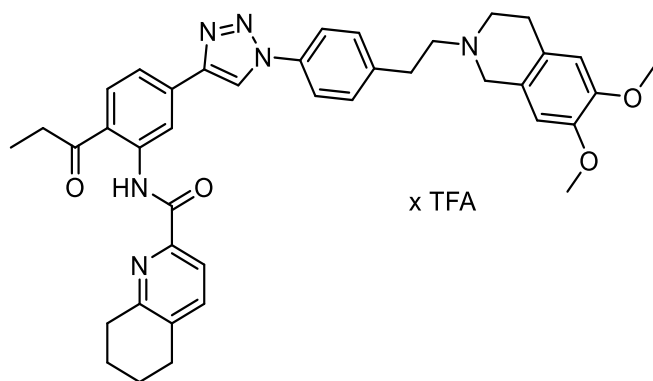
**3.58** was prepared according to the general procedure 1 for N-acylation of anilines. The reaction was carried out using benzofuran-2-carboxylic acid (827 mg, 5.10 mmol, 1.5 eq), TBTU (1638 mg, 5.10 mmol, 1.5 eq), DIPEA (1777  $\mu$ L, 10.20 mmol, 3.0 eq) and 1-(2-amino-4-ethynylphenyl)propan-1-one (**3.37**) (589 mg, 3.40 mmol, 1.0 eq) and DMF (9 mL). Dilution with DCM preceded the washing steps. Purification by column chromatography (eluent: PE/EtOAc = 6:1,  $R_f$  = 0.3) afforded **3.58** as a brownish solid (400 mg, 1.26 mmol, 37%), **mp** 144-148 °C.  $^1\text{H NMR}$  (300 MHz,  $\text{CDCl}_3$ )  $\delta$  (ppm) 12.91 (s, 1H), 9.10 (d,  $J$  = 1.6 Hz, 1H), 7.94 (d,  $J$  = 8.3 Hz, 1H), 7.75-7.68 (m, 2H), 7.62 (m, 1H), 7.51-7.43 (m, 1H), 7.35-7.25 (m, 2H, signals interfering with the solvent signal), 3.27 (s, 1H), 3.11 (q,  $J$  = 7.2 Hz, 2H), 1.29 (t,  $J$  = 7.3 Hz, 3H).  $^{13}\text{C NMR}$  (75 MHz,  $\text{CDCl}_3$ )  $\delta$  (ppm) 204.9, 157.8, 155.4, 148.9, 140.4, 130.8, 128.7, 127.7, 127.4, 126.4, 124.7, 123.9, 122.8, 121.7, 112.6, 111.8, 82.7, 80.9, 33.5, 8.8. **HRMS** (ESI):  $m/z$   $[M+H]^+$  calcd. for  $\text{C}_{20}\text{H}_{16}\text{NO}_3^+$ : 318.1125, found: 318.1127.  $\text{C}_{20}\text{H}_{15}\text{NO}$  (317.34).

***N*-(5-(1-(4-(2-(6,7-Dimethoxy-3,4-dihydroisoquinolin-2(1*H*)-yl)ethyl)phenyl)-1*H*-1,2,3-triazol-4-yl)-2-propionylphenyl)-2-naphthamide hydrotrifluoroacetate (3.59)**

**3.59** was prepared according to the general procedure for the CuAAC. The reaction was carried out using *N*-(5-ethynyl-2-propionylphenyl)-2-naphthamide (**3.51**) (30.0 mg, 0.092 mmol, 1.0 eq), 2-(4-azidophenethyl)-6,7-dimethoxy-1,2,3,4-tetrahydroisoquinoline (**3.09**) (37.2 mg, 0.110 mmol, 1.2 eq),  $\text{CuSO}_4 \cdot 5\text{H}_2\text{O}$  (3.4 mg, 0.014 mmol, 0.15 eq), sodium ascorbate (12.7 mg, 0.064 mmol, 0.7 eq) and TBTA (7.3 mg, 0.014 mmol, 0.15 eq) in  $\text{CHCl}_3$  (3 mL). Refluxing

lasted for 3 d. Flash column chromatography (4 g column, gradient: 0-20 min: DCM/MeOH 100:0-95:5,  $R_f = 0.4$  in DCM/MeOH 95:5) followed by preparative HPLC (gradient: 0-30 min: MeCN/ 0.1% aq TFA 51:49-87:13,  $t_R = 14.2$  min) afforded the product as a yellowish solid (14.2 mg, 0.018 mmol, 20%), **mp** 91-104 °C.  **$^1\text{H}$  NMR** (600 MHz,  $\text{CDCl}_3$ )  $\delta$  (ppm) 13.35 (br s, 1H), 13.06 (s, 1H), 9.42 (s, 1H), 8.60 (s, 1H), 8.44 (s, 1H), 8.12 (dd,  $J = 1.3, 8.6$  Hz, 1H), 8.09 (d,  $J = 8.3$  Hz, 1H), 8.04 (d,  $J = 7.9$  Hz, 1H), 7.99 (d,  $J = 8.5$  Hz, 1H), 7.94 (d,  $J = 8.2$  Hz, 1H), 7.91 (d,  $J = 7.9$  Hz, 1H), 7.76 (d,  $J = 7.9$  Hz, 2H), 7.59 (m, 2H), 7.42 (d,  $J = 7.9$  Hz, 2H), 6.64 (s, 1H), 6.54 (s, 1H), 4.67 (d,  $J = 14.2$  Hz, 1H), 4.08 (d,  $J = 14.2$  Hz, 1H), 3.86 (s, 3H), 3.84 (s, 3H), 3.79 (m, 1H), 3.44 (m, 2H), 3.35 (m, 1H), 3.27 (m, 3H), 3.15 (q,  $J = 7.2$  Hz, 2H), 2.98 (d,  $J = 15.4$  Hz, 1H), 1.29 (t,  $J = 7.2$  Hz, 3H).  **$^{13}\text{C}$  NMR** (151 MHz,  $\text{CDCl}_3$ )  $\delta$  (ppm) 205.4, 166.6, 149.5, 148.8, 147.4, 142.0, 137.1, 136.3, 136.2, 135.2, 132.9, 132.0, 131.9, 130.4 (2C), 129.6, 129.0, 128.8, 128.2, 127.9, 127.0, 123.7, 122.4, 121.4, 121.1 (2C), 119.9, 119.4, 118.2, 117.7, 111.3, 109.3, 56.2, 56.1, 55.6, 52.5, 49.4, 33.4, 30.5, 24.1, 8.8. **RP-HPLC** (220 nm): 99% ( $t_R = 7.7$  min,  $k = 6.4$ ). **HRMS** (ESI):  $m/z$   $[M+H]^+$  calcd. for  $\text{C}_{41}\text{H}_{39}\text{N}_5\text{O}_4^+$ : 666.3075, found: 666.3087.  $\text{C}_{41}\text{H}_{39}\text{N}_5\text{O}_4 \cdot \text{C}_2\text{HF}_3\text{O}_2$  (665.79 + 114.02).

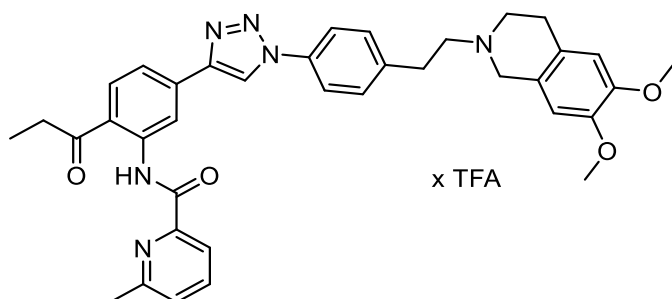
***N*-(5-(1-(4-(2-(6,7-Dimethoxy-3,4-dihydroisoquinolin-2(1*H*)-yl)ethyl)phenyl)-1*H*-1,2,3-triazol-4-yl)-2-propionylphenyl)-5,6,7,8-tetrahydroquinoline-2-carboxamide hydrotrifluoroacetate (3.60)**



**3.60** was prepared according to the general procedure for the CuAAC. The reaction was carried out using *N*-(5-ethynyl-2-propionylphenyl)-5,6,7,8-tetrahydroquinoline-2-carboxamide (**3.52**) (50.0 mg, 0.150 mmol, 1.0 eq), 2-(4-azidophenethyl)-6,7-dimethoxy-1,2,3,4-tetrahydroisoquinoline (**3.09**) (76.4 mg, 0.226 mmol, 1.5 eq),  $\text{CuSO}_4 \cdot 5\text{H}_2\text{O}$  (5.6 mg, 0.023 mmol, 0.15 eq), sodium ascorbate (20.9 mg, 0.105 mmol, 0.7 eq) and TBTA (12.0 mg, 0.023 mmol, 0.15 eq) in  $\text{CHCl}_3$  (3 mL). Refluxing lasted for 3 d. Column chromatography (eluent: DCM/MeOH 19:1,  $R_f = 0.3$ ) followed by preparative HPLC (gradient: 0-30 min: MeCN/ 0.1% aq TFA 51:49-87:13,  $t_R = 15.0$  min) afforded the product as a beige-colored solid (46.9 mg, 0.060 mmol, 40%), **mp** 83-92 °C.  **$^1\text{H}$  NMR** (600 MHz,  $\text{CDCl}_3$ )  $\delta$  (ppm) 13.63 (s, 1H), 11.80 (br s, 1H), 9.34 (s, 1H), 8.54 (s, 1H), 8.07 (d,  $J = 8.0$  Hz, 1H), 7.96 (d,  $J = 7.7$  Hz, 1H), 7.91 (d,

$J = 7.6$  Hz, 1H), 7.79 (d,  $J = 6.7$  Hz, 2H), 7.66 (d,  $J = 7.7$  Hz, 1H), 7.40 (d,  $J = 5.6$  Hz, 2H), 6.64 (s, 1H), 6.55 (s, 1H), 4.71 (d,  $J = 12.9$  Hz, 1H), 4.13 (d,  $J = 12.2$  Hz, 1H), 3.86 (s, 3H), 3.84 (m, 4H), 3.49 (m, 2H), 3.40 (m, 1H), 3.27 (m, 3H), 3.19 (t,  $J = 6.2$  Hz, 2H), 3.11 (q,  $J = 7.1$  Hz, 2H), 3.00 (d,  $J = 15.9$  Hz, 1H), 2.90 (t,  $J = 6.1$  Hz, 2H), 1.99 (m, 2H), 1.89 (m, 2H), 1.29 (t,  $J = 7.1$  Hz, 3H).  $^{13}\text{C}$  NMR (151 MHz,  $\text{CDCl}_3$ )  $\delta$  (ppm) 204.5, 164.0, 161.0 (TFA), 160.8 (TFA), 157.2, 149.6, 148.9, 147.3, 146.1, 140.5, 139.4, 137.4, 136.8, 136.1, 135.7, 131.9, 130.4 (2C), 122.5, 122.2, 121.0 (2C), 120.3, 120.1, 119.7, 118.0, 118.0, 116.6 (TFA), 114.7 (TFA), 111.3, 109.3, 56.2, 56.1, 55.9, 52.9, 49.9, 33.5, 32.0, 30.5, 29.0, 24.1, 22.7, 22.4, 8.8. **RP-HPLC** (220 nm): 99% ( $t_R = 7.5$  min,  $k = 6.2$ ). **HRMS** (ESI):  $m/z$   $[M+H]^+$  calcd. for  $\text{C}_{40}\text{H}_{43}\text{N}_6\text{O}_4^+$ : 671.3340, found: 671.3349.  $\text{C}_{40}\text{H}_{42}\text{N}_6\text{O}_4 \cdot \text{C}_2\text{HF}_3\text{O}_2$  (670.81 + 114.02).

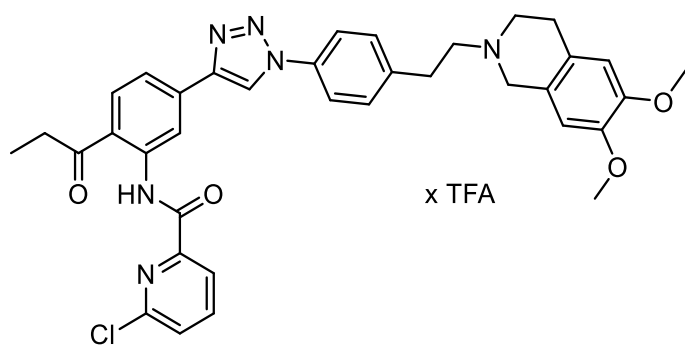
***N*-(5-(1-(4-(2-(6,7-Dimethoxy-3,4-dihydroisoquinolin-2(1*H*)-yl)ethyl)phenyl)-1*H*-1,2,3-triazol-4-yl)-2-propionylphenyl)-6-methylpicolinamide hydrotrifluoroacetate (3.61)**



**3.61** was prepared according to the general procedure for the CuAAC. The reaction was carried out using *N*-(5-ethynyl-2-propionylphenyl)-6-methylpicolinamide (**3.53**) (60.0 mg, 0.205 mmol, 1.0 eq), 2-(4-azidophenethyl)-6,7-dimethoxy-1,2,3,4-tetrahydroisoquinoline (**3.09**) (104.2 mg, 0.308 mmol, 1.5 eq),  $\text{CuSO}_4 \cdot 5\text{H}_2\text{O}$  (7.7 mg, 0.031 mmol, 0.15 eq), sodium ascorbate (28.5 mg, 0.114 mmol, 0.7 eq) and TBTA (16.3 mg, 0.031 mmol, 0.15 eq) in DMSO/isopropanol 3:1 (5 mL). Refluxing lasted for 2 d. The mixture was diluted with DCM (100 mL) and washed with  $\text{H}_2\text{O}$  (3 x 100 mL). The organic layer was dried over  $\text{Na}_2\text{SO}_4$  and the solvent evaporated. Column chromatography (eluent: DCM/MeOH 19:1,  $R_f = 0.4$ ) followed by preparative HPLC (gradient: 0-30 min: MeCN/ 0.1% aq TFA 42:58-78:22,  $t_R = 14.5$  min) afforded the product as a yellow solid (18.56 mg, 0.025 mmol, 12%), **mp** 121-132 °C.  $^1\text{H}$  NMR (600 MHz,  $\text{CDCl}_3$ )  $\delta$  (ppm) 13.69 (s, 1H), 12.96 (br s, 1H), 9.40 (s, 1H), 8.44 (s, 1H), 8.04 (m, 2H), 7.89 (d,  $J = 7.9$  Hz, 1H), 7.76 (m, 3H), 7.41 (m, 2H), 7.35 (d,  $J = 7.6$  Hz, 1H), 6.63 (s, 1H), 6.54 (s, 1H), 4.67 (m, 1H), 4.10 (m, 1H), 3.85 (s, 3H), 3.84-3.74 (m, 4H), 3.54-3.18 (m, 6H), 3.11 (q,  $J = 7.2$  Hz, 2H), 2.99 (m, 1H), 2.77 (s, 3H), 1.29 (t,  $J = 7.2$  Hz, 3H).  $^{13}\text{C}$  NMR (151 MHz,  $\text{CDCl}_3$ )  $\delta$  (ppm) 203.0, 163.7, 157.0, 148.6, 148.4, 147.8, 146.5, 139.8, 136.8, 136.0, 135.1, 134.7, 130.8, 129.4 (2C), 125.5, 121.6, 121.4, 120.0 (2C), 119.0, 118.8, 118.3, 117.2,

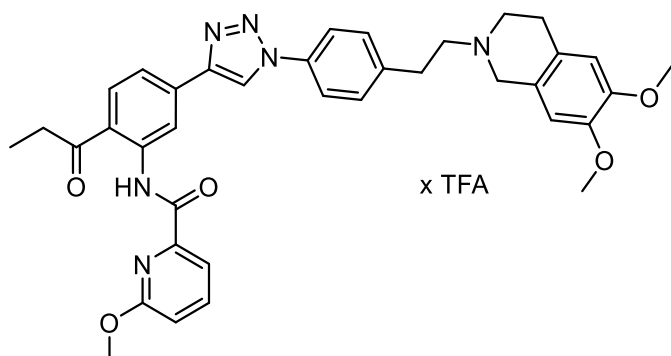
116.9, 110.3, 108.3, 55.2, 55.1, 54.7, 51.6, 48.5, 32.5, 29.5, 23.6, 23.1, 7.8. **RP-HPLC** (220 nm): 97% ( $t_R$  = 6.5 min,  $k$  = 5.2). **HRMS** (ESI):  $m/z$   $[M+H]^+$  calcd. for  $C_{37}H_{39}N_6O_4^+$ : 631.3027, found: 631.3038.  $C_{37}H_{38}N_6O_4 \cdot C_2HF_3O_2$  (630.75 + 114.02).

**6-Chloro-*N*-(5-(1-(4-(2-(6,7-dimethoxy-3,4-dihydroisoquinolin-2(1*H*)-yl)ethyl)phenyl)-1*H*-1,2,3-triazol-4-yl)-2-propionylphenyl)picolinamide hydrotrifluoroacetate (3.62)**



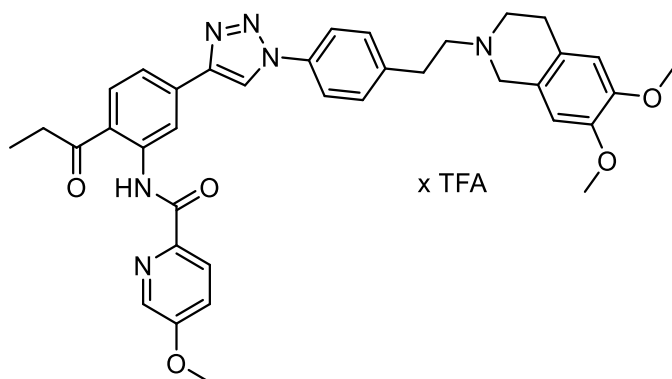
**3.62** was prepared according to the general procedure for the CuAAC. The reaction was carried out using 6-chloro-*N*-(5-ethynyl-2-propionylphenyl)picolinamide (**3.54**) (60.0 mg, 0.192 mmol, 1.0 eq), 2-(4-azidophenethyl)-6,7-dimethoxy-1,2,3,4-tetrahydroisoquinoline (**3.09**) (97.4 mg, 0.288 mmol, 1.5 eq),  $CuSO_4 \cdot 5H_2O$  (7.2 mg, 0.029 mmol, 0.15 eq), sodium ascorbate (26.6 mg, 0.134 mmol, 0.7 eq) and TBTA (15.3 mg, 0.029 mmol, 0.15 eq) in  $CHCl_3$  (2 mL). Refluxing lasted for 1 d. Column chromatography (eluent: DCM/MeOH 19:1,  $R_f$  = 0.3) followed by preparative HPLC (gradient: 0-30 min: MeCN/ 0.1% aq TFA 46:54-82:18,  $t_R$  = 13.0 min) afforded the product as a yellowish solid (64.1 mg, 0.084 mmol, 44%), **mp** 148-154 °C.  **$^1H$  NMR** (600 MHz,  $CDCl_3$ )  $\delta$  (ppm) 13.59 (s, 1H), 12.79 (br s, 1H), 9.34 (s, 1H), 8.41 (s, 1H), 8.15 (d,  $J$  = 7.4 Hz, 1H), 8.07 (d,  $J$  = 8.3 Hz, 1H), 7.92-7.84 (m, 2H), 7.75 (d,  $J$  = 7.7 Hz, 2H), 7.54 (d,  $J$  = 7.9 Hz, 1H), 7.41 (d,  $J$  = 7.6 Hz, 2H), 6.64 (s, 1H), 6.54 (s, 1H), 4.68 (d,  $J$  = 12.3 Hz, 1H), 4.10 (d,  $J$  = 12.1 Hz, 1H), 3.86 (s, 3H), 3.83 (s, 3H), 3.80 (m, 1H), 3.54-3.21 (m, 6H), 3.12 (q,  $J$  = 7.2 Hz, 2H), 3.00 (m, 1H), 1.30 (t,  $J$  = 7.2 Hz, 3H).  **$^{13}C$  NMR** (151 MHz,  $CDCl_3$ )  $\delta$  (ppm) 204.2, 162.9, 161.9 (TFA), 161.7 (TFA), 150.9, 150.8, 149.5, 148.8, 147.3, 140.6, 140.2, 137.0, 136.1, 135.7, 131.9, 130.4 (2C), 127.6, 122.5, 122.4, 121.4, 121.1 (2C), 120.4, 119.3, 118.1, 117.9, 111.3, 109.3, 56.2, 56.1, 55.7, 52.6, 49.6, 33.5, 30.5, 24.1, 8.9. **RP-HPLC** (220 nm): 98% ( $t_R$  = 6.6 min,  $k$  = 5.3). **HRMS** (ESI):  $m/z$   $[M+H]^+$  calcd. for  $C_{36}H_{36}ClN_6O_4^+$ : 651.2481, found: 651.2505.  $C_{36}H_{35}ClN_6O_4 \cdot C_2HF_3O_2$  (651.15 + 114.02).

***N*-(5-(1-(4-(2-(6,7-Dimethoxy-3,4-dihydroisoquinolin-2(1*H*)-yl)ethyl)phenyl)-1*H*-1,2,3-triazol-4-yl)-2-propionylphenyl)-6-methoxypicolinamide hydrotrifluoroacetate (3.63)**



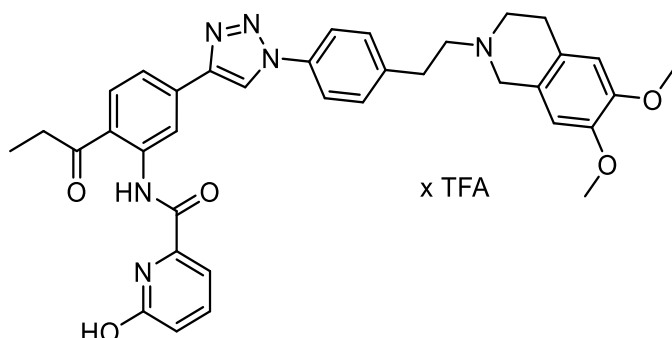
**3.63** was prepared according to the general procedure for the CuAAC. The reaction was carried out using *N*-(5-ethynyl-2-propionylphenyl)-6-methoxypicolinamide (**3.55**) (40.0 mg, 0.130 mmol, 1.0 eq), 2-(4-azidophenethyl)-6,7-dimethoxy-1,2,3,4-tetrahydroisoquinoline (**3.09**) (65.8 mg, 0.195 mmol, 1.5 eq), CuSO<sub>4</sub>·5H<sub>2</sub>O (4.9 mg, 0.019 mmol, 0.15 eq), sodium ascorbate (18.0 mg, 0.091 mmol, 0.7 eq) and TBTA (10.3 mg, 0.019 mmol, 0.15 eq) in CHCl<sub>3</sub> (2 mL). Refluxing lasted for 3 d. Column chromatography (eluent: DCM/MeOH 19:1, *R<sub>f</sub>* = 0.2) followed by preparative HPLC (gradient: 0-30 min: MeCN/ 0.1% aq TFA 46:54-82:18, *t<sub>R</sub>* = 15.0 min) afforded the product as a yellowish solid (52.11 mg, 0.068 mmol, 53%), **mp** 127-136 °C. **<sup>1</sup>H NMR** (600 MHz, CDCl<sub>3</sub>) δ (ppm) 13.64 (s, 1H), 12.86 (br s, 1H), 9.41 (s, 1H), 8.45 (s, 1H), 8.05 (d, *J* = 8.2 Hz, 1H), 7.94 (d, *J* = 8.0 Hz, 1H), 7.83 (d, *J* = 7.2 Hz, 1H), 7.80-7.73 (m, 3H), 7.43 (d, *J* = 7.6 Hz, 2H), 6.96 (d, *J* = 8.2 Hz, 1H), 6.65 (s, 1H), 6.55 (s, 1H), 4.69 (d, *J* = 12.8 Hz, 1H), 4.32 (s, 3H), 4.10 (d, *J* = 12.2 Hz, 1H), 3.87 (s, 3H), 3.84 (s, 3H), 3.81 (m, 1H), 3.51-3.24 (m, 6H), 3.10 (q, *J* = 7.2 Hz, 2H), 3.00 (m, 1H), 1.24 (t, *J* = 7.2 Hz, 3H). **<sup>13</sup>C NMR** (151 MHz, CDCl<sub>3</sub>) δ (ppm) 203.7, 164.4, 163.4, 162.0 (TFA), 161.7 (TFA), 149.5, 148.9, 147.7, 147.5, 140.7, 139.8, 137.0, 136.2, 135.7, 131.6, 130.4 (2C), 122.8, 122.4, 121.1 (2C), 120.1, 119.3, 118.1, 117.8, 116.0, 115.2, 111.3, 109.4, 56.2, 56.1, 55.6, 54.6, 52.7, 49.6, 33.4, 30.5, 24.1, 8.5. **RP-HPLC** (220 nm): 99% (*t<sub>R</sub>* = 7.1 min, *k* = 5.8). **HRMS** (ESI): *m/z* [*M*+*H*]<sup>+</sup> calcd. for C<sub>37</sub>H<sub>39</sub>N<sub>6</sub>O<sub>5</sub><sup>+</sup>: 647.2976, found: 647.2970. C<sub>37</sub>H<sub>38</sub>N<sub>6</sub>O<sub>5</sub> · C<sub>2</sub>HF<sub>3</sub>O<sub>2</sub> (646.75 + 114.02).

***N*-(5-(1-(4-(2-(6,7-Dimethoxy-3,4-dihydroisoquinolin-2(1*H*)-yl)ethyl)phenyl)-1*H*-1,2,3-triazol-4-yl)-2-propionylphenyl)-5-methoxypicolinamide hydrotrifluoroacetate (3.64)**



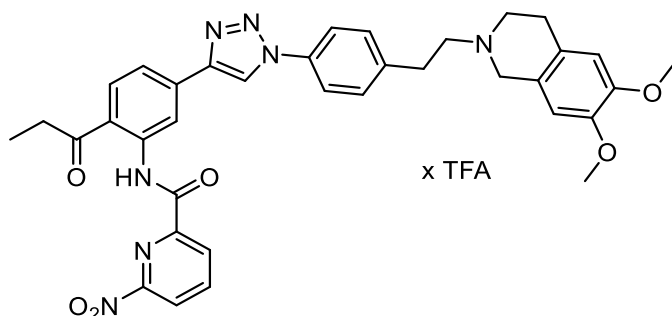
**3.64** was prepared according to the general procedure for the CuAAC. The reaction was carried out using *N*-(5-ethynyl-2-propionylphenyl)-5-methoxypicolinamide (**3.56**) (25.0 mg, 0.081 mmol, 1.0 eq), 2-(4-azidophenethyl)-6,7-dimethoxy-1,2,3,4-tetrahydroisoquinoline (**3.09**) (41.2 mg, 0.122 mmol, 1.5 eq), CuSO<sub>4</sub>·5H<sub>2</sub>O (3.0 mg, 0.012 mmol, 0.15 eq), sodium ascorbate (11.2 mg, 0.057 mmol, 0.7 eq) and TBTA (6.5 mg, 0.012 mmol, 0.15 eq) in DMSO/isopropanol 3:1 (3 mL). Refluxing lasted for 1 d. The mixture was diluted with DCM (50 mL) and washed with H<sub>2</sub>O (3 x 50 mL). The organic layer was dried over Na<sub>2</sub>SO<sub>4</sub> and the solvent evaporated. Column chromatography (eluent: DCM/MeOH 19:1, *R<sub>f</sub>* = 0.3) followed by preparative HPLC (gradient: 0-30 min: MeCN/ 0.1% aq TFA 42:58-78:22, *t<sub>R</sub>* = 13.5 min) afforded the product as a yellowish solid (6.86 mg, 0.009 mmol, 11%), **mp** 110-130 °C. <sup>1</sup>H NMR (600 MHz, CDCl<sub>3</sub>) δ (ppm) 13.56 (s, 1H), 12.91 (br s, 1H), 9.42 (s, 1H), 8.51 (d, *J* = 2.5 Hz, 1H), 8.46 (s, 1H), 8.21 (d, *J* = 8.6 Hz, 1H), 8.09 (d, *J* = 8.3 Hz, 1H), 7.95 (d, *J* = 8.2 Hz, 1H), 7.79 (d, *J* = 7.7 Hz, 2H), 7.44 (d, *J* = 7.4 Hz, 2H), 7.35 (dd, *J* = 2.6, 8.6 Hz, 1H), 6.66 (s, 1H), 6.55 (s, 1H), 4.69 (d, *J* = 13.8 Hz, 1H), 4.09 (d, *J* = 11.3 Hz, 1H), 3.96 (s, 3H), 3.87 (s, 3H), 3.85 (s, 3H), 3.80 (m, 1H), 3.53-3.25 (m, 6H), 3.14 (q, *J* = 7.2 Hz, 2H), 3.00 (s, 1H), 1.31 (t, *J* = 7.2 Hz, 3H). <sup>13</sup>C NMR (151 MHz, CDCl<sub>3</sub>) δ (ppm) 204.4, 164.5, 158.3, 149.6, 148.9, 147.6, 143.0, 141.1, 137.1, 137.0, 136.3, 135.8, 131.9, 130.4 (2C), 124.1, 122.4, 122.3, 121.2 (2C), 120.9, 119.9, 119.3, 118.1, 117.9, 111.3, 109.4, 56.2, 56.2, 56.0, 55.6, 52.6, 49.6, 33.5, 30.5, 24.0, 8.9. **RP-HPLC** (220 nm): 99% (*t<sub>R</sub>* = 6.1 min, *k* = 4.9). **HRMS** (ESI): *m/z* [*M*+H]<sup>+</sup> calcd. for C<sub>37</sub>H<sub>39</sub>N<sub>6</sub>O<sub>5</sub><sup>+</sup>: 647.2976, found: 647.2984. C<sub>37</sub>H<sub>38</sub>N<sub>6</sub>O<sub>5</sub> · C<sub>2</sub>HF<sub>3</sub>O<sub>2</sub> (646.75 + 114.02).

***N*-(5-(1-(4-(2-(6,7-Dimethoxy-3,4-dihydroisoquinolin-2(1*H*)-yl)ethyl)phenyl)-1*H*-1,2,3-triazol-4-yl)-2-propionylphenyl)-6-hydroxypicolinamide hydrotrifluoroacetate (3.65)**



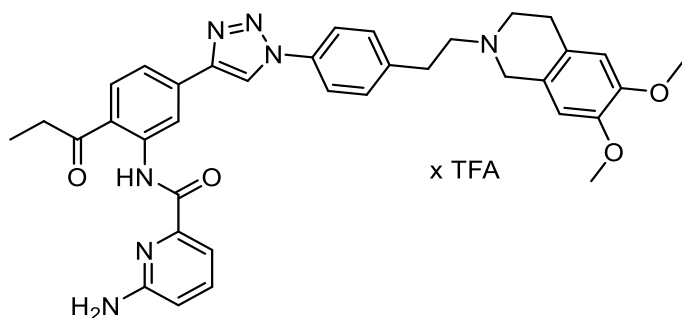
**3.65** was prepared according to the general procedure 1 for N-acylation of anilines. The reaction was carried out using 1-(2-amino-4-(1-(4-(2-(6,7-dimethoxy-3,4-dihydroisoquinolin-2(1*H*)-yl)ethyl)phenyl)-1*H*-1,2,3-triazol-4-yl)phenyl)propan-1-one (**3.69**) (60.0 mg, 0.096 mmol, 1.0 eq), 6-hydroxypicolinic acid (26.7 mg, 0.192 mmol, 2.0 eq), TBTU (61.6 mg, 0.192 mmol, 2.0 eq), DIPEA (100  $\mu$ L, 0.576 mmol, 6.0 eq) and DMF (2 mL). Dilution with DCM preceded the washing steps. The crude product was subjected to flash column chromatography (4 g column, gradient: 0-20 min: DCM/MeOH 100:0-95:5,  $R_f$  = 0.2 in DCM/MeOH 95:5) and for further purification to preparative HPLC (gradient: 0-30 min: MeCN/ 0.1% aq TFA 33:67-69:31,  $t_R$  = 17.0 min). Removal of the solvent from the eluate through evaporation and lyophilization afforded **3.65** as a yellow solid (3.9 mg, 0.005 mmol, 5%), **mp** 162-173  $^{\circ}$ C.  **$^1\text{H}$  NMR** (600 MHz, DMSO- $d_6$ )  $\delta$  (ppm) 12.94 (s, 1H), 11.26 (br s, 1H), 10.10 (s, 1H), 9.48 (s, 1H), 9.40 (s, 1H), 8.29 (d,  $J$  = 8.5 Hz, 1H), 8.02 (d,  $J$  = 8.4 Hz, 2H), 7.89 (m, 1H), 7.81 (dd,  $J$  = 1.6, 8.3 Hz, 1H), 7.67 (m, 1H), 7.60 (d,  $J$  = 8.5 Hz, 2H), 6.97 (d,  $J$  = 7.7 Hz, 1H), 6.85 (s, 1H), 6.81 (s, 1H), 4.56 (d,  $J$  = 15.1 Hz, 1H), 4.32 (m, 1H), 3.81\* (m, 1H), 3.76\* (s, 3H), 3.75\* (s, 3H), 3.54\* (m, 2H), 3.37 (m, 1H), 3.20 (m, 4H), 3.13-2.98 (m, 2H), 1.16 (t,  $J$  = 7.1 Hz, 3H) (\*signals interfering with the water signal).  **$^{13}\text{C}$  NMR** (151 MHz, DMSO- $d_6$ )  $\delta$  (ppm) 203.8, 162.8, 158.1 (TFA), 157.8 (TFA), 148.5, 147.8, 146.3, 140.7, 139.7, 137.7, 135.4, 135.3, 132.3, 130.3 (2C), 123.1, 122.8, 121.0, 120.4 (2C), 120.0, 119.8, 117.2, 111.5, 109.7, 55.6, 55.6, 55.5, 51.9, 49.3, 32.9, 29.2, 24.6, 8.5 (two tertiary and two quaternary carbons not apparent). **RP-HPLC** (220 nm): 98% ( $t_R$  = 5.0 min,  $k$  = 3.7). **HRMS** (ESI):  $m/z$  [ $M+H$ ] $^+$  calcd. for  $\text{C}_{36}\text{H}_{37}\text{N}_6\text{O}_5^+$ : 633.2820, found: 633.2829.  $\text{C}_{36}\text{H}_{36}\text{N}_6\text{O}_5 \cdot \text{C}_2\text{HF}_3\text{O}_2$  (632.72 + 114.02).

***N*-(5-(1-(4-(2-(6,7-Dimethoxy-3,4-dihydroisoquinolin-2(1*H*)-yl)ethyl)phenyl)-1*H*-1,2,3-triazol-4-yl)-2-propionylphenyl)-6-nitropicolinamide hydrotrifluoroacetate (3.66)**



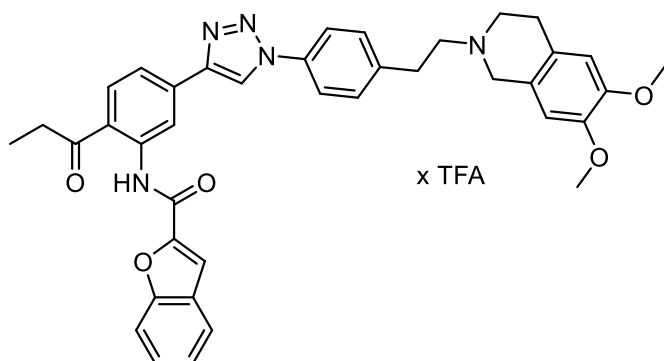
**3.66** was prepared according to the general procedure for the CuAAC. The reaction was carried out using *N*-(5-ethynyl-2-propionylphenyl)-6-nitropicolinamide (**3.57**) (70.0 mg, 0.217 mmol, 1.0 eq), 2-(4-azidophenethyl)-6,7-dimethoxy-1,2,3,4-tetrahydroisoquinoline (**3.09**) (109.9 mg, 0.433 mmol, 1.5 eq), CuSO<sub>4</sub>·5H<sub>2</sub>O (8.1 mg, 0.032 mmol, 0.15 eq), sodium ascorbate (30.0 mg, 0.152 mmol, 0.7 eq) and TBTA (17.2 mg, 0.032 mmol, 0.15 eq) in DMSO/isopropanol 3:1 (5 mL). Refluxing lasted for 2 d. The mixture was diluted with DCM (100 mL) and washed with H<sub>2</sub>O (3 x 100 mL). The organic layer was dried over Na<sub>2</sub>SO<sub>4</sub> and the solvent evaporated. Column chromatography (eluent: DCM/MeOH 19:1, *R<sub>f</sub>* = 0.3) followed by preparative HPLC (gradient: 0-30 min: MeCN/ 0.1% aq TFA 42:58-78:22, *t<sub>R</sub>* = 12.0 min) afforded the product as a light yellow solid (59.13 mg, 0.076 mmol, 35%), **mp** 107-117 °C. **<sup>1</sup>H NMR** (600 MHz, CDCl<sub>3</sub>) δ (ppm) 13.79 (s, 1H), 13.38 (br s, 1H), 9.35 (s, 1H), 8.61 (d, *J* = 7.4 Hz, 1H), 8.45 (d, *J* = 7.9 Hz, 1H), 8.41 (m, 1H), 8.28 (s, 1H), 8.09 (d, *J* = 8.2 Hz, 1H), 7.91 (d, *J* = 8.0 Hz, 1H), 7.76 (d, *J* = 7.6 Hz, 2H), 7.42 (d, *J* = 7.6 Hz, 2H), 6.64 (s, 1H), 6.55 (s, 1H), 4.66 (m, 1H), 4.09 (m, 1H), 3.86 (s, 3H), 3.84 (s, 3H), 3.79 (m, 1H), 3.52-3.23 (m, 6H), 3.14 (q, *J* = 7.0 Hz, 2H), 2.99 (m, 1H), 1.32 (t, *J* = 7.1 Hz, 3H). **<sup>13</sup>C NMR** (151 MHz, CDCl<sub>3</sub>) δ (ppm) 204.5, 161.8, 155.5, 150.3, 149.5, 148.8, 147.2, 141.9, 140.4, 137.1, 136.1, 135.9, 131.9, 130.4 (2C), 128.0, 122.5, 122.5, 121.1 (2C), 120.7, 120.6, 119.3, 118.2, 117.9, 111.3, 109.3, 56.2, 56.1, 55.6, 52.5, 49.4, 33.5, 30.5, 24.1, 8.7. **RP-HPLC** (220 nm): 95% (*t<sub>R</sub>* = 5.9 min, *k* = 4.7). **HRMS** (ESI): *m/z* [*M*+*H*]<sup>+</sup> calcd. for C<sub>36</sub>H<sub>36</sub>N<sub>7</sub>O<sub>6</sub><sup>+</sup>: 662.2722, found: 662.2732. C<sub>36</sub>H<sub>35</sub>N<sub>7</sub>O<sub>6</sub> · C<sub>2</sub>HF<sub>3</sub>O<sub>2</sub> (661.72 + 114.02).

**6-Amino-*N*-(5-(1-(4-(2-(6,7-dimethoxy-3,4-dihydroisoquinolin-2(1*H*)-yl)ethyl)phenyl)-1*H*-1,2,3-triazol-4-yl)-2-propionylphenyl)picolinamide hydrotrifluoroacetate (3.67)**



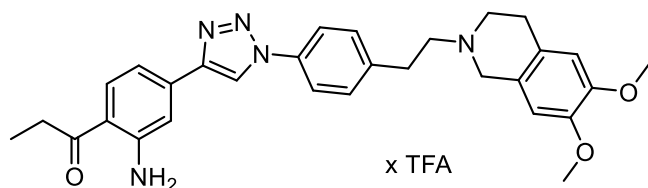
*N*-(5-(1-(4-(2-(6,7-Dimethoxy-3,4-dihydroisoquinolin-2(1*H*)-yl)ethyl)phenyl)-1*H*-1,2,3-triazol-4-yl)-2-propionylphenyl)-6-nitropicolinamide (**3.66**) (13.0 mg, 0.017 mmol, 1.0 eq) was suspended in THF/MeOH 2:1 (6 mL) and ammonium formate (21.1 mg, 0.335 mmol, 20 eq) was added, causing the starting material to go into solution. Palladium on carbon (10 wt. % loading; 2 mg) was added and the mixture refluxed overnight. The reflux cooler was equipped with a balloon to collect the nascent hydrogen. The solids were removed by filtration and the volatiles evaporated. Preparative HPLC (gradient: 0-30 min: MeCN/ 0.1% aq TFA 33:67-60:40,  $t_R$  = 14.0 min) afforded the product as a yellowish solid (6.5 mg, 0.009 mmol, 52%), **mp** 183-190 °C. **<sup>1</sup>H NMR** (600 MHz, DMSO-*d*<sub>6</sub>)  $\delta$  (ppm) 12.99 (s, 1H), 10.17 (br s, 1H), 9.47 (s, 1H), 9.40 (d,  $J$  = 1.4 Hz, 1H), 8.28 (d,  $J$  = 8.4 Hz, 1H), 8.03 (d,  $J$  = 8.3 Hz, 2H), 7.79 (dd,  $J$  = 1.6, 8.3 Hz, 1H), 7.66 (m, 1H), 7.60 (d,  $J$  = 8.5 Hz, 2H), 7.36 (d,  $J$  = 7.1 Hz, 1H), 6.85 (s, 1H), 6.81 (s, 1H), 6.78 (d,  $J$  = 8.3 Hz, 1H), 4.55 (d,  $J$  = 15.0 Hz, 1H), 4.32 (m, 1H), 3.80 (s, 1H), 3.76 (s, 3H), 3.75 (s, 3H), 3.54 (m, 2H), 3.37 (m, 1H), 3.25-3.15 (m, 4H), 3.11-2.98 (m, 2H), 1.17 (t,  $J$  = 7.1 Hz, 3H) (the NH<sub>2</sub> protons appear as a very broad signal at about 4.6-6.0 ppm interfering with the broad water signal). **<sup>13</sup>C NMR** (151 MHz, DMSO-*d*<sub>6</sub>)  $\delta$  (ppm) 203.8, 163.6, 158.5, 158.3 (TFA), 158.0 (TFA), 148.5, 147.8, 146.3, 139.7, 138.7, 137.7, 135.4, 135.3, 132.2, 130.3 (2C), 123.1, 122.8, 121.0, 120.4 (2C), 119.8, 119.8, 117.1, 116.8, 114.9, 111.5, 110.9, 109.6, 55.6, 55.6, 55.5, 51.8, 49.3, 32.9, 29.2, 24.5, 8.6. **RP-HPLC** (220 nm): 100% ( $t_R$  = 4.3 min,  $k$  = 3.1). **HRMS** (ESI):  $m/z$  [ $M+H$ ]<sup>+</sup> calcd. for C<sub>36</sub>H<sub>38</sub>N<sub>7</sub>O<sub>4</sub><sup>+</sup>: 632.2980, found: 632.2982. **C<sub>36</sub>H<sub>37</sub>N<sub>7</sub>O<sub>4</sub> · C<sub>2</sub>HF<sub>3</sub>O<sub>2</sub>** (631.74 + 114.02).

***N*-(5-(1-(4-(2-(6,7-Dimethoxy-3,4-dihydroisoquinolin-2(1*H*)-yl)ethyl)phenyl)-1*H*-1,2,3-triazol-4-yl)-2-propionylphenyl)benzofuran-2-carboxamide hydrotrifluoroacetate (**3.68**)**



**3.68** was prepared according to the general procedure for the CuAAC. The reaction was carried out using *N*-(5-ethynyl-2-propionylphenyl)benzofuran-2-carboxamide (**3.58**) (300 mg, 0.945 mmol, 1.0 eq), 2-(4-azidophenethyl)-6,7-dimethoxy-1,2,3,4-tetrahydroisoquinoline (**3.09**) (480 mg, 1.418 mmol, 1.5 eq), CuSO<sub>4</sub>·5H<sub>2</sub>O (35.4 mg, 0.142 mmol, 0.15 eq), sodium ascorbate (131 mg, 0.662 mmol, 0.7 eq) and TBTA (75.2 mg, 0.142 mmol, 0.15 eq) in CHCl<sub>3</sub> (8 mL). Refluxing lasted for 1 d. Column chromatography (eluent: DCM/MeOH 19:1, *R<sub>f</sub>* = 0.3) followed by preparative HPLC (gradient: 0-30 min: MeCN/ 0.1% aq TFA 55:45-90:10, *t<sub>R</sub>* = 12.0 min) afforded the product as a yellowish solid (318 mg, 0.413 mmol, 44%), **mp** 217-219 °C. <sup>1</sup>H NMR (600 MHz, DMSO-*d*<sub>6</sub>) δ (ppm) 12.83 (s, 1H), 10.11 (s, 1H), 9.50 (s, 1H), 9.35 (d, *J* = 1.6 Hz, 1H), 8.32 (d, *J* = 8.5 Hz, 1H), 8.02 (d, *J* = 8.4 Hz, 2H), 7.87 (d, *J* = 7.7 Hz, 1H), 7.84-7.78 (m, 3H), 7.60 (d, *J* = 8.5 Hz, 2H), 7.58-7.54 (m, 1H), 7.44-7.39 (m, 1H), 6.85 (s, 1H), 6.81 (s, 1H), 4.56 (d, *J* = 14.1 Hz, 1H), 4.32 (d, *J* = 13.8 Hz, 1H), 3.80 (m, 1H), 3.76 (s, 3H), 3.75 (s, 3H), 3.53 (m, 2H), 3.37 (s, 1H, signal interfering with the water signal (identified by <sup>1</sup>H-COSY and HSQC)), 3.26-3.17 (m, 4H), 3.15-2.96 (m, 2H), 1.18 (t, *J* = 7.1 Hz, 3H). <sup>13</sup>C NMR (151 MHz, DMSO-*d*<sub>6</sub>) δ (ppm) 205.1, 157.9 (TFA), 157.7 (TFA), 156.7, 154.6, 148.5, 148.4, 147.8, 146.1, 139.7, 137.8, 135.6, 135.4, 132.4, 130.3 (2C), 127.8, 127.2, 124.1, 123.2, 122.2, 121.2, 120.4 (2C), 120.3, 119.8, 118.3, 116.8, 112.1, 111.7, 111.5, 109.7, 55.6, 55.6, 55.5, 51.9, 49.3, 32.8, 29.2, 24.6, 8.5. **RP-HPLC** (220 nm): 99% (*t<sub>R</sub>* = 7.1 min, *k* = 5.8). **HRMS** (ESI): *m/z* [*M*+H]<sup>+</sup> calcd. for C<sub>39</sub>H<sub>38</sub>N<sub>5</sub>O<sub>5</sub><sup>+</sup>: 656.2867, found: 656.2882. C<sub>39</sub>H<sub>37</sub>N<sub>5</sub>O<sub>5</sub> · C<sub>2</sub>HF<sub>3</sub>O<sub>2</sub> (655.74 + 114.02).

**1-(2-Amino-4-(1-(4-(2-(6,7-dimethoxy-3,4-dihydroisoquinolin-2(1H)-yl)ethyl)phenyl)-1H-1,2,3-triazol-4-yl)phenyl)propan-1-one hydrotrifluoroacetate (3.69)**



**3.69** was prepared according to the general procedure for the CuAAC. The reaction was carried out using 1-(2-amino-4-ethynylphenyl)propan-1-one (**3.37**) (150 mg, 0.866 mmol, 1.0 eq), 2-(4-azidophenethyl)-6,7-dimethoxy-1,2,3,4-tetrahydroisoquinoline (**3.09**) (440 mg, 1.299 mmol, 1.5 eq), CuSO<sub>4</sub>·5H<sub>2</sub>O (32.4 mg, 0.130 mmol, 0.15 eq), sodium ascorbate (120 mg, 0.606 mmol, 0.7 eq) and TBTA (68.9 mg, 0.130 mmol, 0.15 eq) in CHCl<sub>3</sub> (5 mL). Refluxing lasted for 3 d. Column chromatography (eluent: DCM/MeOH 19:1, *R<sub>f</sub>* = 0.3) followed by preparative HPLC (gradient: 0-30 min: MeCN/ 0.1% aq TFA 33:67-69:31, *t<sub>R</sub>* = 13.0 min) afforded the product as a yellow solid (164 mg, 0.262 mmol, 30%), **mp** 121-125 °C. **<sup>1</sup>H NMR** (400 MHz, DMSO-*d*<sub>6</sub>) δ (ppm) 10.56 (s, 1H), 9.32 (s, 1H), 7.97 (d, *J* = 8.5 Hz, 2H), 7.89 (d, *J* = 8.5 Hz, 1H), 7.58 (d, *J* = 8.6 Hz, 2H), 7.45 (d, *J* = 1.5 Hz, 1H), 7.08 (dd, *J* = 1.5, 8.3 Hz, 1H), 6.84 (s, 1H), 6.80 (s, 1H), 4.57 (d, *J* = 14.7 Hz, 1H), 4.32 (d, *J* = 13.1 Hz, 1H), 3.79\* (m, 1H), 3.75\* (s, 3H), 3.74\* (s, 3H), 3.53\* (d, *J* = 7.0 Hz, 2H), 3.37\* (m, 1H), 3.21 (t, *J* = 8.3 Hz, 2H), 3.15-2.92 (m, 4H), 1.08 (t, *J* = 7.2 Hz, 3H) (\*signals interfering with the NH<sub>2</sub> signal; the NH<sub>2</sub> protons appear as a very broad signal between 4.2 and 3.3 ppm). **<sup>13</sup>C NMR** (101 MHz, DMSO-*d*<sub>6</sub>) δ 202.1, 151.4, 148.5, 147.8, 146.7, 137.7, 135.5, 135.0, 132.2, 130.3 (2C), 123.2, 120.6, 120.3 (2C), 119.8, 116.1, 112.9, 112.0, 111.5, 109.7, 55.6, 55.6, 55.5, 51.7, 49.2, 31.7, 29.2, 24.5, 8.8. **HRMS** (ESI): *m/z* [*M*+H]<sup>+</sup> calcd. for C<sub>30</sub>H<sub>34</sub>N<sub>5</sub>O<sub>3</sub><sup>+</sup>: 512.2656, found: 512.2664. **C<sub>30</sub>H<sub>33</sub>N<sub>5</sub>O<sub>3</sub> · C<sub>2</sub>HF<sub>3</sub>O<sub>2</sub>** (511.63 + 114.02).

### 3.4.2 Molecular Docking

**ABCG2 transporter and ligand preparation.** The cryo-EM structure of the human ABCG2 transporter (PDB ID: 5NJ3 [30]) was used as template. To reconstitute missing N-termini and loops, Modeller 9.18 [91-93] was used. The ABCG2 model contained disulfide bridges within each monomer (Cys592 - Cys608) and between the monomers (Cys603 - Cys603). Coordinates of the antibody 5D3-Fab were removed. Protein and ligand preparation (Schrödinger LLC, Portland, OR, USA) including an assignment of protonation states were essentially performed as described [94,95] before. Compounds **3.27**, **3.48** and **3.50** were considered in the unprotonated state.

**Induced-fit docking.** Compounds **3.27**, **3.48**, **3.50** and further potential ligands were docked “flexibly” to the ABCG2 transporter using the induced-fit docking module (Schrödinger LLC). The ligands were docked within a box of  $46 \times 46 \times 46 \text{ \AA}^3$  around the center of mass between N436 of the first and the second monomer, respectively. Redocking was performed in the extended precision mode. From the induced-fit docking results obtained, one pose (ligand-ABCG2 transporter complex) was selected based on low/minimal XP Gscores and reasonability of the ligand binding pose. Ligand-receptor interactions were analyzed using PLIP 1.4.2 [96]. Figures showing molecular structures of the ABCG2 transporter in complex with **3.27** or **3.48** were generated with PyMOL Molecular Graphics system, version 2.2.0 (Schrödinger LLC).

### 3.4.3 Biology

#### 3.4.3.1 General Experimental Conditions

**Materials.** Commodity chemicals and solvents were purchased from commercial suppliers (Sigma Aldrich, Munich, Germany; Merck, Darmstadt, Germany; VWR, Darmstadt, Germany; Thermo Fisher Scientific, Waltham, MA, USA; Invitrogen, Karlsruhe, Germany). Topotecan and vinblastine were obtained from Sigma Aldrich. Hoechst 33342 and calcein-AM were procured from Biotium (Fremont, CA, USA). FTC was from Merck. Tariquidar was synthesized in our laboratory according to literature [97] with slight modifications [98]. Reversan was obtained from Tocris (Wiesbaden-Nordenstadt, Germany). Millipore water was used throughout for the preparation of buffers, aqueous reagent solutions and HPLC eluents. The pH of buffers and aqueous reagent solutions was adjusted with NaOH aq or HCl aq unless stated otherwise. Acetonitrile for HPLC (gradient grade) was obtained from Merck. All cell lines were purchased from the ATCC (American Type Culture Collection; Manassas, VA, USA). Tissue culture flasks were procured from Sarstedt (Nümbrecht, Germany). Dulbecco's Modified Eagle's Medium - high glucose (DMEM/High; with 4500 mg/L glucose, sodium pyruvate and sodium bicarbonate, without L-glutamine, liquid, sterile-filtered, suitable for cell culture) and L-glutamine solution (200 mM, sterile-filtered, BioXtra, suitable for cell culture) were from Sigma Aldrich. Fetal calf serum (FCS) and trypsin/EDTA were from Biochrom (Berlin, Germany). For all assays in microplate format, 96-well plates (PS, clear, F-bottom, with lid, sterile) from Greiner Bio-One (Frickenhausen, Germany) were used. Human CPD (citrate, phosphate, dextrose) plasma was a gift from the Bavarian Red Cross (Regensburg, Germany). Syringe filters (Phenex-RC, 4 mm, 0.2  $\mu\text{m}$ ) used in the chemical stability assay (in blood plasma) were from Phenomenex (Aschaffenburg, Germany).

**Stock solutions.** Topotecan and vinblastine were dissolved in 70% EtOH to give 100  $\mu\text{M}$  stock solutions. Hoechst 33342 stock solution (0.8 mM) was prepared in water and calcein-AM stock solution (100  $\mu\text{M}$ ) in DMSO. The test compounds and the reference compounds

fumitremorgin C, tariquidar, reversan and sulfasalazine were dissolved in DMSO at 100 times the final concentrations in the transport assays and the ATPase assay and at 1000 times the final concentrations in the chemosensitivity assay. For the stability assay in blood plasma, 10 mM stock solutions of the test compounds were prepared in DMSO. If not stated otherwise, millipore water served as solvent for other assay reagents.

**Instruments.** Fluorescence and absorbance measurements in microplates were carried out with a GENios Pro microplate reader (equipped with a Xenon arc lamp; Tecan, Grödig, Austria). Analytical HPLC after incubation in human blood plasma was performed on a system from Agilent described in Section 3.4.1.1. The HPLC conditions were as described, yet with two alterations. The following linear gradient was applied: 0-12 min: A/B 20:80-95:5, 12-15 min: A/B 95:5. The injection volume was 100  $\mu$ L.

**Software.** All biological data were analyzed with GraphPad Prism 5 (GraphPad Software, San Diego, CA, USA).

### 3.4.3.2 Cell Culture

All cells were cultured in DMEM/High supplemented with 2% (v/v) of a 200 mM L-glutamine solution and 10% (v/v) FCS at 37 °C in a water-saturated atmosphere containing 5% CO<sub>2</sub>.

**MCF-7/Topo** cells, an ABCG2-overexpressing variant of the MCF-7 cell line (ATCC<sup>®</sup> HTB-22), were obtained by passaging the MCF-7 cells with increasing amounts of topotecan in the culture medium to achieve a maximum concentration of 550 nM within a period of about 40 d; after 3 passages at the maximum concentration the treated cells expressed sufficient quantities of ABCG2 [99,100]. Cells were cultured in the presence of topotecan (550 nM) to maintain overexpression of the ABCG2 transporter.

**KB-V1** cells, an ABCB1-overexpressing variant of the KB cell line (ATCC<sup>®</sup> CCL-17), were obtained by passaging the KB cells with increasing amounts of vinblastine in the culture medium to achieve a maximum concentration of 330 nM within a period of about 90 d; after 3 passages at the maximum concentration the treated cells expressed sufficient quantities of ABCB1 transporter [98,101]. They were cultured with 330 nM vinblastine to maintain overexpression of the ABCB1 transporter.

**MDCK.2-MRP1** cells were a kind gift from Prof. Dr. P. Borst from the Netherland Cancer Institute (Amsterdam, NL). They were obtained by transfecting MDCK.2 cells (ATCC<sup>®</sup> CRL-2936) with human ABCC1 [102,103]. Due to the strong adherence of this cell line, trypsinization was performed using 2X trypsin/EDTA (0.1%./0.04%) for 30 min.

All cells were routinely monitored for mycoplasma contamination by PCR using the Venor<sup>®</sup>GeM mycoplasma detection kit (Minerva Biolabs, Berlin, Germany) and were negative.

### 3.4.3.3 Inhibition of ABCG2: Hoechst 33342 Transport Assay

The assay was performed as described in our previous report [28] (c.f. Section 2.4.2.3), applying the following modification: cells were seeded into 96-well plates at a density of 18,000 cells per well (instead of 20,000).

### 3.4.3.4 Inhibition of ABCB1: Calcein-AM Transport Assay

The assay was performed as described in our previous report [28] (c.f. Section 2.4.2.4).

### 3.4.3.5 Inhibition of ABCC1: Calcein-AM Transport Assay

The assay was performed as described in our previous report [28] (c.f. Section 2.4.2.5).

### 3.4.3.6 Chemosensitivity Assay

The assay was performed as described in our previous report [28] (c.f. Section 2.4.2.8).

Cytotoxic effects were expressed as corrected T/C-values according to

$$T / C_{corr} [\%] = \frac{T - C_0}{C - C_0} \cdot 100$$

where T is the mean absorbance of the treated cells, C the mean absorbance of the negative controls and  $C_0$  the mean absorbance of the cells at the time of compound addition ( $t_0$ ). When the absorbance of treated cells T was lower than at the beginning of the experiment ( $C_0$ ), the extent of cell killing was calculated as cytotoxic effect according to

$$Cytotoxic\ effect\ [\%] = \frac{T - C_0}{C_0} \cdot 100$$

### 3.4.3.7 ABCG2 ATPase Assay

**Membrane preparation.** The protocol is based on the procedure of Sarkadi et al. [104] and our previous report [28]. MCF-7/Topo cells were harvested after trypsinization by centrifugation at 4 °C and 500 g for 10 min. The cell pellet was re-suspended in Tris mannitol buffer (50 mM Tris, 300 mM mannitol, 0.5 mM phenylmethylsulfonyl fluoride (PMSF), pH 7; 100 mL) and centrifuged again. Then the pellet was lysed and homogenized in TMEP buffer (50 mM Tris, 50 mM mannitol, 1 mM EDTA, 10 µg/mL leupeptin, 10 µg/mL benzamidine, 0.5 mM PMSF, 2 mM DTT, pH 7; 60 mL) by a Potter Elvehjem tissue homogenizer. Undisrupted cells and cellular debris were pelleted by centrifugation at 4 °C and 500 g for 10 min and the supernatant, containing the membranes, was removed carefully. After centrifugation at 4 °C and 100,000 g for 1 h the pellet (containing the membranes) was re-suspended in TMEP buffer (30 mL), giving a protein concentration of 2.0-3.0 mg/mL, and

homogenized with a Potter Elvehjem tissue homogenizer. All procedures during the membrane preparation were performed at 4 °C and aliquots (500-1000 µL) were stored at - 80 °C until use.

**Protein quantification** was performed by the method of Bradford using the Bio-Rad protein assay kit according to the manual.

**Assay procedure.** The assay was performed by analogy with the ABCB1 ATPase assay procedure described by Sarkadi et al. [104] and the procedure described in our previous report [28]. The ATPase activity of the ABCG2 transporter was estimated by measuring inorganic phosphate liberation. It was determined as orthovanadate-sensitive ATPase activity in the presence of inhibitors in ABCG2 MCF-7/Topo membrane preparations.

Membranes containing 2.0-2.5 mg of total soluble protein were thawed on ice and pelleted by centrifugation at 4 °C and 16,200 g for 10 min. Then they were suspended in assay buffer (50 mM MOPS-Tris (100 mM MOPS, pH adjusted to 7.0 with 1.7 M Tris), 50 mM KCl, 5 mM NaN<sub>3</sub>, 2 mM EGTA, 2 mM DTT, 1 mM ouabain; 4.2 mL), mixed with 10% (w/w) CHAPS (42 µL; decreases the high basal ABCG2 ATPase activity) and homogenized using a syringe and a needle (27G). The suspension was split into 2 portions (2.0 mL each) and one portion was supplemented with orthovanadate (100 mM Na<sub>3</sub>VO<sub>4</sub>, pH 10; 50 µL; final conc. 2 mM), the other with the same amount of purified water. The two suspensions (w. and wo. orthovanadate) were transferred into a 96-well plate on ice (40 µL/well; 20-25 µg protein/well) and pre-incubated at 37 °C for 3 min.

The ATPase reaction was started by adding the reference and test compounds in assay buffer containing 20 mM ATP (10 µL/well, giving a final volume of 50 µL/well; final conc. 4 mM) with a multichannel pipette and the plate was incubated at 37 °C in a microplate shaker for 1 h. For this purpose, an ATP solution (200 mM Mg<sub>x</sub>ATP, 400 mM MgCl<sub>2</sub>, pH adjusted to 7.0 with 1.7 M Tris) was diluted 1:10 (v/v) with assay buffer and the test and reference compounds were added 5-fold concentrated. Sulfasalazine at a final concentration of 30 µM served as reference activator (positive control); the vehicle DMSO (1% final content) served as negative control. Each concentration (w. and wo. orthovanadate) was measured in duplicate, positive and negative control in quadruplicate each.

The reaction was stopped by the addition of 10% (w/w) SDS (30 µL/well); background control (phosphate stemming from the assay buffer) (w. and wo. orthovanadate) was stopped before starting the reaction with MgATP and was measured in duplicate.

Phosphate standards (0, 0.05, 0.1, 0.25, 1.5 and 2.0 mM NaH<sub>2</sub>PO<sub>4</sub> in assay buffer; 50 µL/well; each concentration measured in duplicate) were included on each plate for calibration.

The amount of phosphate was determined by adding a colorimetric reagent (1 part of reagent A (35 mM ammonium molybdate, 15 mM zinc acetate) mixed with 4 parts of reagent B (5%

(w/w) ascorbic acid, pH 5.0; freshly prepared); 200  $\mu$ L/well) and by incubating at 37 °C for further 20 min. The absorbance (820 nm) as a parameter proportional to the phosphate amount was measured, using a GENios Pro microplate reader.

The data obtained under the treatment with orthovanadate were subtracted from the data without orthovanadate to obtain phosphate liberation resulting from ABCG2 activity. The ensuing data were normalized relative to the absorbance in the absence of an ABCG2 activator (negative control) and the response elicited by the sulfasalazine (positive) control, which was defined as 100% ATPase activity. IC<sub>50</sub> values were calculated using four parameter sigmoidal fits. Errors were expressed as standard error of the mean (SEM).

### 3.4.3.8 Chemical Stability Assay (in Blood Plasma)

The human CPD (citrate, phosphate, dextrose) blood plasma samples were stored at - 80 °C and thawed before use. Stock solutions of the test compounds (10 mM in DMSO) were diluted 1:50 with blood plasma, giving a concentration of 200  $\mu$ M. The samples were vortexed briefly and incubated at 37 °C. After different periods of time, aliquots were taken and deproteinated by adding three parts of ice-cold MeCN, vortexing and storing at 4 °C for 30 min. Samples were centrifuged at 4 °C and 16,000 g for 5 min and the supernatants were diluted 1:1 with 0.05% TFA aq and stored at - 80 °C until analyzed. They were thawed at room temperature, filtered with syringe filters and analyzed with HPLC.

## 3.4.4 Solubility

### 3.4.4.1 General Experimental Conditions

**Materials.** Chemicals and solvents were purchased from commercial suppliers (Sigma Aldrich, Munich, Germany; Merck, Darmstadt, Germany; VWR, Darmstadt, Germany; Thermo Fisher Scientific, Waltham, MA, USA). Millipore water was used throughout for the preparation of buffers and HPLC eluents. The pH of buffers was adjusted with NaOH aq and HCl aq. Buffers were filtered before use. Acetonitrile for HPLC (gradient grade) was obtained from Merck. Micro tubes were from Sarstedt (Nümbrecht, Germany). 96-Well plates (PS, clear, F-bottom, with lid, sterile) were acquired from Greiner Bio-One (Frickenhausen, Germany). Glass vials (with PE plug) were procured from Altmann Analytik (München, Germany); borosilicate glass centrifuge tubes (without plug) from Thermo Fisher Scientific. Sigmacote® (Sigma Aldrich) was used as siliconizing agent for the vials. Parafilm (Bemis, Neenah, WI, USA) was used to cap the centrifuge tubes.

**Stock solutions.** The test compounds and the reference compound haloperidol were dissolved in DMSO at 1000 times the final concentrations in the thermodynamic solubility assay and for the calibration curve at 100 times the final concentrations. Furthermore, the test compounds

and the reference compound coronene were dissolved at 100 times the final concentrations in the kinetic solubility assay.

**Instruments.** For incubating and shaking vials an MB-102 ThermoCell mixing block (BIOER, Hangzhou, China) was used. Analytical HPLC of the samples from the thermodynamic solubility assay was performed on a system from Agilent, described in Section 3.4.1.1. The HPLC conditions were as described with two alterations. The following linear gradient was applied: 0-8 min: A/B 30:70-73:27, 8-9 min: A/B 73:27-95:5, 9-12 min: A/B 95:5, 12-13 min: A/B 95:5-30:70. The injection volume was 100  $\mu$ L. Absorbance measurements of the microplates were carried out with a GENios Pro microplate reader (Tecan, Männedorf, Switzerland).

**Software.** Data were analyzed with Microsoft Excel and GraphPad Prism 5 (GraphPad Software, San Diego, CA, USA). ClogP values were calculated with ACD/Structure Designer, version 12 (Advanced Chemistry Development, Inc. (ACD/Labs), Toronto, Canada).

#### 3.4.4.2 Kinetic Solubility Assay

**UV-VIS Spectra** of the test compounds were recorded along with the high-resolution mass spectrometry (HRMS) analysis, which was performed on the Agilent LC/MS system described in Section 3.4.1.1; the system was additionally equipped with a 1290 DAD detector (Agilent Technologies, Santa Clara, CA, USA).

**Assay Procedure.** The kinetic solubility was determined turbidimetrically. DMSO stock solutions of the test compound (different concentrations) were diluted 1:100 with the respective buffer (pH 7.4) at 37 °C in a micro tube (10  $\mu$ L stock in 1000  $\mu$ L buffer), giving a final DMSO concentration of 1%. The sample was vortexed and transferred into a 96-well plate (300  $\mu$ L/well, 3 replicate wells). DMSO (1% in buffer; 300  $\mu$ L/well, measured 12-fold) served as vehicle control/ blank value, coronene served as a highly insoluble control compound. After incubating the plate at 37 °C for 2 h, the extinction was measured at 380 nm using a GENios Pro microplate reader. The data were normalized to the blank value and the kinetic solubility limit was estimated as the highest concentration at which more than 95% of the radiation is transmitted (i.e. the extinction is lower than 0.0223).

#### 3.4.4.3 Thermodynamic Solubility Assay

The thermodynamic solubility of the test and reference compounds was determined by the saturation shake-flask method. A DMSO stock solution of the test compound was diluted 1:1000 in PBS (pH 7.4) in a glass vial or glass centrifuge tube, both of which had been treated with a siliconizing agent, giving a final DMSO content of 1‰ (e.g. 0.6  $\mu$ L stock in 600  $\mu$ L PBS). According to solubility, stock solutions of different concentrations were used

(compounds **3.40**, **3.41**, **3.48** and **3.49**: 50 mM, compound **3.65**: 20 mM, all other compounds: 10 mM). The vial was capped, vortexed and shaken at 25 °C for 36-40 h. Shaking was stopped and the precipitate was allowed to sediment at 25 °C for 24 h. In the case of poorly sedimenting compounds, the samples were then centrifuged at 25 °C and 2700 g for 30 min. 2 aliquots of supernatant (100 µL each) were taken carefully from each vial with a micropipette, anxious not to swirl up the sediment, and diluted with MeCN (50 µL). The micropipette tip was rinsed thoroughly in the mixture of supernatant and MeCN to dissolve potential residue adsorbed to the tip surface. The sample was analyzed with HPLC and the peak area was determined. Standard solutions were produced as follows. DMSO stock solutions (5 concentrations) and DMSO were diluted 1:100 in PBS (1% final DMSO content), vortexed and immediately an aliquot (100 µL) from each solution was taken and diluted with MeCN (50 µL) (plus pipette tip was rinsed). The standards were measured by HPLC and the peak areas were used to construct a calibration curve. Solubility of the test compound was determined by quantifying the concentration of the sample using the calibration curve. At least 6 independent experiments were carried out for each reported result. Errors were expressed as standard error of the mean (SEM).

## 3.5 Supplementary Material

### 3.5.1 Figures 3.13, 3.14 and 3.15

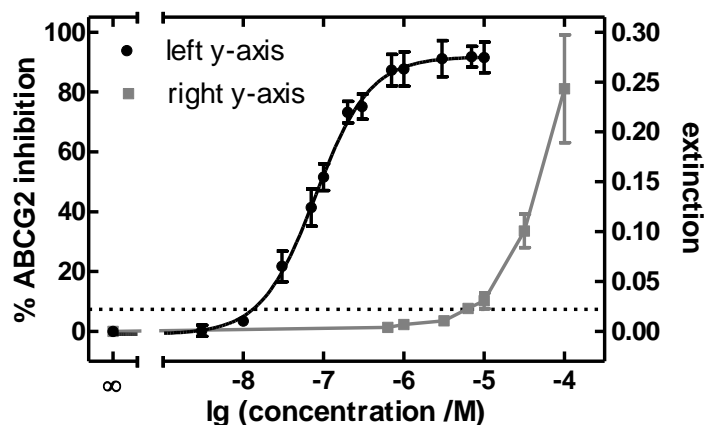


**Figure 3.13.** Comparison of the concentration-dependent inhibition of ABCG2-mediated Hoechst 33342 efflux and the concentration-dependent extinction (at 380 nm) due to scattering in a kinetic solubility assay, both caused by the inhibitor **3.01**.

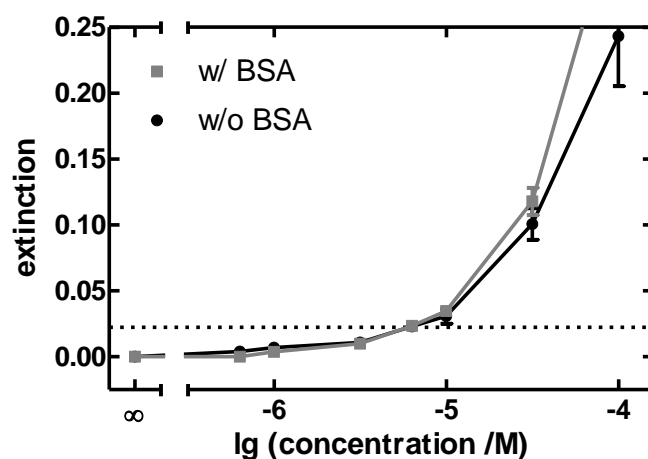


**Figure 3.14.** Concentration-dependent extinction (at 380 nm) due to scattering in a kinetic solubility assay in PBS caused by the inhibitor **3.01** in the absence (w/o) and presence (w/) BSA. The data were normalized to the blank value. Presented are mean values  $\pm$  SEM from two independent experiments, each performed in triplicate.

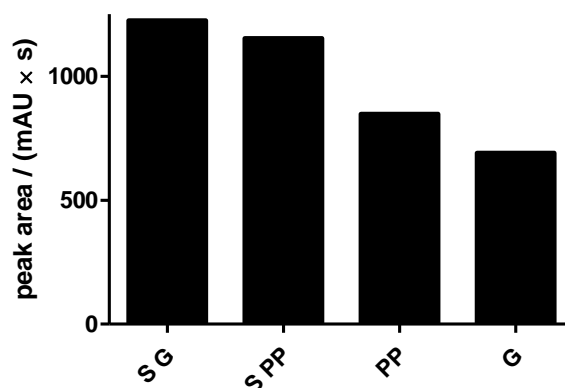
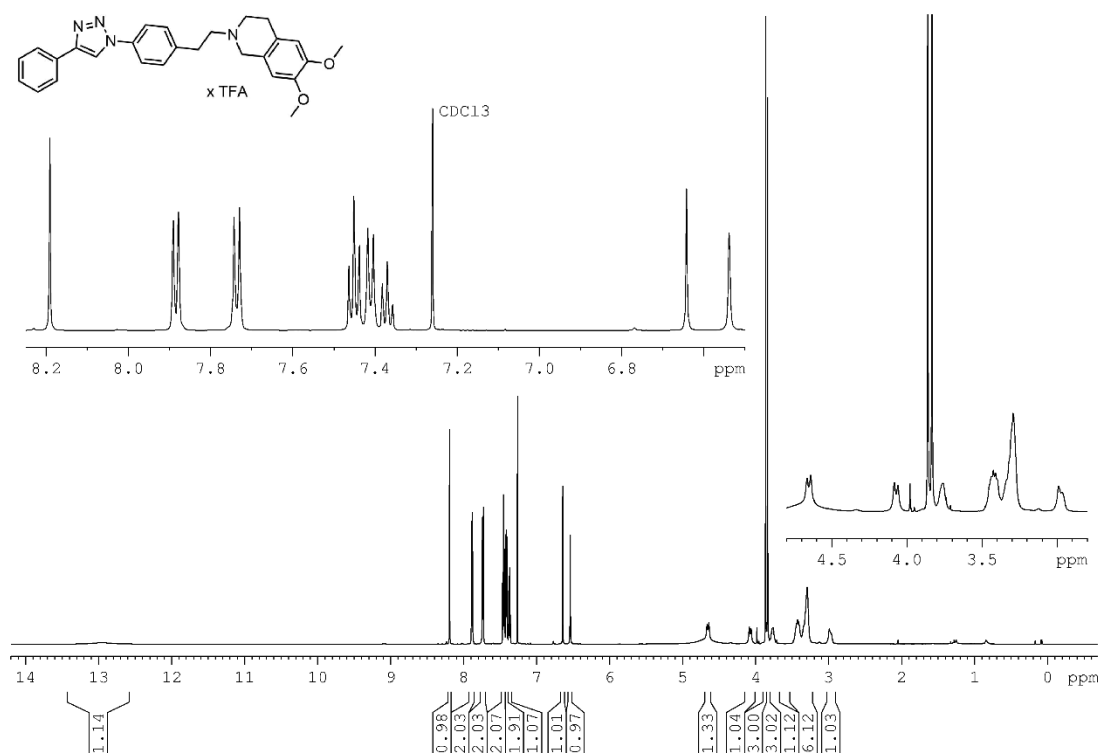
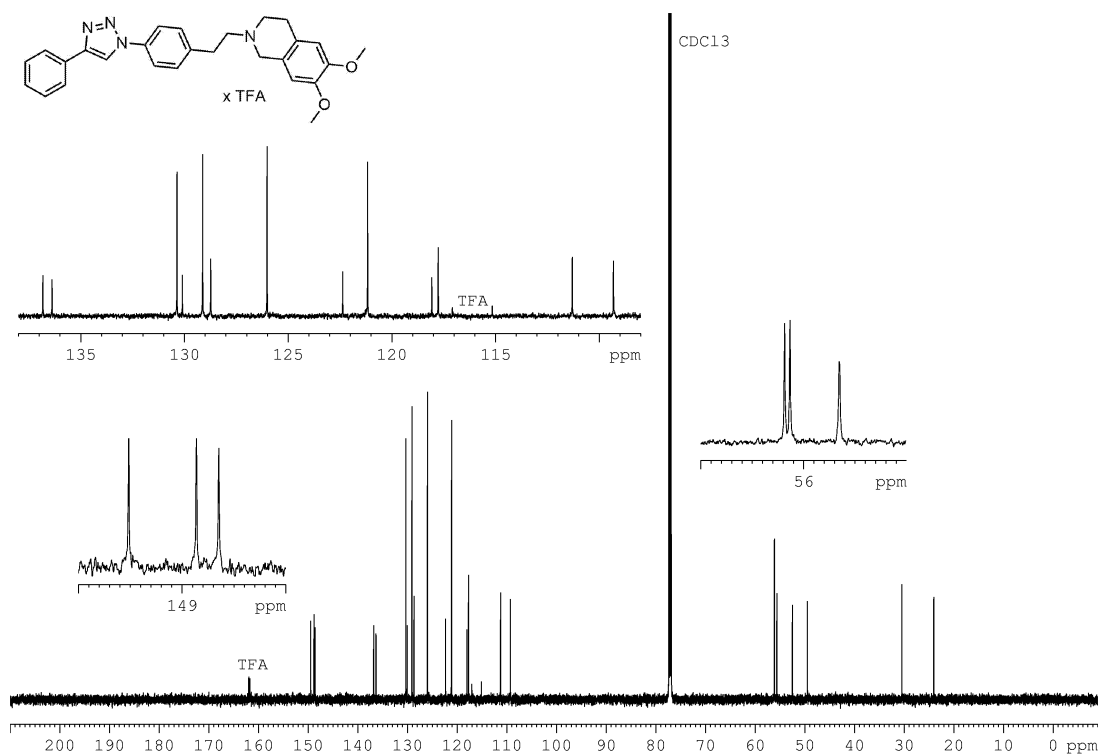


**Figure 3.15.** Influence of the vial material on the adsorption of inhibitor **3.01** to the vial surface. Solutions of **3.01** at a concentration of 7  $\mu$ M in PBS were prepared in vials consisting of glass (G), 'siliconized' glass (S G), polypropylene (PP) or 'siliconized' PP (S PP), vortexed briefly and analyzed by RP-HPLC (UV detection at 220 nm).

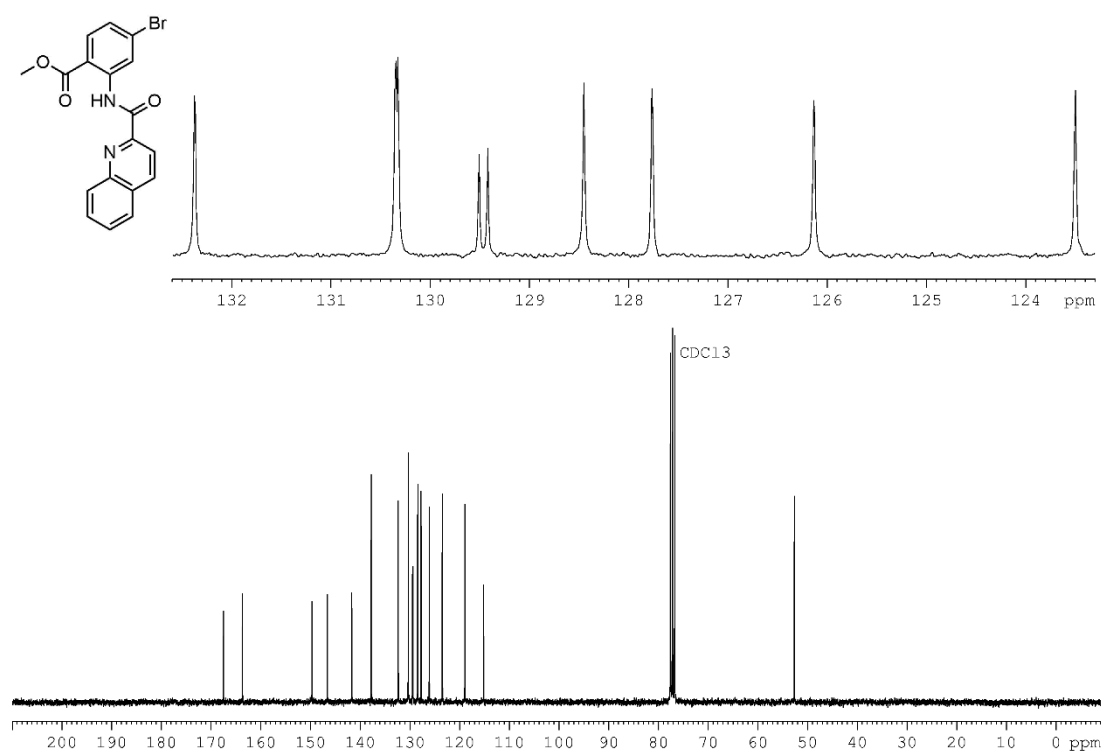
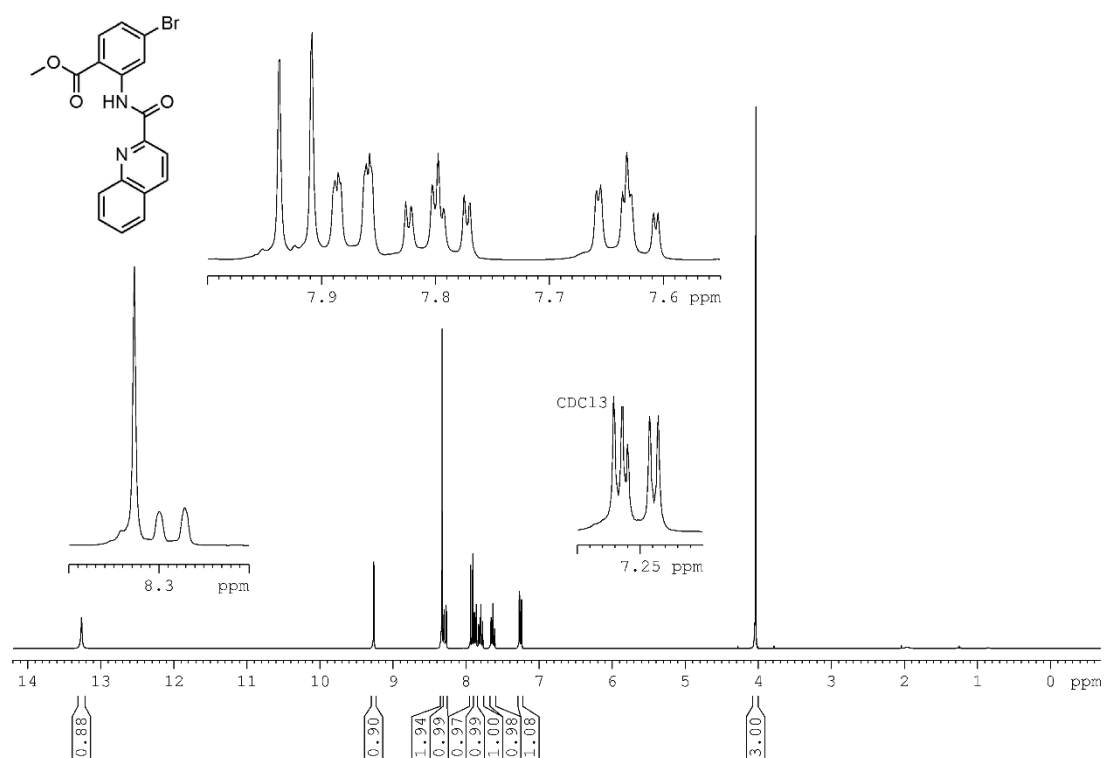
### 3.5.2 NMR Spectra

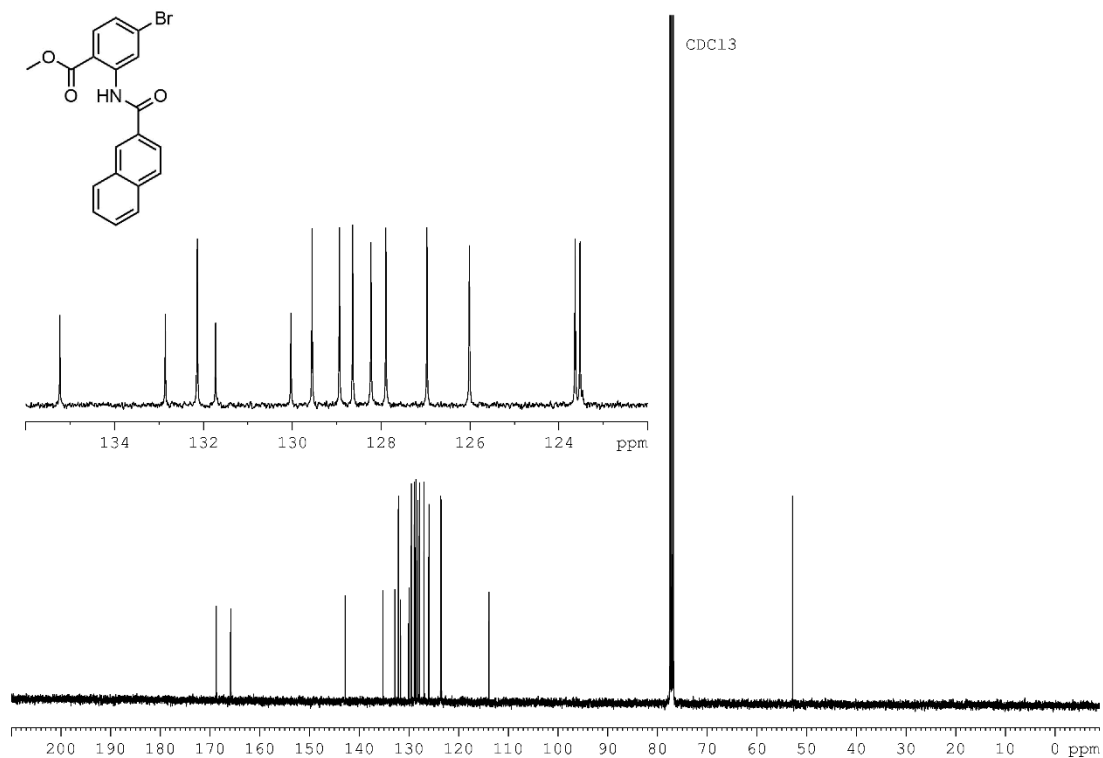
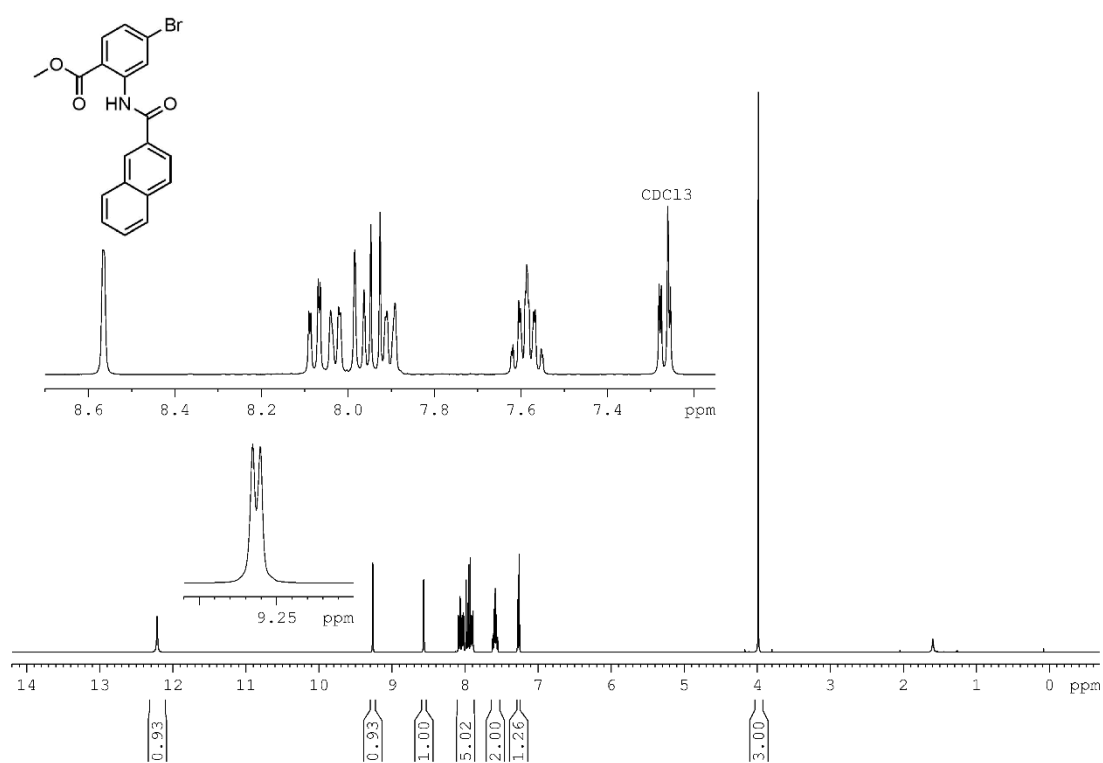


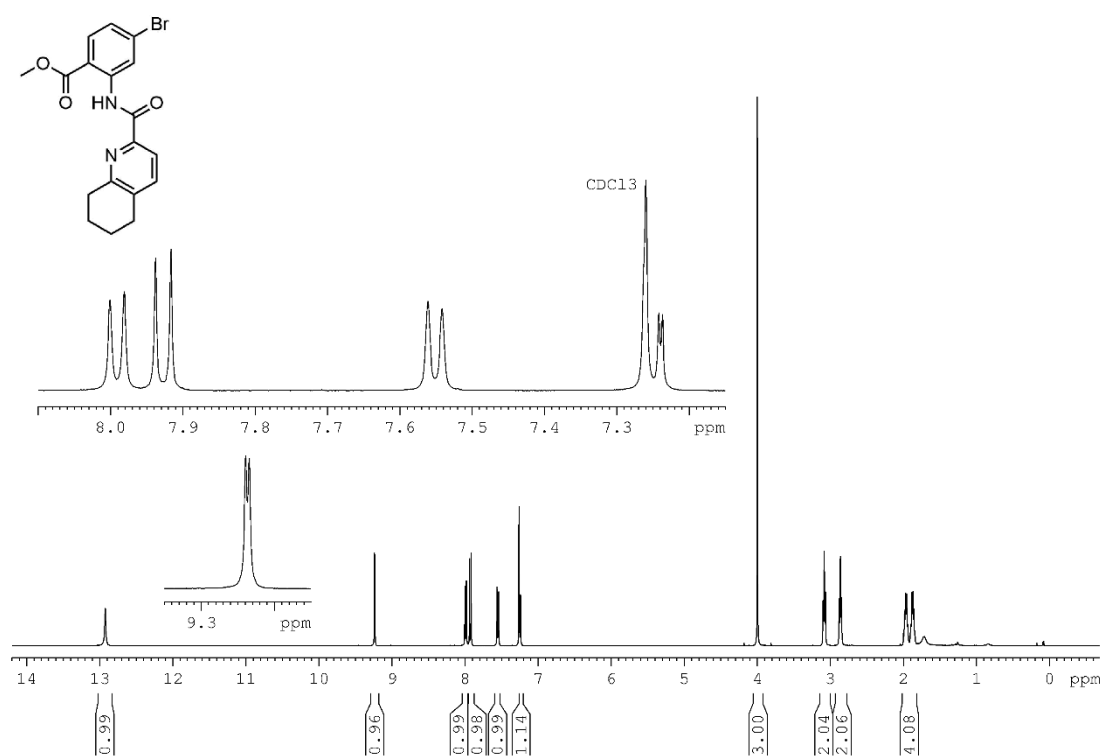
<sup>1</sup>H NMR spectrum (600 MHz, CDCl<sub>3</sub>) of compound **3.03**.



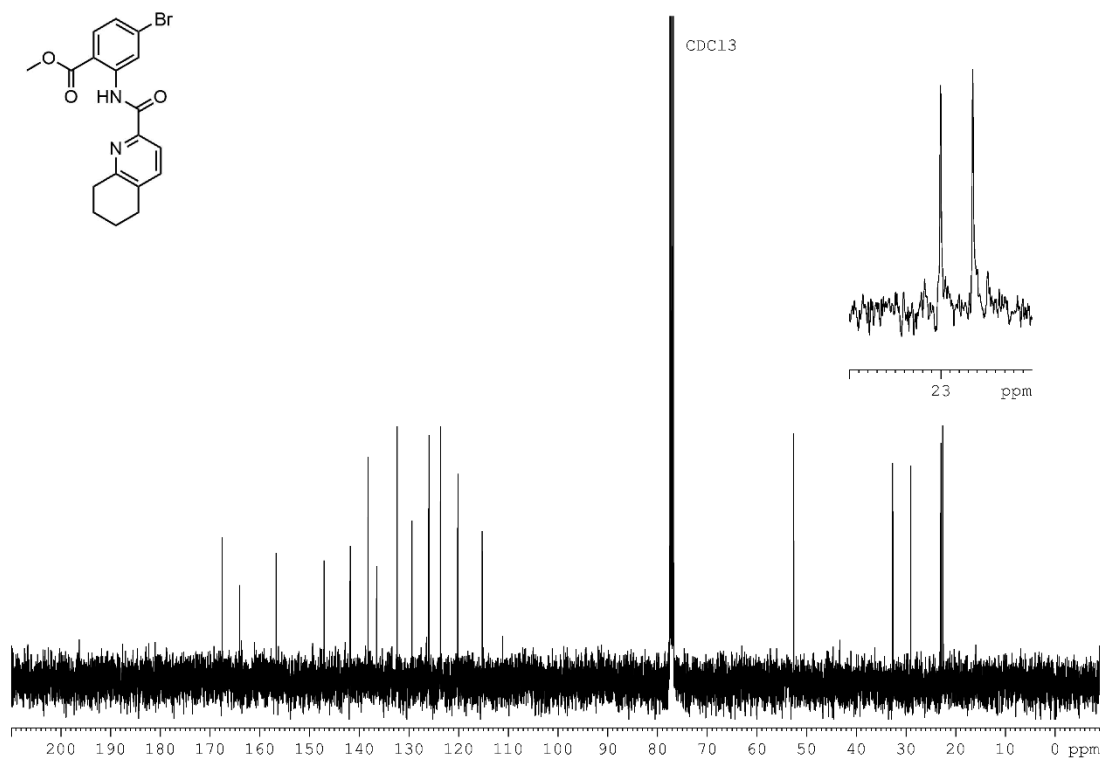
<sup>13</sup>C NMR spectrum (151 MHz, CDCl<sub>3</sub>) of compound **3.03**.



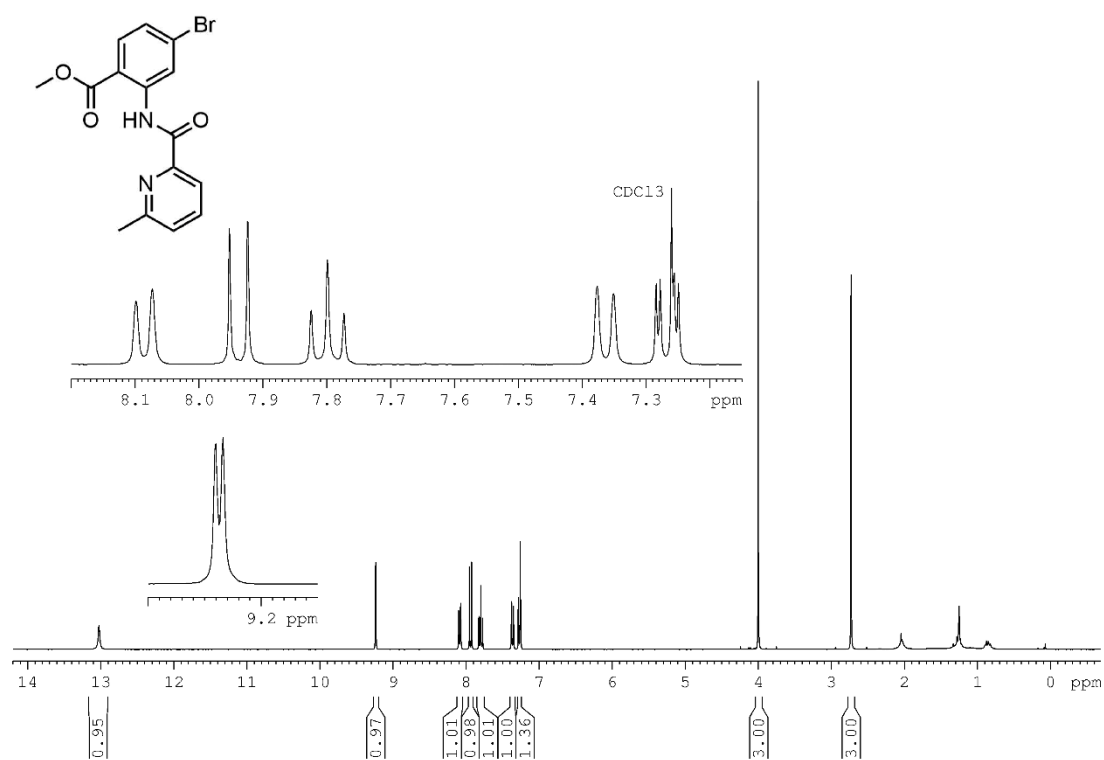




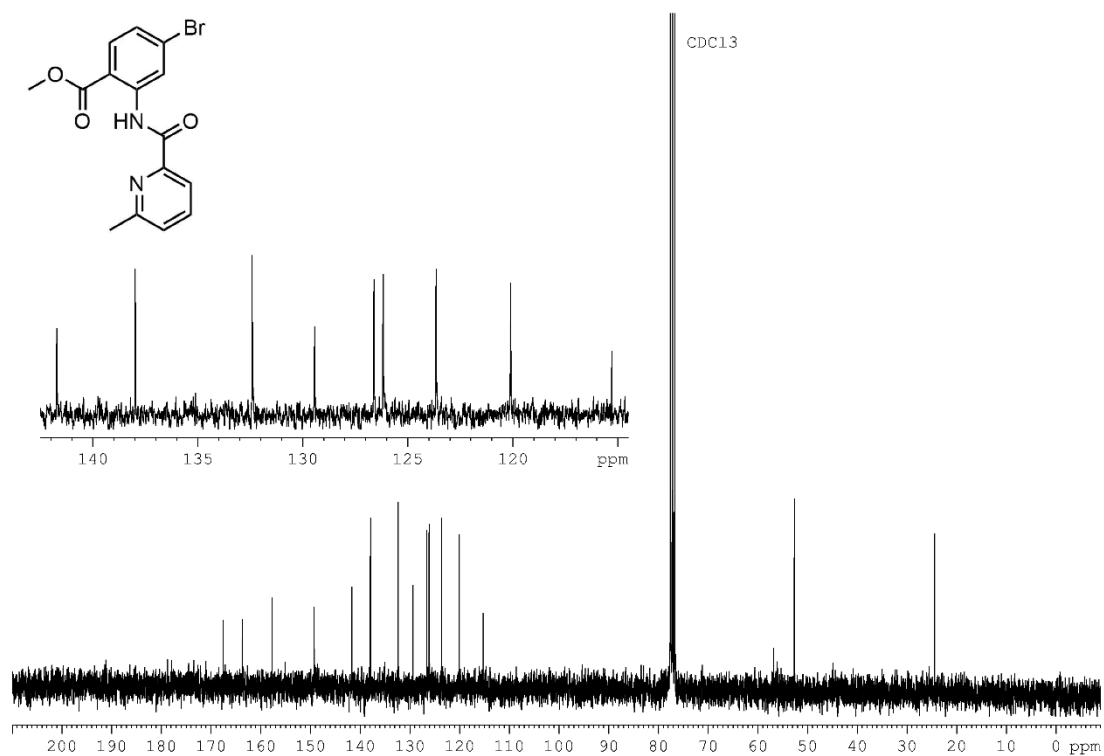
$^1\text{H}$  NMR spectrum (400 MHz,  $\text{CDCl}_3$ ) of compound **3.13**.



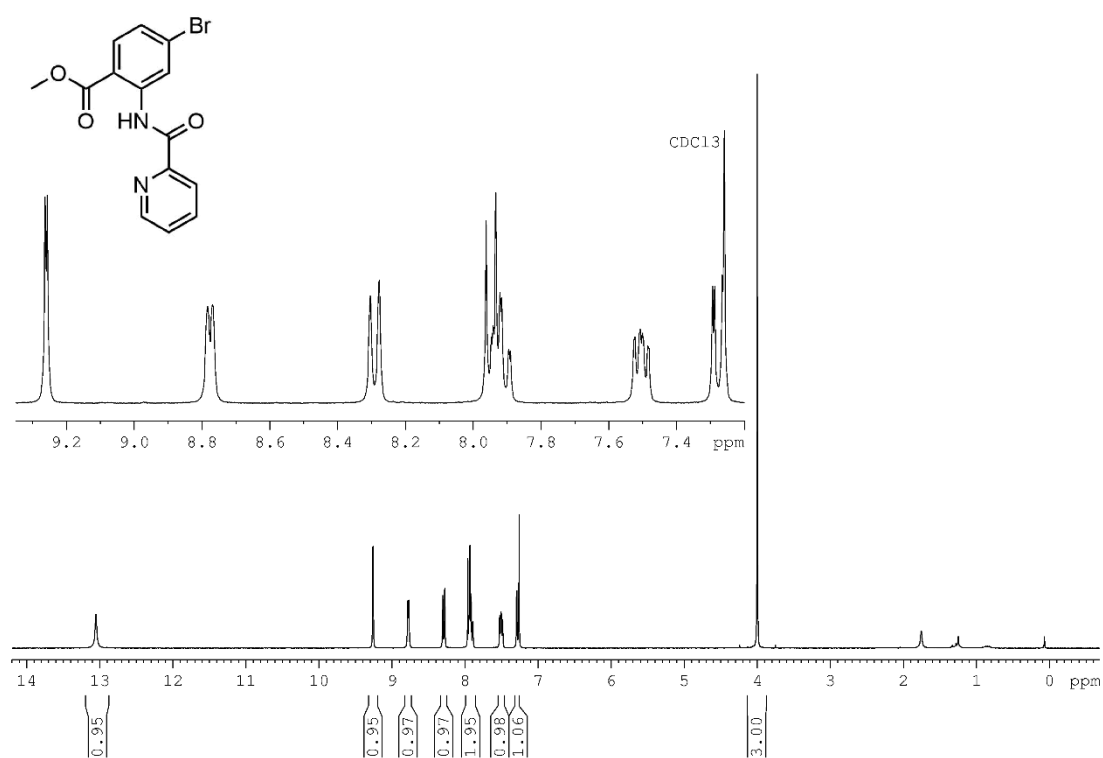
$^{13}\text{C}$  NMR spectrum (101 MHz,  $\text{CDCl}_3$ ) of compound **3.13**.



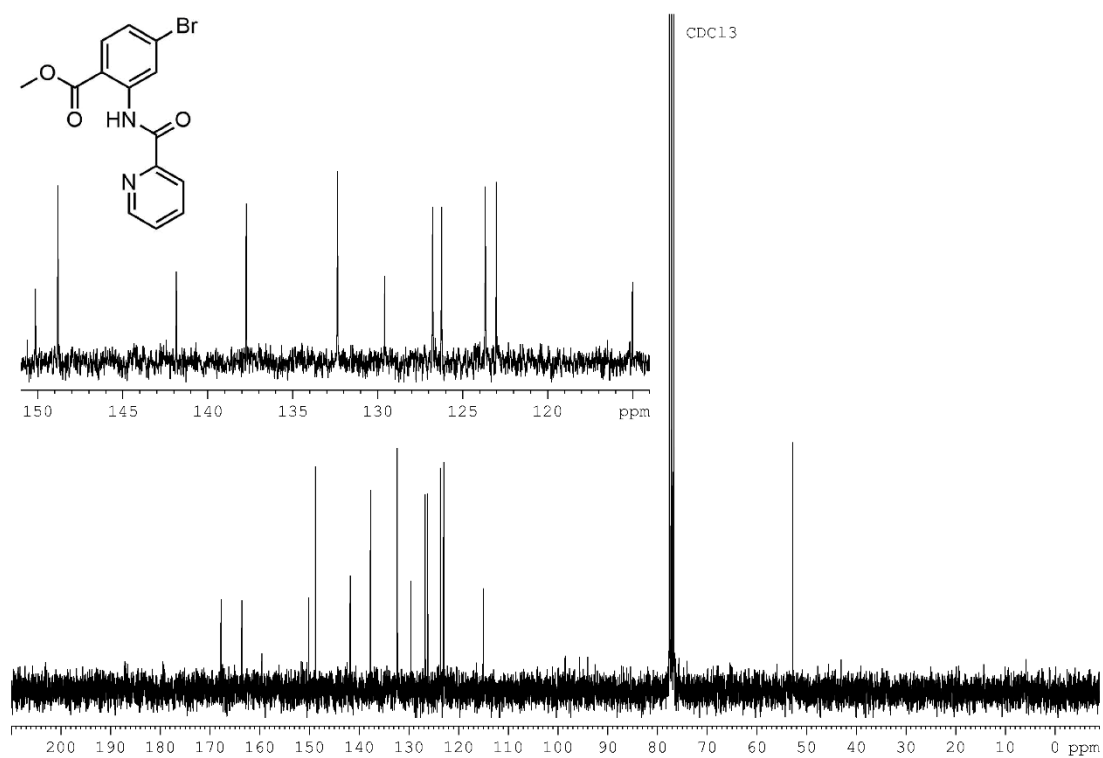
$^1\text{H}$  NMR spectrum (300 MHz,  $\text{CDCl}_3$ ) of compound **3.14**.



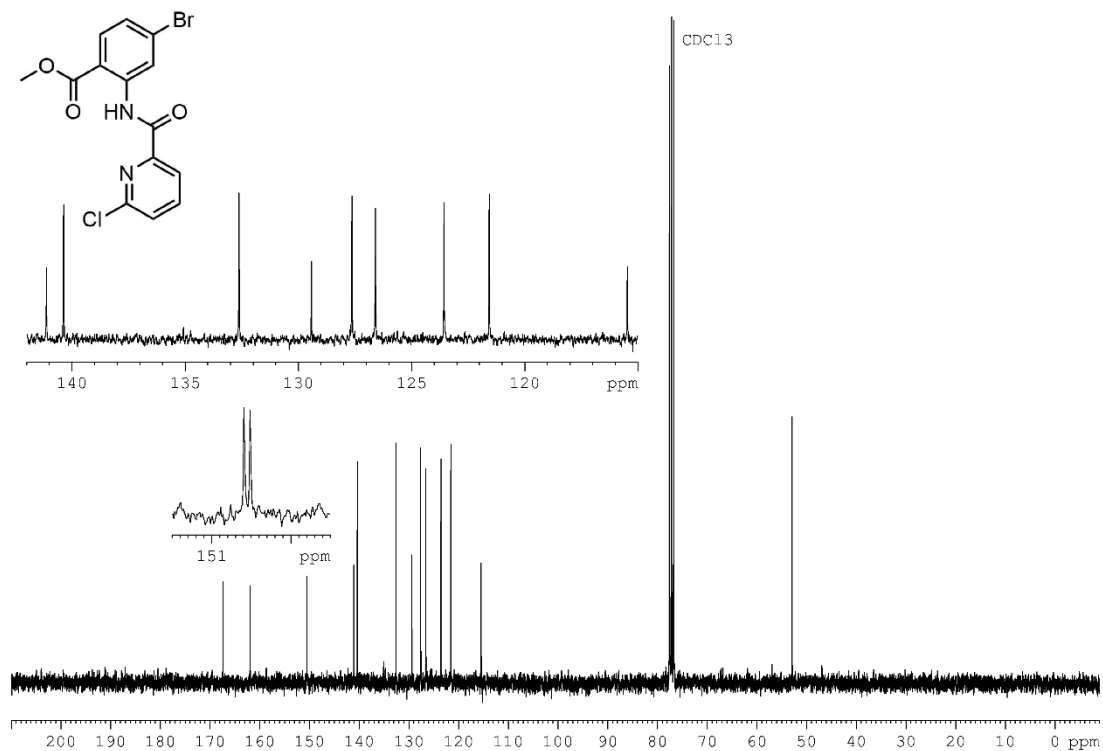
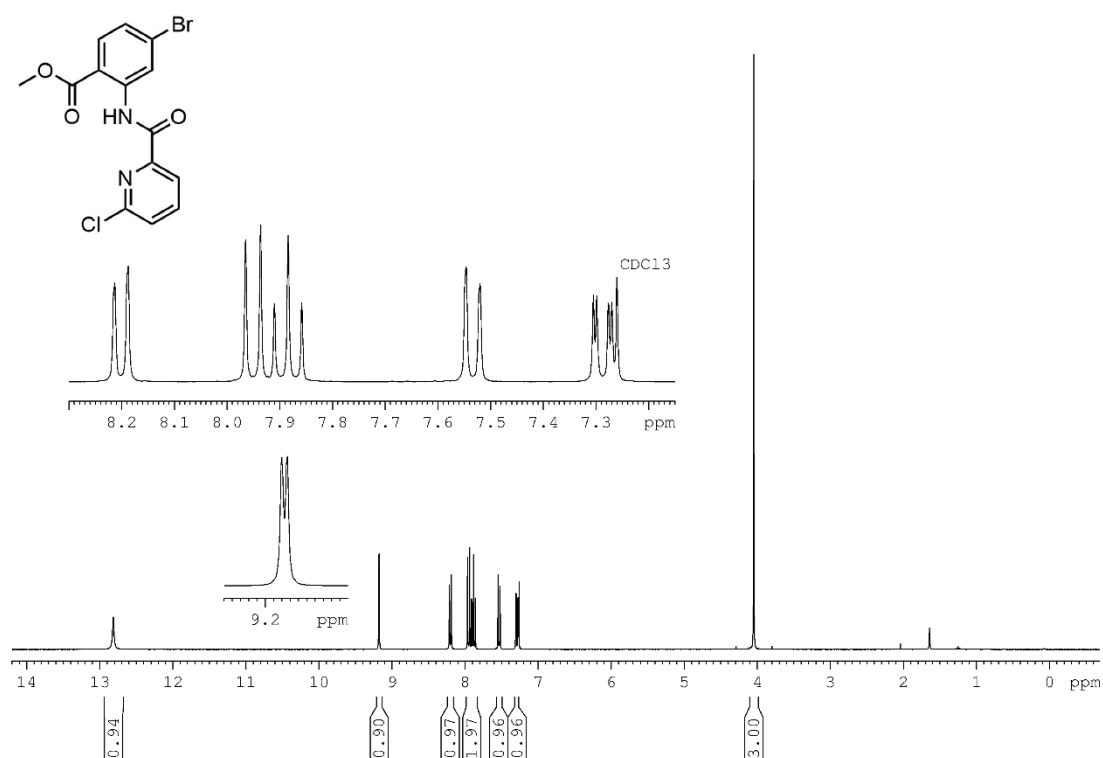
$^{13}\text{C}$  NMR spectrum (75 MHz,  $\text{CDCl}_3$ ) of compound **3.14**.

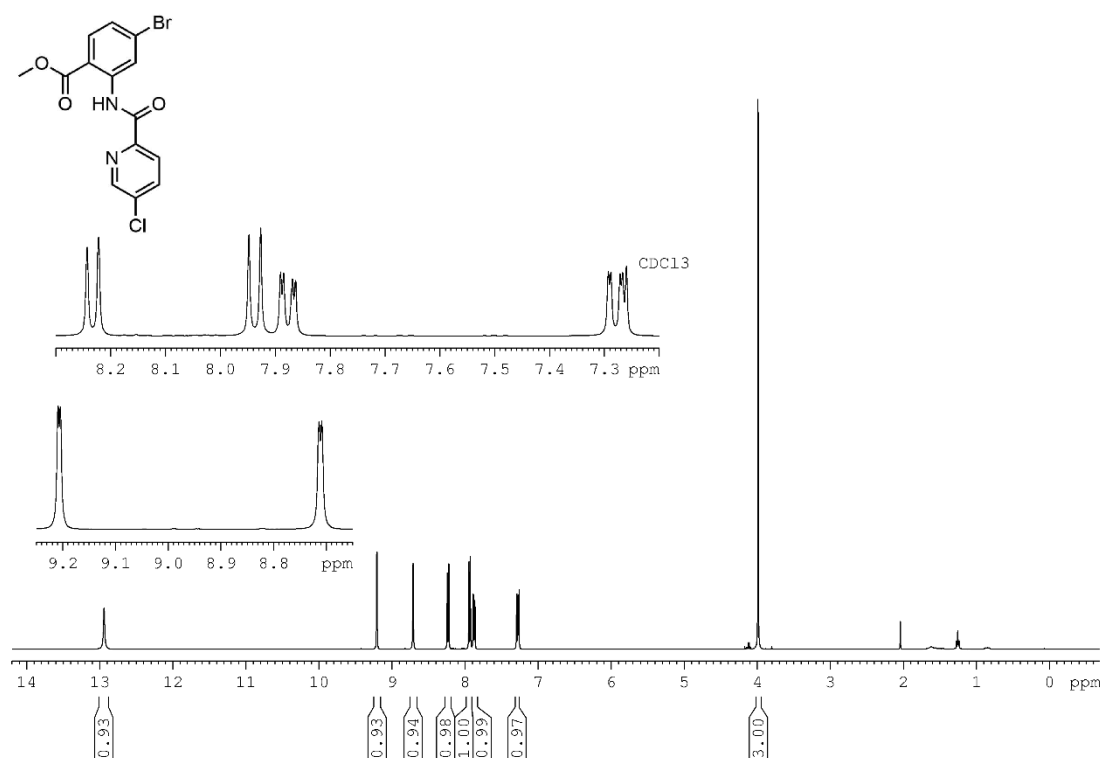


$^1\text{H}$  NMR spectrum (300 MHz,  $\text{CDCl}_3$ ) of compound **3.15**.

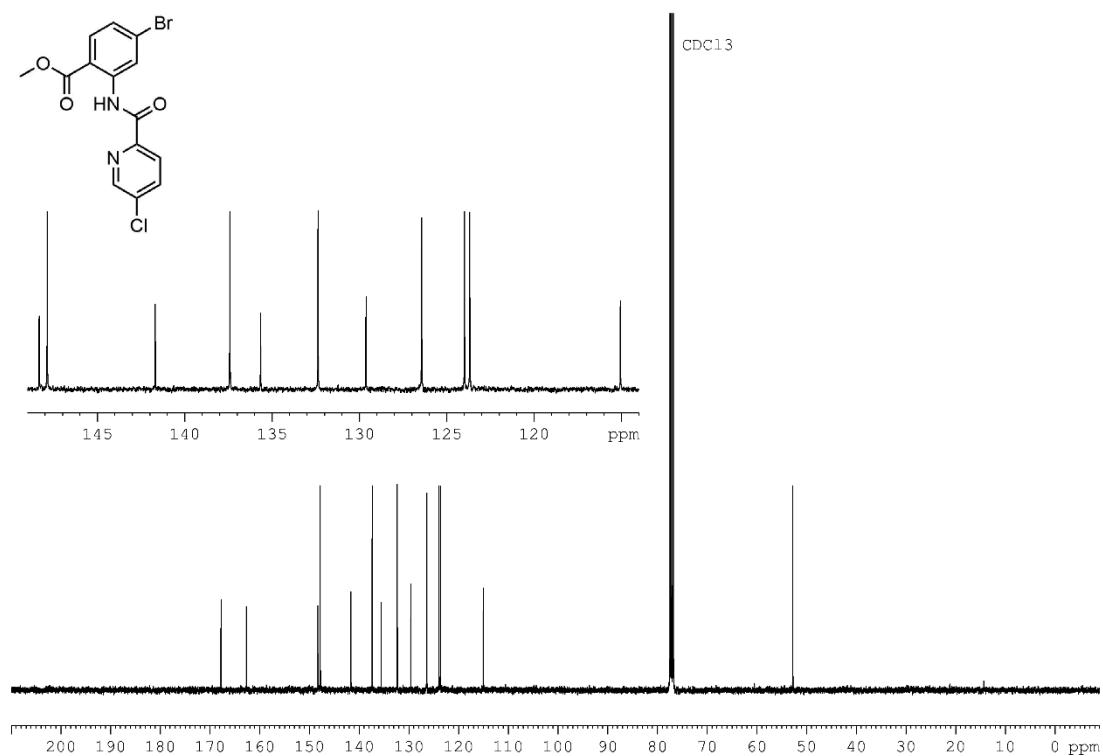


$^{13}\text{C}$  NMR spectrum (75 MHz,  $\text{CDCl}_3$ ) of compound **3.15**.

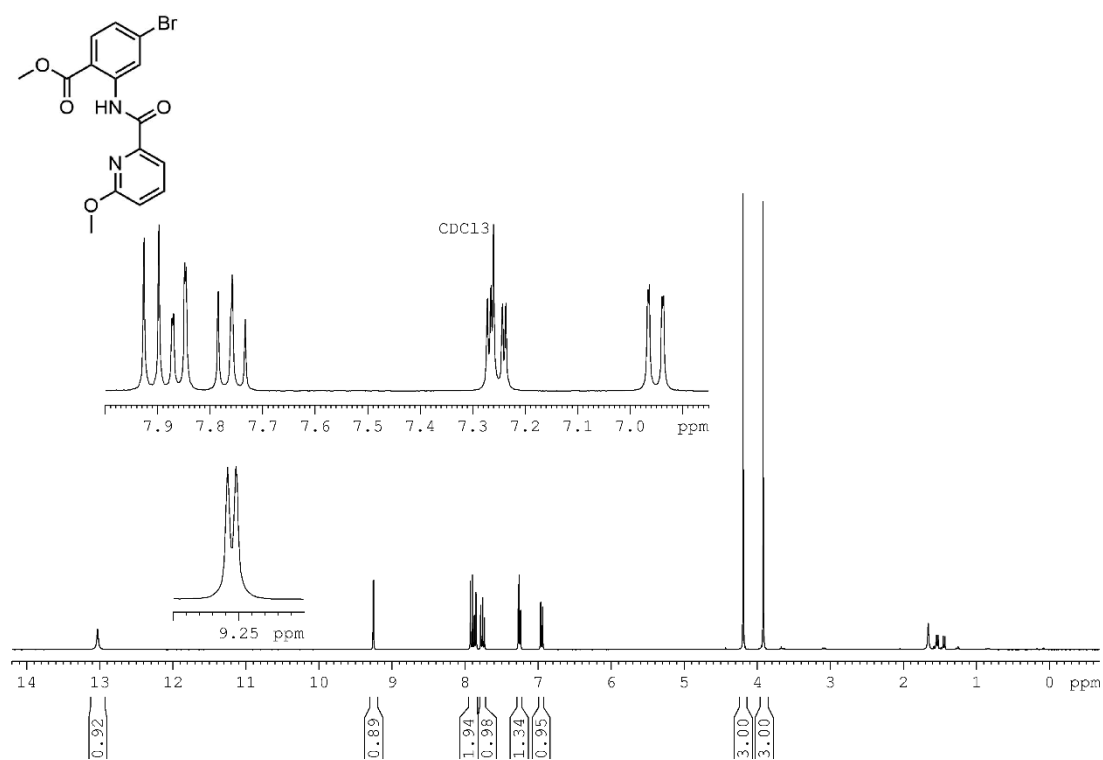




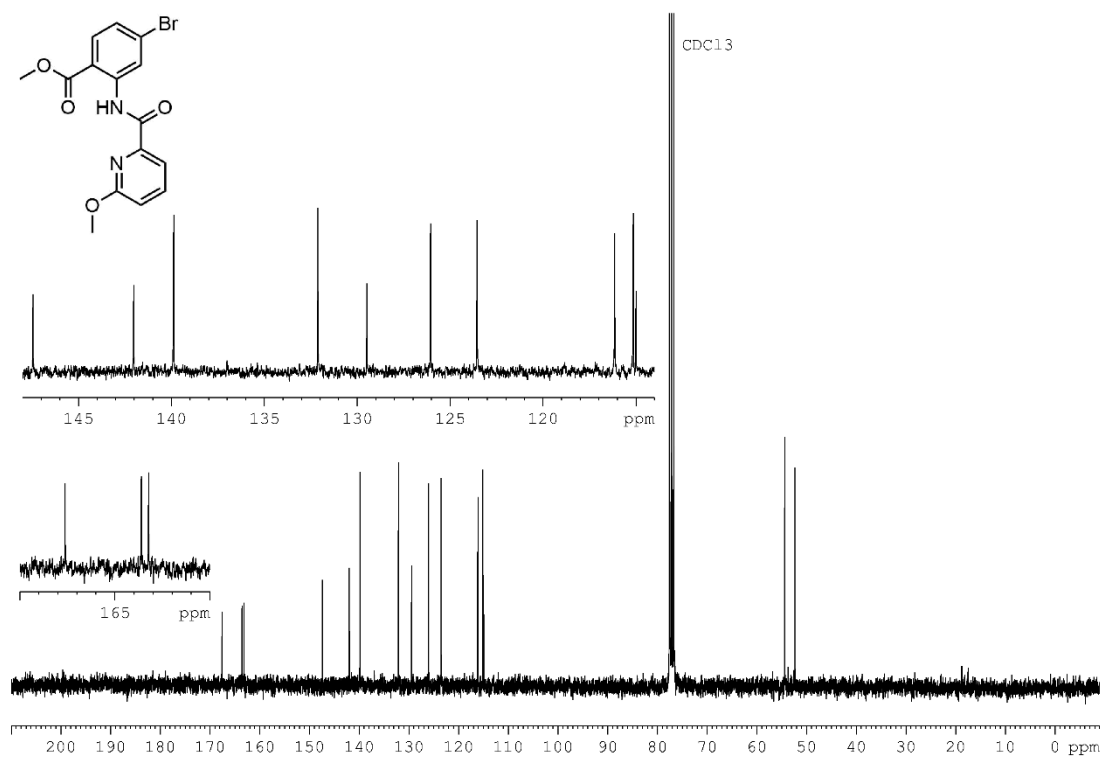
<sup>1</sup>H NMR spectrum (400 MHz, CDCl<sub>3</sub>) of compound **3.17**.



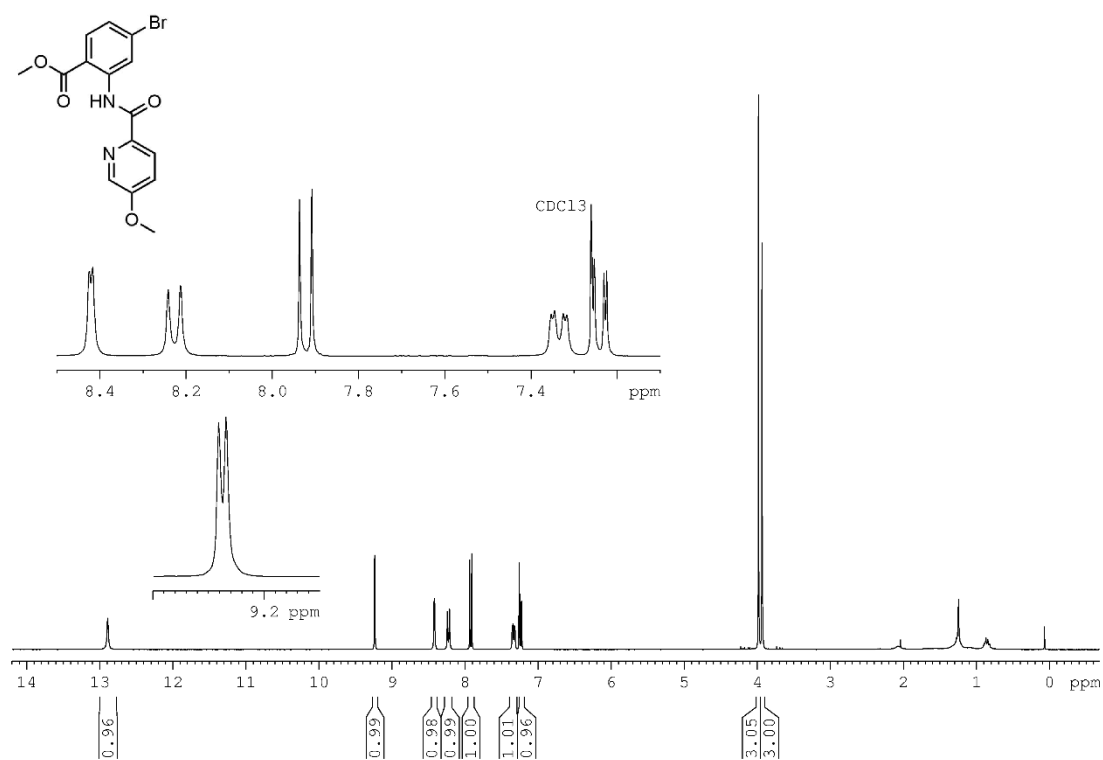
<sup>13</sup>C NMR spectrum (101 MHz, CDCl<sub>3</sub>) of compound **3.17**.



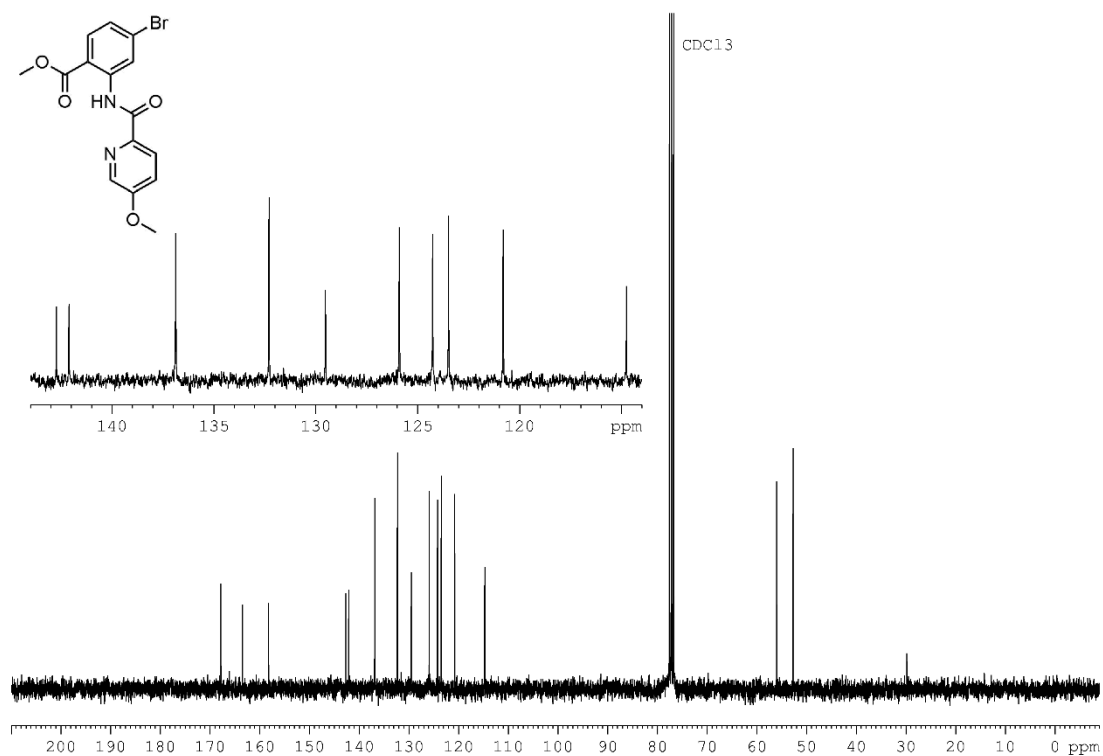
<sup>1</sup>H NMR spectrum (300 MHz, CDCl<sub>3</sub>) of compound **3.18**.



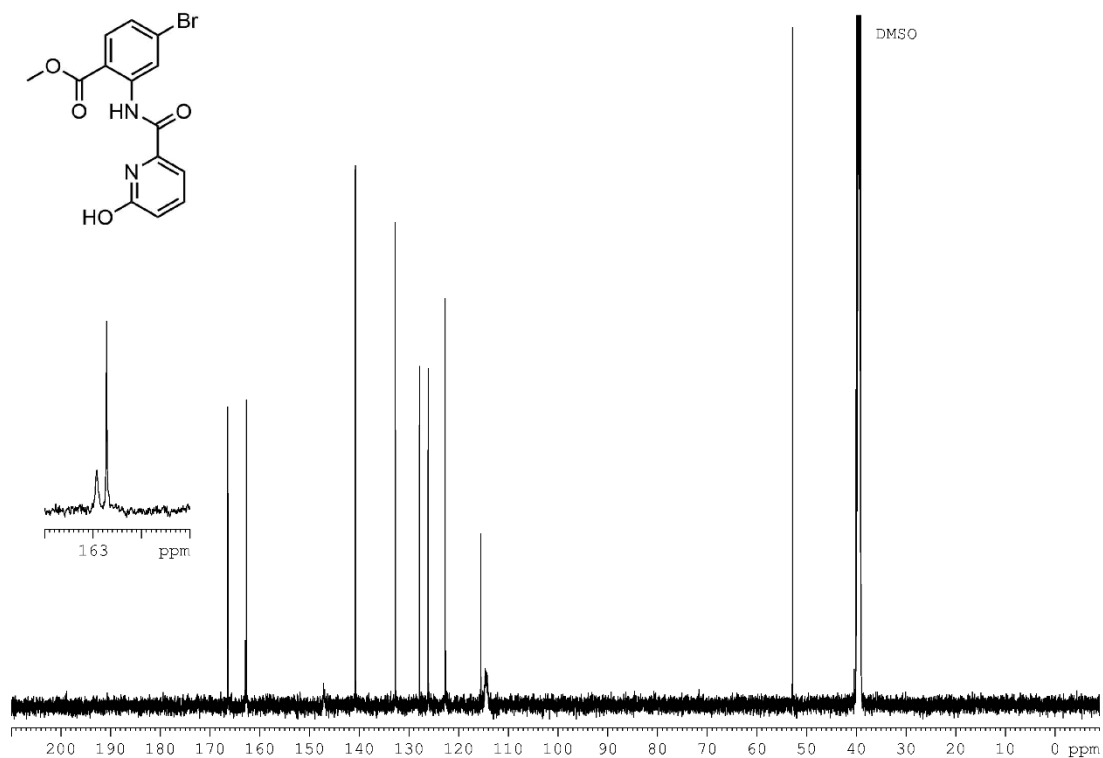
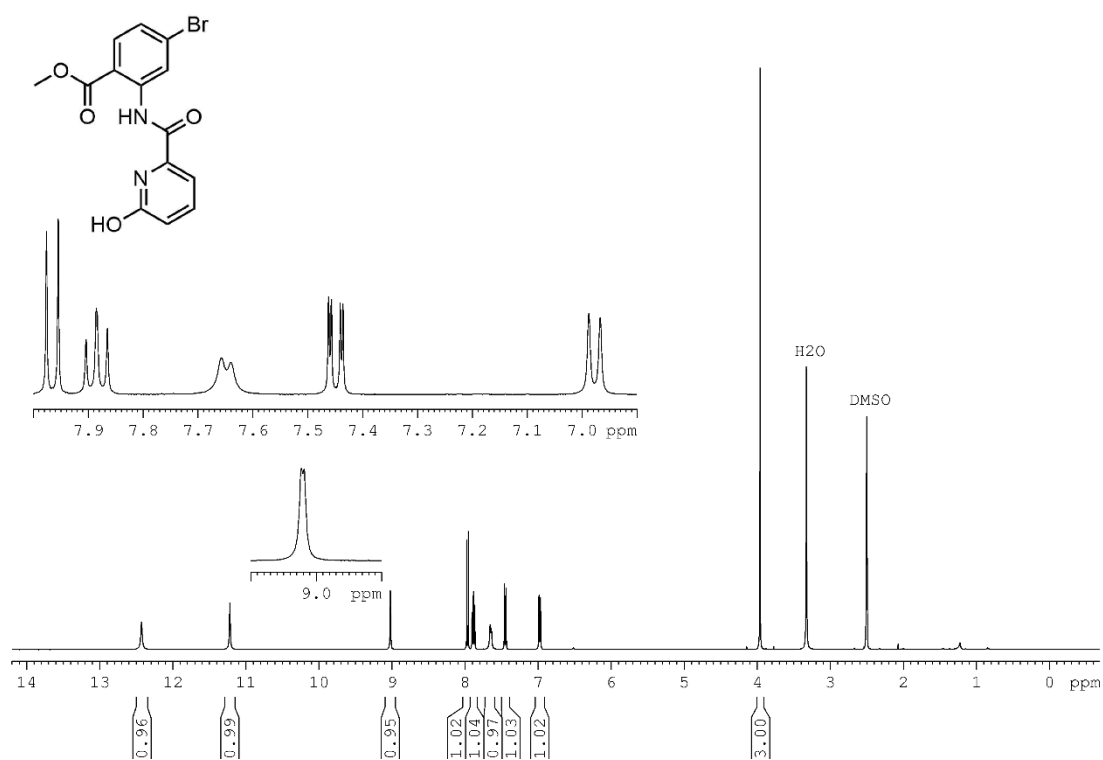
<sup>13</sup>C NMR spectrum (75 MHz, CDCl<sub>3</sub>) of compound **3.18**.

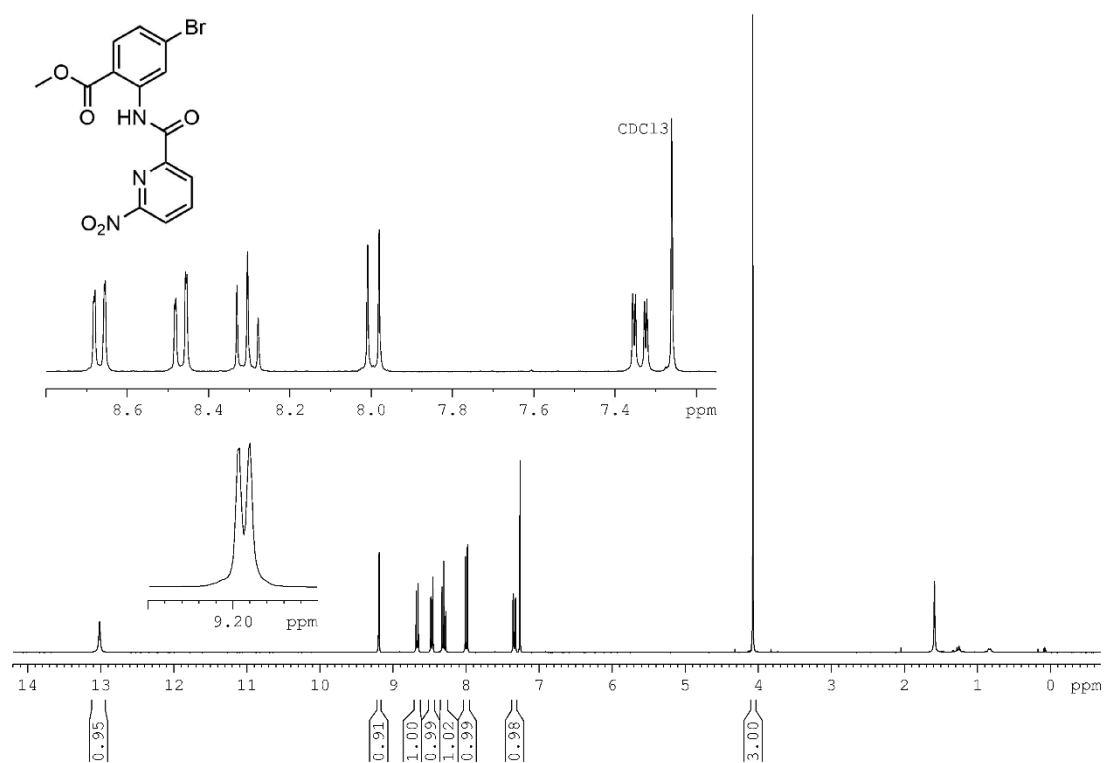


<sup>1</sup>H NMR spectrum (300 MHz, CDCl<sub>3</sub>) of compound **3.19**.

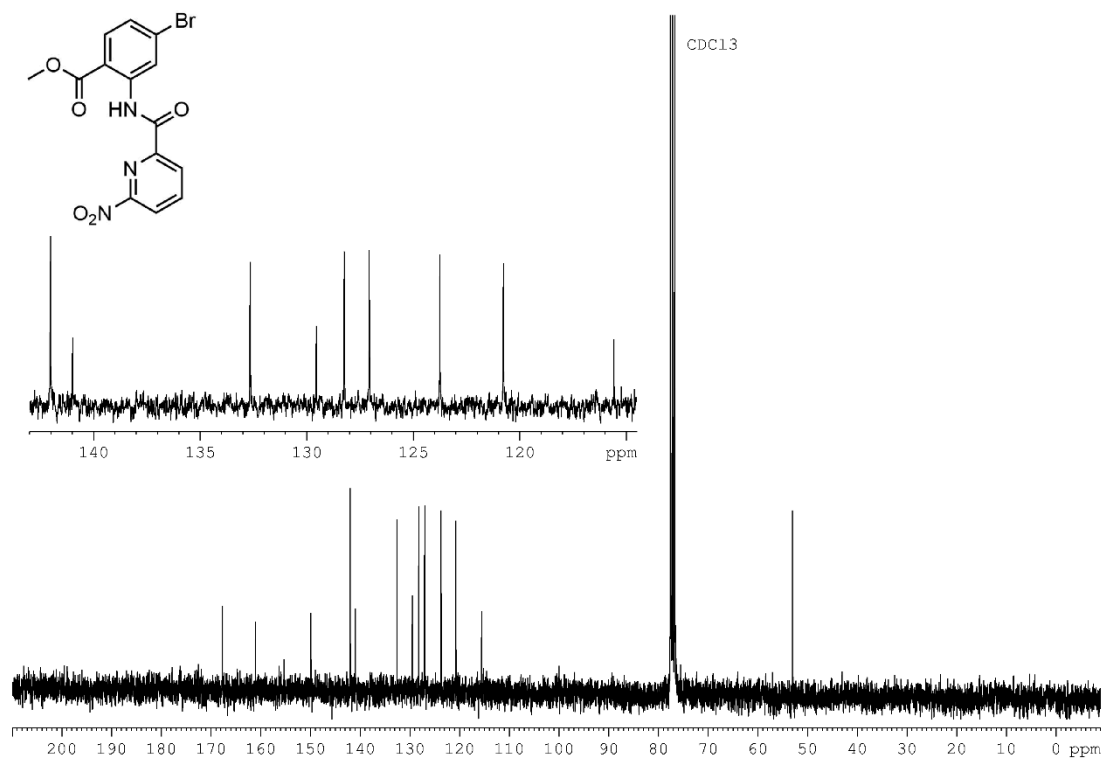


<sup>13</sup>C NMR spectrum (75 MHz, CDCl<sub>3</sub>) of compound **3.19**.

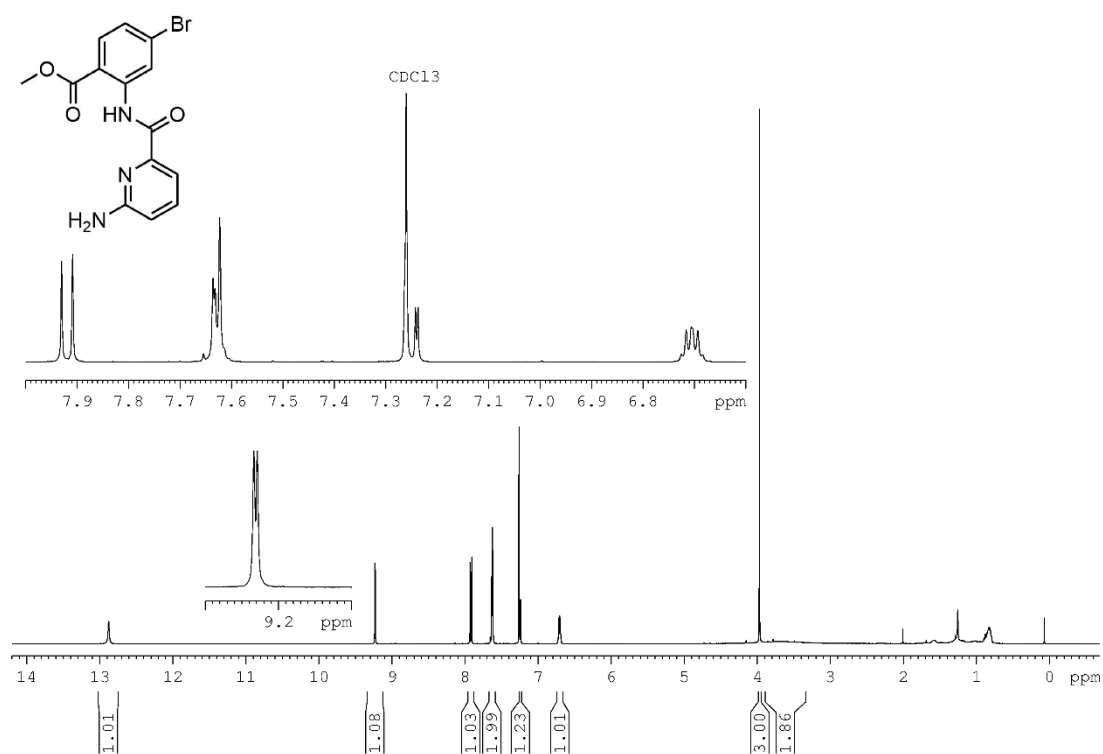




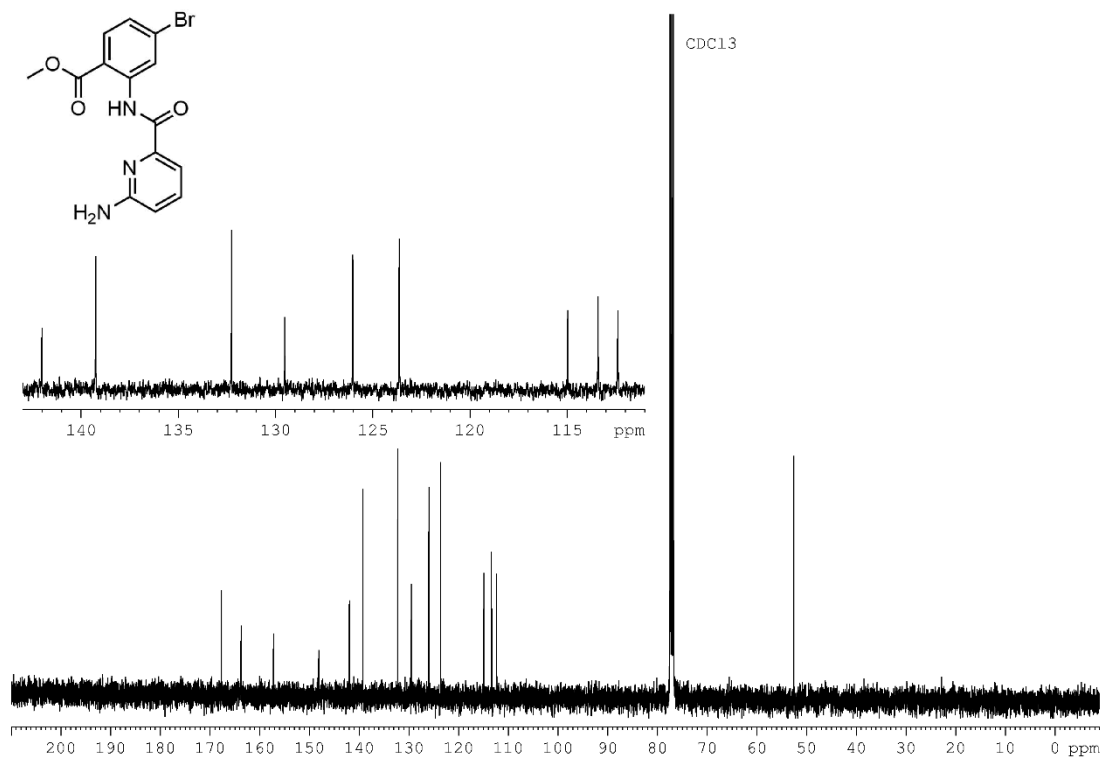
$^1\text{H}$  NMR spectrum (300 MHz,  $\text{CDCl}_3$ ) of compound **3.21**.



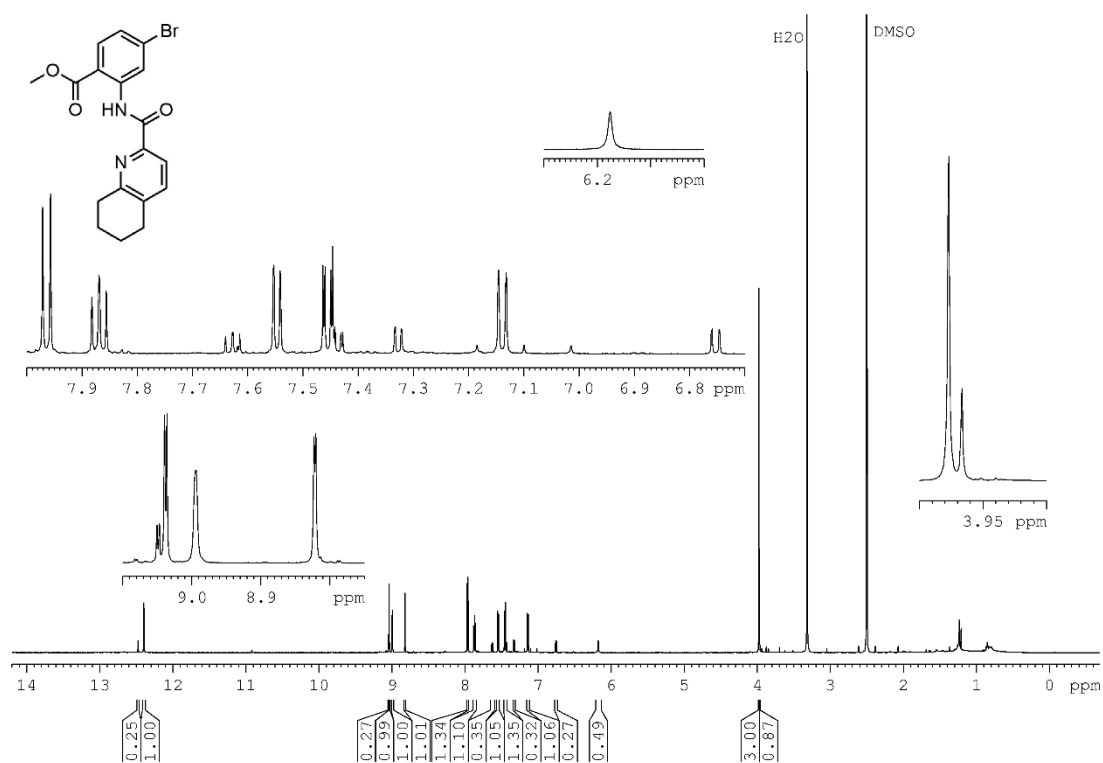
$^{13}\text{C}$  NMR spectrum (75 MHz,  $\text{CDCl}_3$ ) of compound **3.21**.



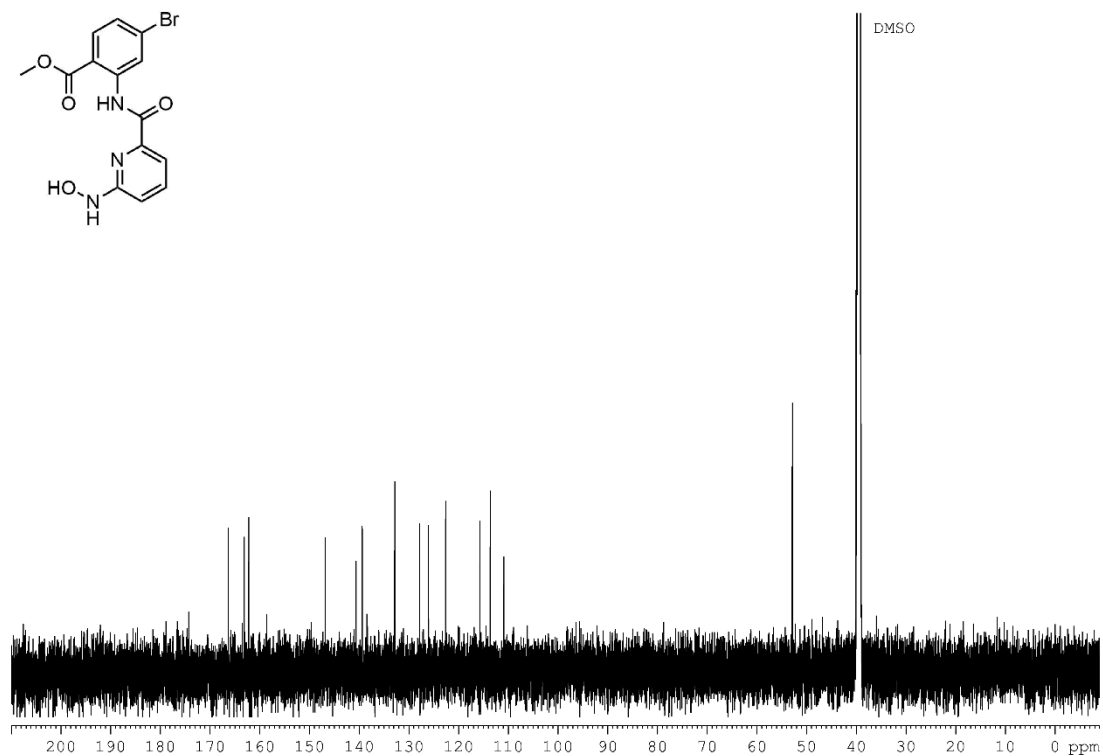
<sup>1</sup>H NMR spectrum (400 MHz, CDCl<sub>3</sub>) of compound **3.22**.



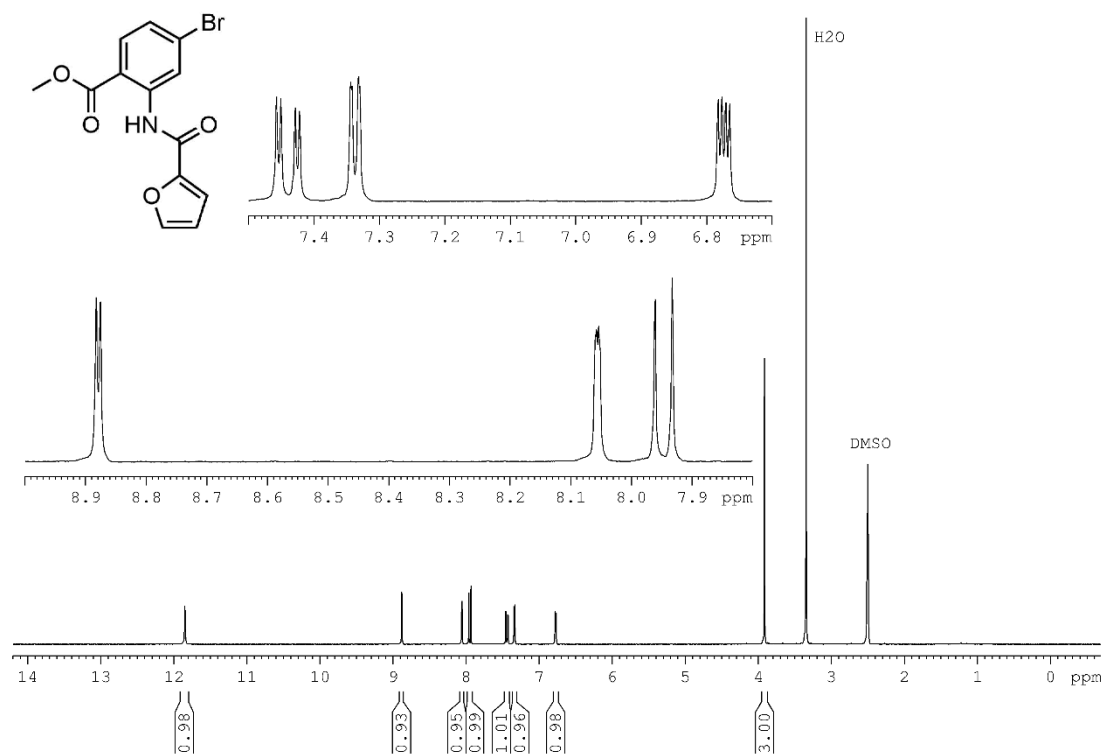
<sup>13</sup>C NMR spectrum (101 MHz, CDCl<sub>3</sub>) of compound **3.22**.



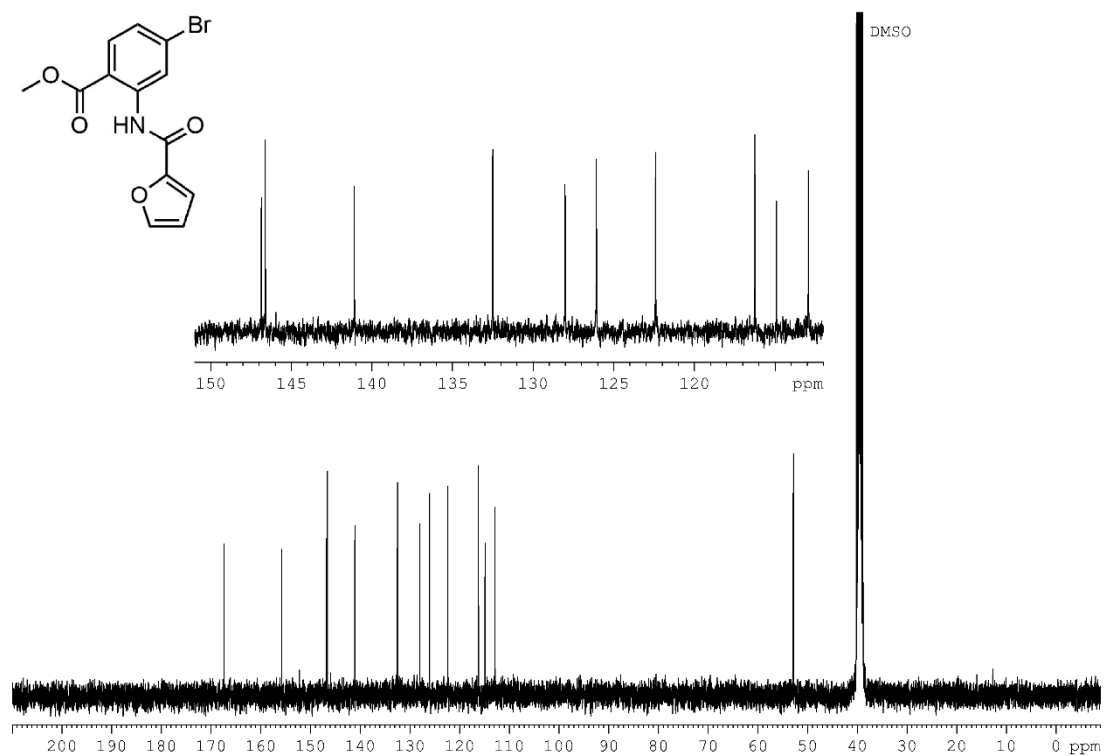
<sup>1</sup>H NMR spectrum (600 MHz, DMSO-*d*<sub>6</sub>) of compound **3.23**.



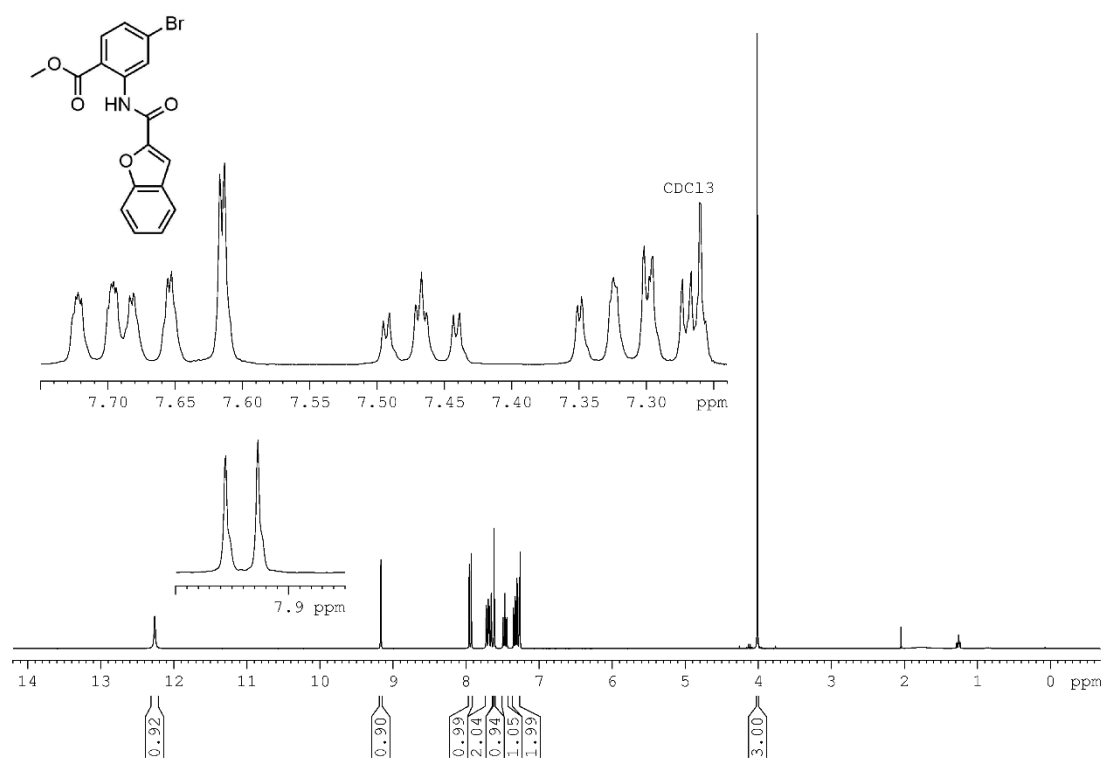
<sup>13</sup>C NMR spectrum (151 MHz, DMSO-*d*<sub>6</sub>) of compound **3.23**.



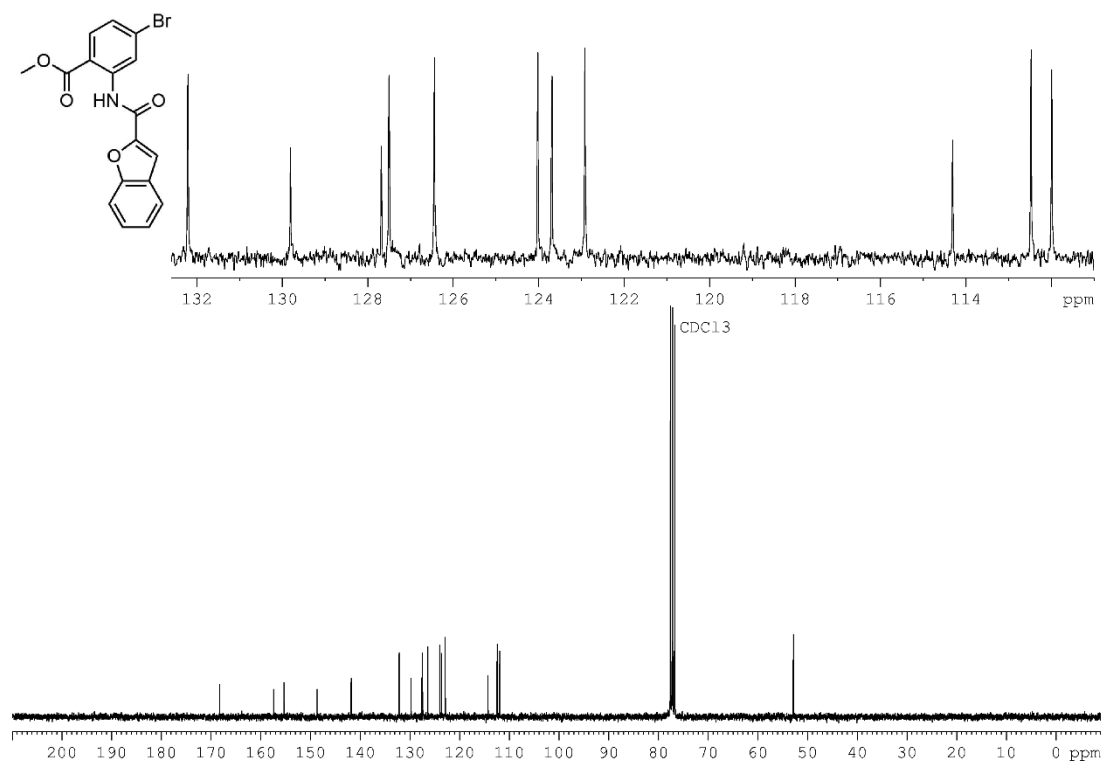
<sup>1</sup>H NMR spectrum (300 MHz, DMSO-*d*<sub>6</sub>) of compound **3.24**.



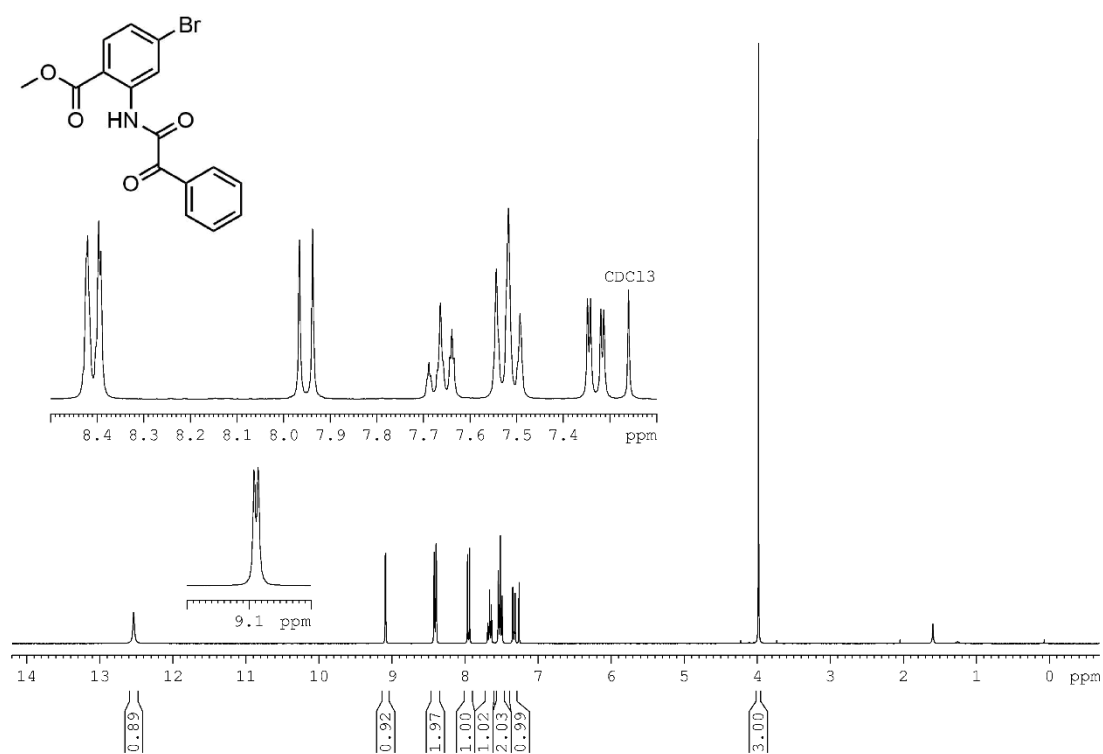
<sup>13</sup>C NMR spectrum (101 MHz, DMSO-*d*<sub>6</sub>) of compound **3.24**.



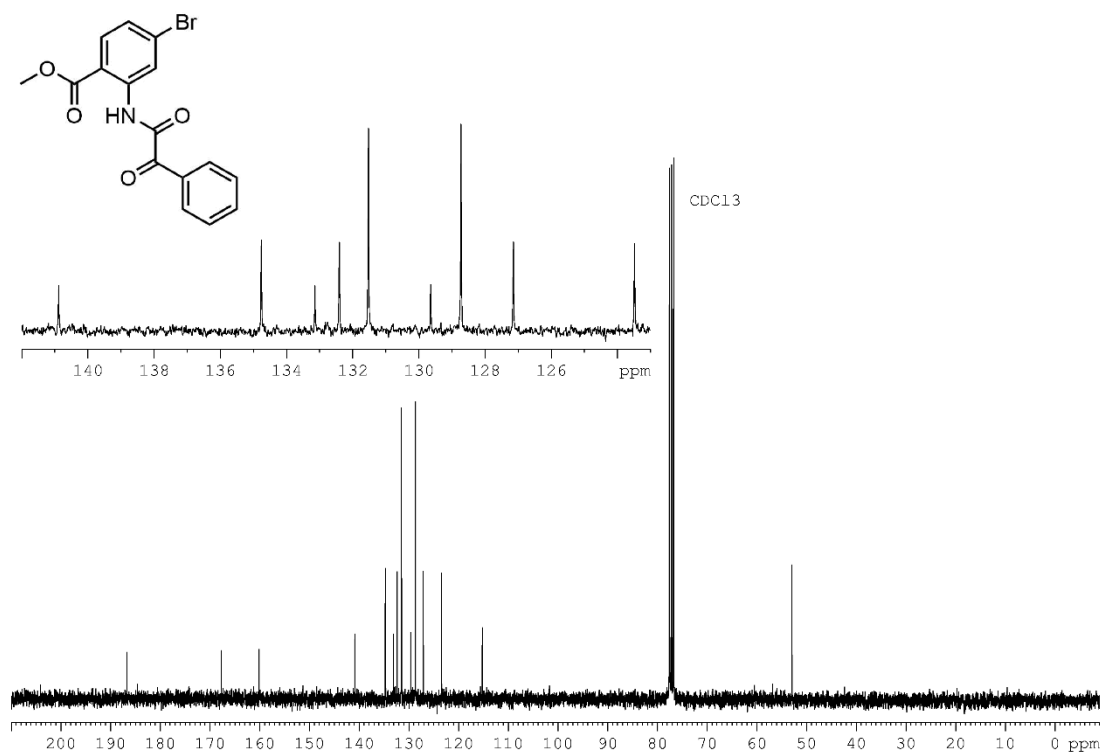
<sup>1</sup>H NMR spectrum (300 MHz, CDCl<sub>3</sub>) of compound **3.25**.



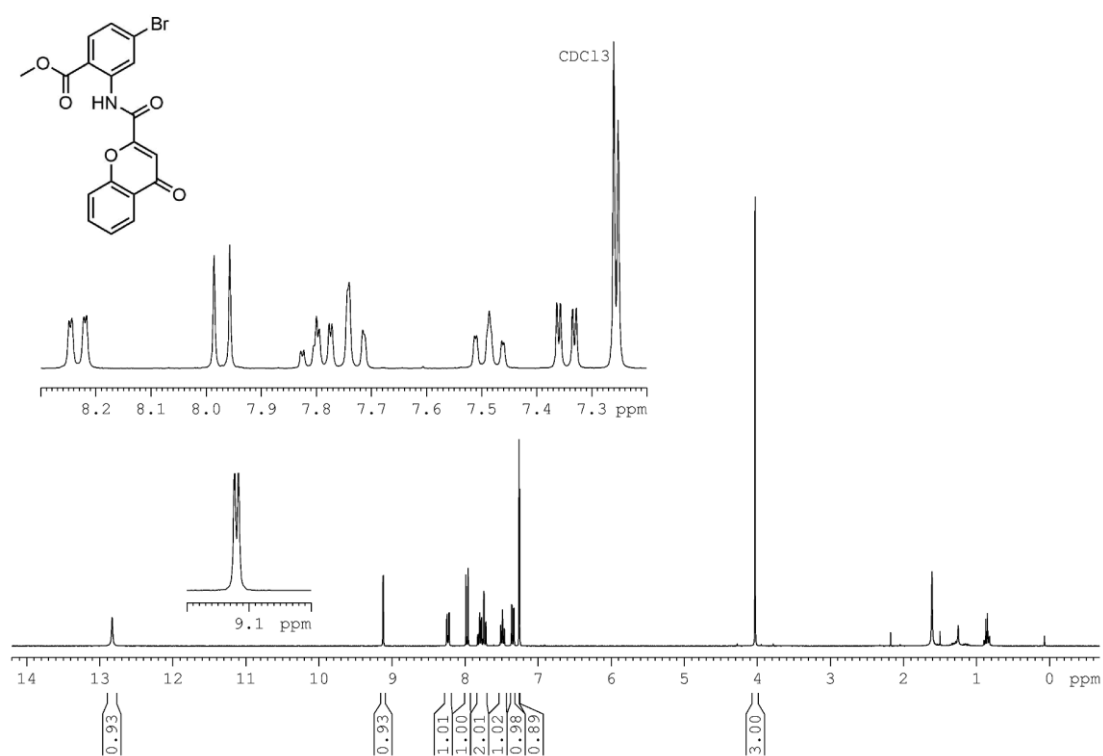
<sup>13</sup>C NMR spectrum (75 MHz, CDCl<sub>3</sub>) of compound **3.25**.



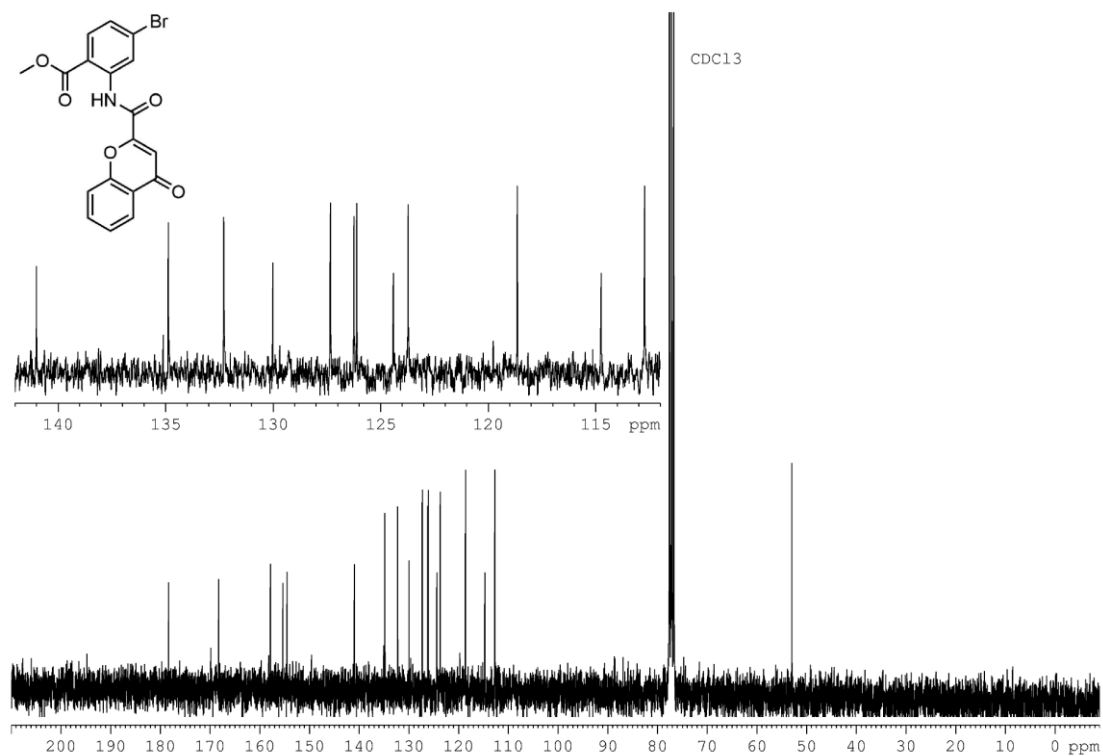
$^1\text{H}$  NMR spectrum (300 MHz,  $\text{CDCl}_3$ ) of compound **3.26**.



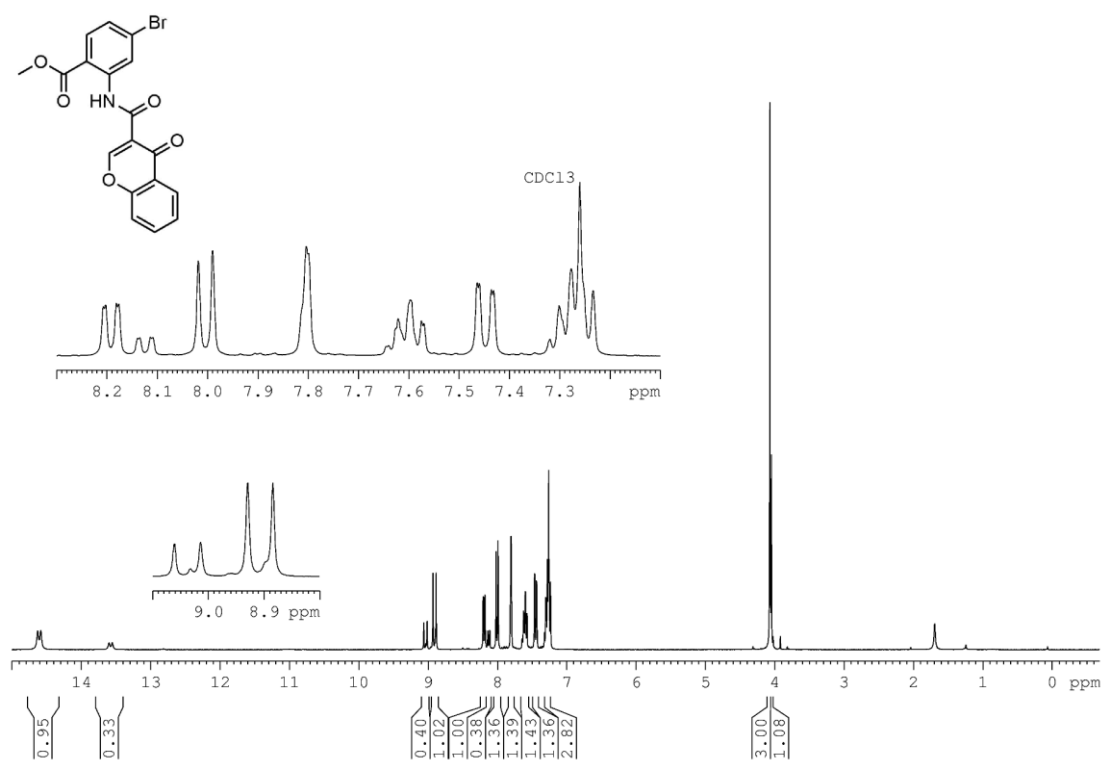
$^{13}\text{C}$  NMR spectrum (75 MHz,  $\text{CDCl}_3$ ) of compound **3.26**.



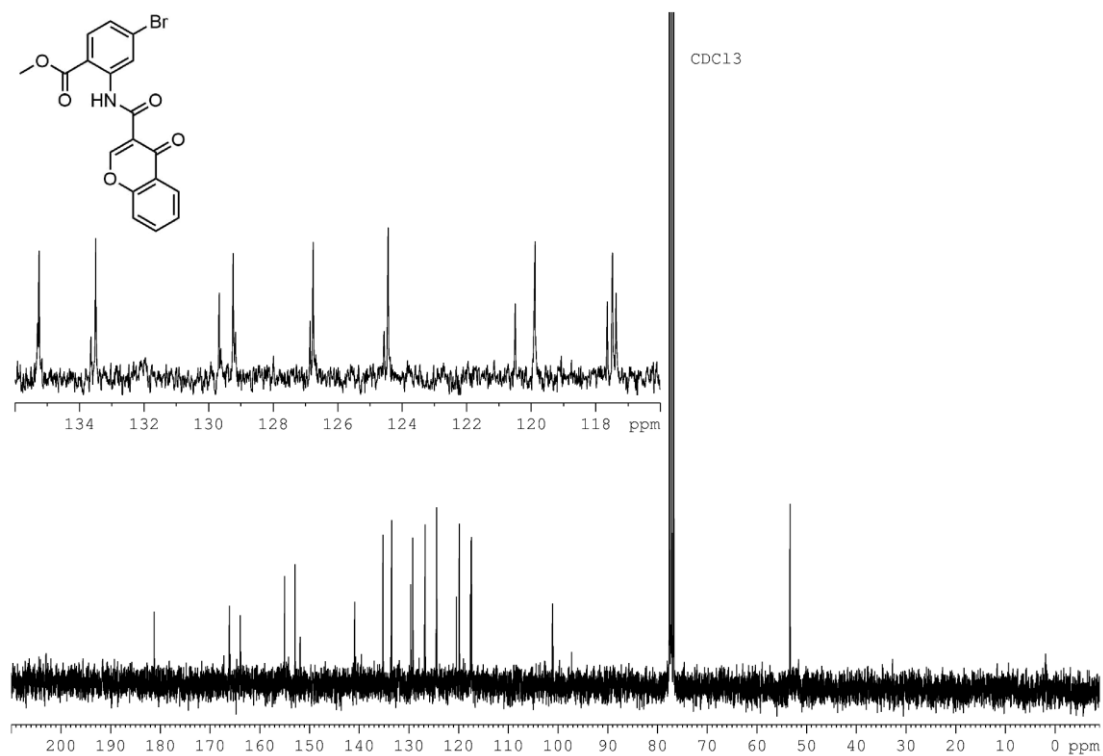
$^1\text{H}$  NMR spectrum (300 MHz,  $\text{CDCl}_3$ ) of compound **3.27**.



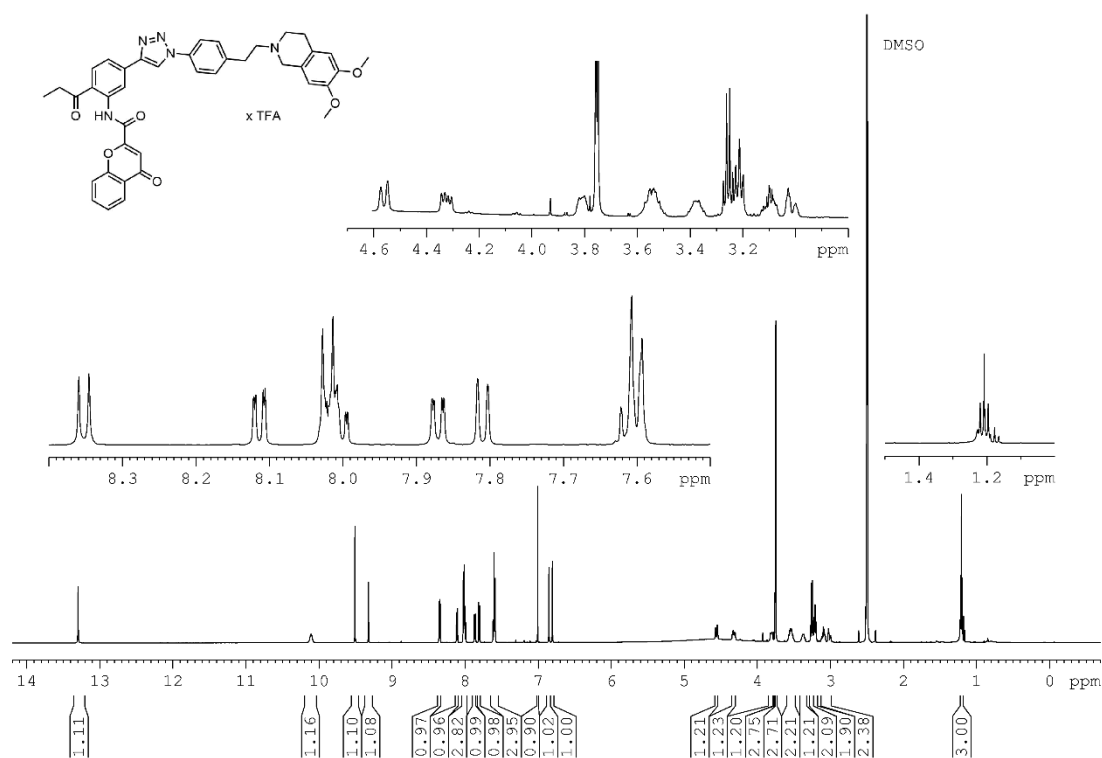
$^{13}\text{C}$  NMR spectrum (75 MHz,  $\text{CDCl}_3$ ) of compound **3.27**.



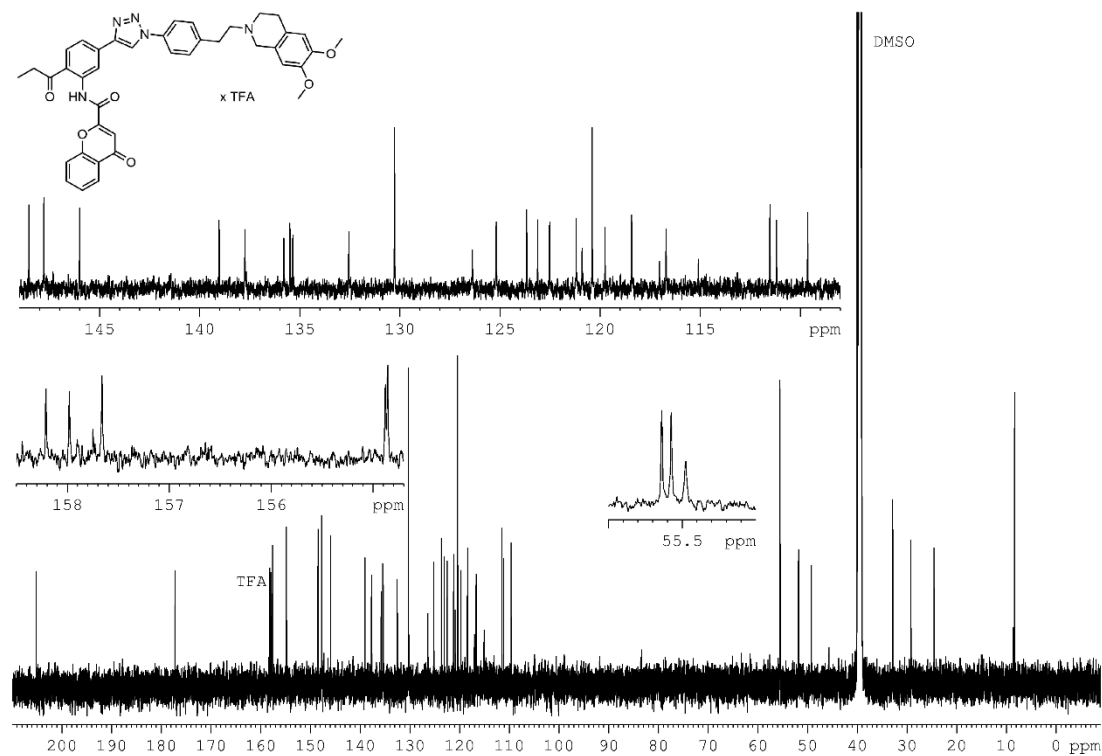
<sup>1</sup>H NMR spectrum (300 MHz, CDCl<sub>3</sub>) of compound **3.28**.



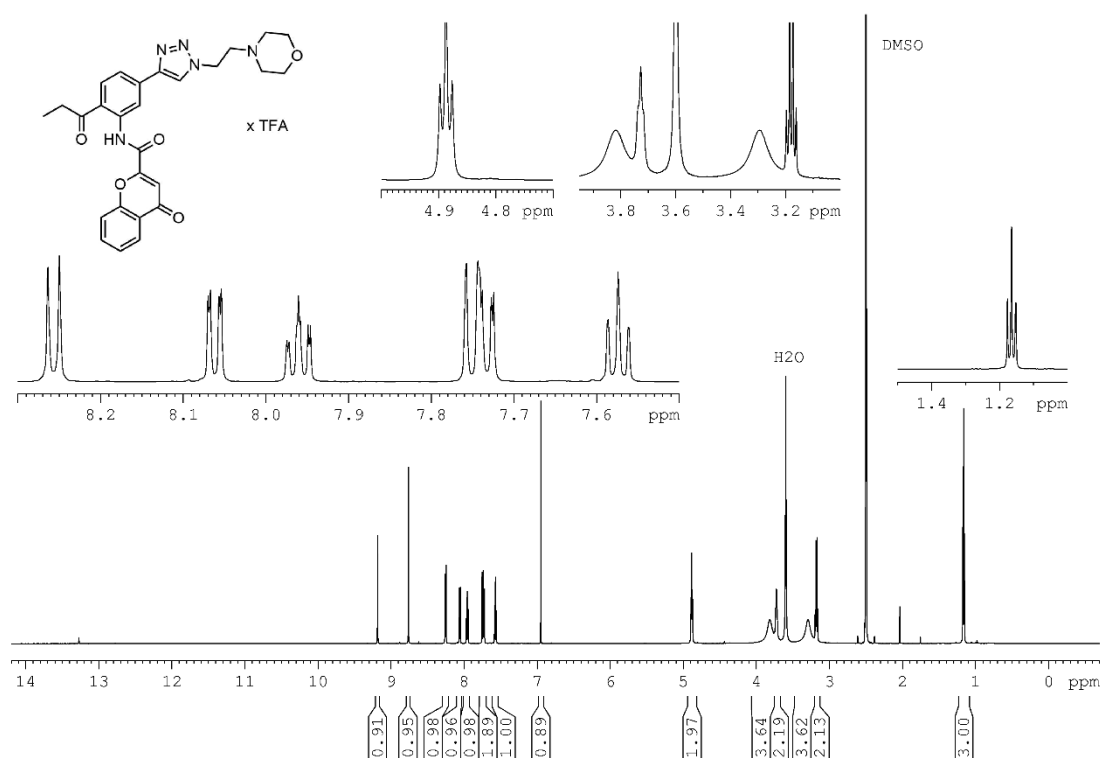
<sup>13</sup>C NMR spectrum (75 MHz, CDCl<sub>3</sub>) of compound **3.28**.



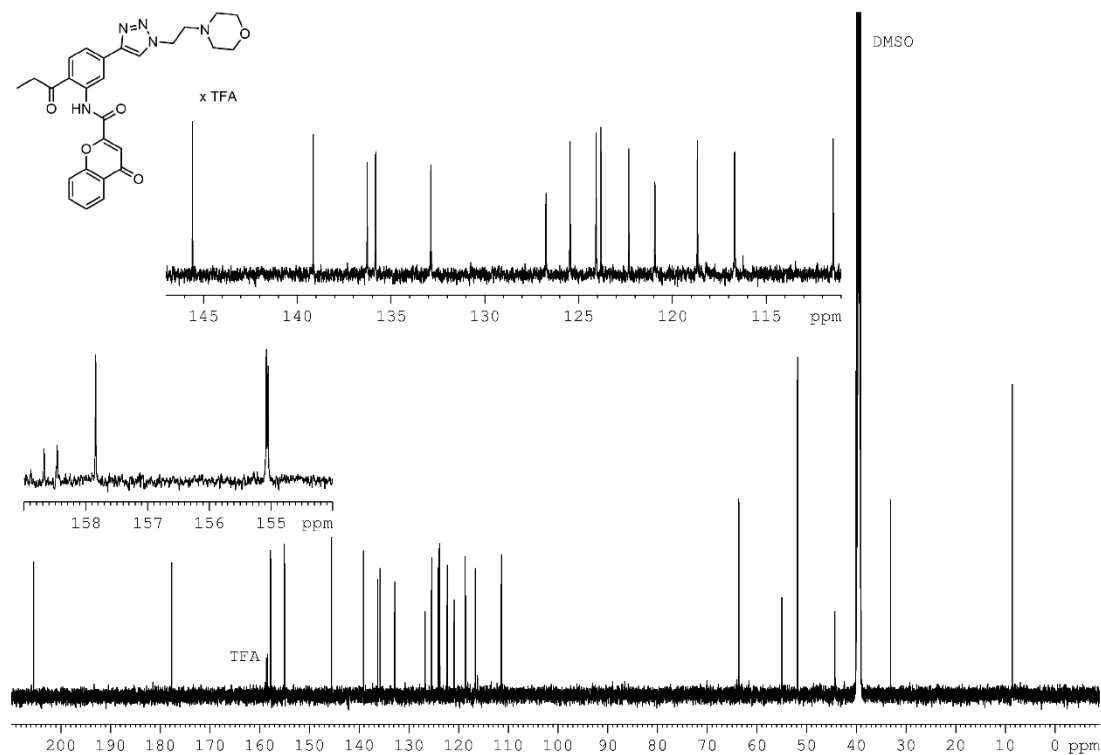
<sup>1</sup>H NMR spectrum (600 MHz, DMSO-*d*<sub>6</sub>) of compound **3.39**.



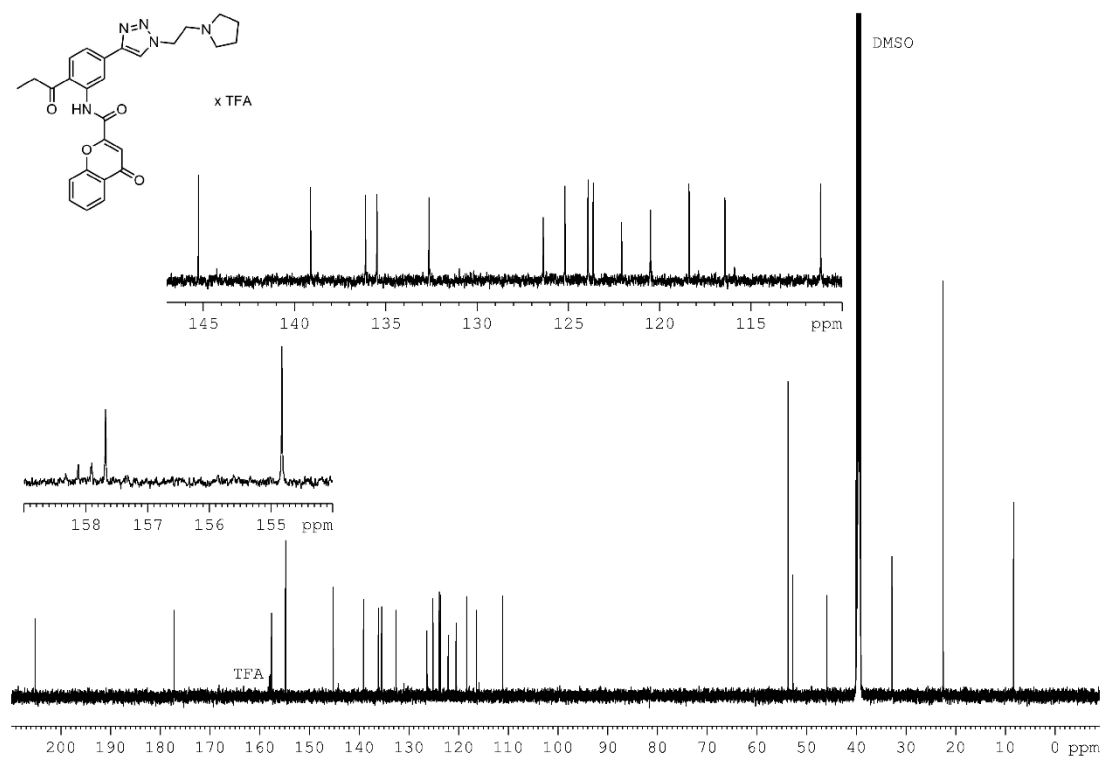
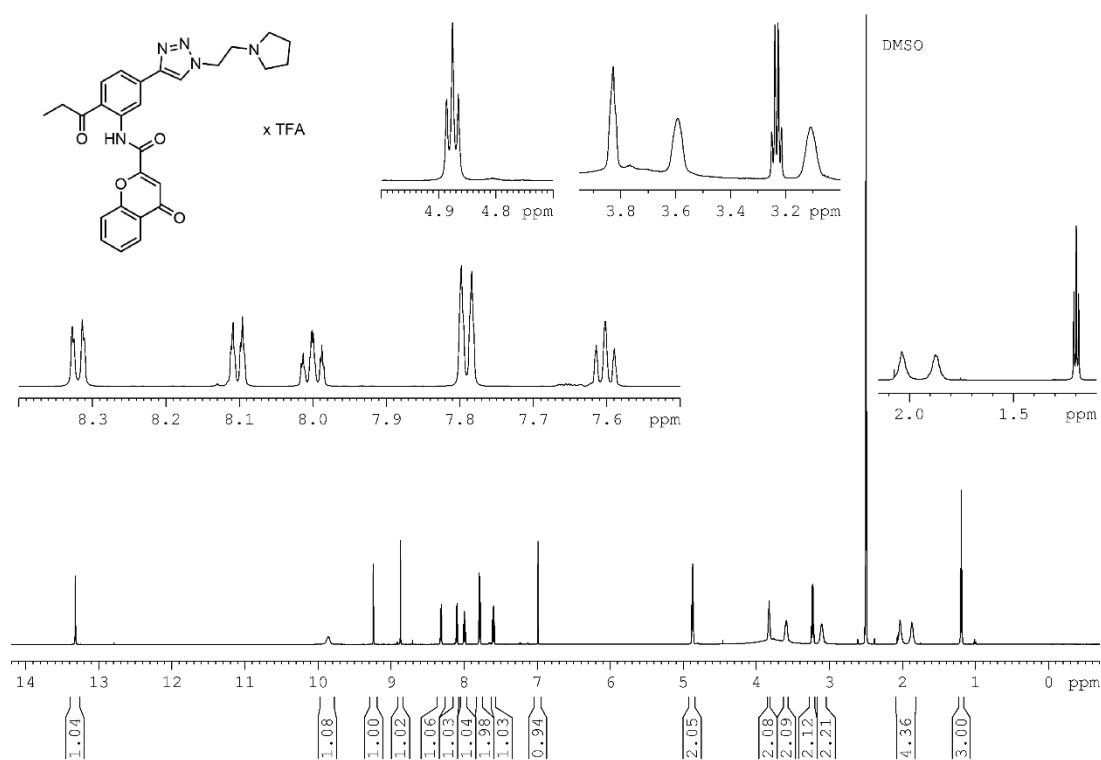
<sup>13</sup>C NMR spectrum (151 MHz, DMSO-*d*<sub>6</sub>) of compound **3.39**.

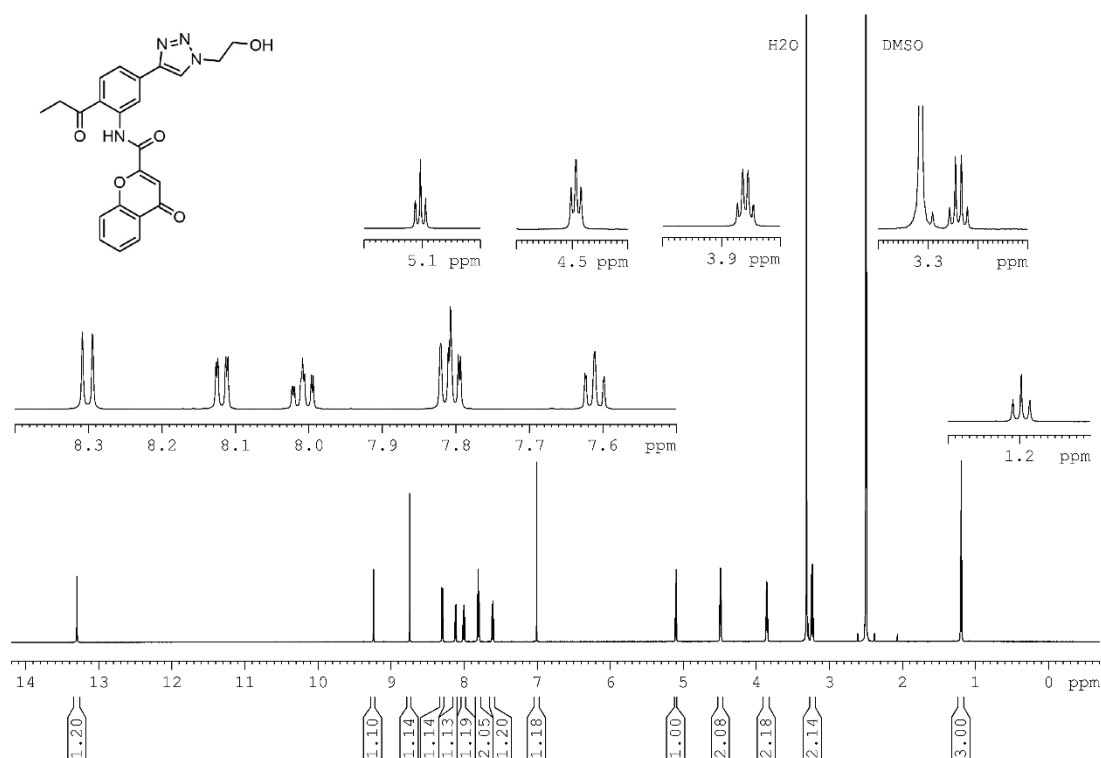


$^1\text{H}$  NMR spectrum (600 MHz,  $\text{DMSO}-d_6$ ,  $\text{D}_2\text{O}$  10%) of compound **3.40**.

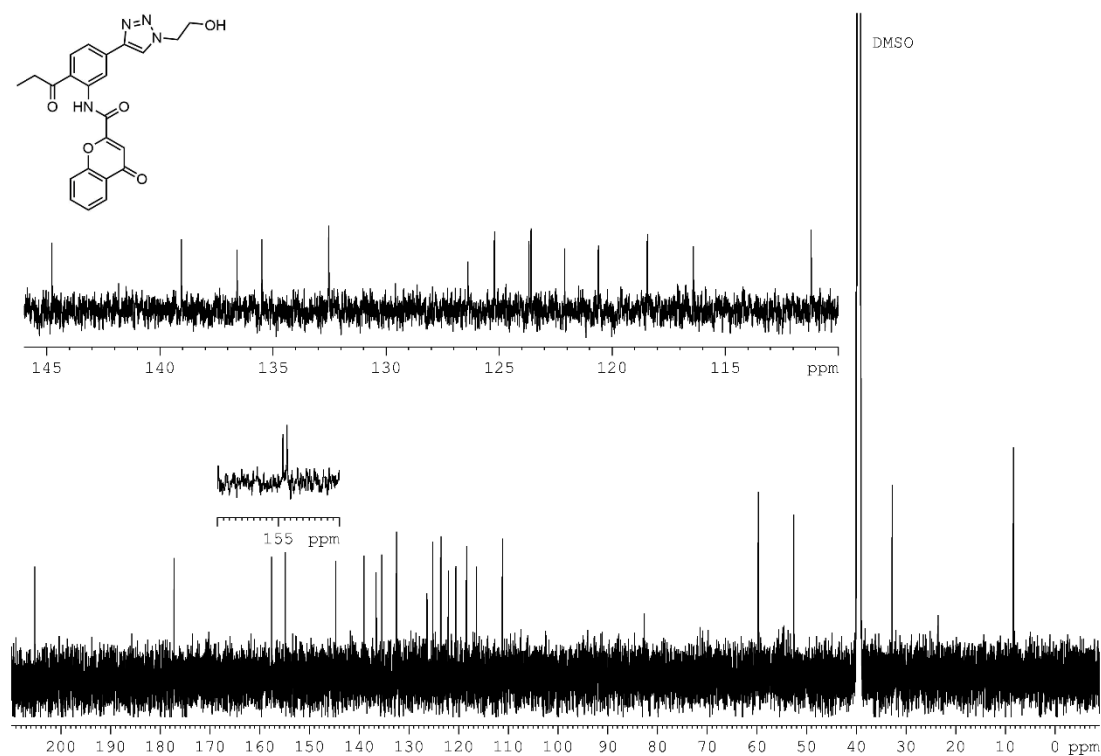


$^{13}\text{C}$  NMR spectrum (151 MHz,  $\text{DMSO}-d_6$ ,  $\text{D}_2\text{O}$  10%) of compound **3.40**.

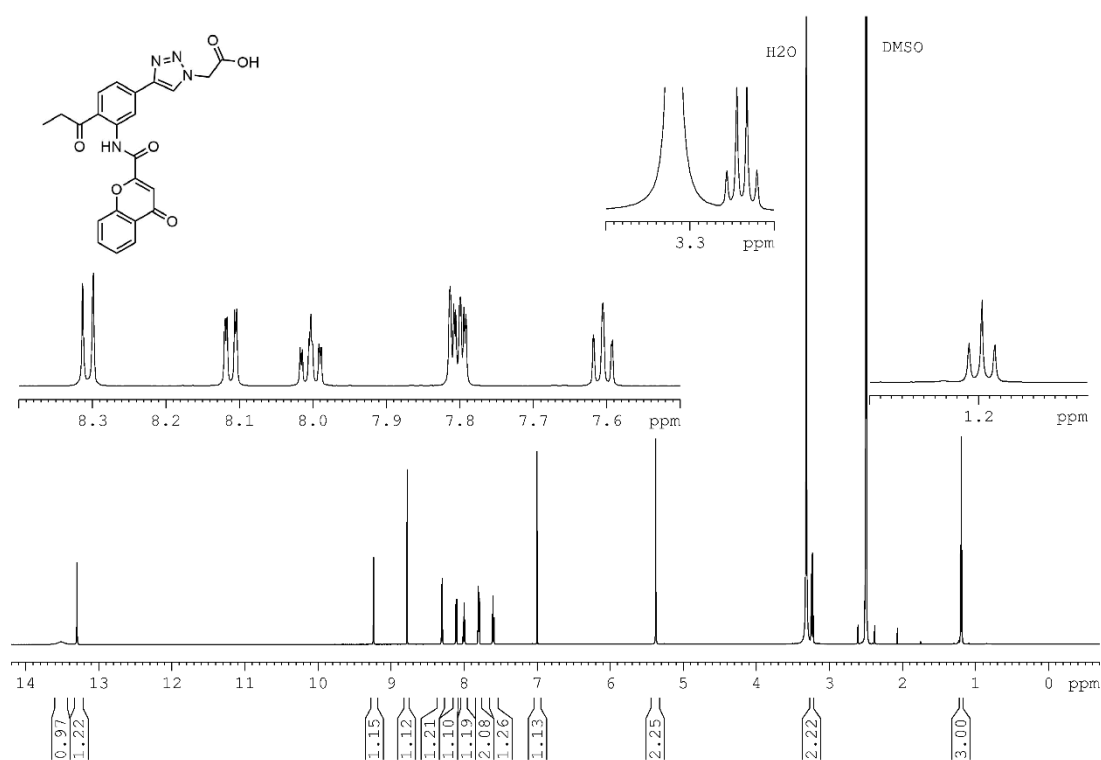




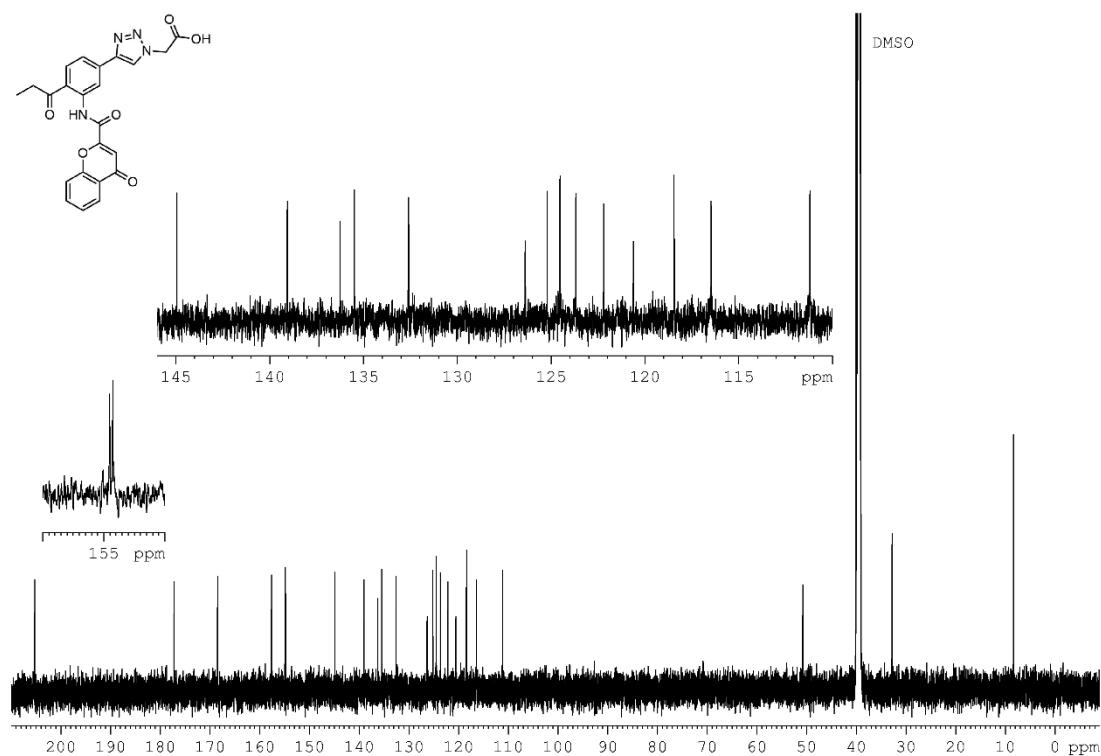
<sup>1</sup>H NMR spectrum (600 MHz, DMSO-*d*<sub>6</sub>) of compound **3.42**.



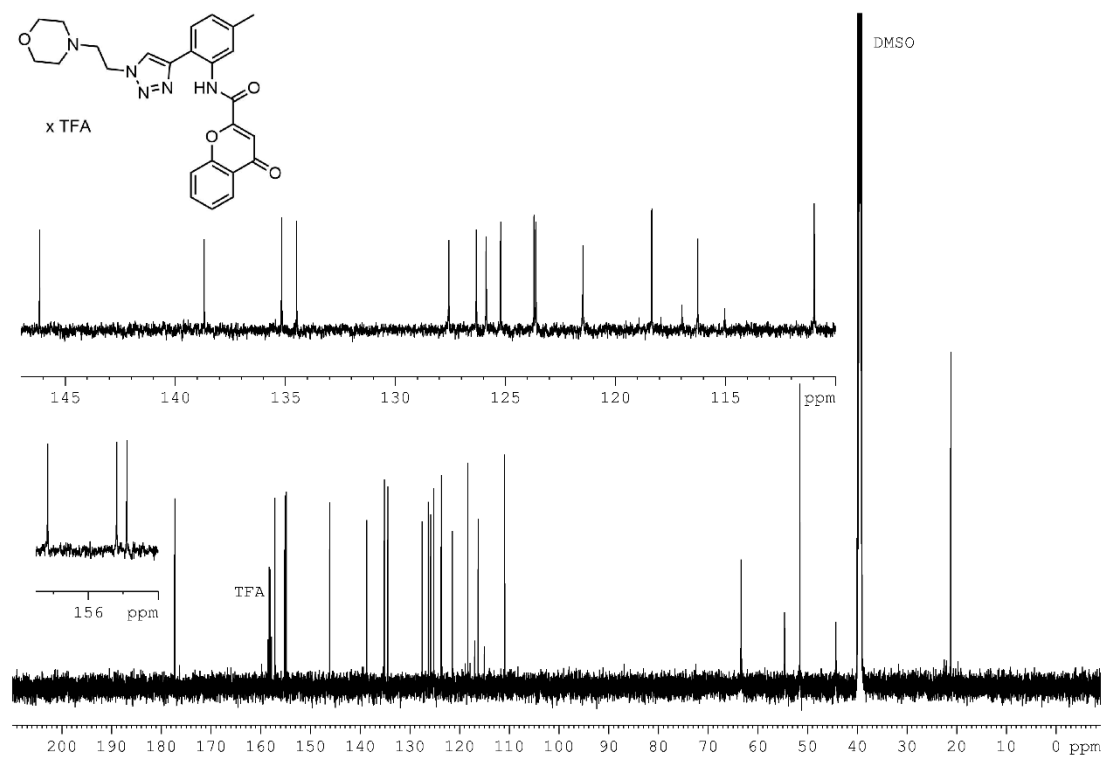
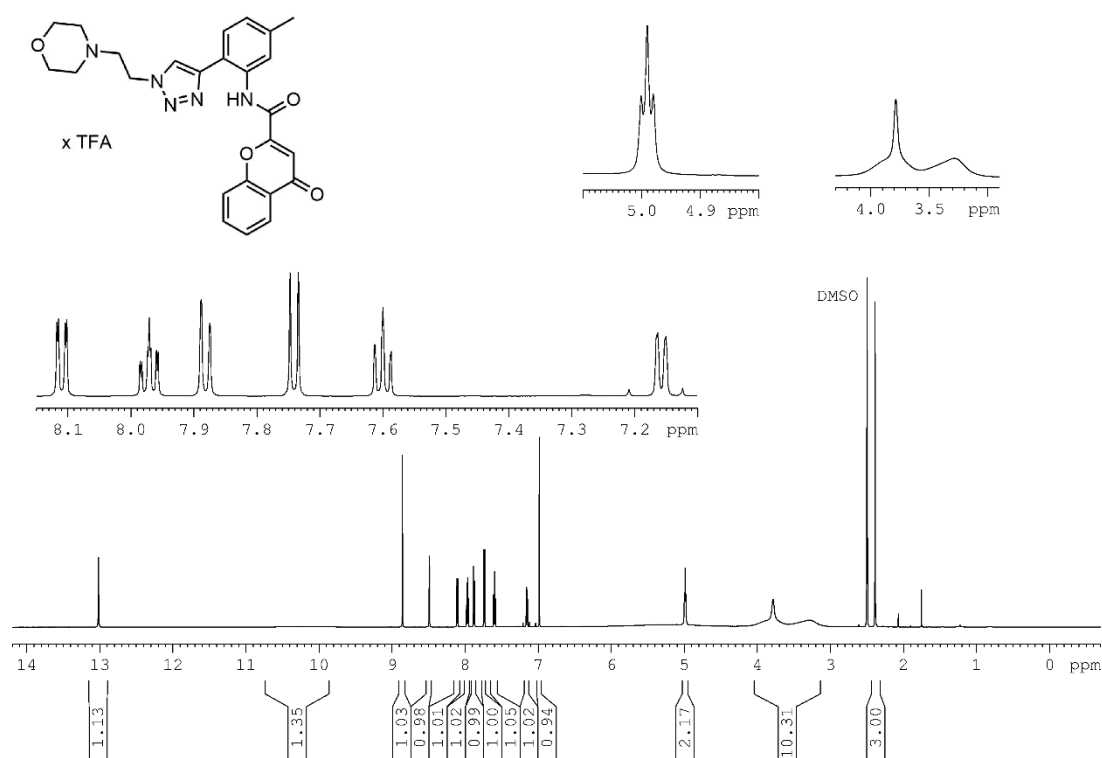
<sup>13</sup>C NMR spectrum (151 MHz, DMSO-*d*<sub>6</sub>) of compound **3.42**.

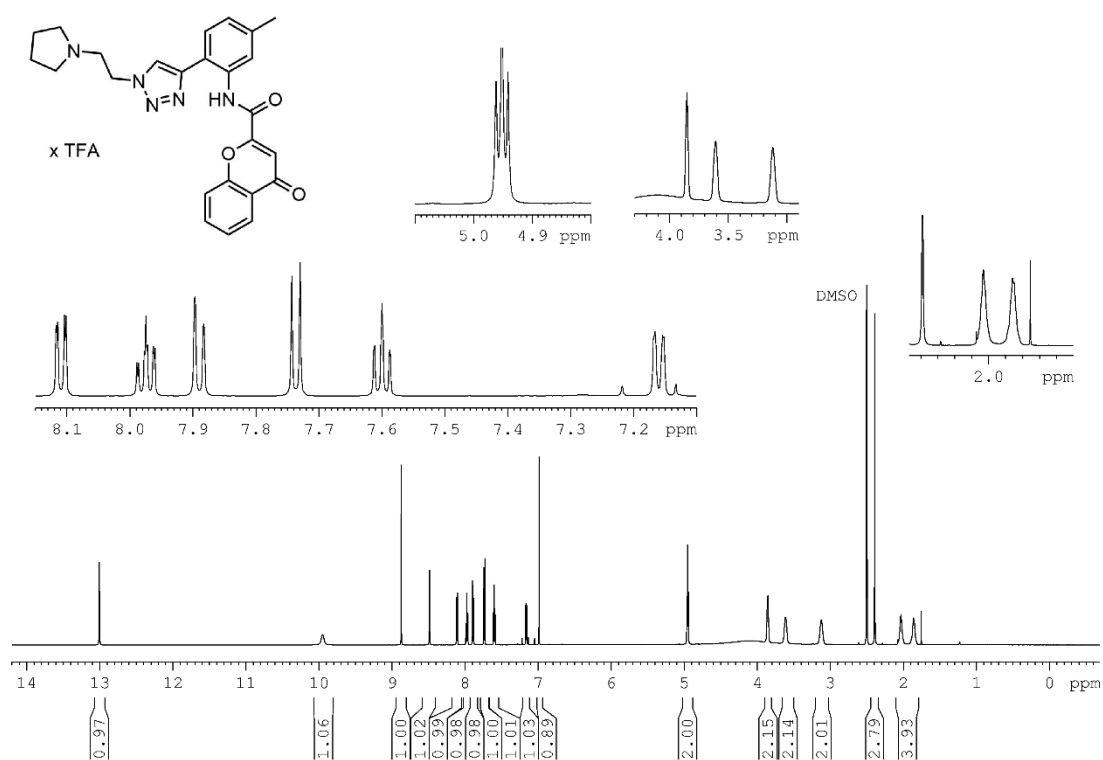


<sup>1</sup>H NMR spectrum (600 MHz, DMSO-*d*<sub>6</sub>) of compound **3.43**.

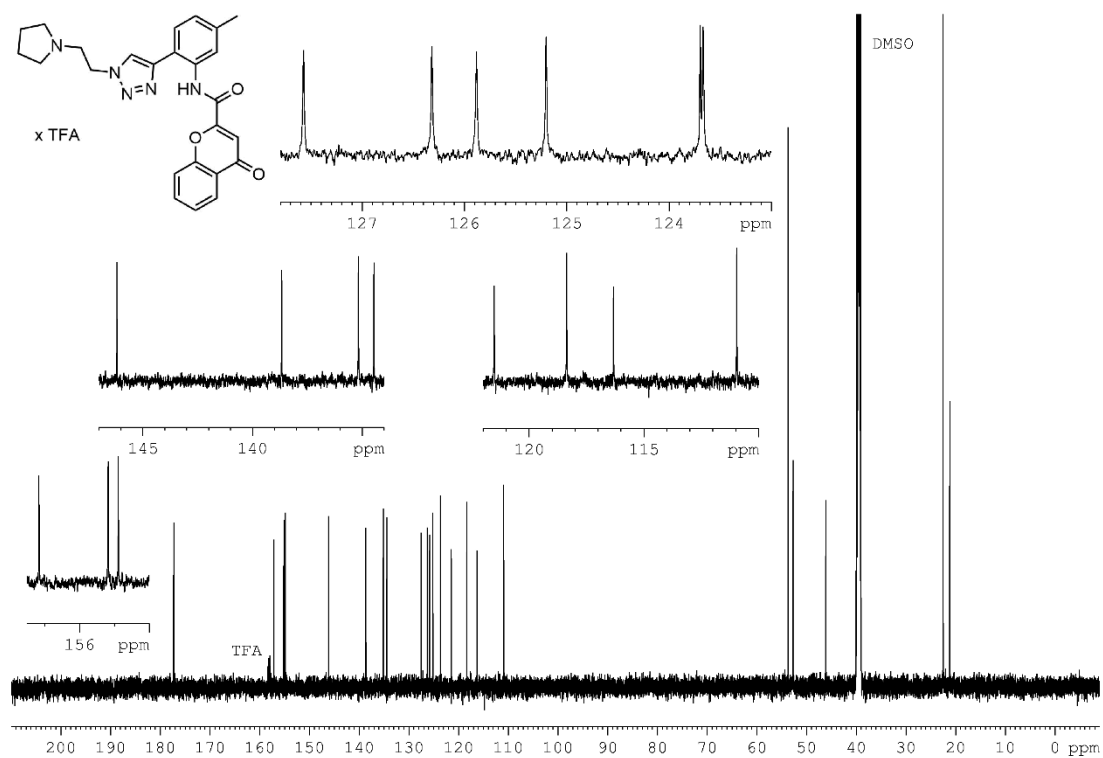


<sup>13</sup>C NMR spectrum (151 MHz, DMSO-*d*<sub>6</sub>) of compound **3.43**.

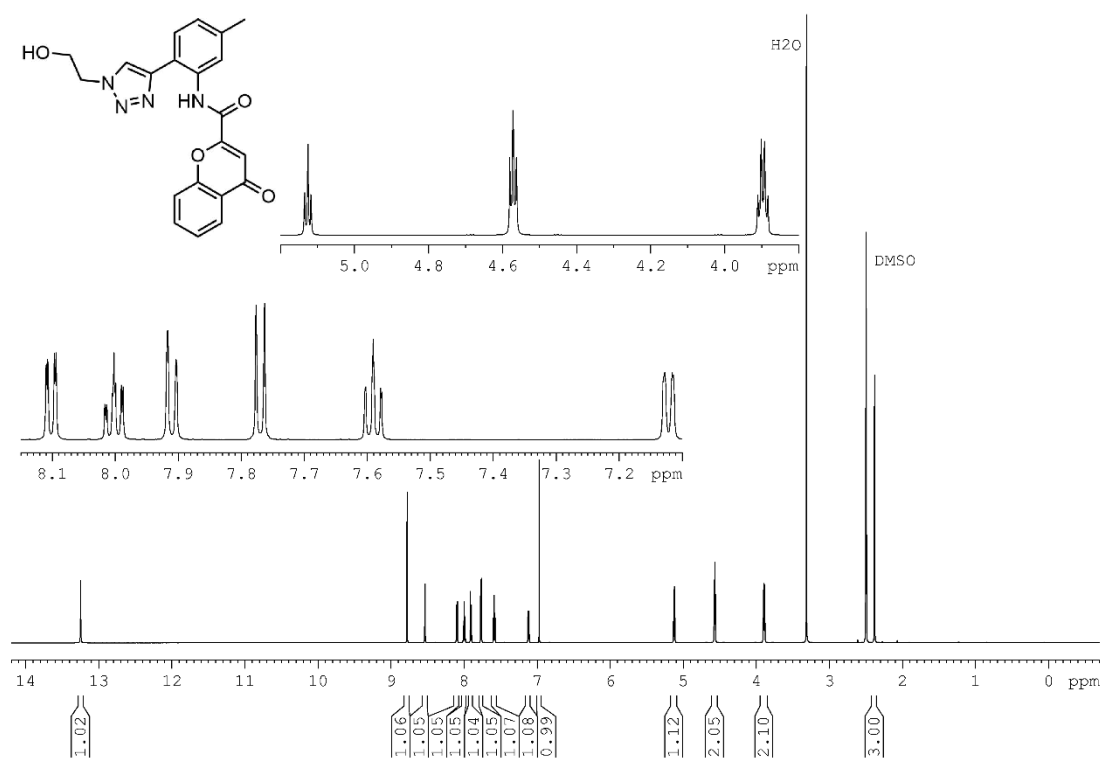




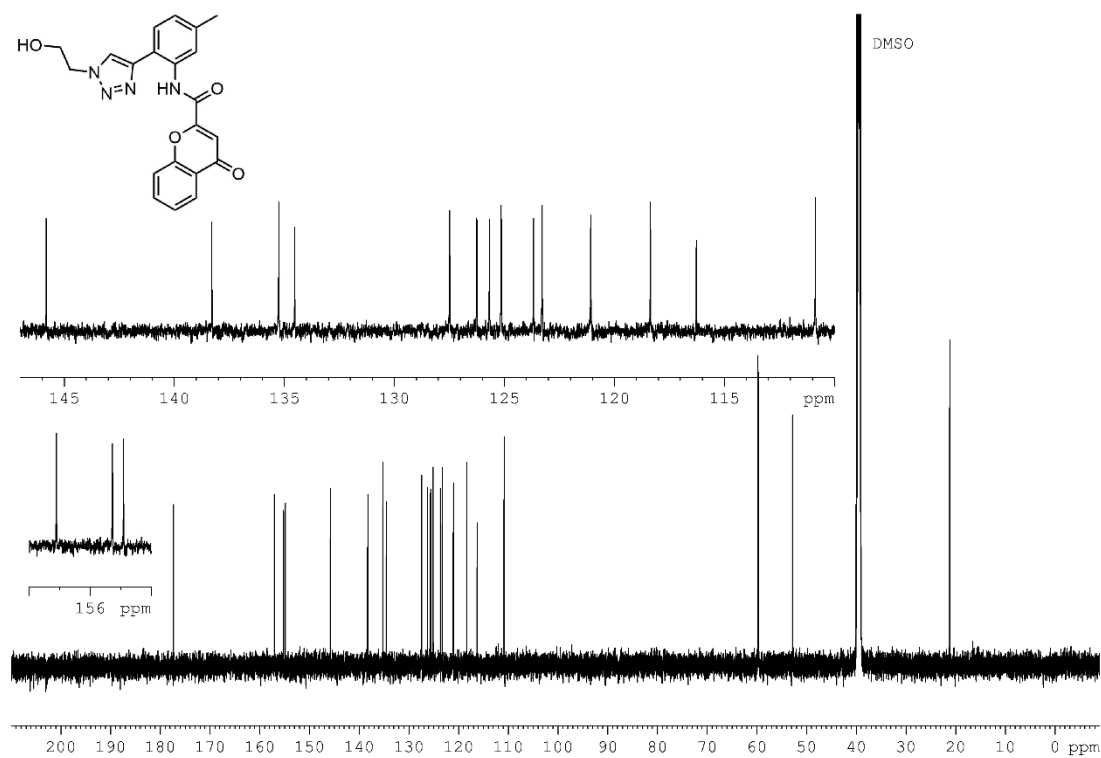
<sup>1</sup>H NMR spectrum (600 MHz, DMSO-*d*<sub>6</sub>) of compound **3.49**.



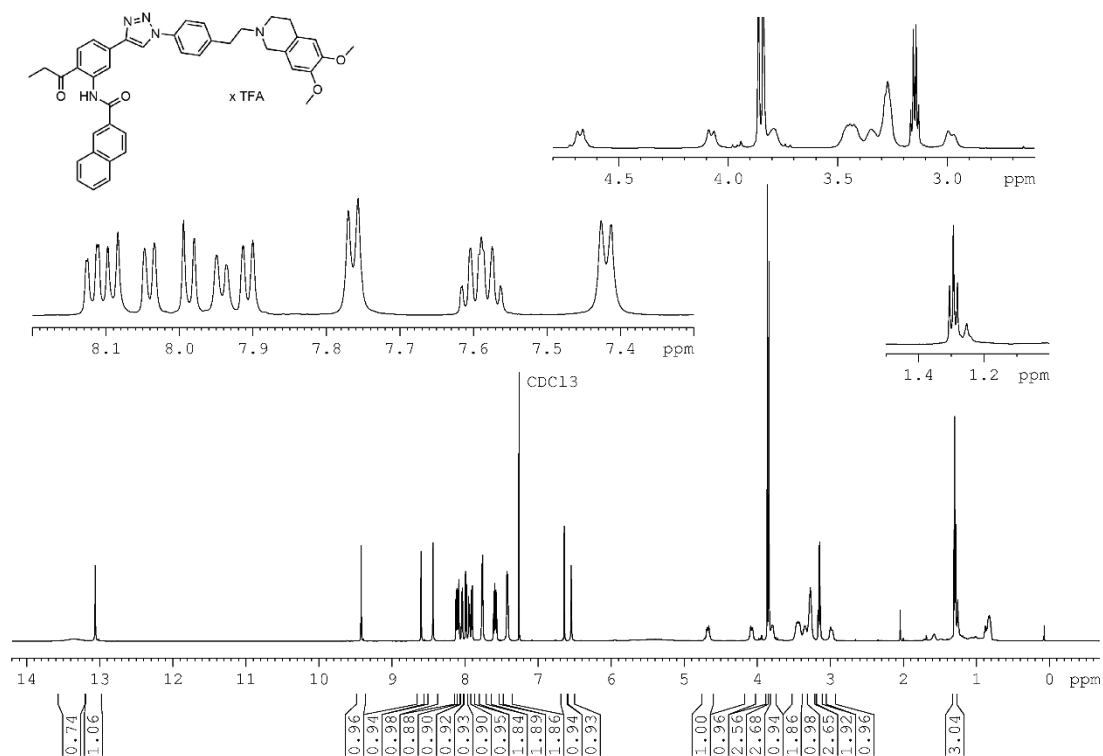
<sup>13</sup>C NMR spectrum (151 MHz, DMSO-*d*<sub>6</sub>) of compound **3.49**.



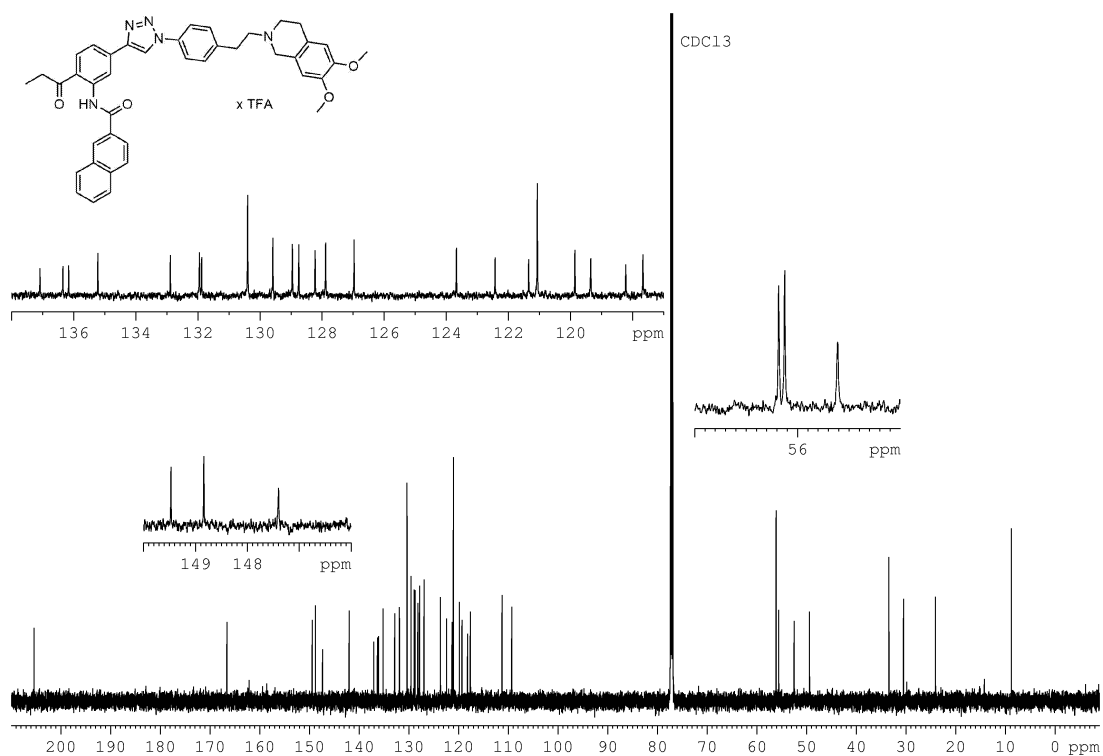
<sup>1</sup>H NMR spectrum (600 MHz, DMSO-*d*<sub>6</sub>) of compound **3.50**.



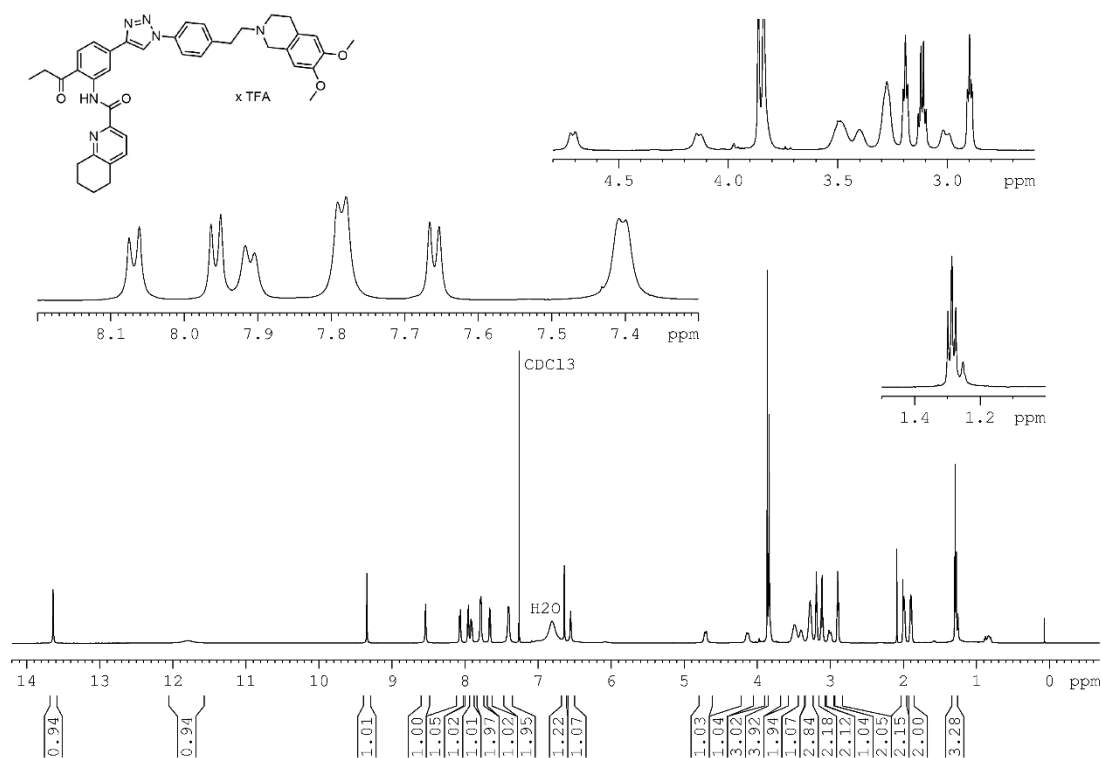
<sup>13</sup>C NMR spectrum (151 MHz, DMSO-*d*<sub>6</sub>) of compound **3.50**.



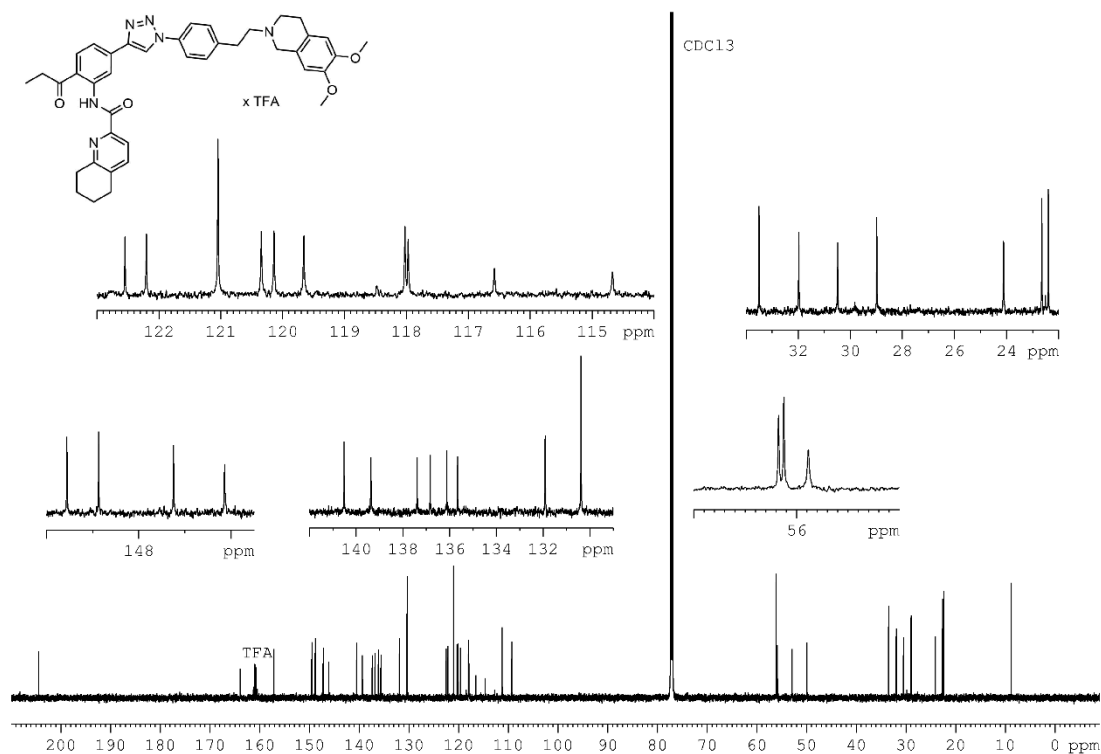
<sup>1</sup>H NMR spectrum (600 MHz, CDCl<sub>3</sub>) of compound **3.59**.



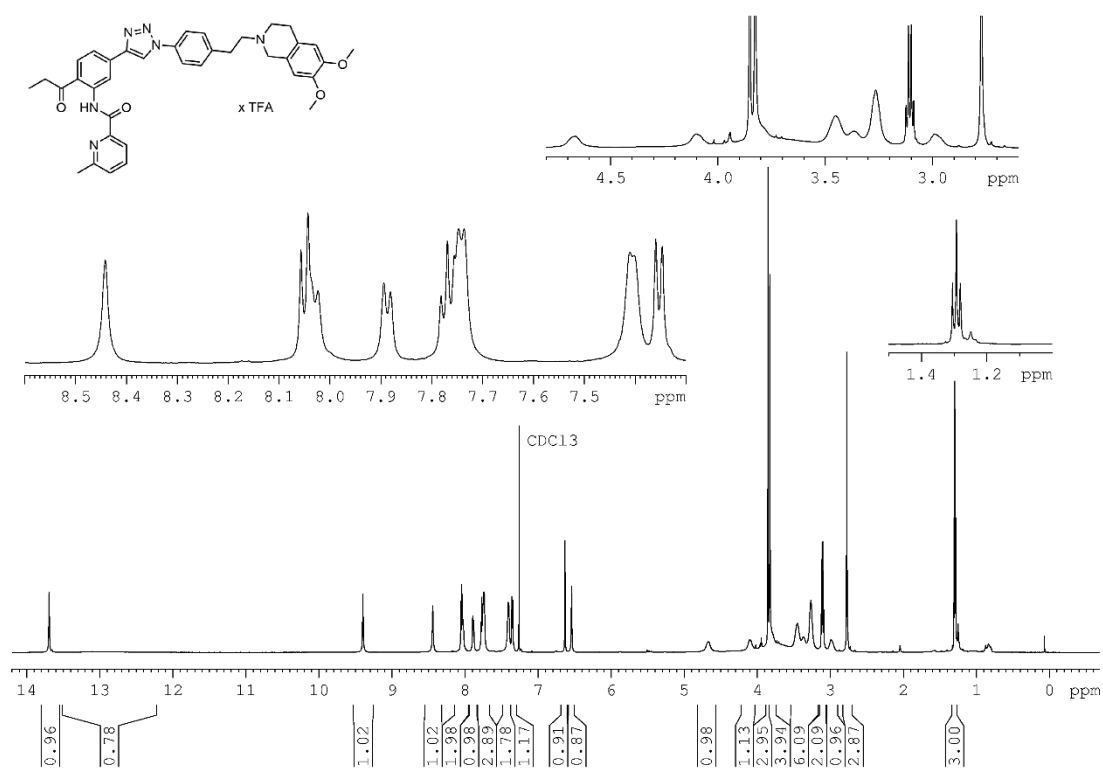
<sup>13</sup>C NMR spectrum (151 MHz, CDCl<sub>3</sub>) of compound **3.59**.



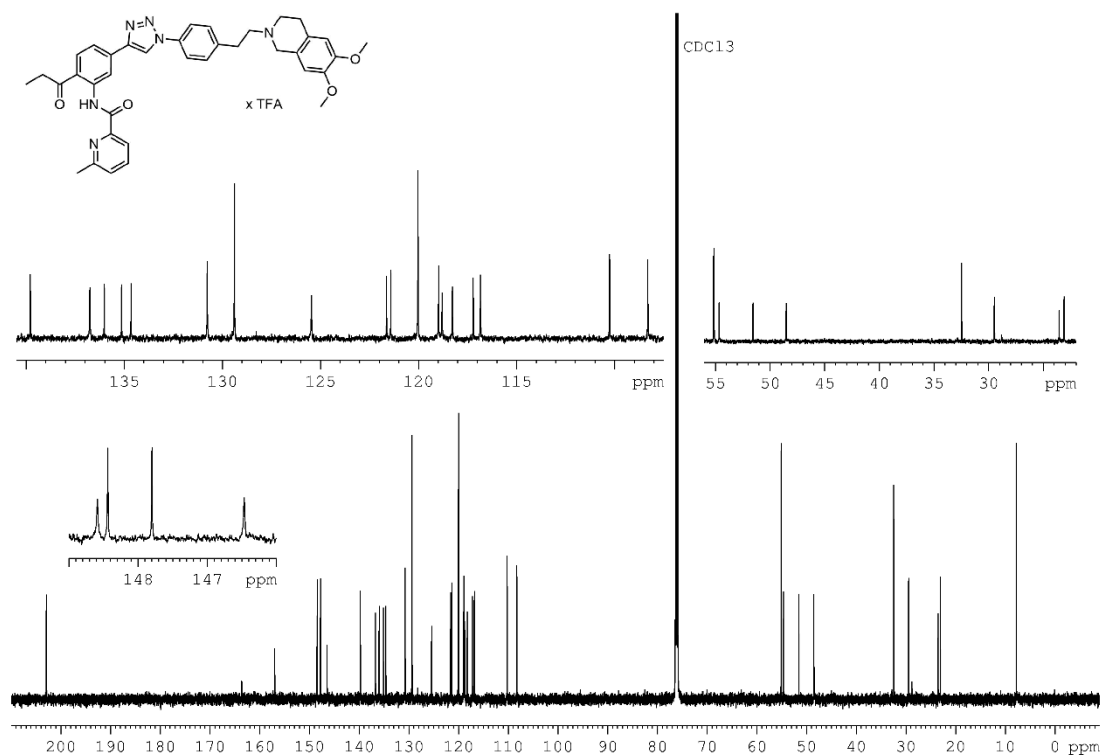
$^1\text{H}$  NMR spectrum (600 MHz,  $\text{CDCl}_3$ ) of compound **3.60**.



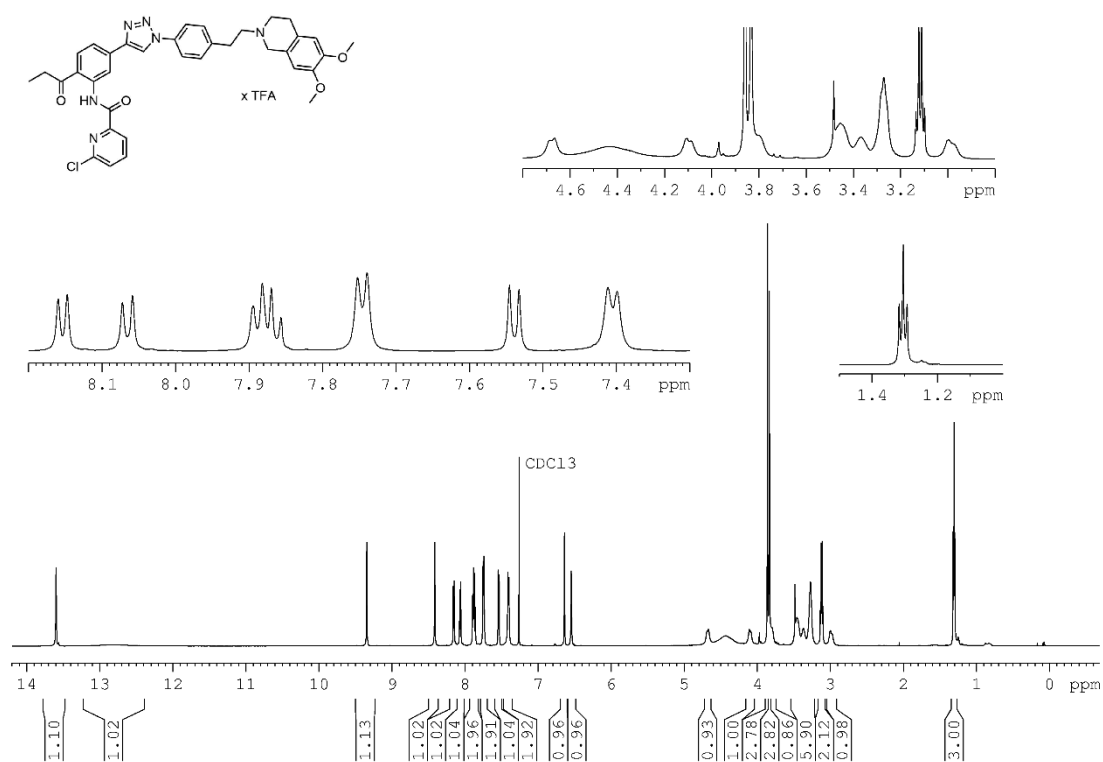
$^{13}\text{C}$  NMR spectrum (151 MHz,  $\text{CDCl}_3$ ) of compound **3.60**.



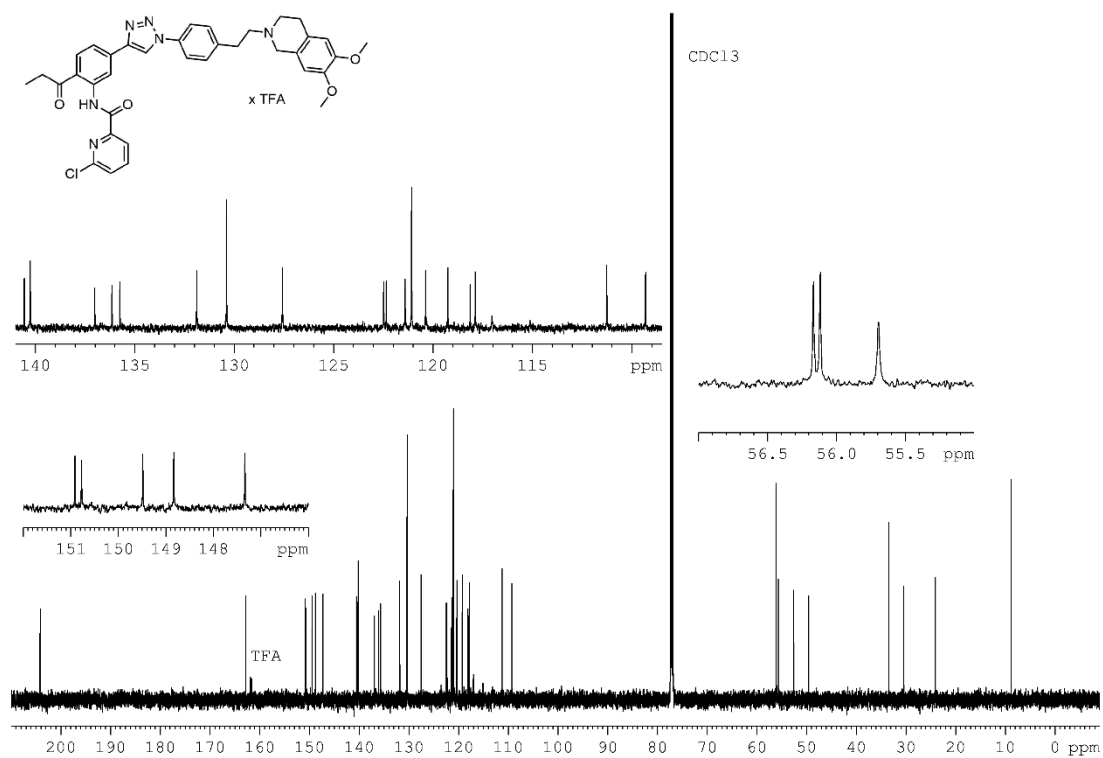
$^1\text{H}$  NMR spectrum (600 MHz,  $\text{CDCl}_3$ ) of compound **3.61**.



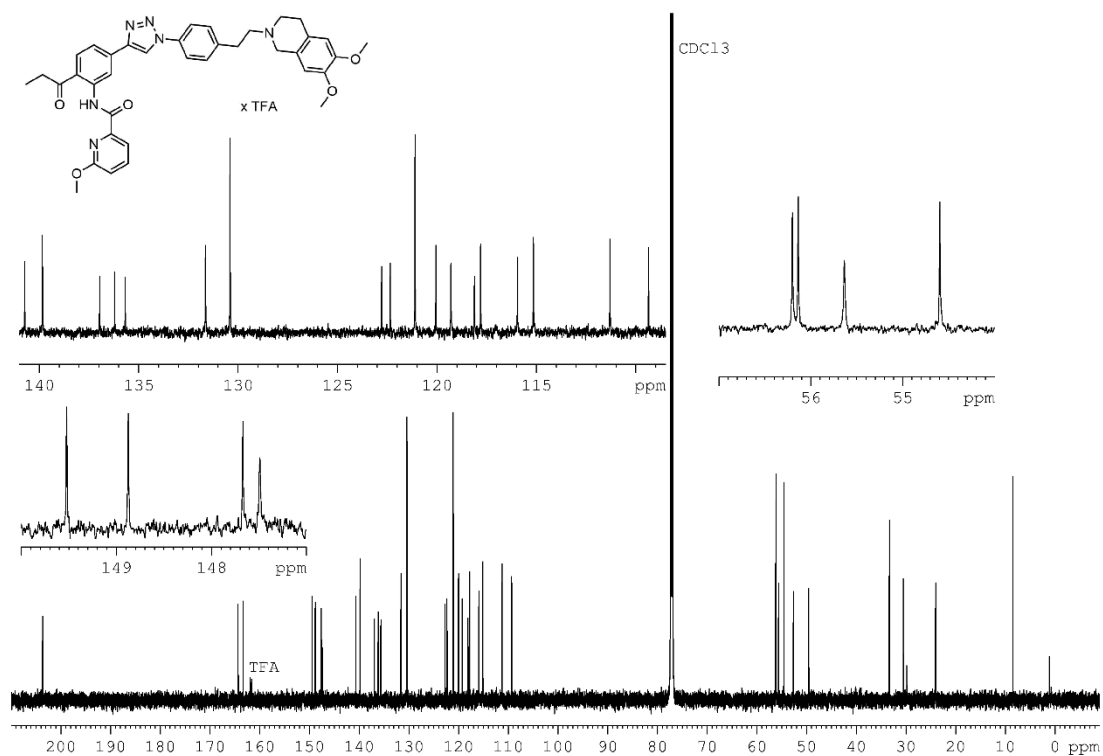
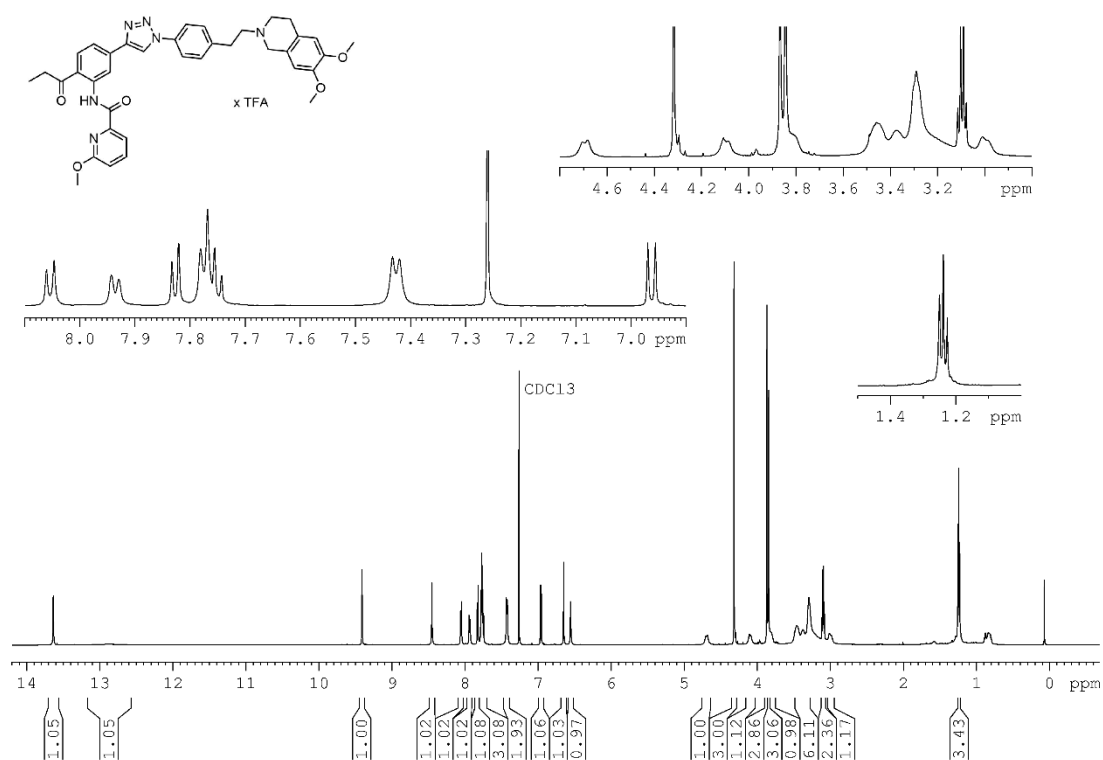
$^{13}\text{C}$  NMR spectrum (151 MHz,  $\text{CDCl}_3$ ) of compound **3.61**.

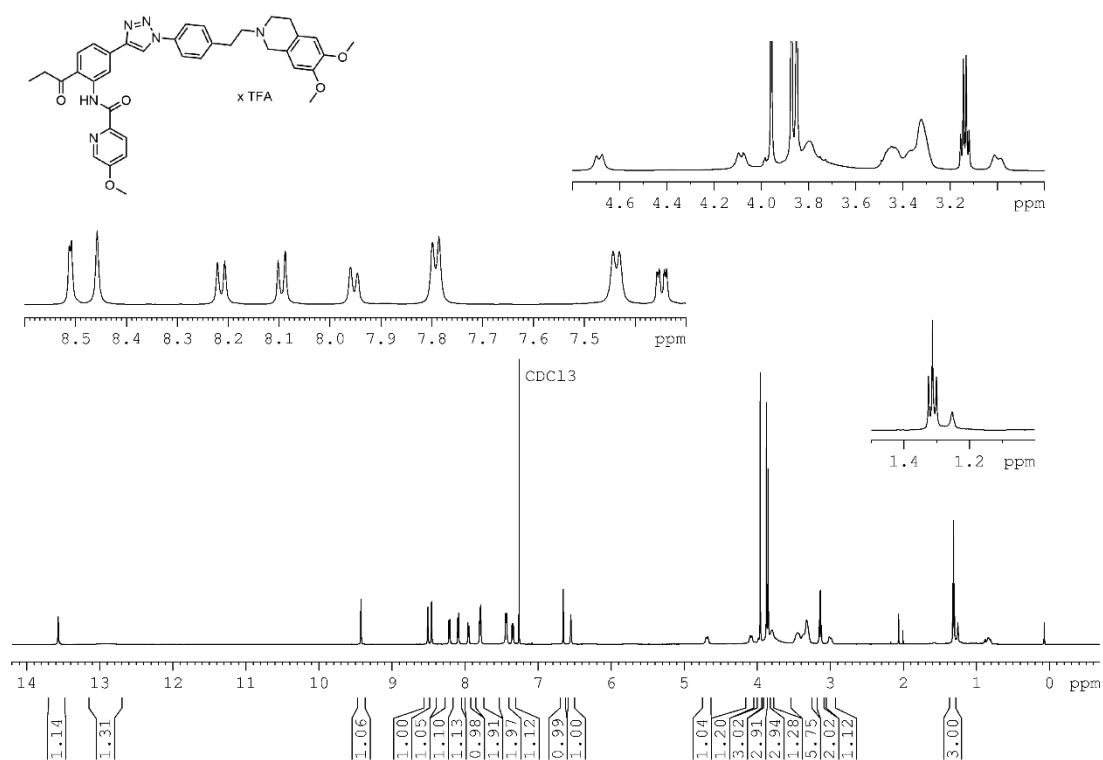


<sup>1</sup>H NMR spectrum (600 MHz, CDCl<sub>3</sub>) of compound **3.62**.

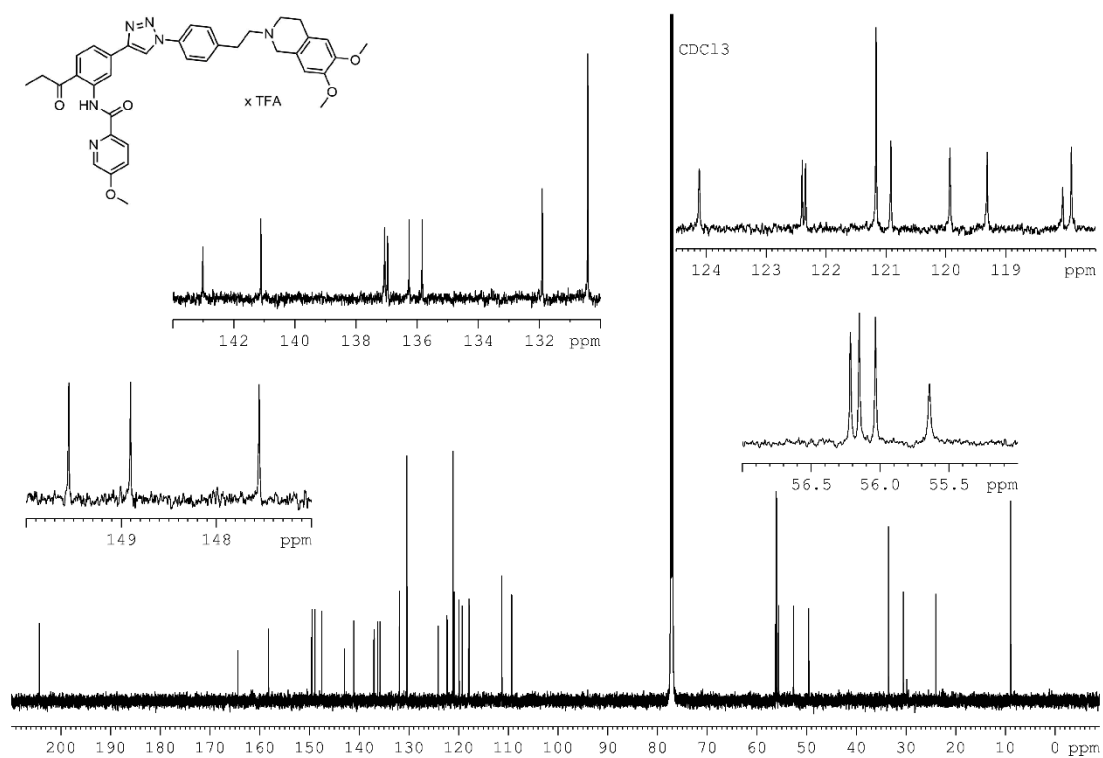


<sup>13</sup>C NMR spectrum (151 MHz, CDCl<sub>3</sub>) of compound **3.62**.

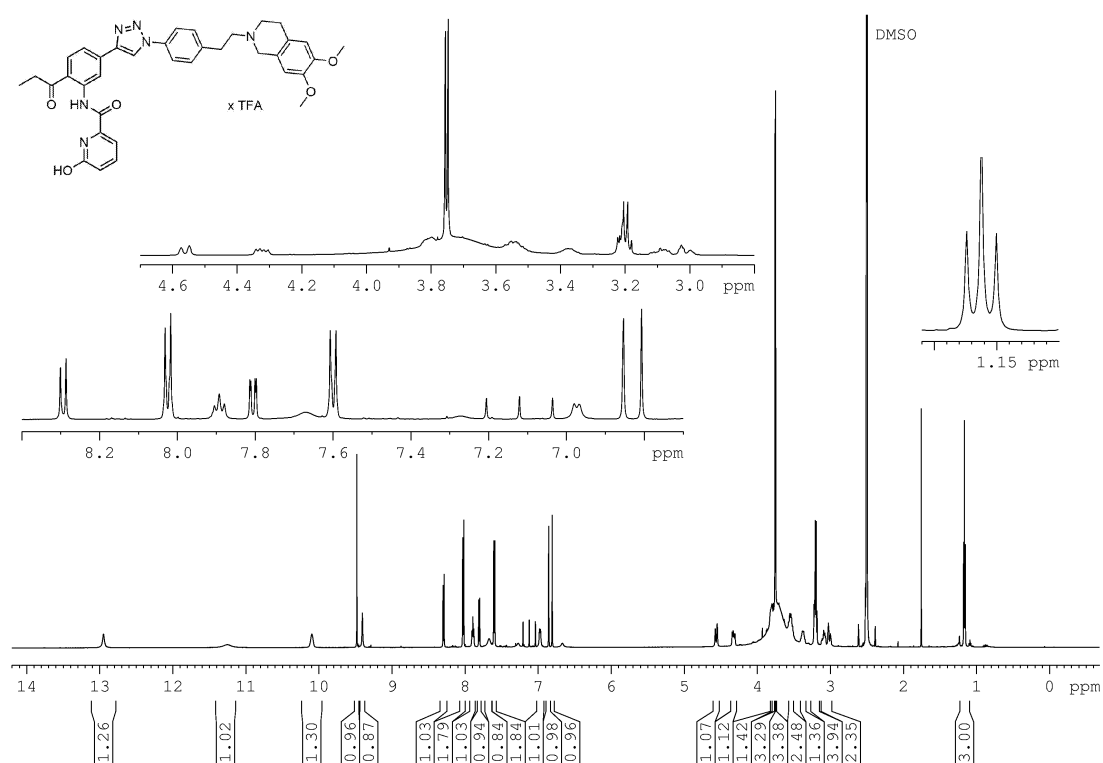




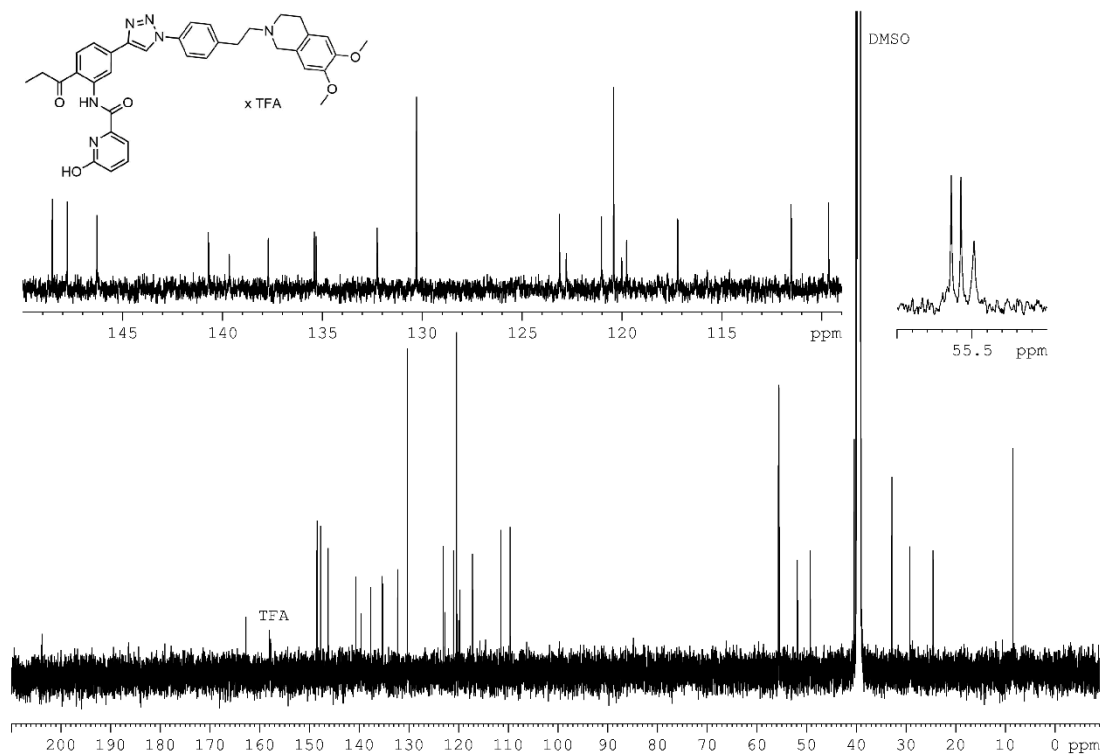
$^1\text{H}$  NMR spectrum (600 MHz,  $\text{CDCl}_3$ ) of compound **3.64**.



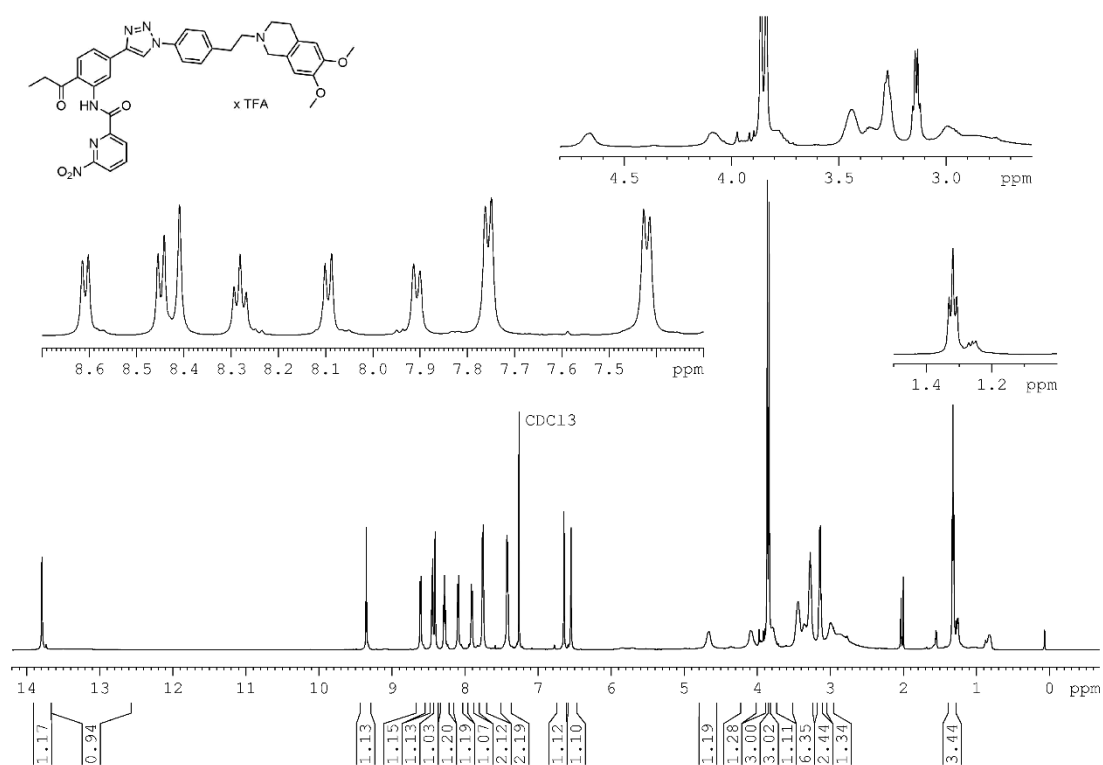
$^{13}\text{C}$  NMR spectrum (151 MHz,  $\text{CDCl}_3$ ) of compound **3.64**.



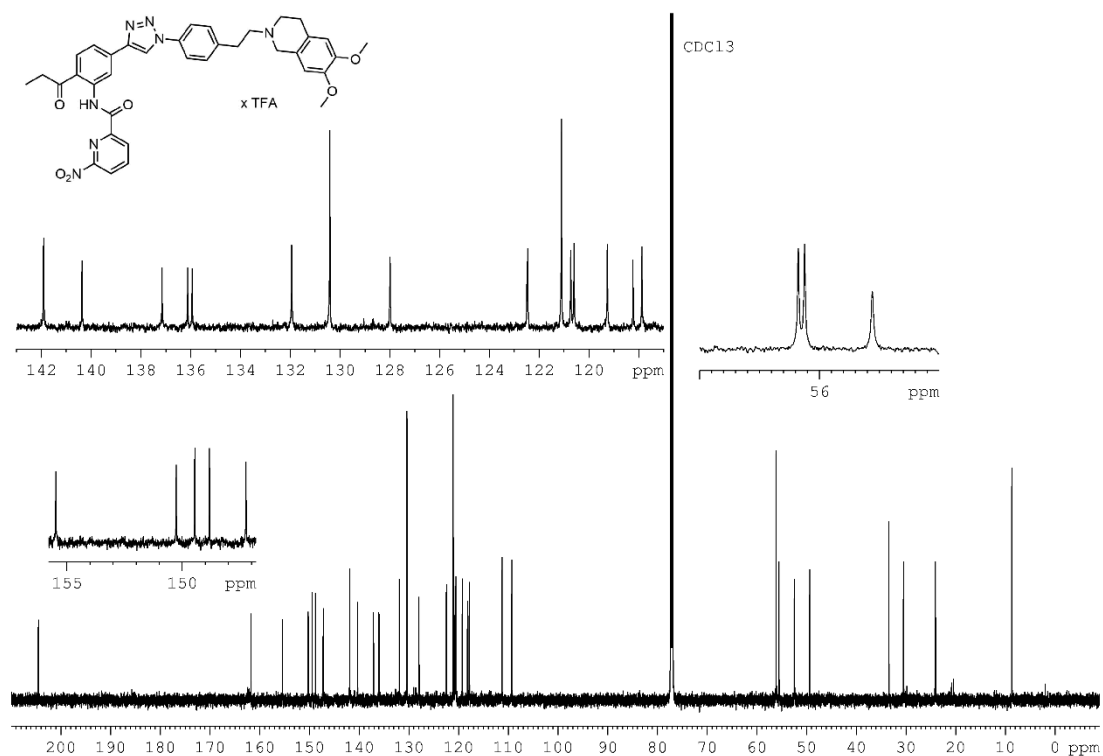
<sup>1</sup>H NMR spectrum (600 MHz, DMSO-*d*<sub>6</sub>) of compound **3.65**.



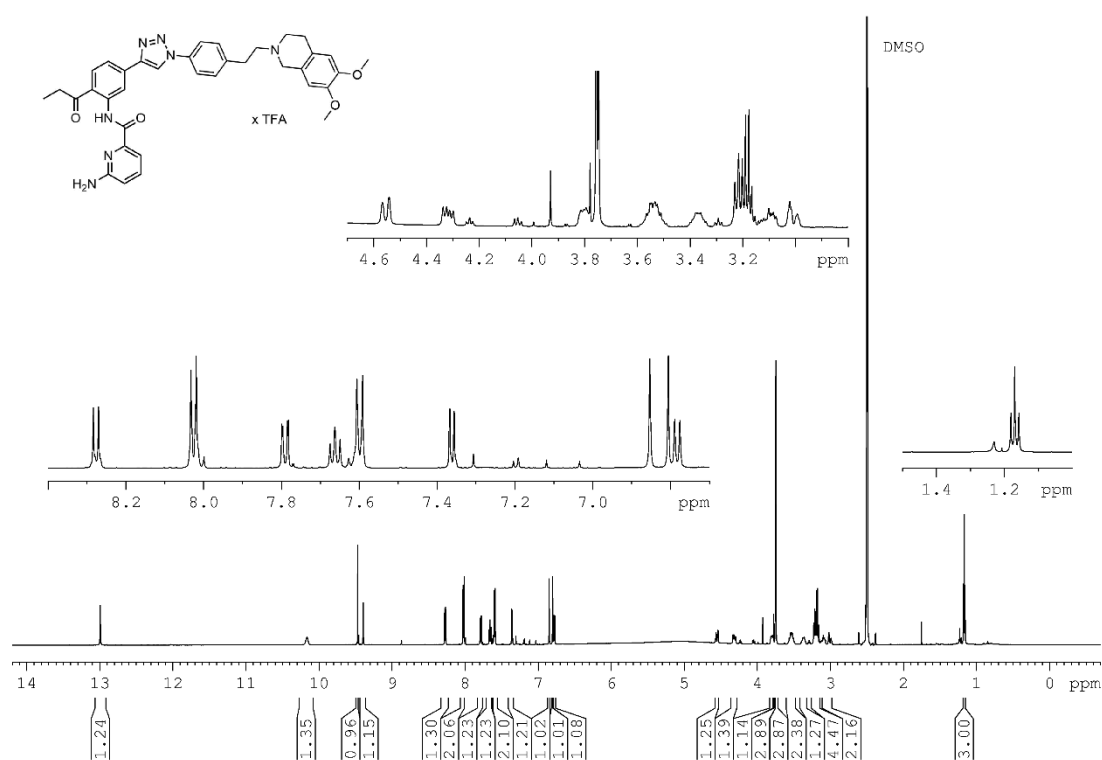
<sup>13</sup>C NMR spectrum (151 MHz, DMSO-*d*<sub>6</sub>) of compound **3.65**.



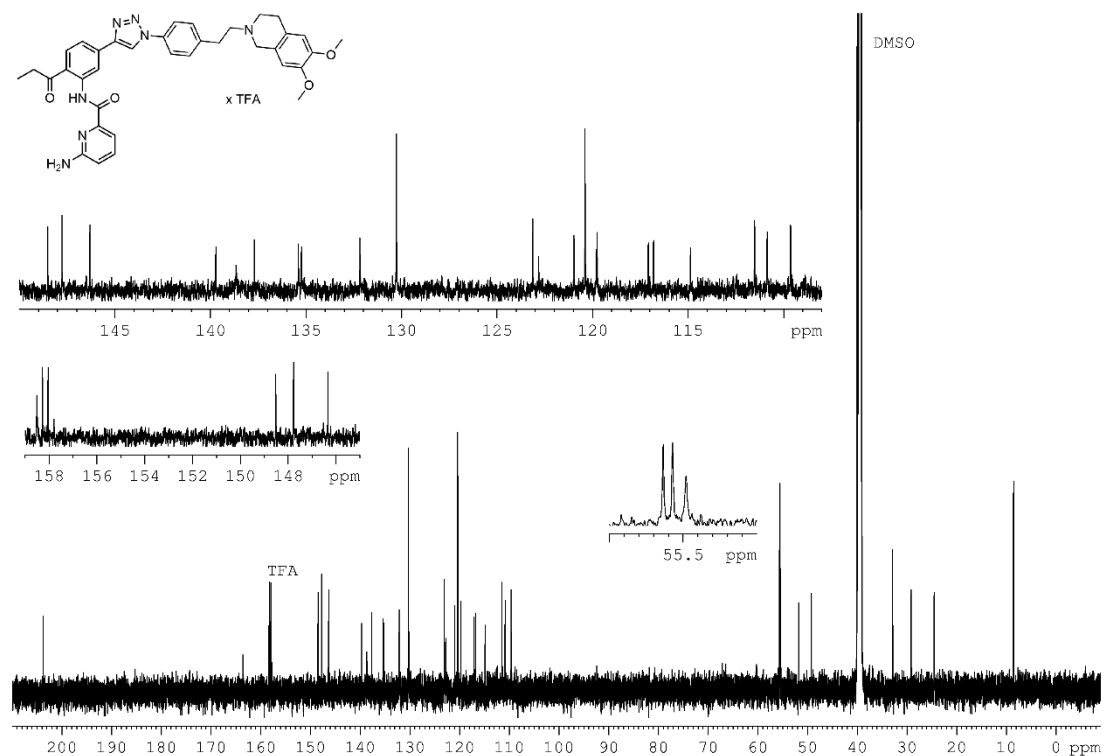
<sup>1</sup>H NMR spectrum (600 MHz, CDCl<sub>3</sub>) of compound **3.66**.



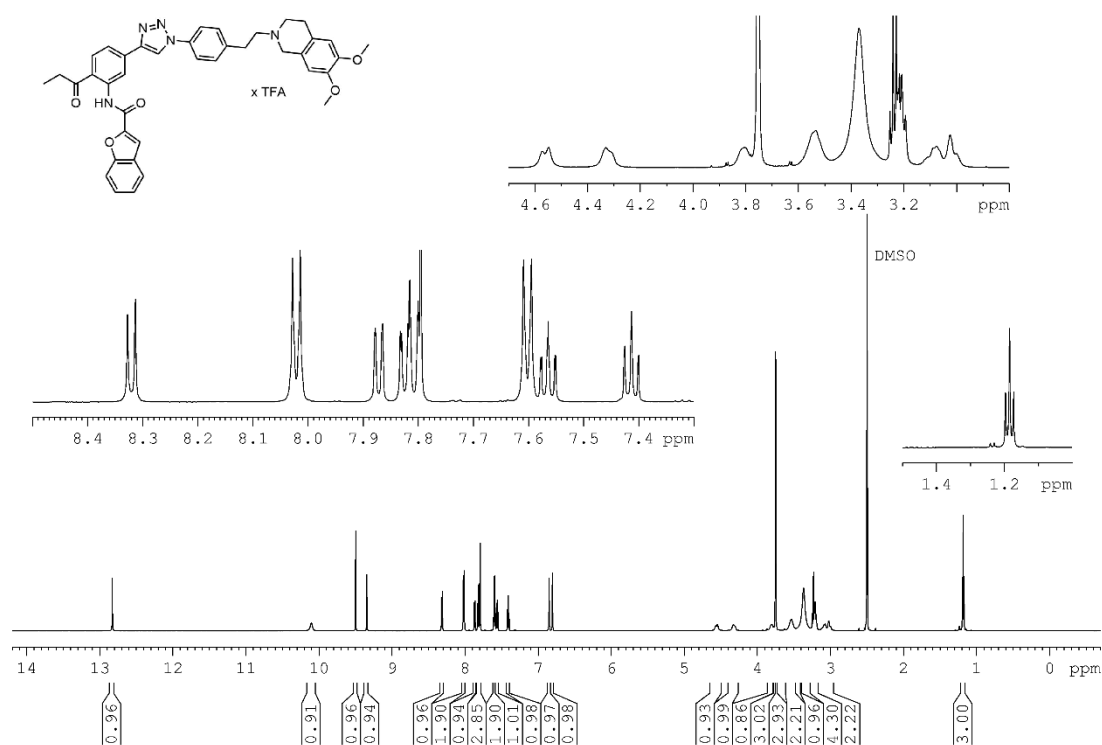
<sup>13</sup>C NMR spectrum (151 MHz, CDCl<sub>3</sub>) of compound **3.66**.



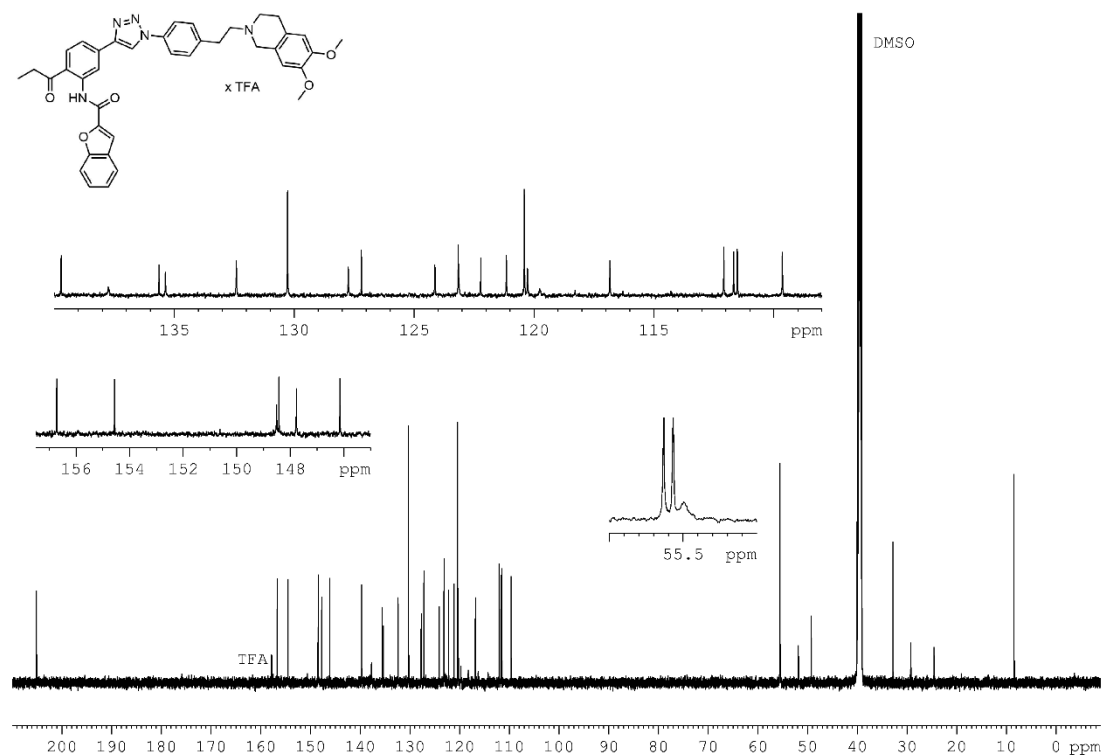
<sup>1</sup>H NMR spectrum (600 MHz, DMSO-*d*<sub>6</sub>) of compound **3.67**.



<sup>13</sup>C NMR spectrum (151 MHz, DMSO-*d*<sub>6</sub>) of compound **3.67**.

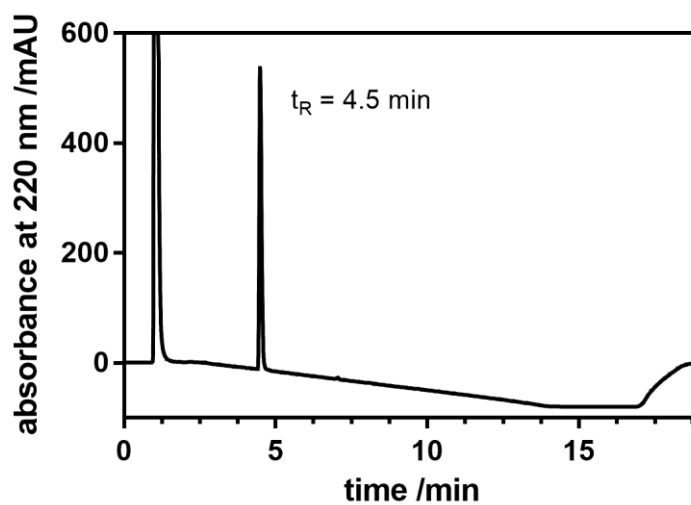


<sup>1</sup>H NMR spectrum (600 MHz, DMSO-*d*<sub>6</sub>) of compound **3.68**.

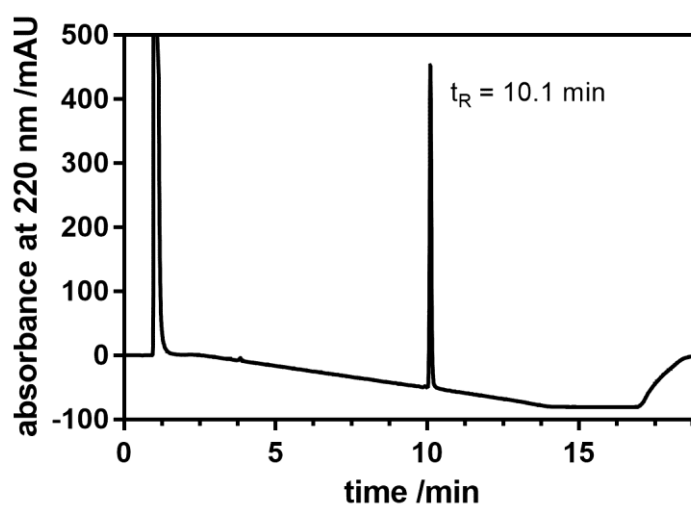


<sup>13</sup>C NMR spectrum (151 MHz, DMSO-*d*<sub>6</sub>) of compound **3.68**.

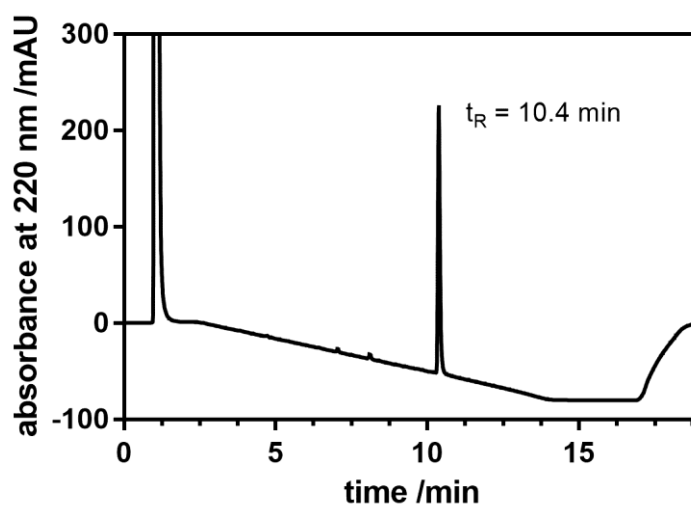
### 3.5.3 Chromatograms (Purity Control)



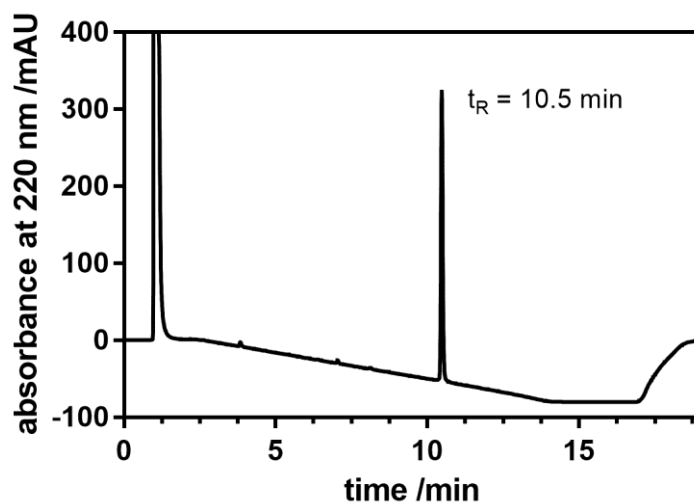
Chromatogram (purity control) of **3.03** (RP-HPLC).



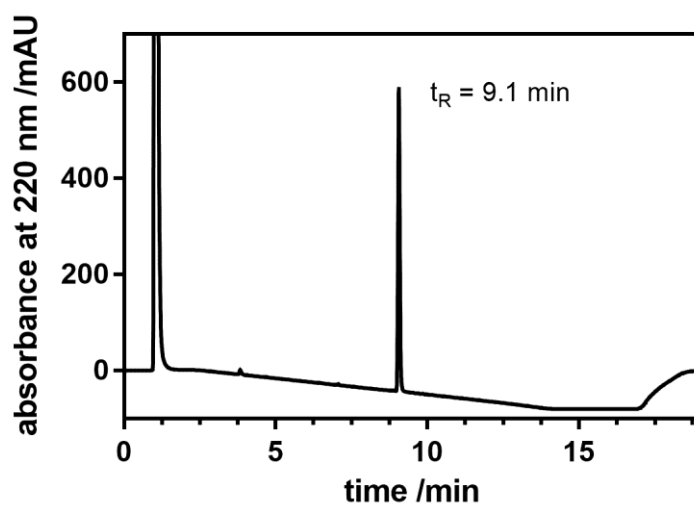
Chromatogram (purity control) of **3.04** (RP-HPLC).



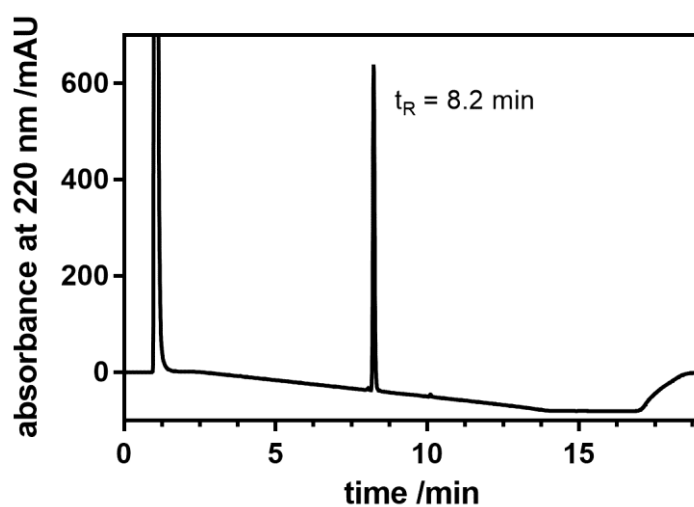
Chromatogram (purity control) of **3.12** (RP-HPLC).



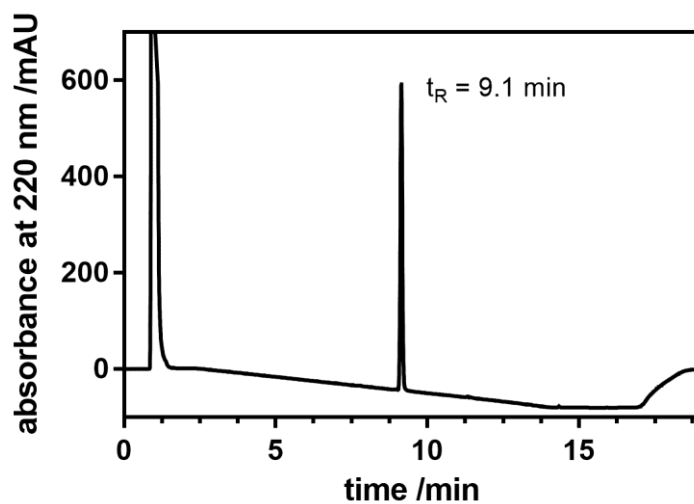
Chromatogram (purity control) of **3.13** (RP-HPLC).



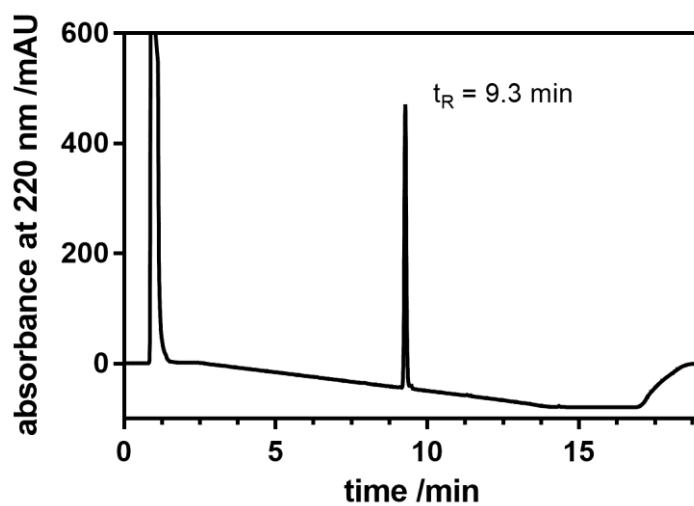
Chromatogram (purity control) of **3.14** (RP-HPLC).



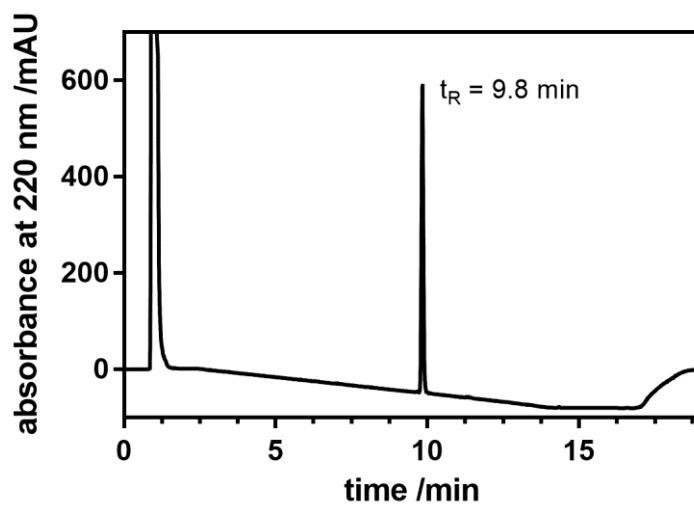
Chromatogram (purity control) of **3.15** (RP-HPLC).



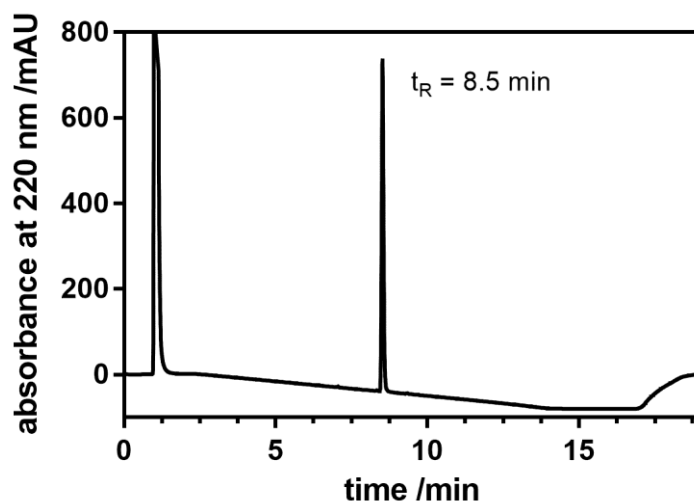
Chromatogram (purity control) of **3.16** (RP-HPLC).



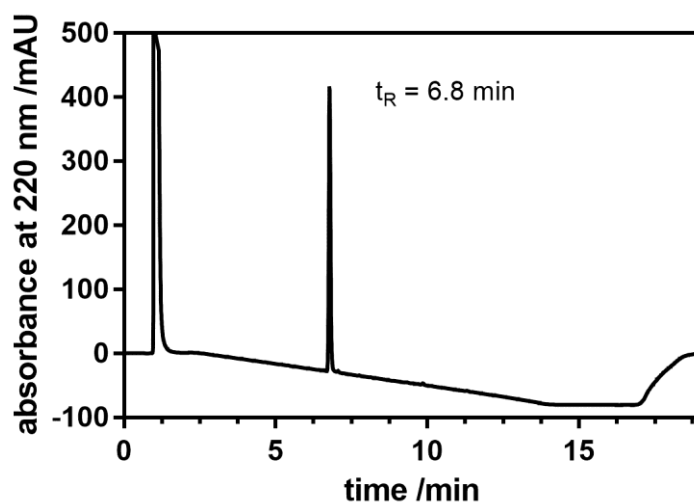
Chromatogram (purity control) of **3.17** (RP-HPLC).



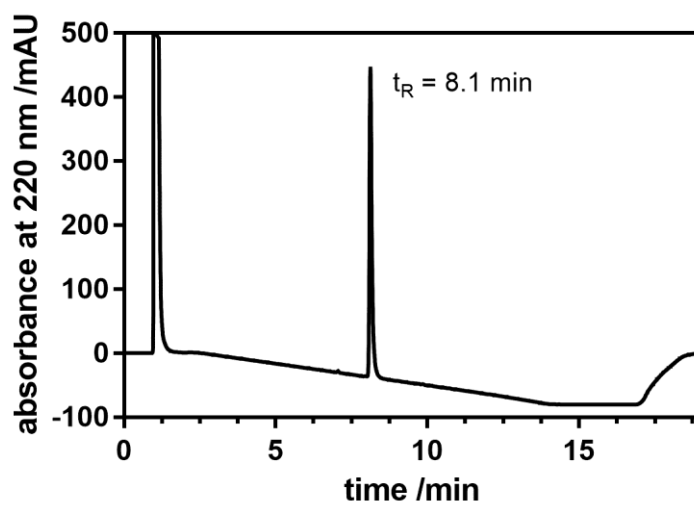
Chromatogram (purity control) of **3.18** (RP-HPLC).



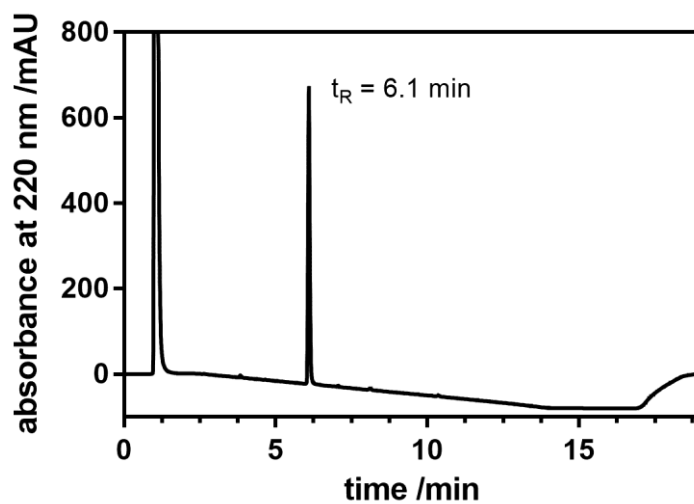
Chromatogram (purity control) of **3.19** (RP-HPLC).



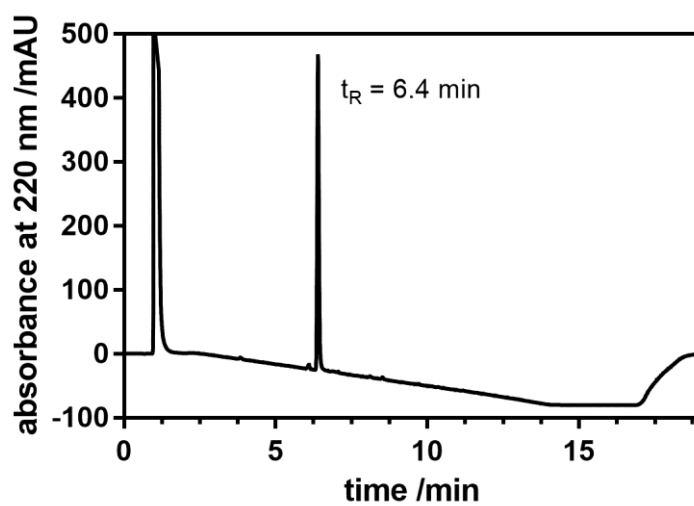
Chromatogram (purity control) of **3.20** (RP-HPLC).



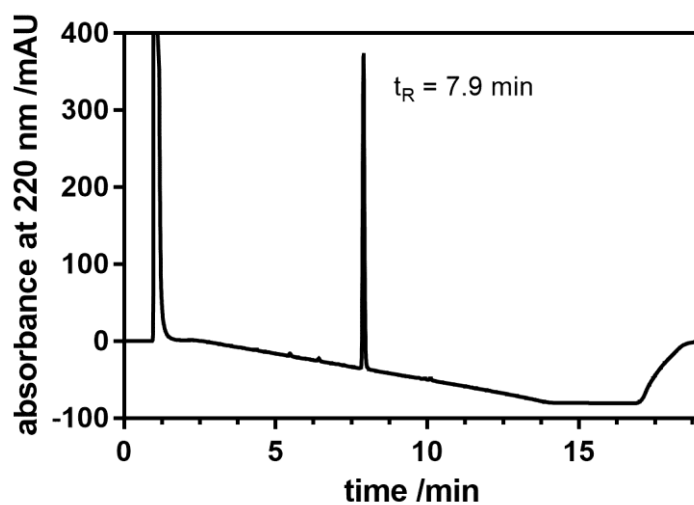
Chromatogram (purity control) of **3.21** (RP-HPLC).



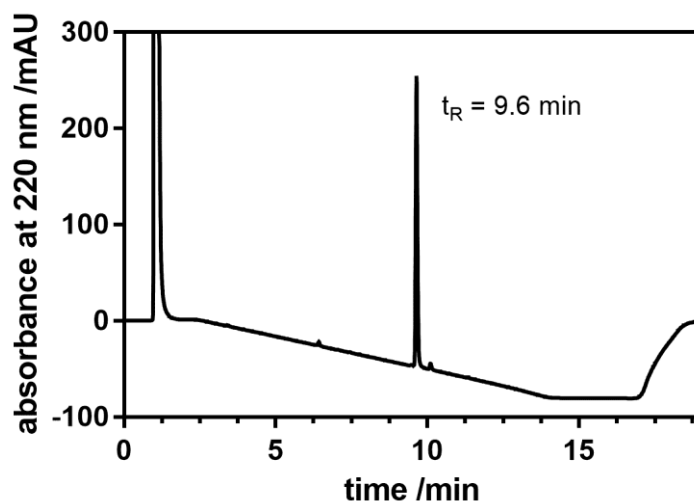
Chromatogram (purity control) of **3.22** (RP-HPLC).



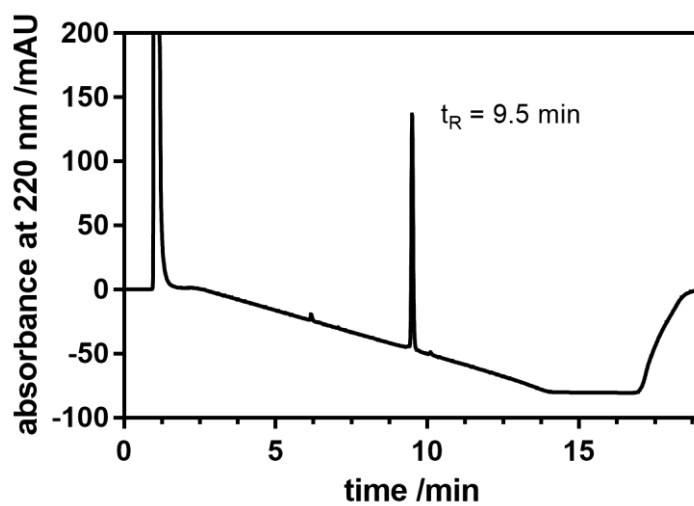
Chromatogram (purity control) of **3.23** (RP-HPLC).



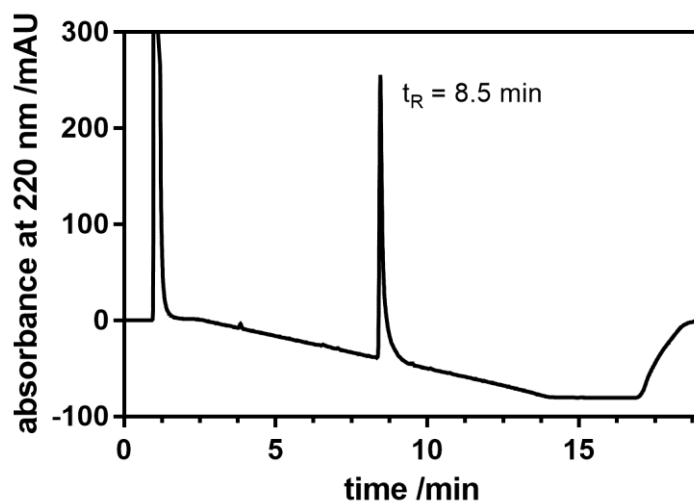
Chromatogram (purity control) of **3.24** (RP-HPLC).



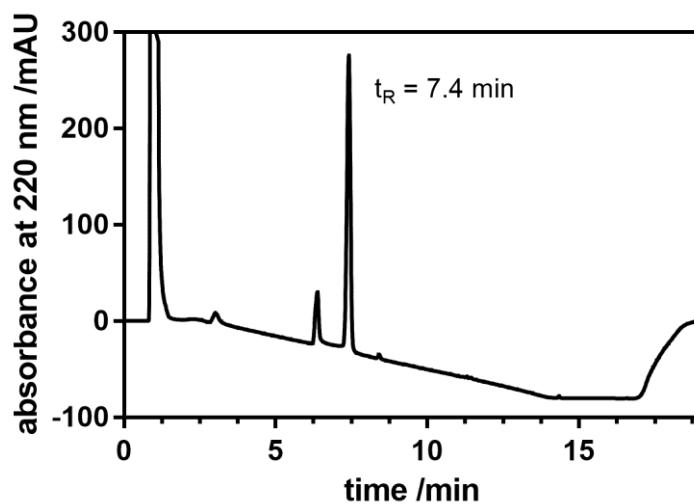
Chromatogram (purity control) of **3.25** (RP-HPLC).



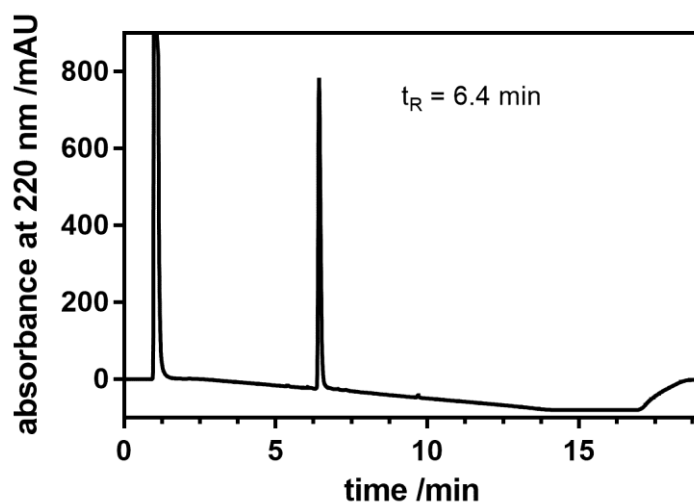
Chromatogram (purity control) of **3.26** (RP-HPLC).



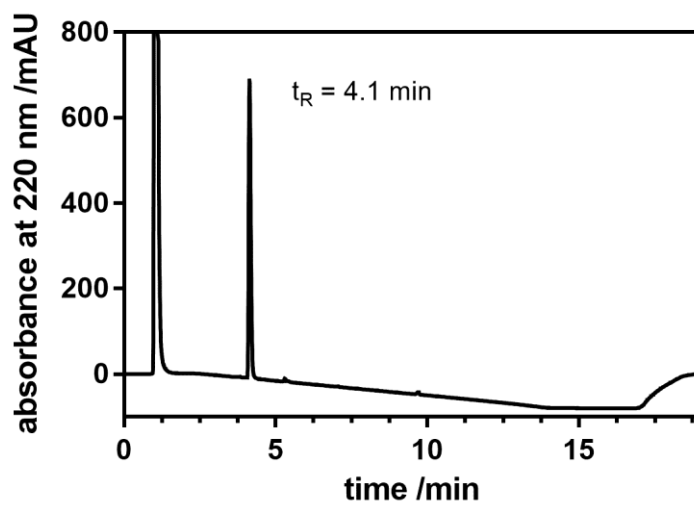
Chromatogram (purity control) of **3.27** (RP-HPLC).



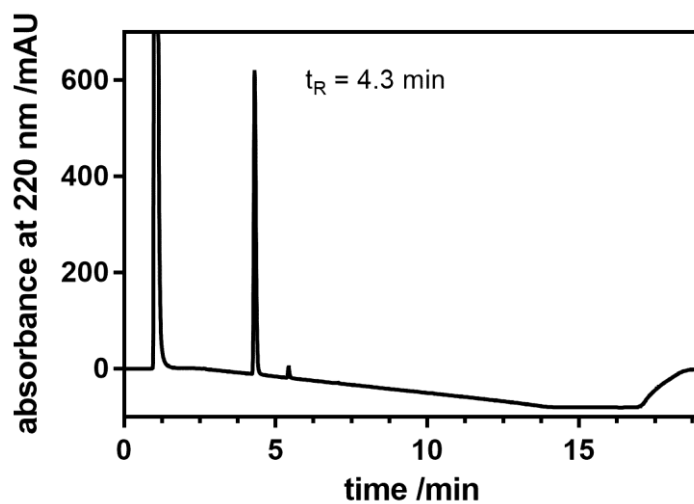
Chromatogram (purity control) of **3.28** (RP-HPLC).



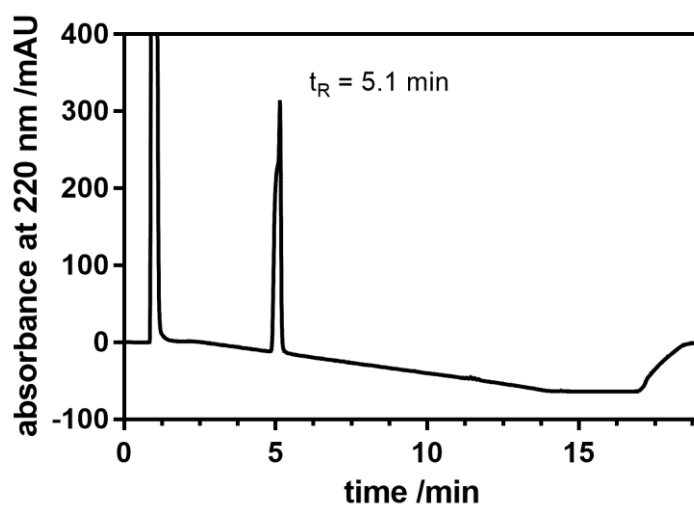
Chromatogram (purity control) of **3.39** (RP-HPLC).



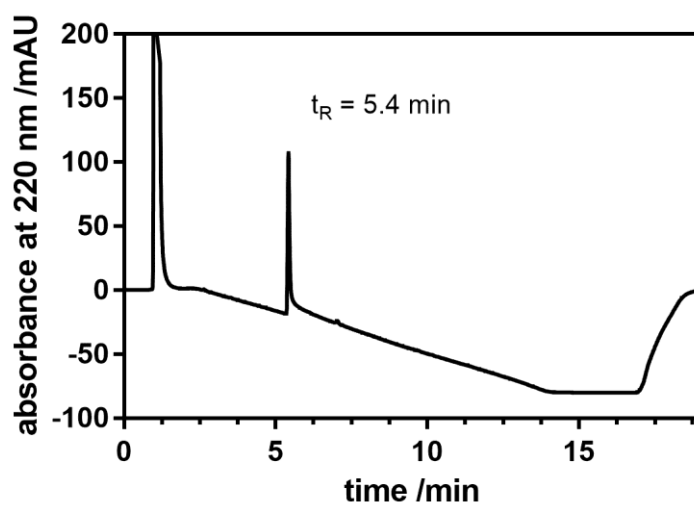
Chromatogram (purity control) of **3.40** (RP-HPLC).



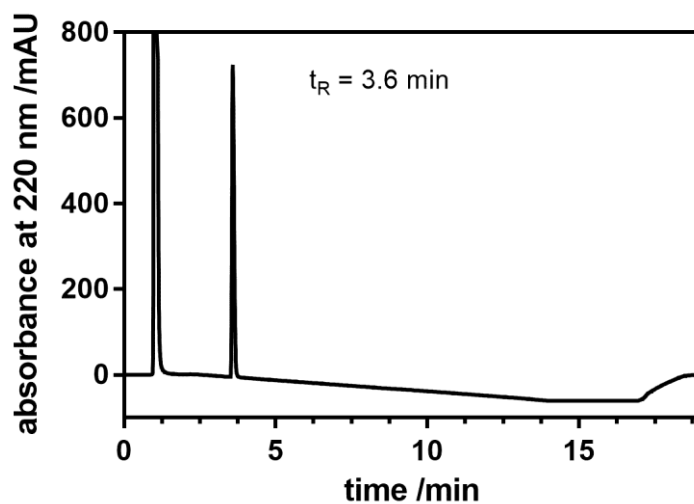
Chromatogram (purity control) of **3.41** (RP-HPLC).



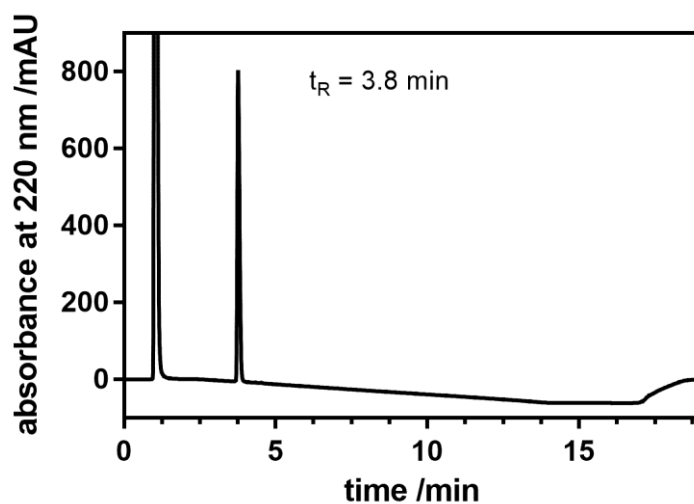
Chromatogram (purity control) of **3.42** (RP-HPLC).



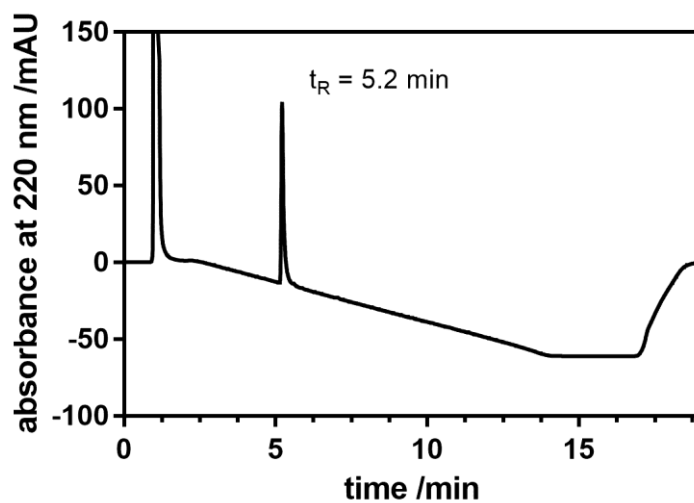
Chromatogram (purity control) of **3.43** (RP-HPLC).



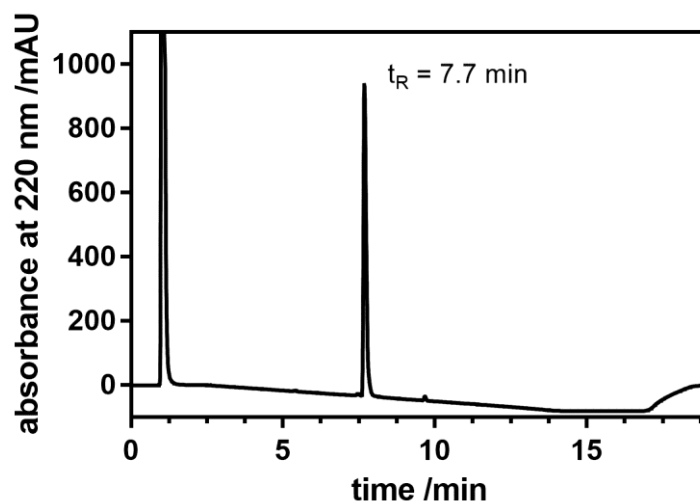
Chromatogram (purity control) of **3.44** (RP-HPLC).



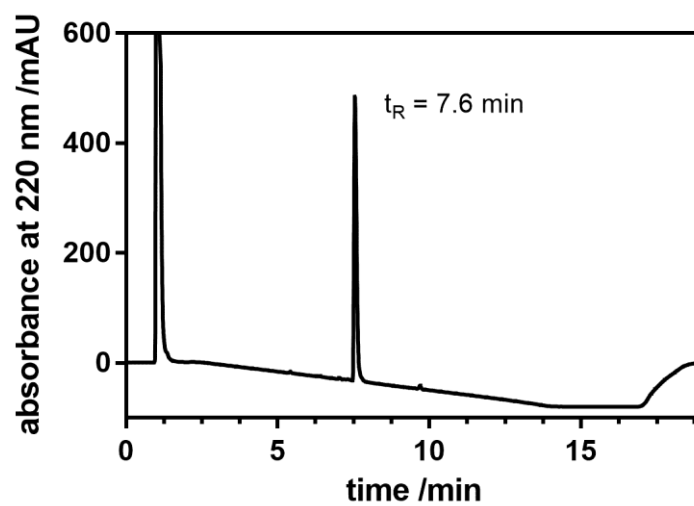
Chromatogram (purity control) of **3.49** (RP-HPLC).



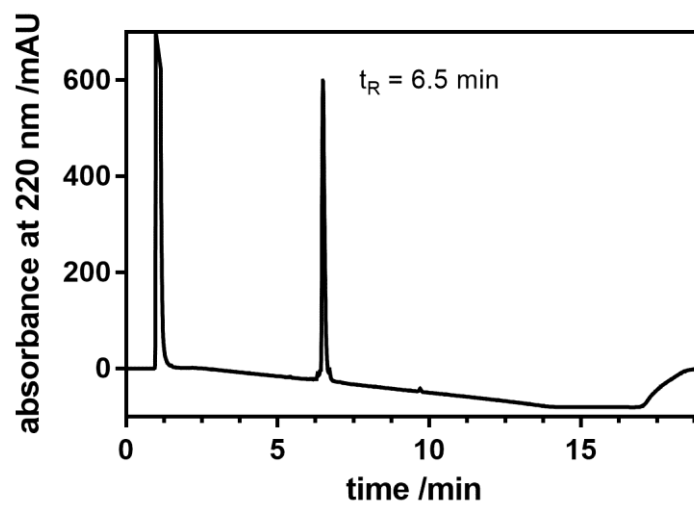
Chromatogram (purity control) of **3.50** (RP-HPLC).



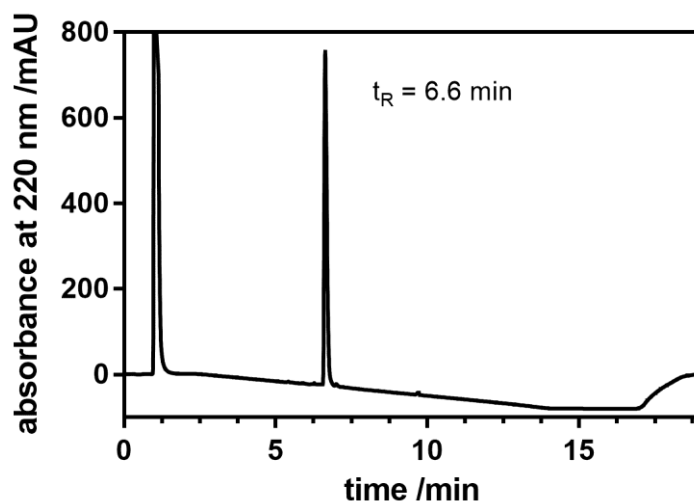
Chromatogram (purity control) of **3.59** (RP-HPLC).



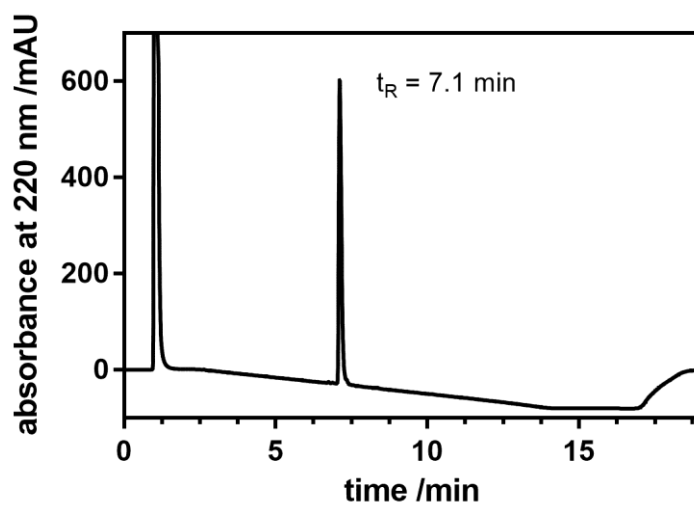
Chromatogram (purity control) of **3.60** (RP-HPLC).



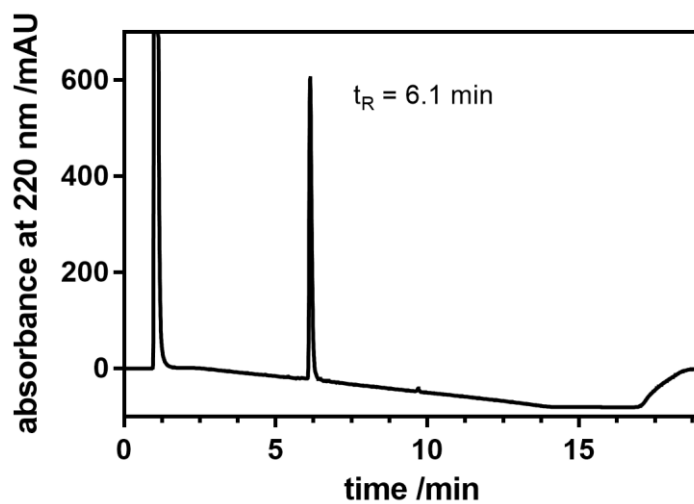
Chromatogram (purity control) of **3.61** (RP-HPLC).



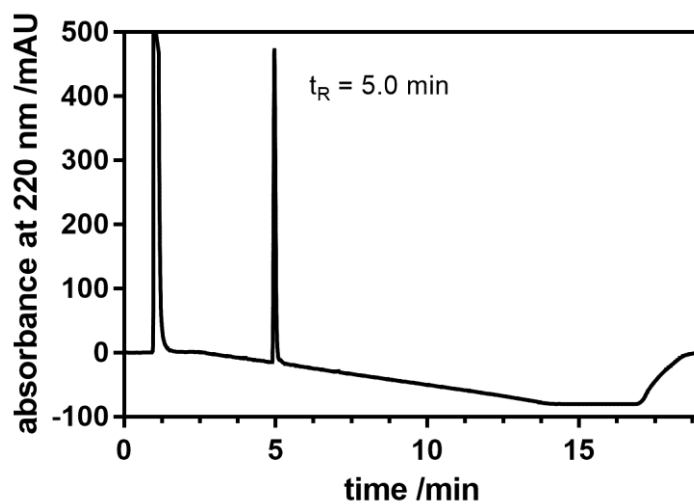
Chromatogram (purity control) of **3.62** (RP-HPLC).



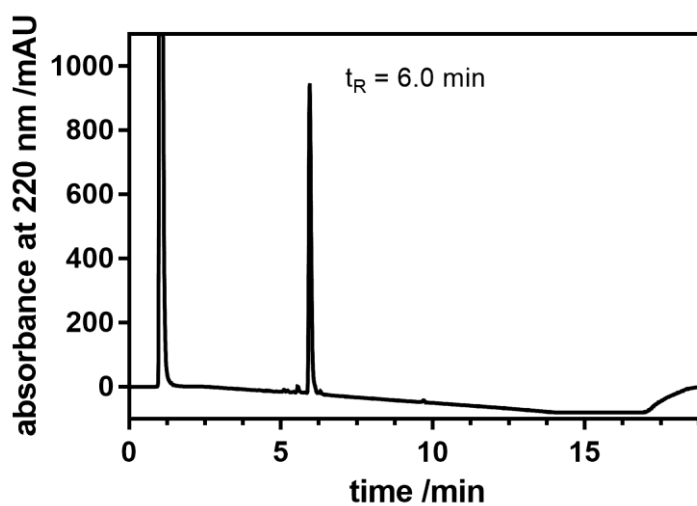
Chromatogram (purity control) of **3.63** (RP-HPLC).



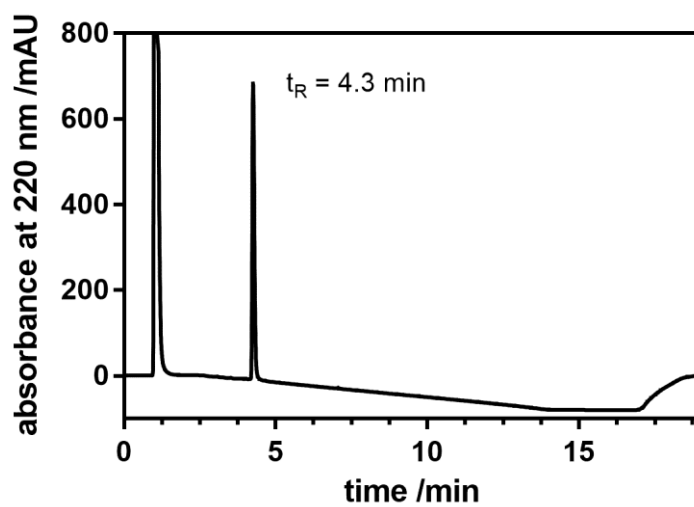
Chromatogram (purity control) of **3.64** (RP-HPLC).



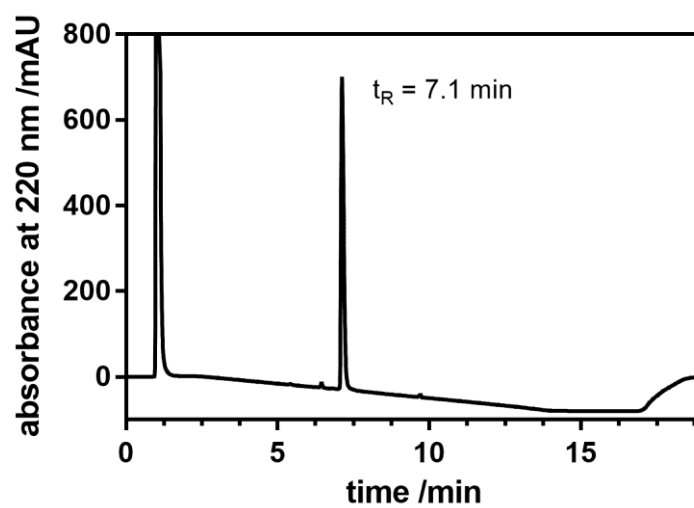
Chromatogram (purity control) of **3.65** (RP-HPLC).



Chromatogram (purity control) of **3.66** (RP-HPLC).



Chromatogram (purity control) of **3.67** (RP-HPLC).



Chromatogram (purity control) of **3.68** (RP-HPLC).

## 3.6 References

- [1] C.A. Lipinski, F. Lombardo, B.W. Dominy, P.J. Feeney, Experimental and computational approaches to estimate solubility and permeability in drug discovery and development settings, *Adv. Drug Delivery Rev.*, 23 (1997) 3-25.
- [2] C. Lipinski, Drug Solubility in Water and Dimethylsulfoxide, in: R. Mannhold, H. Kubinyi, G. Folkers (Eds.) *Molecular Drug Properties*, Wiley-VCH, Weinheim, Germany, 2008, pp. 255-282.
- [3] L. Di, P.V. Fish, T. Mano, Bridging solubility between drug discovery and development, *Drug Discov. Today*, 17 (2012) 486-495.
- [4] R.J. Young, Physical Properties in Drug Design, in: N.A. Meanwell (Ed.) *Tactics in Contemporary Drug Design*, Springer, 2015, pp. 1-68.
- [5] A.M. Davis, S.J. Teague, Hydrogen Bonding, Hydrophobic Interactions, and Failure of the Rigid Receptor Hypothesis, *Angew. Chem., Int. Ed.*, 38 (1999) 736-749.
- [6] Z. Guo, B. Li, L.-T. Cheng, S. Zhou, J.A. McCammon, J. Che, Identification of Protein–Ligand Binding Sites by the Level-Set Variational Implicit-Solvent Approach, *J. Chem. Theory Comput.*, 11 (2015) 753-765.
- [7] L. Zhang, H. Zhu, A. Mathiowetz, H. Gao, Deep understanding of structure–solubility relationship for a diverse set of organic compounds using matched molecular pairs, *Bioorg. Med. Chem.*, 19 (2011) 5763-5770.
- [8] S.N. Bhattachar, L.A. Deschenes, J.A. Wesley, Solubility: it's not just for physical chemists, *Drug Discov. Today*, 11 (2006) 1012-1018.
- [9] B. Faller, P. Ertl, Computational approaches to determine drug solubility, *Adv. Drug Delivery Rev.*, 59 (2007) 533-545.
- [10] K.T. Savjani, A.K. Gajjar, J.K. Savjani, Drug solubility: importance and enhancement techniques, *ISRN Pharm.*, 2012 (2012) 195727-195727.
- [11] S.H. Yalkowsky, J.F. Krzyzaniak, G.H. Ward, Formulation-Related Problems Associated with Intravenous Drug Delivery, *J. Pharm. Sci.*, 87 (1998) 787-796.
- [12] L. Di, E.H. Kerns, G.T. Carter, Drug-like property concepts in pharmaceutical design, *Curr. Pharm. Des.*, 15 (2009) 2184-2194.
- [13] N.M. Ahmad, Solubility-driven lead optimisation: Recent examples and personal perspectives, *Bioorg. Med. Chem. Lett.*, 26 (2016) 2975-2979.
- [14] M. Ishikawa, Y. Hashimoto, Improvement in Aqueous Solubility in Small Molecule Drug Discovery Programs by Disruption of Molecular Planarity and Symmetry, *J. Med. Chem.*, 54 (2011) 1539-1554.
- [15] M.A. Walker, Improving Solubility via Structural Modification, in: N.A. Meanwell (Ed.) *Tactics in Contemporary Drug Design*, Springer, Berlin, Heidelberg, 2015, pp. 69-106.
- [16] S. Höfinger, F. Zerbetto, On the Cavitation Energy of Water, *Chem. – Eur. J.*, 9 (2003) 566-569.
- [17] L. Gandhi, D.R. Camidge, M. Ribeiro de Oliveira, P. Bonomi, D. Gandara, D. Khaira, C.L. Hann, E.M. McKeegan, E. Litvinovich, P.M. Hemken, C. Dive, S.H. Enschede, C. Nolan, Y.-L. Chiu, T. Busman, H. Xiong, A.P. Krivoschik, R. Humerickhouse, G.I. Shapiro, C.M. Rudin, Phase I study of Navitoclax (ABT-263), a novel Bcl-2 family inhibitor, in patients with small-cell lung cancer and other solid tumors, *J. Clin. Oncol.*, 29 (2011) 909-916.
- [18] C.A. Lipinski, Rule of five in 2015 and beyond: Target and ligand structural limitations, ligand chemistry structure and drug discovery project decisions, *Adv. Drug Delivery Rev.*, 101 (2016) 34-41.
- [19] D.A. DeGoey, H.-J. Chen, P.B. Cox, M.D. Wendt, Beyond the Rule of 5: Lessons Learned from AbbVie's Drugs and Compound Collection, *J. Med. Chem.*, 61 (2018) 2636-2651.
- [20] Bradley C. Doak, B. Over, F. Giordanetto, J. Kihlberg, Oral Druggable Space beyond the Rule of 5: Insights from Drugs and Clinical Candidates, *Chem. Biol.*, 21 (2014) 1115-1142.

- [21] A. Klamt, B.J. Smith, Challenge of Drug Solubility Prediction, in: R. Mannhold, H. Kubinyi, G. Folkers (Eds.) *Molecular Drug Properties*, Wiley-VCH, Weinheim, Germany, 2008, pp. 283-311.
- [22] B.E. Blass, In vitro ADME and In vivo Pharmacokinetics, in: B.E. Blass (Ed.) *Basic Principles of Drug Discovery and Development*, Academic Press, Boston, 2015, pp. 245-306.
- [23] L.A. Doyle, W. Yang, L.V. Abruzzo, T. Krogmann, Y. Gao, A.K. Rishi, D.D. Ross, A multidrug resistance transporter from human MCF-7 breast cancer cells, *Proc. Natl. Acad. Sci. U. S. A.*, 96 (1999) 2569.
- [24] E. Rocchi, A. Khodjakov, E.L. Volk, C.-H. Yang, T. Litman, S.E. Bates, E. Schneider, The Product of the ABC Half-Transporter Gene ABCG2 (BCRP/MXR/ABCP) Is Expressed in the Plasma Membrane, *Biochem. Biophys. Res. Commun.*, 271 (2000) 42-46.
- [25] A. Mahringer, G. Fricker, ABC transporters at the blood-brain barrier, *Expert Opin. Drug Metab. Toxicol.*, 12 (2016) 499-508.
- [26] B.C. Baguley, Multiple Drug Resistance Mechanisms in Cancer, *Mol. Biotechnol.*, 46 (2010) 308-316.
- [27] A. Spindler, K. Stefan, M. Wiese, Synthesis and Investigation of Tetrahydro- $\beta$ -carboline Derivatives as Inhibitors of the Breast Cancer Resistance Protein (ABCG2), *J. Med. Chem.*, 59 (2016) 6121-6135.
- [28] F. Antoni, M. Bause, M. Scholler, S. Bauer, S.A. Stark, S.M. Jackson, I. Manolaridis, K.P. Locher, B. König, A. Buschauer, G. Bernhardt, Tariquidar-related triazoles as potent, selective and stable inhibitors of ABCG2 (BCRP), *Eur. J. Med. Chem.*, 191 (2020) 112133.
- [29] S.M. Jackson, I. Manolaridis, J. Kowal, M. Zechner, N.M.I. Taylor, M. Bause, S. Bauer, R. Bartholomaeus, G. Bernhardt, B. Koenig, A. Buschauer, H. Stahlberg, K.-H. Altmann, K.P. Locher, Structural basis of small-molecule inhibition of human multidrug transporter ABCG2, *Nat. Struct. Mol. Biol.*, 25 (2018) 333-340.
- [30] N.M.I. Taylor, I. Manolaridis, S.M. Jackson, J. Kowal, H. Stahlberg, K.P. Locher, Structure of the human multidrug transporter ABCG2, *Nature*, 546 (2017) 504-509.
- [31] G.G. Ferenczy, G.M. Keserű, Enthalpic Efficiency of Ligand Binding, *J. Chem. Inf. Model.*, 50 (2010) 1536-1541.
- [32] G.G. Ferenczy, G.M. Keserű, On the enthalpic preference of fragment binding, *MedChemComm*, 7 (2016) 332-337.
- [33] H.C. Kolb, M.G. Finn, K.B. Sharpless, Click Chemistry: Diverse Chemical Function from a Few Good Reactions, *Angew. Chem., Int. Ed.*, 40 (2001) 2004-2021.
- [34] S. Yang, K.-Y. Lee, R.-J. Chen, P. Lo, S.-Y. Liao, J.-D. Wu, C.-H.R. King, Preparation of 3-(quinolin-4-yl)-linked proline-containing peptidomimetics as HCV protease inhibitors, WO2008095058A1, 2008.
- [35] S. Bauer, C. Ochoa-Puentes, Q. Sun, M. Bause, G. Bernhardt, B. Koenig, A. Buschauer, Quinoline Carboxamide-Type ABCG2 Modulators: Indole and Quinoline Moieties as Anilide Replacements, *ChemMedChem*, 8 (2013) 1773-1778.
- [36] S.C. Köhler, M. Wiese, HM30181 Derivatives as Novel Potent and Selective Inhibitors of the Breast Cancer Resistance Protein (BCRP/ABCG2), *J. Med. Chem.*, 58 (2015) 3910-3921.
- [37] D. Peña-Solórzano, M. Scholler, G. Bernhardt, A. Buschauer, B. König, C. Ochoa-Puentes, Tariquidar-Related Chalcones and Ketones as ABCG2 Modulators, *ACS Med. Chem. Lett.*, 9 (2018) 854-859.
- [38] N.A. Gujarati, L. Zeng, P. Gupta, Z.-S. Chen, V.L. Korlipara, Design, synthesis and biological evaluation of benzamide and phenyltetrazole derivatives with amide and urea linkers as BCRP inhibitors, *Bioorg. Med. Chem. Lett.*, 27 (2017) 4698-4704.
- [39] M.K. Krapf, J. Gallus, V. Namasivayam, M. Wiese, 2,4,6-Substituted Quinazolines with Extraordinary Inhibitory Potency toward ABCG2, *J. Med. Chem.*, 61 (2018) 7952-7976.

- [40] A. Boumendjel, E. Nicolle, T. Moraux, B. Gerby, M. Blanc, X. Ronot, J. Boutonnat, Piperazinobenzopyranones and Phenalkylaminobenzopyranones: Potent Inhibitors of Breast Cancer Resistance Protein (ABCG2), *J. Med. Chem.*, 48 (2005) 7275-7281.
- [41] G. Valdameri, E. Genoux-Bastide, B. Peres, C. Gauthier, J. Guitton, R. Terreux, S.M.B. Winnischofer, M.E.M. Rocha, A. Boumendjel, A. Di Pietro, Substituted Chromones as Highly Potent Nontoxic Inhibitors, Specific for the Breast Cancer Resistance Protein, *J. Med. Chem.*, 55 (2012) 966-970.
- [42] A.d.R.A. Pires, F. Lecerf-Schmidt, N. Guragossian, J. Pazinato, G.J. Gozzi, E. Winter, G. Valdameri, A. Veale, A. Boumendjel, A. Di Pietro, B. Pérès, New, highly potent and non-toxic, chromone inhibitors of the human breast cancer resistance protein ABCG2, *Eur. J. Med. Chem.*, 122 (2016) 291-301.
- [43] A.L. Hopkins, C.R. Groom, A. Alex, Ligand efficiency: a useful metric for lead selection, *Drug Discov. Today*, 9 (2004) 430-431.
- [44] J.D. Allen, A. Van Loevezijn, J.M. Lakhai, M. Van der Valk, O. Van Tellingen, G. Reid, J.H.M. Schellens, G.-J. Koomen, A.H. Schinkel, Potent and specific inhibition of the breast cancer resistance protein multidrug transporter in vitro and in mouse intestine by a novel analogue of fumitremorgin C, *Mol. Cancer Ther.*, 1 (2002) 417-425.
- [45] G. Luurtsema, P. Elsinga, R. Dierckx, R. Boellaard, A. van Waarde, PET Tracers for Imaging of ABC Transporters at the Blood-Brain Barrier: Principles and Strategies, *Curr. Pharm. Des.*, 22 (2016) 5779-5785.
- [46] C. Özvegy, T. Litman, G. Szakács, Z. Nagy, S. Bates, A. Váradi, B. Sarkadi, Functional Characterization of the Human Multidrug Transporter, ABCG2, Expressed in Insect Cells, *Biochem. Biophys. Res. Commun.*, 285 (2001) 111-117.
- [47] T. Litman, T.E. Druley, W.D. Stein, S.E. Bates, From MDR to MXR: new understanding of multidrug resistance systems, their properties and clinical significance, *Cell. Mol. Life Sci.*, 58 (2001) 931-959.
- [48] A. Gaspar, M.J. Matos, J. Garrido, E. Uriarte, F. Borges, Chromone: A Valid Scaffold in Medicinal Chemistry, *Chem. Rev.*, 114 (2014) 4960-4992.
- [49] J. Reis, A. Gaspar, N. Milhazes, F. Borges, Chromone as a Privileged Scaffold in Drug Discovery: Recent Advances, *J. Med. Chem.*, 60 (2017) 7941-7957.
- [50] M.A. Ibrahim, N.M. El-Gohary, S. Said, Ring opening ring closure reactions with 3-substituted chromones under nucleophilic conditions, *Heterocycles*, 91 (2015) 1863-1903.
- [51] IUPAC, Compendium of Chemical Terminology <http://goldbook.iupac.org/terms/view/S05740> (accessed February 24, 2020).
- [52] H. Gamsjäger, J.W. Lorimer, P. Scharlin, D.G. Shaw, Glossary of terms related to solubility (IUPAC Recommendations 2008), *Pure Appl. Chem.*, 80 (2008) 233.
- [53] M. Apley, G.B. Crist, V. Fellner, M.A. Gonzalez, R.P. Hunter, M.N. Martinez, J.R. Messenheimer, S. Modric, M.G. Papich, A.F. Parr, J.E. Riviere, M.R.C. Marques, Determination of thermodynamic solubility of active pharmaceutical ingredients for veterinary species: a new USP general chapter, *Dissolution Technol.*, 24 (2017) 36-39.
- [54] C.D. Bevan, R.S. Lloyd, A High-Throughput Screening Method for the Determination of Aqueous Drug Solubility Using Laser Nephelometry in Microtiter Plates, *Anal. Chem.*, 72 (2000) 1781-1787.
- [55] B. Hoelke, S. Gieringer, M. Arlt, C. Saal, Comparison of Nephelometric, UV-Spectroscopic, and HPLC Methods for High-Throughput Determination of Aqueous Drug Solubility in Microtiter Plates, *Anal. Chem.*, 81 (2009) 3165-3172.
- [56] J. Alsenz, M. Kansy, High throughput solubility measurement in drug discovery and development, *Adv. Drug Delivery Rev.*, 59 (2007) 546-567.
- [57] C. Saal, A.C. Petereit, Optimizing solubility: Kinetic versus thermodynamic solubility temptations and risks, *Eur. J. Pharm. Sci.*, 47 (2012) 589-595.

- [58] D. Mackay, W.Y. Shiu, Aqueous solubility of polynuclear aromatic hydrocarbons, *J. Chem. Eng. Data*, 22 (1977) 399-402.
- [59] M. Abedi, R. Ahangari Cohan, M. Shafiee Ardestani, F. Davami, Comparison of polystyrene versus cycloolefin microplates in absorbance measurements in the UV/VIS region of the spectrum, *J. Shahrekord Univ. Med. Sci.*, 21 (2019) 110-113.
- [60] F. Cataldo, O. Ursini, G. Angelini, S. Iglesias-Groth, On the Way to Graphene: The Bottom-Up Approach to Very Large PAHs Using the Scholl Reaction, *Fullerenes, Nanotubes, Carbon Nanostruct.*, 19 (2011) 713-725.
- [61] J.P.L. Damasceno, C.d.S. Giuberti, R.d.C.R. Gonçalves, R.R. Kitagawa, Preformulation study and influence of DMSO and propylene glycol on the antioxidant action of isocoumarin paepalantine isolated from *Paepalanthus bromelioides*, *Rev. Bras. Farmacogn.*, 25 (2015) 395-400.
- [62] E. Huber, M. Frost, Light scattering by small particles, *J. Water Supply: Res. Technol. - Aqua*, 47 (1998) 87-94.
- [63] M.I. Jeraal, K.J. Roberts, I. McRobbie, D. Harbottle, Process-Focused Synthesis, Crystallization, and Physicochemical Characterization of Sodium Lauroyl Isethionate, *ACS Sustainable Chem. Eng.*, 6 (2018) 2667-2675.
- [64] Y.W. Alelyunas, R. Liu, L. Pelosi-Kilby, C. Shen, Application of a Dried-DMSO rapid throughput 24-h equilibrium solubility in advancing discovery candidates, *Eur. J. Pharm. Sci.*, 37 (2009) 172-182.
- [65] L. Zhou, L. Yang, S. Tilton, J. Wang, Development of a high throughput equilibrium solubility assay using miniaturized shake-flask method in early drug discovery, *J. Pharm. Sci.*, 96 (2007) 3052-3071.
- [66] E. Baka, J.E.A. Comer, K. Takács-Novák, Study of equilibrium solubility measurement by saturation shake-flask method using hydrochlorothiazide as model compound, *J. Pharm. Biomed. Anal.*, 46 (2008) 335-341.
- [67] NIH PubChem, Haloperidol: CID=3559, <https://pubchem.ncbi.nlm.nih.gov/compound/Haloperidol> (accessed February 24, 2020).
- [68] K. Valkó, Application of high-performance liquid chromatography based measurements of lipophilicity to model biological distribution, *J. Chromatogr. A*, 1037 (2004) 299-310.
- [69] N.M. Kershaw, G.S.A. Wright, R. Sharma, S.V. Antonyuk, R.W. Strange, N.G. Berry, P. M. O'Neill, S.S. Hasnain, X-ray Crystallography and Computational Docking for the Detection and Development of Protein–Ligand Interactions, *Curr. Med. Chem.*, 20 (2013) 569-575.
- [70] X. Guo, K.K.W. To, Z. Chen, X. Wang, J. Zhang, M. Luo, F. Wang, S. Yan, L. Fu, Dacomitinib potentiates the efficacy of conventional chemotherapeutic agents via inhibiting the drug efflux function of ABCG2 in vitro and in vivo, *J. Exp. Clin. Cancer Res.*, 37 (2018) 31/31-31/13.
- [71] M. Hubensack, C. Mueller, P. Hoecherl, S. Fellner, T. Spruss, G. Bernhardt, A. Buschauer, Effect of the ABCB1 modulators elacridar and tariquidar on the distribution of paclitaxel in nude mice, *J. Cancer Res. Clin. Oncol.*, 134 (2008) 597-607.
- [72] E.M. Leslie, R.G. Deeley, S.P.C. Cole, Multidrug resistance proteins: role of P-glycoprotein, MRP1, MRP2, and BCRP (ABCG2) in tissue defense, *Toxicol. Appl. Pharmacol.*, 204 (2005) 216-237.
- [73] V.V. Rostovtsev, L.G. Green, V.V. Fokin, K.B. Sharpless, A stepwise Huisgen cycloaddition process: copper(I)-catalyzed regioselective "ligation" of azides and terminal alkynes, *Angew. Chem., Int. Ed.*, 41 (2002) 2596-2599.
- [74] T.R. Chan, R. Hilgraf, K.B. Sharpless, V.V. Fokin, Polytriazoles as Copper(I)-Stabilizing Ligands in Catalysis, *Org. Lett.*, 6 (2004) 2853-2855.
- [75] T.A. Davidson, R.C. Griffith, N-[Amino(or hydroxy)phenethyl]-1,2,3,4-tetrahydroisoquinolines and precursors, EP51190A2, 1982.

- [76] W. Klinkhammer, H. Mueller, C. Globisch, I.K. Pajeva, M. Wiese, Synthesis and biological evaluation of a small molecule library of 3rd generation multidrug resistance modulators, *Bioorg. Med. Chem.*, 17 (2009) 2524-2535.
- [77] N. Dodic, B. Dumaitre, A. Daugan, P. Pianetti, Synthesis and Activity against Multidrug Resistance in Chinese Hamster Ovary Cells of New Acridone-4-carboxamides, *J. Med. Chem.*, 38 (1995) 2418-2426.
- [78] B. Liu, Q. Qiu, T. Zhao, L. Jiao, J. Hou, Y. Li, H. Qian, W. Huang, Discovery of Novel P-Glycoprotein-Mediated Multidrug Resistance Inhibitors Bearing Triazole Core via Click Chemistry, *Chem. Biol. Drug Des.*, 84 (2014) 182-191.
- [79] T.L. Lemke, T.W. Shek, L.A. Cates, L.K. Smith, L.A. Cosby, A.C. Sartorelli, Synthesis of 5,6-dihydro-8(7H)-quinolinone thiosemicarbazones as potential antitumor agents, *J. Med. Chem.*, 20 (1977) 1351-1354.
- [80] S. Kaiser, S.P. Smidt, A. Pfaltz, Iridium catalysts with bicyclic pyridine-phosphinite ligands: asymmetric hydrogenation of olefins and furan derivatives, *Angew. Chem., Int. Ed.*, 45 (2006) 5194-5197.
- [81] W. Giencke, J. Vermehren, Process for the preparation of substituted 2-cyanopyridines, EP551831A1, 1993.
- [82] S. Higashibayashi, T. Mori, K. Shinko, K. Hashimoto, M. Nakata, Synthetic studies on thiostrepton family of peptide antibiotics: synthesis of the tetrasubstituted dihydroquinoline portion of siomycin D1, *Heterocycles*, 57 (2002) 111-122.
- [83] B.T. Hopkins, B. Ma, T.R. Chan, G. Kumaravel, H. Miao, A. Bertolotti-Ciarlet, K. Otipoby, Preparation of pyrrolopyrimidinylbenzylpicolimamide derivatives and analogs for use as Bruton's tyrosine kinase inhibitors, WO2015089327A1, 2015.
- [84] T. Suzuki, Y. Ota, M. Ri, M. Bando, A. Gotoh, Y. Itoh, H. Tsumoto, P.R. Tatum, T. Mizukami, H. Nakagawa, S. Iida, R. Ueda, K. Shirahige, N. Miyata, Rapid Discovery of Highly Potent and Selective Inhibitors of Histone Deacetylase 8 Using Click Chemistry to Generate Candidate Libraries, *J. Med. Chem.*, 55 (2012) 9562-9575.
- [85] C. Xiao, Y. Cheng, Y. Zhang, J. Ding, C. He, X. Zhuang, X. Chen, Side chain impacts on pH- and thermo-responsiveness of tertiary amine functionalized polypeptides, *J. Polym. Sci., Part A: Polym. Chem.*, 52 (2014) 671-679.
- [86] G.-C. Kuang, H.A. Michaels, J.T. Simmons, R.J. Clark, L. Zhu, Chelation-Assisted, Copper(II)-Acetate-Accelerated Azide-Alkyne Cycloaddition, *J. Org. Chem.*, 75 (2010) 6540-6548.
- [87] T. Sugawara, T. Toyoda, M. Adachi, K. Sasakura, Aminohaloborane in organic synthesis. 1. Specific ortho substitution reaction of anilines, *J. Am. Chem. Soc.*, 100 (1978) 4842-4852.
- [88] Y. Tokimizu, S. Oishi, N. Fujii, H. Ohno, Gold-Catalyzed Cascade Cyclization of (Azido)ynamides: An Efficient Strategy for the Construction of Indoloquinolines, *Org. Lett.*, 16 (2014) 3138-3141.
- [89] K. Sonogashira, Y. Tohda, N. Hagihara, Convenient synthesis of acetylenes. Catalytic substitutions of acetylenic hydrogen with bromo alkenes, iodo arenes, and bromopyridines, *Tetrahedron Lett.*, (1975) 4467-4470.
- [90] E. Kumaran, W.Y. Fan, W.K. Leong, [Cp\*IrCl<sub>2</sub>]<sub>2</sub> Catalyzed Formation of 2,2'-Biindoles from 2-Ethynylanilines, *Org. Lett.*, 16 (2014) 1342-1345.
- [91] M.A. Martí-Renom, A.C. Stuart, A. Fiser, R. Sánchez, F. Melo, A. Šali, Comparative Protein Structure Modeling of Genes and Genomes, *Annu. Rev. Biophys. Biomol. Struct.*, 29 (2000) 291-325.
- [92] A. Šali, T.L. Blundell, Comparative Protein Modelling by Satisfaction of Spatial Restraints, *J. Mol. Biol.*, 234 (1993) 779-815.
- [93] A. Fiser, R.K.G. Do, A. Šali, Modeling of loops in protein structures, *Protein Sci.*, 9 (2000) 1753-1773.

- [94] A. Pegoli, X. She, D. Wifling, H. Hübner, G. Bernhardt, P. Gmeiner, M. Keller, Radiolabeled Dibenzodiazepinone-Type Antagonists Give Evidence of Dualsteric Binding at the M2 Muscarinic Acetylcholine Receptor, *J. Med. Chem.*, 60 (2017) 3314-3334.
- [95] A. Pegoli, D. Wifling, C.G. Gruber, X. She, H. Hübner, G. Bernhardt, P. Gmeiner, M. Keller, Conjugation of Short Peptides to Dibenzodiazepinone-Type Muscarinic Acetylcholine Receptor Ligands Determines M2R Selectivity, *J. Med. Chem.*, 62 (2019) 5358-5369.
- [96] S. Salentin, S. Schreiber, V.J. Haupt, M.F. Adasme, M. Schroeder, PLIP: fully automated protein-ligand interaction profiler, *Nucleic Acids Res.*, 43 (2015) W443-W447.
- [97] M. Roe, A. Folkes, P. Ashworth, J. Brumwell, L. Chima, S. Hunjan, I. Pretswell, W. Dangerfield, H. Ryder, P. Charlton, Reversal of P-glycoprotein mediated multidrug resistance by novel anthranilamide derivatives, *Bioorg. Med. Chem. Lett.*, 9 (1999) 595-600.
- [98] M. Hubensack, Approaches to Overcome the Blood-Brain Barrier in the Chemotherapy of Primary and Secondary Brain Tumors: Modulation of P-glycoprotein 170 and Targeting of the Transferrin Receptor, Dissertation, University of Regensburg, 2005, <https://epub.uni-regensburg.de/10297/>.
- [99] C.-H. Yang, E. Schneider, M.-L. Kuo, E.L. Volk, E. Rocchi, Y.-C. Chen, BCRP/MXR/ABCP expression in topotecan-resistant human breast carcinoma cells, *Biochem. Pharmacol.*, 60 (2000) 831-837.
- [100] M. Kühnle, M. Egger, C. Müller, A. Mahringer, G. Bernhardt, G. Fricker, B. König, A. Buschauer, Potent and Selective Inhibitors of Breast Cancer Resistance Protein (ABCG2) Derived from the p-Glycoprotein (ABCB1) Modulator Tariquidar, *J. Med. Chem.*, 52 (2009) 1190-1197.
- [101] K. Kohno, J. Kikuchi, S. Sato, H. Takano, Y. Saburi, K. Asoh, M. Kuwano, Vincristine-resistant human cancer KB cell line and increased expression of multidrug-resistance gene, *Jpn. J. Cancer Res.*, 79 (1988) 1238-1246.
- [102] R. Evers, M. Kool, L. van Deemter, H. Janssen, J. Calafat, L.C. Oomen, C.C. Paulusma, R.P. Oude Elferink, F. Baas, A.H. Schinkel, P. Borst, Drug export activity of the human canalicular multispecific organic anion transporter in polarized kidney MDCK cells expressing cMOAT (MRP2) cDNA, *J. Clin. Invest.*, 101 (1998) 1310-1319.
- [103] E. Bakos, R. Evers, G. Szakacs, G.E. Tusnady, E. Welker, K. Szabo, M. De Haas, L. Van Deemter, P. Borst, A. Varadi, B. Sarkadi, Functional multidrug resistance protein (MRP1) lacking the N-terminal transmembrane domain, *J. Biol. Chem.*, 273 (1998) 32167-32175.
- [104] B. Sarkadi, E.M. Price, R.C. Boucher, U.A. Germann, G.A. Scarborough, Expression of the human multidrug resistance cDNA in insect cells generates a high activity drug-stimulated membrane ATPase, *J. Biol. Chem.*, 267 (1992) 4854-4858.



## 4 Summary

ATP-binding cassette (ABC) transporters are gatekeepers at all major physiological barriers, such as the intestinal barrier, the hepatic barrier or the blood-brain barrier (BBB). On one hand, these proteins extrude endogenous substrates like bile salts, and on the other hand, they protect cells against the entry of numerous xenobiotics, including a variety of drugs such as anticancer and anti-HIV agents or neuropharmaceuticals. The three main drug transporters are ABCB1, ABCC1 and ABCG2, with ABCG2 being predominant at the human BBB. They constitute a severe impediment for the oral bioavailability and brain penetration of drugs, and confer multidrug resistance (MDR) to cancer cells. Thus, inhibitors of ABCG2 are required as molecular tools for examinations on the patho(physiological) role of this transporter, for (clinical) studies on drug-drug interactions (DDIs) during drug development and as potential drugs to overcome tissue barriers (especially the BBB) and MDR in cancer.

Heretofore, the discovery of ABCG2 inhibitors had largely been driven by potency, while drug-like properties – imperative for application in vivo – had been overlooked. Moreover, the mechanism of transport inhibition had still been enigmatic. Therefore, the present thesis aimed at creating novel ABCG2 inhibitors with improved drug-like properties, in particular stability in blood plasma and water solubility, and at elucidating the underlying transport inhibition mechanism.

Tariquidar analogs had been described as potent and selective ABCG2 inhibitors by our working group. However, their susceptibility to hydrolysis limited their applicability in vivo. Chapter 2 of this thesis comprises the synthesis (performed by Prof. König's group) and characterization (performed by our group, including the author of this thesis) of new tariquidar-related inhibitors, obtained by bioisosteric replacement of the labile moieties in the previous tariquidar analog UR-ME22-1. CuAAC ("click" reaction) gave convenient access to a triazole core as a substitute for the labile amide group and the unstable ester moiety was replaced by different acyl groups in a Sugasawa reaction. An HPLC assay proved the enhancement of the stability in murine blood plasma. Compounds UR-MB108 and UR-MB136 inhibited ABCG2 in a Hoechst 33342 transport assay with an  $IC_{50}$  value of about 80 nM and thus belong to the most potent ABCG2 inhibitors described so far (Figure 4.1). Compound UR-MB108 was highly selective for ABCG2, whereas its PEGylated analog UR-MB136 showed some potency at ABCB1. Both UR-MB108 and UR-MB136 produced an ABCG2 ATPase-depressing effect, which is in agreement with a precedent cryo-EM study identifying UR-MB136 as an ATPase inhibitor that exerts its effect via locking the inward-facing conformation of ABCG2. Thermostabilization of ABCG2 by UR-MB108 and UR-MB136 (performed by Prof. Locher's group) can be taken as a hint to comparable binding to ABCG2. As reference substances, compounds UR-MB108 and UR-MB136 allow additional mechanistic studies on ABCG2 inhibition. Due to their stability in blood plasma, they are also applicable in vivo. The highly

specific inhibitor UR-MB108 is suited for PET labeling, helping to further clarify the (patho)physiological role of ABCG2, e.g. at the BBB.

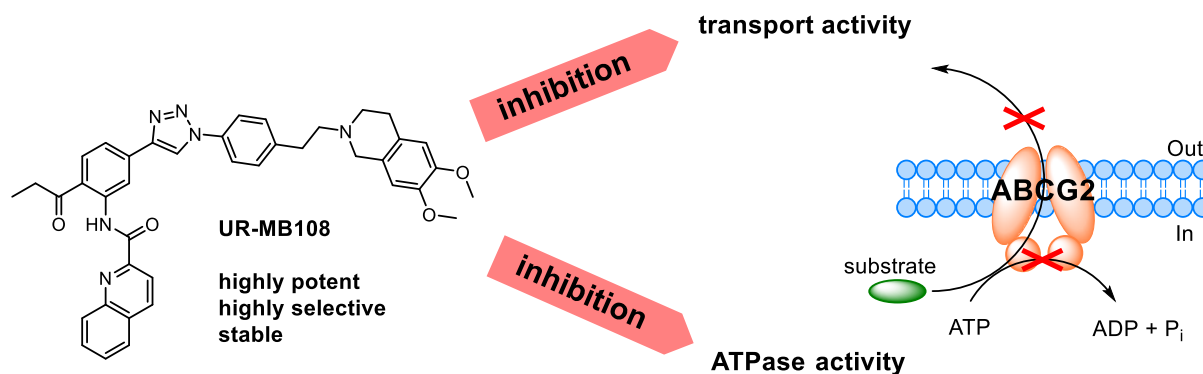


**Figure 4.1.** Graphical summary of Chapter 2 on tariquidar-related triazoles as potent, selective and stable inhibitors of ABCG2.

Chapter 3 of this thesis is focused on water solubility. The latter is an indispensable prerequisite for all bioactive compounds – seemingly trivial, however often underestimated. Many drug development failures have been attributed to poor aqueous solubility. ABCG2 inhibitors are especially prone to be insoluble since they have to address the extremely large and hydrophobic multidrug binding site in ABCG2. A case in point is UR-MB108, which showed high potency (79 nM), but very low aqueous solubility (78 nM; determined in Chapter 3 of this thesis). To discover novel potent ABCG2 inhibitors with improved solubility, a fragment-based approach was pursued. Substructures of UR-MB108 were optimized and the fragments ‘enlarged’ to obtain inhibitors, in part supported by molecular docking studies. Syntheses were achieved, i.a., via Sonogashira coupling, click chemistry and amide coupling. A kinetic solubility assay revealed that UR-MB108 and most of the new inhibitors did not precipitate during the short time period of the applied biological assays (up to two hours). The solubility of the compounds in aqueous media at equilibrium was investigated in a thermodynamic solubility assay, where UR-Ant116, UR-Ant121, UR-Ant131 and UR-Ant132 excelled with solubilities between 1  $\mu$ M and 1.5  $\mu$ M – an up to 19-fold improvement compared to UR-MB108 (Figure 4.2). Moreover, these novel *N*-phenyl-chromone-2-carboxamides inhibited ABCG2 in a Hoechst 33342 transport assay with potencies in the low three-digit nanomolar range, reversed MDR in ABCG2-overexpressing cancer cells, were non-toxic and proved stable in blood plasma. Altogether, the aforementioned compounds are attractive candidates especially for in vivo studies, but also for in vitro assays requiring long-term incubation, both needing sufficient solubility at equilibrium. UR-Ant121 and UR-Ant132 were highly ABCG2-selective, a precondition for developing PET tracers. The triple ABCB1/ABCC1/ABCG2 inhibitor UR-Ant116 qualifies for potential therapeutic applications, given the concerted role of the three transporter subtypes at many tissue barriers, e.g. the BBB.

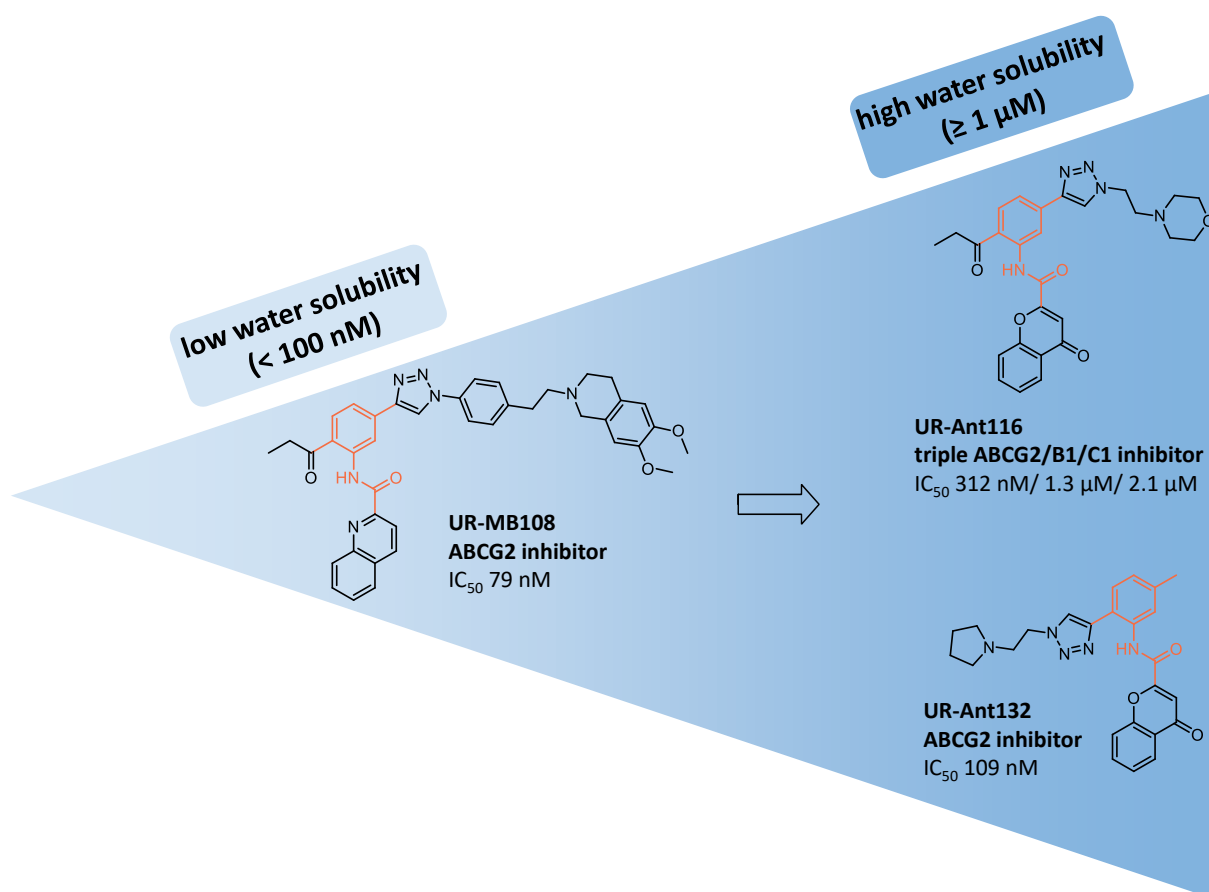


**Figure 4.2.** Graphical summary of Chapter 3 on water-soluble inhibitors of ABCG2, obtained by a fragment-based and computational approach.

Taken together, this thesis provides ABCG2 inhibitors that are both potent and effective as well as water-soluble, stable in blood plasma and nontoxic – important drug-like properties. These novel compounds may be of broad interest as molecular biological tools to scientists in fundamental ABCG2 research and to pharmaceutical companies assessing DDIs, and possibly even as diagnostic tools or drugs for patients with cancer or brain disorders.

# **5 Annex: Derivatives of Nitrogen Mustard Anticancer Agents with Improved Cytotoxicity**

Prior to the submission of this thesis, this chapter was submitted slightly modified for publication:

F. Antoni\*, G. Bernhardt, Derivatives of nitrogen mustard anticancer agents with improved cytotoxicity, Arch. Pharm., n/a (2020) e2000366.

<https://doi.org/10.1002/ardp.202000366>

Author contributions:

F.A. conceived the project with input from G.B. F.A. performed the synthesis, the cytotoxicity assays, and the data analysis with G.B. as a supervisor. F.A. wrote the manuscript with input from G.B.

\*Corresponding author

## 5.1 Introduction

Cancer is the second leading cause of death worldwide [1]. Surgery and radiation are local therapies and cannot eradicate metastatic cancer, where every organ in the body needs to be reached [2]. By contrast, chemotherapy works systemically and is the most effective treatment for disseminated tumors [2,3]. The era of chemotherapy began in 1942 with the discovery of nitrogen mustards – originally produced as chemical warfare agents – as a remedy for cancer [2,4]. A basic chemical reaction underlies the mechanism of action of nitrogen mustards, namely the intramolecular cyclization in a polar solvent to form an aziridinium cation, which reacts readily with bionucleophiles (Figure 5.1), e.g. nitrogen in the DNA. This reaction leads to the formation of DNA interstrand crosslinks, which prevents cell replication and ultimately causes cell death [4,5].

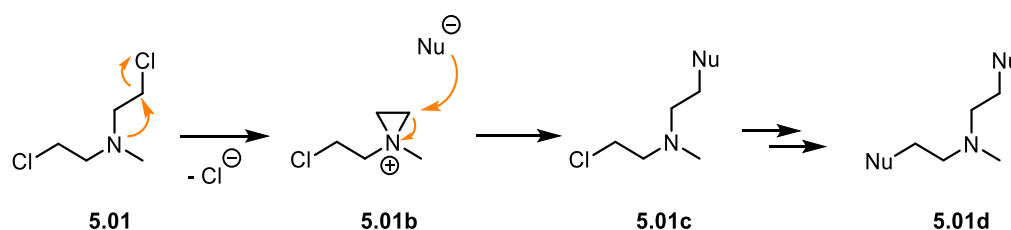


**Figure 5.1.** Mechanism of the reaction of nitrogen mustards with nucleophiles (Nu<sup>-</sup>), here shown for mechlorethamine (**5.01**).

Inspired by this success, further, improved DNA-alkylating agents of the nitrogen mustard type were developed as chemotherapeutics, such as chlorambucil, melphalan or bendamustine.

Chlorambucil (**5.02**) (Figure 5.2) was first synthesized by Everett et al. in 1953 [6]. The nitrogen mustard moiety (i.e. the bis(2-chloroethyl)amino moiety, also called N-lost moiety) was attached to a phenyl ring, which withdraws electrons from the nitrogen atom, thereby disfavoring aziridinium ion formation, which renders the nitrogen mustard moiety less reactive towards nucleophilic attack [7]. Therefore, Chlorambucil and other aromatic analogs are sufficiently deactivated so that they can reach their target DNA sites before being degraded by reacting with collateral nucleophiles, resulting in reduced toxic side effects and allowing oral administration [7]. The butanoic acid side chain makes the compound hydrophilic [8]. Chlorambucil is sold, e.g., under the brand name of Leukeran and is indicated in the treatment of chronic lymphocytic leukemia (CLL), Hodgkin and non-Hodgkin lymphomas (HL and NHL) as well as breast and ovarian carcinomas [5,9,10].

Melphalan (**5.03**) (Figure 5.2) differs from chlorambucil in the length of the alkanolic acid side chain and in the amino group attached to the latter – the amino acid L-phenylalanine is the ‘carrier’ of the N-lost moiety. Melphalan was first synthesized in 1954 by Bergel et al., aiming at increased tumor-selectivity [11]. Indeed melphalan is imported by amino acid transporters

[12], whose expression is up-regulated in cancer cells [13]. Melphalan is used for treating various malignancies including multiple myeloma (MM), ovarian cancer, breast cancer and melanoma and is sold, among others, under the trade name of Alkeran [14,15].

Bendamustine (**5.04**) (Figure 5.3) was initially synthesized in 1963 by Ozegowski et al. [16,17] in the former German Democratic Republic and was introduced into the market there [18,19]. It distinguishes itself from chlorambucil in the central benzimidazole ring, which is unique to bendamustine and was intended to include antimetabolite properties, which, however, have not yet been confirmed [17,18]. Nevertheless, bendamustine displays a unique mechanism of action, as it inhibits mitotic checkpoints, causes inefficient DNA repair and induces the expression of the protein p53, a tumor suppressor, which initiates apoptosis [20,21]. Bendamustine was approved in the Federal Republic of Germany after the iron curtain had fallen and today it is sold, e.g., under the brand name of Ribomustin for CLL, indolent NHL and MM [19,22]. In the USA, the drug is marketed, among others, under the brand name of Treanda and is approved for CLL and indolent NHL [18,19]. The assets of bendamustine are a favorable side-effect profile [18], the lack of cross-resistances with many other alkylating agents [19] and its superiority to chlorambucil in previously untreated patients with CLL [22].

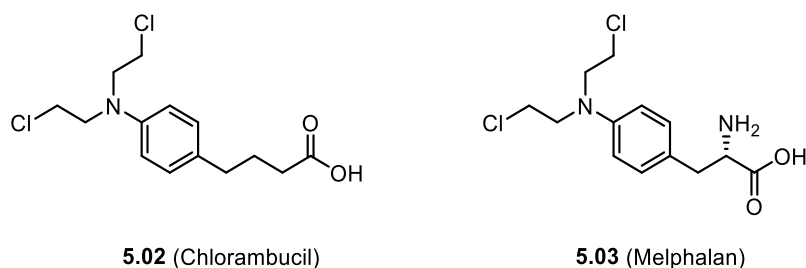


**Figure 5.2.** Structures of the nitrogen mustard anticancer agents chlorambucil (**5.02**) and melphalan (**5.03**).

Bendamustine is usually dosed intravenously, however there have been a couple of patent applications aiming at formulations for oral administration [23,24]. Esterification of the carboxylic acid moiety may increase the chances of oral application and, furthermore, has been reported to enhance the hydrolytic stability of the N-lost moiety (for different reasons) [25-27]. The increasing interest in esters of bendamustine prompted our working group to perform a study on the pharmacological properties of the latter. It was revealed that esters of bendamustine are by far more potent cytotoxic agents than the parent compound, in particular esters comprising basic moieties, which are charged under physiological conditions, e.g. the 2-pyrrolidinoethyl ester **5.05** (Figure 5.3) [28]. The basic esters show pronounced cellular accumulation for reasons not yet identified, but transport proteins may be involved [28]. However, the basic esters turned out to be especially prone to hydrolysis at the ester bond in blood plasma, which was attributed to their similarity to substrates of unspecific cholinesterases [29]. We were able to overcome this obstacle by substituting the linear ester moiety in **5.05** by

a branched ester (compound **5.06**), which increased the stability to an acceptable level [29], and so did replacement of the ester by an amide bond (compound **5.07**; unpublished data). Bendamustine, its derivatives **5.05-5.07**, as well as their respective half-lives in human blood plasma are depicted in Figure 5.3. As a note, the decomposition of bendamustine is due to the hydrolysis of the carbon-chlorine bonds of the N-lost moiety.

The preparation of **5.07** and the cytotoxicity analysis of **5.06** and **5.07** have not yet been reported and are part of the present study.

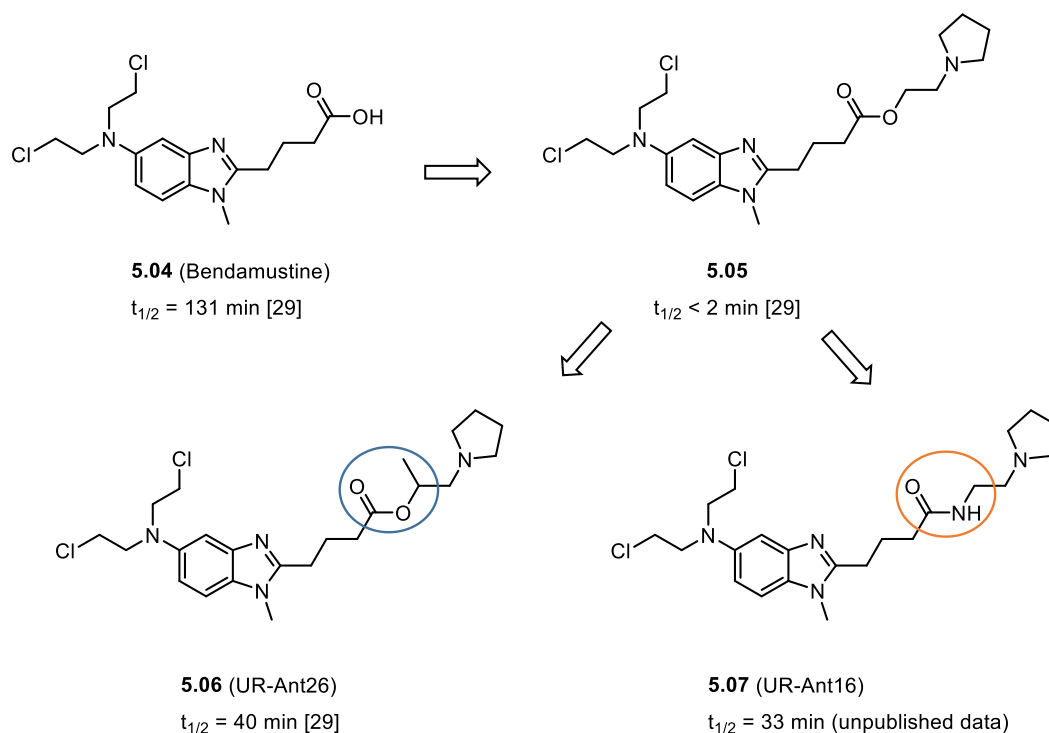


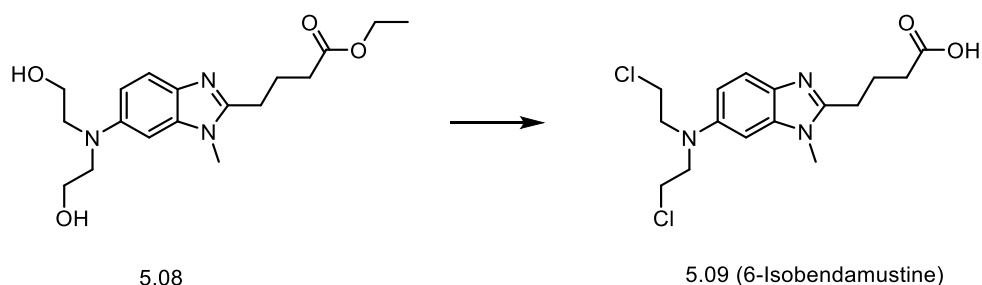
**Figure 5.3.** Structures of the nitrogen mustard anticancer agent bendamustine (**5.04**) and its derivatives **5.05**, **5.06** and **5.07**, as well as their corresponding half-lives in human blood plasma.

Since other anticancer agents are structurally very similar to bendamustine, it is conceivable that these can be improved by the same modification. Aiming at increased cytotoxicity, the present study comprises the synthesis and cytotoxicity analysis of basic derivatives of further members of the nitrogen mustard family, in particular an isomer of bendamustine we recently described (6-isobendamustine) [30,31], chlorambucil and melphalan. A pyrrolidino alkyl chain was introduced via amide or branched ester formation, since these moieties previously proved superior to a linear ester group in terms of stability in blood plasma [29].

## 5.2 Results and Discussion

### 5.2.1 Synthesis

The anticancer agents bendamustine, chlorambucil and melphalan are marketed drugs. 6-Isobendamustine (**5.09**) [30,31] (here short: isobendamustine), which, by contrast with conventional bendamustine, bears the N-lost moiety in 6-position – instead of 5-position – of the benzimidazole ring, is not commercially available. The latter was prepared from 4-(1-methyl-6-bis(2-hydroxyethyl)aminobenzimidazol-2-yl)butyric acid ethyl ester (**5.08**), which we received as a kind gift from Gemini PharmChem. Compound **5.08** was first treated with the chlorinating agent thionyl chloride and then with hydrochloric acid to hydrolyze the ester bond (Scheme 5.1).



**Scheme 5.1.** Synthesis of 6-isobendamustine (**5.09**). Reagents and conditions: (I)  $\text{SOCl}_2$ , DCM, reflux, 60 min; (II) 6 M HCl aq., 90 °C, 2 h.

The esters and amides were prepared from their respective parent compounds and a pyrrolidinoalkyl alcohol or amine. The bendamustine ester **5.06** was synthesized with the help of the coupling reagent DCC, as we described previously [29]; for the preparation of the novel bendamustine amide **5.07** the coupling reagents TBTU and DIPEA were used (Scheme 5.2). Isobendamustine was converted to the ester **5.10** and the amide **5.11** in the same way as compounds **5.06** and **5.07**, respectively (Scheme 5.2). The chlorambucil ester **5.12** could not be synthesized with DCC, but coupling with TBTU and DIPEA was successful, and the same reagents were used to prepare the chlorambucil amide **5.13** (which is already known in literature [32]) (Scheme 5.2). Melphalan was first boc-protected (to compound **5.14**), then treated with the respective alcohol or amide and the established coupling reagents TBTU and DIPEA, and subsequently deprotected to the melphalan ester **5.15** or the amide **5.16** (Scheme 5.2).

### 5.2.2 Cytotoxicity

242

### 5.2.2.1 Bendamustine and Derivatives

In accordance with our previous report [28], bendamustine proved ineffective against HT-29 carcinoma cells (Figure 5.4). Also the chemosensitivity of MG-63 osteosarcoma and SK-MEL-3 melanoma cells was very low with slight cytotoxic effects at concentrations above 30  $\mu$ M. By contrast, the branched ester **5.06** and the amide **5.07** exhibited a distinct increase in cytotoxicity compared to the parent compound, showing cytocidal effects against the treated cancer cells at concentrations of 10-30  $\mu$ M. This is in good accordance with our previously examined, linear esters of bendamustine [28]. Thus, the replacement of the linear ester moiety by a branched ester or an amide group did not only increase the stability in human blood plasma, but also proved to be bioisosteric.

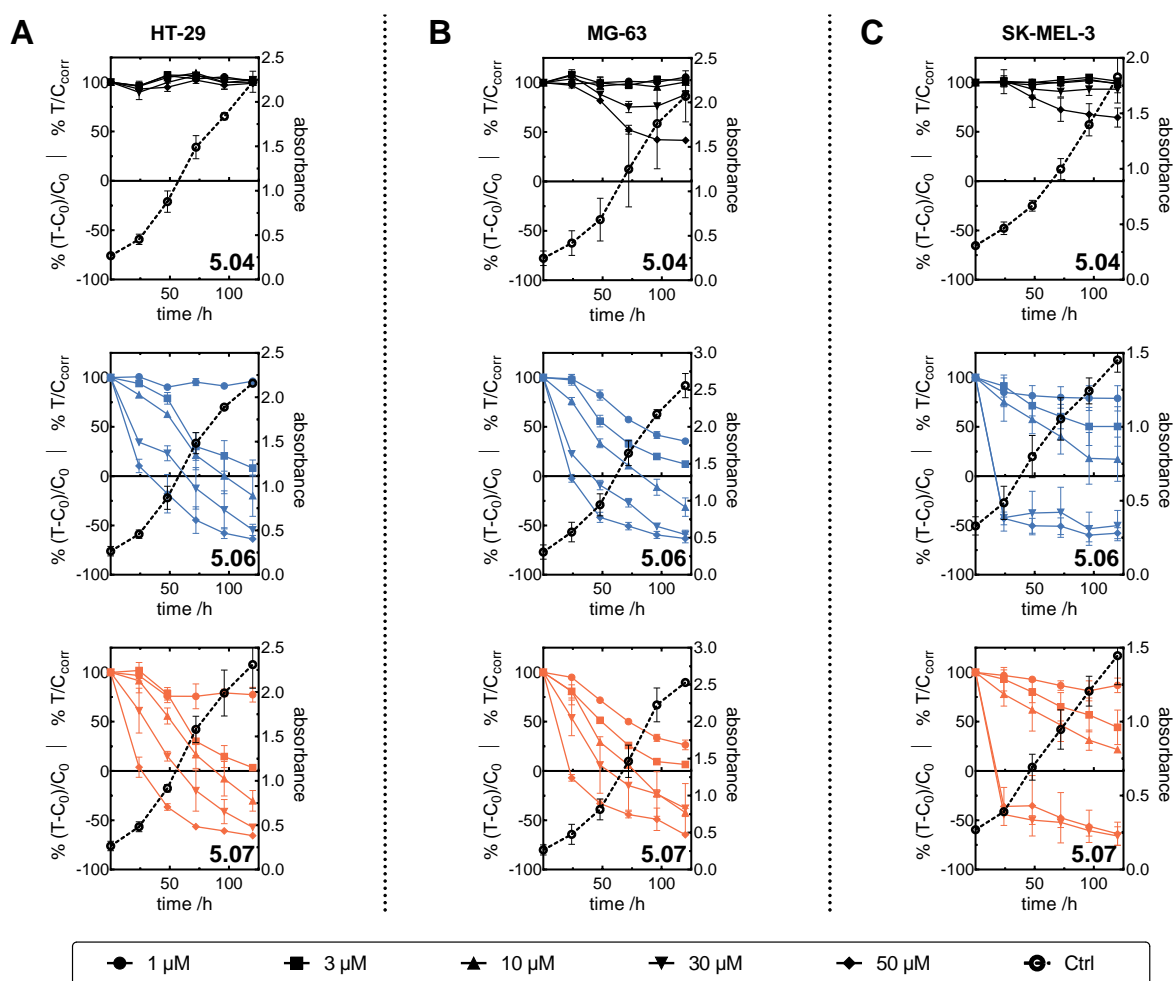


**Figure 5.4.** Cytotoxicity of bendamustine (**5.04**), its ester **5.06** and its amide **5.07** against HT-29 cells (A), MG-63 cells (B) and SK-MEL-3 cells (C). Cytotoxic/ cytocidal effects correspond to the left y-axes. The growth curves of untreated control cells (open circles) correspond to the right y-axes. Data are mean values  $\pm$  SEM of two to four independent experiments, each performed in octuplicate.

### 5.2.2.2 Isobendamustine and Derivatives

The comportment of isobendamustine in the chemosensitivity assay was almost identical to its isomer bendamustine – all three cell lines were refractory against treatment with isobendamustine (Figure 5.5). By contrast, the basic derivatives **5.10** and **5.11** exerted a pronounced effect against the three cell lines (cytotoxic at concentrations between 10–30  $\mu\text{M}$ ), which is in analogy with the basic derivatives of bendamustine. Hence, the method of increasing the cytotoxicity by the introduction of a basic moiety was successfully applied to the 6-isomer of bendamustine and it became obvious that changing the position of the nitrogen mustard moiety at the benzimidazole ring is well-tolerated.

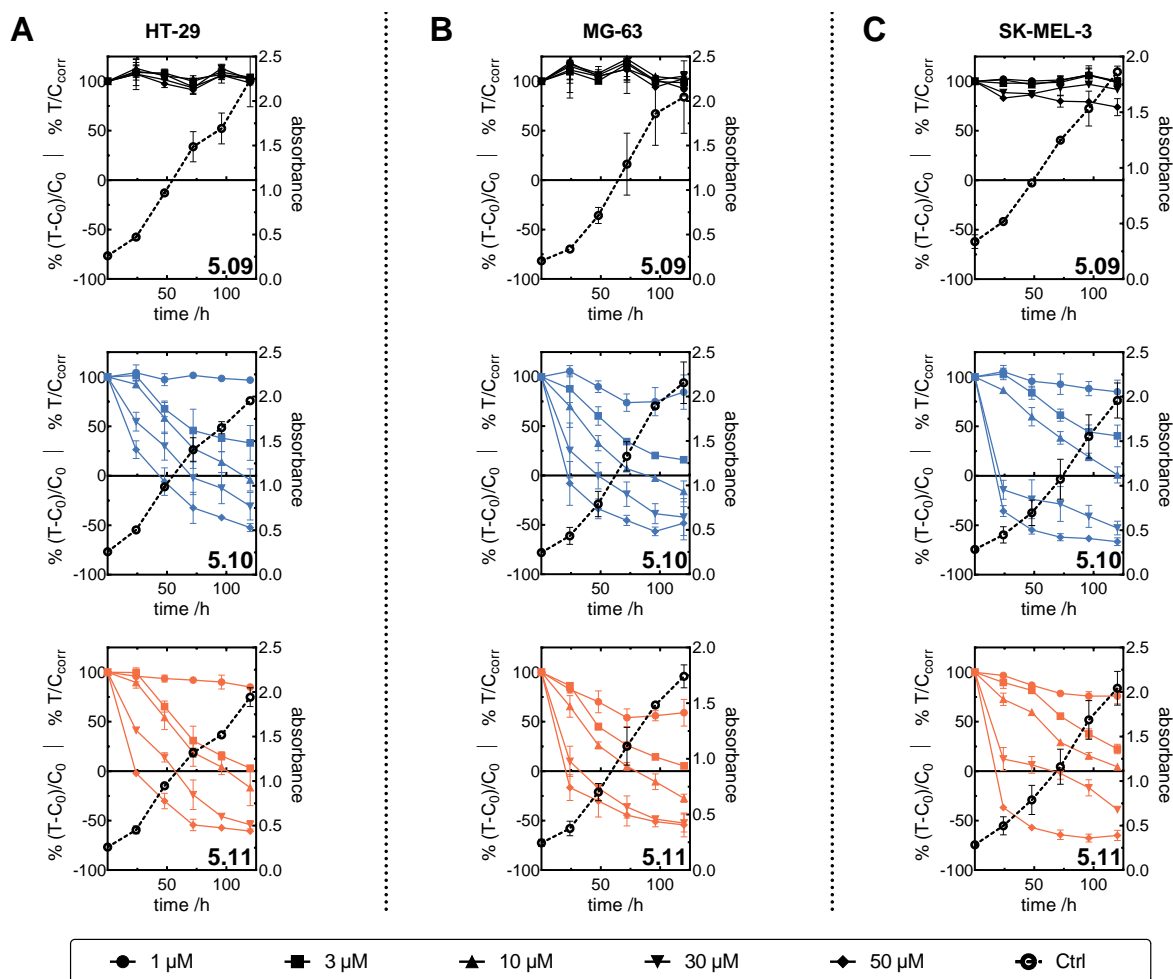


**Figure 5.5.** Cytotoxicity of isobendamustine (**5.09**), its ester **5.10** and its amide **5.11** against HT-29 cells (**A**), MG-63 cells (**B**) and SK-MEL-3 cells (**C**). Cytotoxic/ cytotoxic effects correspond to the left y-axes. The growth curves of untreated control cells (open circles) correspond to the right y-axes. Data are mean values  $\pm$  SEM of two to four independent experiments, each performed in octuplicate.

### 5.2.2.3 Chlorambucil and Derivatives

Chlorambucil displays a pronounced structural difference from bendamustine, as it bears a phenyl ring instead of a benzimidazole moiety. Its effect against HT-29 carcinoma cells and SK-MEL-3 melanoma cells was rather weak, whereas it showed a cytocidal effect against MG-63 osteosarcoma cells at a concentration of 30  $\mu\text{M}$  (Figure 5.6). The conversion into the basic ester **5.12** or amide **5.13** markedly increased the cytotoxicity compared to the parent compound, both derivatives showing cytocidal effects against HT-29 and MG-63 cells at concentrations of 1–10  $\mu\text{M}$  and against SK-MEL-3 cells, which were refractory against treatment with chlorambucil, at concentrations of 10–30  $\mu\text{M}$ . The chlorambucil amide was more potent than the ester; for instance the amide exhibited a cytocidal effect against MG-63 osteosarcoma cells at a concentration as low as 1  $\mu\text{M}$ , whereas a concentration of 10  $\mu\text{M}$  of the ester was necessary to achieve the same effect. Taken together, the introduction of a basic moiety via an ester or amide bond turned out an effective means to increase the potency of chlorambucil.

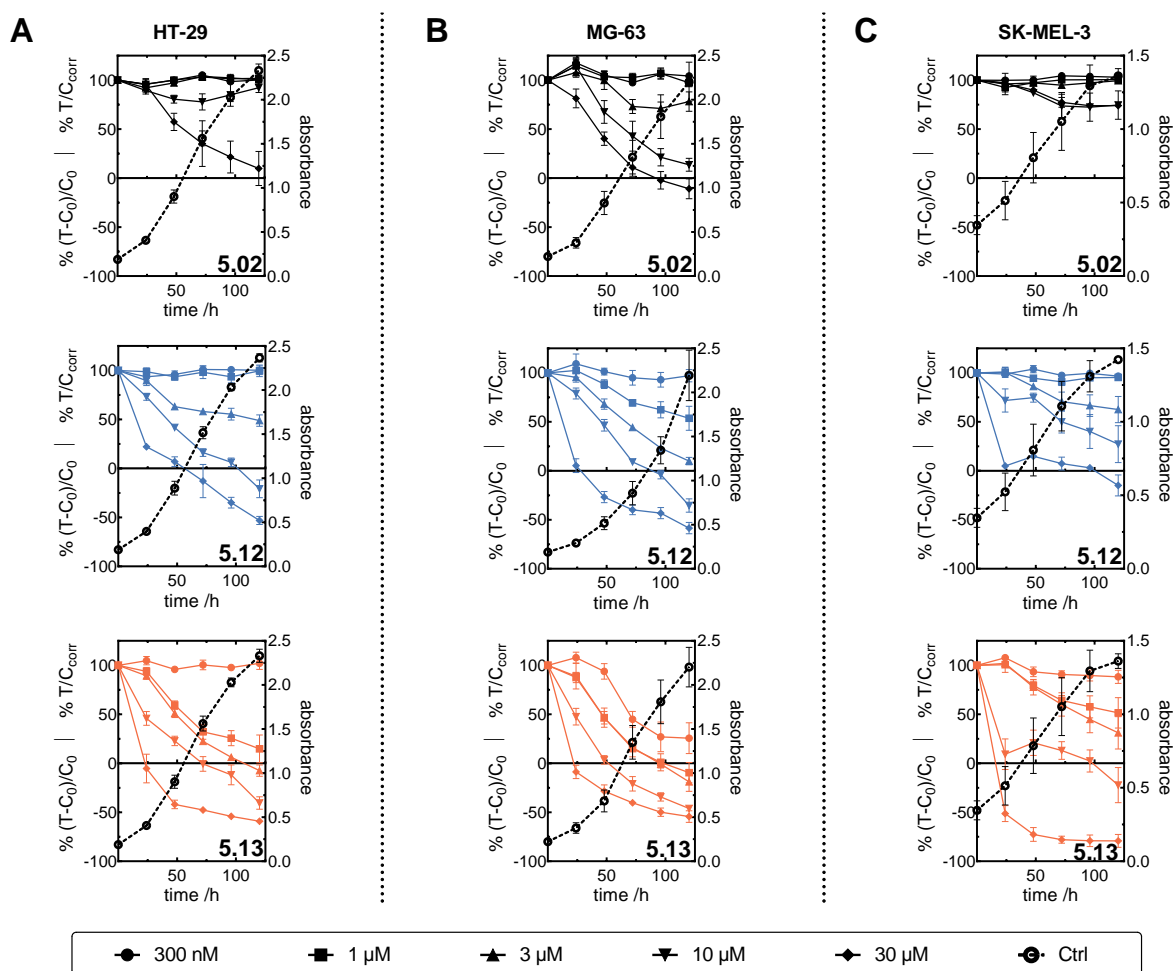


**Figure 5.6.** Cytotoxicity of chlorambucil (**5.02**), its ester **5.12** and its amide **5.13** against HT-29 cells (**A**), MG-63 cells (**B**) and SK-MEL-3 cells (**C**). Cytotoxic/ cytocidal effects correspond to the left y-axes. The growth curves of untreated control cells (open circles) correspond to the right y-axes. Data are mean values  $\pm$  SEM of two to four independent experiments, each performed in octuplicate.

### 5.2.2.4 Melphalan and Derivatives

Melphalan, an L-phenylalanine-nitrogen mustard, was more effective against the three cell lines than bendamustine, isobendamustine or chlorambucil, which may be due to its property as an amino acid transporter substrate, causing increased cellular uptake. Melphalan showed a cytotoxic effect on carcinoma HT-29 and osteosarcoma MG-63 cells at concentrations of 30  $\mu\text{M}$  and 10  $\mu\text{M}$ , respectively (Figure 5.7). The chemosensitivity of SK-MEL-3 cells was lower, with a cytostatic effect at a concentration of 30  $\mu\text{M}$ . The basic ester **5.15** and amide **5.16** showed effects similar to the parent compound against MG-63 cells. However, HT-29 and SK-MEL-3 cells exhibited a higher response upon treatment with **5.15** and **5.16** than when treated with melphalan (cytotoxic effects at concentrations of 3–30  $\mu\text{M}$ ). As in the case of the chlorambucil derivatives, the amide was somewhat more potent than the ester. All in all, only a slight improvement in cytotoxicity of melphalan could be achieved by the introduction of a basic moiety.

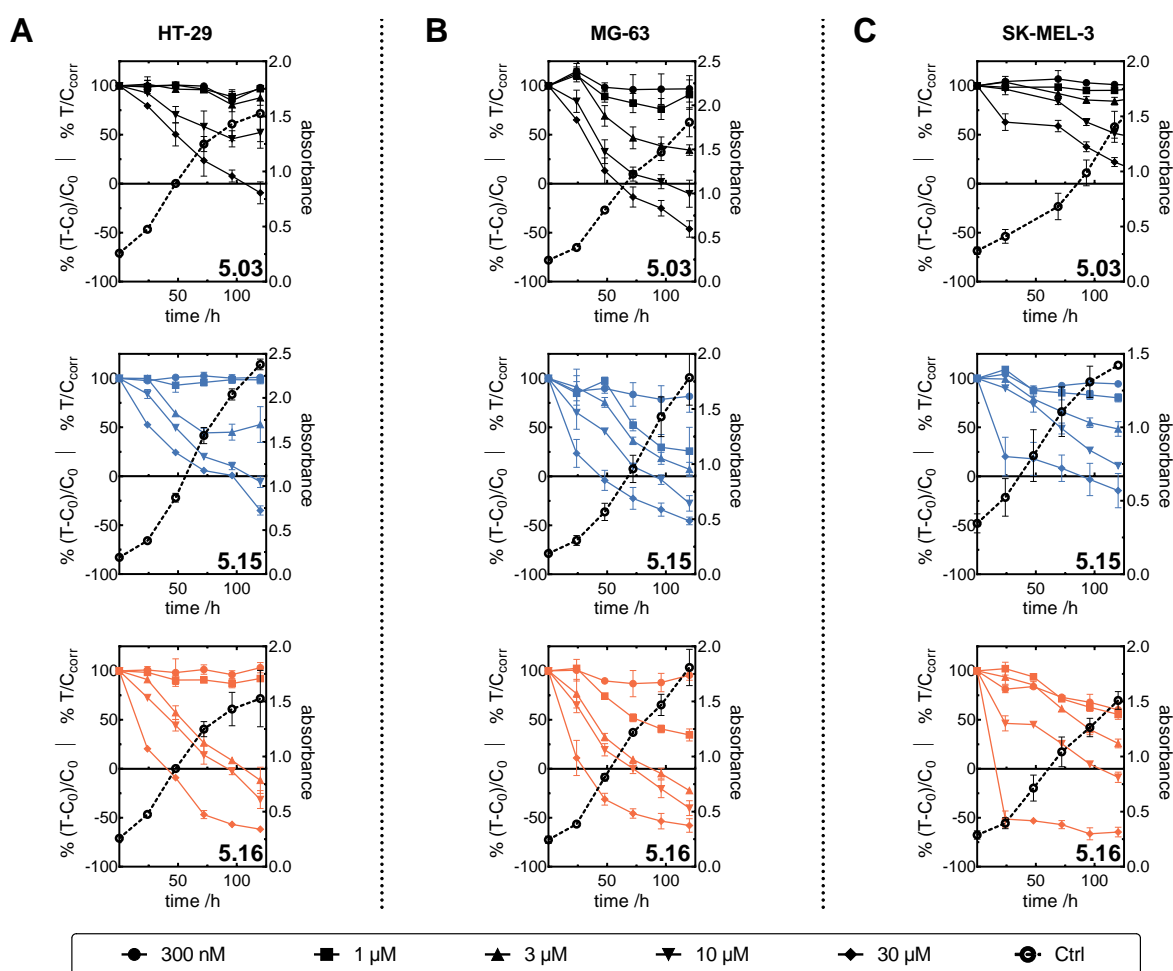


**Figure 5.7.** Cytotoxicity of melphalan (**5.03**), its ester **5.15** and its amide **5.16** against HT-29 cells (**A**), MG-63 cells (**B**) and SK-MEL-3 cells (**C**). Cytotoxic/ cytotoxic effects correspond to the left y-axes. The growth curves of untreated control cells (open circles) correspond to the right y-axes. Data are mean values  $\pm$  SEM of two to four independent experiments, each performed in octuplicate.

Comparing the basic derivatives of bendamustine, isobendamustine, chlorambucil and melphalan, it becomes apparent that they all display similar potencies – the growth curves of the individual cell lines upon treatment with **5.06**, **5.07**, **5.10-5.13**, **5.15** and **5.16** are very much alike. This can be taken as a hint that the enhancement of cytotoxicity is due to the same mechanism, for instance increased cellular uptake. Since the basic pyrrolidine ring is protonated under physiological conditions, the involvement of cation transporters is conceivable. This would also explain the smaller potency difference between melphalan and its derivatives – contrary to bendamustine and chlorambucil, melphalan is imported into the cell by amino acid transporters [12], which is why the cellular uptake does not leave much room for optimization.

## 5.3 Conclusion

Previously, we showed that esters of bendamustine are by far more cytotoxic anticancer agents than their parent compound, in particular ones containing a basic moiety. Since the latter were rapidly cleaved in human blood plasma, the labile ester moiety was substituted by a branched ester, resulting in compound UR-Ant26 (**5.06**), or an amide group, yielding UR-Ant16 (**5.07**), both of which markedly increased the stability. In the current study, the cytotoxicity of the compounds **5.06** and **5.07** was examined. By analogy with the previous linear esters, they showed cytocidal effects at concentrations between 10  $\mu\text{M}$  and 30  $\mu\text{M}$  – a striking increase in cytotoxicity compared to bendamustine, which was practically ineffective against the treated cells. These results verify that the replacement of the labile ester moiety by a branched ester or an amide was bioisosteric.

In the hope that this approach of increasing the cytotoxicity would be applicable to other, related nitrogen mustard anticancer agents, basic esters and amides of 6-isobendamustine (compounds UR-Ant45 (**5.10**) and UR-Ant48 (**5.11**)), chlorambucil (compounds UR-Ant66 (**5.12**) and UR-Ant55 (**5.13**)) and melphalan (compounds UR-Ant65 (**5.15**) and UR-Ant39 (**5.16**)) were synthesized. The reaction of the respective parent compound with a pyrrolidino alkyl alcohol or amide and the coupling reagent DCC or TBTU gave access to the target compounds. Cytotoxicity against carcinoma, sarcoma and melanoma cells was assessed in a kinetic chemosensitivity assay. The novel derivatives showed cytotoxic or cytocidal effects at concentrations above 1  $\mu\text{M}$ . This constitutes a striking enhancement over 6-isobendamustine, which was ineffective against the selected cancer cells. These results are very similar to bendamustine and its derivatives, which shows that the constitution isomerism, i.e. the change in the position of the N-lost moiety, is well-tolerated. Also an ample improvement over chlorambucil was achieved, which only showed weak potency against the sarcoma cells. Melphalan was almost as effective as the target compounds – derivatization provided only a small increase in cytotoxicity. It can be speculated that the introduction of a basic moiety

confers substrate properties of (cation) transporters, thereby increasing cellular uptake and ultimately cytotoxicity. This would explain the comparable meager enhancement achieved by derivatization of melphalan – the latter already exploits membrane transport systems, as it is a substrate of amino acid transporters [12].

Taken together, the novel nitrogen mustard chemotherapeutics can be considered interesting molecular tools for the analysis of a correlation between cytotoxicity and membrane transport mechanisms. Furthermore, the increased antiproliferative activity suggests higher efficacy in the treatment of malignancies for which the parent compound is approved, and a possible extension of the scope of indications.

## 5.4 Experimental Section

### 5.4.1 Chemistry

#### 5.4.1.1 General Experimental Conditions

**Chemicals and solvents** were purchased from commercial suppliers (Sigma Aldrich, Munich, Germany; Merck, Darmstadt, Germany; VWR, Darmstadt, Germany; Thermo Fisher Scientific, Karlsruhe, Germany; TCI, Eschborn, Germany) and used without further purification unless stated otherwise. Bendamustine was a kind gift from Arevipharma (Radebeul, Germany). 4-(1-Methyl-6-bis(2-hydroxyethyl)aminobenzimidazol-2-yl)butyric acid ethyl ester was a kind gift from Gemini PharmChem (Mannheim, Germany). Reactions requiring anhydrous conditions were carried out in dried reaction vessels under an atmosphere of argon and anhydrous solvents were used. Millipore water was used throughout for the preparation of buffers and HPLC eluents. Acetonitrile for HPLC (gradient grade) was obtained from Merck.

**Microwave** reactions were carried out in an Initiator 8 microwave reactor (Biotage, Uppsala, Sweden).

**Thin layer chromatography** was performed on TLC Silica gel 60 F<sub>254</sub> aluminium plates (Merck, Darmstadt, Germany). Visualization was accomplished by UV irradiation at wavelengths of 254 nm and 366 nm or by staining with ninhydrin (1.5 g ninhydrin, 5 mL acetic acid, 500 mL 95% ethanol).

**NMR spectra** were recorded on an Avance 400 instrument (9.40 T, <sup>1</sup>H: 400 MHz, <sup>13</sup>C: 101 MHz) or an Avance 600 instrument with cryogenic probe (14.1 T, <sup>1</sup>H: 600 MHz, <sup>13</sup>C: 151 MHz) (Bruker, Karlsruhe, Germany) with TMS as external standard.

**High-resolution mass spectrometry** (HRMS) analysis was performed on an Agilent 6540 UHD Accurate-Mass Q-TOF LC/MS system (Agilent Technologies, Santa Clara, CA, USA) using an ESI source.

**Preparative HPLC** was performed on a system from Knauer (Berlin, Germany) consisting of two K-1800 pumps and a K-2001 detector. A Nucleodur 100-5 C18 (5 µm, 110 Å, 250 mm x 21 mm; Macherey-Nagel, Düren, Germany) (compound **5.07**) or a Kinetex<sup>®</sup> XB-C18 (5 µm, 100 Å, 250 mm x 21.2 mm; Phenomenex, Aschaffenburg, Germany) (all other compounds) served as RP-columns at flow-rates of 16 mL/min and 15 mL/min, respectively. Mixtures of acetonitrile and 0.1% aq TFA were used as mobile phase. The detection wavelength was set to 220 nm throughout. The solvent mixtures were removed by lyophilization using an Alpha 2-4 LD lyophilization apparatus (Christ, Osterode am Harz, Germany) equipped with an RZ 6 rotary vane vacuum pump (Vacuubrand, Wertheim, Germany).

**Analytical HPLC** of all compounds, except for **5.12** and **5.15**, was performed on a system from Thermo Separation Products (Dreieich, Germany), composed of an SN400 controller, a P4000 pump, a Degassex DG-4400 degasser (Phenomenex, Aschaffenburg, Germany), an AS3000 autosampler and a Spectra Focus UV-VIS detector. A Nucleodur 100-5 C18 (5  $\mu\text{m}$ , 250 mm x 4.0 mm; Macherey-Nagel, Düren, Germany) (compound **5.07**) or a Kinetex<sup>®</sup> XB-C18 (5  $\mu\text{m}$ , 100 Å, 250 mm x 4.6 mm; Phenomenex) (all other compounds) served as RP-columns at a flow rate of 0.75 mL/min. Oven temperature was set to 30 °C throughout. Mixtures of acetonitrile (A) and 0.05% aq TFA (B) were used as mobile phase and degassed with Helium. The detection wavelength was set to 220 nm throughout. Solutions for injection (100  $\mu\text{M}$ ) were prepared in a mixture of A and B corresponding to the mixture at the start of the gradient. The following linear gradient was applied: 0-30 min: A/B 20:80-95:5, 30-35 min: A/B 95:5. Analytical HPLC of compounds **5.12** and **5.15** was performed on a system from Agilent Technologies (Santa Clara, CA, USA) (Series 1100) composed of a G1312A binary pump equipped with a G1379A degasser, a G1329A ALS autosampler, a G1316A COLCOM thermostated column compartment and a G1314A VWD detector. A Kinetex<sup>®</sup> C18 (2.6  $\mu\text{m}$ , 100 Å, 100 mm x 3 mm; Phenomenex, Aschaffenburg, Germany) served as RP-column at a flow rate of 0.4 mL/min. Oven temperature was set to 30 °C throughout. Mixtures of acetonitrile (A) and 0.05% aq TFA (B) were used as mobile phase. The detection wavelength was set to 220 nm throughout. Solutions for injection (100  $\mu\text{M}$ ) were prepared in a mixture of A and B corresponding to the mixture at the start of the gradient. The following linear gradient was applied: 0-12 min: A/B 20:80-95:5, 12-15 min: A/B 95:5. Retention (capacity) factors were calculated from retention times ( $t_R$ ) according to  $k = (t_R - t_0)/t_0$  ( $t_0$  = dead time of the respective HPLC-system).

#### 5.4.1.2 Synthesis Protocols and Analytical Data

##### General Procedure 1 for Ester Bond Formation

The respective carboxylic acid (1.0 eq) was dissolved in anhydrous DMF (0.2-0.3 M) in a microwave reaction vessel. 1-(Pyrrolidin-1-yl)propan-2-ol (1.5 eq) was added and the stirred mixture was cooled down to 0 °C using an ice bath. DCC (1.1 eq) was added and stirring was continued at 0 °C for 15 min and at 80 °C in a microwave reactor for 30 min. The mixture was subjected to preparative HPLC (eluent: MeCN/0.1% aq TFA) and the eluate lyophilized.

##### General Procedure 2 for Ester Bond Formation

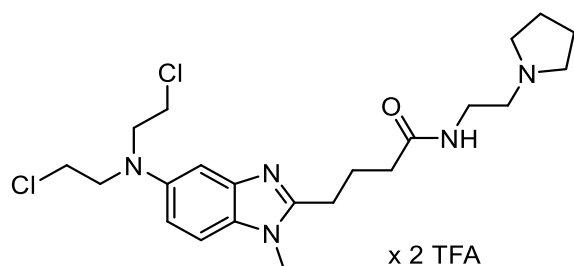
Under dry conditions the respective carboxylic acid (1.0 eq) was dissolved in anhydrous DMF (0.2-0.3 M) in a microwave reaction vessel. DIPEA (2.0 eq) and the coupling reagent TBTU (1.0 eq) were added and the solution was stirred at rt for 5 min. 1-(Pyrrolidin-1-yl)propan-2-ol (1.5 eq) was added and stirring was continued for another 45 min at 80 °C in a microwave reactor. The mixture was subjected to preparative HPLC (eluent: MeCN/0.1% aq TFA) and the

eluate lyophilized. In the case of boc-protected compounds, work-up and deprotection preceded purification of the final product by preparative HPLC.

### General Procedure for Amide Bond Formation

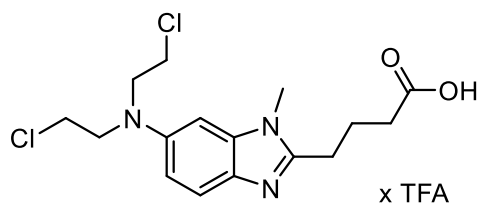
Under dry conditions the respective carboxylic acid (1.0 eq) was dissolved in anhydrous DMF (0.2-0.3 M) in a microwave reaction vessel or a round bottom flask. DIPEA (2.0-3.0 eq) and the coupling reagent TBTU (1.0 eq) were added and the solution was stirred at rt for 5 min. The according amine (1.0-1.1 eq) was added and stirring was continued for another 45-120 min at 60-80 °C in a microwave reactor or at rt overnight. The mixture was subjected to preparative HPLC (eluent: MeCN/0.1% aq TFA) and the eluate lyophilized. In the case of boc-protected compounds, work-up and deprotection preceded purification of the final product by preparative HPLC.

### 4-(5-(Bis(2-chloroethyl)amino)-1-methyl-1*H*-benzo[*d*]imidazol-2-yl)-*N*-(2-(pyrrolidin-1-yl)ethyl)butanamide (isobendamustine 2-pyrrolidinoethyl amide) (**5.07**)



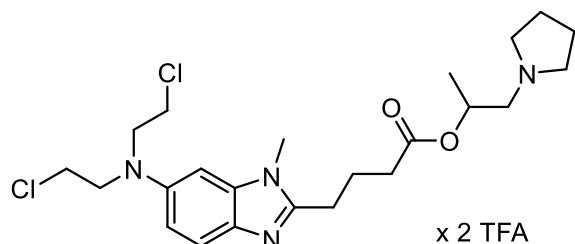
Compound **5.07** was prepared according to the general procedure for amide bond formation (in a round bottom flask with stirring overnight). The reaction was carried out using, bendamustine (100 mg, 0.279 mmol, 1.0 eq), TBTU (98.6 mg, 0.307 mmol, 1.1 eq), DIPEA (52.2  $\mu$ L, 0.307 mmol, 1.1 eq), 2-(pyrrolidin-1-yl)ethan-1-amine (35.4  $\mu$ L, 0.279 mmol, 1.0 eq) and DMF (1 mL). Preparative HPLC (0-30 min: MeCN/ 0.1% aq TFA 19:81-55:45,  $t_R$  = 13.0 min) yielded **5.07** as a yellowish resin (97.5 mg, 0.143 mmol, 51%). **<sup>1</sup>H NMR** (600 MHz, CDCl<sub>3</sub>):  $\delta$  (ppm) = 11.43 (s, 1H), 8.24 (t,  $J$  = 4.9 Hz, 1H), 7.39 (d,  $J$  = 9.2 Hz, 1H), 6.98 (d,  $J$  = 2.3 Hz, 1H), 6.95 (dd,  $J$  = 9.2 Hz,  $J$  = 2.3 Hz, 1H), 3.89 (s, 3H), 3.81 (t,  $J$  = 6.6 Hz, 6H), 3.67 (t,  $J$  = 6.6 Hz, 4H), 3.49 (q,  $J$  = 5.4 Hz, 2H), 3.24 (t,  $J$  = 5.4 Hz, 2H), 3.19 (t,  $J$  = 7.4 Hz, 2H), 2.89 (br s, 2H), 2.39 (t,  $J$  = 6.7 Hz, 2H), 2.18 (qi,  $J$  = 7.1 Hz, 2H), 2.08 (br s, 4H). **<sup>13</sup>C NMR** (150 MHz, CDCl<sub>3</sub>):  $\delta$  (ppm) = 173.0, 162.1 (TFA), 161.9 (TFA), 161.6 (TFA), 161.4 (TFA), 151.5, 146.1, 132.8, 125.1, 117.5 (TFA), 115.5 (TFA), 112.9, 112.3, 96.4, 55.0, 54.4 (2C), 54.1 (2C), 40.6 (2C), 35.7, 34.3, 31.0, 24.7, 23.2 (2C), 22.5. **RP-HPLC** (220 nm): 99% ( $t_R$  = 7.8 min,  $k$  = 2.3). **HRMS** (ESI):  $m/z$  [ $M+H$ ]<sup>+</sup> calcd. for C<sub>22</sub>H<sub>34</sub>Cl<sub>2</sub>N<sub>5</sub>O<sup>+</sup>: 454.2135, found: 454.2135. C<sub>22</sub>H<sub>33</sub>Cl<sub>2</sub>N<sub>5</sub>O • C<sub>4</sub>H<sub>2</sub>F<sub>6</sub>O<sub>4</sub> (454.44 + 228.05).

**4-(6-(Bis(2-chloroethyl)amino)-1-methyl-1*H*-benzo[d]imidazol-2-yl)butanoic acid (6-isobendamustine) hydrotrifluoroacetate (5.09) [30,31]**



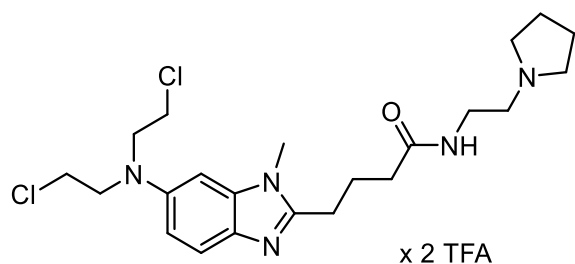
4-(1-Methyl-6-bis(2-hydroxyethyl)aminobenzimidazol-2-yl)butyric acid ethyl ester (800 mg, 2.29 mmol, 1.0 eq) was dissolved in DCM and the chlorinating agent thionyl chloride (498  $\mu$ L, 6.87 mmol, 3.0 eq) was added dropwise. The mixture was refluxed for 60 min and the volatiles were removed under reduced pressure. The ester bond was hydrolyzed with 6 M HCl aq (4 mL) 90 °C for 2 h. The mixture was washed with DCM to remove lipophilic impurities and isobendamustine hydrochloride was precipitated by adding 10 M NaOH aq until a pH of 0-1 was reached. Recrystallization in isopropanol yielded isobendamustine free base as a brownish solid (346 mg, 0.966 mmol, 42%). For further purification, 50 mg of the substance were subjected to preparative HPLC (gradient: 0-30 min: MeCN/ 0.1% aq TFA 25:75-55:45,  $t_R$  = 13.0 min) and the eluate was lyophilized, yielding compound **5.09** as a brownish resin (61.8 mg, 0.131 mmol, 94%). Analytical and pharmacological characterization was performed with the HPLC-purified substance. **<sup>1</sup>H NMR** (600 MHz, DMSO- $d_6$ ):  $\delta$  (ppm) = 14.70 (br s, 1H), 12.26 (br s, 1H), 7.58 (d,  $J$  = 9.03 Hz, 1H), 7.11 (d,  $J$  = 2.28 Hz, 1H), 7.08 (dd,  $J$  = 9.03 Hz,  $J$  = 2.28 Hz, 1H), 3.90 (s, 3H), 3.86 (t,  $J$  = 6.57 Hz, 2H), 3.80 Hz (t,  $J$  = 6.66 Hz, 4H), 3.15 (t,  $J$  = 7.74 Hz, 2H), 2.41 (t,  $J$  = 7.1 Hz, 2H), 2.00 (qi,  $J$  = 7.56 Hz, 2H). **<sup>13</sup>C NMR** (151 MHz, DMSO- $d_6$ ):  $\delta$  (ppm) = 173.7, 158.5 (TFA), 158.3 (TFA), 158.1 (TFA), 157.8 (TFA), 151.8, 145.4, 134.3, 121.9, 117.5 (TFA), 115.6 (TFA), 114.5, 112.7, 94.0, 52.4 (2C), 41.2 (2C), 32.5, 30.8, 24.2, 21.4. **RP-HPLC** (220 nm): 98% ( $t_R$  = 11.7 min,  $k$  = 2.9). **HRMS** (ESI):  $m/z$  [ $M+H$ ]<sup>+</sup> calcd. for C<sub>16</sub>H<sub>22</sub>Cl<sub>2</sub>N<sub>3</sub>O<sub>2</sub><sup>+</sup>: 358.1084, found: 358.1104. C<sub>16</sub>H<sub>21</sub>Cl<sub>2</sub>N<sub>3</sub>O<sub>2</sub> • C<sub>2</sub>HF<sub>3</sub>O<sub>2</sub> (358.26 + 114.02).

**1-(Pyrrolidin-1-yl)propan-2-yl 4-(6-(bis(2-chloroethyl)amino)-1-methyl-1H-benzo[d]imidazol-2-yl)butanoate (isobendamustine 1-methyl-2-pyrrolidinoethyl ester) bis(hydrotrifluoroacetate) (5.10)**



Compound **5.10** was prepared according to the general procedure 1 for ester bond formation. The reaction was carried out using isobendamustine (75 mg, 0.209 mmol, 1.0 eq), 1-(pyrrolidin-1-yl)propan-2-ol (40.6 mg, 0.314 mmol, 1.5 eq), DCC (47.5 mg, 0.230 mmol, 1.1 eq) and DMF (0.5 mL). A yellow coloration and a white precipitate could be observed. Preparative HPLC (0-30 min: MeCN/ 0.1% aq TFA 20:80-55:45,  $t_R$  = 14.5 min) yielded **5.10** as a brownish resin (32.8 mg, 0.047 mmol, 22%). More than one diastereoisomer was evident in the NMR spectra.  **$^1\text{H}$  NMR** (600 MHz, DMSO- $d_6$ ):  $\delta$  (ppm) = 15.03 (br s, 1H), 10.18 (s, 1H), 7.59 (d,  $J$  = 9.13 Hz, 1H), 7.12 (d,  $J$  = 2.23 Hz, 1H), 7.08 (dd,  $J$  = 9.13 Hz,  $J$  = 2.23 Hz, 1H), 5.13 (m, 1H), 3.91 Hz (s, 3H), 3.86 (t,  $J$  = 6.58 Hz, 4H), 3.80 (t,  $J$  = 6.58 Hz, 4H), 3.54 (br s, 2H), 3.38 (m, 2H), 3.16 (t,  $J$  = 7.56 Hz, 2H), 3.10 (br s, 2H), 2.55 (m, 2H), 2.04 (m, 2H), 1.92 (br s, 4H), 1.18 (d,  $J$  = 6.25 Hz, 3H).  **$^{13}\text{C}$  NMR** (151 MHz, DMSO- $d_6$ ):  $\delta$  (ppm) = 171.7, 158.8 (TFA), 158.5 (TFA), 158.3 (TFA), 158.1 (TFA), 151.7, 145.4, 134.3, 122.0, 117.4 (TFA), 115.5 (TFA), 114.6, 112.7, 94.0, 66.5, 57.4, 54.9 and 53.3 (the two carbons adjacent to the pyrrolidine nitrogen yielded two signals), 52.4 (2C), 41.2 (2C), 32.4, 30.8, 24.1, 22.6 (2C), 21.1, 17.7. **RP-HPLC** (220 nm): 96% ( $t_R$  = 10.2 min,  $k$  = 2.4). **HRMS** (ESI):  $m/z$  [ $M+H$ ] $^+$  calcd. for  $\text{C}_{23}\text{H}_{35}\text{Cl}_2\text{N}_4\text{O}_2^+$ : 469.2132, found: 469.2137.  $\text{C}_{23}\text{H}_{34}\text{Cl}_2\text{N}_4\text{O}_2 \cdot \text{C}_4\text{H}_2\text{F}_6\text{O}_4$  (469.45 + 228.05).

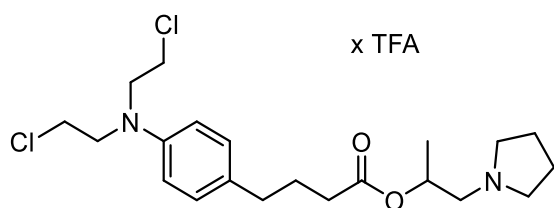
**4-(6-(Bis(2-chloroethyl)amino)-1-methyl-1H-benzo[d]imidazol-2-yl)-N-(2-(pyrrolidin-1-yl)ethyl)butanamide (isobendamustine 2-pyrrolidinoethyl amide) bis(hydrotrifluoroacetate) (5.11)**



Compound **5.11** was prepared according to the general procedure for amide bond formation (in the microwave). The reaction was carried out using isobendamustine (100 mg, 0.279 mmol, 1.0 eq), TBTU (89.6 mg, 0.279 mmol, 1.0 eq), DIPEA (97.2  $\mu\text{L}$ , 0.558 mmol, 2.0 eq),

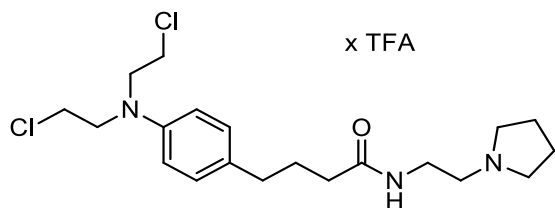
2-(pyrrolidin-1-yl)ethan-1-amine (38.9  $\mu$ L, 0.279 mmol, 1.0 eq) and DMF (1 mL). Preparative HPLC (0-30 min: MeCN/ 0.1% aq TFA 15:85-55:45,  $t_R$  = 14.2 min) yielded **5.11** as a yellow resin (77.2 mg, 0.113 mmol, 41%). **<sup>1</sup>H NMR** (600 MHz, DMSO-*d*<sub>6</sub>):  $\delta$  (ppm) = 14.98 (br s, 1H), 10.02 (s, 1H), 8.24 (t,  $J$  = 5.69 Hz, 1H), 7.58 (d,  $J$  = 9.07 Hz, 1H), 7.11 (d,  $J$  = 2.25 Hz, 1H), 7.08 (dd,  $J$  = 9.07 Hz,  $J$  = 2.25, 1H), 3.91 (s, 3H), 3.86 (t,  $J$  = 6.51 Hz, 4H), 3.80 (t,  $J$  = 6.51 Hz, 4H), 3.57 (br s, 2H), 3.36 (m, 2H), 3.17 (s, 2H), 3.13 (t,  $J$  = 7.71 Hz, 2H), 2.99 (br s, 2H), 2.27 (t,  $J$  = 7.24 Hz, 2H), 2.01 (m, 2H), 1.92 (m, 4H). **<sup>13</sup>C NMR** (151 MHz, DMSO-*d*<sub>6</sub>):  $\delta$  (ppm) = 171.9, 158.8 (TFA), 158.6 (TFA), 158.4 (TFA), 158.1 (TFA), 151.9, 145.4, 134.3, 122.0, 117.6 (TFA), 115.6 (TFA), 114.6, 112.7, 94.0, 53.3(2C), 53.1, 52.4 (2C), 41.2 (2C), 35.0, 33.7, 30.8, 24.3, 22.5 (2C), 21.8. **RP-HPLC** (220 nm): 96% ( $t_R$  = 9.0 min,  $k$  = 2.0). **HRMS** (ESI):  $m/z$  [ $M+H$ ]<sup>+</sup> calcd. for C<sub>22</sub>H<sub>34</sub>Cl<sub>2</sub>N<sub>5</sub>O<sup>+</sup>: 454.2135, found: 454.2135. C<sub>22</sub>H<sub>33</sub>Cl<sub>2</sub>N<sub>5</sub>O · C<sub>4</sub>H<sub>2</sub>F<sub>6</sub>O<sub>4</sub> (454.44 + 228.05).

**1-(Pyrrolidin-1-yl)propan-2-yl 4-(4-(bis(2-chloroethyl)amino)phenyl)butanoate (chlorambucil 1-methyl-2-pyrrolidinoethyl ester) hydrotrifluoroacetate (**5.12**)**



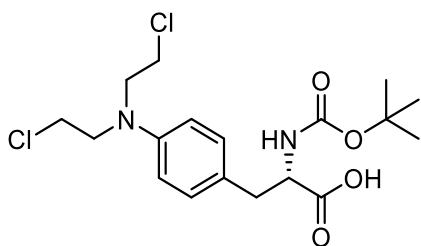
Compound **5.12** was prepared according to the general procedure 2 for ester bond formation. The reaction was carried out using chlorambucil (80 mg, 0.263 mmol, 1.0 eq), TBTU (84.4 mg, 0.263 mmol, 1.0 eq), DIPEA (89.4  $\mu$ L, 0.526 mmol, 2.0 eq), 1-(pyrrolidin-1-yl)propan-2-ol (51.0  $\mu$ L, 0.394 mmol, 1.5 eq) and DMF (1 mL). Preparative HPLC (0-30 min: MeCN/ 0.1% aq TFA 33:67-69:31,  $t_R$  = 15.5 min) yielded **5.12** as a brownish resin (49.2 mg, 0.093 mmol, 35%). More than one diastereoisomer was evident in the NMR spectra. **<sup>1</sup>H NMR** (600 MHz, DMSO-*d*<sub>6</sub>)  $\delta$  (ppm) 9.99 (br s, 1H), 7.02 (d,  $J$  = 8.6 Hz, 2H), 6.67 (d,  $J$  = 8.8 Hz, 2H), 5.13 (m, 1H), 3.69 (m, 8H), 3.59-3.45 (m, 2H), 3.44-3.30 (m, 2H), 3.12-3.99 (m, 2H), 2.49-2.45 (m, 2H), 2.38-2.27 (m, 2H), 1.99 (m, 2H), 1.86 (m, 2H), 1.77 (m, 2H), 1.20 (d,  $J$  = 6.3 Hz, 3H). **<sup>13</sup>C NMR** (151 MHz, DMSO-*d*<sub>6</sub>)  $\delta$  (ppm) 172.3, 158.6 (TFA), 158.3 (TFA), 158.1 (TFA), 157.9 (TFA), 144.5, 129.4, 129.3 (2C), 117.5 (TFA), 115.6 (TFA), 111.9 (2C), 66.1, 57.4, 54.9 and 53.3 (the two carbons adjacent to the pyrrolidine nitrogen yielded two signals), 52.2 (2C), 41.2 (2C), 33.2, 33.0, 26.3, 22.7 and 22.5 (the two pyrrolidine carbons not adjacent to the nitrogen yielded two signals), 17.7. **RP-HPLC** (220 nm): 92% ( $t_R$  = 9.2 min,  $k$  = 6.2) (the second peak in the chromatogram is not due to impurity but to decomposition in the aqueous HPLC eluent). **HRMS** (ESI):  $m/z$  [ $M+H$ ]<sup>+</sup> calcd. for C<sub>21</sub>H<sub>33</sub>Cl<sub>2</sub>N<sub>2</sub>O<sub>2</sub><sup>+</sup>: 415.1914, found: 415.1924. C<sub>21</sub>H<sub>32</sub>Cl<sub>2</sub>N<sub>2</sub>O<sub>2</sub> · C<sub>2</sub>HF<sub>3</sub>O<sub>2</sub> (414.18 + 114.02).

**4-(4-(Bis(2-chloroethyl)amino)phenyl)-N-(2-(pyrrolidin-1-yl)ethyl)butanamide (chlorambucil 2-pyrrolidinoethyl amide) hydrotrifluoroacetate (5.13) [32]**



Compound **5.13** was prepared according to the general procedure for amide bond formation (in the microwave). The reaction was carried out using chlorambucil (100 mg, 0.329 mmol, 1.0 eq), TBTU (105.5 mg, 0.329 mmol, 1.0 eq), DIPEA (111.8  $\mu$ L, 0.657 mmol, 2.0 eq), 2-(pyrrolidin-1-yl)ethan-1-amine (45.8  $\mu$ L, 0.362 mmol, 1.1 eq) and DMF (1 mL). Twofold purification by preparative HPLC (0-30 min: MeCN/ 0.1% aq TFA 28:72-68:32,  $t_R$  = 13.5 min) yielded **5.13** as a yellowish resin (75.5 mg, 0.147 mmol, 45%).  **$^1\text{H}$  NMR** (600 MHz, DMSO- $d_6$ )  $\delta$  (ppm) 9.80 (br s, 1H), 8.07 (m, 1H), 7.01 (d,  $J$  = 8.6 Hz, 2H), 6.66 (d,  $J$  = 8.6 Hz, 2H), 3.69 (m, 8H), 3.57 (m, 2H), 3.36 (q,  $J$  = 6.1 Hz, 2H), 3.18 (q,  $J$  = 6.0 Hz, 2H), 3.00 (m, 2H), 2.44 (t,  $J$  = 7.7 Hz, 2H), 2.10 (t,  $J$  = 7.4 Hz, 2H), 1.99 (m, 2H), 1.85 (m, 2H), 1.74 (m, 2H).  **$^{13}\text{C}$  NMR** (151 MHz, DMSO- $d_6$ )  $\delta$  (ppm) 172.8, 158.6 (TFA), 158.4 (TFA), 158.2 (TFA), 158.0 (TFA), 144.4, 129.8, 129.3 (2C), 117.6 (TFA), 115.6 (TFA), 111.9 (2C), 53.4 (2C), 53.3, 52.2 (2C), 41.2 (2C), 35.0, 34.8, 33.6, 27.0, 22.5 (2C). **RP-HPLC** (220 nm): 92% ( $t_R$  = 14.3 min,  $k$  = 3.7) (the second peak in the chromatogram is not due to impurity but to decomposition in the aqueous HPLC eluent). **HRMS** (ESI):  $m/z$   $[M+H]^+$  calcd. for  $\text{C}_{20}\text{H}_{32}\text{Cl}_2\text{N}_3\text{O}^+$ : 400.1917, found: 400.1925.  $\text{C}_{20}\text{H}_{31}\text{Cl}_2\text{N}_3\text{O} \cdot \text{C}_2\text{HF}_3\text{O}_2$  (399.18 + 114.02).

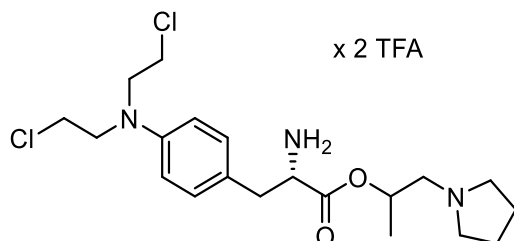
**(S)-3-(4-(Bis(2-chloroethyl)amino)phenyl)-2-((tert-butoxycarbonyl)amino)propanoic acid (boc-melphalan) (5.14) [34,35]**



Melphalan (38.0 mg, 0.125 mmol, 1.0 eq) and  $\text{NaHCO}_3$  (31.4 mg, 0.374 mmol, 3.0 eq) were dissolved in THF/ $\text{H}_2\text{O}$  1:1 (1 mL),  $\text{Boc}_2\text{O}$  (42.9  $\mu$ L, 0.1787 mmol, 1.5 eq) was added and the mixture stirred at rt for 30 min. The suspension was diluted with EtOAc and the organic layer was washed with 1 M HCl aq and brine, dried over  $\text{Na}_2\text{SO}_4$  and concentrated under reduced pressure to a brown oil which was used in subsequent reactions without further purification.  **$^1\text{H}$  NMR** (400 MHz,  $\text{CDCl}_3$ )  $\delta$  (ppm) 9.79 (s, 1H), 7.07 (d,  $J$  = 7.8 Hz, 2H), 6.62 (d,  $J$  = 8.6 Hz, 2H), 4.96 (d,  $J$  = 7.4 Hz, 1H), 4.55 (m, 1H), 3.70 (m, 4H), 3.61 (m, 4H), 3.13-2.96 (m, 2H),

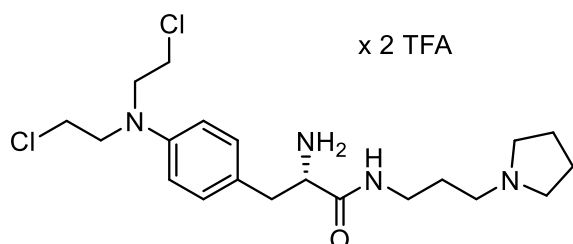
1.52 (s, 9H). **HRMS** (ESI):  $m/z$   $[M+H]^+$  calcd. for  $C_{22}H_{34}Cl_2N_5O^+$ : 454.2135, found: 454.2135.  $C_{18}H_{26}Cl_2N_2O_4$  (504.32).

**1-(Pyrrolidin-1-yl)propan-2-yl (2S)-2-amino-3-(4-(bis(2-chloroethyl)amino)phenyl)-propanoate (melphalan 1-methyl-2-pyrrolidinoethyl ester) bis(hydrotrifluoroacetate) (5.15)**



Compound **5.15** was prepared according to the general procedure 2 for ester bond formation. The reaction was carried out using boc-melphalan (133 mg, 0.328 mmol, 1.0 eq), TBTU (105 mg, 0.328 mmol, 1.0 eq), DIPEA (111  $\mu$ L, 0.655 mmol, 2.0 eq), 1-(pyrrolidin-1-yl)propan-2-ol (63.5  $\mu$ L, 0.491 mmol, 1.5 eq) and DMF (3 mL). The mixture was diluted with brine (50 mL) and the product extracted with EtOAc (3 x 50 mL). The combined organic layers were dried over  $Na_2SO_4$  and concentrated under reduced pressure. For *N*-boc deprotection, the residue was dissolved in DCM (2 mL), TFA (0.5 mL) was added and the solution was stirred at rt for 2 h. Evaporation of the volatiles and purification by preparative HPLC (0-30 min: MeCN/ 0.1% aq TFA 21:79-57:43,  $t_R$  = 13.5 min) yielded **5.15** as a brown resin (20.2 mg, 0.031 mmol, 10% for protection, coupling and deprotection). More than one diastereoisomer was evident in the NMR spectra.  **$^1H$  NMR** (600 MHz,  $DMSO-d_6$ )  $\delta$  (ppm) 10.07 (br s, 1H), 8.57 (m, 3H), 7.08 (m, 2H), 6.72 (m, 2H), 5.16 (m, 1H), 4.33-4.15 (m, 1H), 3.72 (m, 8H), 3.62-3.31 (m, 4H), 3.12-2.91 (m, 4H), 2.05-1.74 (m, 4H), 1.27-1.12 (m, 3H).  **$^{13}C$  NMR** (151 MHz,  $DMSO-d_6$ )  $\delta$  (ppm) 168.7, 168.0, 158.8 (TFA), 158.6 (TFA), 158.4 (TFA), 158.2 (TFA), 145.7, 145.7, 130.7, 130.6 (2C), 122.3, 122.0, 117.6 (TFA), 115.6 (TFA), 112.0 (2C), 68.9, 68.6, 57.1, 57.0, 54.8, 53.7, 53.5, 53.3, 53.0, 52.0 (2C), 41.1 (2C), 34.8, 34.8, 22.6 (2C), 17.3, 17.2. **RP-HPLC** (220 nm): 98% ( $t_R$  = 5.5 min,  $k$  = 3.4). **HRMS** (ESI):  $m/z$   $[M+H]^+$  calcd. for  $C_{20}H_{32}Cl_2N_3O_2^+$ : 416.1866, found: 416.1871.  $C_{20}H_{31}Cl_2N_3O_2 \cdot C_4H_2F_6O_4$  (416.39 + 228.05).

**(S)-2-Amino-3-(4-(bis(2-chloroethyl)amino)phenyl)-N-(3-(pyrrolidin-1-yl)propyl)-propanamide (melphalan 3-pyrrolidinopropyl amide) bis(hydrotrifluoroacetate) (5.16)**



Compound **5.16** was prepared according to the general procedure for amide bond formation (in the microwave). The reaction was carried out using boc-melphalan (64.2 mg, 0.125 mmol, 1.0 eq), TBTU (40.0 mg, 0.125 mmol, 1.0 eq), DIPEA (65.1  $\mu$ L, 0.374 mmol, 3.0 eq), 3-(pyrrolidin-1-yl)propan-1-amine (47.3  $\mu$ L, 0.374 mmol, 3.0 eq) and DMF (1 mL). The mixture was diluted with brine (20 mL) and the product extracted with EtOAc (3 x 20 mL). The combined organic layers were dried over  $\text{Na}_2\text{SO}_4$  and concentrated under reduced pressure. For *N*-boc deprotection, the residue was dissolved in DCM (0.5 mL), TFA (0.5 mL) was added and the solution was stirred at rt for 2 h. Evaporation of the volatiles and purification by preparative HPLC (0-30 min: MeCN/ 0.1% aq TFA 15:85-55:45,  $t_R$  = 14.4 min) yielded **5.16** as a brownish resin (22.9 mg, 0.036 mmol, 29% for protection, coupling and deprotection). More than one diastereoisomer was evident in the NMR spectra.  **$^1\text{H}$  NMR** (600 MHz,  $\text{DMSO}-d_6$ )  $\delta$  (ppm) 10.08 (s, 1H), 8.59 (t,  $J$  = 5.8 Hz, 1H), 8.20 (br s, 3H), 7.06 (d,  $J$  = 8.7 Hz, 2H), 6.71 (d,  $J$  = 8.8 Hz, 2H), 3.86 (m, 1H), 3.71 (s, 8H), 3.51 (m, 2H), 3.21-3.09 (m, 2H), 3.07-2.98 (m, 2H), 2.95-2.83 (m, 4H), 2.03-1.82 (m, 4H), 1.79-1.67 (m, 2H).  **$^{13}\text{C}$  NMR** (151 MHz,  $\text{DMSO}-d_6$ )  $\delta$  (ppm) 168.3, 158.8 (TFA), 158.6 (TFA), 158.4 (TFA), 158.2 (TFA), 145.5, 130.5 (2C), 122.8, 117.8 (TFA), 115.9 (TFA), 112.0 (2C), 53.9, 53.3 and 53.2 (the two carbons adjacent to the pyrrolidine nitrogen yielded two signals), 52.1 (2C), 51.8, 41.2 (2C), 36.1, 35.9, 25.4, 22.6 (2C). **RP-HPLC** (220 nm): 97% ( $t_R$  = 8.9 min,  $k$  = 1.9). **HRMS** (ESI):  $m/z$  [ $M+\text{H}$ ] $^+$  calcd. for  $\text{C}_{20}\text{H}_{33}\text{Cl}_2\text{N}_4\text{O}^+$ : 415.2026, found: 415.2034.  **$\text{C}_{20}\text{H}_{32}\text{Cl}_2\text{N}_4\text{O} \cdot \text{C}_4\text{H}_2\text{F}_6\text{O}_4$**  (415.40 + 228.05).

## 5.4.2 Biology

### 5.4.2.1 General Experimental Conditions

**Materials.** Commodity chemicals and solvents were purchased from commercial suppliers (Sigma Aldrich, Munich, Germany; Merck, Darmstadt, Germany; VWR, Darmstadt, Germany; Thermo Fisher Scientific, Waltham, MA, USA; Invitrogen, Karlsruhe, Germany; Serva, Heidelberg, Germany). Millipore water was used throughout for the preparation of buffers and aqueous reagent solutions. The pH of buffers was adjusted with NaOH aq or HCl aq. All cell lines were purchased from the ATCC (American Type Culture Collection; Manassas, VA,

USA). Tissue culture flasks were procured from Sarstedt (Nümbrecht, Germany). RPMI-1640 medium was from Sigma Aldrich. Fetal calf serum (FCS) and trypsin/EDTA solution were from Biochrom (Berlin, Germany). 96-Well microplates (PS, clear, F-bottom, with lid, sterile) were purchased from Greiner Bio-One (Frickenhausen, Germany).

**Stock solutions.** The test compounds were dissolved in DMSO at 1000 times the final concentrations in the chemosensitivity assay.

**Instruments.** Absorbance measurements were carried out with a GENios Pro microplate reader (equipped with a Xenon arc lamp; Tecan, Grödig, Austria).

**Software.** All biological data were analyzed with GraphPad Prism 5 (GraphPad Software, San Diego, CA, USA).

#### 5.4.2.2 Cell Culture

All cell lines were cultured in RPMI-1640 medium containing 110 mg/L sodium pyruvate, 2.4 g/L HEPES and 2.0 g/L NaHCO<sub>3</sub> and supplemented with 10% (v/v) FCS at 37 °C in a water-saturated atmosphere containing 5% CO<sub>2</sub>. Cells were passaged following treatment with a solution containing 0.05% trypsin and 0.025% EDTA. All cells were routinely monitored for mycoplasma contamination by PCR using the Venor<sup>®</sup>GeM mycoplasma detection kit (Minerva Biolabs, Berlin, Germany) and were negative.

#### 5.4.2.3 Chemosensitivity Assay [33]

Cells were seeded into 96-well plates at a density of 1500 cells per well (MG-63 and HT-29 cells) or a density of 3000 cells per well (SK-MEL-3 cells) (100 µL/well) and allowed to attach to the surface of the microplates in a water-saturated atmosphere containing 5% CO<sub>2</sub> at 37 °C overnight. The next day, fresh medium containing the test compounds at 2-fold final concentrations was added (100 µL/well; giving a final volume of 200 µL/well). On each plate, vinblastine at a final concentration of 300 nM served as reference cytostatic (positive control); the vehicle DMSO (0.1%) served as negative control to monitor cell growth in the absence of a drug. Each concentration was measured in octuplicate, the negative control in 16-fold replication. Growth of the cells was stopped after different periods of time by removal of medium and fixation with 2% (v/v) glutardialdehyde in PBS (100 µL/well). All the plates were stored at 4 °C until the end of the experiment and afterwards stained with 0.02% crystal violet in water (100 µL/well) for 20 min. Excess dye was removed by rinsing the plates with water three times. Crystal violet bound by the fixed cells was re-dissolved in 70% EtOH (180 µL/well) while shaking the microplates for 2-3 h. The absorbance (580 nm) as a parameter proportional to the cell mass was measured using a GENios Pro microplate reader.

Cytotoxic effects were expressed as corrected T/C-values according to

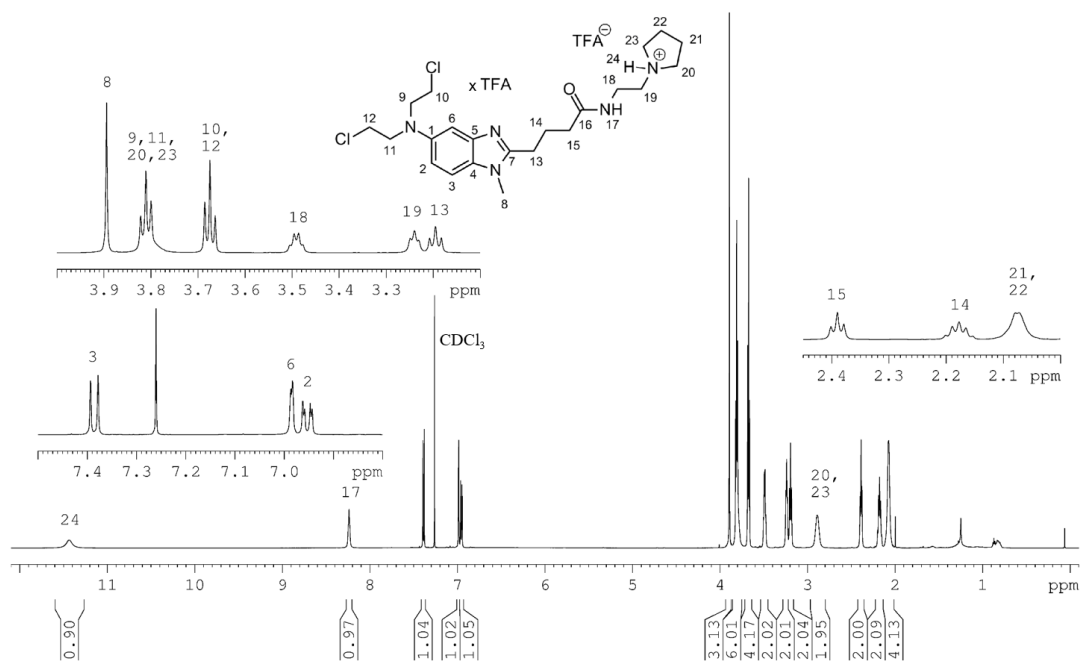
$$T / C_{corr} [\%] = \frac{T - C_0}{C - C_0} \cdot 100$$

where T is the mean absorbance of the treated cells, C the mean absorbance of the negative controls and  $C_0$  the mean absorbance of the cells at the time of compound addition ( $t_0$ ). When the absorbance of treated cells T was lower than at the beginning of the experiment ( $C_0$ ), the extent of cell killing was calculated as cytocidal effect according to

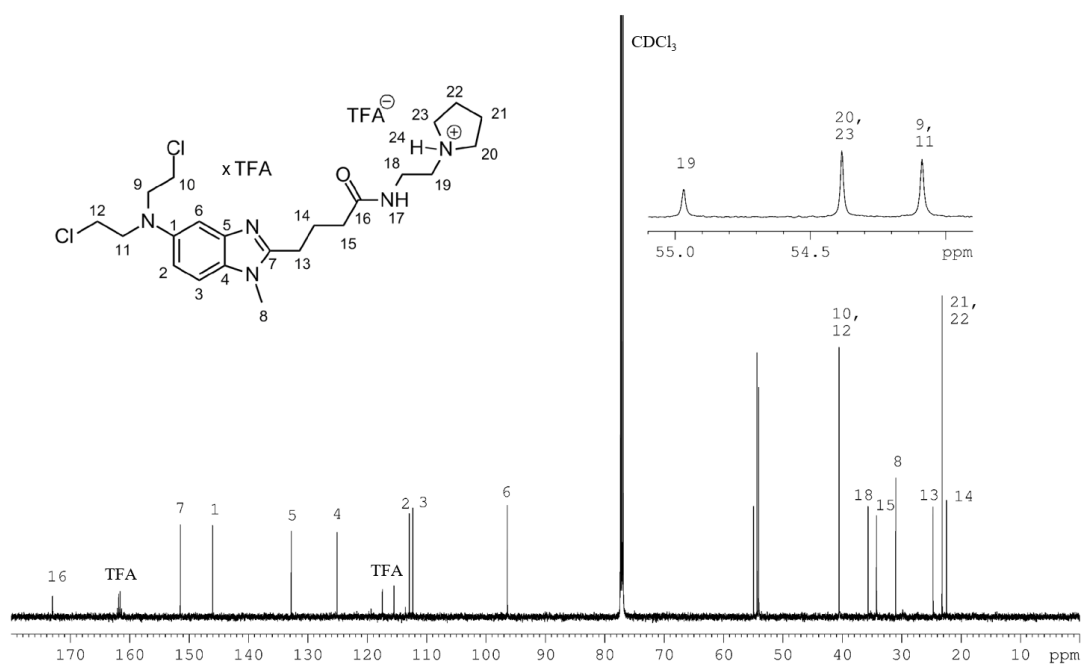
$$Cytocidal\ effect\ [\%] = \frac{T - C_0}{C_0} \cdot 100$$

## 5.5 Supplementary Material

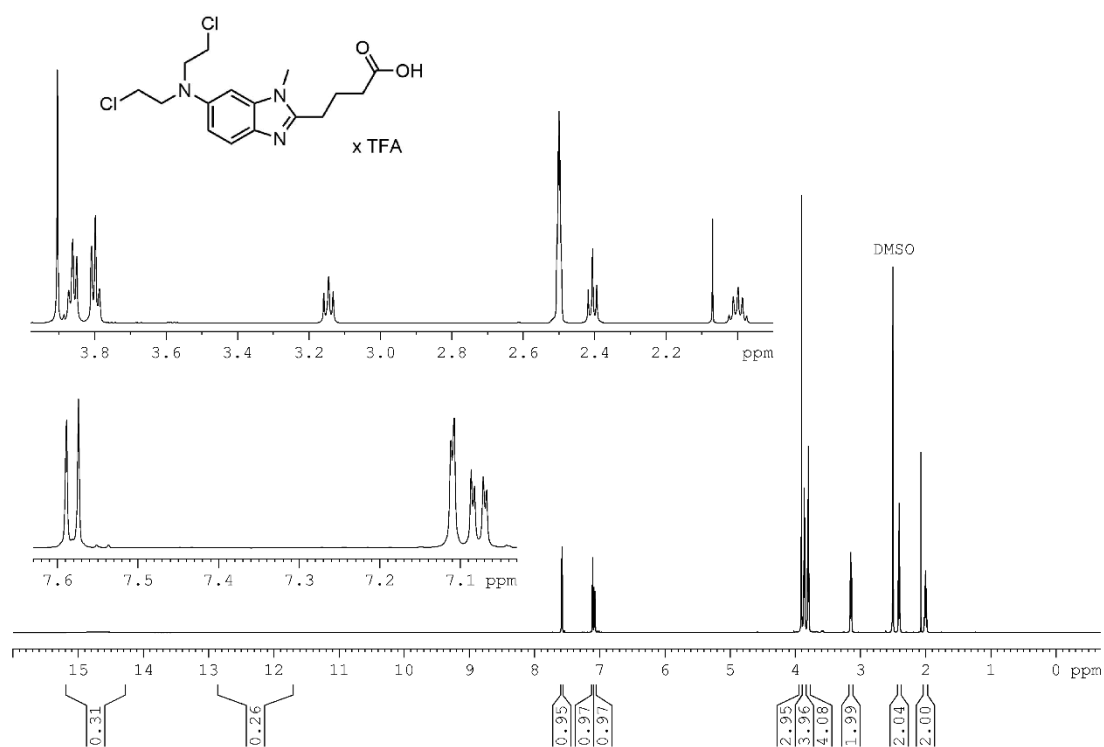
### 5.5.1 NMR Spectra



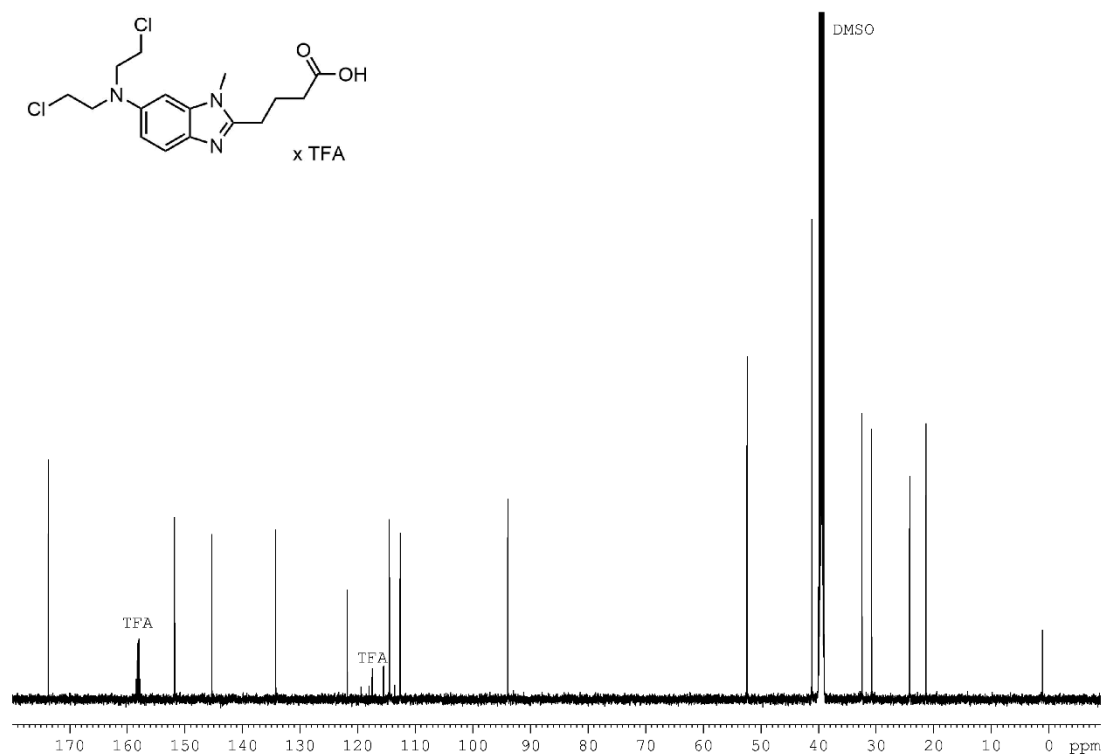
<sup>1</sup>H NMR spectrum (600 MHz, CDCl<sub>3</sub>) of compound **5.07**.



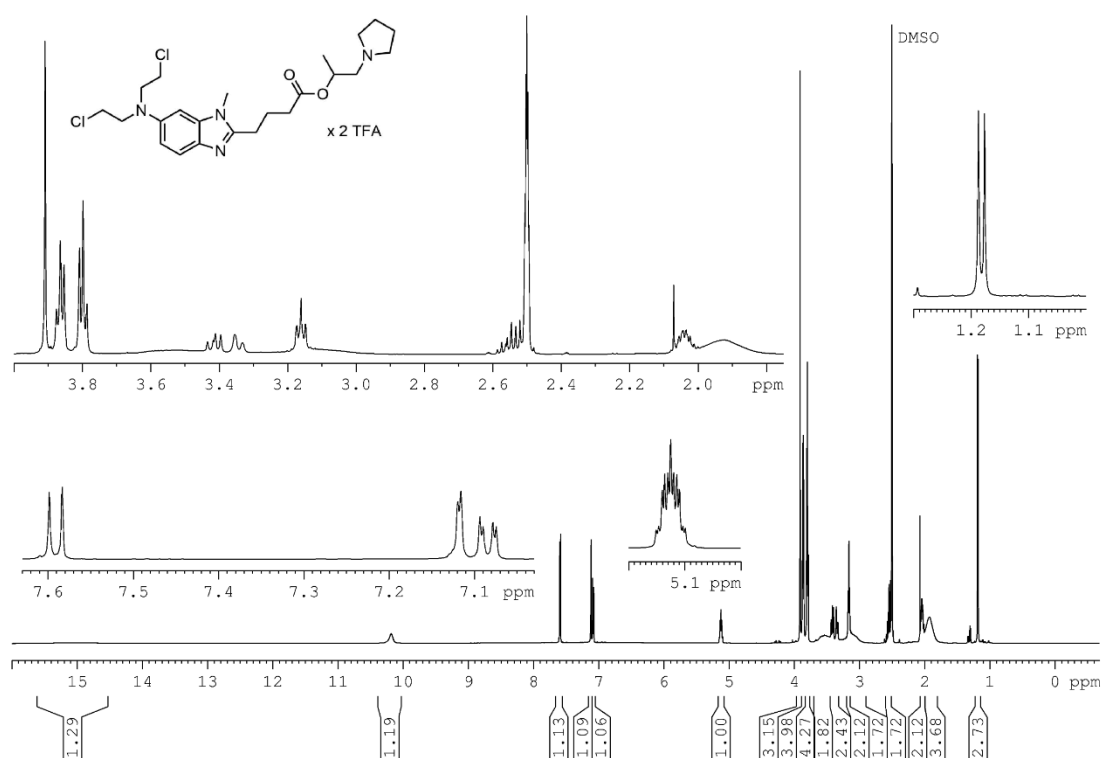
<sup>13</sup>C NMR spectrum (151 MHz, CDCl<sub>3</sub>) of compound **5.07**.



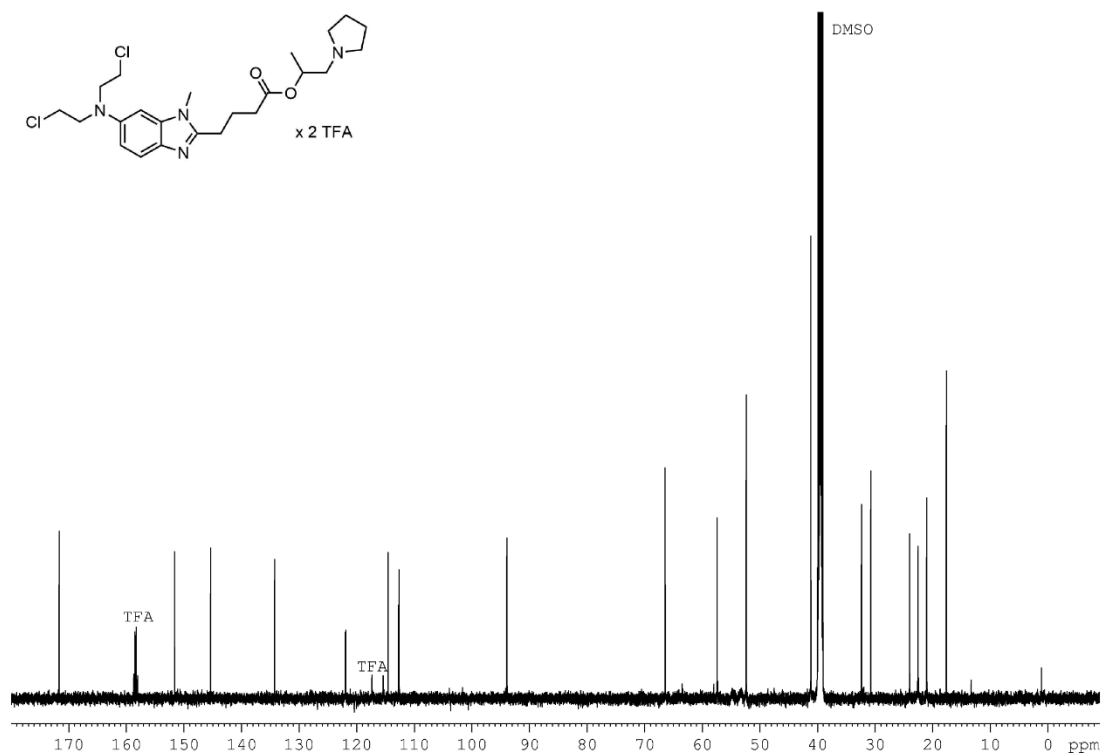
<sup>1</sup>H NMR spectrum (600 MHz, DMSO-*d*<sub>6</sub>) of compound **5.09**.



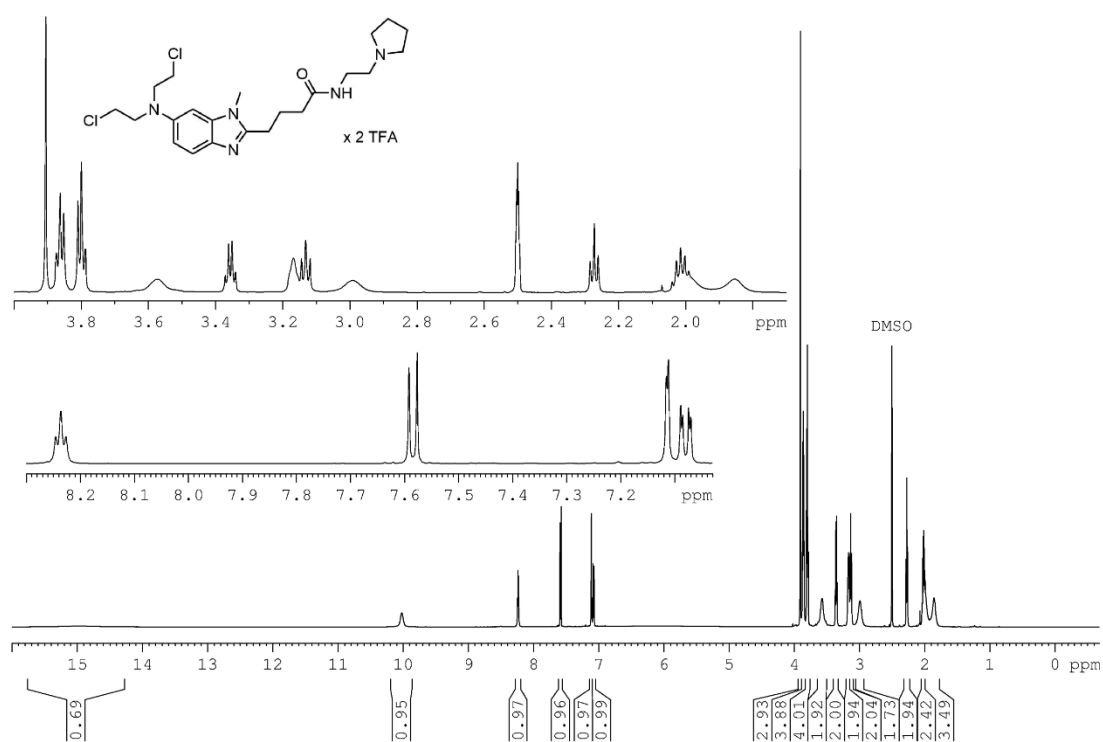
<sup>13</sup>C NMR spectrum (151 MHz, DMSO-*d*<sub>6</sub>) of compound **5.09**.



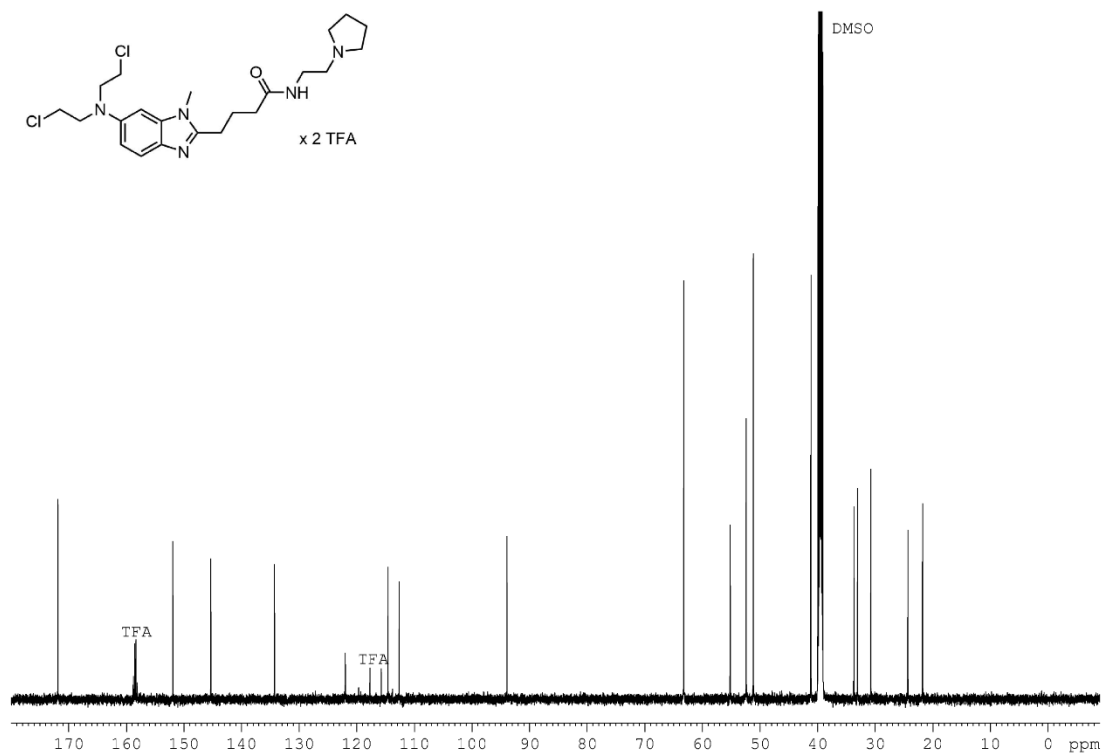
<sup>1</sup>H NMR spectrum (600 MHz, DMSO-*d*<sub>6</sub>) of compound **5.10**.



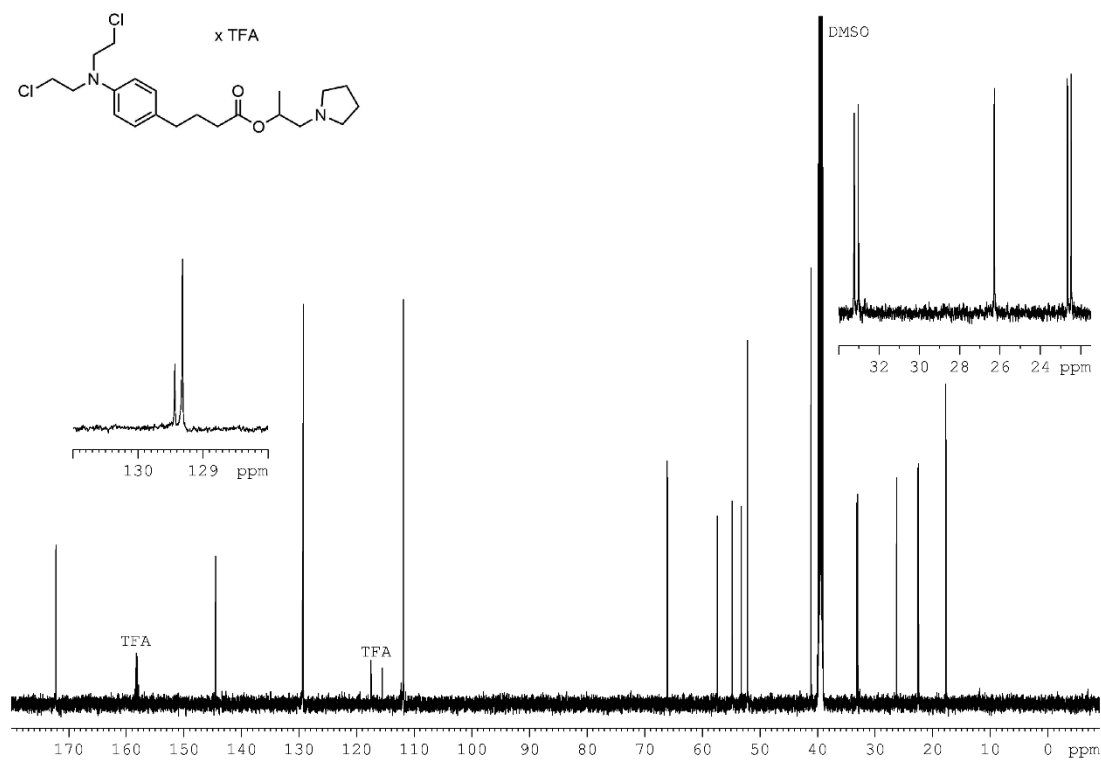
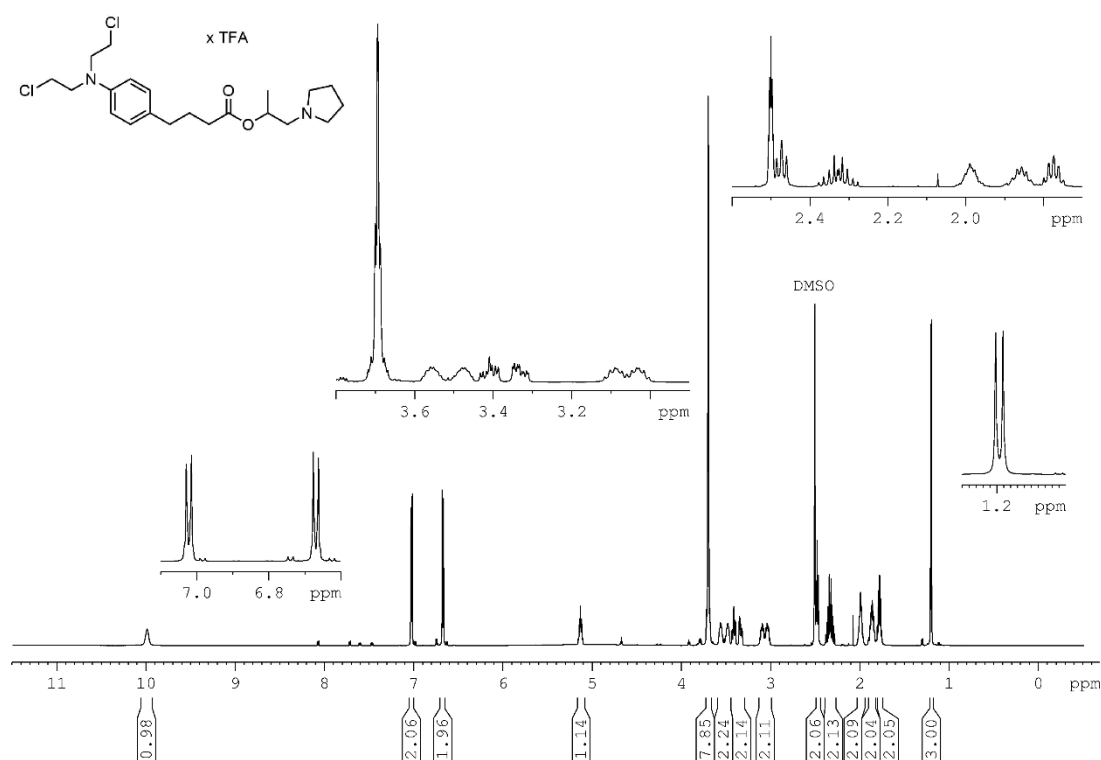
<sup>13</sup>C NMR spectrum (151 MHz, DMSO-*d*<sub>6</sub>) of compound **5.10**.

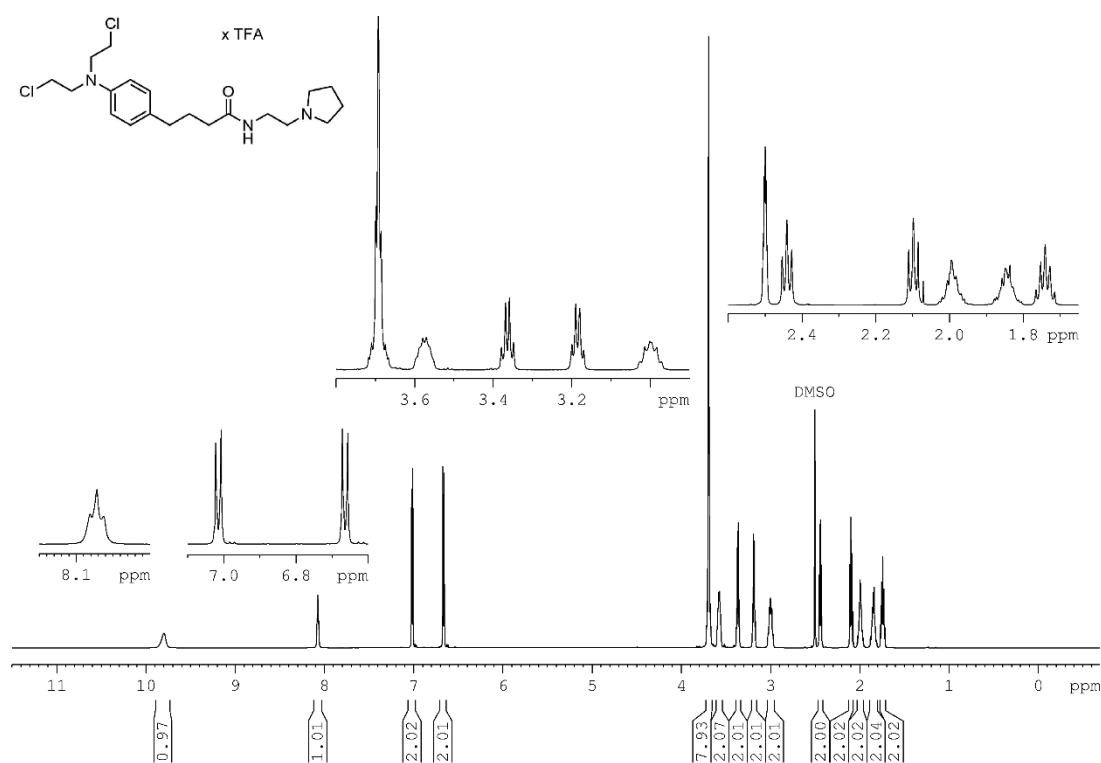


<sup>1</sup>H NMR spectrum (600 MHz, DMSO-*d*<sub>6</sub>) of compound **5.11**.

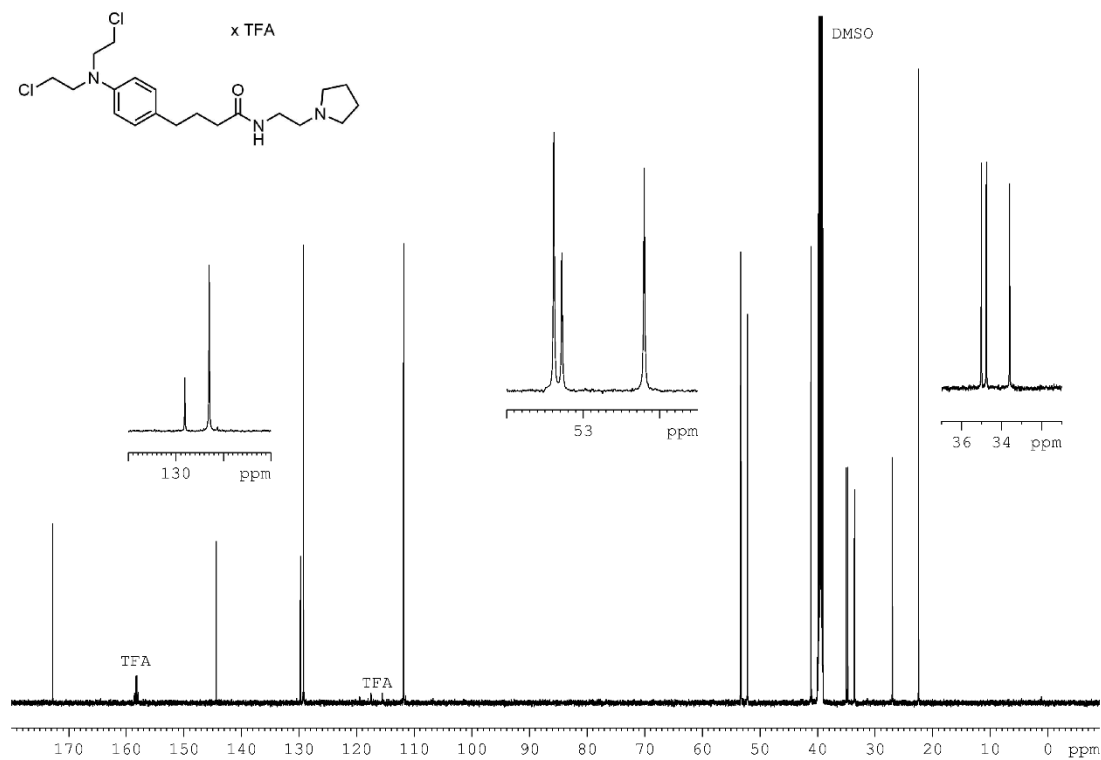


<sup>13</sup>C NMR spectrum (151 MHz, DMSO-*d*<sub>6</sub>) of compound **5.11**.

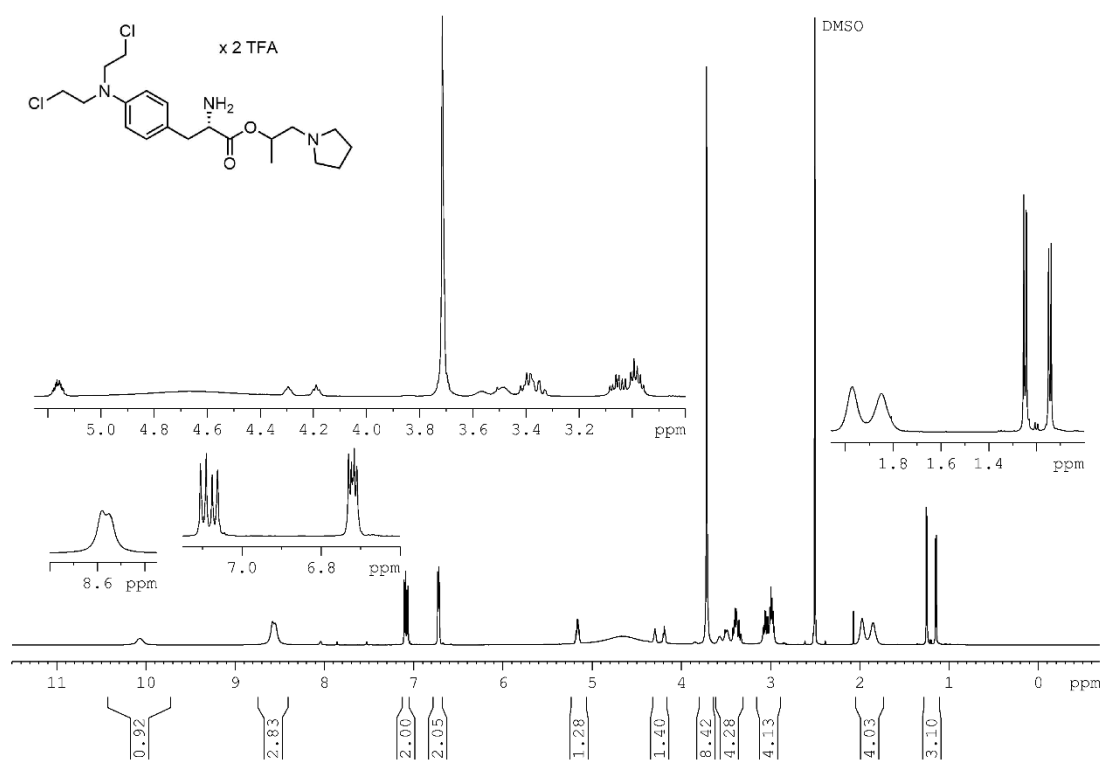




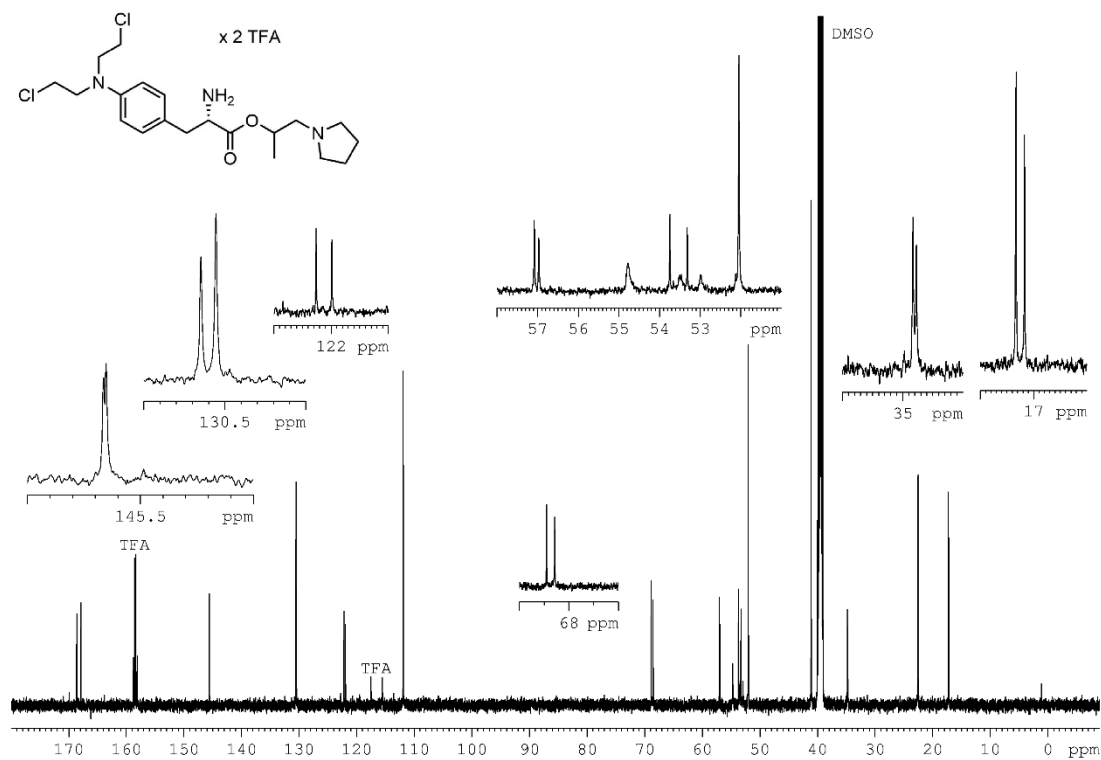
<sup>1</sup>H NMR spectrum (600 MHz, DMSO-*d*<sub>6</sub>) of compound **5.13**.



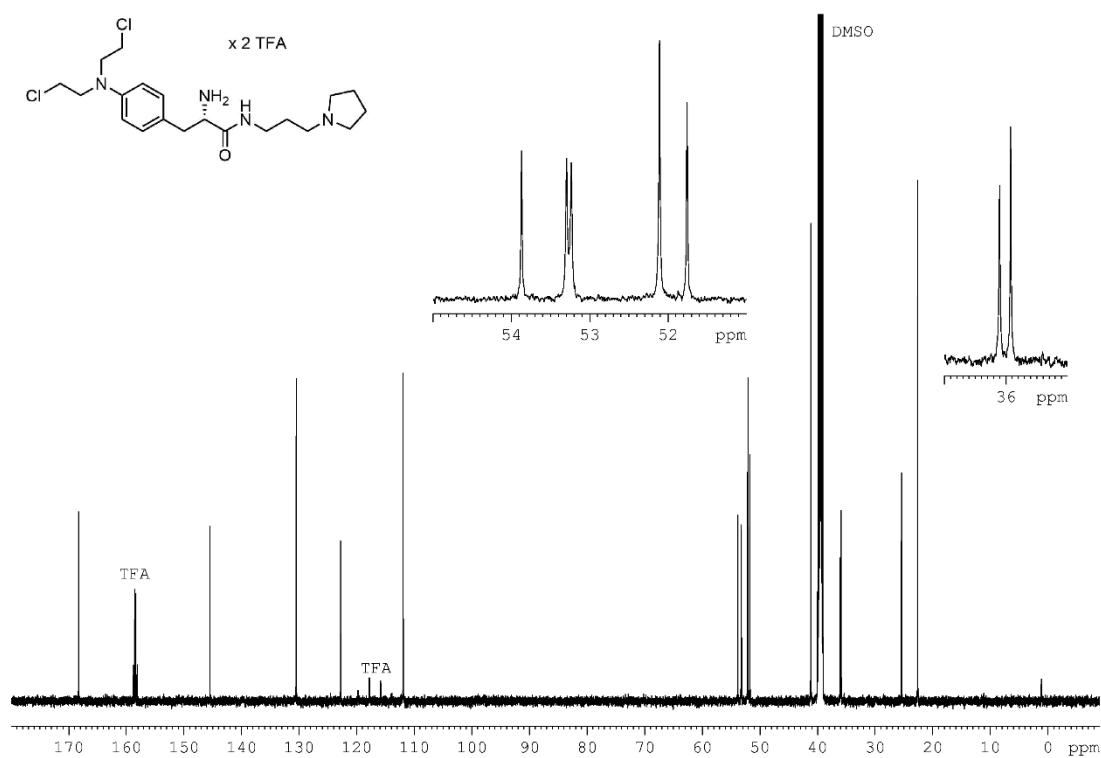
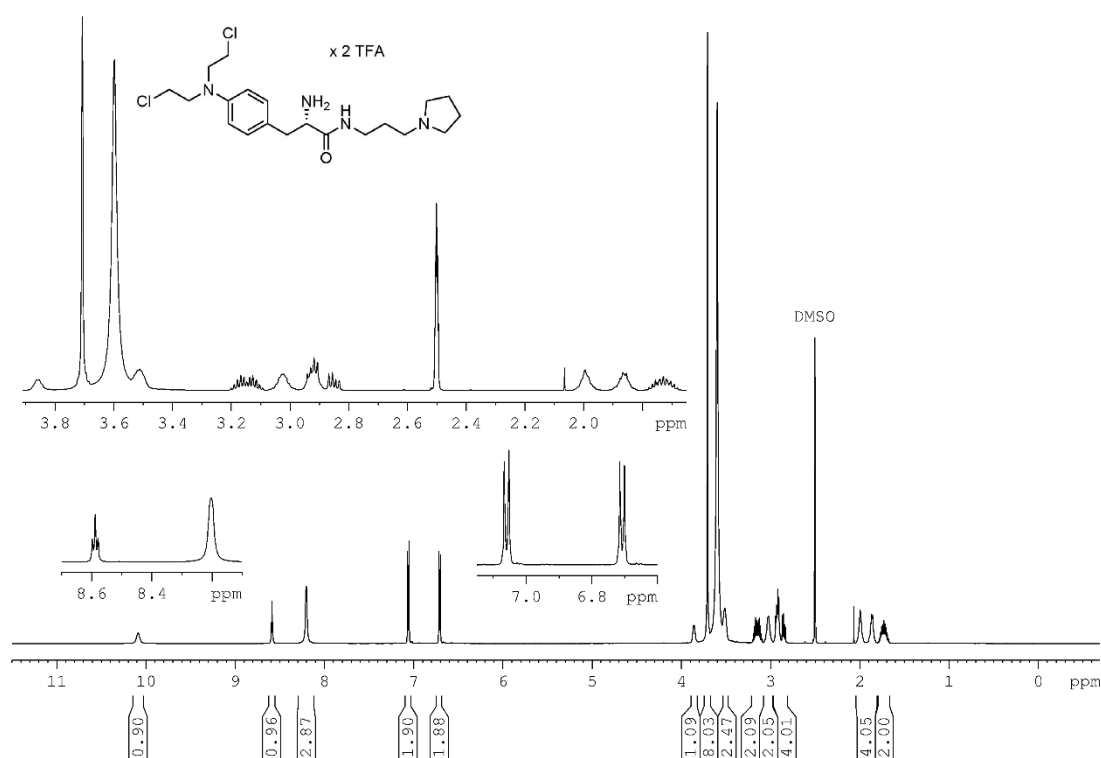
<sup>13</sup>C NMR spectrum (151 MHz, DMSO-*d*<sub>6</sub>) of compound **5.13**.



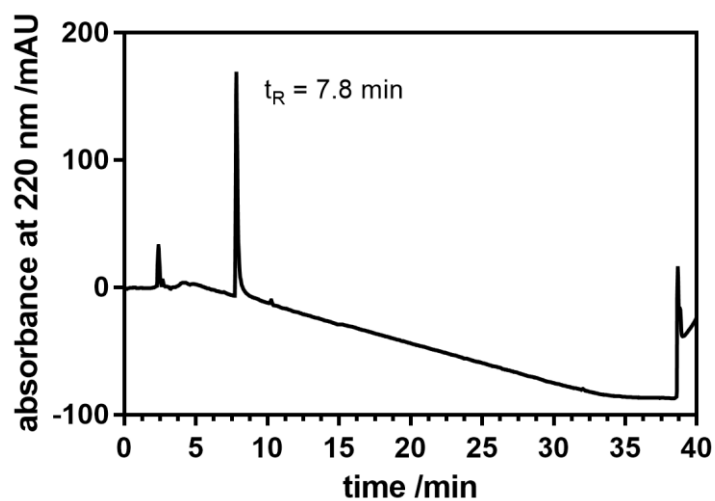
<sup>1</sup>H NMR spectrum (600 MHz, DMSO-*d*<sub>6</sub>) of compound **5.15**.



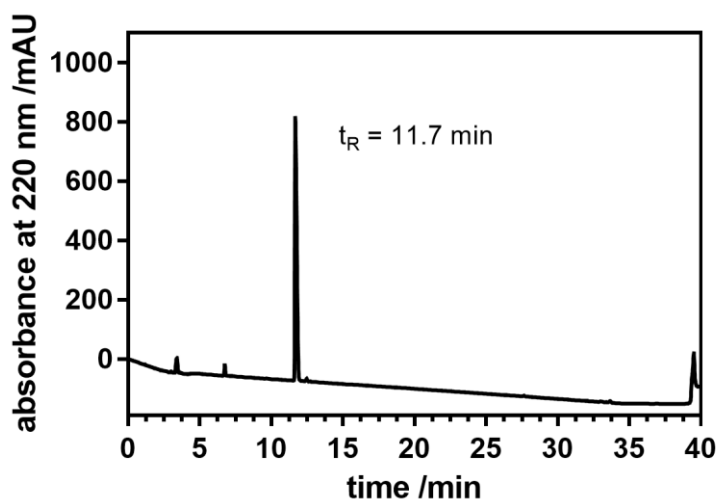
<sup>13</sup>C NMR spectrum (151 MHz, DMSO-*d*<sub>6</sub>) of compound **5.15**.



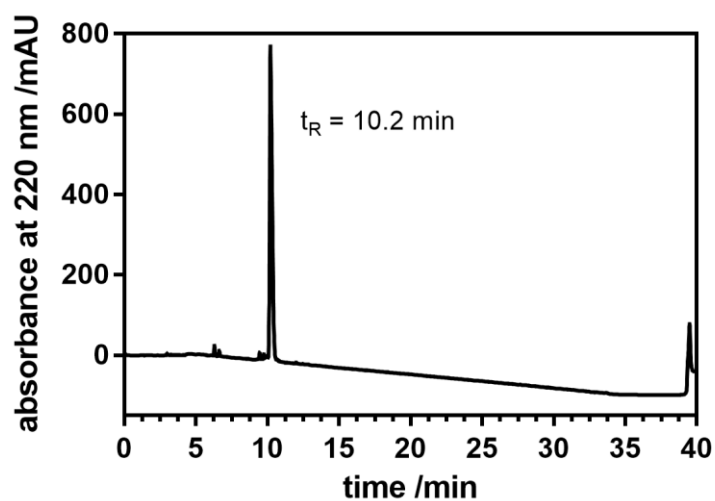
### 5.5.2 Chromatograms (Purity Control)



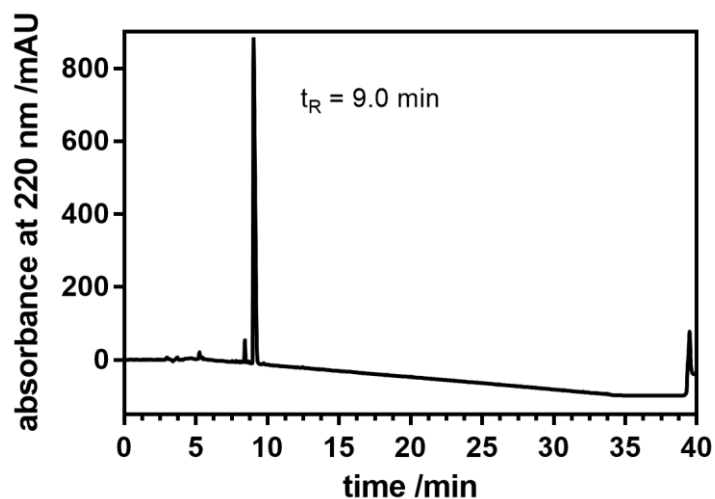
Chromatogram (purity control) of **5.07** (RP-HPLC).



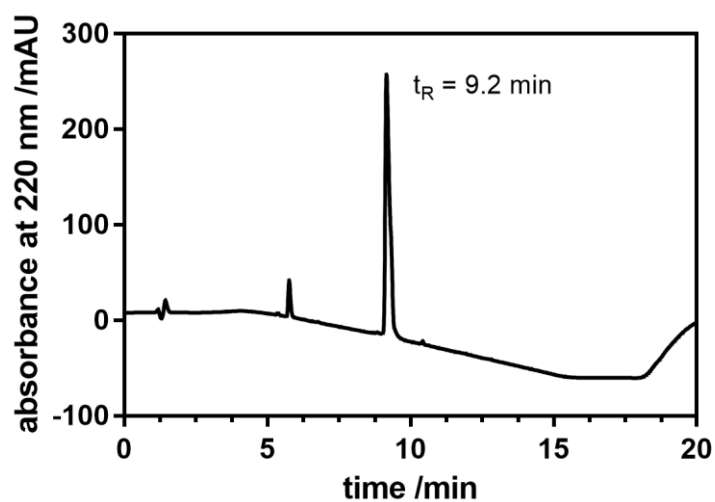
Chromatogram (purity control) of **5.09** (RP-HPLC).



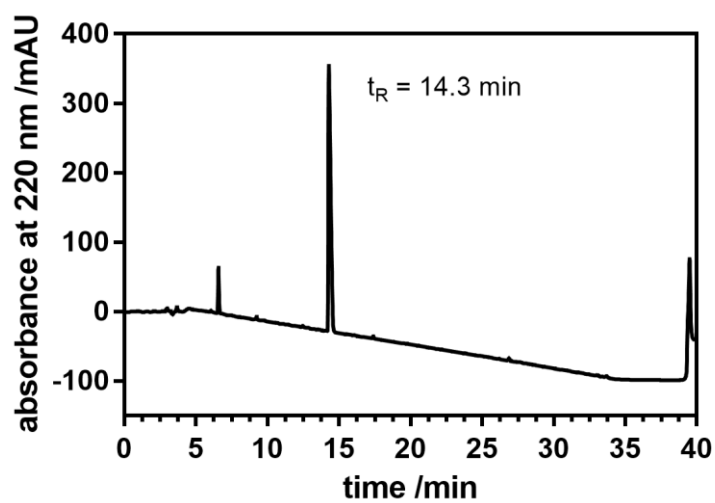
Chromatogram (purity control) of **5.10** (RP-HPLC).



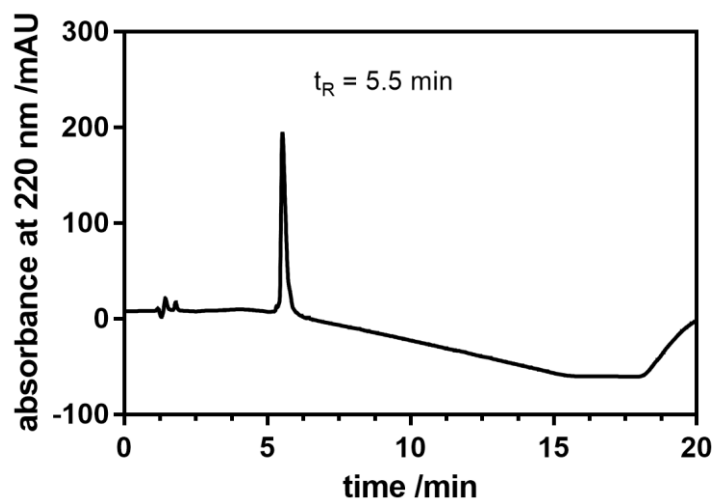
Chromatogram (purity control) of **5.11** (RP-HPLC).



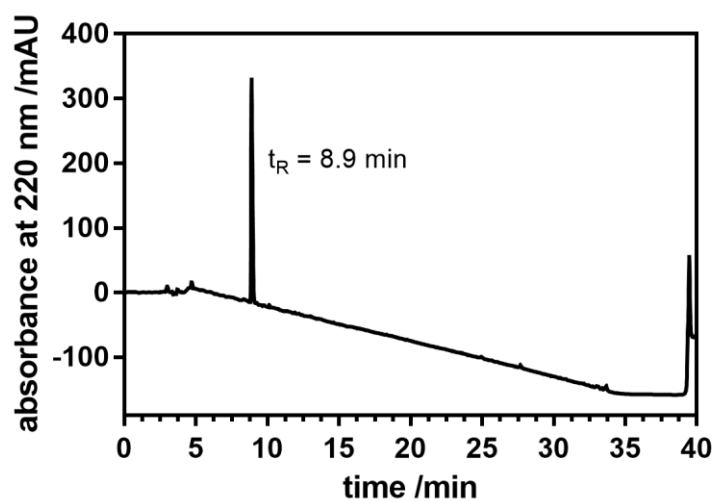
Chromatogram (purity control) of **5.12** (RP-HPLC).



Chromatogram (purity control) of **5.13** (RP-HPLC).



Chromatogram (purity control) of **5.15** (RP-HPLC).



Chromatogram (purity control) of **5.16** (RP-HPLC).

## 5.6 References

- [1] H. Nagai, Y.H. Kim, Cancer prevention from the perspective of global cancer burden patterns, *J. Thorac. Dis.*, 9 (2017) 448-451.
- [2] B.A. Chabner, T.G. Roberts, Chemotherapy and the war on cancer, *Nat. Rev. Cancer*, 5 (2005) 65-72.
- [3] M.M. Gottesman, T. Fojo, S.E. Bates, Multidrug resistance in cancer: role of ATP-dependent transporters, *Nat. Rev. Cancer*, 2 (2002) 48-58.
- [4] A. Gilman, F.S. Philips, The Biological Actions and Therapeutic Applications of the B-Chloroethyl Amines and Sulfides, *Science*, 103 (1946) 409.
- [5] R.K. Singh, S. Kumar, D.N. Prasad, T.R. Bhardwaj, Therapeutic journey of nitrogen mustard as alkylating anticancer agents: Historic to future perspectives, *Eur. J. Med. Chem.*, 151 (2018) 401-433.
- [6] J.L. Everett, J.J. Roberts, W.C.J. Ross, Aryl-2-halogenoalkylamines. Part XII. Some carboxylic derivatives of NN-di-2-chloroethylaniline, *J. Chem. Soc.*, (1953) 2386-2392.
- [7] S. Neidle, D.E. Thurston, Chemical approaches to the discovery and development of cancer therapies, *Nat. Rev. Cancer*, 5 (2005) 285-296.
- [8] D. Godenèche, J.C. Madelmont, M.F. Moreau, R. Plagne, G. Meyniel, Comparative physico-chemical properties, biological effects, and disposition in mice of four nitrogen mustards, *Cancer Chemother. Pharmacol.*, 5 (1980) 1-9.
- [9] S. Genka, J. Deutsch, U.H. Shetty, P.L. Stahle, V. John, I.M. Lieberburg, F. Ali-Osmant, S.I. Rapoport, N.H. Greig, Development of lipophilic anticancer agents for the treatment of brain tumors by the esterification of water-soluble chlorambucil, *Clin. Exp. Metastasis*, 11 (1993) 131-140.
- [10] D. Steinritz, A. Schmidt, T. Simons, M. Ibrahim, C. Morguet, F. Balszuweit, H. Thiermann, K. Kehe, W. Bloch, B. Bölck, Chlorambucil (nitrogen mustard) induced impairment of early vascular endothelial cell migration – Effects of  $\alpha$ -linolenic acid and N-acetylcysteine, *Chem.-Biol. Interact.*, 219 (2014) 143-150.
- [11] F. Bergel, J.A. Stock, Cyto-active amino-acid and peptide derivatives. Part I. Substituted phenylalanines, *J. Chem. Soc.*, (1954) 2409-2417.
- [12] D.T. Vistica, Cytotoxicity as an indicator for transport mechanism. Evidence that melphalan is transported by two leucine-preferring carrier systems in the L1210 murine leukemia cell, *Biochim. Biophys. Acta, Biomembr.*, 550 (1979) 309-317.
- [13] T.B. Salisbury, S. Arthur, The Regulation and Function of the L-Type Amino Acid Transporter 1 (LAT1) in Cancer, *Int. J. Mol. Sci.*, 19 (2018) 2373.
- [14] I.D. Davies, J.P. Allanson, R.C. Causon, Rapid determination of the anti-cancer drug Melphalan (Alkeran<sup>TM</sup>) in human serum and plasma by automated solid phase extraction and liquid chromatography tandem mass spectrometry, *Chromatographia*, 52 (2000) 92-97.
- [15] U.D. Bayraktar, Q. Bashir, M. Qazilbash, R.E. Champlin, S.O. Ciurea, Fifty Years of Melphalan Use in Hematopoietic Stem Cell Transplantation, *Biology of Blood and Marrow Transplantation*, 19 (2013) 344-356.
- [16] W. Ozegowski, D. Krebs, Aminosäureantagonisten. III.  $\omega$ -[Bis-( $\beta$ -chloräthyl)-amino-benzimidazolyl-(2)]-propion- bzw. -buttersäuren als potentielle Cytostatika, *J. Prakt. Chem.*, 20 (1963) 178-186.
- [17] W. Ozegowski, D. Krebs, IMET 3393,  $\gamma$ -[1-Methyl-5-bis-( $\beta$ -chloräthyl)-amino-benzimidazolyl-(2)]-buttersäurehydrochlorid, ein neues Zytostatikum aus der Reihe der Benzimidazol-Loste, *Zbl. Pharm.*, 110 (1971) 1013-1019.
- [18] M. Kalaycio, Bendamustine: a new look at an old drug, *Cancer*, 115 (2009) 473-479.
- [19] L.M. Leoni, Bendamustine: rescue of an effective antineoplastic agent from the mid-twentieth century, *Semin. Hematol.*, 48 (Suppl 1) (2011) 4-11.

- [20] L.M. Leoni, B. Bailey, J. Reifert, H.H. Bendall, R.W. Zeller, J. Corbeil, G. Elliott, C.C. Niemeyer, Bendamustine (Treanda) displays a distinct pattern of cytotoxicity and unique mechanistic features compared with other alkylating agents, *Clin. Cancer Res.*, 14 (2008) 309-317.
- [21] L.M. Leoni, J.A. Hartley, Mechanism of action: the unique pattern of bendamustine-induced cytotoxicity, *Semin. Hematol.*, 48 (Suppl 1) (2011) 12-23.
- [22] B.D. Cheson, M.J. Rummel, Bendamustine: rebirth of an old drug, *J. Clin. Oncol.*, 27 (2009) 1492-1501.
- [23] J. Colledge, Oral dosage forms of bendamustine, WO2010063493A1, 2010.
- [24] R.Y. LaBell, P.R. Patel, Oral formulations of bendamustine, US20120157505A1, 2012.
- [25] I. Pencheva, A. Bogomilova, N. Koseva, D. Obreshkova, K. Troev, HPLC study on the stability of bendamustine hydrochloride immobilized onto polyphosphoesters, *J. Pharm. Biomed. Anal.*, 48 (2008) 1143-1150.
- [26] A.M. Scutaru, M. Wenzel, H. Scheffler, G. Wolber, R. Gust, Optimization of the N-Lost Drugs Melphalan and Bendamustine: Synthesis and Cytotoxicity of a New Set of Dendrimer–Drug Conjugates as Tumor Therapeutic Agents, *Bioconjugate Chem.*, 21 (2010) 1728-1743.
- [27] R.P. Bakale, P.D. Brown, J. Chen, A.S. Drager, R.Y. LaBell, R.E. McKean, P.R. Patel, R.C. Roemmele, Bendamustine derivatives and methods of using same, WO2014075035A1, 2015.
- [28] S. Huber, J.P. Huettner, K. Hacker, G. Bernhardt, J. König, A. Buschauer, Esters of Bendamustine Are by Far More Potent Cytotoxic Agents than the Parent Compound against Human Sarcoma and Carcinoma Cells, *PLOS ONE*, 10 (2015) e0133743.
- [29] S. Huber, F. Antoni, C. Schickaneder, H. Schickaneder, G. Bernhardt, A. Buschauer, Stabilities of neutral and basic esters of bendamustine in plasma compared to the parent compound: Kinetic investigations by HPLC, *J. Pharm. Biomed. Anal.*, 104 (2015) 137-143.
- [30] H. Schickaneder, C. Schickaneder, A. Buschauer, G. Bernhardt, S. Huber, M. Limmert, M. Lubbe, H. Hofmeier, Bendamustine derivatives and related compounds, and medical use thereof in cancer therapy, WO2013189847A1, 2013.
- [31] H. Schickaneder, C. Schickaneder, A. Buschauer, G. Bernhardt, S. Huber, F. Antoni, Preparation of bendamustine derivatives and related compounds for use in treating cancer, WO2015091827A1, 2015.
- [32] M. Wolf, U. Bauder-Wüst, A. Mohammed, F. Schönsiegel, W. Mier, U. Haberkorn, M. Eisenhut, Alkylating benzamides with melanoma cytotoxicity, *Melanoma Research*, 14 (2004).
- [33] G. Bernhardt, H. Reile, H. Birnböck, T. Spruß, H. Schönenberger, Standardized kinetic microassay to quantify differential chemosensitivity on the basis of proliferative activity, *J. Cancer Res. Clin. Oncol.*, 118 (1992) 35-43.
- [34] K.-H. Hsieh, G.R. Marshall, Alkylating angiotensin II analogs: Synthesis, analysis, and biological activity of angiotensin II analogs containing the nitrogen mustard melphalan in position 8, *J. Med. Chem.*, 24 (1981) 1304-1310.
- [35] B.E. Toki, P.D. Senter, Preparation of melphalan prodrugs for use in Antibody-Directed Enzyme Prodrug Therapy, WO2005070457A1, 2005.

## Abbreviations

ABC	ATP-binding cassette transporter
ABCB1	ATP-binding cassette transporter, subfamily B, member 1
ABCC1	ATP-binding cassette transporter, subfamily C, member 1
ABCG2	ATP-binding cassette transporter, subfamily G, member 2
ABCP	placenta-specific ATP-binding cassette transporter
ADME-Tox	absorption, distribution, metabolism, excretion and toxicity
ADP	adenosine diphosphate
AML	acute myeloid leukemia
ATP	adenosine triphosphate
BBB	blood-brain barrier
BCRP	breast cancer resistance protein
boc	<i>tert</i> -butyloxycarbonyl
boc <sub>2</sub> O	di- <i>tert</i> -butyl dicarbonate
calcein-AM	calcein acetoxymethyl ester
CHAPS	3-((3-cholamidopropyl)dimethylammonio)-1-propanesulfonate
CLL	chronic lymphocytic leukemia
clogP	calculated logP value
cryo-EM	cryogenic electron microscopy
CuAAC	copper-catalyzed azide-alkyne cycloaddition
DCC	<i>N,N'</i> -Dicyclohexylcarbodiimide
DCM	dichloromethane
DDI	drug-drug interaction
DHEAS	dehydroepiandrosterone sulfate
DIPEA	<i>N,N</i> -diisopropylethylamine
DMEM	Dulbecco's modified Eagle's medium
DMF	dimethylformamide
DMSO	dimethylsulfoxide
DNA	deoxyribonucleic acid
DTT	dithiothreitol
E <sub>1</sub> S	estrone 3-sulfate
EC <sub>50</sub>	concentration of compound required to give 50% maximal effect on activity
EDTA	ethylenediaminetetraacetic acid
EL	extracellular loop

EMA	European Medicines Agency
EtOH	ethanol
FCS	fetal calf serum
FDA	US Food and Drug Administration
FTC	fumitremorgin C
GBB	gut-blood barrier
HBTU	hexafluorophosphate benzotriazole tetramethyl uronium
HIV	human immunodeficiency virus
HL	Hodgkin lymphoma
HPLC	high pressure liquid chromatography
HRMS	high-resolution mass spectrometry
HTS	high-throughput screening
HUGO	Human Genome Organization
IC <sub>50</sub>	concentration of inhibitor required to give 50% inhibition of activity
IR	infrared
kb	kilobase
kDa	kilodalton
mAU	milli-absorbance units
MDR	multidrug resistance
MeCN	acetonitrile
MeOH	methanol
MM	multiple myeloma
MRP1	multidrug resistance associated protein 1
MS	(low resolution) mass spectrometry
MWT	molecular weight
NBD	nucleotide binding domain
NHL	non-Hodgkin lymphoma
NMR	nuclear magnetic resonance
NMRI	Naval Medical Research Institute
PBS	phosphate buffered saline
PCR	polymerase chain reaction
Pd/C	palladium on activated charcoal
PEG	polyethylene glycol
PET	positron emission tomography
P-gp	permeability glycoprotein
PhIP	2-amino-1-methyl-6-phenylimidazo(4,5-b)pyridine

P <sub>i</sub>	inorganic phosphate
PMSF	phenylmethanysulfonyl fluoride
PP	polypropylene
RAMEB	randomly methylated β-cyclodextrins
RNA	ribonucleic acid
Ro5	rule of five
RP-HPLC	reversed-phase high pressure liquid chromatography
SDS	sodium dodecyl sulfate
SEC-TS	size-exclusion chromatography-based thermostability assay
SEM	standard error of the mean
SPECT	single-photon emission computed tomography
t <sub>1/2</sub>	half-life
TBAF	tetra- <i>n</i> -butylammonium fluoride
TBTA	tris((1-benzyl-4-triazolyl)methyl)amine
TBTU	2-(1 <i>H</i> -benzotriazole-1-yl)-1,1,3,3-tetramethylaminium tetrafluoroborate
TFA	trifluoroacetic acid
THF	tetrahydrofuran
TLC	thin layer chromatography
TM	transmembrane helix
TMD	transmembrane domain
TMEP	Tris, mannitol, EDTA, leupeptin, benzamidine, PMSF, DTT (buffer ingredients)
TMS	trimethylsilyl
Tris	tris(hydroxymethyl)aminomethane
UV	ultraviolet
VIS	visible



# Acknowledgements

I would like to take this opportunity to express my gratitude to all the people who contributed to the realization of this doctoral thesis. I would like to thank:

Prof. Dr. Armin Buschauer, who gave me the opportunity to work freely and independently on a topic of my choosing. Unfortunately he passed away far too early (July 2017).

Prof. Dr. Günther Bernhardt for his reliable support, especially for his advice on the preparation of the manuscripts for publication and of this thesis.

Prof. Dr. Pierre Koch, Prof. Dr. Joachim Wegener and Prof. Dr. Dominik Horinek for kindly agreeing to be part of the examination board.

Matthias Scholler for being my ABC buddy in a group of GPCR researchers, for ABC-related discussions and for the excellent collaboration on tariquidar-related triazoles as ABCG2 inhibitors. For the latter I would also like to thank Dr. Manuel Bause and the other co-authors.

Dr. David Wifling for performing the molecular docking studies and for always having a friendly word on his lips.

Dr. Max Keller for helpful pieces of advice on miscellaneous matters.

Maria Beer-Krön and Lydia Schneider for excellent technical assistance and friendly conversations.

Peter Richthammer for helpful IT support and for spreading good mood.

The employees of the analytical department of the University of Regensburg for measuring NMR and mass spectra. Special thanks goes to Fritz Kastner for his competent help with several NMR-related problems and his friendliness.

The students who supported me with my lab work and showed great interest in my research.

The members of my working group for moral support, in particular the following persons:

Franziska Naporra, who I could always turn to when I needed someone to talk to, who never let me down in difficult situations, and who was my steady companion throughout the time of my dissertation.

Edith Bartole, who I admire for her ability to stand up for herself and who I turned to when I needed a push.

Sabrina Biselli, who helped me with all sorts of questions and with whom I enjoyed many Yoga sessions together.

Jonas Buschmann, a person with integrity, who always offered me an open ear.

Andrea Pegoli, my favorite Italian guy, with whom I laughed so much and who is the most patient listener I have ever met.

And of course all the colleagues with whom I shared the lab 14.2.23 for the entertaining time together.

For moral support I would also like to thank the following persons:

My “Regensburg-Chemistry-Crew”, especially Monika Enzinger, Maria Landa, Judith Böhm, and Christian Iffelsberger, who I could always count on when the shit hit the fan. I apologize for using such words in my thesis.

My dear friends and companions through life Cornelia Kruse, Nadja Busch, Simone Hoffmann, Simone Thonn and Anne Assmann.

Last but not least, I would like to express my deep gratitude to my family, to whom I dedicate this thesis. During all the ups and downs that are implied when embarking on the adventure that is a doctoral dissertation, I was always sure to have a safety net. This made being successful possible in the first place. Very special thanks goes to my mother, who not only supported me mentally, but also contributed to this thesis through her expertise. As a former English teacher, she proofread every page and gave me valuable linguistic advice.

A heartfelt thank you!

# Eidesstattliche Erklärung

Ich erkläre hiermit an Eides statt, dass ich die vorliegende Arbeit ohne unzulässige Hilfe Dritter und ohne Benutzung anderer als der angegebenen Hilfsmittel angefertigt habe; die aus anderen Quellen direkt oder indirekt übernommenen Daten und Konzepte sind unter Angabe des Literaturzitats gekennzeichnet.

Einige der experimentellen Arbeiten wurden in Zusammenarbeit mit anderen Personen und Institutionen durchgeführt. Vermerke zu den Beiträgen der betreffenden Personen finden sich in den jeweiligen Kapiteln.

Weitere Personen waren an der inhaltlich-materiellen Herstellung der vorliegenden Arbeit nicht beteiligt. Insbesondere habe ich hierfür nicht die entgeltliche Hilfe eines Promotionsberaters oder anderer Personen in Anspruch genommen. Niemand hat von mir weder unmittelbar noch mittelbar geldwerte Leistungen für Arbeiten erhalten, die im Zusammenhang mit dem Inhalt der vorgelegten Dissertation stehen.

Die Arbeit wurde bisher weder im In- noch im Ausland in gleicher oder ähnlicher Form einer anderen Prüfungsbehörde vorgelegt.

Regensburg den 30. September 2020

---

Frauke Antoni